Flinders University

Identifying and interrogating human host factors associated with dengue virus non-structural protein 1 secretion and internalisation

By

Stephen Matthew Rodgers Johnson
Bachelor of Science (Honours)

Thesis
Submitted to Flinders University
for the degree of Doctor of Philosophy in Biological Sciences

Doctor of Philosophy
College of Medicine and Public Health
15 October 2025

TABLE OF CONTENTS

ABSTRACT

As the most prevalent arthropod-borne viral pathogen, dengue virus (DENV) is estimated to infect nearly 400 million people each year. Clinical manifestations encompass a wide disease spectrum ranging from mild febrile illness to more serious complications including haemorrhage, shock and death. No DENV-specific therapeutics are currently available to prevent dengue disease progression, thus necessitating a deeper understanding of DENV-human host molecular interactions. A key DENV virulence factor is its non-structural protein 1 (NS1). This multifunctional viral protein performs a variety of roles that are indispensable to DENV and critical for dengue disease. Within infected cells, intracellular NS1 is essential for viral genome replication and virion morphogenesis. NS1 is also secreted from infected cells, and this secreted NS1 (sNS1) form has been identified as a key mediator of dengue pathogenesis. In the extracellular environment, the highly immunogenic sNS1 can elicit the production of both protective and pathogenic antibodies. sNS1 can also interfere with components of the complement system and modulate their activity. Importantly, sNS1 can bind to immune cells and potently induce the production of proinflammatory and vasoactive cytokines that can influence endothelial cell permeability and contribute to vascular leakage – a key hallmark of severe dengue disease. Moreover, sNS1 can bind and internalise into a variety of uninfected target host cell types and enhance their susceptibility to infection. The binding and internalisation of sNS1 by endothelial cells directly contributes to endothelial cell hyperpermeability and vascular leakage. While much research has been conducted on the synthesis, structure, and key functional residues of this viral virulence factor, major gaps exist in our understanding of the molecular mechanisms that are exploited by DENV to achieve NS1 secretion and sNS1 internalisation. As such, the focus of this work was to identify the human host molecular machinery that are involved in NS1 secretion and sNS1 internalisation. First, to identify and interrogate the human host factors involved in NS1 secretion, we employed a customised membrane-trafficking siRNA screen targeting ~180 human host factors in cells infected with an NS1-tagged luciferase reporter virus. Our screen identified COPA, COPB2, and COPG1 as the top ranking host determinants of NS1 secretion efficiency. These proteins are three of the seven subunits of the coatomer protein complex I (COPI) that coat intracellular transport vesicles, implicating COPI machinery and associated pathways as being involved in NS1 secretion. Validation studies employing COPI gene knockdown in DENV-infected cells confirmed that COPI components are required for efficient NS1 secretion but are dispensable for infectious virus secretion. Similar reductions in NS1 secretion were observed when COPI components were depleted in cells infected with the related West Nile virus Kunjin subtype (WNV/KUNV), indicating that the exploitation of COPI to achieve efficient NS1 secretion may be a feature conserved within the Orthoflavivirus genus. Overexpression of wildtype and pathogenic COPI variants in DENV NS1-NS5 polyprotein expressing cells altered NS1 secretion profiles suggesting that allelic variants or COPI expression levels influence NS1 secretion. To functionally inhibit the formation of COPI vesicles, we employed

Golgicide A, a potent and specific inhibitor of GBF1 – a master regulator of COPI vesicle biogenesis. Our results revealed that when GCA is applied late in infection, the catalytic activity of GBF1 is dispensable for DENV genome replication but is required for infectious virus production and efficient NS1 secretion. Interestingly, while virion secretion was reduced by GCA treatment in a dose-dependent manner, NS1 secretion was only reduced at the highest dose applied, indicating that multiple mechanisms may be exploited by DENV to achieve NS1 secretion. Next, to identify the human host molecular machinery associated with sNS1 internalisation, we employed an APEX2-based proximity labelling strategy. APEX2 is an engineered plant peroxidase that can catalyse the biotinylation of proximal proteins within live cells. We utilised our previously characterised DENV2-NS1-APEX2 virus that secretes sNS1-APEX2 fusion protein from infected cells. sNS1-APEX2-containing cell culture supernatants were inoculated onto naïve human cells to allow sNS1-directed host cell binding and internalisation. Following APEX2-catalysed biotinylation of sNS1 proximal proteins, enriched biotinylated proteins were identified by mass spectrometry, revealing a broad range of candidate human host proteins associated with the early events of sNS1 internalisation. Comparisons of these sNS1 proximal proteins with previous NS1 proteomic studies revealed substantial overlap, confirming the validity of our approach. The identification of multiple proteins that are known to directly interact with sNS1 to induce important biological effects, or to associate with sNS1 in DENV infected patients, confirmed the biological and physiological relevance of our novel data set. Gene ontology analyses revealed an enrichment of host factors associated with extracellular vesicles, suggesting that sNS1 may hijack these intercellular communication vehicles to facilitate sNS1 host cell binding and internalisation. Protein-protein interaction network analyses revealed several functional and/or physical associations that connect many of our identified proteins involved in intracellular trafficking pathways, suggesting that these host factors may be involved in the early events of internalised sNS1 trafficking. Taken together, this work has revealed COPI as a key factor in NS1 secretion and identified a range of host factors associated with sNS1 internalisation. Together, this understanding may aid in the identification of novel targets for NS1-targeting antiviral drug development.

DECLARATION

I certify that this thesis:

1. does not incorporate without acknowledgment any material previously submitted for a degree or diploma in any university

2. and the research within will not be submitted for any other future degree or diploma without the permission of Flinders University

3. to the best of my knowledge and belief, does not contain any material previously published or written by another person except where due reference is made in the text; and

4. has been completed without the use of generative artificial intelligence tools.

This research was supported by an Australian Government Research Training Program (RTP) Scholarship *doi.org/10.82133/C42F-K220*.

Signed: Stephen Johnson

Date: 9th May 2025

ACKNOWLEDGEMENTS

I would like to express my sincerest gratitude to Dr Nicholas Eyre, not only for the opportunity to undertake a PhD but for the privilege of your mentorship. Your overwhelming contribution to my professional development has been invaluable. I'd also like to convey my appreciation to Professor Jill Carr. Thank you for your ever-insightful wisdom, you have been instrumental to my progress. Indeed, my time here would not have been nearly as enjoyable without the support and camaraderie of my Molecular Virology Group lab mates. To Nick, Tom, Brandon, Siena, Rosa, Marie, Laurelle, Roman, Bracho, Travis, and Aiden, thank you!! Big thanks are certainly extended to my colleagues from the Carr Lab: Evie, Josh, Amy, Valeria, Timothy, Luke, and Hawraa. Additionally, thank you to Professor Briony Forbes, Associate Professor Michael Michael, and Professor Eric Gowans for your contribution and assistance which helped me achieve my candidature milestones. Beyond the lab and office, I'd like to express my debt of gratitude to my parents, Helen and Vince, and to my partner, Yasmin. Without your outstanding contribution to my happiness and wellbeing, this PhD would not have been achieved.

LIST OF FIGURES AND TABLES

ABBREVIATIONS

bp	base pair
C	Capsid
COPI	Coatomer protein complex I
COPII	Coatomer protein complex II
DAPI	4', 6-Diamidino-2-pheylinodole
DENV	Dengue Virus
DF	Dengue fever
DHF	Dengue haemorrhagic fever
DMEM	Dulbecco's modified eagle medium
DMSO	Dimethyl sulfoxide
DNA	Deoxyribonucleic acid
DPBS	Dulbecco's PBS
ds	double stranded
DSS	Dengue shock syndrome
E	Envelope
ER	Endoplasmic reticulum
ERES	ER exit sites
ERGIC	ER intermediate Golgi complex
FBS	foetal bovine serum
FFA	Focus forming assay
FFU	Focus forming units
Hr	hour

hpi	hours post-infection
hpt	hours post-transfection
iNS1	intracellular NS1
JEV	Japanese encephalitis virus
kb	kilobase
kDa	kiloDalton
LB	Lauria Bertani Broth
LPS	lipopolysaccharide
Luc	Luciferase
µg	microgram
µL	microlitre
MOI	Multiplicity of infection
MW	Molecular weight
NanoLuc	NanoLuciferase
ng	nanogram
NS	Non-structural
NS1	Non-structural protein 1
NS2A	Non-structural protein 2A
NS2B	Non-structural protein 2B
NS3	Non-structural protein 3
NS4A	Non-structural protein 4A
NS4B	Non-structural protein 4B
NS5	Non-structural protein 5
ORF	Open reading frame

PAGE	Polyacrylamide gel electrophoresis
PBS	Phosphate buffered saline
PCR	Polymerase chain reaction
RC	Replication complex
RdRp	RNA-dependent RNA polymerase
RNA	ribonucleic acid
RT	Root temperature
SDS	sodium dodecyl sulfate
sNS1	secreted NS1
ss	single stranded
TGN	trans Golgi network
UTR	Untranslated region
vRNA	viral RNA
WHO	World Health Organisation
WNV/KUNV	West Nile virus (Kunjin strain)
WT	Wildtype
ZIKV	Zika virus

Chapter 1

Introduction

1: Introduction

1.1: History

The first records of a dengue-like disease were reported in China in the 3rd century AD in the Chinese 'encyclopedia of disease symptoms and remedies', with subsequent events of similar diseases described in the 7th and 10th centuries [1]. The disease, designated 'water poison', was connected with water-associated flying insects. By the 17th century, dengue-like disease epidemics were being recorded in the Caribbean (Martinique and Guadeloupe in 1635) and Central America (Panama 1699) and by the 18th century, similar disease outbreaks had been observed in Southeast Asia (Batavia, now Jakarta, Indonesia 1779) and Africa (Egypt, Cairo 1779) [2]. Ascribing these dengue-like cases to dengue virus (DENV), however, is impracticable due to a paucity of detailed clinical documents and the likely co-circulation of other arboviral pathogens for which infections result in similar clinical presentations [3]. The clinical picture described by Benjamin Rush detailing an outbreak in Philadelphia, United States, in 1780 is widely accepted as being of DENV aetiology, with 'break-bone fever' symptoms compatible with dengue haemorrhagic fever (DHF) [4]. Dengue-like diseases were recorded in the Americas during the 1800's across a wide geographical expanse encompassing regions as far north as the United States to as far south as Chile [5]. These outbreaks, most frequently connected with port cities, have been associated with historical global shipping expansion and urbanisation, in particular, facilitating the geographical expansion of an African mosquito, *Aedes aegypti*, aided by the slave trade disseminating this vector from West Africa to the New World during the 17th century [2, 6]. The ability of this mosquito to adapt to a human and urban environment has allowed it to become an efficient vector of several viruses. More recently, in the late 19th and early 20th centuries, dengue-like haemorrhagic disease outbreaks were identified in Australia (1897), Lebanon (1910), Taiwan (1916 and 1931), and Greece (1928) [2], suggesting that major dengue epidemics had been observed on all populated continents and that DENV may have had achieved a global distribution.

Virological investigations in the early 1900's had provided some observations that dengue disease may be of mosquito origin and viral in aetiology [7]. In 1906, the Australian naturalist Thomas L. Bancroft implicated *Ae. aegypti* as a vector of dengue transmission [8]. *Ae. aegypti*-mediated transmission of dengue-like disease was subsequently confirmed in 1918 by the Australian pathologist and naturalist J. Burton Cleland [9]. The viral aetiology of dengue was established in the 1940's when the first DENV's were isolated [10, 11]. It was recognised by Sabin and Schlesinger in 1952 that DENV's isolated from three geographically separated locations (Hawaii, India, and New Guinea) were antigenically similar, yet antigenically distinct strains could also be isolated from the same locations [12]; the two immunologically distinct variants were subsequently designated DENV1 and DENV2. Further, two more antigenically distinct DENV's were isolated from patients in Thailand and the Philippines, DENV3 and DENV4 [13], thus giving rise to the identification of all four DENV

serotypes. The World War II period ushered in a rapid acceleration of our understanding of DENV, particularly as experimental medical research studies were being conducted on human participants [12]. This period, however, introduced catastrophic consequences for the spread of DENV as increased human incursion within and between countries facilitated DENV dispersal. In the years following, rapid population growth, heavy urbanisation, modern transportation and globalisation facilitated increased DENV transmission and endemicity. This was particularly prominent within the south-eastern region of Asia, where densely populated cities facilitated the co-circulation of multiple DENV serotypes [14]. The first recorded epidemic of DHF occurred in the Philippines in 1953/1954, and by the 1970's DHF had become one of the leading causes of hospitalisation and death of children within Southeast Asia [1]. Despite a near-absence of DENV in the Pacific Island countries and territories in the years following WWII, the 1970's saw a resurgence and serious dengue outbreaks and epidemics occurred in the region [15]. In the Americas, however, a yellow fever virus (YFV)-focussed program designed to eliminate the *Ae. aegypti* vector commenced in 1947. The program employed the use of a DDT-based strategy to successfully eradicate this mosquito vector from 18 countries by 1962 [5]. Disappointingly, following the loosening of the strategies involved in the eradication program during the 1970's, the mosquito vector repopulated these geographical regions leading to the re-emergence of DHF epidemics in the Americas [16].

1.2: Epidemiology

DENV is the most prevalent arthropod-borne human viral pathogen. It is transmitted by mosquitoes and maintained in two transmission cycles (Figure 1.1). In the sylvatic cycle, DENV circulates between non-human primates and arboreal mosquitoes of the *Aedes* species. This cycle is found primarily in Africa and Southeast Asia, where spill-over events into humans have been recorded [17-19]. In the urban endemic/epidemic cycle, DENV circulates between humans and *Aedes* species, primarily the domestic *Ae. aegypti* and the peridomestic *Ae. albopictus*. Transmission of DENV to humans is predicted to occur throughout the tropical and subtropical world, with estimates suggesting that one-third to half of the world's population live in at-risk areas [20, 21]. Modelling studies investigating the global occurrence and distribution of dengue suggest that the current total human infection burden averages approximately 100 million human infections annually [21-23]. Other studies suggest the number may be closer to 400 million human infections each year, with Asia, Africa, the Americas and Oceania bearing approximately 70%, 16%, 14%, 0.2% of the global dengue burden, respectively [24]. The data used to build these modelling estimates of the global distribution and health burden are based primarily on recorded dengue cases and include additional factors known or suspected to influence DENV transmission. Despite being sound, evidence-based models, mapping the precise distribution of DENV is inherently difficult, given factors such as a lack of reporting, misdiagnosis or misreporting, particularly during coincident epidemics of related

orthoflaviviruses that result in similar clinical presentation [25]. Nonetheless, evidence-based studies that take into consideration some of these limitations have identified 128 countries where evidence strongly suggests DENV is present, including 36 more than those recorded by the World Health Organisation (WHO) at the time of the study [26]. Over the last two decades, the WHO has reported a ten-fold increase in the reported cases of dengue [27], resulting in the emergence of dengue as a global health problem. In 2019, 129 countries reported incidents of dengue, with approximately 56 million new cases and 36,000 deaths reported [27, 28]. This increase in incidents has been attributed to factors such as rapid population growth, heavy urbanisation, and increased international travel that have contributed to the geographical expansion of DENV and its mosquito vector. Urban centres provide an environment enabling maintenance of DENV through low-level silent transmission. Further, increasing numbers of metropolises are experiencing hyperendemicity with multiple DENV serotypes becoming established [14]. These densely populated hyperendemic urban areas provide an environment conducive to producing dengue epidemics, resulting in increased viral resilience and epidemic potential that can be transported to other destinations via viraemic individuals. Indeed, DENV is spreading into regions previously considered DENV-free, including Europe where local transmission has been observed since 2010 [29]. Moreover, in Queensland, Australia, of the 1,773 dengue cases reported between 2010 and 2015, 632 were locally acquired [30]. This is clear evidence that the recent and historical demographic and societal factors that have contributed to the geographical expansion of DENV are not confined to the past. Moreover, the influence of increased temperature and erratic rainfall patterns due to climate change further threatens the geographical expansion and intensification of DENV [31]. Hence, there is a real need to understand biological, chemical, and environmental strategies to reduce the further expansion of dengue, which currently appears set to continue as a global health problem.

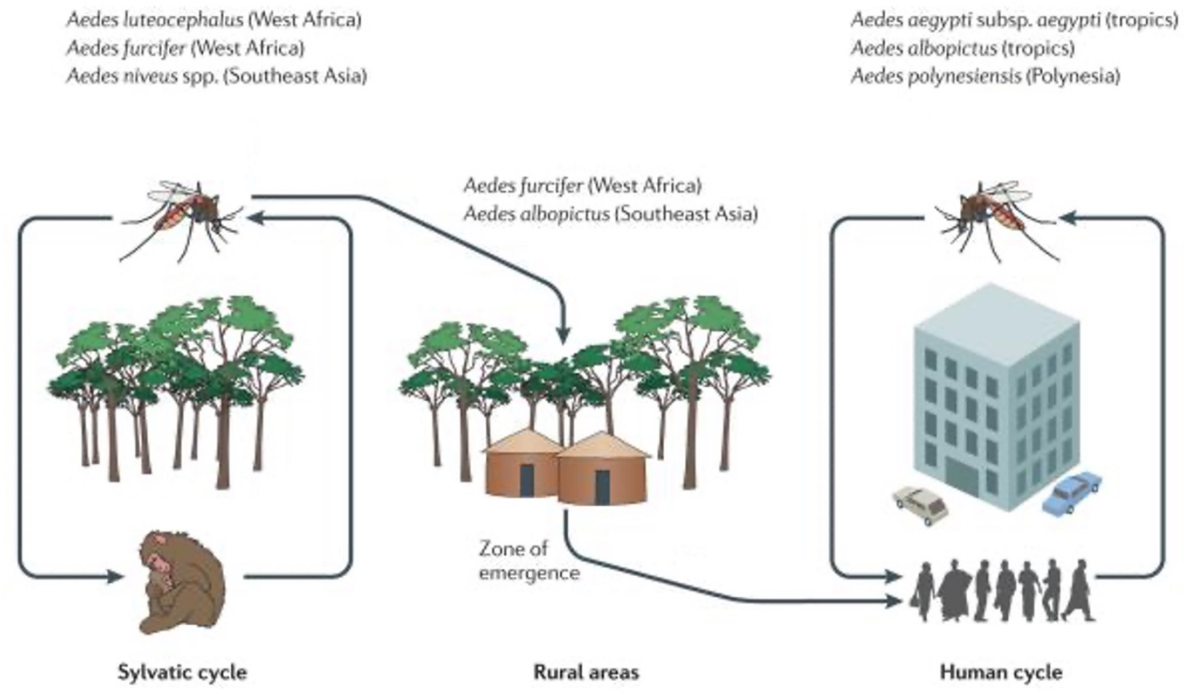

Figure 1.01: Sylvatic and human dengue virus transmission cycles.

Two transmission cycles enable the maintenance of DENV. In the sylvatic cycle, DENV transmission occurs between arboreal *Aedes* mosquito species and non-human primates. In the human endemic/epidemic cycle, DENV transmission occurs between (peri-) domestic *Aedes* mosquito species and humans. Spill-over events have been documented. (Adapted from Vasilakis et al., 2011 [32]).

1.3: Clinical Manifestation

All four serotypes of DENV can cause systemic disease. Around 75% of DENV infections are asymptomatic. However, approximately 96 million infections are estimated to result in disease each year [24], with clinical manifestations encompassing a wide spectrum. Previously, the WHO categorised dengue into three classifications based on severity: dengue fever (DF), dengue haemorrhagic fever (DHF) and dengue shock syndrome (DSS) [33]. The current classification system [34] is similarly based on severity, however, it is aimed towards guiding improved clinical management of patients. This revised dengue case classification system includes dengue with and without warning signs and severe dengue. The current classification system is summarised in Figure 1.2. Following an incubation period of 4-10 days, symptomatic individuals may experience an acute, and mild to debilitating, febrile illness lasting 2-7 days [35]. This febrile phase of dengue is characterised by the rapid onset of high fever and may also include severe headache, myalgia or arthralgia, retro-orbital discomfort, photophobia, and minor haemorrhage including petechia, epistaxis or gingival bleeding [34]. Defervescence usually occurs around days 3-7 of illness, and those who improve at this stage are considered to have non-severe dengue. However, warning signs can occur during the defervescence stage that can be indicative of the potential progression to more severe disease; this is classified as dengue with warning signs. These warning signs include persistent vomiting, clinical fluid accumulation, mucosal bleeding, liver enlargement, and postural hypotension [34]. This critical phase of dengue is characterised by an increase in capillary permeability that can lead to plasma leakage; the critical phase usually lasts for 1 to 2 days, and the majority of patients improve. However, depending upon the extent of plasma leakage, the development of severe dengue and life-threatening complications can occur rapidly. Additional complications can manifest as severe changes in haematocrit, pathological accumulations of fluid around the lungs or within the peritoneal cavity, severe haemorrhaging, and severe organ involvement which can be evidenced by elevated liver enzymes (e.g.: alanine transaminase [ALT] and aspartate transaminase [AST]) present in the blood [36]. If appropriate medical intervention is not received, shock can set in due to severe plasma leakage, the pulse and blood pressure become undetectable, and death can occur. However, if a patient's health improves and plasma leakage resolves, the extravasated fluids recede, the patient's haematocrit stabilises, and white cell and platelet counts recover; this phase is known as the recovery phase. There are no dengue-specific therapeutics currently available that can help prevent uncomplicated dengue from progressing to more serious forms. Early recognition of the warning signs that are suggestive of the progression to severe dengue are key, as the provision of supportive therapy can greatly reduce the risk of death [34]. This is of particular importance in regions where other pathogens (e.g.: Zika virus, chikungunya virus, malaria) that induce similar pathologies co-circulate, as disease management strategies differ [37].

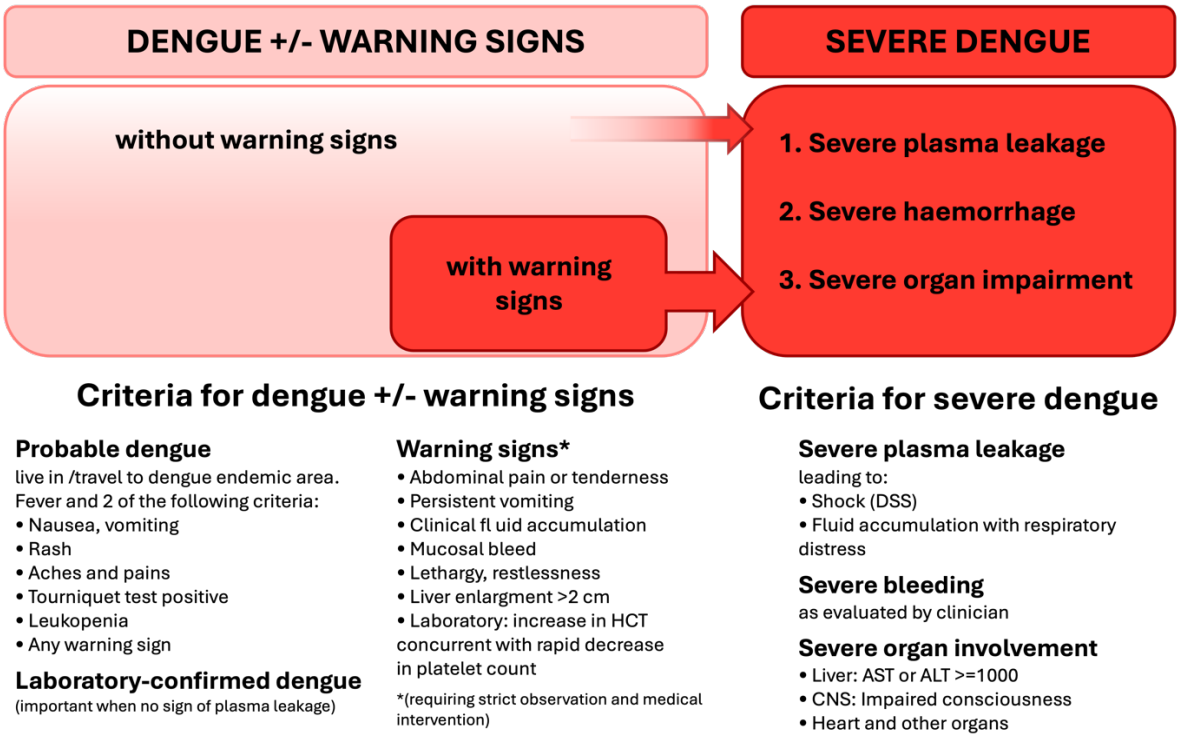

Figure 1.02: World Health Organization's dengue case classification system.

The current WHO dengue classification system is based on severity and designed to aid clinicians in dengue diagnosis to guide clinical management and improve patient outcomes. (Adapted from: Dengue Guidelines for diagnosis, treatment, prevention and control, New Edition. Geneva: WHO; 2009 [34]. Reproduced with permission of the World Health Organization).

1.4: DENV Genome Organisation

Belonging to the *Orthoflavivirus* genus of the *Flaviviridae* family, DENV shares a high level of genetic similarity with other genera members including the Australian-endemic Kunjin virus (KUNV), Zika virus (ZIKV), and Japanese encephalitis virus (JEV). There are four antigenically related yet distinct serotypes of DENV, DENV1-4 [38]. A potential fifth serotype, tentatively termed DENV5, was detected in Malaysia in 2007 and reported in 2013 [39]. However, whether this variant constitutes a novel human transmission cycle serotype or a sylvatic cycle spill-over event is contentious [40], and the inclusion of this serotype has not yet been accepted into the nomenclature set by the International Committee on Taxonomy of Viruses (ICTV) [ICTV_Master_Species_List_ 2022_MSL38.v3]. Sharing approximately 65% genetic homology, genetic variation exists between and within these serotypes. The highly condensed ~11 kb positive sense single stranded RNA (+ssRNA) genome encodes a single open reading frame (ORF) (Figure 1.3). Flanking the ORF are two structurally and functionally complex untranslated regions (UTRs) that act as master regulators of viral processes. The 5'-UTR is ~100 nucleotides (nt) in length and plays important roles in viral RNA stability, localisation, and translation. The 5'-UTR contains: a type I cap structure (7 methyl guanosine) for cap-dependent translation; a competent internal ribosomal entry site (IRES), for cap-independent translation [41, 42] and; two stem-loop structures, stem loop A and stem loop B (5' SLA and 5'SLB), that are ~70 and ~30 nt in length, respectively. 5'SLA is recognised by the viral RNA-dependent RNA polymerase (RdRp), NS5, and acts as a promoter or viral RNA synthesis [43]. 5'SLB contains the 5' upstream AUG region (5'AUG) nucleotide sequence that is complementary to a region within the 3' end of the viral RNA molecule. This complementarity allows long-range viral RNA-RNA interactions to facilitate genome cyclisation that is required for genome replication [44]. The 3'-UTR is ~400-450 nt in length and is divided into three domains (I-III) based on secondary structure. Domain I contains two stem-loop structures that are both partially resistant to the host 5'-3' exoribonuclease, Xrn1, that is responsible for the degradation of viral RNA. This resistance to degradation results in the amassing of two long non-coding RNAs, subgenomic flaviviral RNA (sfRNA1 and sfRNA2), that can mediate proviral, immunomodulatory, and pathogenic effects [45]. Domain II contains two dumbbell structures (DBs) that contain conserved regions: repeated conserved sequence 2 (RCS2) and conserved sequence 2 (CS2). Motifs contained within the DBs play crucial sequence-dependent roles in viral replication, and the DBs also appear to play a synergistic role in viral RNA translation [46]. Two additional sfRNAs (sfRNA3 and sfRNA4) arise from the abortion of Xrn1-mediated exoribonuclease activity immediately upstream of each DB [47]. Domain III comprises the last ~100 nt's and is a crucial determinant of viral RNA replication capability [48]. This domain contains a short hairpin (sHP) and a large stem loop at the 3' terminal (3'SL). Two elements within this domain, 3' conserved sequence (3'CS) and the 3' upstream AUG region (3'UAR), exhibit sequence complementarity to regions in the 5'UTR. This cyclisation brings the 3' end of the viral genome into close proximity with the 5' NS5-SLA complex, allowing the synthesis of a negative-sense single stranded RNA (-ssRNA) intermediate [43]. This domain is indispensable for viral RNA replication. The single ORF encodes a

3,411 amino acid polyprotein which is co- and post- translationally cleaved by viral and cellular proteases to produce ten proteins. The N-terminal region codes for three structural proteins (Capsid, precursor-Membrane and Envelope) followed by seven non-structural proteins (NS1, NS2A, NS2B, NS3, NS4A, NS4B and NS5).

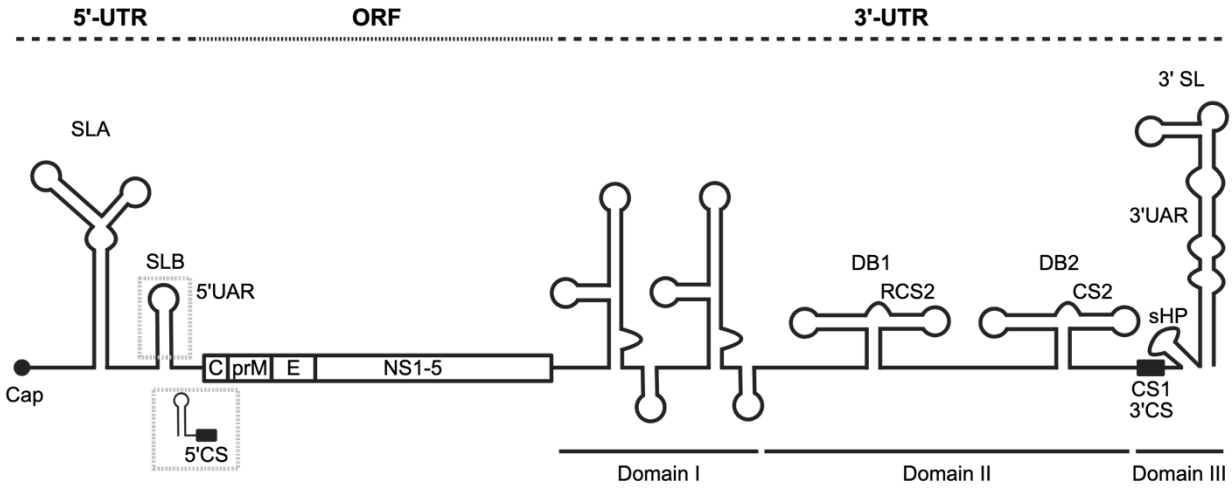

Figure 1.03: Structural organisation of the dengue virus genome

Schematic representation of the organisation of the dengue virus genome. The viral genome contains a single open reading frame (ORF) that codes for three structural proteins (C, prM, E) and seven non-structural proteins (NS1-5) and is flanked by 5' and 3' untranslated regions (UTR). Elements within the 5' UTR include: type I cap structure (Cap), stem loop A (SLA), stem loop B (SLB) and 5' upstream AUG region (5'UAR). The 3' UTR is divided into three domains: domain I contains sfRNA1 and sfRNA2 (see text), domain II contains two dumbbell structures with conserved and repeat conserved sequences (CS2 and RCS2) and domain III consists of short hairpin (sHP) and 3' stem loop (3'SL) that contains CS1, 3'CS, and 3'UAR. (Adapted from Ng et al., 2017 [49]).

1.5: DENV Proteins

The DENV genome encodes a single ORF that encodes a 3,411 amino acid polyprotein that consists of three structural and seven non-structural proteins (Figure 1.4). The structural proteins (Capsid, precursor-Membrane, and Envelope) are components of the virus particle that provide order and stability to the virion, encapsidate the genomic RNA and help define host cell tropism [50]. The non-structural proteins (NS1-5) are responsible for the induction of membrane rearrangements, genome replication, viral polyprotein cleavage, modification of host gene expression, recruitment of proviral host factors, inhibition of antiviral host cell defences, and packaging of the viral genome for virion assembly [50, 51]. Considering the highly condensed nature of the DENV genome, it is not surprising that most of these proteins are multifunctional and able to interact with multiple host factors [51]. Each protein is critical for the establishment of a productive viral infection. The structural properties and primary functional roles of individual DENV proteins are summarized below.

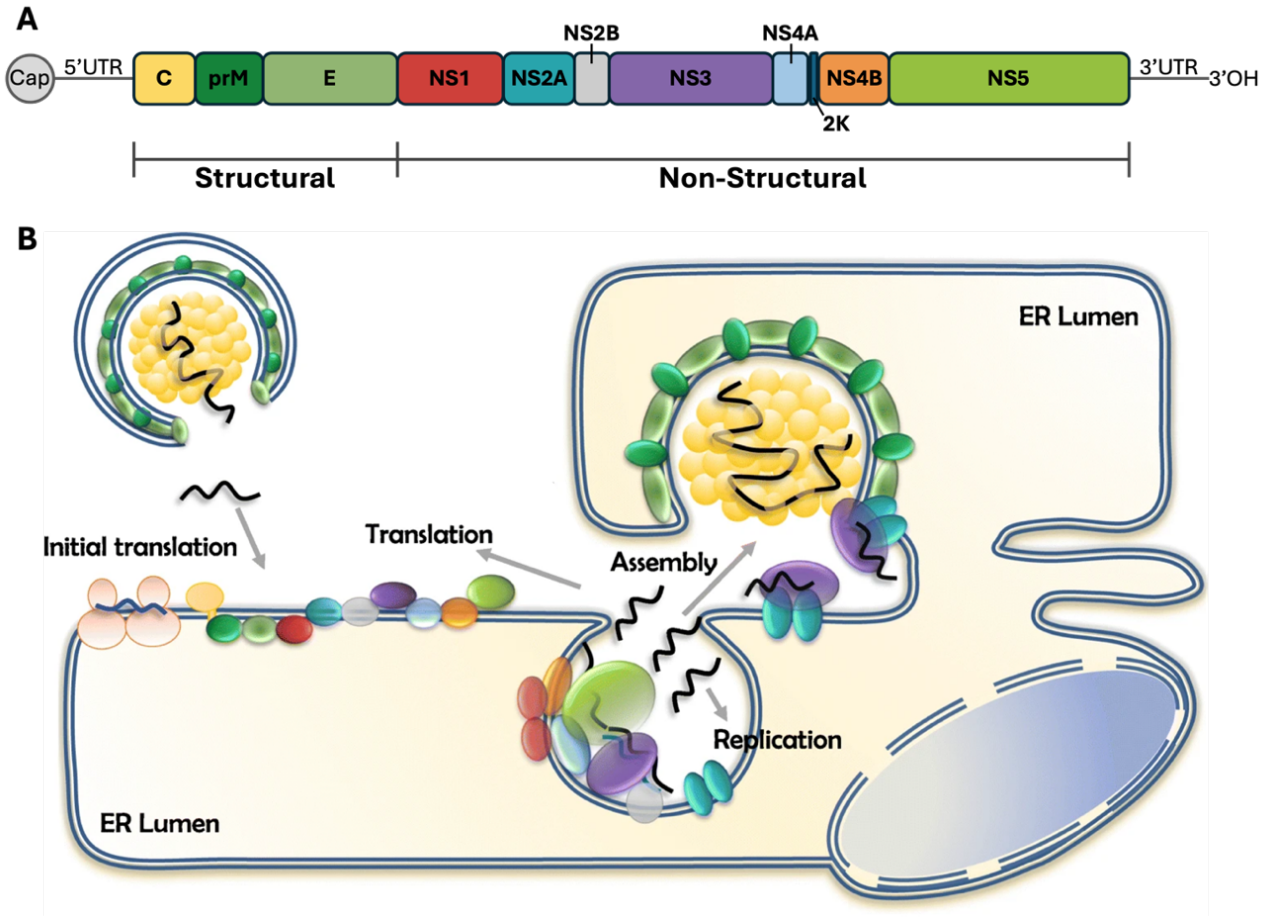

Figure 1.04: Organisation of the DENV polyprotein and primary roles of the structural and non-structural proteins in genome replication and virion assembly

(A) Schematic representation of the DENV polyprotein. (B) Illustration of the primary roles of viral proteins. The DENV genome encodes 10 proteins that are translated by the host ribosomal machinery and co- and post-translationally cleaved by viral and host proteases. The N-terminal end contains 3 structural proteins that form the virion; the C-terminal end contains 7 non-structural proteins that are predominantly involved in viral genome replication. (Adapted from Zhang et al., 2023[52] and Diosa-Toro et al., 2020[53]).

1.5.1: Capsid

The principal function of capsid (C) protein is to package the viral genome [54]. The mature DENV C monomer is composed of 100 residues and forms four α-helices. It is a highly basic 12 kDa protein that homodimerizes in solution. The 3D solution structure was solved using nuclear magnetic resonance spectroscopy [55], identifying a large dimerization surface contributed by two pairs of helices. The C dimer structure exhibits an asymmetric distribution of basic residues along one face of the molecule; this region has been proposed to interact with the viral RNA. The opposite face of the molecule has an extensive apolar surface formed by a conserved hydrophobic region; this region has been proposed to interact with membranes [55]. Within the cytoplasm of infected cells, C is found on endoplasmic reticulum (ER) membranes, on the surface of lipid droplets (LD), and in the nucleus. During infection, C accumulates on lipid droplets [56]. This trafficking of C from the ER where it is synthesised to LDs has been shown to be driven in a GBF1-Arf-COPI-dependent manner [57]. This has been proposed as a mechanism to store C protein, regulating its availability, and sequestering it away from sites of viral RNA synthesis. However, C-LD association may be a mechanism to modulate lipid metabolism during infection. C is also detected in the nucleus of infected cells, a feature well-conserved within the *Orthoflavivirus* genus [58-60]. The translocation of C from the cytoplasm to the nucleus is proposed to be driven by nuclear localisation sequences (NLS). Three NLSs are predicted [61, 62], and mutations within these regions significantly reduce nuclear localisation [63]. The functional significance of nucleoli-localised C remains poorly understood, however, given the histone binding properties of C [64], its presence within the nucleoli may affect host gene transcription. The ER-localised C protein is found near to vesicle packet RNA exit sites within close proximity to viral budding particles. The first step in viral particle assembly requires the formation of the nucleocapsid. For nucleocapsid assembly, a single viral genome is complexed with multiple C copies. While no RNA encapsidation signals have been identified in the DENV genome, C has high affinity and low specificity for ribonucleic acid and acts as an RNA chaperone *in vitro* [56, 65, 66]. Recent studies have demonstrated that the formation of DENV nucleocapsid-like particles require the neutralisation of C protein positive charges, presumably by RNA or negatively charged interfaces [67]. Despite intensive research, a detailed understanding of the molecular mechanism of nucleocapsid assembly remains elusive [68].

1.5.2: Precursor Membrane

The DENV precursor Membrane (prM) protein is initially synthesised as a pre-protein of 166 amino acid residues composed of two components: the precursor (pr) peptide, consisting of amino acid residues 1-91 and; the structural membrane (M) protein, consisting of amino acid residues 92-166 that interacts with the lipid membrane in the virion [69]. The pr peptide contains seven, mostly antiparallel, β strands stabilised by three disulfide bonds and is glycosylated at Asn69 [69]. The M

protein contains an N-terminal loop, an alpha-helical domain, and two transmembrane domains [70]. Following synthesis in the ER, prM plays a critical chaperone role for the proper folding of the viral Envelope protein and in the prevention of the premature fusion of the Envelope protein with host membranes during viral release [71, 72]. During virion maturation within the secretory pathway, the low pH environment of the trans-Golgi network (TGN) induces a conformational change in prM, making prM cleavage sites accessible to the host protease furin [73]. prM is proteolytically cleaved by furin, and this cleavage releases the 91 N-terminal pr residues, leaving the ectodomain and C-terminal transmembrane regions of the mature M protein – residues 92 to 130 and 131 to 166, respectively [69]. The pr peptides dissociate from the mature virion in the neutral pH extracellular environment, while the membrane-anchored M protein provides structural integrity to the mature virion [74].

1.5.3: Envelope

The mature DENV virion contains 180 copies of the Envelope (E) protein, a 53-56 kDa membrane-bound glycoprotein, existing as 90 E homodimers arranged in a herringbone pattern [75]. This protein is a major determinant of host cell tropism and a major target of neutralising antibodies. E is a class II fusion protein involved in target host cell receptor binding, internalisation, and fusion of the viral envelope with the host endosomal membrane [76]. E contains a transmembrane anchor domain in the C-terminal region that anchors E to the viral membrane [74]. There is a flexible region linking the transmembrane domain to a soluble ectodomain. This soluble ectodomain contains three globular domains (D-I, D-II, and D-III), which are connected by flexible interdomain linkers that undergo major conformational changes at different stages during the viral life-cycle [74, 77]. D-I is situated at the centre of the monomer, assumes a β-barrel-like conformation and joins at one end to D-II. D-II contains a ‘finger-like’ domain that contains a glycine-rich region which plays a key role in fusion loop formation, facilitating viral fusion with the host endosome. The opposite end of D-I connects to D-III, a domain that forms an immunoglobulin-like structure. D-III contains amino acid residues that are important for electrostatically-mediated interactions with cell-surface glycosaminoglycans [78], and is proposed to be the region responsible for host cell receptor interaction [79]. E is a major target of neutralising antibodies, and neutralising antibodies have been mapped to all three domains of E [80]. The lateral ridge of domain III, however, is the core of the serotype-specific sequences that are conserved within each DENV serotype and therefore contains the main serotype-defining epitopes of the virus [81]. There are two *N*-linked glycosylation sites within E. The Asn-67 site is unique to DENV, while the Asn-153 site is conserved within many Orthoflaviviruses [82]. The presence of carbohydrate moieties has been demonstrated to be important for the receptor-binding properties of E [83-85]. During the viral life-cycle, E undergoes various structural alterations [86]. At neutral pH, E exists in a dimer configuration [82]. Following acidification of the virion-containing endosome, the

low pH environment triggers E to attain a trimeric configuration allowing fusion of the viral lipid envelope with the endosomal membrane [87]. Following initial synthesis, E is cleaved from the nascent polypeptide within the ER by the host signal peptidase. Newly synthesised E rapidly heterodimerises with prM, with prM performing a chaperone role to ensure the proper folding of E [69]. prM/E heterodimers coalesce on the luminal side of the ER membrane forming heterotrimeric spikes, which may be important for inducing ER membrane curvature to allow nascent immature virion budding into the ER [88]. During transit through the secretory pathway, the immature virion is exposed to progressively more acidic environments, with the low pH inducing prM/E rearrangements allowing furin-mediated cleavage of prM [73]. Under low pH conditions, pr remains bound to E to prevent premature membrane fusion [71, 89]. Following release of the virion into the pH-neutral extracellular milieu, pr is released to produce fully infectious mature virions containing E and M.

1.5.4: Non-structural protein 1

Non-structural protein 1 (NS1) is discussed in detail below (see section: Non-structural protein 1, DENVs virulence factor). In short, this multifunctional 45-55 kDa protein is composed of 352 amino acids. The monomer is translated directly in the ER where it is *N*-glycosylated at two conserved residues, Asn130 and Asn207 (Figure 1.5). NS1 monomers rapidly dimerise forming a membrane-associated NS1 dimer, the predominant intracellular form [90-92]. NS1 colocalises with dsRNA – a marker of viral genome replication – at both the ER-lumenal and cytoplasmic sides of the virus-induced replication complexes [93, 94] where NS1 plays an essential role in viral RNA replication [95, 96]. Recent evidence has demonstrated a role of NS1 in viral particle assembly [97]. NS1 is also secreted from infected cells as a small soluble hexamer, with an open barrel-shaped form, the central channel of which is stabilised by a lipid component [92, 98, 99]. The structure of this secreted form of NS1 has recently been questioned, however, with evidence suggesting it may be secreted in multiple oligomeric states [100, 101]. This secreted form of NS1 plays an important role in immune evasion and pathogenesis [95, 96].

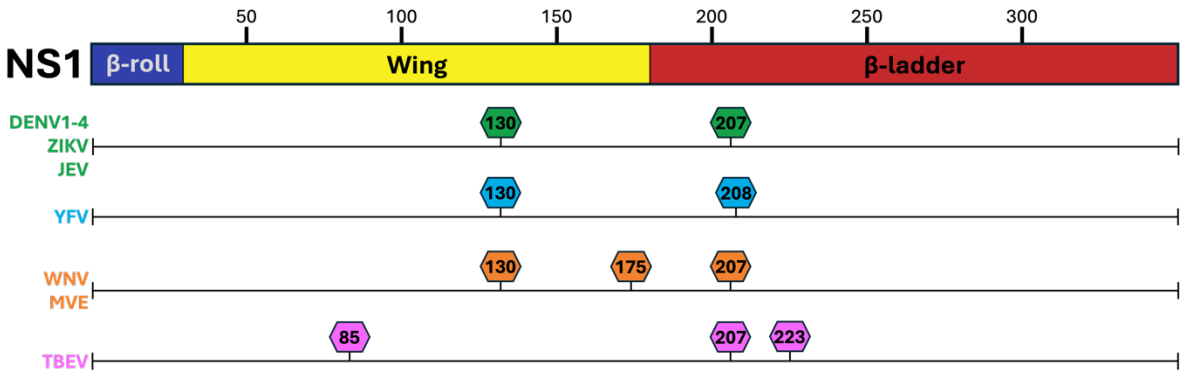

Figure 1.05: *N*-linked glycosylation sites within non-structural protein 1

DENV NS1 is glycosylated at two conserved residues, N130 and N207. Defined and/or putative sites are shown for alternative Orthoflaviviruses. ZIKV: Zika virus, JEV: Japanese encephalitis virus, YFV: yellow fever virus, WNV: West Nile virus, MVE: Murray Valley encephalitis virus, TBEV: tick-borne encephalitis virus. (Adapted from Carpio et al., 2021[102]).

1.5.5: Non-structural protein 2A

Non-structural protein 2A (NS2A) is a 22 kDa hydrophobic transmembrane protein composed of 218 amino acids. The monomer is cleaved at the N-terminal end by an as yet unidentified host protease, while cleavage at the C-terminal end is mediated by the viral protease NS2B-3 complex [103]. NS2A has five integral transmembrane segments that span the ER lipid bilayer and a further three predicted non-integral transmembrane segments interact with, but do not traverse, the ER membrane [104]. The membrane topology model reported by Xie and colleagues indicates that the N-terminal 68 amino acid residues are present within the ER lumen [104]. This region contains two predicted non-integral transmembrane domains, pTMS1 and pTMS2. The five integral transmembrane segments span amino acids 69 to 209. This region further contains the third predicted non-integral transmembrane domain pTMS5 located within the ER lumen. The C-terminal amino acids 210 to 218 are located within the cytosol. pTMS1 and pTMS5 are not believed to be membrane-associated; pTMS2 peripherally associates with the ER membrane, an interaction that is proposed to occur via membrane interface partitioning or electrostatic interactions with phospholipids or membrane-bound proteins [105, 106]. Flavivirus NS2A is a component of the viral replication complex [107], and mutational analyses have defined distinct roles of NS2A in DENV RNA replication and virion assembly and secretion [108, 109]. This protein recruits viral RNA and structural proteins to the sites of virus assembly to coordinate virion assembly [110]. NS2A, in conjunction with NS4B, plays a role in immune evasion by inhibiting RIG-I/MAVS-driven (retinoic acid-inducible gene-I / mitochondrial antiviral-signaling protein) type I interferon (IFN) responses by blocking TBK1/IRF3 (TANK-binding kinase / interferon regulatory factor 3) activation [111].

1.5.6: Non-structural protein 2B

Non-structural protein 2B (NS2B) is a 15 kDa protein composed of 130 amino acids. It is a hydrophobic protein that is proposed to form a helical bundle composed of four transmembrane alpha-helices with the flanking N- and C-terminal regions present in the cytosol [112]. NS2B's main function is to regulate the serine-protease activity of NS3, which it achieves through a highly dynamic hydrophilic region between alpha helices 2 and 3 [112-114]. This 40-residue hydrophilic region between helices 2 and 3 allows NS2B and NS3 heterodimerisation (NS2B3), an interaction that is necessary for the formation of a functional two-component serine protease complex [115]. The protease activity of NS2B-3 is necessary for the maturation of the viral polyprotein precursor by cleaving the NS2A/NS2B, NS2B/NS3, NS3/NS4A, and NS4B/NS5 junctions [116, 117]. In addition to its critical role in viral polypeptide cleavage, the NS2B-3 protease complex plays a role in immune suppression by inhibiting type I interferon signalling through the proteolytic degradation of human host antiviral proteins [118, 119]. Moreover, NS2B itself has recently been shown to play a role in

immune evasion by targeting the DNA sensor cyclic GMP-AMP synthase (cGAS) for degradation to antagonise the interferon-induced antiviral response to DENV infection [120].

1.5.7: Non-structural protein 3

Non-structural protein 3 (NS3) is a 69 kDa soluble protein composed of 618 amino acids and is highly conserved within the *Orthoflavivirus* genus. This large multifunctional enzymatic protein has serine protease, helicase, nucleoside 5'-triphosphatase (NTPase), and 5'-terminal RNA triphosphatase (RTPase) activity [121, 122]. NS3 is present in the cytosol of infected cells and localises to replication complexes, however recent evidence indicates NS3 may also be present in the nucleus at early time points during DENV infection [123]. The N-terminal region, amino acid residues 1-168, contains the serine protease domain which is responsible for the proteolytic processing of the viral polyprotein [121]. This proteolytic activity requires NS3 to be complexed with NS2B, which acts as an NS3 co-factor and provides anchoring of the NS2B-3 complex to the ER membrane [112]. An 11 amino acid linker region separates the protease and helicase regions of NS3 providing flexibility between these two domains [124]. The C-terminal domain, amino acids 180 to 618, contains the helicase, NTPase and RTPase domains [121, 122, 125]. The helicase and NTPase activities are responsible for unwinding the dsRNA intermediate and/or disrupting secondary structures formed by single stranded RNA (ssRNA) to allow NS5-mediated viral RNA replication [122, 126]. The RTPase activity is required for priming progeny viral genomes for NS5-mediated 5' capping [127]. In addition to the NS2B-3 protease-mediated inhibition of host antiviral signalling described above, NS3 possesses protease-independent immune evasion properties. The protease domain of NS3 exhibits 14-3-3ε binding capability which acts to inhibit the translocation of activated RIG-I to the mitochondrion-associated adaptor protein MAVS, thus preventing antiviral signalling [128].

1.5.8: Non-structural protein 4A

Non-structural protein 4A (NS4A) is a 16 kDa hydrophobic membrane protein composed of 127 amino acids. Within the cytoplasm, NS4A is cleaved at its N-terminal end by the NS2B-3 two-component viral protease. A 23 amino acid residue sequence within the C-terminal end of NS4A acts as a signal sequence to translocate NS4B to the lumen of the ER [129]. Within the ER, this signal sequence fragment, designated 2K, is cleaved from NS4A and NS4B by the NS2B-3 viral protease and host signalase, respectively [130]. The NS4A protein comprises six alpha-helices and contains three integral transmembrane segments [129, 131]. The N- and C-terminal regions are located in the cytosol and ER lumen, respectively. The N-terminal end, amino acid residues 1-48, contains three membrane-interacting hydrophobic regions that act as a curvature-sensitive

membrane anchor [132]. The intracellular expression of DENV NS4A alone has been shown to induce membrane alterations characteristic of virus-induced structures indicating a role of NS4A in host membrane remodelling [129]. This is in contrast to the situation for KUNV, where host membrane remodelling is also induced by NS4A but is more pronounced and reminiscent of virus-induced structures when co-expressed with the C-terminal 2K fragment [133]. Nonetheless, both DENV and KUNV NS4A proteins localise to ER-derived vesicle packets, where NS4A provides a major structural role as a part of the replication complex. Several host proteins are hijacked to facilitate membrane remodelling and regulation of replication complex formation and maintenance. In this context, DENV NS4A interacts with vimentin, a protein important for vesicular and organelle positioning, and this NS4A-vimentin interaction is critical for replication complex maintenance [134]. The host protein reticulon 3.1 is also recruited to flavivirus replication complexes with recruitment facilitated by NS4A of KUNV but not DENV [135], highlighting species-specific NS4A protein functions. NS4A also plays a role in innate immune evasion by suppressing IFN production through the direct binding of MAVS [136]. Further, NS4A from DENV1, but not DENV2 or DENV4, inhibits TBK1-directed IFN-β transcription [111], emphasising unique serotype-specific NS4A protein functions.

1.5.9: Non-structural protein 4B

Non-structural protein 4B (NS4B) is a 27 kDa hydrophobic integral membrane protein composed of 248 amino acid residues. Following cleavage from NS4A, 2K-NS4B is directed to the lumen of the ER by virtue of the 2K fragment that acts as a signal peptide. This 2K fragment is subsequently cleaved by the host signalase. NS4B is predicted to contain eleven helices, five of which form integral membrane regions [137], with membrane integration being orchestrated by the C-terminal transmembrane regions [138]. DENV NS4B contains two conserved *N*-glycosylation sites at Asn58 and Asn62 that are important for viral RNA replication, likely through affecting NS4B folding as genetic ablation of these sites has been shown to result in the generation of compensatory mutations within NS4B [139, 140]. NS4B is recruited by NS4A to viral replication complexes where it plays an essential role in viral replication [138, 141]. The N-terminal end is located in the ER lumen; the C-terminal region is localised in the cytosol [137, 138]. NS4B has been shown to interact with NS3 to influence NS3 localisation and to act as an NS3 co-factor to regulate the NS3 helicase activity [142]. Both the N-terminal region and the flexible cytoplasmic loop of NS4B have been shown to be important determinants of this NS4B-NS3 interaction [143, 144]. Further, NS4B plays important roles in facilitating DENV replication by antagonising the host innate immune response. NS4B acts in innate immune evasion by regulating RIG-I/MDA5/MAVS/TBK1-directed responses to reduce IFN-β transcription, with functional determinants mapped to the N-terminal region of NS4B [111].

1.5.10: Non-structural protein 5

Non-structural protein 5 (NS5) is the largest and most highly conserved viral protein, showing approximately 70% sequence identity among the four DENV serotypes. Encoded at the C-terminal region of the viral polyprotein, NS5 is a 104 kDa protein composed of 900 amino acids. NS5 is liberated from the viral polyprotein by the NS2B-3 two-component viral protease complex. The N-terminal region contains a methyltransferase (MTase) domain [145]. This MTase domain is critical for generating the 5' cap structure of progeny viral genomes which is recognised by the host cellular translation machinery, thus allowing viral polyprotein translation [146]. The formation of this cap structure also provides a mechanism to protect against viral RNA recognition by the host cellular machinery [147]. The C-terminal domain contains the RNA-dependent RNA polymerase (RdRp) [148]. This RdRp domain is responsible for carrying out the de novo synthesis of viral RNA. The SLA within the 5'-UTR acts as a promoter sequence to facilitate NS5-RNA binding [43, 149]. DENV RNA replication critically depends on circularisation of the viral genome, a property afforded by complementary RNA sequences within the 5'- and 3'-UTR. This is proposed to bring the SLA-bound NS5 protein into close proximity with the 3' end of the viral genome to initiate viral genome replication [43, 150]. Critical to viral genome replication are the RNA-binding and enzymatic activities of NS3, which have been shown to be regulated by NS5 [151]. The helicase/NTPase/RTPase activities of NS3 together with the MTase/RdRp activities of NS5 contain all the enzymatic functions required to synthesise type-I capped viral RNA genomes [152, 153]. Two NLSs have been identified between amino acid residues 320 and 405, and recognition of these sequence signals by cellular factors allow NS5 translocation to the nucleus [154]. While nuclear localisation of NS5 is not strictly essential for viral RNA replication *in vitro* [155] and indeed serotype-specific differences in the levels of NS5 nuclear accumulation exist [156], most mutations within this region that reduce the nuclear accumulation of NS5 also impair viral RNA replication and infectious virus production [155, 157]. Nuclear localisation of NS5 has been shown to create a cellular environment that is less restrictive to viral replication by antagonising the expression of antiviral genes [158] and interfering with the proper processing of precursor mRNA [159]. Moreover, DENV NS5 promotes viral replication by disrupting host cellular immune signalling pathways. Of particular significance, NS5 binds STAT2 (signal transducer and activator of transcription 2) and targets it for proteasomal degradation thus inhibiting IFN-I signalling [160-162].

1.6: The Viral Replication Cycle in Human Hosts

In the urban transmission cycle, DENV employs a complex dual-host lifecycle alternating between mosquitoes and humans. Transmission to a human host is achieved through the bite of an infected female mosquito. In a primary infection, DENV initiates an intimate association with a target cell via its envelope glycoprotein (E). DENV displays a wide host-cell tropism *in vitro* [163], suggesting that E may bind a ubiquitously expressed host cell receptor. However, no universal factor has been identified, rather, experimental evidence indicates that E is able to interact with a wide variety of surface-exposed host cell factors [164]. Glycosaminoglycans, including heparin sulfate, and C-type lectins, including DC-SIGN and the mannose receptor, have been extensively studied as human host cell (co-)receptors for DENV infection [163, 165, 166]. The promiscuous nature of E likely serves to concentrate viral particles at the cell surface, affording the virus two options (i) through low-affinity interactions, diffuse along the cell surface and become deposited in a pre-existing clathrin coated pit, or (ii) initiate a stronger, high-affinity interaction with specific receptors to induce uptake. In the skin epidermis and dermis, DENV encounters permissive cells including keratinocytes and Langerhans cells [167]. DENV internalisation into a host cell has been shown to occur by clathrin-dependent endocytosis, however studies have demonstrated that DENV can also exploit additional clathrin-independent pathways [164, 168]. Internalised DENV virions traffic to early (Rab5-positive) endosomes which subsequently mature into late (Rab7-positive) endosomes [169]. However, this Rab7 endosomal maturation sorting event may be DENV strain-specific [170]. The low pH environment of the endosome causes E to undergo conformational changes resulting in fusion of the viral envelope with the endosomal membrane [77]. This releases the nucleocapsid – a single viral genome in complex with multiple copies of viral capsid protein – into the cytosol [171]. Through an unknown mechanism, dissociation of the nucleocapsid occurs, releasing the viral genome. By virtue of the 7-methylguanosine cap at the 5' end of the genome, the positive-sense single stranded RNA (+ssRNA) genome is misconstrued as mRNA by the host cell machinery and translation is initiated. The nascent polypeptide is delivered to the ER membrane, and it is co- and post-translationally cleaved by viral and cellular proteases to produce the 3 structural proteins (Capsid [C], precursor membrane [prM], and envelope [E]) and 7 non-structural proteins (NS1, NS2A, NS2B, NS3, NS4A, NS4B, NS5). The non-structural proteins are all essential for viral genome replication and, together with usurped host factors, induce membrane remodelling to establish ER-derived replication complexes (RCs) [172]. These RCs contain NS3 and NS5, the viral proteins that contain all the enzymatic functions required for the synthesis of type-I capped viral RNA genomes, and dsRNA and are likely the sites of active viral genome replication [173]. Viral genome replication begins with the +ssRNA genome that acts as template for the synthesis of a -ssRNA molecule, forming a dsRNA intermediate. The dsRNA intermediate is used as template for the asymmetric synthesis of +ssRNA molecules that can then be further utilised as protein-coding molecules or genomic RNA for virion assembly. Virion assembly occurs on ER membranes that are tightly opposed to RCs [173], and a recent study has highlighted that this assembly process is heavily

coordinated by several NS proteins [110]. NS2A has been shown to bind DENV genomic RNA and translocate it from the RCs to the sites of virion assembly [110]. NS2A also recruits the C-prM-E polyprotein along with the catalytically active viral protease complex, NS2B-3, allowing the coordinated cleavage of the DENV structural proteins [110]. Together, these processes facilitate the association of newly synthesised viral genomes with capsid protein to form the nucleocapsid. The nucleocapsid then buds into prM- and E-rich microdomains in the ER, collecting the viral envelope. Interestingly, DENV NS1 was recently shown to interact with the structural proteins, and mutations within the NS1 protein have been shown to produce replication-competent but assembly/egress-defective mutants, suggesting that NS1 may play an additional intracellular role in virion morphogenesis [97]. However, the precise involvement of NS1 in DENV virion assembly or egress remains to be determined. Assembled immature virions then traffic through the secretory pathway where furin-mediated cleavage of prM to mature M occurs [174], allowing the virus to leave the cell as a fully infectious mature virion.

1.7: Non-Structural Protein 1 – a Key Virulence Factor

1.7.1: Background

An important orthoflavivirus virulence factor is the non-structural protein 1 (NS1). NS1 was first identified over 50 years ago as a non-hemagglutinating, soluble complement-fixing antigen in the brain and serum of DENV2 infected mice [175]. In 1985 the first complete genome sequence for the orthoflavivirus yellow fever virus (YFV) was obtained and, based on the genomic organisation, this protein acquired its NS1 nomenclature [176]. All orthoflavivirus genomes contain an approximately 1,056 nucleotide sequence that codes for a 352 amino acid NS1 protein. Dependent upon its glycosylation status, the NS1 protein has a molecular weight of 45-55 kDa. This multifunctional protein assumes multiple oligomeric states and is found in a variety of intra- and extracellular locales: (i) NS1 exhibits an intracellular form that plays a critical role in viral RNA replication and virion morphogenesis; (ii) it has a cell surface-exposed form that can stimulate cellular signal transduction; (iii) it is secreted from infected cells into the extracellular environment where it plays several roles in pathogenesis and; (iv) secreted NS1 is efficiently endocytosed by a variety of uninfected cell types – a process that contributes to vascular permeability [95]. A phylogenetic analysis of the NS1 protein sequences from 11 representative orthoflaviviruses (8 species including DENV1-4) revealed that these viruses cluster into 4 groups and share 50 – 80% sequence similarity [177]. Particular regions within NS1 show high sequence conservation, indicating that NS1 from multiple orthoflaviviruses maintain shared and conserved functions. Regions of higher variability are indicative of unique group-specific functions and characteristics. Given the diverse and essential roles of NS1 in orthoflavivirus biology, understanding this multifaceted protein is of critical importance.

1.7.2: NS1 synthesis and structure

Upon translation of the viral polypeptide, nascent NS1 is targeted to the ER lumen by a signal peptide of 24 amino acids encoded in the C-terminal region of the Envelope protein [178]. NS1 is released from the viral polypeptide at its N-terminal end by a host signal peptidase [179]. Cleavage from the C-terminal end is achieved by an as yet unidentified protease but appears to require a minimum of 8 amino acids present in the NS1 C-terminus, representing an orthoflavivirus-conserved octapeptide (L/M-V-X-S-X-V-X-A) [103, 180]. Within the ER, DENV NS1 is subjected to *N*-linked glycosylation, with Asn130 and Asn207 representing conserved sites for the addition of high-mannose moieties. This hydrophilic NS1 monomer contains 12 cysteine residues and six discrete intramolecular disulphide bonds are formed [92, 181]. Mutational studies have demonstrated that the three C-terminal cysteines are essential for NS1 homodimerisation, which occurs rapidly within 20 to 40 minutes [90, 91, 182]. NS1 dimerisation occurs in the absence of other DENV proteins, suggesting that NS1 contains all the information required for this process [182]. Dimeric NS1 is the predominant intracellular form, with monomeric NS1 existing at a low-level steady-state concentration [90], and presumed to be of low biological importance [183].

The recently solved crystal structures of the full-length glycosylated NS1 from DENV and WNV has provided much insight into the three-dimensional architectural arrangement of the NS1 dimer (and hexamer, see below) (Figure 1.06a) [92]. The crystal structure of the NS1 dimer has revealed the presence of three distinct domains within each NS1 protomer: a β-roll dimerisation domain, a wing domain, and a β-ladder domain. The β-roll domain (1-29 aa) is composed of two β-hairpins that are stabilised by a disulfide bond (Cys4-Cys15). In the dimer, the two β-hairpins contributed by each monomer intertwine to form a four-stranded β-sheet that is curved into a 'roll-like' structure. The wing domain (30-180 aa), which projects from the central β-ladder, contains a glycosylation site at Asn130, and a second glycosylation site at Asn175 in WNV, and is stabilised by a disulfide bond (Cys55-Cys143). This wing domain contains a further two subdomains; the α/β subdomain (38-151 aa) and the discontinuous connector subdomain (30-37 aa and 152-180 aa). The α/β subdomain is composed of a four-stranded β-sheet, two α-helicies and a 20-residue disordered distal tip. The discontinuous connector subdomain packs against the small β-roll domain and joins the wing domain to the β-ladder domain by a disulfide bond (Cys179-Cys223). The β-ladder domain (181-352 aa), which contains the Asn207 glycosylation site, forms a central β-sheet and is the predominant structural feature of NS1. Within the dimer, this continuous β-sheet is composed of 18 β-strands that are arranged in an antiparallel 'ladder rung' fashion with nine 'rungs' contributed by each monomer. The β-roll and connector subdomain produce a hydrophobic protrusion that extends from one face of the dimer, and this is proposed to be the region of the NS1 dimer responsible for membrane association.

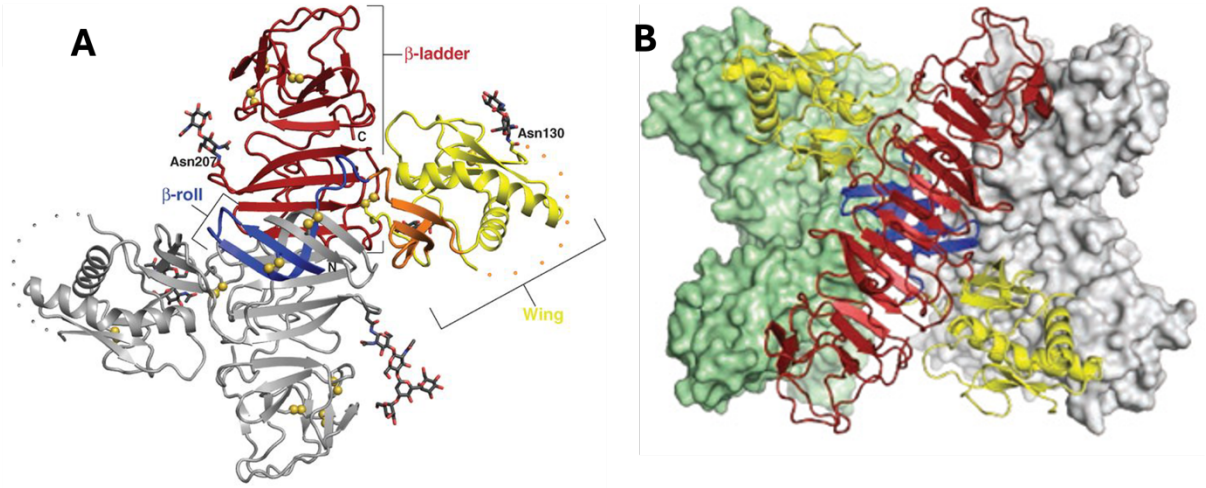

Figure 1.06: Structural organisation of the NS1 dimer and hexamer

(A) NS1 dimer organisation. One NS1 protomer is colour coded to highlight the distinct domains (β-roll domain in blue; wing domain and connector subdomain in yellow and orange, respectively; β-ladder in red), the second NS1 protomer is in grey for clarity. Disulfide bonds are represented as yellow spheres. Glycosylation sites are displayed as stick structures. (B) NS1 hexamer organisation. The hexamer is composed of a trimer of NS1 dimers. For clarity, two dimers are shown in green and white. The third and front-most dimers is colour coded as in A. (Adapted from Akey et al., 2014 [92])

1.7.3: Intracellular NS1

Intracellular NS1 (iNS1) is a key factor that performs a variety of roles in the DENV life cycle. iNS1 is well-documented as being essential for orthoflaviviral RNA replication [97, 184-189]. iNS1 colocalises with dsRNA and other constituents of the replication complex in virus-induced ER-derived membranous structures called vesicle packets (VP) [93, 94, 173]. It has been proposed that NS1's hydrophobic protrusion formed by the β-roll and the connector subdomain, and in particular the amino acid residues 10-11 and 159-162, respectively, associates iNS1 with the ER membrane [183]. This orientation would likely position the hydrophilic portion of the iNS1 dimer within the ER luminal side of the VPs. The presence of ER-luminal exposed iNS1 dimers has been suggested to provide positive membrane curvature to the VPs to support the negative membrane bending curvature induced by NS4A, NS4B, and potentially NS2A, indicating that iNS1 may play a structural role to induce or maintain VP architecture [172]. This is supported by data implicating genetic and physical interactions of iNS1 with other viral components of the replication complex [190-192] and NS1's ability to interact with and remodel membranes [92, 188]. A recent report, however, indicates that the role of iNS1 in viral RNA replication may extend beyond a structural role in the VP architecture [192]. Plaszczyca *et al* identified a novel interaction between DENV NS1 and the viral polyprotein NS4A-2K-4B cleavage intermediate [192]. It was demonstrated that mutations within NS1 that abrogate the NS1 and NS4B-2K-4B interaction are dispensable for VP formation but critical for viral RNA amplification, arguing that iNS1 also contributes directly to DENV RNA replication via a mechanism that is distinct from its role in VP formation.

A role for iNS1 in the assembly and maturation of orthoflaviviruses has long been hypothesised [193-195]. However, given the importance of iNS1 in viral RNA replication, interrogating this has been difficult. In this context, Scaturro and colleagues employed alanine scanning mutagenesis to interrogate functional residues within DENV NS1 [97]. Of the 46 mutations introduced into NS1, 23 were found to have minimal or no impact on viral RNA amplification. These RNA replication-competent NS1 mutants provided a platform to interrogate the roles of iNS1 in additional and alternative aspects of the DENV replication cycle. When mutated, several key residues (S114, W115, D180 and T301) were identified as causing a defect in infectious virus production and, interestingly, a T117A mutant exhibited enhanced infectious virus production. Further, iNS1 was shown to colocalise and interact with the DENV structural proteins C and E. This work has revealed a previously unappreciated role of iNS1 as a critical factor for infectious DENV particle production, providing evidence that iNS1 modulates the assembly or release of infectious virus particles through interactions with the viral structural proteins.

Despite an abundance of work highlighting the importance of iNS1 as indispensable for viral RNA replication, and emerging evidence that iNS1 is a critical determinant of infectious particle production, a complete understanding of the underlying mechanisms is lacking. Further, the

identification of a multitude of host proteins as iNS1 interacting partners (see below) in both fully infectious or NS1-expressing cell culture systems indicates that some key functions mediated by iNS1 may involve the manipulation of iNS1-interacting host factors. Future work determining the precise molecular functions of iNS1 and iNS1-usurped host factors will provide important insights into orthoflavivirus biology.

1.7.4: Cell surface-exposed NS1

In orthoflavivirus infected cells, a minority of NS1 is plasma membrane-associated and cell surface-exposed [196]. An elegant study by Jacobs *et al* identified a 26 amino acid segment in the N-terminus of NS2A to be required and sufficient for this NS1 localisation [197]. This hydrophobic segment, immediately downstream of NS1 contains the characteristic features of a carboxy-terminal glycosylphosphatidylinositol (GPI) anchor signal sequence. This allows a portion of NS1 to be post-translationally processed to incorporate a GPI anchor attachment, which is then targeted to and expressed at the cell surface in association with lipid rafts [198]. Given that NS1 is a major target of humoral immunity during DENV infection, this cell-associated surface-exposed form is subject to antibody recognition. While the functional purpose of this form of NS1 has not been determined, it has been shown to elicit important biological functions in response to anti-NS1 antibody stimulation. First, this GPI-anchored form of NS1 stimulates signal transduction mechanisms that induce phosphorylation of cellular proteins, but how this affects the virus and/or the host remains to be determined [197]. Second, in the presence of anti-NS1 antibodies, cell surface-exposed NS1 triggers antibody-dependent complement activation resulting in the deposition of lysis-inducing membrane attack complexes [199]. Third, antibody recognition of cell surface-exposed NS1 from WNV can trigger Fc-**γ** receptor-mediated phagocytosis and clearance of infected cells [200]. The small minority of plasma membrane-associated cell surface-exposed NS1 relative to the more abundant intracellular and secreted NS1 may explain the paucity of research conducted on this form. Nonetheless, given the cellular proteome-modifying and both pathological and protective responses elicited, this NS1 species should not be overlooked.

1.7.5: Secreted NS1 (sNS1)

NS1 is secreted from DENV-infected mammalian and mosquito cells [98, 201]. sNS1 is released into the blood stream of infected individuals and accumulates to significant levels in the sera of infected individuals (up to approximately 50 ug/mL) [199, 202-204]. While useful as a diagnostic marker of DENV infection [95, 205], this secreted form of NS1 acts as a DENV virulence factor and it has been linked to dengue disease pathogenesis through a variety of pathways [95, 96]. Indeed, high levels

of sNS1 in hospitalised DENV-infected individuals have been correlated with adverse disease outcomes [206]. In the extracellular environment, the highly immunogenic sNS1 can elicit the production of cross-reactive antibodies that recognise host factors expressed on endothelial cells and platelets [96]. sNS1 can interfere with components of the complement system and modulate their activity to modify the host immune response [207]. Moreover, sNS1 is bound and endocytosed by a variety of uninfected cell types [208, 209]. Through binding to immune cells, sNS1 is able to induce the production of proinflammatory cytokines and disrupt endothelial cell integrity [210]. Importantly, sNS1 is bound and internalised by endothelial cells, a process which promotes endothelial glycocalyx degradation and disrupts the endothelial cell-barrier integrity [211]. Through these pathways, sNS1 is able to contribute to endothelial cell permeability and vascular leakage: a hallmark of severe dengue disease. Additionally, the endocytosis of sNS1 has been shown to enhance cellular susceptibility to infection. These attributes indicate that sNS1 acts to favour DENV replication and longevity and directly contributes to advanced dengue disease. As such, dissecting the structural properties and key functional residues of the sNS1 protein and how they contribute to its secretion has been the focus of intensive research.

1.7.6: sNS1 Structure

Influential work by Flamand *et al* demonstrated that DENV1 NS1 is secreted from infected cells as a unique soluble hexameric species composed of a trimer of NS1 dimers that are held together by weak hydrophobic interactions and exhibits a molecular weight of approximately 310 kDa [98] . Using electron microscopy (EM) and single particle analysis of DENV1 and DENV2 sNS1, two groups independently determined that the trimer of dimers associate along narrow lateral surfaces to create a barrel-shaped hexameric protein with a prominent central cavity [99, 212]. These two reconstructions, however, exhibit a major structural difference. In the cryo-EM work of Gutsche *et al*, which was refined with D3 symmetry and resolved at ~30 Å resolution, sNS1 was shown to exhibit an open barrel-structure with a wide central channel. In the negative-stain EM work provided by Muller *et al*, which was refined with C3 symmetry and resolved to a resolution of ~23Å, the sNS1 barrel was revealed to be closed at one end. In addition to demonstrating that the sNS1 hexamer is composed of three NS1 dimers, the crystal structure of DENV sNS1 has provided atomic-resolution information (Figure 1.06b) [92]. As described by Akey *et al*, DENV2 sNS1 is arranged as an open hexamer with full D3 symmetry [92]. Within the hexamer, the spaghetti loop, glycosylation sites, and the wing-domain loop are oriented towards the outer surface, while the three β-rolls are oriented towards the interior. The hydrophobic protrusions contributed by each dimer are oriented towards the interior of the hexamer and generate a hydrophobic interior surface. The central cavity has been shown to contain a lipid component [99, 212]. In the open barrel structure, the central cavity exhibits triangular openings of approximately 9 nm^2 at each end. This open central channel has an estimated

volume of approximately 80 nm^3, is lipid-rich and rich in triglycerides. Additional lipid components include cholesterol esters and phospholipids. The lipid component, which is reminiscent of high-density lipoproteins, is proposed to contribute further stability to the non-covalently bound sNS1 hexamer. The purification of NS1 from both human serum and insect cells transduced with baculovirus vectors suggests that DENV NS1 is secreted as a homogeneous hexameric species [98, 99, 212]. However, the homogeneous hexameric nature of DENV sNS1 has recently been questioned. Specifically, high-resolution cryo-EM structures of sNS1 from recombinantly expressed C-terminal His-tagged NS1 from DENV2 [100] and DENV1-4 [101] have been presented. These high-resolution reconstructions have revealed that sNS1 may exist in the extracellular environment as a heterogeneous population of different oligomeric states including hexamers, tetramers, and dimers. Moreover, hexameric sNS1 from DENV4 was shown to exist in two different conformational arrangements [101]. Interestingly, crystal structures of sNS1 from WNV have also been observed to adopt two different conformational forms [92]. Whether this is an indication that DENV NS1 is secreted in multiple oligomeric states, or whether DENV NS1 is secreted as a unique and homogenous hexameric lipoparticle that can acquire different conformations and oligomeric states in the extracellular environment, remains an open question. Nonetheless, how the oligomeric states of sNS1 differ between serotypes and strains, how their state is impacted by the presence and relative abundance of host factors, how this changes during the course of infection, and how this impacts the biological functions of sNS1 will continue to present challenges and opportunities to the DENV research field.

1.7.7: sNS1 Glycosylation

Seminal work by Winkler *et al* demonstrated that intracellular and extracellular (i.e.: secreted) DENV NS1 exhibit different *N*-glycosylation patterns [90]. Whereas intracellular NS1 (iNS1) contains high-mannose moieties at both N130 and N207 glycosylation sites, sNS1 retains the high-mannose type chain at N207 but undergoes additional processing to a complex oligosaccharide form at N130 [213]. The different glycosylation patterns that exist between iNS1 and sNS1 suggest that the additional processing of the N130 glycan may be an important feature for the maturation of secretion-destined NS1. Given the influence of glycosylation on viral protein folding, stability and solubility, however, interrogating the importance of *N*-linked glycosylation of NS1 in the context of viral infection has been complicated due to the detrimental – but not necessarily lethal – impact of NS1 deglycosylation on viral growth characteristics [214-217]. As such, studying NS1 *N*-linked glycosylation has been somewhat restricted to transgenic NS1 expression systems to bypass confounding effects. Several groups have employed a number of different approaches, often yielding dissimilar observations. In mammalian cells expressing DENV NS1 N130 glycosylation mutants, namely N130A or N130Q substitutions, the accumulation of extracellular NS1 has been observed albeit at reduced levels

relative to wildtype NS1 [213, 218]. Similar results have been observed in mammalian cells transfected with a full-length infectious DENV clone lacking N130 glycosylation due to an N130Q mutation [215]. These studies determined that the presence of the *N*-linked glycan at N130 is dispensable for DENV NS1 secretion from mammalian cells, but that this N130 carbohydrate addition does appear to influence the stability of sNS1. In contrast, Wang *et al* reported that their recombinant DENV NS1 construct bearing a N130Q substitution was associated with inefficient secretion of NS1 from transfected mammalian cells [219]. It has been shown that the N130Q mutation used by this group results in the accumulation of sNS1 that is dominated by a higher order oligomer formation in excess of the hexameric form (i.e.: > 675 kDa), although sNS1 purification strategies may explain this discrepancy. The ablation of *N*-linked glycans at N207 does, however, appear to reduce NS1 secretion levels. This was proposed to be due to the reduced stability of the NS1 dimer under the loss of N207 glycosylation incurred by N207A mutagenesis as reported by Pryor *et al* [213]. In this context, Tan *et al* demonstrated that N130A and N207A mutations in NS1 had little impact on DENV2 RNA replication or infectious virus production as determined using subgenomic replicon and full-length infectious DENV2 constructs, respectively, while N130A was associated with no appreciable effect on NS1 secretion and N207A moderately impaired NS1 secretion, when examined in the context of a DENV2 NS1-NS5 polyprotein expression system [188]. Furthermore, Somnuke and colleagues, using an N207Q NS1 mutant, demonstrated that the reduced NS1 secretion phenotype was not the result of instability of the nascently generated intracellular NS1, but was likely due to a negative impact on the NS1 secretion rate and extracellular stability of this NS1 mutant [218]. In contrast, employing a similar N207Q mutational approach to generate N-glycosylation deficient mutants using a DENV NS1 expression construct, Wang *et al* found that the N207Q mutant displays efficient secretion of NS1 from mammalian cells [219]. Taken together, *N*-glycosylation of NS1 does not appear to be required for its secretion although it may be important for the stability of sNS1.

While *N*-glycosylation of NS1 does not appear to be a fundamental requirement for NS1 secretion, glycosylation does appear to impact the extracellular accumulation of sNS1. Despite intensive research into the impact of *N*-linked glycans on DENV NS1 secretion, clear discrepancies exist in the literature. The study of *N*-linked glycosylation on NS1 secretion, even in the context of NS1 expression in cell culture, is complicated by several factors: (i) NS1 dimer stability [91, 213]; (ii) misfolding [218] and; (iii) the extracellular accumulation of multiple NS1 species [218]. A comprehensive study of the impact of *N*-linked glycosylation on DENV NS1 secretion that accounts for the associated complexities will be invaluable.

1.7.8: Important sNS1 residues

Given the importance of sNS1 in DENV pathogenesis, several groups have recently investigated NS1 to identify functionally critical residues that are important molecular determinants of NS1

secretion. Expanding upon a repertoire of 18 replication-impaired NS1 mutants generated by colleagues, Plasczcyza *et al* explored the impact of alanine substitutions on NS1 secretion [192]. To circumvent the negative impact of these mutations on viral RNA replication, various NS1 mutant constructs were generated and employed in the context of a T7 RNA polymerase-driven NS1-NS5 expression system. Six mutations (D136A, W311A, P319A, P320A, E334A, R336A) were identified as almost completely blocking NS1 secretion. These residues that are essential for NS1 secretion largely cluster to the C-terminal domain of the β-ladder. Tan *et al* further interrogated NS1 to identify key functional residues that are essential for NS1 secretion. Using a C-terminal HiBiT luminescent peptide-tagged NS1 expression construct, PCR-based random point mutagenesis was employed to develop a library of NS1 mutants with each bearing a single amino acid substitution [189]. In this system, the luminescent HiBiT peptide tag enabled the rapid quantification of intracellular and secreted NS1 abundance from transfected cells. Ten mutations (E139K, S152L, D180Y, V220D, A248V, T283A, L298W, C313S, I335T, and R336S) were identified as essential for NS1 secretion. Consistent with the findings of Plasczcyza *et al*, most of these mutations were enriched within the β-ladder domain and highly conserved amongst DENV1-4, WNV and YFV, further reinforcing the interpretation that the β-ladder domain is key to efficient DENV NS1 secretion.

1.8: Current understanding of the NS1 secretion pathway in infected mammalian cells

Seminal studies from the late 1980's and early 1990's revealed that the intracellular and secreted forms of Orthoflavivirus NS1 exhibit different N-linked glycosylation patterns [90, 194, 195, 220]. While the intracellular form of NS1 exhibits high-mannose moieties, the secreted form of NS1 undergoes further processing to a complex-type sugar on at least one of those moieties. Additionally, intracellular NS1 exists primarily as a partially hydrophobic membrane-associated dimer, whereas NS1 is secreted as a lipid-associated higher-order oligomer. Given that DENV NS1 is a secretory glycoprotein that has a high-mannose oligosaccharide processed to a complex sugar, this has led to the current dogma that NS1 is secreted from infected mammalian cells via the canonical secretion pathway. Specifically, NS1 is synthesised in the ER and then trafficked to the Golgi for *N*-linked glycosylation and maturation. From the Golgi or trans-Golgi network (TGN), NS1 is trafficked to the plasma membrane where it exits the cell as a mature lipid-associated hexamer. Several lines of evidence support this hypothesis and are discussed below. However, many molecular details remain undefined.

NS1 is translated directly into the ER where it is cleaved from the viral polypeptide into a hydrophilic water-soluble monomer [90, 91, 178]. DENV NS1 is decorated with *N*-linked high-mannose glycans at two conserved residues, Asn130 and Asn207 [90, 213, 221]. The addition of these high-mannose glycans to NS1 is catalysed by the ER-localised oligosaccharyltransferase (OST) complex [222], and addition of these glycans to NS1 can be impaired by pharmacological treatment with tunicamycin or

NGI-1, which inhibit glycosylation completely or OST activity, respectively [91, 221, 222]. The newly synthesised soluble NS1 monomer very quickly homodimerizes to become a partially hydrophobic membrane-associated dimer, the predominant intracellular NS1 form [90, 91]. The high-mannose moieties on the intracellular form of NS1 can be removed by treatment with endoglycosidase H (Endo H), which cleaves high-mannose but not complex glycans [90, 195, 220, 223, 224]. The secreted form of DENV NS1, however, displays an Endo H-resistant complex-type glycan at N130, while the high-mannose addition at N207 remains unchanged [213], indicating that the secreted form of NS1 undergoes additional *N*-linked glycan maturation. It should be noted that the genetic ablation of *N*-linked glycosylation at N130 has been shown to reduce but not abolish recombinant NS1 secretion from NS1-expressing mammalian cells, confirming that neither *N*-linked glycosylation nor the additional processing of the N130 glycan are a strict prerequisite for NS1 secretion [213, 218]. Glycosylation mutations at N130 and N207 do, however, impact the stability, oligomeric state, and extracellular interactions of secreted NS1 [213, 218, 219], raising the possibility that *N*-linked glycosylation may be more critical to the biological function of secreted NS1 rather than the secretion process itself. Nonetheless, in DENV-infected cell culture systems, secreted NS1 displays a complex-type glycan at N130. Given that in uninfected cells the glycosidase and glycosyltransferase machinery responsible for high-mannose trimming and complex glycan addition resides in the Golgi, it has been claimed that the additional processing of NS1 at N130 occurs following ER-to-Golgi translocation [90, 224, 225]. While this hypothesis remains to be validated experimentally, it is supported by a recent proteomic analysis that identified several Golgi components in the interactome of DENV NS1 in DENV replicon-harbouring mammalian cells [222]. In addition to differential glycosylation patterns, intracellular and secreted NS1 exhibit different oligomeric forms. NS1 is traditionally accepted as being secreted from infected cells as a soluble lipid-associated hexameric species composed of a trimer of NS1 dimers [92, 98, 99, 212], suggesting that higher-order oligomerisation of NS1 dimers is essential for NS1 secretion. More recently it was revealed that, in the extracellular environment, secreted NS1 may exist in a highly dynamic equilibrium as dimers, tetramers, hexamers, filamentous polymers, and in complex with human host serum components including high-density lipoproteins [92, 100, 101, 226-229]. Importantly, these recent structural studies have provided insight into how NS1 dimers may assemble into higher-order oligomeric structures. Atomic resolution structural information suggests that this flexibility to transition between oligomeric states may be conferred by the relatively weak intermolecular bonds that are formed between the relatively stable NS1 dimer subunits [92, 101, 229]. The β-roll domain appears to play a key role in the higher-order assembly process by contributing hydrogen bonds and hydrophobic interactions between the dimer subunits. Moreover, the β-roll domain forms hydrophobic interactions with the central lipid component of hexameric NS1 [101], supporting the understanding that the lipid component helps to stabilise the secreted hexameric NS1 form [92, 99]. Highlighting the importance of the lipid component is that NS1 secretion is reduced in cells pharmacologically treated with chemical inhibitors that target lipidic components of lipid droplets and lipid rafts, suggesting that lipid-

NS1 interactions are required for the efficient assembly and secretion of the NS1 lipoprotein particle [99]. Given that secreted NS1 has been shown to be a lipoprotein with a lipid component rich in triglycerides, cholesterol esters and phospholipids [99, 212], and that purified NS1 possesses the ability to bind lipid bilayers and remodel liposomes into lipoprotein particles [92], it has been proposed that NS1 dimers preferentially localise to the sites of nascent lipid droplets on the luminal side of the ER [99]. This has been suggested as a mechanism to concentrate NS1 dimers, with three dimers coming together to associate and pinch off from the membrane, converting them into a soluble hexamer and collecting the lipid component that fills the hexamers central cavity [99]. However, cholesterol-rich microdomains in the Golgi have also been proposed as the site of NS1 dimer association and hexamer formation [95, 98, 230]. Despite its importance, the intracellular location where higher-order oligomerisation of NS1 dimers occurs remains elusive. Nonetheless, regardless of the chronological order and cellular compartments involved in the higher-order oligomerisation and maturation of the N130 glycan processes, NS1 is understood to traffic from the Golgi or TGN to the plasma membrane where it exits the cell as a hexameric glycolipoprotein. This classical secretion pathway hypothesis is regarded as the mechanism that multiple Orthoflaviviruses exploit to achieve NS1 secretion from infected mammalian cells [52, 95, 230-232].

1.9 Extracellular sNS1 and its role in pathogenesis

1.9.1: Background

In the extracellular environment, the complex interplay between sNS1 and numerous host cells and host factors provokes a variety of responses to DENV infection. The highly immunogenic sNS1 elicits an antibody response that can produce both protective and pathogenic consequences [102]. Anti-NS1 antibodies can activate complement and contribute to complement-mediated neutralisation of infected cells, however, the sNS1 protein itself can directly bind and interfere with the proper functioning of several components of the complement system to evade complement-mediated neutralisation [207]. sNS1 is able to bind a variety of cell types which can provoke various biological activities. Several host cell factors have been implicated in the binding of sNS1 to uninfected mammalian cells, including the glycosaminoglycans heparin sulfate and chondroitin sulfate E [209], the pattern recognition receptor Toll-like receptor 4 (TLR4) [210], and the high-density lipoprotein receptor, scavenger receptor class B type I (SR-BI) [233]. Through binding to immune cells, sNS1 is able to induce the production of proinflammatory cytokines [210]. Moreover, sNS1 has been shown to bind and invade endothelial cells, a process which promotes endothelial glycocalyx degradation [211]. Through these two independent pathways, sNS1 is able to contribute to endothelial cell permeability and vascular leakage; a hallmark of severe dengue disease. Additionally, the binding and endocytosis of sNS1 by uninfected cells has been shown to enhance cellular susceptibility to

infection. Understanding the diverse roles of sNS1 and how it favours viral propagation and contributes to viral pathogenesis is of great importance.

1.9.2: Protective and pathogenic anti-sNS1 antibodies

In DENV-infected patients, sNS1 activates a potent humoral immune response leading to the production of anti-NS1 antibodies. These anti-NS1 antibodies can elicit both protective and pathogenic outcomes [234]. Anti-NS1 antibodies raised in mice have been demonstrated to bind to human endothelial cells, platelets, plasminogen, and thrombin [235, 236]. Studies in mouse models have indicated that cross-reactive anti-NS1 antibodies contribute to pathogenesis by inducing liver cell damage and thrombocytopenia [236-238]. This cross-reactivity, however, is not limited to antibodies generated in mice. Studies have shown that anti-NS1 antibodies from DENV-infected patients can cross-react with endothelial cells and induce endothelial cell damage *in vitro* [239]. Similarly, anti-NS1 antibodies from DENV-infected patients have been shown to bind platelets causing platelet dysfunction and inhibiting platelet aggregation [240]. Collectively, these data suggest that anti-NS1 antibodies play a direct role in dengue disease pathogenesis. Indeed, cross-reactive anti-NS1 antibodies have been shown to be higher in patients with severe dengue disease compared to control patients [241]. Importantly however, it is well documented that both passive and active immunization of mice against sNS1 can offer protection against DENV challenge [242-246], highlighting the potential for the development of an NS1-based vaccine. Crucial to the development of an NS1-based vaccine, key epitopes that elicit protective or pathogenic responses are continuing to be identified and mapped to the NS1 protein [96]. Employing a proteomics approach, Cheng *et al* identified several human host cell factors that are target proteins recognised by anti-NS1 antibodies, and sequence homology analysis identified the C-terminal region of NS1 as containing cross-reactive epitopes [247]. Antibodies generated against a C-terminally truncated form of NS1 (deletion of aa 271-352) exhibited reduced platelet cross-reactivity and reduced platelet aggregation [248]. Further, in DENV-infected endothelial cells, antibodies directed towards this truncated form of NS1 were shown to induce complement-mediated cytolysis and inhibit viral replication [249]. Moreover, the active immunization of mice with the C-terminally truncated NS1 protein or a chimeric DENV NS1 protein containing the C-terminal (aa 271-352) amino acid sequence of JEV, was shown to reduce DENV-induced bleeding time, haemorrhage, and viral load [249]. As such, this modified DENV NS1 protein may be a promising candidate for an NS1-based DENV vaccine.

1.9.3: sNS1 and complement

A crucial link between the innate and adaptive immune system is the complement system. The complement system comprises a family of over 50 serum and cell surface-associated proteins that interact with each other to help fight infection [250]. Activation of the complement system occurs via three pathways that involve a cascade of events where complement components interact sequentially and converge to generate inflammatory, vasoactive, and opsonic factors, and a terminal membrane attack complex (MAC) that can directly lyse pathogens and infected target cells [251]. In response to these protective functions, DENV has evolved strategies to modulate complement activity [207, 252, 253]. Importantly, given the potency of the complement system, the dysregulation and/or overactivation of complement can be damaging to host cells. DENV sNS1 was first identified as a soluble complement fixing antigen in 1970 [175]. Anti-NS1 antibodies have been shown to activate complement and can directly target host cell surface-expressed NS1 to induce complement-dependent cytolysis of DENV-infected cells, thus providing a protective role against DENV infection [249, 254]. Both cell surface-associated and sNS1 activate complement to completion, and this activation is enhanced in the presence of anti-NS1 antibodies [199]. Importantly, in DENV-infected patients, plasma levels of sNS1 and terminal complement complexes C5b-9 have been shown to correlate with dengue disease severity [199]. Given that DENV sNS1 can bind to a variety of uninfected endothelial cells in a manner reflecting disease tropism [208, 209], these data suggest that anti-NS1 antibody-dependent hyperactivation of complement may contribute to vascular leakage – a key symptom of severe dengue disease.

Numerous studies have revealed that DENV sNS1 can directly interact with various complement components to modulate complement activity as an immune evasion strategy. DENV sNS1 binds to mannose-binding lectin (MBL), a pattern recognition molecule that recognises specific carbohydrates expressed on the surface of many pathogens including DENV [255]. sNS1 competitively binds MBL, thus helping to prevent DENV virion detection from MBL recognition and protecting DENV from complement activation via the lectin pathway [256]. DENV sNS1 also binds C4 and its complement-specific serine protease C1s [254]. By forming this tripartite C4-NS1-C1s/pro-C1s complex in solution, sNS1 promotes the degradation of C4 to C4b, thus minimising the concentrated deposition of active C4b on DENV virions and DENV-infected cells [254]. Further, DENV sNS1 reduces the functional capacity of C4b in complement activation by interacting directly with the complement regulatory protein, C4b binding protein (C4BP) [257]. sNS1 exploits the cofactor activity of C4BP to recruit the complement-specific serine protease Factor I (FI) for the cleavage and inactivation of C4b in solution and on the cell surface [257]. Through these mechanisms sNS1 attenuates both the classical and lectin complement pathways, thus protecting both DENV virions and DENV-infected cells from complement-mediated neutralisation. DENV sNS1 has also been shown to directly bind to the terminal MAC components C5, C6, C7, and C9 and the complement regulatory factor vitronectin (VN) [258]. Through interactions with these components, sNS1 is able

to inhibit MAC formation and prevent complement-mediated cell lysis. This NS1-VN complex has been observed in DENV-infected patient plasma [258]. Clearly, sNS1 can interfere with the proper functioning of a variety of complement proteins that act at multiple stages within the complement cascade. Through these mechanisms, sNS1 can attenuate each of the classical, alternative and lectin pathways, thus offering DENV virions and DENV-infected cells protection from complement-mediated neutralisation.

1.9.4: sNS1 and proinflammatory cytokine dysregulation

An exacerbated and aggressive release of proinflammatory and vasoactive cytokines, termed 'cytokine storm', is proposed to play a major role in severe dengue disease by contributing to vascular leakage. TNF-α, IFN-ɣ, IL-6, IL-8, IL-10, MIF, VEGF, and IP-10 have been found to be significantly higher in the sera of patients experiencing severe dengue compared to those with non-severe dengue [259-263]. TLR4 is a membrane-spanning pattern recognition receptor (PRR) that recognises evolutionarily conserved components – pathogen-associated molecular patterns (PAMPs) – on invading microorganisms. TLR4 is a key activator of the innate immune response, and its activation leads to cellular signalling pathways that induce the production of proinflammatory cytokines, chemokines, and type I interferons to facilitate clearance of the invading pathogen.

In 2015, Modhiran *et al* identified sNS1 as a TLR4-activating PAMP [210]. Specifically, the binding and activation of TLR4 on mouse bone marrow-derived macrophages or human peripheral blood mononuclear cells by highly purified sNS1 was shown to potently induce the transcription of TNF-α, IL-6, IL-1β, and IL-8. It was also demonstrated that sNS1-induced activation of TLR4 results in human microvascular endothelial cell monolayer disruption and that this could be blocked by the use of a TLR4 antagonist (LPS-RS) or an anti-TLR4 antibody. In addition to the enhanced production of TNF-α, IL-6, and MIF, vascular leakage has been observed in mice inoculated with sNS1 alone, supporting a direct link between circulating sNS1-induced vasoactive cytokine dysregulation and vascular leakage *in vivo* [246, 264]. Moreover, the level of vascular leakage seen in mice co-inoculated with sNS1 and a sub-lethal dose of DENV can be greatly reduced by treatment with LPS-RS or anti-NS1 antibodies [210, 246], further confirming the role of sNS1-induced TLR4 activation as an important determinant of severe dengue disease. sNS1 also binds and activate platelets via TLR4 [265], and this results in the release of stored cytokines (MIF) and chemokines (CXCL4 and CCL5) [266], indicating that sNS1-induced activation of platelets may play a role in amplifying inflammation in DENV infection. In this context, synthesis of pro-IL-1β, the inactive precursor that is subsequently processed into the proinflammatory cytokine IL-1β, is increased in sNS1-activated platelets, although this does not translate into the enhanced secretion of IL-1β that is observed in DENV-infected platelets and correlated with increased vascular leakage [266, 267]. Interestingly, while DENV-infected platelets sustain viral RNA replication, viral protein synthesis and NS1

secretion, they do not support the release of infectious virus [268]. As such, it has been proposed that sNS1-induced activation of TLR4 acts through an autocrine loop in infected platelets, to further enhance the inflammatory phenotype of DENV-infected platelets [266]. Importantly, however, sNS1-induced activation of platelets has been shown to enhance platelet aggregation, adhesion to and permeability of endothelial cells, and phagocytosis by macrophages [265]. This suggests that, in addition to contributing to proinflammatory cytokine dysregulation, sNS1-induced activation of platelets can contribute directly to the thrombocytopenia and haemorrhage observed in dengue disease. Human monocyte-derived dendritic cells (mo-DCs), a primary target of DENV infection, bind and internalise sNS1 [269]. It has been shown that mo-DCs pre-treated with sNS1 prior to infection exhibit enhanced susceptibility to infection, increased viral RNA replication, and increased production of IL-6 and the monocyte chemoattractant CCL2 [269]. It is not clear, however, whether the increased IL-6 and CCL2 production is a direct result of sNS1 pretreatment and/or enhanced viral replication. However, these data suggest that sNS1 may act to recruit proinflammatory-secreting DENV primary target cells to sites of infection, thereby contributing to the exacerbated 'cytokine storm' that is seen in severe dengue cases.

These studies provide evidence that sNS1 is able to contribute to the dysregulation of proinflammatory cytokines that can influence endothelial cell permeability and vascular leakage. However, these permeability-enhancing impacts occur rapidly upon exposure to sNS1 whereas the plasma leakage observed in severe dengue disease occurs after circulating sNS1 has been largely cleared. Clearly, the role of sNS1 in contributing to proinflammatory cytokine dysregulation is multifactorial and complex, particularly in the context of a full viral infection.

1.9.5: sNS1 and vascular leakage

Severe dengue disease is characterised by an increase in vascular permeability that can lead to plasma leakage. Lining the blood vessels is the vascular endothelium, where endothelial cells, and the tight junctions (TJs) and adherens junctions (AJs) between them, act as the gatekeepers to control the extravasation of leukocytes and plasma proteins. In addition to the intercellular junction proteins providing endothelial cell-cell adhesion, many of the transmembrane proteins confer intracellular signalling functions through cytoplasmic-localised scaffolding proteins. Moreover, lining the luminal side of the vascular endothelium is the endothelial glycocalyx layer (EGL), a proteoglycan- and glycosaminoglycan-rich network that confers critical functions in circulatory homeostasis. The binding and internalisation of sNS1 has recently been shown to modify the molecular organisation of the EGL and endothelial cell-cell junctions and contribute directly to endothelial cell permeability *in vitro* and vascular leakage *in vivo*. [219].

Importantly, specific lineages of endothelial cells differentially bind and internalise Orthoflavivirus sNS1 proteins in a tissue-specific manner that largely reflects the pathophysiology of each virus [208]. The internalisation of DENV sNS1 by diverse endothelial cells has been shown to induce changes in gene expression, with endothelial cell-specific pathway analysis indicating that sNS1 internalisation can modify the expression of genes that confer key roles in vascular homeostasis [270]. The upregulation of the sialidases Neu1, Neu2, and Neu3, result in the cleavage of sialic acid from the endothelial cell surface [211, 219]. sNS1 internalisation also leads to the activation of lysosomal proteases, including Cathepsin L, which in turn induces the expression and activation of heparinase, resulting in the cleavage of heparan sulfate proteoglycans from the EGL [211, 271]. Given that sNS1 can induce the activation of endothelial cell enzymes, including heparinase and sialidases, which cleave cell surface expressed EGL factors, and that these EGL factors perform key roles in the regulation of vascular permeability, their sNS1-induced removal likely plays a key role in dengue disease pathology. Indeed, circulating EGL degradation products have been detected in DENV-infected patients with elevated levels of these circulating products correlating with disease severity [272, 273]. Recently, it was demonstrated that sNS1 is able to bind and activate MMP-9 [274], a matrix metalloprotease that is involved in the disassembly of the extracellular matrix. Endothelial cells treated with sNS1 and MMP-9 display an altered distribution of the AJ and TJ proteins, β-catenin and ZO-1. In this work, Pan and colleagues were able to demonstrate that sNS1 can activate and recruit MMP-9 to the endothelial cell surface where MMP-9 acts to degrade endothelial cell junctions leading to endothelial hyperpermeability *in vitro* and vascular leakage *in vivo* [274]. β-catenin is a phospho-regulated multifunctional protein that plays roles in endothelial cell adhesion and signal transduction by linking the cell-cell junction protein, VE-cadherin, to the cytoskeleton. In endothelial cells inoculated with sNS1, VE-cadherin colocalises with clathrin heavy chains indicating that sNS1 may induce VE-cadherin internalisation in a clathrin-dependent manner. Moreover, sNS1 stimulation induces changes in the phosphorylation status of β-catenin in a glycogen synthase kinase-3B (GSK-3B)-dependent manner. Puerta-Guardo *et al* revealed that NS1-induced endothelial barrier dysfunction and vascular leakage could be blocked by the pharmacological inhibition of GSK-3β [275].

The ability of sNS1 to selectively bind and be internalised by lineage-specific endothelial cells and trigger endothelial barrier dysfunction and vascular leakage in a manner that reflects disease tropism indicates that sNS1 is directly responsible, at least in part, for the pathologies associated with Orthoflavivirus infection. Importantly, the sNS1-induced vascular leakage observed in many of these studies can be reduced by inhibiting components of these molecular pathways, suggesting that they may provide targets for therapeutic intervention.

1.9.6: sNS1 internalisation enhances susceptibility to infection

Despite the complex dual-host lifecycle that requires DENV to replicate in both mosquitoes and humans, two organisms that are more than 500 million years diverged [276], it is estimated that DENV infects approximately 400 million humans each year [24]. The multifunctional viral virulence factor, sNS1, provides numerous proviral fitness advantages that enhances intra-host viral replication and inter-species transmission.

In 2005, Alcon-LePoder and colleagues reported that purified sNS1 of mammalian origin is efficiently endocytosed by human hepatocytes and, further, that sNS1 treatment enhances their endocytic activity [277]. Moreover, it was shown that when hepatocytes were pre-treated with sNS1 prior to DENV challenge, a substantial increase in infectious virus production was observed [277], suggesting that the pre-exposure of uninfected cells to sNS1 may enhance cellular susceptibility to DENV infection. Purified sNS1 of mammalian origin is also efficiently endocytosed by human monocyte-derived dendritic cells (mo-DCs) [269]. The pre-treatment of mo-DCs with sNS1 prior to DENV challenge results in a greater proportion of infected cells and enhances DENV genome replication at the early stage of infection [269], thus supporting the conclusion that sNS1 enhances cellular susceptibility to DENV infection. While this did not translate to an increase in infectious virus production in mo-DCs, alterations in cytokine gene expression profiles were observed [269], suggesting that the biological impact of sNS1 internalisation may be cell-type dependent. Mechanistically, it has also been demonstrated that the treatment of uninfected murine macrophages with purified sNS1 of insect origin promotes plasma membrane lipid raft accumulation in a TLR4-dependent manner, and that this facilitates DENV cell surface attachment following DENV challenge [226]. While viral RNA replication and infectious virus production were not assessed, this work provides evidence to indicate that pre-exposure of mammalian cellular membranes to insect-derived sNS1 can alter plasma membrane composition and that this may provide a mechanism to facilitate DENV infection. Alcala *et al* demonstrated that purified sNS1 of insect origin is efficiently endocytosed by mosquito cells, and that the pre-treatment of mosquito cells with sNS1 prior to DENV infection also results in a significant increase in infectious DENV production [233]. Similar results were also observed in experiments using ZIKV sNS1. Importantly, it was revealed that sNS1 from both DENV and ZIKV can exploit SR-BI to bind to human hepatocytes, and an SR-BI-like receptor to bind to mosquito cells [233]. In addition to identifying a novel receptor that allows sNS1-host cell binding, this work confirms that sNS1-induced enhancement of infection occurs in both human and mosquito cells and that this may be a conserved feature amongst Orthoflaviviruses to favour replication in two evolutionarily divergent host organisms. Indeed, it has been shown that the presence of sNS1 in infected mammalian host sera facilitates viral acquisition by mosquitoes. In a series of elegant experiments, Liu and colleagues demonstrated that the presence of sNS1 in DENV-infected human blood significantly increases the percentage of infected *Ae. aegypti* mosquitoes following an *in vitro* membrane blood meal [278]. RNA-Seq analysis focussing on immune-related

genes revealed that genes related to reactive oxygen species production and the JAK/STAT pathway were downregulated, indicating that mammalian-derived sNS1 can suppress multiple mosquito antiviral strategies. Importantly, *in vivo* experiments confirmed that the passive transfer of anti-NS1 antibodies reduces the percentage of infected *Ae. aegypti* and *Ae. albopictus* mosquitoes after feeding on DENV-infected mice. Moreover, similar results were observed in *Culex pipiens pallens* mosquitoes after feeding on JEV-infected mice, confirming that this phenomenon of sNS1-enhanced acquisition of viral infection following inter-species transmission may represent a conserved role of Orthoflavivirus sNS1.

1.10: Current understanding of the mechanism of DENV sNS1 internalisation in mammalian cells

DENV sNS1 is able to associate with a variety of tissues and cell types both *in vitro* and *in vivo*. In mice intravenously inoculated with sNS1, Alcon-LePoder *et al* found that sNS1 was massively associated with the liver and localised in discreet punctate structures within hepatocytes [277]. Through *in situ* histological analysis, Avirutnan *et al* found DENV sNS1 bound to endothelial cells within the liver and lung [209]. More recently, Puerta-Guardo and colleagues have shown that sNS1 proteins from different Orthoflaviviruses bind endothelial cells, including liver, lung, skin, umbilical vein, and brain in a virus-specific manner, and induce endothelial barrier dysfunction in a tissue-specific manner that largely reflects disease pathophysiology [208]. Importantly, the ability of sNS1 to induce endothelial barrier dysfunction and vascular leakage is dependent upon the cellular internalisation of sNS1 [219]. As such, defining the molecular mechanisms that sNS1 exploits to achieve internalisation is of paramount importance.

sNS1 can initiate an intimate association with a target cell through interactions with a variety of extracellular matrix and plasma-membrane-associated host factors. The near-ubiquitously expressed glycosaminoglycans (GAG), heparin sulfate and chondroitin sulfate E, have been shown to allow sNS1 binding to the surface of a range of epithelial and mesenchymal cells [209]. This sNS1-GAG interaction appears to be more dependent on sulfation rather than negative charge, with highly sulfated motifs required for optimal binding [209]. As described above, sNS1 is also able to bind and activate TLR4 [210, 265], a pattern recognition receptor that is primarily expressed on cells of myeloid origin. It has also been suggested that DENV sNS1 may bind and activate TLR2 and TLR6 [279], however the validity of this interaction has been challenged [280]. The HDL receptor SR-BI, which is highly expressed in the liver and, to a lesser extent, in macrophages, endothelial cells, and lung tissue [281], was recently demonstrated to act as an sNS1 binding receptor [233]. Importantly, chemical treatment [209, 219], competitive binding assays [233], and genetic knockout experiments [265] designed to inhibit sNS1 binding to these host factors have been shown to reduce but not ablate sNS1-host cell binding, indicating that sNS1 is likely promiscuous in its binding and host cell

attachment may occur via a diverse repertoire of host cell-surface exposed factors. Beyond attachment, Wang and colleagues explored the process of DENV sNS1 internalisation in lung and brain endothelial cells [219]. The binding of sNS1 to these endothelial cells recruits clathrin to the plasma membrane and sNS1 is internalised in a clathrin-dependent and dynamin-dependent manner. Intriguingly, this group revealed that an sNS1-N207Q glycosylation mutant can bind to endothelial cells comparably to wildtype sNS1, however it fails to be internalised, indicating that sNS1 binding and internalisation may be distinct processes. Moreover, the internalisation process appears to be quite rapid. Using an sNS1 internalisation temperature-shift assay, which involves incubating cells with sNS1 at 4°C to allow binding, washing to remove unbound sNS1, then incubating at 37°C to allow internalisation, and monitoring the sNS1 lifespan within endothelial cells by confocal immunofluorescence microscopy, Wang *et al* revealed that sNS1 accumulates to a maximum peak in endothelial cells within 15 minutes. At 90 minutes post-internalisation, sNS1 colocalises with the early endosome markers Rab5 and EEA1, the lysosomal marker Lamp1, and the lysosomal cysteine protease cathepsin L. Interestingly, following sNS1 internalisation in lung and brain endothelial cells, the intracellular sNS1 signal was lost within 3 hours, suggesting that it may be degraded. In umbilical vein endothelial cells, Barbachano-Guerrero *et al* found that DENV1 sNS1 similarly colocalises with Rab5 and also with the late endosome marker Rab7 at 2 hours post-inoculation [270]. In these experiments, where sNS1-containing inoculum remained on the cells for the duration of the experiment, sNS1 was found to steadily accumulate over several hours, with discreet sNS1 puncta coalescing to form larger structures [270]. In experiments of longer duration, it has been found that internalised sNS1 exhibits marked stability in human Huh-7 and HepG2 hepatocyte-derived cells, with sNS1 being detected for at least 48 hours post-internalisation [277]. To track internalised sNS1 distribution along the endolysosomal pathway, Alcon-LePoder and colleagues incubated hepatocyte-derived cells with sNS1 for 6 hours and examined intracellular sNS1 distribution relative to early endosomes, late endosomes, and late endosomes/lysosomes. After this incubation, sNS1 was found to exhibit partial colocalisation with LBPA, a specific lipid component of late endosomes. At 24- and 48-hours post-internalisation, sNS1 and LBPA signals were indistinguishable, indicating near-complete colocalisation of sNS1 with late endosomes. Collectively, these data indicate that internalised sNS1 is targeted to the late endosome where it is remarkably resistant to degradation. Supporting this, ultrastructural analysis by electron microscopy revealed that internalised sNS1 was present in 0.5 – 1 μM cytoplasmic vacuoles, many of which contained internal membranes characteristic of late endosomes [277].

Clearly, our understanding of the molecular mechanisms involved in sNS1 host cell binding and internalisation is evolving. Several cell surface factors have been implicated in sNS1 attachment, and it has been revealed that sNS1 internalisation is clathrin- and dynamin-dependent. The upregulation of heparinases and sialidases have provided insight into how sNS1 internalisation can contribute to EGL disruption. Nonetheless, the exact molecular details of sNS1 binding, internalisation, and how this contributes sNS1-induced pathological phenotypes remain unclear.

Given the pathological consequences of sNS1 host cell binding and internalisation, identifying the repertoire of host cell attachment factors, further defining the molecular mechanisms of internalisation, revealing the internalised sNS1-associated cellular proteome, and understanding how this exerts specific cellular responses is of critical importance. Defining these processes will contribute to our understanding of how internalised sNS1 influences cell signalling pathways, enhances cellular susceptibility to infection, and contributes to cytokine dysregulation and selective vascular leakage – a hallmark of severe dengue disease.

1.11: Molecular techniques to interrogate virus-host interactions

As non-metabolic, obligate intracellular parasites that harbour small genomes that encode limited proteomes, viruses must hijack host cellular factors and pathways to support their replication. The exploitation of host cell proteins is critical for viral entry, genome replication, protein synthesis, virion assembly, and egress. Additionally, virus-host protein-protein interactions (PPI) are critical for virus-induced manipulation of the host to generate an environment conducive to productive viral infection. As such, identifying the host proteins and pathways that are usurped by viruses are key to understanding the molecular mechanisms of virus replication and pathogenesis. Several powerful tools that enable the identification of virus-host interactions are available in the virological toolbelt. This section discusses the two main techniques used in this thesis to identify the human host cell factors associated with DENV NS1 secretion and sNS1 internalisation.

1.11.1: siRNA screening

One molecular biological approach that allows the interrogation of host protein function is gene silencing through RNA interference (RNAi) [282]. Given that mammalian cells naturally possess all of the cellular machinery required for siRNA-mediated gene silencing, the experimental interrogation of gene function simply requires gene-specific siRNA or shRNA to be introduced into the target cell cytoplasm [283]. As such, genome-wide or targeted siRNA libraries are commercially available and can be readily customised. It should be noted that while siRNA screening is a valuable tool for studying genotype-phenotype relationships, this technique is not equivalent to genetic approaches that introduce gene-disrupting mutations into the host genome. As such, siRNA screens often suffer from lack of sensitivity due to incomplete suppression of host gene expression. Moreover, while siRNAs require near-perfect complementary base pairing for mRNA suppression, the presence of siRNAs can activate alternative endogenous RNAi pathways (e.g.: microRNA) that can suppress gene expression by imperfect base pairing, potentially leading to off-target effects via suppression of multiple mRNA species [284]. Therefore, independent experimental validation of the results of

high-throughput siRNA screens using complementary genetic and/or pharmacological approaches is of critical importance [284-287]. Nonetheless, the simplicity and reproducibility of siRNA screening makes it a valuable and effective approach to rapidly probe gene function in virus infected cells [288].

1.11.2: APEX2-based proximity-dependent labelling for proteomic profiling

Proximity-dependent labelling utilises enzymes to create highly reactive radicals that can covalently tag proximal proteins in live cells [289]. When coupled with mass spectrometry, this approach allows the identification and characterisation of protein interactome networks in a high-throughput format. Several enzyme systems are available (BioID, TurboID, APEX, HRP, and PUP-IT) [290], and these enzymes can be fused to a viral protein of interest to identify virus-host PPIs to understand how viral proteins behave in host cells [291]. Importantly, however, given that the enzyme must be genetically fused to the viral protein of interest, it is essential to confirm that the fusion of this enzyme does not significantly impact the function of the viral protein of interest. Indeed, several recent studies have utilised this approach to interrogate the viral-host proteomes of DENV [292], ZIKV [293], and Hepatitis C virus [294]. The APEX2 enzyme is a next-generation engineered plant-based peroxidase that provides the added advantage over alternative enzyme labelling systems in that it remains active in the reducing environment of the cellular cytosol [295]. Moreover, the biotin-phenol radicals are not membrane permeable, making APEX2 an excellent tool to study the proteomic profiles of membrane-bound organelles. Further, the APEX2 enzyme can be utilised for electron microscopy, thus providing the added advantage of allowing the confirmation of cellular localisation at high resolution [295]. Experimentally, through the addition of biotin-phenol and H_2O_2, APEX2 catalyses biotin-phenol to short-lived biotin-phenol radicals [296]. These radicals tag electron-dense amino acids in proteins within close proximity (~20 nm) [297], thus only tagging the immediately proximal environment thus reducing non-specific labelling. Further, the rapid labelling kinetics (<1 min) provides temporal resolution [296], making this enzyme useful for the study of dynamic changes in protein complex arrangement [298]. As tagged proteins are biotinylated, they can be efficiently recovered by affinity purification using streptavidin-coated beads and stringent washing and identified by mass spectrometry.

1.12: Research Objectives

sNS1 is an important DENV pathogenic factor and sNS1 levels in patient serum is correlated with adverse patient outcomes. As detailed above, extracellular sNS1 can induce the production of autoantibodies, attenuate complement pathways, and contribute to the dysregulation and exacerbation of proinflammatory cytokine production. Moreover, sNS1 has been shown to be internalised by a variety of cell types. This internalisation of sNS1 can contribute to transmission, enhanced infection, and vascular leakage - a key symptom of severe dengue disease. Given the pathological effects of sNS1, much research has focussed on the molecular determinants of NS1 that facilitate sNS1 secretion and contribute to disease. However, a detailed understanding of the molecular mechanisms exploited by DENV to achieve sNS1 secretion and internalisation are lacking. Therefore, the research objectives of this thesis are to identify and interrogate the host cellular factors that are essential to DENV sNS1 secretion and internalisation.

1.12.1: Hypothesis

Identifying the human host molecular machinery that are exploited by DENV to achieve NS1 secretion and sNS1 internalisation may contribute towards the development of NS1-targeting anti-orthoflaviviral therapies.

1.12.2: Aim 1

To identify host cellular factors that are important determinants of DENV NS1 secretion using a high-throughput siRNA screen approach and to interrogate and confirm their role in validation studies.

1.12.3: Aim 2

To create a comprehensive protein interactome of human host factors involved in the early events of sNS1 internalisation using a proximity-based proteomics approach in live cells.

Chapter 2

Materials and Methods

2: Materials and Methods

2.1: Molecular biology techniques

2.1.1: Synthetic oligonucleotides

Synthetic oligonucleotides for PCR, Sanger sequencing and cloning and gene fragments for cloning (Appendix II) were purchased from Integrated DNA Technologies or Sigma-Aldrich. DNA oligonucleotides were resuspended at 100 µM in DNase/RNase-free water and working stocks were prepared at 20 µM by diluting in DNase/RNase-free water.

2.1.2: Plasmids

The plasmid pFK-DVs which contains a full-length DENV2 genome (16681) [299], a pFK-DVs subgenomic replicon derivative encoding a *Renilla* luciferase cassette (pFK-sgDVs-R2A) [299], a pFK-sgDVs-R2A replication-defective NS5 mutant derivative (pFK-sgDVs-GND-R2A) [299], and a replication-independent T7 RNA polymerase-driven DENV2 non-structural protein 1-5 expression plasmid (pIRO-D) [300] were provided by Ralf Bartenschlager (University of Heidelberg, Heidelberg, Germany). The pFK-DVs derivative encoding a NanoLuc luciferase tag embedded within NS1 between Lys-175 and Gln-176 (pFK-DVs-NS1-NLuc), and the pFK-DVs derivative encoding the engineered plant peroxidase APEX2 at the same site within NS1 (pFK-DVs-NS1-APEX2) were previously described [94]. GFP-tagged wildtype COPA, COPB2, and COPG1 cDNA constructs that were cloned into a pLenti6/V5-D-TOPO (Thermo Fisher Scientific) backbone were created as previously described [301]. For single nucleotide polymorphism (SNP) incorporation, wildtype GFP-tagged COPA, COPB2, COPG1 cDNA constructs were modified using QuikChange II site-directed mutagenesis (Agilent) in conjunction with the appropriate SNP-containing primers (Appendix II), as described in 2.1.12. The DENV2-IgK-APEX2-myc construct was generated using NEB HiFi DNA Assembly. Briefly, our laboratory's previously generated DENV2-T2A-APEX2-P2A was modified to incorporate an IgK chain leader sequence at the N-terminal end of APEX2 and a myc-tag epitope sequence at the C-terminal end. The plasmid map and annotated nucleotide sequence is shown in Appendix IV. The GeCKO LentiCRISPRv2 plasmid [302], the psPAX2 lentiviral packaging plasmid, and the VSV-G Envelope expression plasmid pMD2.G were purchased from Addgene (Addgene plasmid numbers 52961, 12260, and 12259, respectively).

2.1.3: Bacterial transformation

NEB® 5-alpha Competent High-Efficiency *E. coli* chemically competent cells were purchased from New England Biolabs and stored at -80°C. For transformation, 50 µL aliquots of NEB® 5-alpha

Competent High-Efficiency *E. coli* cells were thawed on ice, mixed with 5 ng of plasmid DNA, 2 µL NEB HiFi DNA Assembly reaction or 2 µL of ligation product and incubated on ice for 30 minutes. Cells were then heat shocked at 42°C for 30 seconds and immediately returned to ice for a further 5 minutes. 950 µL of SOC outgrowth media (New England Biolabs) was added to each sample and incubated at 37°C for 60 minutes with agitation on an orbital shaker. Cells were then centrifuged at 2,000 x g for 5 minutes at room temperature. 800 µL of SOC media was removed and the cell pellet was resuspended by gentle pipetting in the remaining volume of SOC media. 50 µL and 150 µL aliquots of each sample were then spread onto prewarmed Luria Bertani agar plates supplemented with 100 ug/mL ampicillin (Appendix I) and incubated at 37°C overnight.

2.1.4: Small-scale (Mini-prep) plasmid DNA preparation

For small scale plasmid preparations, single colonies of bacterial transformants were picked and inoculated into 10 mL Luria Bertani broth supplemented with 100 ug/mL ampicillin. These cultures were then incubated at 37°C overnight with agitation on an orbital shaker. Following sufficient growth (often ≥24 hours for pFK-DVs and derivative plasmids), cells were briefly chilled on ice and then centrifuged at 5,000 x g for 15 minutes at 4°C (Microfuge X Pro Series, Thermo Fisher Scientific). Bacterial pellets were then processed for plasmid DNA extraction using the NucleoSpin® Plasmid EasyPure Kit (Macherey-Nagel) according to the manufacturer's instructions. Plasmid DNA quantity was estimated as described in 2.1.6. Purified DNA was verified by diagnostic restriction enzyme digestion (2.1.7) or Sanger sequencing (2.1.10). DNA was stored at -20°C.

2.1.5: Large-scale (Midi/Maxi-prep) plasmid DNA preparation

For large-scale plasmid preparations, diagnostic digest- or Sanger sequencing-verified plasmid DNA (2.1.4) was used for bacterial transformation as described in 2.1.3. Single colonies were then inoculated into 10 mL Luria Bertani broth supplemented with 100 ug/mL ampicillin. These starter cultures were incubated at 37°C for approximately 4-8 hours with agitation, and then used to inoculate 200 mL or 500 mL (Midi- and Maxi-Prep, respectively) of Luria Bertani broth supplemented with 100 ug/mL ampicillin. These larger-scale cultures were incubated at 37°C overnight with shaking. Following sufficient growth, cultures were chilled on ice and centrifuged at 4,000 x g for 30 minutes at 4°C (Multifuge X Pro Series, Thermo Fisher Scientific). Bacterial pellets were processed for plasmid DNA extraction using the NucleoBond® Xtra Midi/Maxi Kit (Macherey-Nagel) following the high copy plasmid purification protocol (mammalian expression plasmids) or the low copy plasmid purification protocol (DENV2 plasmids), with the following exceptions: after pelleting the DNA precipitate (Step 13 of the protocol), all but 1 mL of the supernatant was removed, the pellet

was resuspended in this remaining 1 mL and transferred to a DNase/RNase-free 1.5 mL microcentrifuge tube. This was centrifuged at 15,000 x g for 5 minutes at 4°C and the supernatant was discarded. The DNA pellet was then washed in 1 mL of 70% ethanol and centrifuged at 15,000 x g for 5 minutes at room temperature. This was step was repeated. Ethanol was removed by careful pipetting and the DNA pellet was resuspended in an appropriate volume of DNase/RNase-free water. Plasmid DNA quantity was estimated as described in 2.1.6. Purified DNA was verified by diagnostic restriction enzyme digestion (2.1.7) or Sanger sequencing (2.1.10). DNA was stored at -20°C.

2.1.6: Estimation of DNA and RNA concentrations

DNA and RNA concentration and purity (OD260nm/OD280nm; OD260nm/OD230nm) were determined via UV spectrophotometry (NanoDrop 2000/One, Thermo Fisher Scientific).

2.1.7: Restriction endonuclease digestion

For restriction enzyme digestion of plasmid DNA, 1 µg of plasmid DNA was mixed with 2 µL of 10x CutSmart buffer (New England Biolabs), 1 µL of restriction enzyme (New England Biolabs) and DNase/RNase-free water to a final volume of 20 µL. Following assembly, reactions were pulse-centrifuged, vortexed, centrifuged briefly and incubated at 37°C overnight in an S1000™ Thermal Cycler (Bio-Rad). Digested samples were then assessed by agarose gel electrophoresis as described in 2.1.8.

2.1.8: Agarose gel electrophoresis

Agarose gel electrophoresis was performed using 0.7 – 2.5 % (w/v) agarose gels. Gels were prepared by dissolving an appropriate weight of molecular grade agarose powder (Bioline) in 1x TAE buffer (Appendix I) supplemented with a 1:20,000 dilution of RedSafe™ Nucleic Acid Staining Solution (Intron Biotechnology). Gels were cast in Mini- or Midi-Gel Casters (Bio-Rad). Samples were diluted with an appropriate volume of 6 x Blue/Purple loading dye (New England BioLabs) and separated by electrophoresis alongside a 100 bp or 1 kb DNA ladder (New England Biolabs) in 1x TAE buffer in a Mini-Sub® Cell GT Agarose Gel Electrophoresis System (Bio-Rad) at 80 – 100V for 40 – 90 minutes to achieve appropriate separation. DNA-containing gels were visualised using the ChemiDoc MP Imaging System (Bio-Rad) coupled with Imaging Lab Software using the default settings for RedSafe™-stained nucleic acid visualisation. For DNA extraction and purification from agarose gels, DNA bands were excised using a disposable scalpel blade, and then placed in a weighed DNase/RNase-free microcentrifuge tube and then processed as described in 2.1.9.

2.1.9: Gel and PCR Purification

DNA purification of PCR products, restriction enzyme digests, and DNA bands excised from agarose gels were performed using the NucleoSpin® Gel and PCR Clean-Up Kit (Macherey-Nagel) following the manufacturer's protocol with the following exceptions: for elution, elution buffer or DNase/RNase-free H2O was pre-warmed to 70°C and incubated on the column membrane for 5 – 10 minutes at 50°C. Samples were then centrifuged at 12,000 x g for 1 minute at room temperature. DNA quantity was estimated as described in 2.1.6.

2.1.10: Sanger Sequencing

DNA Sequencing was performed by the Australian Genome Research Facility (AGRF, Urrbrae, South Australia). Samples were prepared by combining target DNA (400 – 800 ng plasmid; 30 – 75 ng PCR product) with 0.5 µL of 20 µM sequencing primer (Appendix II) and DNase/RNase-free water added to a final volume of 12uL. FASTA and .ab1 format files were analysed using Benchling software.

2.1.11: Polymerase Chain Reaction

Primers were designed manually using Benchling software to visualise the DNA sequences. Self-complementarity was assessed using the online oligonucleotide properties calculator: OligoCalc (BioTools, North Western University, Illinois, USA). Annealing temperatures were assessed using the NEB Tm Calculator (New England Biolabs). PCR reactions were performed using Q5® High-Fidelity DNA Polymerase (New England Biolabs). PCR reactions were assembled on ice to a final volume of 25 µL using DNase/RNase-free H2O with the following: an appropriate volume of template DNA (~1 ng plasmid DNA; ~500 ng genomic DNA), forward and reverse primers were each added at a final concentration 0.5 µM, and 12.5 µL of Q5® 2x Master Mix (New England Biolabs). Samples were briefly vortexed and pulse-centrifuged. PCR reactions were carried out using an S1000™ Thermal Cycler (Bio-Rad) using the following conditions (unless otherwise specified): initial denaturation 98°C for 30 seconds; 18 – 35 cycles of 98°C for 10 seconds, 50-72°C for 10 – 30 seconds, 72°C for 20 – 30 seconds per kb; final extension of 72°C for 2 minutes; samples were then held at 4°C. Where appropriate, PCR products were visualised using agarose gel electrophoresis (2.1.8) and purified using the NuceloSpin® Gel and PCR Clean-Up Kit (Macherey-Nagel), as detailed in section 2.1.9.

2.1.12: Site-Directed Mutagenesis

Site-Directed Mutagenesis was employed to modify GFP-tagged COPA, COPB2, and COPG1 cDNA plasmids. This was performed using the QuikChange II XL Site-Directed Mutagenesis Kit (Agilent), as per the manufacturer's instructions. Briefly, 50 µL Mutant Strand PCR Synthesis Reactions were assembled on ice using the following components: 5 µL 10x Reaction Buffer (Agilent), 10 ng of dsDNA plasmid template, 125 ng of each forward and reverse mutagenic primers (Appendix II), 1 µL dNTP mix, 3 µL QuikSolution Reagent (Agilent), and DNase/RNase-free water added to 50 µL. Samples were briefly vortexed and pulse-centrifuged prior to the addition of 1 µL PfuUltra HF DNA polymerase (Agilent). This assembled reaction mix was then mixed by gentle pipetting. Site-directed mutagenesis PCR reactions were carried out using an S1000™ Thermal Cycler (Bio-Rad) with the following conditions: initial denaturation 95°C for 60 seconds; 18 cycles of 95°C for 50 seconds, 60°C for 50 seconds, 68°C for 13 minutes; final extension of 68°C for 7 minutes, and samples were then briefly held at 4°C. 1 µL of *Dpn*I restriction enzyme (10 U/uL) (Agilent) was then added to each reaction. Samples were then briefly vortexed, pulse-centrifuged and incubated at 37°C for 1 hour to digest the parental plasmid. For each sample, 2 µL of the *Dpn*I-treated PCR reaction was used for bacterial transformation (2.1.3). The following day, single colonies were processed for small-scale plasmid DNA extraction as described in 2.1.4. Plasmids were then verified by Sanger sequencing (2.1.10) using the sequencing primers listed in Appendix II. Sanger sequencing-verified plasmids were then subjected to large-scale plasmid DNA preparation as described in 2.1.5, with the following exceptions: for each sample, a single colony was picked and inoculated directly into 200 mL Luria Bertani broth supplemented with 100 ug/mL ampicillin. These cultures were incubated at 37°C overnight with shaking. Following sufficient growth (~16 hours), cultures were chilled on ice and centrifuged at 4,000 x g for 30 minutes at 4°C. Bacterial pellets were processed for plasmid DNA extraction using the NucleoBond® Xtra Midi Kit (Macherey-Nagel) following the manufacturer's recommendations for high copy plasmid purification. Plasmid DNA quantity was estimated as described in 2.1.6 and stored at -20°C.

2.1.13: NEBuilder HiFi DNA Assembly

For various cloning assemblies, the NEBuilder HiFi DNA Assembly kit (New England BioLabs) was utilised. As recommended by the manufacturer, the NEBioCalculator tool was employed to determine the appropriate quantity of vector and insert DNA for a molar ratio of 1:2 (vector:insert). Vector and insert were then added to a DNase/RNase-free PCR tube and NEBuilder HiFi DNA assembly reactions were assembled ice. For this, the vector (50 ng), insert and appropriate volume of DNase/RNase-free water were added to a final volume of 5 µL. Samples were briefly vortexed and pulse-centrifuged-centrifuged. 5 µL of 2x NEBuilder HiFi DNA Assembly Master Mix (New England BioLabs) was then added to the PCR tube, briefly vortexed and pulse-centrifuged. Reactions were

incubated at 50°C for 1 hour (S1000™ Thermal Cycler, Bio-Rad) and then briefly stored on ice prior to transformation. 2 µL of NEBuilder HiFi DNA Assembly reactions was used for bacterial transformation as described in 2.1.3.

2.1.14: Generating COPI component CRISPR-Cas9 plasmids

2.1.14.1: Guide RNA design

Two predesigned single guide RNAs (sgRNAs) targeting distinct loci within each gene of interest (COPA, COPB2, COPG1 and GBF1) were selected using the Alt-R CRISPR-Cas9 online tool (Integrated DNA Technologies). Single guide RNA oligonucleotides were further designed using Benchling to incorporate *Bsm*BI-v2 overhangs (Appendix II) for integration into *Bsm*BI-V2-digested pLentiCRISPRv2 plasmid. These were purchased as single stranded DNA oligonucleotides (Sigma-Aldrich).

2.1.14.2: Plasmid Backbone

pLentiCRISPRv2 plasmid was digested using the *Bsm*BI-v2 restriction enzyme (New England Biolabs), as described in 2.1.7, and dephosphorylated using Antarctic Phosphatase (New England Biolabs), as per the manufacturer's instructions. DNA was separated by agarose gel electrophoresis (2.1.8) and the digested pLentiCRISPRv2 vector backbone was recovered by gel purification (2.1.9). Purified *Bsm*BI-v2-digested linear pLentiCRISPRv2 backbone was stored at -20°C.

2.1.14.3: Annealing oligonucleotides

Single stranded oligonucleotides (2.1.14.1) were annealed and 5'-phosphorylated using the T4 Polynucleotide Kinase (New England Biolabs). For this, the following reagents were assembled on ice: 2 µL of 20 µM oligonucleotide #1, 2 µL of 20 µM oligonucleotide #2, 13 µL of DNase/RNase-free H2O, 2 µL 10x T4 Ligase Buffer (New England Biolabs), and 1 µL of T4 PNK (New England Biolabs). Samples were briefly vortexed, pulse-centrifuged and transferred to an S1000™ Thermal Cycler (Bio-Rad) for sequential incubations according to the following conditions: 37°C for 30 minutes, 95°C for 5 minutes, 70°C for 10 minutes, and cooled to room temperature over 60 minutes (~1°C per minute). These annealed oligonucleotide complexes were diluted 1:40 in DNase/RNase-free water.

2.1.14.4: Ligation

To ligate the oligonucleotide complexes (2.1.14.3) into the *Bsm*BI-v2-digested pLentiCRISPRv2 backbone (2.1.14.2), the following reaction was assembled on ice: 1 µL (50 ng) of digested pLentiCRISPRv2 plasmid, 1 µL diluted oligonucleotide complex, 2 µL 10× T4 Ligase Buffer (New England Biolabs), 16.5 µL of DNase/RNase-free water, 0.5 µL T4 DNA Ligase (New England

Biolabs). Samples were briefly vortexed, pulse-centrifuged and incubated at 16°C for 60 minutes in an S1000™ Thermal Cycler (Bio-Rad). Following bacterial transformation (2.1.3) and small-scale plasmid preparation (2.1.4), purified plasmid DNA was subjected to restriction enzyme diagnostic digestion (2.1.7) and sgRNA cassette-containing plasmids were verified by DNA sequencing (2.1.10). Sanger sequencing-verified plasmids were then used for large-scale plasmid DNA preparation (2.1.5). These COPI sgRNA pLentiCRISPRv2 plasmids were subsequently utilised for lentivirus production as described in 2.3.5.1.

2.1.15: *In vitro* transcription of viral RNA

5 µg of viral cDNA-containing pFK- plasmid was linearised by *Xba*I (New England Biolabs) restriction enzyme digestion at 37°C overnight (2.1.7). The next morning, digested plasmid DNA was directly purified using the NucleoSpin Gel and PCR Clean-Up kit (Macherey-Nagel), as per the manufacturer's instructions and eluted in 10 µL DNase/RNase-free water. DNA quantity and purity was estimated as described in 2.1.6. The linearised vector was then used as template to transcribe viral RNA using the mMessage mMachine™ SP6 Transcription Kit (Thermo Fisher Scientific). Reactions were assembled at room temperature to a final volume of 20 µL using an appropriate volume of DNase/RNase-free water, 1.5 µL SP6 GTP, 10 µL 2x SP6 NTP/CAP, 1 µg cDNA template, 2 µL 10x SP6 buffer and 2 µL of SP6 Enzyme Mix. Following assembly, reagents were extensively mixed, pulse-centrifuged and incubated at 37°C for 3 hours in an S1000™ Thermal Cycler (Bio-Rad). To degrade the DNA template, 1 µL of Turbo DNase was added, extensively mixed, pulse-centrifuged and incubated at 37°C for 15 minutes. Samples were then transferred to a fresh DNase/RNase-free 1.5 mL microcentrifuge tube and *in* vitro transcribed (IVT) RNA was immediately purified, as described in 2.1.16.

2.1.16: Isolation of *in vitro* transcribed viral RNA

1 mL of TRI-reagent® (Sigma Aldrich) was added to the IVT RNA reaction product generated in 2.1.15 and samples were incubated for 5 minutes at room temperature. 200 µL of chloroform was added to each sample, shaken vigorously for 15 seconds, and then incubated for 5 minutes at room temperature. Samples were then centrifuged at 12,000 x g for 15 minutes at 4°C. The RNA-containing upper aqueous phase was then transferred to a fresh DNase/RNase-free microcentrifuge tube. To precipitate the IVT RNA, 500 µL of isopropanol was added to each sample, mixed by inversion, pulse-centrifuged and then incubated for 10 minutes at room temperature. Samples were then centrifuged at 12,000 x g for 30 minutes at 4°C. Supernatant was then removed, and the RNA-containing pellet was washed twice in 75% ethanol and centrifuged at 7,500 x g for 5 minutes at 4°C.

Ethanol was removed by careful pipetting and the RNA pellet was air-dried and resuspended in 50uL DNase/RNase-free water. RNA quantity and purity was estimated as detailed in 2.1.6. 5 µg aliquots of IVT viral RNA were dispensed into DNase/RNase-free PCR tubes and stored at -80°C.

2.1.17: Quantification of mRNA and viral RNA by RT-qPCR

Total cellular RNA was extracted from cell culture monolayers, as described in 2.2.17, and diluted to a final concentration of 2.5 ng/uL in DNase/RNase-free water. First-strand cDNA synthesis and RT-qPCR was performed using the Luna® Universal One-Step RT-qPCR Kit (New England Biolabs) in 384-well plates using a CFX-Opus (Bio-Rad) or QuantStudio 7 Flex (Life Technologies) thermal cycler according to the manufacturer's instructions. For each sample and each primer pair, 10 µL reactions were prepared in technical duplicate. Each reaction contained 5 ng of total RNA, 0.2 µL of 20 µM forward primer, 0.2 µL of 20 µM reverse primer, 5 µL of Luna Universal One-Step 2x Reaction Mix, 0.5 µL Luna WarmStart RT 20x Enzyme Mix, and 2.1 µL DNase/RNase-free water. All samples were additionally processed to quantify *RPLP0* mRNA (housekeeping gene). For melt curve analysis, the qPCR instrument default settings were utilised. mRNA or DENV RNA levels were expressed as a percentage of those of the experimental control (non-targeting control [NTC] siRNA-transfected or 0.1% [v/v] DMSO carrier control-treated, as indicated) following normalisation to *RPLP0* mRNA, by using the threshold cycle (ΔΔCT) method. Primer sequences are detailed in Appendix II.

2.1.18: SDS-PAGE and Western blotting

SDS-PAGE-buffered cell culture lysates or cell culture supernatants, prepared as described in 2.2.18, were separated by SDS-PAGE alongside Precision PlusProtein® Kaleidoscope® Pre-stained protein standards (Bio-Rad) using a precast 4-20% Mini-PROTEAN® TGX gel (Bio-Rad) in 1x SDS-PAGE running buffer (Appendix I) at 100V for 50 – 70 minutes in a Mini PROTEAN® Tetra cell (Bio-Rad). Samples were then transferred to a nitrocellulose membrane at 100V for 60 minutes in a Mini-PROTEAN cell (Bio-Rad) containing ice-cold wet transfer buffer (Appendix I), submerged ice pack, and magnetic stirrer to prevent overheating. Alternatively, samples were transferred to a nitrocellulose membrane using a Trans-Blot Turbo Transfer System (Bio-Rad) and the default mixed molecular weight transfer setting (7 min), as per the manufacturer's instructions. For cell culture supernatant Western blot normalisation, see 2.1.19. Following protein transfer, nitrocellulose membranes were blocked in 5% (w/v) skim milk in TBS (Appendix I) for 60 minutes with gentle agitation on an orbital shaker. For immunoblotting, primary antibodies targeting the protein of interest were diluted to the appropriate concentration (Appendix III) in 1% (w/v) skim milk in TBS-T (Appendix

I). This solution was incubated with the membrane overnight at 4°C with gentle agitation. The following day, antibody-containing solution was removed, and the membranes were washed three times in TBS-T, each for 5 minutes with gentle agitation. Secondary antibodies (Appendix III) diluted in 1% (w/v) skim milk in TBS-T were then incubated with the membrane for 60 minutes in the dark at room temperature. Secondary antibody-containing solution was then removed, and the membranes were washed three times in TBS-T for 5 minutes in the dark at room temperature with gentle agitation. Membranes were then imaged using an Odyssey CLx Imaging system (LI-COR) using the default settings.

2.1.19: Total Protein Stain for quantitative Western blot analysis of extracellular NS1

For quantitative Western blot analysis of sNS1-containing cell culture supernatants, Revert™ 700 Total Protein Stain (LI-COR) was employed for Western blot normalisation. As noted in 2.1.18, prior to blocking in 5% skim milk in TBS, protein-containing nitrocellulose membranes were incubated with 3-5mL of Revert™ 700 Total Protein Stain solution for 5 minutes in the dark at room temperature with gentle agitation. Total Protein Stain solution was then removed, and the membrane was washed with 5 mL of Revert™ 700 Wash solution for 30 seconds in the dark at room temperature with gentle agitation. This wash step was performed twice. Wash solution was then removed, the membrane was immersed in MQ water and then immediately imaged using an Odyssey CLx Imaging system (LI-COR) using the default settings. Following imaging (imaging acquisition time ~8 min/membrane), membranes were immediately blocked in 5% (w/v) skim milk in TBS and processed for immunoblotting as described in 2.1.18.

2.1.20: Western blot image analysis and quantitation

For Western blot image analysis and quantitation, signal intensities were quantified using Image Studio Lite (version 5.2.5). For quantitative analysis of NS1 protein secretion efficiency, intracellular NS1 (iNS1) signal intensities were first normalised to those of the loading control β-actin, and secreted NS1 (sNS1) signal intensities were normalised to those of the entire lane Total Protein Stain (TPS) values. Subsequently, normalised sNS1 values were divided by the normalised iNS1 values and expressed as a percentage of that of the relevant negative control for that experiment.

2.2: Cell culture techniques

2.2.1: Cell Lines

2.2.1.1: Huh-7.5:

A derivative of the Huh-7 human hepatocellular carcinoma cell line that was originally isolated from a well-differentiated hepatocellular carcinoma from a 57 year old Japanese male [303]. The Huh-7.5 cell line has been cured by IFN-α treatment of an HCV sub-genomic replicon that was artificially introduced into the Huh-7 cell line [304]. This Huh-7.5 cell line allows high levels of orthoflavivirus production due to defects in innate immune signalling. Huh-7.5 cells were generously provided by Charles M. Rice (Rockefeller University, New York, USA).

2.2.1.2: Huh-7.5+Fluc:

A derivative of the Huh-7.5 cell line that has been engineered for the stable expression of the Firefly luciferase gene has been previously described [305]. Firefly luciferase protein expression is maintained by blasticidin selection (5 ug/mL).

2.2.1.3: Huh-7.5+T7:

A derivative of the Huh-7.5 cell line that has been engineered for the stable expression of the bacteriophage T7 RNA Polymerase, as previously described [305]. T7 RNA polymerase expression is maintained under puromycin antibody selection (3 µg/mL).

2.2.1.4: HEK 293FT:

The HEK 293FT cell line (Thermo Fisher Scientific) is a fast-growing variant of the HEK 293T cell line which is of human embryonal kidney cell origin and engineered to express the SV40 large T-antigen.

2.2.2: Maintenance of cell cultures

Mammalian cells were maintained in tissue culture-treated sterile plastic 75 cm^2 U-Shaped Canted Neck cell culture flasks (Corning). Cell culture media consisted of Dulbecco's Modified Eagle Medium (DMEM) containing 4.5g/L D-Glucose, 25mM HEPES, 2mM L-glutamine (Life Technologies), supplemented with 100 U/mL penicillin, 100 ug/mL streptomycin and 10% heat-inactivated foetal bovine serum, referred to as 'complete DMEM'. Complete DMEM was supplemented with blasticidin (5 µg/mL) or puromycin (3 µg/mL) as required. Cells were cultured at 37°C in a humidified 5% CO_2 atmosphere.

2.2.3: Cell Passaging

Cells were passaged at 80% confluency. For this, spent culture media was aspirated, cells were washed once in PBS and detached by trypsinisation by incubating in 0.5 – 1 mL trypsin-EDTA at 37°C in 5% CO_2 for approximately 5 minutes. Cells were then resuspended in approximately 5 mL of complete DMEM, and an appropriate volume of cell suspension (containing approximately 1 x 10^6 cells) was transferred to a new 75 cm^2 culture flask containing approximately 10 mL of pre-warmed complete DMEM. These cells were then incubated at 37°C in 5% CO_2.

2.2.4: Seeding Cells in tissue culture plates

Near-confluent cells were harvested as described in 2.2.3. Resuspended cells were harvested for enumeration using the Trypan blue exclusion method. For this, an aliquot of cells was diluted in Trypan blue stain solution, mixed by pipetting, and loaded onto a haemocytometer (Hirschmann, Neubauer improved bright line). The number of live cells (cells that excluded trypan blue) were enumerated using the following formula:

live cells/mL = Average cell count x dilution factor x 10,000

Cells were then seeded into complete DMEM-containing Costar Clear TC-treated multiple well plates (Corning) according to the details below and then returned to culture at 37°C in 5% CO_2.

Table 2.01. Useful numbers for propagating human cells in tissue culture plates (adapted from Thermo Fisher Scientific).

Culture plates	Surface area (cm^2)	Seeding density (cells)	Cells at confluency	Complete DMEM (mL)
6-well	9.6	0.3 x 10^6	1.2 x 10^6	1 to 3
12-well	3.5	0.1 x 10^6	0.5 x 10^6	1 to 2
24-well	1.9	0.05 x 10^6	0.24 x 10^6	0.5 to 1
48-well	1.1	0.03 x 10^6	0.12 x 10^6	0.2 to 0.4
96-well	0.32	0.01 x 10^6	0.04 x 10^6	0.1 to 0.2

2.2.5: Seeding cells on glass coverslips for high-resolution microscopy

Sterile 13 mm #1.5 circular coverslips were placed into the wells of a 12-well plate. Alternatively, #1.5 coverglass-bottomed µ-Slide 8-well chamber slides (ibidi Gmbh, Germany) were employed. For coating, 0.2% (w/v) gelatin in PBS was added to each well and incubated for 1 – 2 hours at room temperature. During this time, cells were harvested as described in the indicated experiments. Gelatin solution was then removed from the plates and the wells were washed with PBS. Cells were then added to each well and maintained and processed as described in the indicated experiments.

2.2.6: Cryopreservation of cells

Semi-confluent cells were harvested as described in 2.2.3. Resuspended cells were centrifuged at 200 x g for 5 minutes at room temperature. Supernatants were discarded and cell pellets were resuspended in 3 mL of complete DMEM. 3 mL of 0.2 µm filtered 2x Freezing Mix (Appendix I) was added to the cell suspension, thoroughly mixed, and 1 mL aliquots were transferred into cryogenic vials. Cryogenic vials were then placed in a Mr Frosty freezing container (Thermo Fisher Scientic) and transferred to a -80°C freezer where they were stored for 48 – 72 hours before being transferred to liquid nitrogen for long-term storage.

2.2.7: Resuscitation of frozen cells

Cryopreserved cells were resuscitated by rapid thawing in a 37°C water bath. Thawed cells were added to a 75cm^2 cell culture flask containing approximately 10 mL of pre-warmed complete DMEM and incubated at 37°C in 5% CO_2 for approximately 4 hours. DMSO-containing cell culture media was then removed and replaced with 10 mL complete DMEM. Cells were then maintained as described in previous sections (2.2.2 and 2,2.3, respectively).

2.2.8: Transfection using Lipofectamine 2000

Cells were seeded into 6-well tissue culture plates as described in 2.2.4. The following day, 100 µL of Opti-MEM (Thermo Fisher Scientific) was mixed with 3 µL of room temperature Lipofectamine 2000 (Thermo Fisher Scientific) in a microcentrifuge labelled ‘A’, flick mixed and pulse-centrifuged. In a separate microcentrifuge tube labelled ‘B’, 2 µg of plasmid DNA was diluted in 100 µL of Opti-MEM (Thermo Fisher Scientific), flick mixed and pulse-centrifuged. Tubes ‘A’ and ‘B’ were combined, flick mixed, pulse-centrifuged, and incubated at room temperature for 15 minutes. 200 µL of the

transfection mixture was added dropwise to each well to be transfected. The plate was gently rocked briefly before being returned to incubate at 37°C in 5% CO_2.

2.2.9: Transfection using Lipofectamine 3000

Huh-7.5 or Huh-7.5+T7 cells (2.2.1.3) were seeded into 24-well tissue culture plates as described in 2.2.4. The following day, I µL of room temperature Lipofectamine 3000 (Thermo Fisher Scientific) was diluted in 25 µL Opti-MEM (Thermo Fisher Scientific) in a microcentrifuge labelled 'A', flick mixed and pulse-centrifuged. In a separate microcentrifuge tube labelled 'B', I µL of room temperature p3000 Reagent (Thermo Fisher Scientific) was diluted in 25 µL Opti-MEM (Thermo Fisher Scientific), this was flick mixed and briefly pulse-centrifuged, then 0.5 µg of plasmid DNA was added and immediately flick mixed and pulse-centrifuged. Tubes 'A' and 'B' were combined, flick mixed, briefly pulse-centrifuged, and incubated at room temperature for 10 – 15 minutes. 50 µL of this plasmid DNA/lipofectamine/p3000/Opti-MEM mixture was added dropwise to each well to be transfected. The plate was gently rocked before being returned to incubate at 37°C in 5% CO_2. At 3 hours post-transfection, transfection reagent-containing media was replaced with complete DMEM and cells were then returned to culture at 37°C in 5% CO_2.

2.2.10: Reverse transfection using DharmaFECT 4

The following methods describe the siRNA reverse transfection protocol for a 12-well plate. For alternative sized plates, this protocol was scaled accordingly. In a microcentrifuge tube labelled 'A', 3 µL of DharmaFECT 4 (Dharmacon, Horizon Discovery) was diluted in 97 µL of Opti-MEM (Thermo Fisher Scientific), flick mixed and pulse-centrifuged. In a separate microcentrifuge tube labelled with the appropriate target (i.e.: 'COPA', 'COPB2', 'COPG1', 'GBF1', or 'NTC'), 2 µL of siRNA (20 µM) was added to 98 µL of Opti-MEM (Thermo Fisher Scientific), flick mixed and pulse-centrifuged. Tubes 'A' and 'target' were combined, flick mixed and briefly pulse-centrifuged. 200 µL of this siRNA/DharmaFECT4/Opti-MEM mixture was added to each well to be transfected and the plate was incubated for 20 – 30 minutes at room temperature. Huh-7.5 cells were then PBS-washed, trypsinised, and live cells were enumerated using Trypan blue as described in 2.2.4. After the 20 – 30 minute incubation, 800 µL of cell suspension was added to each well to be transfected (40 nM siRNA final concentration). The plate was briefly rocked before being returned to incubate at 37°C in 5% CO_2. At 3 hours post-transfection, transfection reagent-containing media was replaced with complete DMEM, and cells were then returned to culture at 37°C in 5% CO_2 and processed further as described in the indicated 2.3.3.1 and 2.3.4.

2.2.11: Transfection of *in vitro* transcribed viral RNA using DMRIE-C

Cells were seeded into 6-well tissue culture plates as indicated in 2.2.4. The following day, cell culture media was replaced with 1 mL complete DMEM lacking penicillin and streptomycin and incubated at 37°C in 5% CO_2 for 2 hours. Transfection mixture was assembled using the following: 1 mL of Opti-MEM, 6 µL of room temperature DMRIE-C, 5 µg SP6-generated *in vitro* transcribed viral RNA (as described in 2.1.15 and 2.1.16). This was flick mixed and pulse-centrifuged. Cells were then washed in PBS, the transfection mixture was added to each well to be transfected and cells were incubated at 37°C in 5% CO_2. At 4 hours post-transfection, transfection reagent-containing media was replaced with complete DMEM and cells were returned to culture at 37°C in 5% CO_2.

2.2.12: Orthoflavivirus infection of Huh-7.5 cells for NS1 secretion experiments

Semi-confluent Huh-7.5 cells were harvested and enumerated as described in 2.2.4. 5 x 10^6 cells were then seeded into a 75cm^2 tissue culture flask and returned to culture overnight in complete DMEM at 37°C in 5% CO_2. The following morning, cell viability and seeding density were assessed by light microscopy. Under the assumption of a ~1.5x doubling of Huh-7.5 cells following a 16-hour overnight incubation at 37°C in 5% CO_2 (5 x 10^6 cells x 1.5 = 7.5 x 10^6 cells), cells were inoculated with DENV or KUNV at an MOI ~1. Specifically, 7.5 x 10^6 FFU of DENV or KUNV virions were diluted in 8 mL of pre-warmed complete DMEM, thoroughly mixed and used as inoculum. At 4 hours-post-infection, virus-containing cell culture media was removed. Cells were then washed with PBS, trypsinised and enumerated (2.2.4), and cell suspensions were immediately used for downstream experiments (as described in 2.3.4 and 2.3.6). Additionally, as an uninfected negative control for downstream experiments, a 75cm^2 flask of Huh-7.5 cells was processed in parallel, however, these cells were mock-inoculated with 8 mL of complete DMEM lacking orthoflavivirus.

2.2.13: Cell Viability Assays

Cell viability assays were performed using the CellTiter-Glo 2.0 luminescent cell viability assay (Promega), as per the manufacturer's instructions. For GCA experiments, cells were treated as described in 2.3.6. For COPI siRNA experiments, cells were treated as per 2.3.4. At the cessation of each experiment (18 hours post-GCA treatment or 48 hours post-siRNA treatment), cell culture supernatants were removed and replaced with complete DMEM (40 µL/well). The plate was then equilibrated to room temperature for approximately 30 minutes prior to the addition of precisely 40 µL/well of CellTiter-Glo 2.0 Reagent. The plate was mixed gently and incubated for 10 minutes at room temperature. Luminescence was then determined using a Cytation 5 Multimode Reader equipped with a Dual-Reagent Injector Module (BioTek), as per the manufacturer's instructions.

2.2.14: Infectivity Assays

Virus-containing cell culture supernatants were recovered, where indicated, at the specified timepoints. These were clarified by centrifugation (15,000 x g for 15 minutes at room temperature) to remove cellular debris, and clarified supernatants were stored at -80°C. Infectivity was assessed by focus forming assay (FFA). For this, Huh-7.5 cells were seeded into 96-well plates at 2 x 10^4 cells/well (as described in 2.2.4). The following day, virus-containing cell culture supernatants were serially diluted in complete DMEM. Huh-7.5 cells were washed in PBS and inoculated with serially diluted virus-containing cell culture supernatants at 40 µL/well in technical duplicate and incubated at 37°C in 5% CO_2 for 3 hours. At 3 hours post-infection, virus-containing inoculum was removed, cells were washed with PBS and returned to culture in complete DMEM (100 µL/well) at 37°C in 5% CO_2 for 3 days. At 3 days post-infection, cells were then washed in PBS and fixed and labelled for immunofluorescence microscopy (2.2.19 and 2.2.20, respectively) using an anti-capsid primary antibody (Appendix III). DENV-positive foci were defined as ≥3 capsid-positive cells arranged as a distinct cluster. Foci were enumerated and infectivity titers were determined using the following formula:

Focus forming units/mL = Average number of foci x dilution factor x 25

2.2.15: Quantification of subgenomic DENV RNA replication by luciferase assay

Purified *in vitro* transcribed (IVT) pFK-sgDVs-R2A and pFK-sgDVs-GND-R2A RNA (generated as per 2.1.15 and 2.1.16) were transfected into Huh-7.5 cells in 12-well plates as described in 2.2.11. At 24 hours post-transfection, cells were washed in PBS and returned to culture in complete DMEM supplemented with GCA (1 µM, 2.5 µM, or 5 µM) or 0.5% (v/v) DMSO carrier control at 37°C in 5% CO_2 for 18 hours. At 18 hours post-GCA treatment, cells were washed with PBS and lysed in 1x *Renilla* Luciferase Lysis Buffer (250 µL/well) (Promega) with gentle agitation. Plates were then sealed with parafilm and stored at -20°C. For each sample, 10 µL of thawed cell lysate was dispensed into a single well of a white-walled 96-well plate. Luminescence was then determined using a Cytation 5 Multimode Reader equipped with a Dual-Reagent Injector Module (BioTek), following automated injections with 50 µL of *Renilla* Luciferase Assay Reagent (prepared by diluting 100x Renilla Luciferase Assay Substrate at 1 in 100 in Renilla Luciferase Assay Buffer; Promega) per well and an integration time of 10 s, following a 2 s delay. Unless otherwise indicated, luciferase signals (relative light units [RLU]) were expressed as a percentage of average values for values associated with lysates that were prepared at 3 hour time-points following IVT RNA transfection (‘input’).

2.2.16: Genomic DNA extraction

Huh-7.5 cells were resuspended as described in 2.3.5.4. 1 mL of cell suspension (~1 x 10^6 cells) was transferred to a 1.5 mL microcentrifuge tube. Cells were clarified by centrifugation at 1000 x g for 5 minutes at room temperature. Cell culture supernatant was removed, and the cell pellet was processed using NucleoSpin® Tissue Mini kit (Macherey-Nagel) for DNA extraction (2.2.16), as per the manufacturer's instructions. DNA quantity and purity was estimated as described in 2.1.6, and stored at -20°C.

2.2.17: Total cellular RNA extraction

Total cellular RNA was extracted from cell culture monolayers grown in a 24-well plate (as detailed in the indicated experiments). For this, cell culture supernatants were removed, and 250 µL NucleoZOL (Macherey-Nagel) was added to each well. Plates were then briefly stored on ice and samples in each well were homogenised by pipetting several times to ensure complete lysis. Lysates were then transferred to ice-cold DNase/RNase-free microcentrifuge tubes and stored at -80°C. For processing, NucleoZOL lysates were defrosted on ice. 100 µL of DNase/RNase-free water was added to each sample and samples were shaken vigorously for 15 seconds and then incubated for 5 minutes at room temperature. Samples were then centrifuged at 12,000 x g for 15 minutes at room temperature. 500 µL of RNA-containing supernatant was transferred to a fresh microcentrifuge tube. To precipitate RNA, 500 µL of isopropanol was added to each sample and samples were incubated for 10 minutes at room temperature. To pellet RNA precipitates, samples were then centrifuged at 12,000 x g for 10 minutes at room temperature and then the supernatant was aspirated and discarded. The RNA pellet was washed in 1 mL of 75% ethanol and centrifuged at 8,000 x g for 5 minutes. Ethanol was removed by careful pipetting. This wash step was performed twice. Following removal of the supernatant, the RNA pellet was air-dried for approximately 5 minutes and then resuspended in an appropriate volume (20-50 µL) of DNase/RNase-free water. RNA quantity and purity was estimated using a NanoDrop 2000 spectrophotometer, as detailed below. Samples were then stored at -80°C.

2.2.18: Extraction of cell culture protein for SDS-PAGE

For whole cell lysates, cell culture monolayers were extensively washed in PBS, lysed in protease inhibitor-supplemented NP-40 lysis buffer or protease inhibitor-supplemented RIPA lysis buffer, as detailed in the indicated experiments, and stored on ice for 30 mins. Whole cell lysates were then homogenised by passing through a 25 G needle with a 1 cc/mL syringe (Terumo), clarified by centrifugation (15,000 x g 15 minutes at 4°C) and the debris-free cell lysis supernatant was then

transferred to a fresh ice-cold microcentrifuge tube. For cell culture supernatants, culture media was recovered from cells and placed on ice. Ice-cold supernatants were then clarified by centrifugation (15,000 x g for 15 min) and debris-free supernatant was then transferred to a fresh ice-cold microcentrifuge tube. Clarified lysate and clarified supernatant samples were mixed with SDS-PAGE 4x reducing or non-reducing buffer (Appendix I) and boiled at 95°C for 5 minutes in an S1000™ Thermal Cycler (Bio-Rad) and stored at -20°C or used immediately for SDS-PAGE as described in 2.1.18.

2.2.19: Fixing cells for immunofluorescence microscopy

2.2.19.1: Acetone:Methanol Fixation

Cells were grown on 0.2% (w/v) gelatin-coated 13mm #1.5 circular coverslips in 24-well plates, #1.5 glass coverslip-bottom chamber slides (µ-Slide 8 Well Glass Bottom chamber slides; Ibidi) or TC treated (uncoated) multi-well cell culture plates, as appropriate. Cell culture media was removed, and cells were extensively washed with PBS. Cell culture monolayers were fixed in ice-cold acetone:methanol (1:1) and plates were incubated on ice for 5 minutes. Fixative was then removed and replaced with PBS. Plates were stored at 4°C or immediately processed for immunofluorescent labelling as described in 2.2.20.

2.2.19.2: 4% Paraformaldehyde Fixation

Cells were grown on 0.2% (w/v) gelatin-coated 13mm #1.5 circular coverslips in 24-well plates, #1.5 glass coverslip-bottom chamber slides (µ-Slide 8 Well Glass Bottom chamber slides; Ibidi) or TC treated (uncoated) multi-well cell culture plates, as appropriate. Cell culture media was removed, and cells were extensively washed with PBS. Cell culture monolayers were fixed 4% PFA fixation solution (Appendix I) and incubated for 20 minutes at room temperature. Cells were washed in PBS and then permeabilised by incubating cells in 0.1% (v/v) Triton X-100 in PBS for 10 minutes at room temperature. Cells were then washed in PBS, and plates were stored at 4°C or immediately processed for immunofluorescent labelling as described in 2.2.20.

2.2.20: Immunofluorescent labelling of fixed cells for immunofluorescence microscopy

Cell culture monolayers from indicated experiments were fixed as described in 2.1.19. PBS was removed from cell culture monolayers, replaced with 5% (w/v) BSA in PBS (Appendix I), and incubated for 30 minutes at room temperature. 5% BSA blocking reagent was removed and replaced with the indicated primary antibody diluted in 1% BSA according to the primary antibody dilutions

detailed in Appendix III. Plates were then incubated overnight at 4°C. The following day, cells were then washed twice (or as indicated) in PBS. PBS was removed and replaced with AlexaFluor-conjugated secondary antibody appropriately diluted in 1% BSA in PBS (Appendix III) and plates were incubated for 1 – 2 hours in the dark at 4°C. Cells were then washed twice (or as indicated) in PBS. PBS was removed and replaced with DAPI (1 ug/mL) in PBS and incubated for 10 minutes in the dark at 4°C. DAPI solution was removed and replaced with PBS. Plates were then stored at 4°C in the dark or imaged immediately, as detailed in the indicated experiments. Where appropriate, coverslips were mounted onto glass microscope slides using ProLong Diamond Antifade Mountant (Thermo Fisher Scientific), sealed using clear nail varnish and stored in the dark prior to imaging.

2.2.21: ZEISS LSM 880 + Fast Airyscan confocal microscopy

Cell culture monolayers from indicated experiments were fixed and labelled for immunofluorescence microscopy, as detailed in 2.2.19 and 2.2.20, respectively. Samples were imaged using a ZEISS LSM 880 Fast Airyscan confocal fluorescence microscope system using a C-Plan-Apochromatic 63× (NA: 1.4) oil immersion objective (Flinders Microscopy and Microanalysis, Flinders University, Australia). Laser lines 405 nm, 488 nm and 561 nm were used at 2% maximal power with appropriate detector master gain settings to enable signal visualisation with minimal saturation. Pinhole sizes were set to 1.0 Airy units for the longest-wavelength fluorophore and matched for all tracks. Unless otherwise indicated, images were processed and analysed using ZEN Blue v.2.3 software (ZEISS)

2.3: Project-Specific Experimental Techniques

2.3.1: Customised membrane-trafficking siRNA Screen

2.3.1.1: siRNA library

Detailed experimental methods and analysis of the customised membrane-trafficking siRNA screen are provided in Appendix V. Briefly, the siRNA library comprised a commercially available siRNA library targeting membrane trafficking proteins (Human ON-TARGETplus siRNA Library – Membrane trafficking – SMARTpool, Dharmacon Cat# G-105500) and an additional 37 siRNA SMARTpools (Dharmacon, Horizon Discovery) targeting previously identified proviral host factors that may be manipulated by NS1. Each siRNA SMARTpool consists of four siRNAs that target distinct loci within the same gene. A scrambled non-targeting control (NTC) siRNA was employed as a negative control. Additionally, siRNAs targeting Firefly luciferase (FLuc) and NanoLuc luciferase (NLuc) were employed as technical controls for measures of cell viability (FLuc) and inhibition of DENV replication (NLuc), respectively. The siRNA library was prepared at 1 μM in 1x siRNA buffer

(Dharmacon Cat # B-002000-UB-100) and this was pre-arrayed in 96-well plates at a volume of 4 µL/well for the screening experiments. Pre-arrayed siRNA-containing plates were stored at -80ºC until required. siRNA screening and screen data analysis was performed at Cell Screen SA (Flinders Centre for Innovation in Cancer, Flinders University, Australia).

2.3.1.2: siRNA screen

Huh-7.5+Fluc (2.2.1.2) cells were seeded into 75cm^2 flasks at 1.56 x 10^6 cells/flask and cultured at 37°C in 5% CO_2. The following day, cells were transfected with *in vitro* transcribed DENV2-NS1-NLuc RNA using DMRIE-C (Thermo Fisher Scientific) (specifically, for each flask, the transfection mixture included: 8 mL Opti-MEM, 47 µL DMRIE-C and 39.6 µg IVT DENV2-NS1-NLuc RNA) and was incubated for 3 hours at 37°C in 5% CO_2. At 3 hours post-transfection, transfection reagent-containing media was replaced with complete DMEM, and cells were returned to culture at 37°C in 5% CO_2. At 48 hours post-transfection, cells were collected (PBS-washed, trysinised, and resuspended), and reverse transfected with the siRNA SMARTPool library in 96-well plates at a final siRNA concentration of 40 nM. Specifically, 96-well plates pre-arrayed with 4 µL/well 1 µM siRNA (2.3.1.1) were incubated with 15.7 µL Opti-MEM and 0.3 µL DharmaFECT 4 (Dharmacon, Horizon Discovery) for 20 minutes at room temperature. Following this incubation, the DENV2-NS1-NLuc transfected cell suspension was added at 1.25 x 10^4 cells/well/80µL. At 3 hours post-siRNA reverse transfection, transfection reagent-containing media was replaced with complete DMEM (100 µL/well) and cells were returned to culture at 37°C in 5% CO_2. For each experiment, each experimental siRNA SMARTpool was transfected in triplicate, and 3 independent experimental replicate screens were performed. At 48 hours post-siRNA treatment, cell culture supernatants were collected and centrifuged at 500 x g for 5 minutes at 15°C. Clarified cell culture supernatants were then mixed 1:1 with 2x Passive Lysis Buffer (Promega). Cell culture monolayers were washed in PBS and lysed in 1x Passive Lysis Buffer (Promega). Cell culture lysates and lysed supernatants were then stored at -20°C. To determine the impact of siRNA treatment on the intracellular and extracellular levels of NS1, thawed lysed samples were assayed using the Nano-Glo Dual-luciferase reporter (NanoDLR) assay (Promega). Cell lysates or lysed supernatants were mixed with OneGlo reagent (Promega) and incubated for 45 minutes at room temperature. FLuc luminescence was then quantified using an EnSight multimode plate reader (PerkinElmer) as a measure of Huh-7.5+Fluc cell viability. After plate reading, NanoDLR Stop&Glo (Promega) was added to each sample, mixed, and then incubated for 45 minutes at room temperature. NLuc luminescence was then quantified using an EnSight multimode plate reader (PerkinElmer) as a measure of intracellular (cell lysate) and extracellular (lysed supernatant) NS1-associated NLuc luminescence. For each siRNA treatment, FLuc-associated luminescence values and NLuc-associated luminescence values were expressed as a percentage of the corresponding average NTC siRNA-associated values. Mean, S.D., and % CV were calculated on these normalised values and the experimental siRNAs were scored to identify criteria-matching hits as detailed in the Appendix V.

2.3.2: Deconvolution siRNA Screen

Detailed experimental methods and analysis are provided in Appendix V. Briefly, the deconvolution siRNA screen library comprised siRNAs (Dharmacon, Horizon Discovery) targeting the 8 criteria-matching hits identified in the customised membrane-trafficking siRNA screen, and the Golgi Brefeldin A Resistant Guanine Nucleotide Exchange Factor 1 (GBF1). Each of the four siRNA duplexes that comprised the experimental siRNA SMARTpool (Dharmacon, Horizon Discovery) was assayed in triplicate, and two independent experiments were performed. A similar experimental approach as described in 2.3.1.2 was employed. Additionally, for this deconvolution screen, cell viability was additionally measured using CellTiter-Blue (Promega), according to the manufacturer's instructions. The experimental procedure and data analysis were performed at Cell Screen SA (Flinders Centre for Innovation in Cancer, Flinders University, Australia).

2.3.3: Quantification of protein knockdown by indirect immunofluorescence microscopy

2.3.3.1: siRNA-treated Huh-7.5 cells

As described in 2.2.10, Huh-7.5 cells were reverse transfected in 12-well plates at 1 x 10^5 cells/well with COPI or NTC siRNA SMARTpools (Dharmacon, Horizon Discovery) at a final concentration of 40 nM. At 24 hours post-transfection, cells were washed with PBS, trypsinised, and re-seeded into 96-well black-walled imaging plates (PerkinElmer PhenoPlate-96) at 1 x 10^4 cells/well and returned to culture in complete DMEM at 37°C in 5% CO_2. At 48 hours post-transfection, cells were extensively washed with PBS prior to acetone:methanol fixation (2.2.19) and processed for immunofluorescent labelling, imaging and analysis as described in 2.3.3.3.

2.3.3.2: CRISPR-Cas9-treated Huh-7.5 cells

As described in 2.3.5, COPI CRISPR-Cas9-treated Huh-7.5 cells were resuscitated and maintained for 5 days in complete DMEM at 37°C in 5% CO_2. After 5 days of maintenance, cells were washed with PBS, trypsinised, and re-seeded into 96-well black-walled imaging plates (PerkinElmer PhenoPlate-96) at 1 x 10^4 cells/well and returned to culture in complete DMEM at 37°C in 5% CO_2 for 24 hours. Cells were then extensively washed with PBS prior to acetone:methanol fixation (2.2.19) and processed for immunofluorescent labelling, imaging and analysis as described in 2.3.3.3.

2.3.3.3: Immunofluorescent labelling, imaging and analysis

Following acetone:methanol fixation of cell culture monolayers as described in 2.3.3.1 and 2.3.3.2, immunofluorescent labelling was performed as described in 2.2.20. Specifically, samples were

labelled with the indicated primary antibodies anti-COPA (1:50), anti-COPB2 (1:100), anti-COPG1 (1:100), or anti-GBF1 (1:100) (Appendix III) diluted in 1% BSA in PBS at 4°C overnight. Samples were then washed three times in PBS before incubation for 2 h in the dark at 4°C with Alexa Fluor 488-conjugated anti-rabbit IgG or Alexa Fluor 488-conjugated anti-mouse IgG antibodies (Thermo Fisher Scientific), diluted to 1:500 and 1:2000, respectively (Appendix III). Samples were then washed three times in PBS and counter stained with DAPI (Sigma-Aldrich) diluted to 1 µg/mL in PBS for 10 minutes in the dark at room temperature before being washed three times in PBS. Samples were then imaged using a BioTek Cytation 5 Multimode Reader. Wells were imaged using a 10x objective across a 7x7 montage. The images were processed and analysed using BioTek Gen5 software (version 3.08.01). Briefly, cellular analysis was performed by defining individual cells using a primary mask based on DAPI fluorescence and an appropriate object selection size (10 µm – 50 µm) and a secondary mask expanding from the DAPI-defined nuclear membrane by 30 µm. The sum intensity of COPI labelling-associated green fluorescence (AFU) within the secondary mask was measured for each cell as a measure of protein abundance.

2.3.4: COPI siRNA treatment of orthoflavivirus infected Huh-7.5 cells

2.3.4.1: COPI siRNA reverse transfection of orthoflavivirus infected Huh-7.5 cells

Orthoflavivirus-infected or mock-infected Huh-7.5 cells (as described in 2.2.12) were reverse transfected with COPI siRNA SMARTpools (Dharmacon, Horizon Discovery) at a final concentration of 40 nM (as described in 2.2.10). Specifically, DENV-, KUNV-, or mock-infected Huh-7.5 cells were added at 1.8 x 10^5 cells/well/800µL to 12-well plates containing 200 µL of siRNA transfection mix and incubated for 3 hours at 37°C in 5% CO_2. At 3 hours post-transfection, transfection reagent-containing media was replaced with 2 mL of complete DMEM and cells were returned to culture at 37°C in 5% CO_2.

2.3.4.2: Intracellular and extracellular NS1 protein recovery

At 24 hours post-infection, cell culture media was removed, and cells were extensively washed in PBS. PBS was thoroughly removed and replaced with complete DMEM at 400 µL/well and cells were returned to culture for a further 24 hours at 37°C in 5% CO_2. At 48 hours post-infection, cell culture monolayers and cell culture supernatants were processed for protein recovery as described in 2.2.17 to measure intracellular and extracellular NS1 abundance, respectively, by quantitative Western blot analysis (as described in 2.1.18 and 2.1.19).

2.3.4.3: Viability

At 24 hours post-infection, cells were washed with PBS, harvested by trypsinisation, and live cells were enumerated using Trypan blue as described in 2.2.4. Cells were then reseeded into 96-well plates at $2x10^4$ cell/mL and cultured for a further 24 hours at 37°C. At 48 hours post-infection, cells were then processed to measure cell viability as described in 2.2.13.

2.3.4.4: Viral RNA, host mRNA, and Infectivity

At 48 hours post-infection, virus-containing cell culture supernatants were recovered to assess infectivity by focus forming assay (as described in 2.2.14), and total cellular RNA was extracted (as described in 2.2.17) to measure intracellular viral RNA abundance and host mRNA expression levels by RT-qPCR (as described in 2.1.17).

2.3.5: Generating COPI CRISPR-Cas9-treated Huh-7.5 Cells

2.3.5.1: Lentivirus Production

HEK 293FT cells (2.2.1.4) were seeded in 6-well plates as described in 2.2.4. The following day, cells were transfected with an equimolar ratio of COPI guide cDNA-containing pLentiCRISPRv2 (2.1.14.1), psPAX2, and pMDG.2 using Lipofectamine 2000 as described in 2.2.8. As a control, cells were transfected with pLenti6-mCherry. At 3 hours post-transfection, cell culture media was replaced with 2 mL/well complete DMEM and cells were returned to culture for 24 hours at 37°C in 5% CO_2. Lentivirus-containing cell culture supernatant was then recovered, stored in a sterile 15 mL centrifuge tube (Corning), sealed with parafilm and stored in a secondary container at 4°C. Cell culture media was replaced with 2 mL complete DMEM and cells were returned to culture for a further 24 hours at 37°C in 5% CO_2. Lentivirus-containing cell culture supernatant was again recovered from transfected cells and mixed with the previously collected supernatant. The 4 mL volume of lentivirus-containing cell culture supernatant was then clarified by centrifugation (1,000 x g for 5 minutes at room temperature) and filtered using a 0.4 µM filter and syringe. 1 mL aliquots of filtered lentivirus-containing supernatant were then stored at -80°C until utilised for lentivirus transduction (2.3.5.2).

2.3.5.2: Lentivirus Transduction

Huh-7.5 cells were seeded in 6-well plates as described in 2.2.4. The following day, lentivirus-containing supernatant (see 2.3.5.1) was diluted 1:3 in complete DMEM supplemented with 10 µg/mL polybrene (Sigma-Aldrich). Huh-7.5 cell culture media was replaced with 2 mL/well of lentivirus transduction media and cells were returned to culture for 72 hours at 37°C in 5% CO_2. At 72 hours post-transduction, cell culture media was replaced with complete DMEM supplemented with 3 µg/mL puromycin and cells were returned to culture at 37°C in 5% CO_2. At ~80% confluency,

cells were washed in PBS, trypsinised, and transferred into a 25cm^2 tissue culture flask containing complete DMEM supplemented with 3 ug/mL puromycin and returned to culture at 37°C in 5% CO_2. At ~80% confluency, cells were then similarly harvested and transferred to a 75cm^2 tissue culture flask containing pre-warmed DMEM supplemented with 3 ug/mL puromycin and cells were maintained under antibiotic selection at 37°C in 5% CO_2. Mock-transduced Huh-7.5 cells were used as a negative control for plasmid-induced puromycin resistance. The lentivirus-transduced cells were considered polyclonal COPI CRISPR-Cas9-treated Huh-7.5 cells when the negative control (mock-transduced) Huh-7.5 cells completely died under antibiotic selection (approximately 2 weeks).

2.3.5.3: Expansion of COPI CRISPR-Cas9-treated Huh-7.5 cells

Following antibiotic-induced negative selection of mock-transduced control cells (~2 weeks), polyclonal COPI CRISPR-Cas9-treated Huh-7.5 cells (as described in 2.3.5.2) were then expanded. Specifically, when cells reached 80% confluency in their 75cm^2 tissue culture flask, spent culture media was aspirated, cells were washed in PBS, and detached by trypsinisation by incubating in 0.5 – 1mL trypsin-EDTA at 37°C in 5% CO_2 for approximately 5 minutes. Cells were then resuspended in approximately 5 mL of complete DMEM and transferred to a 175cm^2 tissue culture flask containing approximately 20 mL of pre-warmed complete DMEM and cultured for 7 days at 37°C in 5% CO_2. After 7 days of expansion, cells were cryopreserved as described in 2.2.6.

2.3.5.4: Preparation of COPI CRISPR-Cas9-treated Polyclonal Huh-7.5 cells for analysis

Cryopreserved polyclonal COPI CRISPR-Cas9-treated Huh-7.5 cells (2.3.5.3) were resuscitated (as described in 2.2.7) and maintained for 5 days at 37°C in 5% CO_2. After 5 days, cells were washed with PBS, harvested by trypsinisation, and live cells were enumerated as detailed in 2.2.4. Cells were then processed for genomic DNA extraction (as described in 2.2.16) to assess the CRISPR-Cas9-based genome editing efficiency by TIDE analysis. Additionally, cells also processed to assess the impact of CRISPR-Cas-9 treatment on target protein abundance by quantitative indirect immunofluorescence microscopy as described in 2.3.3.2 and 2.3.3.3.

2.3.5.4: Preparation of COPI CRISPR-Cas9-treated Polyclonal Huh-7.5 cells for analysis

Cryopreserved polyclonal COPI CRISPR-Cas9-treated Huh-7.5 cells (2.3.5.3) were resuscitated (as described in 2.2.7) and maintained for 5 days at 37°C in 5% CO_2. After 5 days, cells were washed with PBS, harvested by trypsinisation, and live cells were enumerated as detailed in 2.2.4. Cells were then processed for genomic DNA extraction (as described in 2.2.16) to assess the CRISPR-Cas9-based genome editing efficiency by TIDE analysis. Additionally, cells also processed to assess the impact of CRISPR-Cas-9 treatment on target protein abundance by quantitative indirect immunofluorescence microscopy as described in 2.3.3.2 and 2.3.3.3.

2.3.6: Golgicide A (GCA) treatment of orthoflavivirus infected Huh-7.5 cells

Orthoflavivirus-infected or mock-infected Huh-7.5 cells (as described in 2.2.12) were seeded into 12-well plates at 1 x 10^5 cells/well and returned to culture in complete DMEM at 37°C in 5% CO_2. At 24 hours post-infection, cell culture media was discarded, and cells were washed in PBS. PBS was thoroughly removed and replaced with 400 µL/well of complete DMEM supplemented with GCA (1 µM, 2.5 µM, or 5 µM in media containing DMSO at a final concentration of 0.5% [v/v]) or 0.5% DMSO carrier control, and cells were returned to culture at 37°C in 5% CO_2. At 18 hours post-GCA treatment, cell culture monolayers and cell culture supernatants were processed for protein recovery as described in 2.2.17 to measure intracellular and extracellular NS1 abundance, respectively, by quantitative Western blot analysis (as described in 2.1.18 and 2.1.19). In parallel plates, cell culture supernatants were collected to measure infectivity by focus forming assay (2.2.14), and total cellular RNA was extracted (as described in 2.2.17) to measure intracellular viral RNA and host mRNA expression levels by RT-qPCR (2.1.17).

2.3.7: sNS1-APEX2-catalysed proximity biotinylation in Huh-7.5 cells

2.3.7.1: sNS1-APEX2 and secreted APEX2-Only protein synthesis and ultrafiltration

To generate sNS1-APEX2 and APEX2-Only cell culture supernatants, Huh-7.5 cells were transfected with *in vitro* transcribed DENV2-NS1-APEX2 and DENV2-IgK-APEX2-myc RNA, respectively, in 6-well plates (as described in 2.2.11). Additionally, to generate a mock (spent culture media) negative control for downstream experiments, untransfected Huh-7.5 cells were processed in parallel. At 4 hours-post transfection, transfection-reagent containing media was removed a replaced with 1 mL/well complete DMEM and cells were returned to culture at 37°C in 5% CO_2. At 3 days post-transfection, cultures were expanded into 175cm^2 tissue culture flasks. For each treatment, cell culture supernatants were recovered, pooled, and transferred to the 175cm^2 flasks. Cell culture monolayers were gently washed in PBS, trypsinised, and resuspended in complete DMEM. Cell suspensions were then pooled, thoroughly mixed by pipetting, and transferred to the 175cm^2 flasks. Complete DMEM (supplemented with 2.5% FCS) was then added to a final volume of 25 mL and flasks were returned to culture at 37°C in 5% CO_2. At 6 days post-transfection, cell culture media was further topped with DMEM (0% FCS). At 7 days post-transfection, cytopathic effects (CPE) were observed in DENV2-NS1-APEX2 infected cell cultures. Cell culture supernatants were then collected, pooled in 50 mL centrifuge tubes, and briefly stored on ice. Ice-cold cell culture supernatants were clarified by centrifugation (3000 x g for 5 minutes at room temperature) and filtered using a 0.45 µM filter and syringe. Clarified supernatants were then transferred to a 100 kDa MWCO centrifuge filter (Pierce™ Protein Concentrators, PES, 5 – 20 mL) and centrifuged at 3000 x

g until supernatants were concentrated approximately 10-fold. Concentrated cell culture supernatants were stored at -80°C until further use as inoculum in biotinylation experiments (2.3.7.2).

2.3.7.2: sNS1-APEX2-catalysed biotinylation of proximal proteins in Huh-7.5 cells

Huh-7.5 cells were seeded into 175cm^2 flasks at 1 x 10^7 cells/flask in complete DMEM and cultured at 37°C in 5% CO_2. The following day, sNS1-APEX2-containing inoculum (as described in 2.3.7.1) was warmed to 37°C. Cell culture media was removed, and cells were washed once in 5mL of pre-warmed complete DMEM. 2.5 mL of sNS1-APEX2-containing inoculum was added to the cells and incubated for 30 minutes at 37°C in 5% CO_2. At 30 minutes post-inoculation, sNS1-APEX2-containing inoculum was removed, cells were washed once in 5mL complete DMEM, and returned to culture in 10 mL of complete DMEM supplemented with biotin-phenol (500 µM) (Appendix I) for 30 minutes at 37°C in 5% CO_2. At 60 minutes post-inoculation, the APEX2-catalysed biotinylation labelling reaction was performed. Specifically, tissue culture flasks were inverted, 100 µL of 30% (v/v) H_2O_2 was added to the cell culture media (1 mM H_2O_2 final concentration) and thoroughly mixed. Tissue culture flasks were then re-oriented to apply the H_2O_2-containing cell culture media to the cell monolayer for precisely 1 minute. Labelling media was then removed, and cells were immediately washed twice in 15 mL of quencher solution, twice in Dulbecco's PBS, and once more in quencher solution. Cell culture monolayers were immediately lysed on ice using 3 mL of quencher solution-supplemented RIPA buffer (Appendix I) for whole cell lysate recovery as described in 2.2.18. In parallel flasks, Huh-7.5 cells were incoulated with spent cell culture media (2.3.7.1) as a negative control. Additionally, Huh-7.5 cells were incoulated with secreted APEX2-containing media (2.3.7.1) to distinguish sNS1-specific from APEX2-specfic interactions. Each treatment was performed in quadruplicate.

2.3.7.3: Enrichment of biotinylated proteins and identification by mass spectrometry

Clarified whole cell lysate samples were sent to collaborators at Flinders Omics for streptavidin bead enrichment of biotinylated proteins and identification by mass spectrometry analysis. Detailed experimental methods are provided in Appendix VI. Briefly, streptavidin-coated magnetic beads were pretreated with Sulfo-NHS-Acetate (5mM final concentration) and resuspended in PBST-azide. To enrich for biotinylated protein, clarified whole cell lysate samples were incubated with S-NHS-Ac-treated magnetic streptavidin beads for 1 hour at 4°C, thoroughly washed, and affinity purified proteins were resuspended in 2 M urea in 50 mM ABC buffer. Next, affinity purified proteins were reduced (0.2mM TCEP, for 30 minutes at room temperature), alkylated (1 mM MMTS for 15 minutes in the dark at room temperature; stopped by 0.1 mM TCEP), and eluted from the streptavidin-coated beads by Lys-C digestion (25°C in the dark overnight). The following day, eluates were subjected to trypsin digestion (5 hours at 37°C; stopped by 0.5% [v/v] TFA) and cleaned using C18 stage tips. Following clean-up, purified peptides were resuspended in 1% TFA supplemented with 0.1% (w/v) DDm and stored at -80°C until mass spectrometry analysis was performed. Peptides were analysed

using a Dionex Ultimate 3000 UPLC coupled with a Thermo Fusion Lumos tandem mass spectrometer (Thermo Fisher Scientific) using data dependent acquisition as detailed in the Appendix VI. Protein identification was determined by matching peptides to a human protein database using the Proteome Discoverer Program (software 2.4.1.15).

Chapter 3

Identifying and interrogating human host cell factors associated with DENV NS1 secretion

3.1: Introduction

DENV non-structural protein 1 (NS1) is a multifunctional protein that performs a variety of roles critical to the viral lifecycle [230]. Following translation in infected cells, this viral virulence factor is targeted to three destinations [96]. In the intracellular environment, NS1 co-localises with dsRNA at the ER luminal side and interior of the virus-induced replication organelles where it plays multiple roles that are essential for viral RNA replication [93, 94, 192]. Additionally, intracellular NS1 (iNS1) has been shown to be involved in virion morphogenesis and viral particle assembly [97]. NS1 exhibits a cell surface-expressed form that functions in immune evasion and may also be involved in signal transduction [197, 198]. Importantly, despite lacking a recognised secretion signal sequence [176], NS1 is efficiently secreted from infected mammalian cells into the extracellular environment [98]. In DENV-infected patients, high free-circulating levels of secreted NS1 (sNS1) have been correlated with adverse patient outcomes [204]. In the extracellular environment, sNS1 serves a range of functions to favour viral propagation: it can act to enhance cellular susceptibility to infection [277]; contribute to immune evasion through multiple mechanisms [207]; and facilitates inter-species transmission [278]. Moreover, sNS1 contributes to dengue pathogenesis through a range of mechanisms: acting as a PAMP, sNS1 contributes to vasoactive cytokine dysregulation [210]; sNS1 can also bind and invade endothelial cells, which promotes endothelial glycocalyx disruption [211]. Both of these processes can lead to endothelial cell permeability and vascular leakage [96]; a hallmark of severe dengue disease. Given the pathological consequences of sNS1, much research has been conducted on the synthesis, structure, and key functional residues that are critical for its secretion [183, 189]. However, major gaps exist in our understanding of the host cellular factors and machinery that DENV exploits to achieve NS1 secretion from infected mammalian cells. As detailed in the Introduction (Chapter 1), the current hypothesis is that NS1 is secreted from mammalian cells via the canonical secretion pathway [52, 90].

The mammalian canonical secretory pathway comprises a network of membrane-bound cellular compartments that are involved in the synthesis, modification, dissemination and export of proteins, lipids, and carbohydrates [306]. This elaborate system comprises the endoplasmic reticulum (ER), ER exit sites (ERES), the ER-Golgi intermediate compartment (ERGIC), the Golgi complex, the trans-Golgi network (TGN), post-Golgi carriers and the plasma membrane [307] (Figure 3.01). The compartmentalisation of the secretory pathway organelles allows fundamental and specialised processes to be achieved with tightly controlled spatial and temporal dynamics [308]. In general, the translation of secretion-destined proteins typically begins on free ribosomes in the cytosol, and the nascent polypeptide is targeted to the ER lumen by an N-terminally encoded signal sequence [309]. Within the ER, the growing polypeptide chain is engaged by chaperones to ensure proper folding [310]. The majority of secreted proteins are glycosylated, and *N*-linked oligosaccharides can be added to the developing protein in the ER [311]. Following proper folding and the completion of ER-derived post-translational modifications, proteins are exported from the ERES to the ERGIC or the

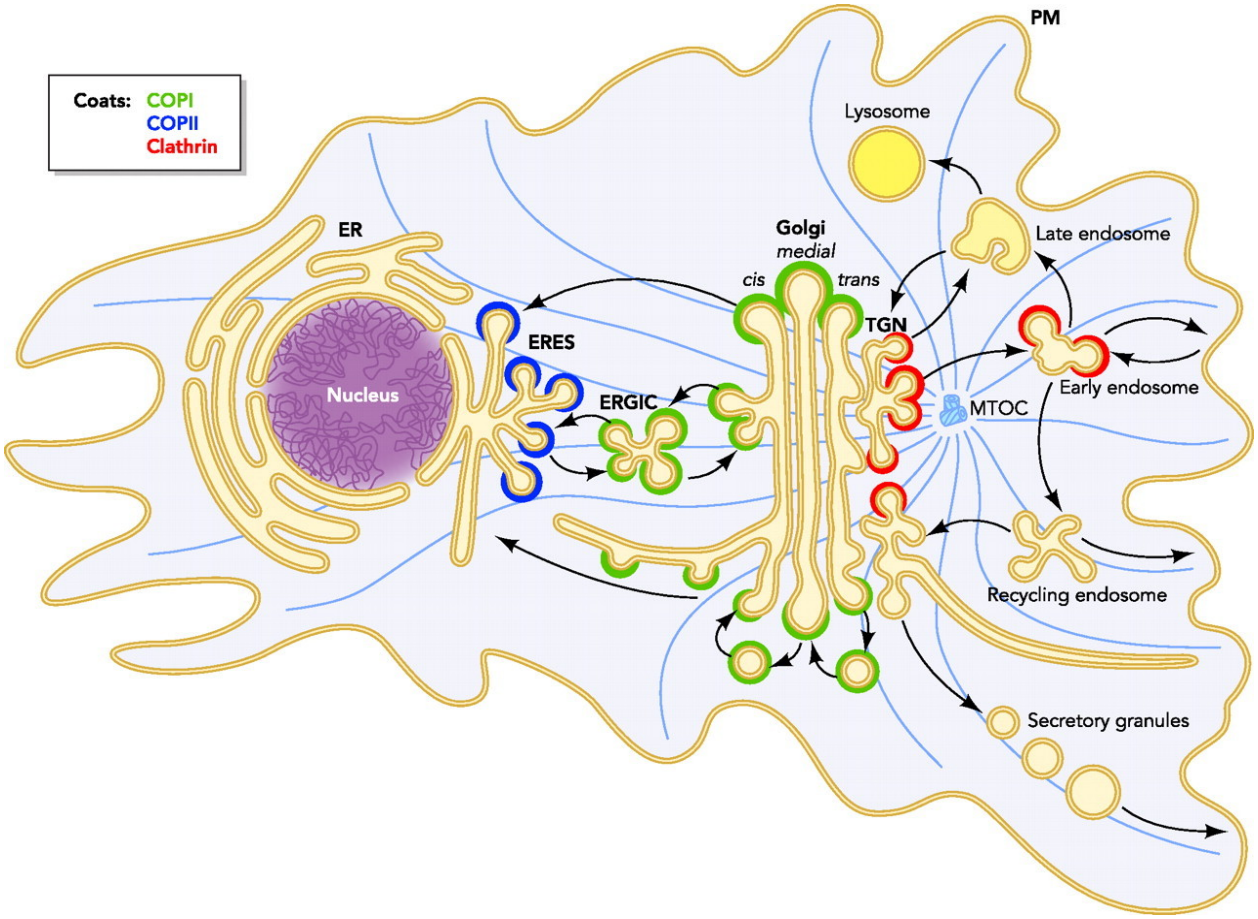

FIGURE 3.01. Schematic overview of the mammalian secretory pathway. Diagram depicts the secretory pathway compartments. In the canonical secretion pathway, secretion-destined proteins are synthesised in the endoplasmic reticulum (ER) and exported from ER exit sites (ERES) to ER Golgi intermediate complex (ERGIC) or the Golgi complex. Following traffic from the cis Golgi, through the medial Golgi and into the trans Golgi, secretion-destined proteins are trafficked to the trans Golgi network (TGN). Proteins are then dispatched to various post-Golgi carriers with secretion-destined protein exiting the cell via the plasma membrane (PM). Adapted from Szul et al., 2011[312].

Golgi [313]. The ERGIC is a major sorting station and secretion-destined proteins generally progress to the Golgi [313]. The Golgi consists of a flattened stack of cisternae and is a central component of the secretory pathway; it plays a major role in the glycosylation and modification of secretory proteins [314]. Following Golgi-derived post-translational modifications, secretion-destined proteins are trafficked to the TGN [315]. The TGN is a highly dynamic tubular reticular network that is involved in the sorting of cargo for delivery to multiple destinations [316]. Here, proteins are packaged into both protein-coated and uncoated membrane carriers for transport to post-Golgi compartments including, but not limited to, the endosome/lysosome system, regulated secretory granules, or to the plasma membrane [316-318]. In addition to this canonical secretory pathway, a multitude of alternative secretory pathways, including Golgi-bypass and autophagy-related pathways, are being unravelled [319-322]. Collectively termed 'unconventional protein secretion', these pathways are largely triggered in response to cellular stresses [306]. Multiple RNA viruses utilise unconventional protein secretion pathways [323-327] and, interestingly, the release of infectious HCV particles by unconventional protein secretion pathways that bypass the Golgi have recently been proposed [328].

The non-contiguous nature of the secretory pathway requires that secretion-destined proteins are trafficked effectively and efficiently between the secretory pathway compartments [308]. This complex process is achieved through membrane-trafficking intermediates, predominantly vesicular carriers, in which proteins are packaged into protein-coated membrane-bound transport vesicles [329, 330]. Three main classes of protein-coated transport vesicles have been well characterised: coatomer protein complex I (COPI)-coated vesicles, coatomer protein complex II (COPII)-coated vesicles, and clathrin-coated vesicles [331]. These three classes of vesicular carriers are defined by the unique composition of their protein coat that surrounds the vesicle membrane [332]. As shown in Figure 3.01 they operate at distinct but overlapping regions within the secretory pathway. COPII coated vesicles facilitate the transport of cargo from the ER to the ERGIC and Golgi [333]. The best characterised roles of COPI coated vesicles is in the bi-directional trafficking of cargo within the early secretory pathway [334]. COPI coated vesicles function in intra- and inter-Golgi trafficking, mediating both anterograde and retrograde transport of secretory cargo and Golgi-resident enzymes including glycosyltransferases [335-337]. They also mediate Golgi-to-ER trafficking of escaped ER resident proteins, thus playing a major role in maintaining the structural and functional integrity of these two organelles [338]. Additionally, several studies have also implicated COPI components as performing roles in endosomal transport and function [339-342]. More recently, COPI has been demonstrated to perform a wealth of processes including in lipid homeostasis [343], autophagy [344], mRNA localisation [345], nuclear envelope disassembly [346], and neurogenesis [347, 348]. Clathrin-coated vesicles mediate the trafficking of cargo between post-Golgi regions, including between the TGN, endosomes, lysosomes, autophagosomes, and the plasma membrane [316, 317, 349]. The biophysical, architectural, functional, and evolutionary limits imposed on a cell may explain why the membrane-manipulating processes involved in vesicle formation and cargo-ferrying are largely performed by a limited repertoire of gene families [350]. Further, despite the use of different protein

coated vesicles at the various stages of the secretory pathway, the structural organisation of the coats and mechanisms of vesicle biogenesis share many similarities [332, 351-353]. For example, COPI is a protein complex that consists of seven core coatomer subunits (COPA, COPB1, COPB2, COPD, COPE, COPG1/COPG2, COPZ1/COPZ2 (paralogous subunits are denoted by a slash; N.B.: COPB1 and COPB2 are not paralogs)) [353-355] . This heptameric complex can be further subdivided into an outer coat (COPA, COPB2, and COPE) and an adapter subcomplex (COPB1, COPD, COPG1/COPG2, and COPZ1/COPZ2) [331] . This cytosolic heptameric coatomer complex is recruited en bloc to a donor membrane to induce the formation of a COPI-coated vesicle [356].

COPI vesicle biogenesis is regulated by the ADP-ribosylation factor (ARF) family of GTPases, which are, in turn, regulated by the Golgi brefeldin A resistant guanine nucleotide exchange factor (GBF1) [357]. ARFs are a family of 6 small GTPases (ARF1-6) that act as molecular switches and control a diverse repertoire of key cellular processes including bidirectional membrane trafficking [358]. Humans have lost ARF2 and, thus, have 5 ARF isoforms [359]. ARFs1-5 primarily localise to the ER, Golgi, and TGN, while ARF6 primarily localises to the plasma membrane [360]. Recombinant ARF1, 4, and 5 have been shown to competitively induce COPI vesicle formation *in vitro*, indicating functional redundancies and differences exist between ARF isoforms [359-361]. Interestingly, the simultaneous siRNA-mediated knockdown of ARF4 and ARF5 has been shown to reduce the secretion of recombinant DENV subviral particles, with data indicating that a pre-Golgi prM-ARF4/5 interaction is critical to the secretion of DENV [362]. A recent study has provided further insight into the specific and redundant roles of ARF1-5 in live cells using systematic CRISPR knockouts, revealing that ARF1 deletion leads to the reduced recruitment of COPI components to the Golgi, and ARF4 deletion leads to the secretion of ER-resident proteins, thus confirming a role of ARF4 in COPI-mediated ER-to-Golgi trafficking [363]. However, given the multitude of effectors that ARFs control beyond COPI, a detailed understanding of the specific and redundant roles or ARF proteins is lacking [358]. Providing further complexity, ARF activation requires the activity of guanine nucleotide exchange factors (GEFs). There are five families of ARF GEFs: GBF1/BIG, F-box, BRAGs, EFA6, cytohesins [364]. The GBF1/BIG family of ARF GEFs is highly conserved in all eukaryotes [365]. These three family members, GBF1, BIG1, and BIG2 are involved in vesicular traffic and their distinct but overlapping subcellular compartment localisation (reviewed in [366]) [358]. COPI vesicle formation requires the GEF activity of GBF1. GBF1 contains the conserved catalytic domain, Sec7d, which is responsible for catalysing GDP-to-GTP conversion of ARFs [367]. GBF1 contains a further 5 non-catalytic domains whose functions largely remain uncategorised but appear to be important for localisation and the regulation of activity [368]. Beyond its well-defined role in regulating COPI vesicle formation and secretory pathway traffic, GBF1 also participates in a multitude of other cellular processes including lipid metabolism, mitochondrial positioning, cell motility, and cytokinesis through alternate effector recruitment [357, 369]. Given its diverse roles, GBF1 is hijacked by a variety of mammalian viruses to perform a multitude of functions (reviewed in [370]). For COPI vesicle formation to occur, the donor membrane-localised GBF1 recruits and activates ARFs by catalysing

the GDP-to-GTP exchange [369, 371, 372]. The activated GTP-bound ARF becomes membrane-associated through the insertion of a myristoylated N-terminal amphipathic helix into the donor membrane [373]. GBF1 also interacts directly with COPG1, thus spatially confining coatomer complexes in close proximity to activated ARFs [374]. Activated ARFs, in turn, anchor coatomer complexes to the membrane through ARF-adapter-coatomer interactions [375]. The building blocks of the COPI coat are three copies of the heptameric coatomer complex and six copies of ARF, which together form a three-fold triad structure linked by flexibly attached domains [376]. Polymerisation of the COPI coat recruits cargo and additional cargo-recognising machinery to the nascent COPI vesicle assembly site [377]. In addition to capturing both membrane-bound and luminal cargo in bulk due to close spatial proximity, selective cargo capture is driven by the recognition of sorting signals in the cytoplasmic domains of cargo proteins [378]. Several classes of sorting signals have been identified: the dilysine motif (KKxx and KxKxx) and the arginine-based motif (ϕRxR) (where ϕ represents a hydrophobic amino acid) are utilised as Golgi-to-ER retrieval signals [379]. Additional proteins can bind coatomer subunits and act as adapters to concentrate cargo [380]. However, the precise nature of how cargo recognition and cargo concentration occurs at COPI assembly sites is still a matter of debate [378]. The continued recruitment of coatomer and ARF-GTP induces positive membrane curvature and membrane destabilisation which results in the recruitment of GTPase activating proteins (ARFGAPs), which provide GTPase activity to ARFs [357], and vesicle scission [381]. It should, however, be noted that additional lipidic and proteinaceous factors (e.g.: acyl-CoA, BARS, LPAATγ) have been implicated in influencing COPI vesicle scission [376]. After scission, COPI coated vesicles traffic via diffusion or motor-mediated transport (e.g.: dynein, kinesis, and myosin) towards the acceptor membrane [382]. Additionally, the COPI coat is shed from the vesicle and the disassembly of the COPI coat requires GTP hydrolysis of ARF by ARFGAPs [381]. Recognition of the acceptor membrane occurs via vesicle and acceptor membrane tethering; target organelles contain large protein tethers (t-SNAREs) that bind cognate partners (v-SNAREs) on transport vesicles [351]. The timing of coat disassembly and acceptor membrane tethering are ill-defined but both processes are necessary for fusion [383]. Fusion of the vesicle with the acceptor membrane results in cargo deposition.

Recently, our group used genome-wide transposon mutagenesis coupled with next-generation DNA sequencing to reveal regions within the DENV genome that are genetically flexible and tolerant to insertions [94]. Our results identified discreet regions within NS1 that exhibit remarkable plasticity, and this information allowed the directed creation of infectious reporter- and epitope-tagged viruses, including a variant encoding the small and sensitive NanoLuc luciferase (NLuc) embedded within NS1 (denoted DENV2-NS1-NLuc) (Figure 3.02 A). This reporter virus has been fully characterised and this infectious NLuc-tagged NS1 variant displays cellular localisation, glycosylation, and secretion profiles similar to the untagged wildtype NS1 protein (Figure 3.02 B-E). Moreover, the DENV2-NS1-NLuc reporter virus allows robust and reproducible quantification of intracellular and secreted NS1 in infected cell cultures by virtue of the NS1-associated NLuc activity. The simple and

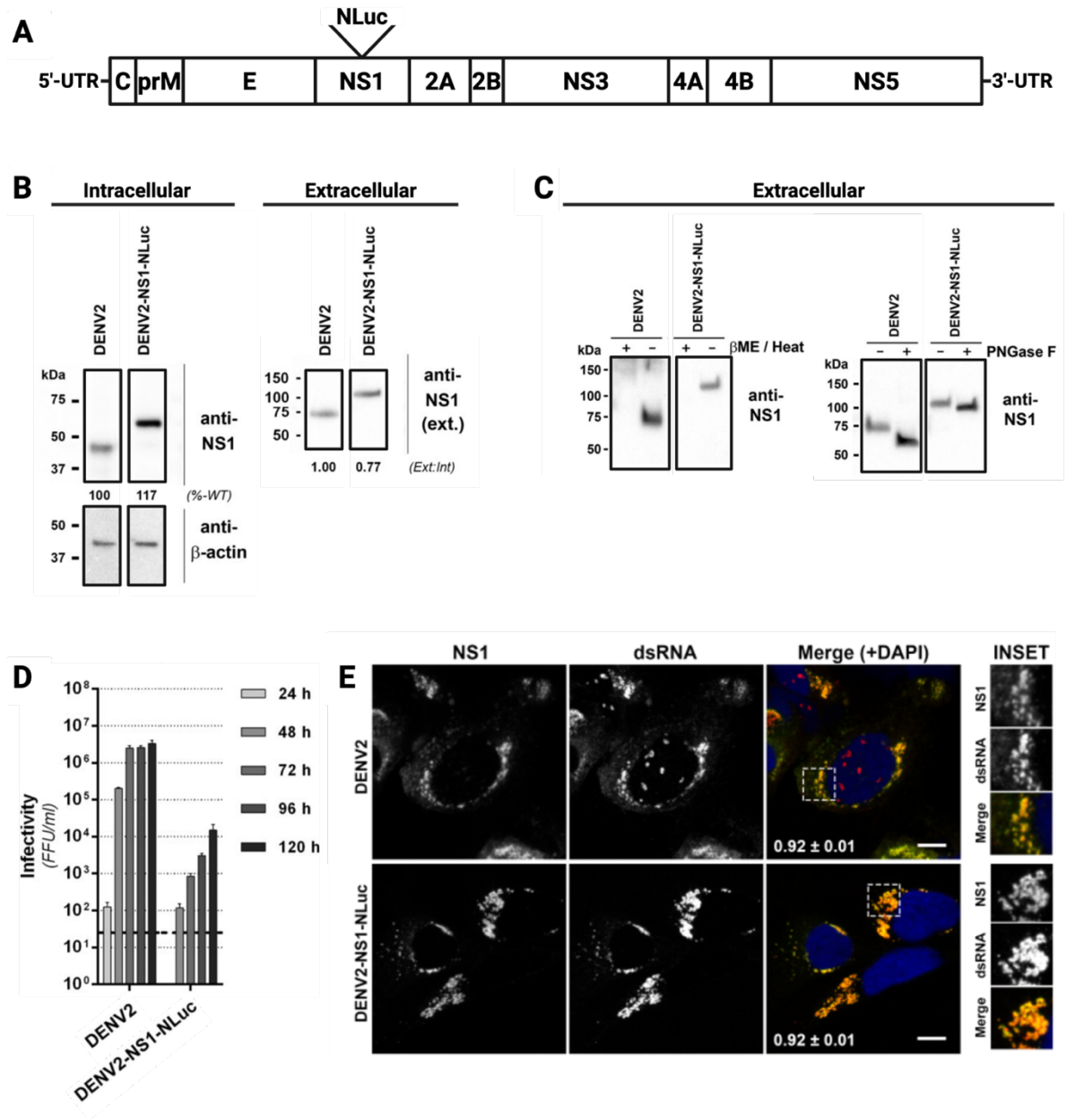

FIGURE 3.02. DENV2-NS1-NLuc reporter virus has been fully characterised. (A) DENV2 (16681) was modified by the insertion of the NLuc reporter insertion (516 nt) within NS1 immediately downstream of Lys-174. To assess the impact of the NLuc insertion on various aspects of DENV2 and NS1 biology, Huh-7.5 cells were electroporated with *in vitro* transcribed DENV2 or DENV—NS1-NLuc RNA and cultured for 4 days. (B) Western blot analysis confirms intracellular and extracellular NS1-NLuc fusion protein is readily detected and contains the expected increase in molecular weight (~19 kDa). (C) NS1-NLuc is recognised by the anti-NS1 MAb 4G4 under nonreducing and nondenaturing conditions, indicating that the fusion protein retains the native epitope conformation that is recognised by 4G4 (left, BME / Heat), and NS1 glycosylation is unaffected by the NLuc reporter insertion (right, PNGase F). (D) DENV2-NS1-NLuc is infectious but appreciably attenuated. (E) NS1-NLuc localisation with respect to dsRNA is unaltered by the NLuc reporter insertion. Adapted from Eyre et al. 2017. For experimental details see referenced article.

reliable quantification of NS1-associated NLuc activity makes this reporter virus amenable to high-throughput functional genomic screens, thus providing a platform to examine the plethora of human host cellular secretory pathway factors that may be required for DENV NS1 secretion. Given the importance of secreted NS1 and the lack of understanding regarding the human host cellular factors involved in NS1 secretion, the focus of this chapter was to identify and interrogate the human host molecular machinery that is exploited by DENV to achieve NS1 secretion.

3.2: Results

3.2.1: High-throughput customised membrane-trafficking siRNA screen

To identify human host membrane-trafficking proteins that may be involved in NS1 secretion, we employed a commercially available membrane-trafficking siRNA library comprising 140 human genes (Dharmacon Human ON-TARGETplus SMARTpool siRNA Library – Membrane Trafficking). This library was customised and curated to include siRNAs targeting a further 37 human genes that have recently been identified as important DENV host-dependency factors that may be manipulated by NS1 [384, 385]**.** The ~180 human host genes targeted in this siRNA screen are shown in Appendix V. To ensure on-target efficacy and to improve the likelihood of effective target gene silencing, each host gene was targeted by a pool of four siRNA duplexes that recognise distinct sequences within each target gene transcript.

To interrogate DENV2 NS1 secretion, we employed our previously designed and characterised infectious DENV2-NS1-NLuc reporter virus that allows the ultra-sensitive detection of intracellular and extracellular NS1- associated NLuc activity in infected cell culture lysates and supernatants, respectively, in a high-throughput manner. Our laboratory routinely utilises the human Huh-7.5 hepatocellular carcinoma cell line to study orthoflavivirus biology. Human liver cells are a major target of DENV [163, 386], and these cells support high levels of DENV2 replication and NS1 secretion [94]. Moreover, these cells are not difficult to transfect, making them well suited to siRNA screening. Additionally, we have a Huh-7.5 cell line that stably expresses Firefly luciferase (Huh-7.5+FLuc) allowing the simple and sensitive detection of FLuc activity as an indirect measure of cell number/viability [387]. This cell line was chosen as it is well-suited to the experimental design as dual-luciferase reporter assay systems would enable the simultaneous phenotypic screening of NS1-associated NLuc luminescence *and* cell number/viability-associated FLuc luminescence in a biologically-relevant cell type.

Figure 3.03 provides a schematic overview of the siRNA screen strategy. Given the importance of membrane-trafficking pathways in replication cycles of orthoflaviviruses [172], we opted to establish DENV2-NS1-NLuc infection in a population of Huh-7.5+FLuc cells prior to introducing the

customised membrane-trafficking siRNA library. The siRNA screening and screen data analysis was performed by collaborators at Cell Screen SA (Flinders Centre for Innovation in Cancer) at Flinders University. Briefly, 1.56 x 10^6 Huh-7.5+Fluc cells were seeded into a T75 flask. The following day, cells were transfected with *in vitro* transcribed infectious DENV2-NS1-NLuc RNA. After 3 hours of incubation at 37°C 5% CO_2, transfection reagent was replaced with complete media and cells were cultured for 2 days to establish infection. Cells were then trypsinised and reverse transfected with the siRNA library pools. A scrambled non-targeting siRNA SMARTpool control (NTC) served as a negative control. siRNAs targeting Firefly luciferase (FLuc) and NanoLuc luciferase (NLuc) served as controls for cell viability and inhibition of DENV2 replication, respectively. Each siRNA pool was reverse transfected in triplicate and three independent experimental replicates were performed. At 3 hours post-siRNA reverse transfection, transfection reagent was replaced with media and cells were cultured for a further 2 days prior to harvest. At 2 days post-siRNA treatment, cell culture lysates and supernatants were recovered to quantitatively analyse intracellular and extracellular NS1-assicated NLuc activity, respectively. Cell lysates or lysed supernatants were also processed to measure cell viability-associated FLuc luminescence and NS1-associated NLuc luminescence using a commercially available dual luciferase assay system.

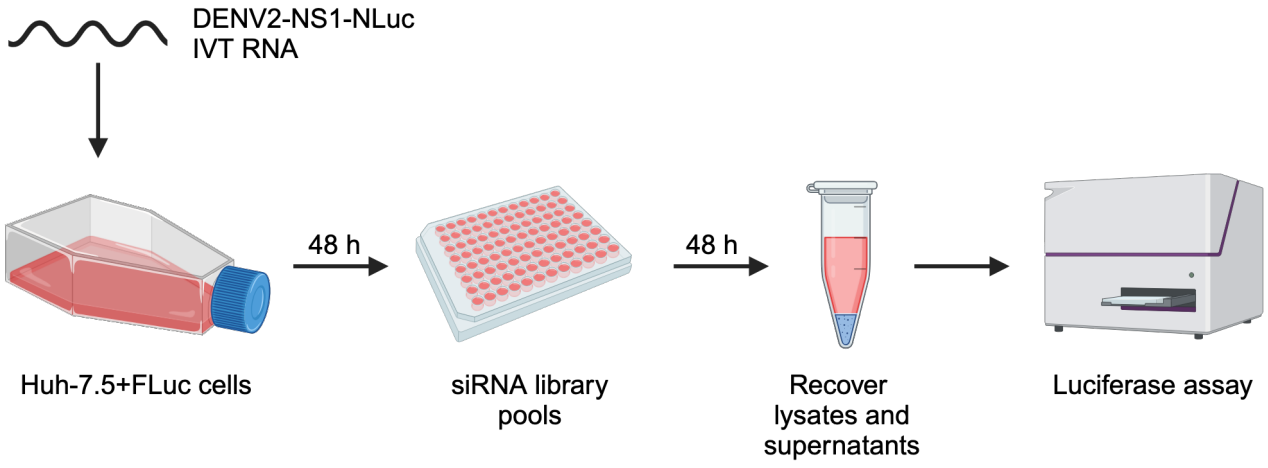

FIGURE 3.03. Schematic overview of the customised membrane-trafficking siRNA screen strategy. Huh-7.5+FLuc cells were transfected with infectious *in vitro* transcribed DENV2-NS1-NLuc RNA. At 48 hours post-transfection, cells were trypsinised and reverse transfected with the siRNA library pools. At 48 hours post-siRNA treatment, cell culture lysates and supernatants were harvested to measure intracellular and extracellular NS1-associated NLuc activity, respectively.

The data analysis and hit selection criteria are detailed in the Materials and Methods section 2.3.1 and Appendix V. Briefly, for each well, the NS1-associated NLuc relative levels (RL) in lysates (NLuc_Lys) and supernatants (NLuc_Sup) were calculated as ratios of their FLuc lysate (FLuc_Lys) values to normalise for variations of the cell densities. Additionally, to assess the effect of siRNA treatment on NS1-associated NLuc secretion efficiency, supernatant-to-lysate NLuc secretion ratios (SR) were determined. Next, NLuc RL and SR values were normalised as percentages of mean values of the NTC siRNA control. To assist in hit identification, 4 effects were defined as possible for any experimental siRNA: (i) cell toxicity, indirectly measured as a decrease of FLuc_Lys values (FLuc knockdown); (ii) inhibition of NLuc activity in lysates, measured as a decrease of NLuc_Lys values (NLuc_Lys knockdown); (iii) inhibition of NLuc activity in supernatants, measured as a decrease of NLuc_Sup values (NLuc_Sup knockdown) and; (iv) inhibition of NLuc secretion, measured as a decrease of Normal_SR-NLuc values (Secretion ratio knockdown). For determining the knockdown effects, thresholds were set for each possible effect and Boolean values (True or False) were assigned to visualise whether the values fell over the respective threshold . Additionally, score values were assigned to the four defined effects with the scores selected such that the sum of each possible effect would provide a unique score value for all possible combinations. Hits were defined as having a score of ≥12; potential hits were defined as having a score value of 5 – 11 (Appendix V).

The experimental siRNA pools that matched our hit selection criteria and their respective impacts on the four defined effects are shown in Figure 3.04 (a final merged data table compiled from the analyses of the three independent experimental replicates is shown in Appendix V). For the controls, siRNAs targeting FLuc and NLuc markedly reduced their respective luciferase values, thus confirming the efficacy of the siRNA transfection process. Moreover, the degree to which luminescence was reduced confirms that the FLuc- and NLuc-associated luminescence is a sensitive and appropriate means to measure reductions in viability and NS1 abundance, respectively. Only 1 experimental siRNA pool, RHOA, reproducibly reduced FLuc luminescence values to 1 standard deviation below the mean of the NTC - the threshold cut-off as defined in Appendix V. This may suggest that the RHOA siRNA pool reduces cell viability under the experimental conditions imposed. Alternatively, one or more of the individual siRNA duplexes comprising the pool may non-specifically target FLuc mRNA thus reducing FLuc protein abundance. Nonetheless, this precluded further analysis of a possible role of RHOA in NS1 secretion. The screen identified 3 siRNA pools that matched our ‘hit’ selection criteria (a score value ≥12), whose depletion reduced NS1-NLuc secretion efficiency to 2 standard deviations below the mean of the NTC. Interestingly, COPA, COPB2, and COPG1 were identified as the top-ranking hits. As detailed above, these proteins are three of the seven subunits of the coatomer protein complex I (COPI) that assembles to coat one of the three main types of cellular transport vesicles [334]. COPI has recently been identified as being involved in various aspects of DENV biology, and a recent study by Iglesias *et al* demonstrated that DENV exploits

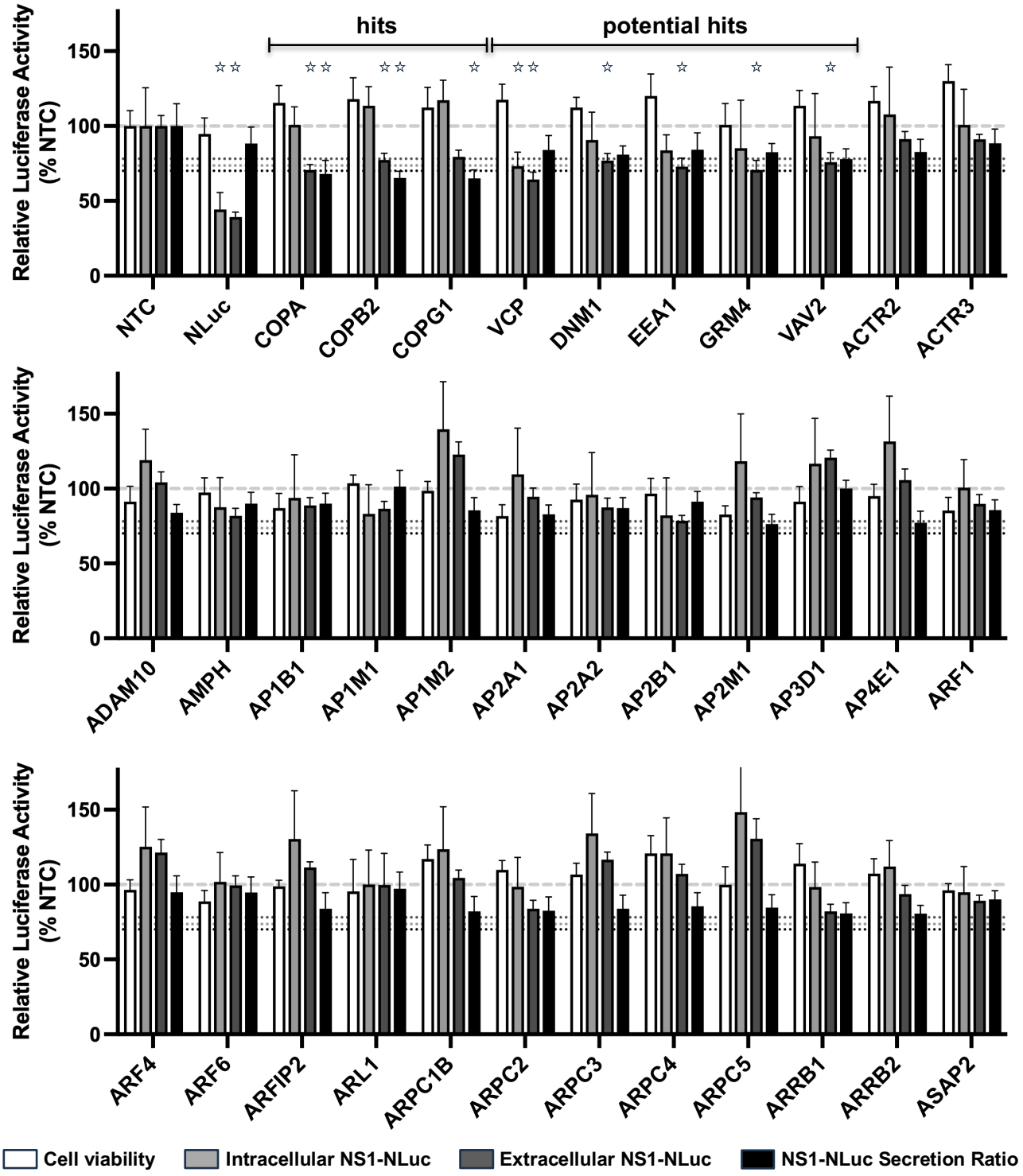

FIGURE 3.04. A customised membrane-trafficking siRNA screen implicates COPI components as important determinants of NS1 secretion. Effect of gene knockdown on on cell viability (FLuc_Lys; white bars), intracellular NS1-NLuc (NLuc_Lys; light grey bars), extracellular NS1-NLuc (NLuc_Sup; dark grey bars), and NS1-NLuc Secretion Ratio (NLuc_Sup / NLuc_Lys; black bars) as a % of the non-targeting control (NTC) siRNA pool (dashed line). Hit selection thresholds are shown as dotted lines (FLuc_Lys = 78%; NLuc_Lys = 74%; NLuc_Sup = 78%; Secretion Ratio = 70%); for clarity, stars above the bars indicate that the respective effect matched the hit selection criteria. Data are means + S.D. from nine measurements from three independent experiments.

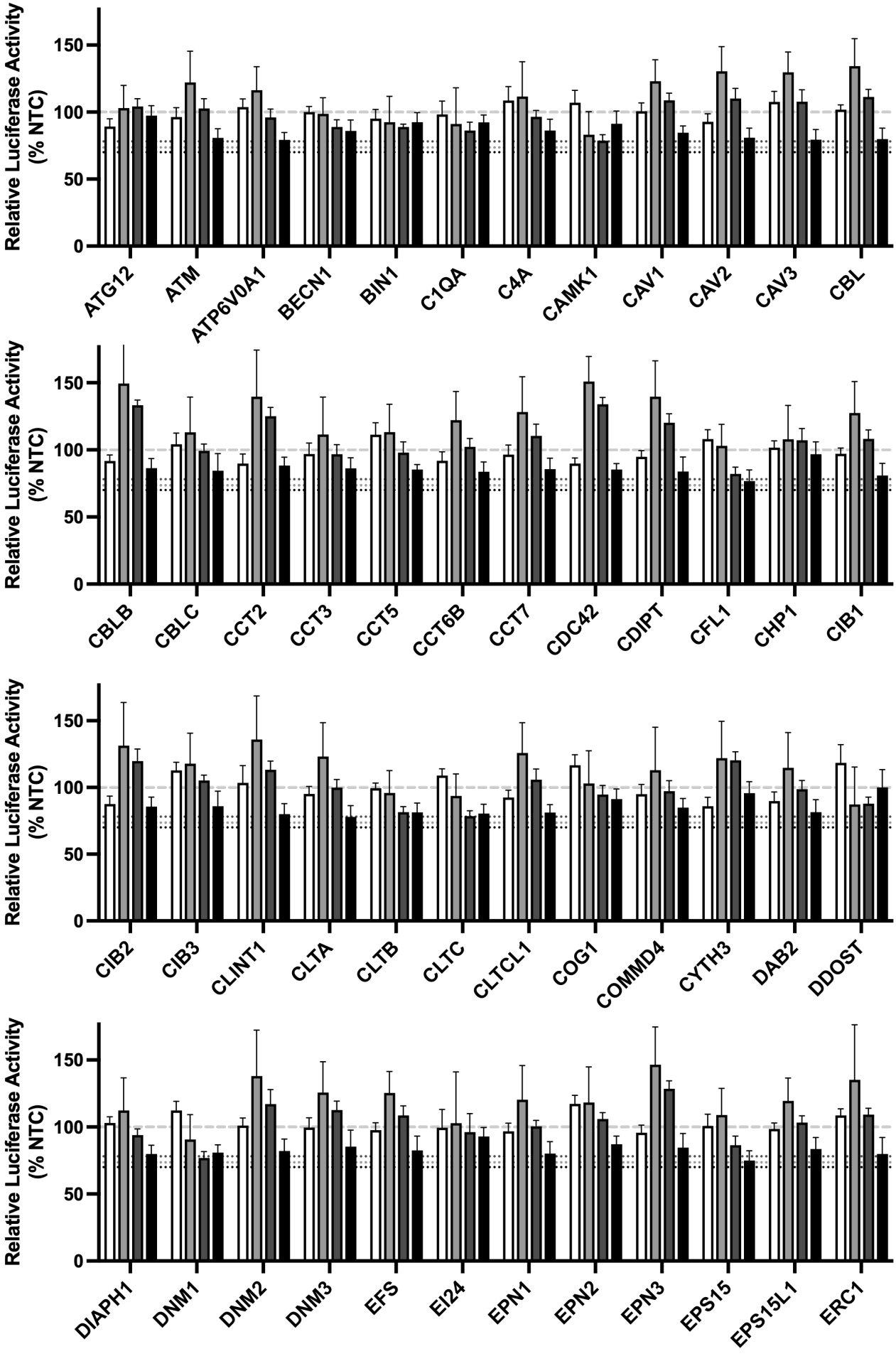
Relative Luciferase Activity (% NTC)
150
100
50
0
ATG12
ATM
ATP6V0A1
BECN1
BIN1
C1QA
C4A
CAMK1
CAV1
CAV2
CAV3
CBL
Relative Luciferase Activity (% NTC)
150
100
50
0
CBLB
CBLC
CCT2
CCT3
CCT5
CCT6B
CCT7
CDC42
CDIPT
CFL1
CHP1
CIB1
Relative Luciferase Activity (% NTC)
150
100
50
0
CIB2
CIB3
CLINT1
CLTA
CLTB
CLTC
CLTCL1
COG1
COMMD4
CYTH3
DAB2
DDOST
Relative Luciferase Activity (% NTC)
150
100
50
0
DIAPH1
DNM1
DNM2
DNM3
EFS
EI24
EPN1
EPN2
EPN3
EPS15
EPS15L1
ERC1

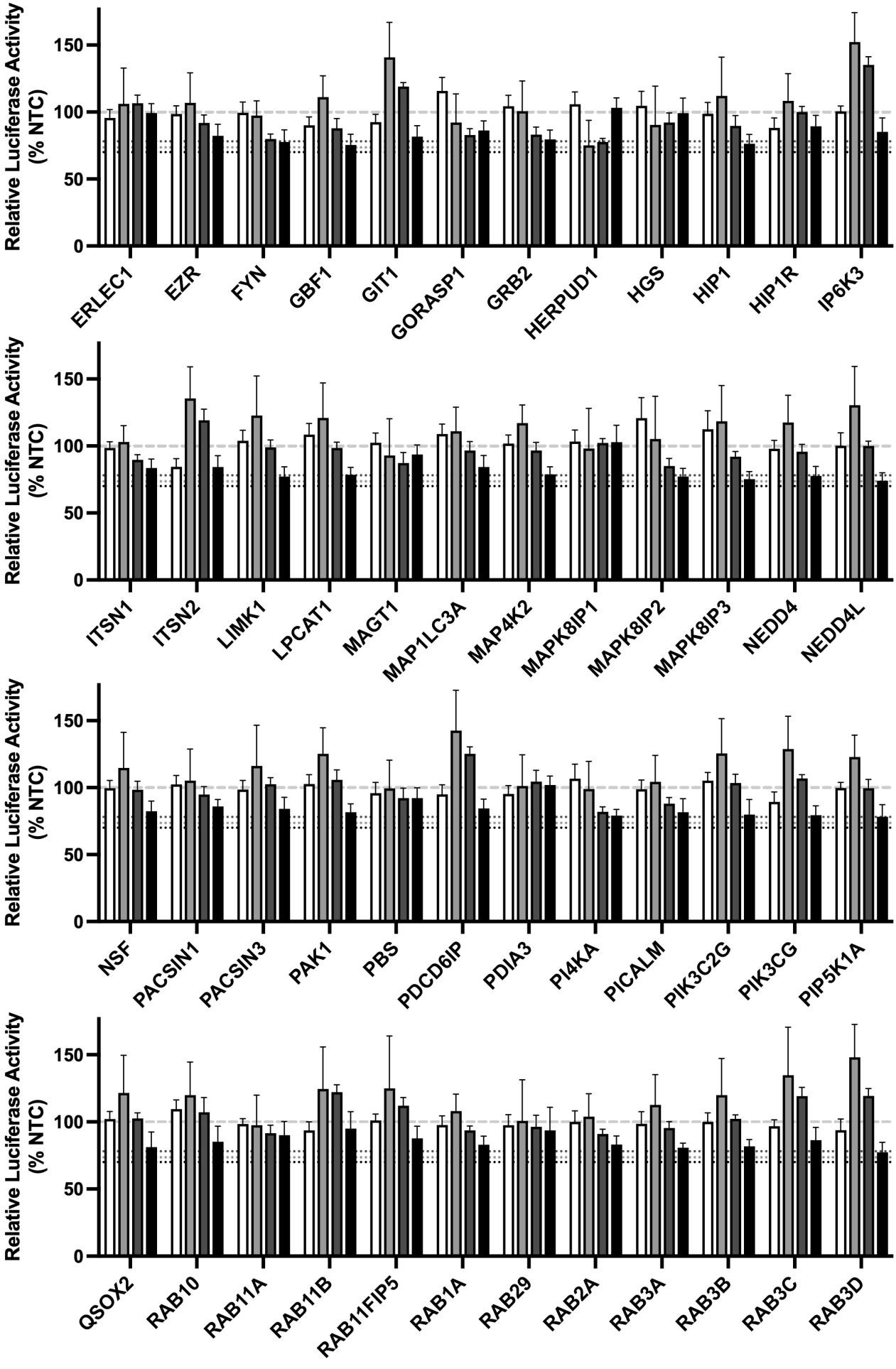
Relative Luciferase Activity (% NTC)
0
50
100
150
ERLEC1
EZR
FYN
GBF1
GIT1
GORASP1
GRB2
HERPUD1
HGS
HIP1
HIP1R
IP6K3
ITSN1
ITSN2
LIMK1
LPCAT1
MAGT1
MAP1LC3A
MAP4K2
MAPK8IP1
MAPK8IP2
MAPK8IP3
NEDD4
NEDD4L
NSF
PACSIN1
PACSIN3
PAK1
PBS
PDCD6IP
PDIA3
PI4KA
PICALM
PIK3C2G
PIK3CG
PIP5K1A
QSOX2
RAB10
RAB11A
RAB11B
RAB11FIP5
RAB1A
RAB29
RAB2A
RAB3A
RAB3B
RAB3C
RAB3D

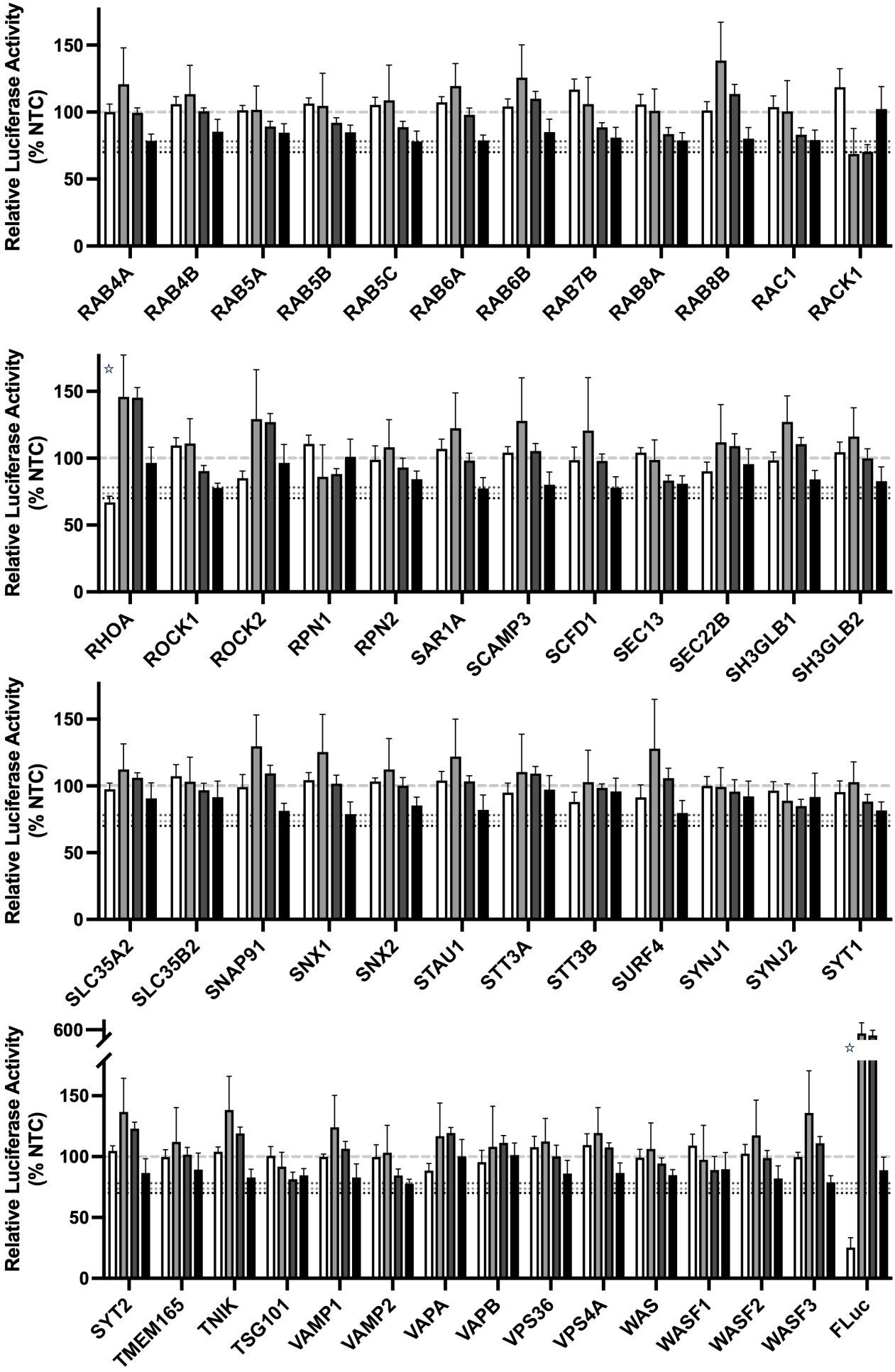
Relative Luciferase Activity (% NTC)
0
50
100
150
RAB4A
RAB4B
RAB5A
RAB5B
RAB5C
RAB6A
RAB6B
RAB7B
RAB8A
RAB8B
RAC1
RACK1
RHOA
ROCK1
ROCK2
RPN1
RPN2
SAR1A
SCAMP3
SCFD1
SEC13
SEC22B
SH3GLB1
SH3GLB2
SLC35A2
SLC35B2
SNAP91
SNX1
SNX2
STAU1
STT3A
STT3B
SURF4
SYNJ1
SYNJ2
SYT1
600
SYT2
TMEM165
TNIK
TSG101
VAMP1
VAMP2
VAPA
VAPB
VPS36
VPS4A
WAS
WASF1
WASF2
WASF3
FLuc

COPI to shuttle the viral capsid protein between the endoplasmic reticulum (ER) and lipid droplets [57, 388]. Additionally, our screen identified a further 5 siRNA pools that matched out 'potential hit' selection criteria (score value 5 – 11), whose depletion reduced the extracellular accumulation of NS1-NLuc to 1 standard deviation below the mean of the NTC. Supporting the validity of our siRNA screen, several of these host gene products have previously been identified as being involved in orthoflavivirus and importantly, NS1 biology. Valosin containing protein (VCP) is an ATPase associated with diverse cellular activities (AAA-ATPase) that plays roles in cellular functions including ER-associated degradation, endosomal trafficking, autophagy, and activation of the NF-κB pathway [389]. VCP has been identified as a critical host factor for multiple orthoflaviviruses [390-393], and it co-localises with NS1 in Japanese encephalitis virus-infected cells [394]. For DENV, the ATPase activity of VCP has been demonstrated to be essential for ER remodelling during VP biogenesis to allow efficient viral genome replication [395]. Intriguingly, two of the 'potential hits', dynamin-1 (DNM1) and early endosome antigen 1 (EEA1), have previously been identified as being involved in the internalisation of secreted DENV NS1 [219]. DNM1 is a member of the dynamin subfamily of GTP-binding proteins and is involved in vesicular trafficking processes including clathrin-dependent and clathrin-independent endocytosis [396]. EEA1 is a marker of early endosomes, it binds phosphatidylinositol 3-phosphate-containing vesicles and participates in endosomal trafficking [397]. The identification here that DNM1 and EEA1 siRNA treatment reduces the extracellular accumulation of NS1-NLuc suggests that DNM1 and EEA1 may be involved in the bi-directional trafficking of both secretion-destined NS1 and internalised sNS1. Glutamate metabotropic Receptor 4 (GRM4), a G-protein-coupled receptor for glutamate that is linked to the inhibition of the cyclic AMP cascade [398], was included as a customised addition in the siRNA library. GRM4 was identified as a potential NS1 interacting protein in an affinity purification-mass spectrometry study by Shah *et al* in 2018, however its biological significance was not explored [384]. GRM4 gene expression has, however, been shown to be downregulated in mice following orthoflavivirus infection [399]. Vav guanine nucleotide exchange factor 2 (VAV2) is a guanine nucleotide exchange factor that activates members of the Rho family of Ras-related GTPases (e.g.: Cdc42, Rac1, and RhoA) which, in turn, act to regulate signalling pathways for various biological processes including cell growth, survival, and differentiation [400, 401]. The implication here that VAV2 may be involved in NS1 secretion may relate to the recently reported involvement of VAV2 in DENV-induced inflammatory responses [402].

3.2.2: Deconvolution siRNA screen on identified hits

To validate the siRNA screen hits, a deconvolution screen was performed. Here, each of the four constituent siRNAs that comprised the siRNA pools were screened individually. Additionally, while GBF1 was not identified as a hit (Figure 3.04), siRNAs targeting GBF1 were also included in this

deconvolution screen given its role as a master regulator of COPI vesicle formation [403]. The deconvolution siRNA screen followed the same experimental approach as shown in Figure 3.03, however, each individual siRNA duplex was reverse transfected in triplicate and two independent experimental replicates were performed. The data analysis and normalisation were largely similar to the original siRNA screen (see Methods section and Appendix V). However, more stringent thresholds for hit identification were applied. Here, the thresholds for each of the four defined effects were set to 2 standard deviations below the mean of the NTC.

While two independent experimental replicates were performed, the second replica displayed severely low NLuc luciferase values with NLuc readings approximately 10-fold lower than those of the first replica (data not shown). This could indicate poor DENV2-NS1-NLuc transfection efficiency or decreased enzyme-substrate activity in the luciferase assay. Accordingly, the results from the second replica were deemed inadequate and excluded from further analysis and only the results from the first replicate were utilised. For each gene targeted, Figure 3.05 shows the impact of the four individual siRNAs on the luciferase values for each of the four defined effects. As expected, the control siRNAs targeting FLuc and NLuc reduced their respective luciferase values. Two individual siRNAs, targeting COPG1 and GBF1, reduced intracellular FLuc luciferase values by 2 standard deviations relative to the NTC (the threshold cut-off as defined in this deconvolution screen), suggesting that the treatment of cells with these siRNAs may negatively impact cell viability or FLuc protein expression. This deconvolution screen identified 11 individual siRNAs that matched our 'hit' selection criteria (a score value ≥12), whose depletion reduced NS1-NLuc secretion efficiency to 2 standard deviations below the mean of the NTC. Interestingly, all four individual siRNAs targeting COPA were identified as hits. Two individual siRNAs were identified as hits for the gene targets COPB2, COPG1, and DNM1. One siRNA targeting EEA1 was identified as a hit. Individual siRNAs targeting VCP, GRM4, VAV2, and GBF1 did not meet the deconvolution screen hit criteria. This may be a result of the increase in stringency for hit identification in the deconvolution screen (2x SD cf. 1x SD). Alternatively, the high-complexity siRNA pool used in the original screen has the advantage of both potency and gene product specificity, which may explain their poorer performance or weaker phenotypic results in the deconvolution screen. Of the COPI components, including GBF1, all but one of the individual siRNAs reduced NS1-NLuc secretion efficiency as inferred from the secretion ratio, lending further support that COPI machinery is involved in DENV NS1 secretion.

Given that multiple individual siRNAs targeting COPA, COPB2, COPG1, and DNM1 induced a strong NS1-NLuc secretion efficiency-reducing phenotype that matched our hit selection criteria, these gene products are considered validated with a high degree of confidence. Moreover, given that several genes that encode components of the multi-subunit COPI complex and associated pathways were identified as important determinants of NS1-NLuc secretion, the interrogation of COPI complex components in orthoflavivirus NS1 secretion was prioritised and forms the basis for the remainder of this chapter of the thesis.

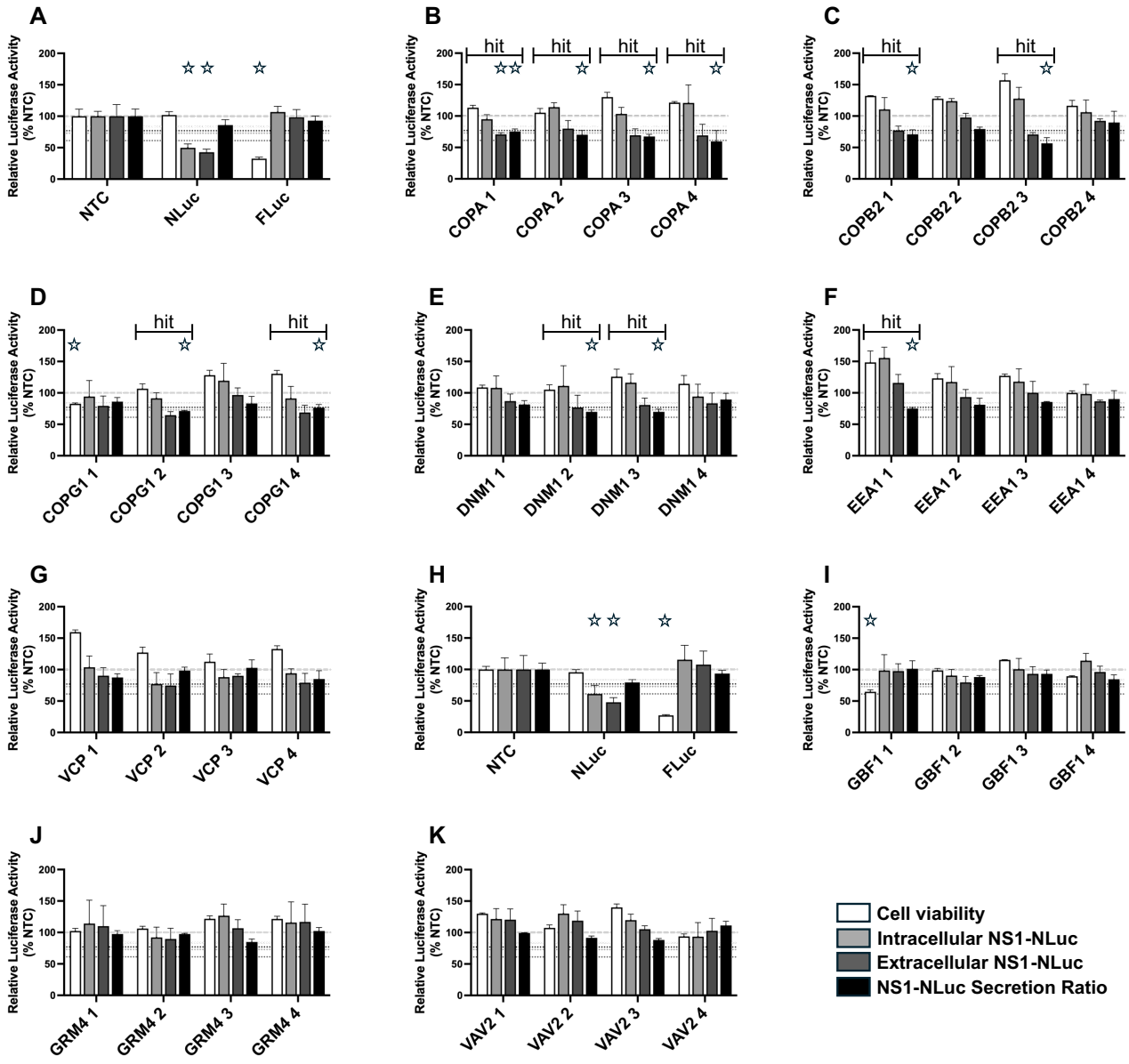

FIGURE 3.05. Deconvolution siRNA screen confirms COPI components as important determinants of NS1-NLuc secretion. Target deconvolution siRNA screen using the 4 individual siRNAs targeting the hits identified in the membrane-trafficking siRNA screen. Effect of knockdown on cell viability (FLuc_Lys; white bars), intracellular NS1-NLuc (NLuc_Lys; light grey bars), extracellular NS1-NLuc (NLuc_Sup; dark grey bars), and NS1-NLuc Secretion Ratio (NLuc_Sup / NLuc_Lys; black bars) as a % of the non-targeting control (NTC) siRNA pool (dashed line). Plate 1 controls (A) were used for normalisation of COPA (B), COPB2 (C), COPG1 (D), DNM1 (E), EEA1 (F), and VCP (G); Plate 2 controls (H) were used for normalisation of GBF1 (I), GRM4 (J), and VAV2 (K). Hit selection thresholds are shown as dotted lines (FLuc_Lys = 84%; NLuc_Lys = 73%; NLuc_Sup = 61%; Secretion Ratio = 77%); for clarity, stars above the bars indicate that the respective effect matched the hit selection criteria. Data are means + S.D. from nine measurements from one experiment.

3.2.3: Validating the involvement of COPI components in wildtype orthoflavivirus NS1 secretion

Our customised membrane-trafficking and deconvolution siRNA screens identified COPA, COPB2, and COPG1 as the top three hits whose depletion reduced the secretion efficiency of the NS1-NLuc fusion protein from DENV2-NS1-NLuc reporter virus-infected Huh-7.5+Fluc cells. Despite the weaker phenotypic results observed in the deconvolution screen, when targeted by a pool of four siRNAs in the original screen, GBF1 silencing increased intracellular NS1-NLuc levels and decreased extracellular NS1-NLuc levels, suggesting that GBF1 inhibition reduced NS1 secretion. Given that this may be a result of reduced COPI vesicle formation we chose to continue to focus on GBF1 and its potential role in NS1 secretion. As such, we next sought to confirm the impact of siRNA-mediated COPI gene knockdown and associated effects on NS1 secretion using wildtype infectious DENV2 and the related orthoflavivirus, Australian-endemic West Nile virus Kunjin subtype (WNV/KUNV).

3.2.4: Assessing the impact of siRNA-mediated knockdown on COPI component mRNA and protein abundance

First, we assessed the efficacy of the COPA, COPB2, COPG1, and GBF1 siRNA pools to knockdown their intended target mRNA expression in Huh-7.5 cells. For this, Huh-7.5 cells were reverse transfected with COPI component or NTC siRNAs and after 3 hours of incubation, transfection media was replaced and cells were returned to culture. At 24-, 48-, and 72-hours post-transfection, total cellular RNA was extracted to quantitatively analyse target gene mRNA expression. The intended gene target mRNA was quantified, relative to that of the NTC, by RT-qPCR. Figure 3.06A shows the impact of siRNA-mediated COPI gene target silencing. All intended target mRNA were reduced relative to that of the NTC, confirming the on-target efficacy and successful delivery of the siRNA pools. Substantial knockdown was observed at 24 hours post-siRNA treatment for each of the gene targets, indicating appropriate dosing of siRNA pools. A time-dependent recovery trend in mRNA abundance was observed at 48- and 72-hours post-siRNA transfection for each of the gene targets. This may be expected given that Huh-7.5 cells are a rapidly dividing cell line that exhibits a doubling time of ~ 1 day, which can lead to siRNA dilution effects in the growing population [404].

Next, to assess whether the observed siRNA-dependent mRNA knockdown was accompanied by a decrease in target protein abundance, we employed quantitative indirect immunofluorescence microscopy using fluorescence intensity as a marker for protein abundance. Huh-7.5 cells were reverse transfected with siRNA pools and at 24 hours post-transfection, cells were fixed and processed for indirect immunofluorescent labelling using anti-COPI antibodies (green) and nuclei were counterstained with DAPI (blue). Samples were then imaged by automated fluorescence microscopy. COPI labelling-associated green fluorescence was measured for each cell as a measure for COPI protein abundance. Reductions in COPI target protein abundance, as inferred

from the reduction in fluorescence intensity relative to the NTC, were observed for each of our COPI siRNA treatments (Figure 3.06B). Residual target protein abundance as a percentage of the NTC were determined as follows: COPA = 73.4%; COPB2 = 81.2%; COPG1 = 40.9%; GBF1 = 83.0%. Despite the large reductions in target mRNA expression following siRNA treatment detailed above, the level of protein knockdown observed by indirect immunofluorescent microscopy was not as pronounced. The incomplete COPI protein knockdown observed here may be explained given that preassembled heptameric COPI complexes are relatively stable and display a half-life of ~ 28 hours in mammalian cells [405]. Nonetheless, these results confirm that COPI siRNA treatment reduced COPI target protein abundance.

Collectively, these data demonstrated that the siRNA-induced silencing of our genes of interest reduced target mRNA and protein abundance when compared to the non-targeting siRNA control, indicating that the experimental design is a suitable approach to study the impact of COPI silencing on DENV biology in Huh-7.5 cells.

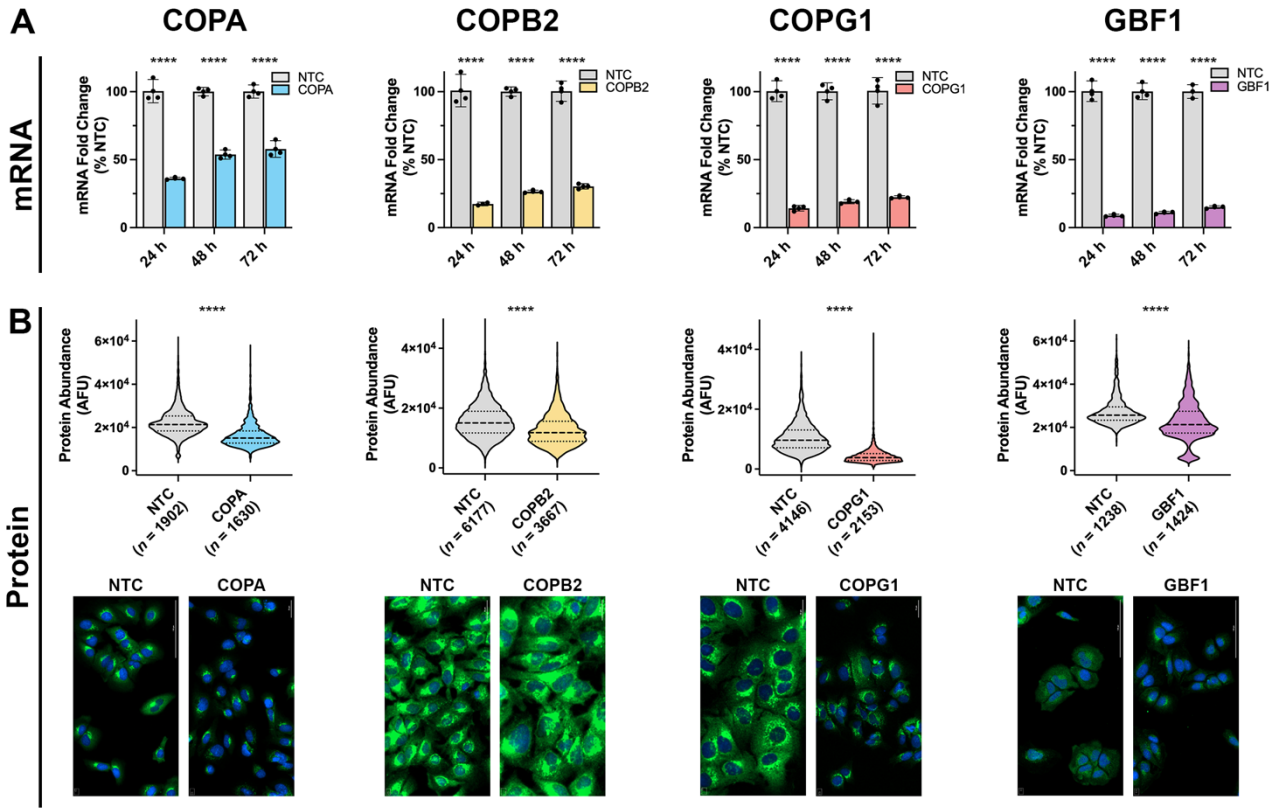

FIGURE 3.06. COPI component mRNA and protein is reduced following siRNA treatment in Huh-7.5 cells. (A) qRT-PCR analysis of COPI component mRNA levels in Huh-7.5 cells at indicated time points following siRNA treatment. Data are normalised to those of the RPLP0 housekeeping gene and expressed as a % of those of the non-targeting control (NTC) siRNA. Data are means + S.D., n = 3, one-way ANOVA. (B) Immunofluorescence microscopy-based quantitative analysis of COPI component protein abundance in Huh-7.5 cells following siRNA treatment. Huh-7.5 cells were reverse transfected with COPI siRNA pools or the NTC siRNA pool as indicated. At 48 h.p.t., cells were fixed and processed for indirect immunofluorescent labelling using anti-COPI antibodies (green) and nuclei were counterstained with DAPI (blue). Fluorescence intensity (AFU) was measured for each cell to determine COPI protein abundance at the single cell level. Violin plots (with light smoothing) display median values (dashed lines) and quartile values (dotted lines) for each data set. Mean fluorescence intensity as a percentage of NTC are displayed on the x-axis. Cell numbers (n) COPA: NTC = 1902, COPA = 1630; COPB2: NTC = 6177, COPB2 = 3667; COPG1: NTC = 4146, COPG1 = 2153; GBF1: NTC = 1238, GBF1 = 1424. The statistical significance of differences between groups was determined using Welch's t-test.

3.2.5: Assessing the impact of COPI silencing on DENV-infected Huh-7.5 cell viability, DENV intracellular viral RNA load, and infectious virus production

Having confirmed siRNA-mediated knockdown of the intended target mRNA and protein, we next sought to investigate the impact of COPI component silencing on DENV-infected Huh-7.5 cell viability, intracellular DENV viral RNA abundance, and infectious virus production. For this, a population Huh-7.5 cells were infected with DENV (MOI ~1.0) and reverse transfected with siRNA pools targeting COPI components or NTC. At 48 hours post-siRNA treatment, cell viability was measured (Figure 3.07A), total cellular RNA was extracted for viral RNA quantification by qRT-PCR (Figure 3.07B), and virus-containing cell culture supernatants were recovered and processed to assess infectivity (Figure 3.07C). Importantly, Huh-7.5 cell viability/metabolic activity was largely unaffected by COPI component silencing, as determined using an ATP-based cell viability assay. There was, however, a small but statistically significant reduction in cell viability/metabolic activity observed in cells treated with siRNAs targeting COPA. Despite this minor impact on COPA-silenced cells, intracellular DENV viral RNA abundance and infectious virus production were observed to be unaltered by any COPI siRNA treatment relative to the NTC. Taken together, these results indicate that, following DENV infection, COPI component gene expression is dispensable for viral RNA replication and infectious virus production in DENV-infected Huh-7.5 cells.

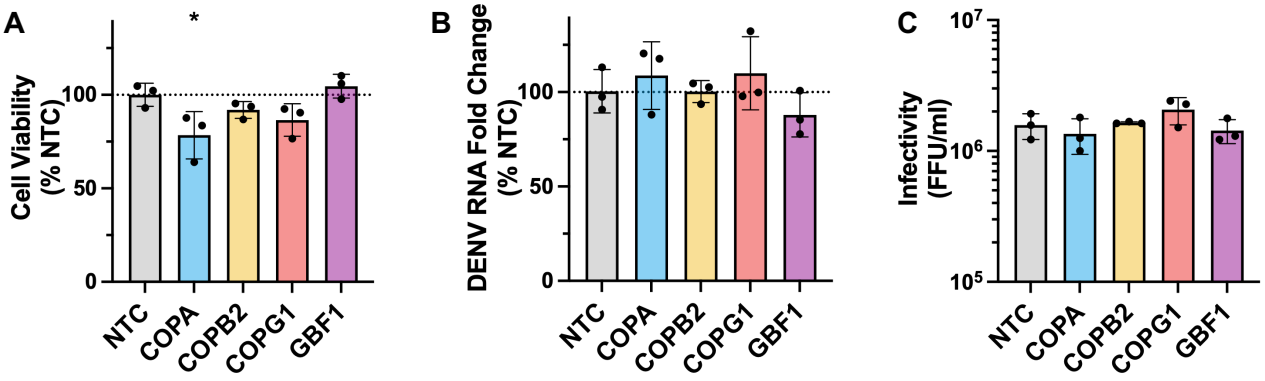

FIGURE 3.07. COPI component silencing does not impact infectious virus production in DENV-infected Huh-7.5 cells. Huh-7.5 cells were infected with DENV2 (MOI ~1) for 4 h and reverse transfected with siRNAs targeting the indicated COPI component or NTC. At 48 hours post-siRNA treatment, cell viability was measured using a CellTiter-Glo 2.0 cell viability assay (A), virus-containing cell culture supernatants were recovered and processed to assess infectivity by focus forming assays (B) and intracellular viral RNA was measured by RT-qPCR analysis (C). For RT-qPCR data are normalised to the RPLP0 housekeeping gene and expressed as a % of the non-targeting control (NTC) siRNA. All data are means + S.D., n = 3 biological triplicates, one-way ANOVA.

3.2.6: Assessing the impact of COPI component silencing on wildtype orthoflavivirus NS1 secretion

Given that COPI component depletion reduced the secretion of NS1-NLuc fusion protein from DENV2-NS1-NLuc-infected cells, we next sought to assess the impact of COPI silencing on NS1 secretion using an un-tagged clinical isolate-derived DENV2 strain and quantitative Western blot analysis (see 2.1.18 for experimental details). Figure 3.08 provides a schematic overview of the experimental approach to assess the impact of COPI component silencing on DENV2 NS1 secretion. Under each of the COPI siRNA treatments, the DENV2 NS1 secretion ratios (sNS1 / iNS1) were reduced relative to that of the non-targeting siRNA control (Figure 3.09A), reflecting the results of the original siRNA screen. These results confirm that the siRNA-mediated silencing of these gene targets in human cells contributes to a reduction in DENV2 NS1 secretion efficiency, further confirming COPI components and associated pathways as an important determinant of NS1 secretion.

To assess whether this reduced NS1 secretion efficiency phenotype is DENV2-specific or a more generalised feature of orthoflavivirus biology, similar experiments were performed in WNV/KUNV-infected Huh-7.5 cells. Similarly to DENV2, a reduction in WNV/KUNV NS1 secretion efficiency was observed in cells treated with siRNAs targeting COPI components (Figure 3.09B), suggesting that these related viruses may utilise similar mechanisms for NS1 secretion. Collectively, these data indicated that while COPI components are dispensable for infectious DENV production, they are required for efficient DENV NS1 secretion. Further, the exploitation of COPI components to achieve efficient NS1 secretion from human cells may be a conserved feature within the Orthoflavivirus genus.

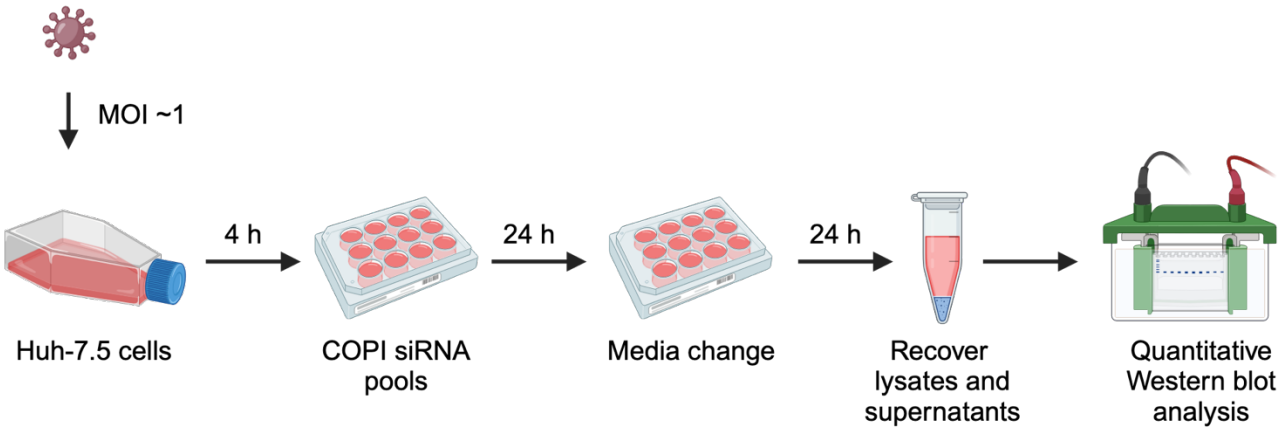

FIGURE 3.08. Schematic overview of the experimental approach to assess the impact of COPI silencing on wildtype DENV2 or WNV/KUNV NS1 secretion. Huh-7.5 cells were infected with DENV2 or WNV/KUNV (MOI ~1), trypsinised at 4 h.p.i., and reverse transfected with siRNAs targeting COPI components or NTC. At 24 hours post-siRNA treatment, cells were extensively washed and returned to culture in complete DMEM for a further 24 hours prior to harvest. Cell culture lysates and supernatants were then recovered to measure intracellular and extracellular NS1 levels, respectively, by quantitative Western blot analysis.

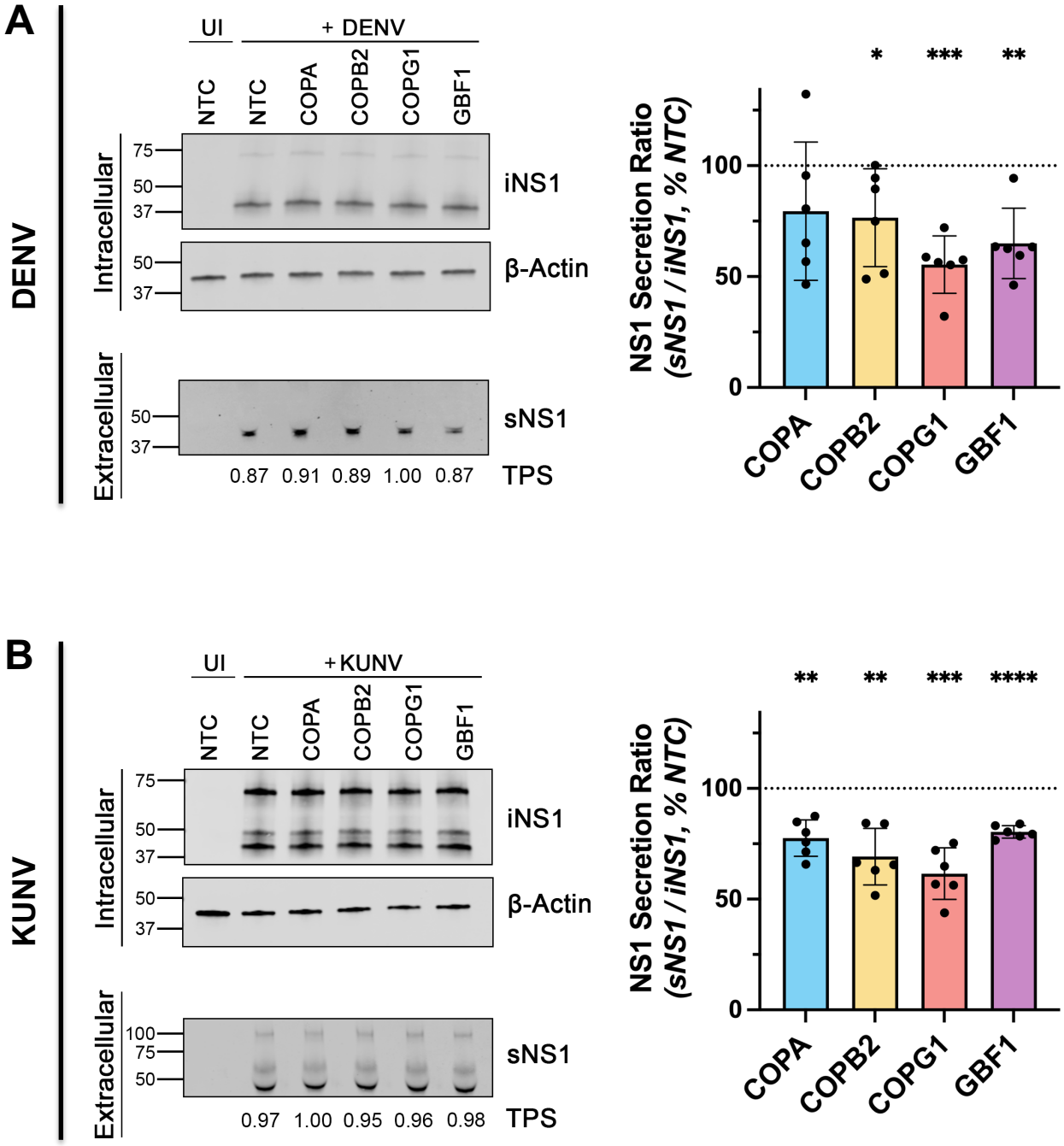

FIGURE 3.09. Orthoflavivirus NS1 secretion is reduced in COPI-silenced Huh-7.5 cells. Quantification of DENV (A) and WNV/KUNV (B) NS1 abundance in cell culture supernatants and lysates by Western blot analysis, displayed as the secretion ratio of NS1 (sNS1 / iNS1) as a % of NTC. Data are means + S.D., n = 3 from two independent experiments, one-sample *t*-test. *p = <0.05, **p = <0.005, ***p = ≤0.0005, ****p = <0.0001.

3.2.7: Attempts to generate COPI component CRISPR-Cas9 knockout Huh-7.5 cell lines

To authenticate the role of COPI components in NS1 secretion using an siRNA-independent approach, we attempted to utilise CRISPR-Cas9 technology to create COPI component knockout Huh-7.5 cell lines. Given the critical roles of COPI components in multiple fundamental processes related to the vesicular trafficking of proteins, lipids and carbohydrates, we first considered whether their knockout may impact upon cell viability and proliferation. In this context, Wang and colleagues performed a genome-wide CRISPR-Cas9 knockout screen in four blood cancer cell lines to identify essential genes in the human genome and identified COPA, COPB2, COPG1 and GBF1 amongst a large list of genes that are 'essential for optimal proliferation' [406]. Nonetheless, their study highlighted some key points: guide RNA choice as well as cell lineage play a major role in the success or failure of CRISPR-Cas9-mediated gene knockout. Given that Huh-7.5 cells were not screened in the study by Wang *et al* and that other studies have reported at least partial CRISPR/Cas9-mediated knockout of COPI genes [348, 407], we endeavoured to create COPI knockout Huh-7.5 cell lines. Two guide RNAs targeting distinct loci within each of our four genes of interest (COPA, COPB2, COPG1, and GBF1) were selected using the predesigned Alt-R CRISPR-Cas9 tool from Integrated DNA Technologies (see Appendix II). Complementary guide oligonucleotides were purchased, annealed, phosphorylated, and ligated into the Cas9- and puromycin resistance gene-encoding lentiCRISPRv2 lentiviral expression construct [302], and bacteria-propagated plasmids were confirmed by Sanger sequencing. These constructs were co-transfected with lentiviral packaging plasmids (psPAX2 and pMD2.G) into HEK293FT cells to produce replication-defective lentiviral particles containing Cas9 and guide RNA expression cassettes [302]. Lentivirus was recovered and clarified by centrifugation and filtration. To generate Huh-7.5 knockout cell lines, Huh-7.5 cells were transduced with filtered lentivirus-containing cell culture media. At 3 days post-transduction, puromycin selection was applied and maintained for approximately 2 weeks, at which point all of the non-transduced negative control Huh-7.5 cells in parallel cultures were dead. Polyclonal cell populations were then expanded for 1 week, at which point, they were trypsinised and prepared for cryopreservation.

To assess the efficacy of the COPI CRISPR-Cas9 treatments on genome editing, we employed the tracking of indels by sequence trace decomposition (TIDE) method developed by Brinkman and colleagues [408]. This assay can quickly and accurately quantify the spectrum and frequency of non-templated CRISPR-Cas9-induced indel mutations within a heterogenous polyclonal population of cells. This approach requires only three steps: (i) genomic DNA PCR amplification of a 0.5-1.5 kb fragment across the expected cut site in the CRISPR-Cas9-targeted pool of cells, accompanied by a parallel PCR of control cells, (ii) conventional capillary (Sanger) sequencing of the PCR amplicons, and (iii) analysis of the quantitative sequence traces using specially designed software that is available as a simple web tool (https://tide.nki.nl/). For this, our 8 polyclonal populations (four genes of interest, two guide RNAs per gene) of cryopreserved COPI CRISPR-Cas9-treated cells and

CRISPR-Cas9-treated control cells (mCherry) were resuscitated and cultured for 5 days. Cells were then trypsinised and genomic DNA was extracted. First, to capture relatively large CRISPR-Cas-induced deletions [409], that may encompass one or both of PCR primer binding sites required for the amplification of the 0.5 – 1.5 kb fragments for TIDE analysis, primers were designed to amplify ~3 kb amplicons surrounding the intended cut sites. Genomic DNA from each of our 8 CRISPR-Cas9-treated cell populations and control cells were PCR amplified using low PCR cycle numbers to maintain genetic diversity. Amplicons were then subjected to standard agarose gel electrophoresis under the assumption that large deletions may have been subject to PCR amplification bias given their relatively small amplicon size and may be visible despite the low-separation and low-resolution of traditional agarose electrophoresis. No DNA fragments significantly smaller than the expected ~3 kb fragment were overtly apparent; thus, no relatively large deletions were identified using this technique (data not shown). This technique, however, likely requires an electrophoresis instrument with high-resolution separation capabilities (e.g.: Fragment Analyzer, BioAnalyzer TapeStation, etc.). Next, these ~3 kb amplicons were subjected to Sanger sequencing using sequencing primers that bind ~500 bp (495 – 536 bp) from the guide RNA PAM site. The sequences from both control- and COPI-CRISPR-Cas9-treated populations (for simplicity, henceforth referred to by the gene target and guide RNA number) were aligned to the reference sequences for manual inspection of the chromatograms, and the sequencing traces were analysed using the online TIDE software (Figure 3.10). Near the intended cut site, marked overlapping peaks in the chromatograms were observed for both COPG1 guides 1 and 2 (Figure 3.10C), and for GBF1 guide 2 (Figure 3.10D), indicating a considerable degree of uncertainty in the nucleotide sequences, suggesting that these polyclonal populations of CRISPR-Cas9-treated cells are heterogeneous at the respective locus of interest. This inference was supported by TIDE analysis, which indicated an editing efficiency of 41%, 32%, and 50%, respectively. As determined by TIDE analysis, the editing efficiency was relatively low (0.7% - 10.4%) for all other COPI CRISPR-Cas9-treated polyclonal populations, indicating that these populations were dominated by cells that do not contain indels near the targeted cut site. These data suggest that these CRISPR-Cas9-treated Huh-7.5 cells are predominantly wildtype at their locus of interest.

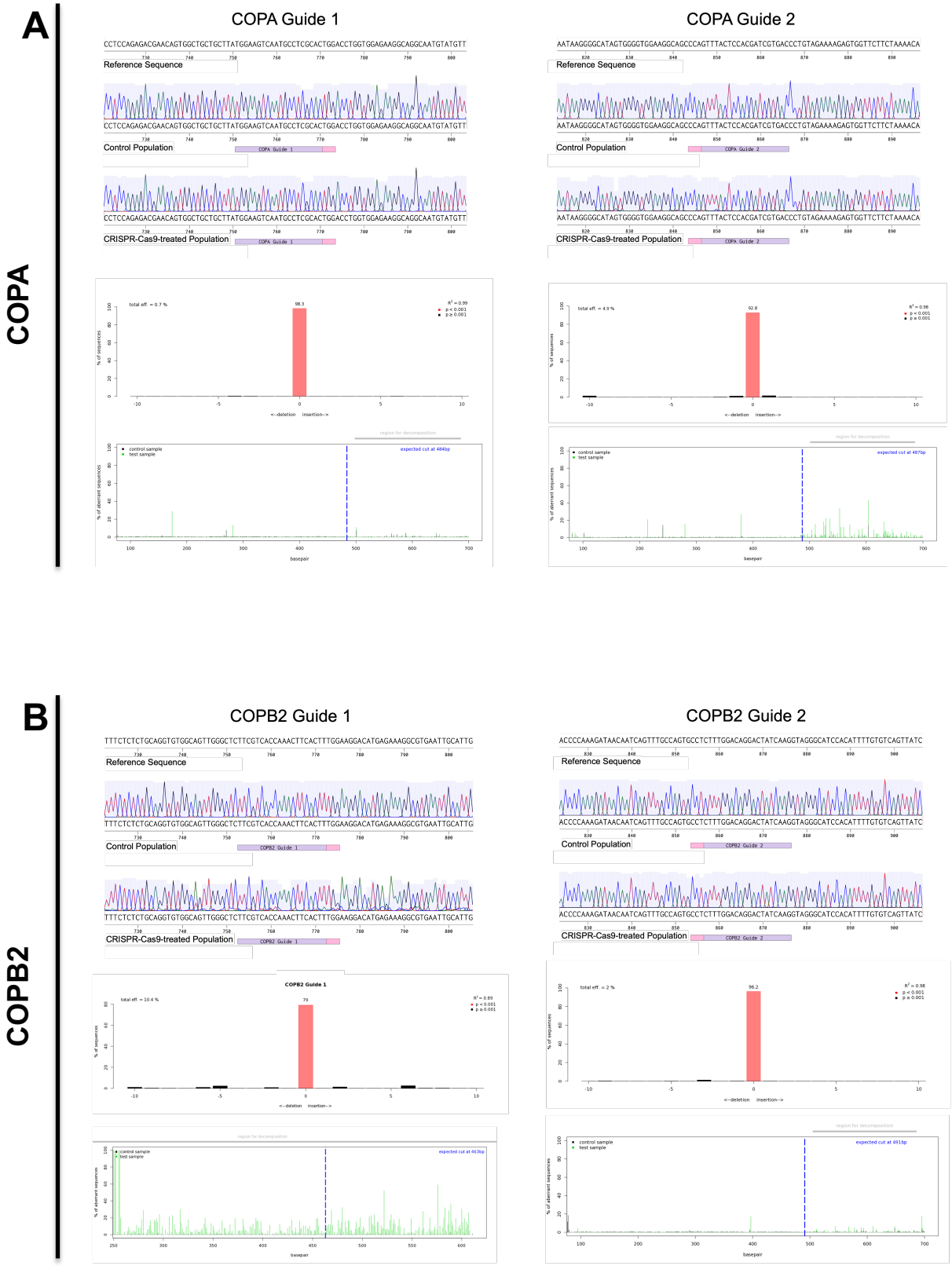

FIGURE 3.10. Impact of COPI CRISPR-Cas9 treatment on genome editing in Huh-7.5 cells. Quantification of genome editing efficiency following CRISPR-Cas9 treatment targeting COPA (A), COPB2 (B), COPG1 (C), and GBF1 (D). Each gene was targeted using two independent guide RNAs: guide 1 (left) and guide 2 (right). Sanger sequencing chromatograms surrounding the

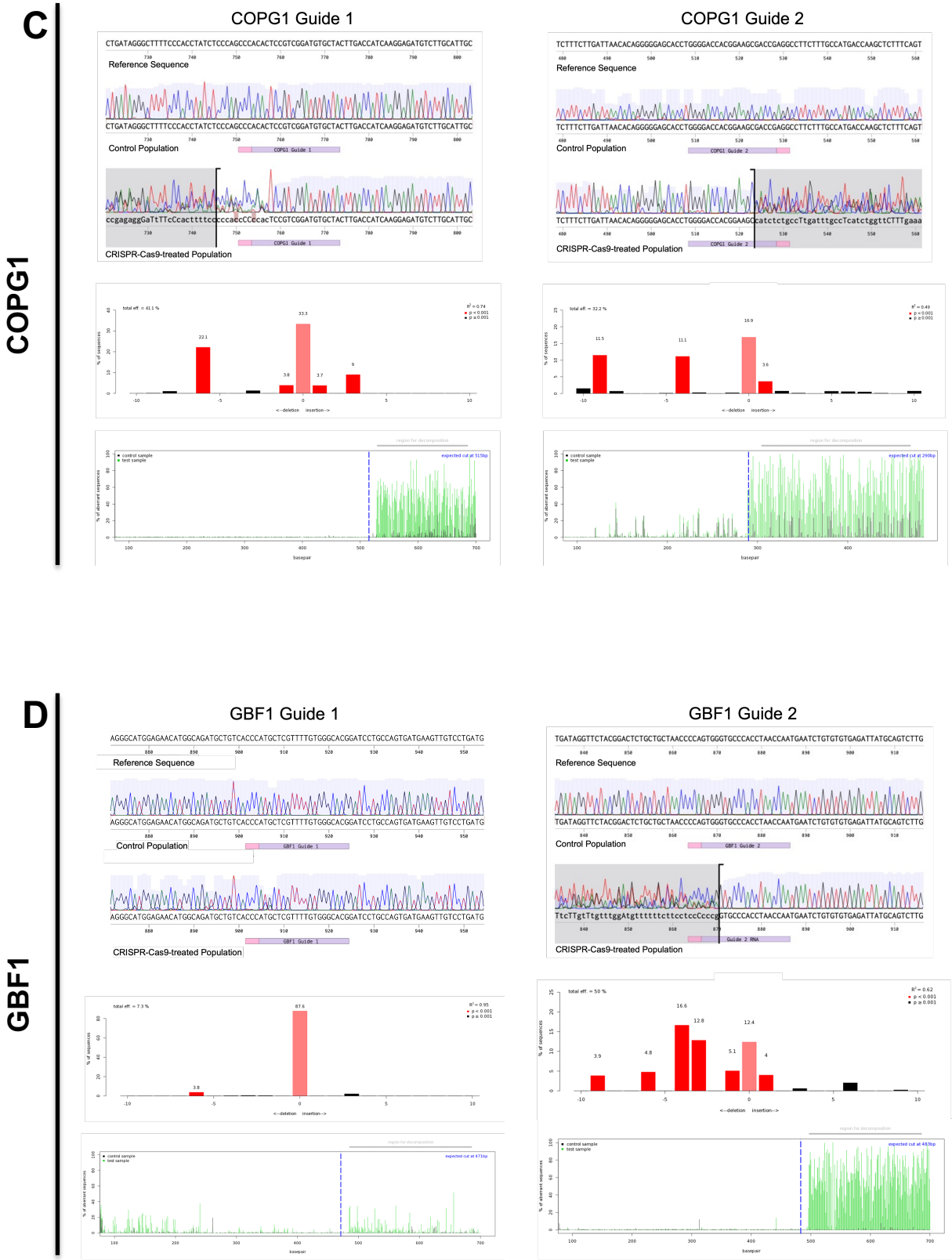

intended cut site are displayed for the control population (top) and CRISPR-Cas9-treated population (bottom), reference sequence is displayed above. TIDE-generated graphs display indel spectrum with their frequencies (middle) and aberrant signal sequence (bottom) with control (black) and CRISPR-treated (green).

We next assessed the impact of COPI CRISPR-Cas9 treatments on target protein abundance by quantitative indirect immunofluorescence microscopy. Cryopreserved COPI CRISPR-Cas9-treated cells and CRISPR-Cas9-treated control cells were resuscitated and cultured for 5 days. Cells were then trypsinised and reseeded into 96-well black-walled imaging plates and returned to culture for 24 hours. Cells were fixed and processed for indirect immunofluorescent labelling using anti-COPI antibodies and nuclei were counterstained with DAPI. Samples were imaged, processed, and analysed as detailed in section 3.2.4. The impact of COPI CRISPR-Cas9 treatment on target protein abundance is shown in Figure 3.11. Consistent with the low editing efficiency observed by TIDE analysis, COPI labelling-associated green fluorescence was largely similar for CRISPR-treated Huh-7.5 cells for COPA guides 1 and 2 (Figure 3.11A) and COPB2 guides 1 and 2 (Figure 3.11B), indicating that the vast majority of cells within these polyclonal populations express their intended target protein at levels comparable to that of the control cells. Also consistent with the TIDE results, COPI labelling-associated green fluorescence was reduced for CRISPR-Cas9-treated Huh-7.5 cells for COPG1 guide 1 (Figure 3.11C) and GBF1 guide 2 (Figure 3.11D) relative to the control, indicating that these polyclonal populations contain cells that express their respective protein at levels that are reduced relative to wildtype cells. Interestingly, a small cohort of COPG1 guide 1 CRISPR-Cas9-treated cells exhibit substantially low COPI labelling-associated fluorescence intensity. Conceivably, these cells may be completely deficient in COPG1 protein and may represent a subpopulation that could be further processed to isolate COPG1-deficient monoclonal cells. Nonetheless, our results indicate that the vast majority of cells within our COPI CRISPR-Cas9-treated polyclonal populations express their protein of interest and, in most cases, at levels comparable to the control. These data suggest that our COPI CRISPR-Cas9-treated Huh-7.5 cells predominantly express wildtype levels of the protein of interest.

Collectively, these data indicate that our attempts to generate Huh-7.5 cell lines deficient in COPA, COPB2, COPG1, or GBF1 protein expression by CRISPR-Cas9-mediated genome editing predominantly failed to yield cells completely deficient in COPI component protein, likely due to the established roles of these genes for optimal cell proliferation [406]. As such, further processing of these cells (i) to generate monoclonal cell lines, or (ii) for NS1 secretion experiments was discontinued.

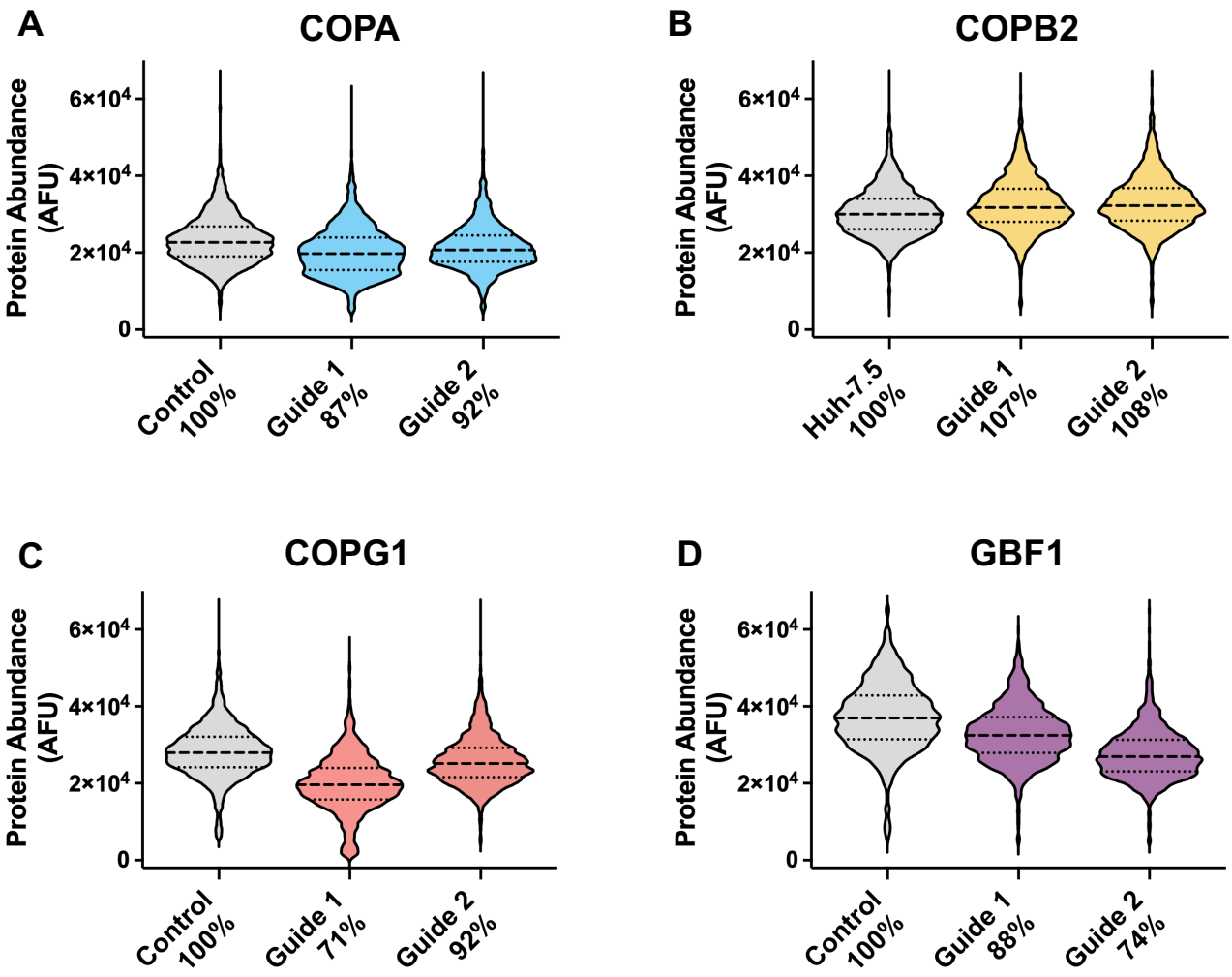

FIGURE 3.11. Impact of COPI CRISPR-Cas9 treatment on target protein abundance. Immunofluorescence microscopy-based quantitative analysis of COPI component protein abundance in 8 polyclonal populations of COPI CRISPR-Cas9-treated Huh-7.5 cells. CRISPR-Cas9-treated (targeting indicated COPI components) Huh-7.5 cells were resuscitated in a T75 flask for 5 days. Cells were then re-seeded into 96-well black plates and returned to culture for a further 24 hours. Cells were then fixed and processed for indirect immunofluorescent labelling using anti-COPI antibodies (green) and nuclei were counterstained with DAPI (blue). Fluorescence intensity was measured for each cell to determine COPI protein abundance at the single cell level. Violin plots (with light smoothing) display median values (dashed lines) and quartile values (dotted lines) for each data set. Mean fluorescence intensity as a percentage of CRISPR-Cas9-treated control cells are displayed on the x-axis. Cell numbers (n) COPA: Control = 2767, Guide 1 = 2162, Guide 2 = 2932; COPB2: Control = 2849, Guide 1 = 2300, Guide 2 = 3243; COPG1: Control = 2348, Guide 1 = 2135, Guide 2 = 2679; GBF1: Control = 2375, Guide 1 = 1819, Guide 2 = 2295.

3.2.8: Exogenous cDNA expression of COPI variants suggests that certain variants and/or expression levels influence NS1 secretion.

Since we were unable to generate Huh-7.5 cells completely deficient in COPI component protein by CRISPR-Cas9 technology, we reasoned that a particularly interesting and complementary approach to achieve an siRNA-independent COPI gene knockout or knockdown approach would be to express loss-of-function variants of our genes of interest in Huh-7.5 cells. Indeed, medically relevant, loss-of-function allelic variants existing as single nucleotide polymorphisms (SNPs) circulating in the human population have recently been identified for COPA-E241K [410], COPB2-R254C [411], and COPG1-K652E [412]. Intriguingly, these variants have been implicated in causing disease phenotypes that are strikingly similar to those associated with orthoflavivirus complications, including arthritis [410], haemorrhage [410], microcephaly [411, 413], and dysregulation of the immune system [412]. From a technical standpoint this approach would be advantageous as these loss-of-function phenotypes may be achieved straightforwardly through exogenous gene expression and could overcome the lethality imposed by essential gene knock-out. Further, these variants would constitute interesting candidates as investigating their impact on NS1 secretion may be of clinical relevance. Accordingly, we investigated the impact of overexpression of wildtype and SNP variants of these genes on NS1 secretion efficiency. Importantly, COPA-E241K is a dominant-negative mutation [410], therefore, exogenous expression from a cDNA vector should interfere with the proper functioning of the endogenously expressed wildtype COPA protein. To date, no dominant-negative SNP mutations have been identified for COPB2 or COPG1. COPB2-R254C and COPG1-K652E are homozygous recessive mutations. Nevertheless, these variants are incorporated into COPI complexes resulting in impaired COPI coated vesicle functioning [412]. As such, we reasoned that under high CMV-driven expression levels, these COPI SNP variant protein products would likely be incorporated into COPI coated vesicles and that this may result in COPI coated vesicle trafficking impairment. To this end, GFP-tagged wildtype COPA, COPB2, and COPG1 cDNA constructs were created and modified variants were generated by site-directed mutagenesis to incorporate these SNPs. To investigate the impact of COPI-WT or COPI-SNP overexpression of NS1 secretion in a manner independent of DENV viral RNA replication and/or spread of infection, we utilised the T7 RNA polymerase-driven pIRO-D expression system, in which heterologously expressed T7 RNA polymerase drives expression of the DENV2 NS1-NS5 polyprotein and induces the formation of replication organelles that are morphologically indistinguishable to those of wildtype DENV infection [414]. COPI-WT, COPI-SNP or GFP-only control cDNA expression plasmids were co-transfected with pIRO-D into T7 RNA polymerase-expressing Huh-7.5 cells (Huh-7.5+T7) [305]. At 18 hours post-transfection, cell culture lysates and supernatants were collected to assess the impact of COPI-WT and COPI-SNP over-expression on intracellular and secreted NS1 abundance by quantitative Western blot analysis. Despite substantial variability of intracellular NS1 levels when either COPA-WT or COPA-SNP cDNA was expressed, the levels of secreted NS1 were relatively consistent within treatment groups (Figure 3.12A). Interestingly, while COPA-WT over-expression had no effect on

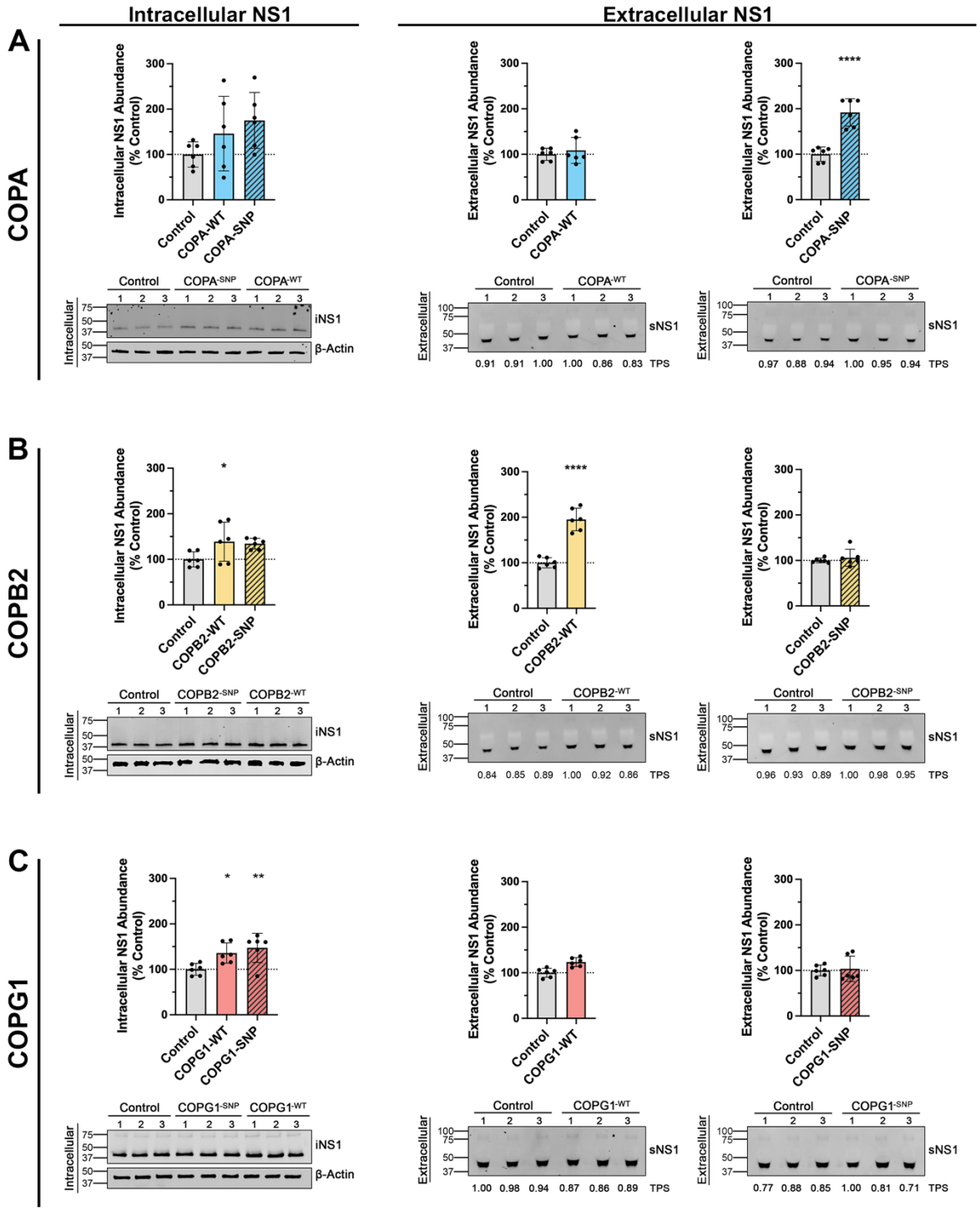

FIGURE 3.12. Ectopic expression of COPI variants indicates that certain variants and over-expression affect DENV NS1 secretion. SNPs were introduced into GFP-tagged wildtype COPA, COPB2, and COPG1 cDNA expression constructs. T7 RNA polymerase-expressing Huh-7.5 cells were co-transfected with COPI expression constructs and a T7 RNA polymerase-driven DENV2 NS1-NS5 polyprotein expression system. At 18 hours post-transfection, cell culture supernatants and lysates were recovered to measure extracellular and intracellular NS1 levels, respectively, by quantitative Western blot analysis. Data are means + SD, n = 3 from two independent experiments, one-way ANOVA, *p = <0.05, **p = <0.01, ***p = <0.005, ****p = <0.0001.

secreted NS1 levels relative to the control, expression of the COPA-E241K construct increased secreted NS1 levels approximately two-fold. Modest increases in intracellular NS1 levels were observed when either COPB2-WT or COPB2-R254C constructs were over-expressed, however, an approximately two-fold increase in secreted NS1 levels was observed in COPB2-WT transfected cells (Figure 3.12B). Similarly, modest increases in the levels of intracellular NS1 were observed in cells over-expressing either COPG1-WT or COPG1-K652E constructs, however, no effect was observed for levels of secreted NS1 (Figure 3.12C). Collectively, the altered NS1 secretion profiles observed here for COPA-E241K and COPB2-WT suggest that allelic variants and/or altered expression levels of COPI components may enhance NS1 secretion.

3.2.9: NS1 secretion is reduced in Golgicide A-treated Huh-7.5 cells

To interrogate the impact of COPI vesicle perturbation on DENV NS1 secretion, we employed the small molecule inhibitor Golgicide A (GCA). GCA is a potent and specific inhibitor of GBF1 catalytic activity that acts by binding to the GBF1-ARF-GDP protein-protein interface, preventing the ARF-GDP/GTP exchange [415]. This results in the prevention of COPI vesicle formation, COPI dissociation from Golgi membranes, disassembly of the Golgi, and swelling of the ER [415]. GBF1 has been demonstrated to perform a variety of roles in many RNA virus lifecycles [370] and much of this information has been garnered through the use of GCA or the related multi-ARF-GEF inhibitor brefeldin A (BFA (which inhibits GBF1, BIG1 and BIG2). Importantly, time of addition studies have shown that these compounds influence multiple aspects of the orthoflavivirus lifecycle. When applied to WNV/KUNV-infected mammalian cells during the 12 – 16 hour latent phase of infection [416], BFA inhibits the formation of virus-induced membrane structures [417], and severely impairs viral protein production and infectious virus release [418]. However, when added late in infection (~20 – 24 hours post-infection), the virus induced membrane structures are relatively stable [417], and only minor effects on viral protein synthesis were observed [418]. Comparatively, GCA pulse-chase experiments performed in DENV-infected mammalian cells indicate that, despite having no impact on DENV internalisation, intracellular viral RNA abundance is significantly reduced when GCA is applied in the first 12 hours of infection, reduced to a lesser extent when applied at 12 hours post-infection, but unaffected when applied at 24 hours post-infection [419]. Indeed, cell culture supernatants of orthoflavivirus-infected mammalian cells treated with high concentrations of BFA or GCA at 1 hour-post infection exhibit reduced abundances of sNS1 compared to untreated vehicle-only control cell culture supernatants [420]. However, given the inhibitory effects of these compounds on orthoflaviviral RNA replication, protein synthesis, and infectious virus production when administered early in infection, a reduction in the extracellular abundance of NS1 is not surprising. Thus, to mitigate the inhibitory effect of GCA on DENV RNA replication, we explored the impact of GCA treatment on NS1 secretion in DENV-infected Huh-7.5 cells when GCA is administered late in infection (Figure 3.13).

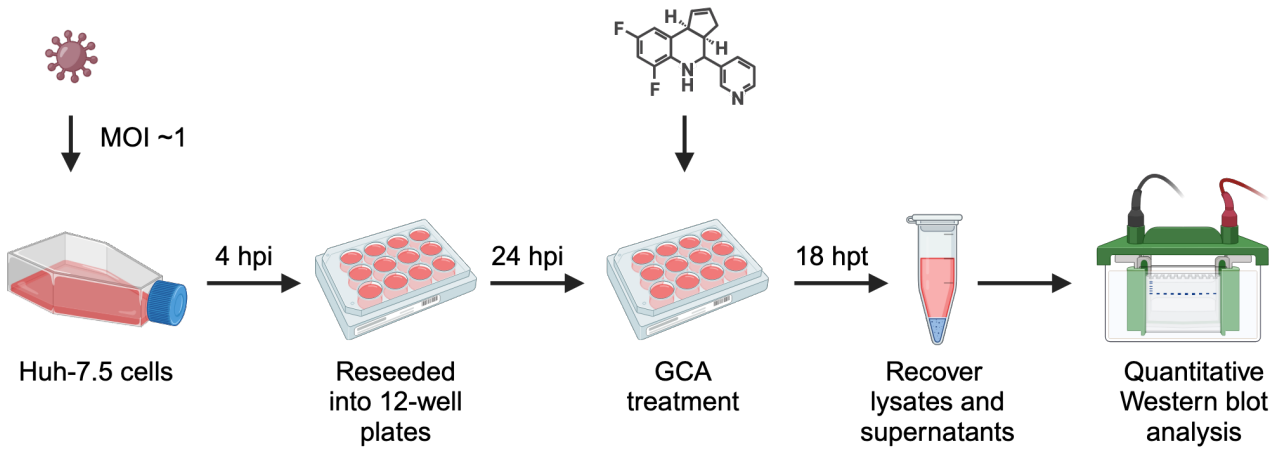

FIGURE 3.13. Schematic overview of the experimental approach to assess the impact of Golgicide A (GCA) treatment on DENV2 or WNV/KUNV NS1 secretion. Huh-7.5 cells were infected with DENV2 or WNV/KUNV (MOI ~1), trypsinised at 4 h.p.i., and re-seeded into 12-well plates. At 24 hours post-infection, cells were extensively washed cultured for a further 18 hours in media supplemented with increasing concentrations of GCA or DMSO control. Cell culture lysates and supernatants were then recovered to measure intracellular and extracellular NS1 levels, respectively, by quantitative Western blot analysis.

To examine the effects of GCA on various aspects of DENV biology in an experimental approach consistent with previous experiments (see Figure 3.13), cells were infected *en masse* with DENV2 (MOI ~1). At 4 hours post-infection, cells were trypsinised and reseeded into 96-well plates for cell viability assays and 12-well plates for analysis of viral RNA, infectious virus production and intracellular and extracellular NS1 abundance. At 24 hours post-infection, cells were extensively washed to remove secreted NS1 and cultured for a further 18 hours in media supplemented with increasing concentrations of GCA (1, 2.5, 5 μM) or DMSO vehicle control. At 18 hours post-GCA treatment, cell viability was measured using an ATP-based cell viability assay, virus-containing cell culture media was recovered and processed to assess infectivity by focus forming assay, and total cellular RNA was extracted for qRT-PCR analysis of intracellular DENV viral RNA levels. No significant effects on DENV-infected Huh-7.5 cell viability/metabolic activity were observed at GCA concentrations ≤ 5 μM (Figure 3.14A). Increasing concentrations of GCA did, however, reveal a dose-dependent reduction in infectious virus production (Figure 3.14B), which was accompanied by increases in intracellular viral RNA abundance (Figure 3.14C). To further interrogate the impact of GCA on intracellular viral RNA abundance independent from infectious virus spread, we employed a *Renilla* luciferase-encoding subgenomic replicon [299]. For this, Huh-7.5 cells were transfected with *in vitro* transcribed RNA from the DENV2 subgenomic replicon (R2A) or the replication-incompetent subgenomic replicon control (GND; input RNA control). At 4 hours post-transfection, transfection reagent was replaced with GCA-supplemented media (1 – 5 μM) or DMSO vehicle, and

cells were returned to culture. At 18 hours post-GCA treatment, cell culture lysates were harvested and processed to quantify *Renilla* luciferase activity as a measure of viral genome replication. *Renilla* luciferase activities were consistent between all GCA- and DMSO control-treated cells indicating that GCA does not impact DENV viral RNA replication. As such, the use of this subgenomic replicon confirmed that the increase in intracellular viral RNA abundance observed in DENV-infected cells treated with GCA was not likely to be the result of changes to DENV RNA replication (Figure 3.14D). Taken together, these results suggest that GCA-mediated GBF1 inhibition does not influence DENV genome replication but, instead, impedes infectious DENV particle release when GCA is applied to cells after 24 hours of DENV infection. Next, to assess the impact of GCA on NS1 secretion, cell culture lysates and supernatants were recovered from DENV2-infected, GCA-treated Huh-7.5 cells to measure intracellular and extracellular NS1 abundance, respectively, by quantitative Western blot analysis. In cells treated with 5 μM GCA, an increase in intracellular NS1 abundance was accompanied by a decrease in extracellular NS1 abundance, indicating that 5 μM GCA reduces NS1 secretion from DENV-infected Huh-7.5 cells (Figure 3.15A). Interestingly, however, no effect was observed on either intracellular or extracellular NS1 levels in cells treated with GCA concentrations below 5 μM. To assess whether GCA treatment reduces NS1 secretion for other orthoflaviviruses, similar experiments were performed in WNV/KUNV-infected Huh-7.5 cells. Comparable reductions in NS1 secretion were observed for WNV/KUNV-infected Huh-7.5 cells treated with 5 μM GCA (Figure 3.15B).

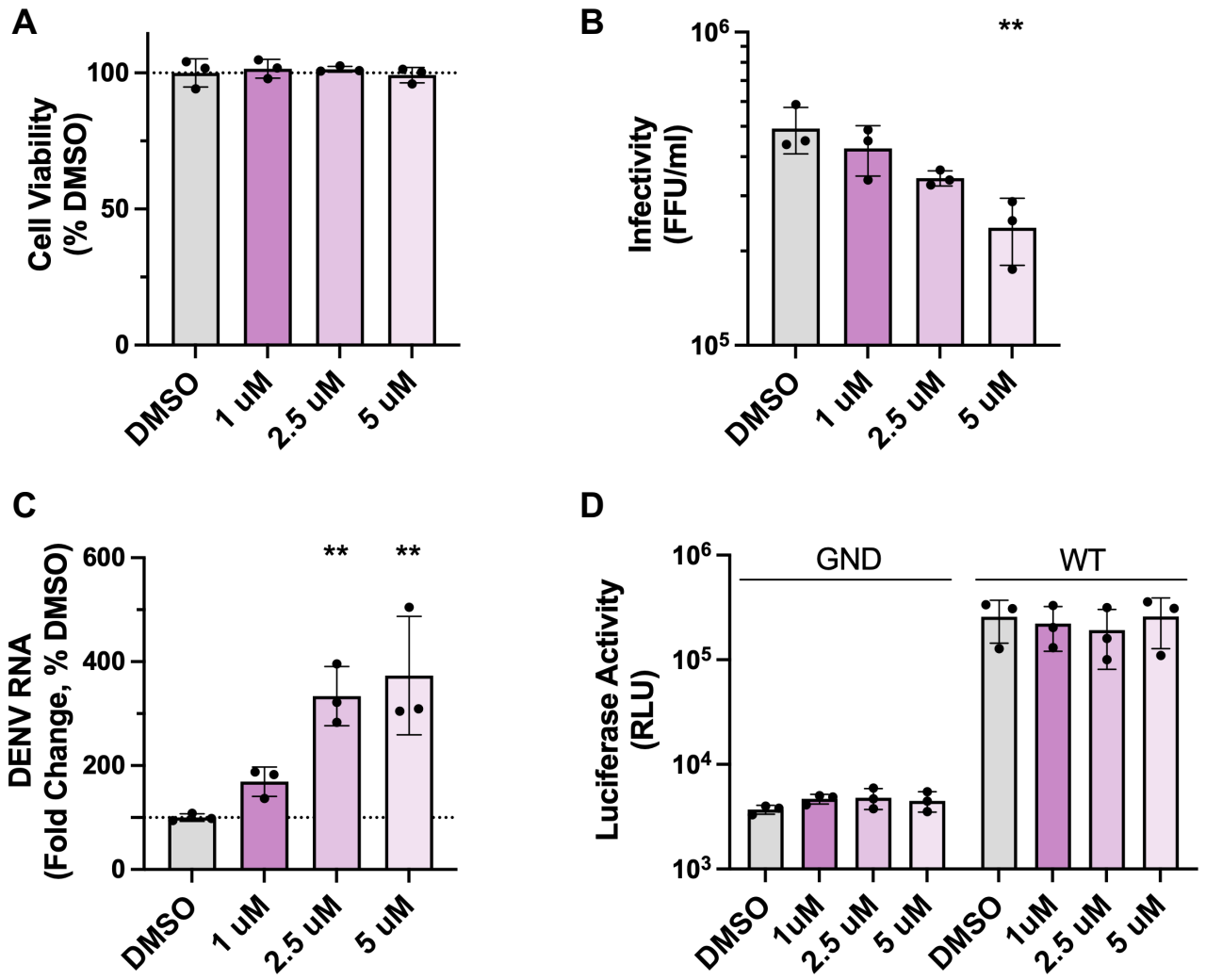

FIGURE 3.14. GCA-mediated GBF1 inhibition does not impact DENV genome replication but does impede infectious virus production. Huh-7.5 cells were cultured as shown in Figure 3.13. At 18 hours post-GCA treatment, cell viability was measured using CellTiter-Glo 2.0 viability assay (A), virus-containing cell culture supernatants were recovered and processed to assess infectivity by focus forming assay (B), and total cellular RNA was collected for qRT-PCR analysis of DENV2 viral RNA levels. For qRT-PCR analysis, data are normalised to the RPLP0 housekeeping gene and expressed as a % of the DMSO-treated mean values (C). (D) Golgicide A does not impact DENV RNA replication. Huh-7.5 cells were transfected with *in vitro* transcribed (IVT) RNA for a DENV2 subgenomic reporter replicon sg-DVs-R2A (WT, or replication-deficient GND control). At 4 hours post-transfection, cells were cultured in GCA at the indicated concentration or DMSO carrier control. At 18 h post-GCA treatment, cell lysates were prepared and luciferase activities were determined as a surrogate marker for viral RNA replication. All data are means + SD, n = 3 biological triplicates, one-way ANOVA, **p= <0.005

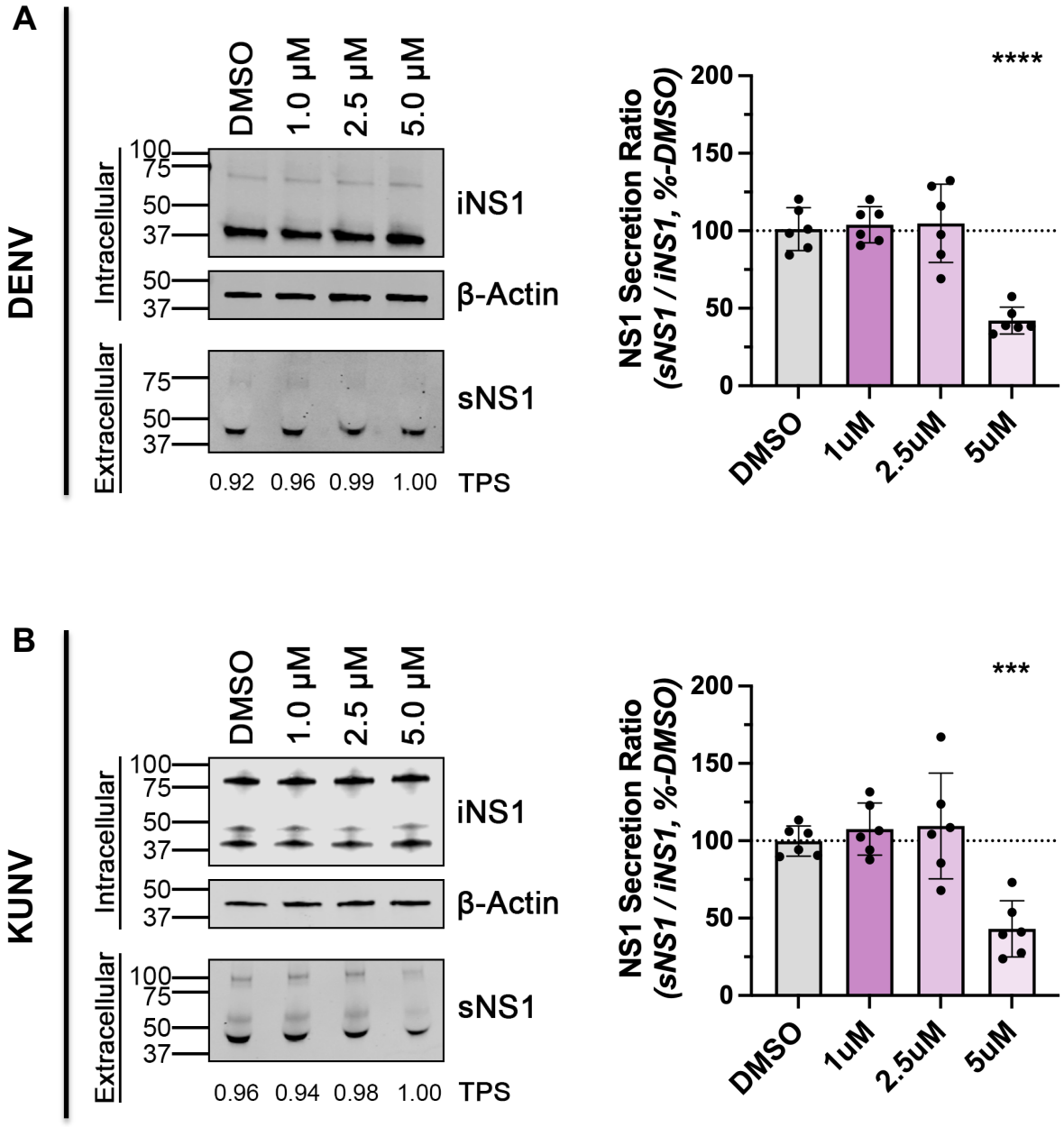

FIGURE 3.15. Orthoflavivirus NS1 secretion is reduced in GCA-treated Huh-7.5 cells. To investigate the impact of GCA treatment of NS1 secretion, the experimental approach depicted in Fig. 3.13 was employed. Quantification of DENV (A) and WNV/KUNV (B) NS1 abundance in cell culture supernatants and lysates by Western blot analysis, displayed as the secretion ratio of NS1 (sNS1 / iNS1) as a % of DMSO control. Data are means + SD, n = 3 from two independent experiments, one-way ANOVA, ***p= <0.001, ****p = <0.0001.

While it was demonstrated that infectious DENV production was reduced in a dose-dependent manner when 1 – 5 μM GCA was applied at 24 hours post-DENV infection, NS1 secretion was only observed to be reduced when cells were treated with 5 μM GCA. This was somewhat surprising given that DENV virion release has been shown to occur via the canonical secretion pathway [421]; the same pathway widely considered to be utilised for NS1 secretion [52]. Given that GCA treatment is known to disrupt Golgi integrity and lead to its disassembly, coupled with the current understanding that the Golgi is a key organelle utilised by DENV for the additional processing of the N130 glycan observed in secreted NS1 [90], we next explored the impact of GCA treatment on intracellular NS1 localisation with respect to the Golgi. At 18 hours post-GCA treatment (0 – 5 μM), DENV-infected Huh-7.5 cells were fixed and processed for indirect immunofluorescent labelling using anti-NS1 and the Golgi marker anti-GM130 antibodies. Samples were counterstained with DAPI and analysed by confocal fluorescence microscopy. No apparent differences in NS1 and the Golgi marker GM130 staining patterns were observed between GCA-treated or DMSO carrier control cells (Figure 3.16), and co-localisation analysis indicated that there was no significant impact on NS1 co-localisation with GM130 in cells treated with ≤ 5 μM GCA (Figure 3.16 inset). These results indicate that the vast majority of intracellular NS1 is spatially detached from the Golgi marker GM130, suggesting that any association that NS1 may have with the Golgi compartment may be infrequent and/or transient. Alternatively, secretion-destined NS1 may represent a relatively small proportion of the total intracellular NS1. Notwithstanding, these results suggest that the 5 μM GCA-induced reduction in NS1 secretion is independent of changes to Golgi morphology.

Collectively, these results indicate that, when GCA is applied at 24 hours post-DENV infection, the catalytic activity of GBF1 is dispensable for DENV genome replication but is critical for infectious virus production and NS1 secretion. Importantly, our results demonstrate that infectious DENV production is more sensitive than NS1 secretion to the impacts of GCA-mediated GBF1 inhibition. Further, GCA-mediated GBF1 inhibition reduces NS1 secretion from cells infected by DENV or WNV/KUNV, indicating that the catalytic activity of GBF1 is likely to be critical for efficient orthoflavivirus NS1 secretion.

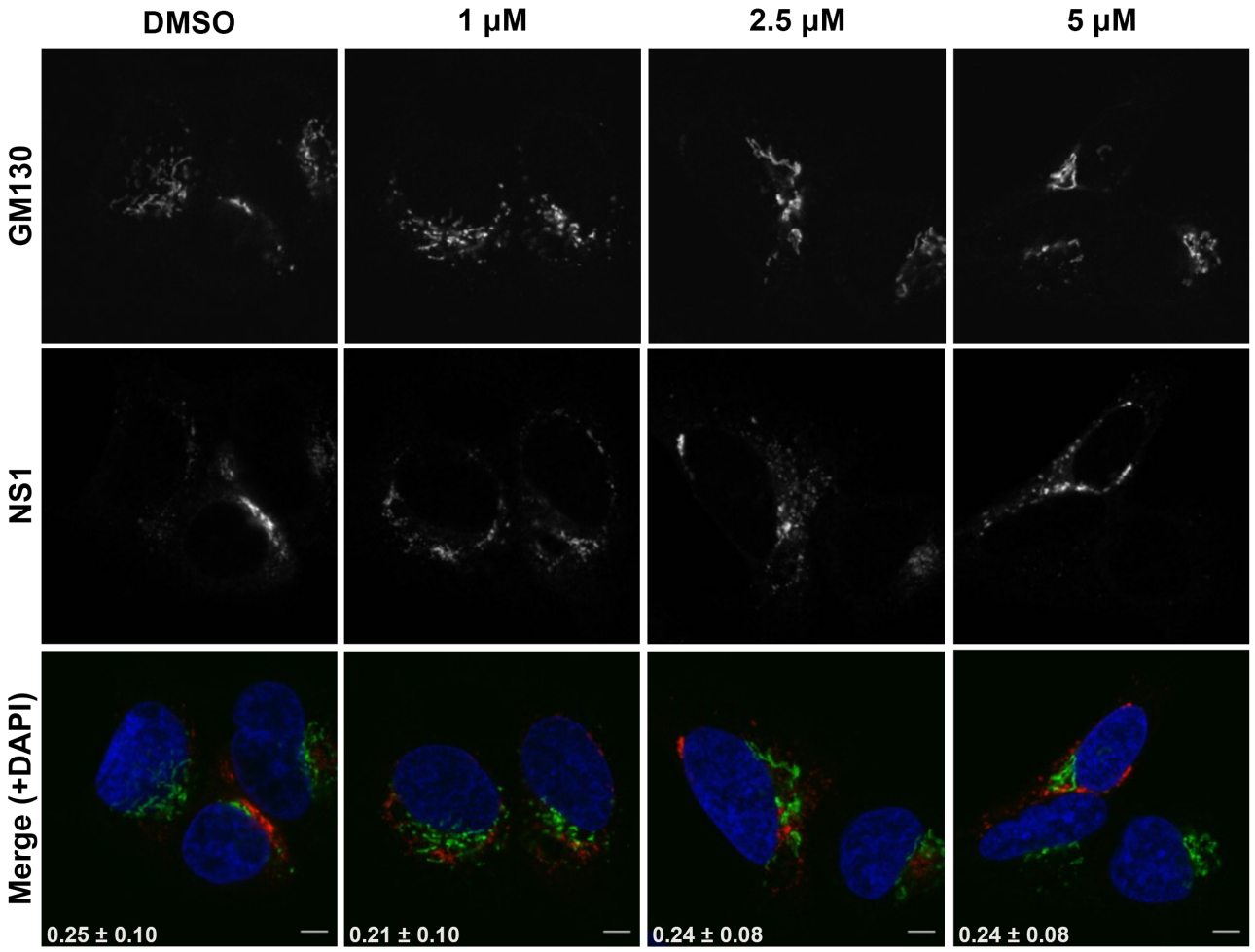

FIGURE 3.16. Confocal analysis of DENV NS1 reveals minimal and infrequent co-localisation with Golgi marker GM130. Huh-7.5 cells were cultured as shown in Figure 3.13. At 18 hours post-GCA treatment, cells were fixed and stained for indirect immunofluorescent labelling using mouse anti-NS1 and rabbit anti-GM130 primary antibodies, followed by AlexaFluor 555-conjugated anti-mouse IgG (red) and AlexaFluor 488-conjugated anti-rabbit IgG (green). Samples were counterstained with DAPI and analysed by confocal fluorescence microscopy. Yellow in the merged images indicates co-localisation. Pearson's co-localisation coefficients are shown in white in the merged images (means + SD, n = >30 cells). Scale bars are 10 µM.

3.3: Discussion

The secreted form of non-structural protein 1 is an important orthoflavivirus virulence factor. In addition to being involved in the enhancement of cellular susceptibility to infection [277], immune evasion [207], and transmission [278], secreted NS1 can disrupt endothelial barrier integrity and induce vascular damage [210, 211]; a key symptom of severe dengue disease. Although extensive research has been conducted on the synthesis, structure, and pathogenic effects of sNS1, the human host cellular machinery and pathways that are involved in NS1 secretion have not been fully investigated. Thus, the focus of this Chapter was to identify and interrogate the human host cellular factors that are required for efficient DENV NS1 secretion.

To gain insight into the human host factors that are involved in the secretion of DENV NS1, we performed a customised membrane-trafficking siRNA screen targeting ~180 human genes in DENV2-NS1-NLuc reporter virus-infected in Huh-7.5 cells. Using this approach, we were able to assess the impact of siRNA treatment on intracellular and secreted NS1 abundances by comparing the NS1-associated NLuc luminescence in cell culture lysates and supernatants, respectively. Of note, no siRNA treatments were observed to abolish NS1 secretion completely, which may at least partially reflect caveats within the experimental design. Given the importance of membrane trafficking pathways in the replication cycles of RNA viruses [326], Huh-7.5 cells were transfected with *in vitro* transcribed DENV2-NS1-NLuc RNA to establish infection prior to siRNA treatment. This methodological approach was employed to balance the focus towards assessing the impact of siRNA treatment on NS1 secretion in infected cells, while mitigating siRNA-mediated confounding effects on critical processes including viral entry, genome replication, and protein synthesis. Importantly, following siRNA treatment, cell culture supernatants remained on cells for two days prior to analysis. Given the temporal lag between siRNA-induced gene knockdown and target protein knockdown [422], sNS1 likely accumulated in cell culture supernatants prior to the occurrence of siRNA-mediated reductions in target protein abundances. Despite these caveats, we identified 3 siRNA pools that matched our ‘hit’ identification criteria of reducing NS1-associated NLuc secretion efficiency to ≥2 SD below the mean of the NTC. These top three hits were COPA, COPB2, and COPG1. These are three of the seven subunits of the coatomer protein complex I (COPI) and identification of multiple subunits of a known complex as the top hits strongly supported the validity of our screen. The screen also identified an additional 5 siRNA pools that met our ‘potential hit’ identification criteria of reducing extracellular NS1-NLuc to ≥1 SD below the mean of the NTC. Many of these genes have been previously identified as host factors involved in various aspects of orthoflavivirus life cycles, thus providing further support to the validity of the screen.

The 8 hits were selected for validation using an siRNA deconvolution screen. Confidence for the involvement of COPI components and associated pathways in NS1 secretion was supported by the demonstration that multiple individual siRNA duplexes targeting these genes resulted in NS1-NLuc secretion efficiency-reducing phenotypes consistent with the original screen. Additionally, multiple individual siRNA duplexes targeting the 'potential hit', DNM1, resulted in a decrease in NS1-NLuc secretion efficiency that matched our hit selection criteria. In this validation round using the criterion of ≥2 individual siRNA duplexes against a given gene of interest that significantly impaired NS1 secretion, COPA, COPB2, COPG1, and DNM1 were considered validated as human host genes that are involved in NS1-NLuc secretion.

It is noteworthy that the majority of the genes identified as potential hits in our original siRNA screen did not meet the hit selection criteria in the deconvolution siRNA screen. This is despite the fact that many of these genes have been previously reported to be involved in orthoflavivirus biology, albeit in aspects of orthoflavirius replication cycles that are not directly related to NS1 secretion. While these siRNAs may represent false positives in our screen (i.e.: they do not target host factors associated with NS1 secretion), they may also represent host factors that are involved in alternative aspects of DENV biology and indirectly impact upon NS1 secretion. For example, our primary screen identified VCP as a potential hit whose depletion reduced the extracellular accumulation of NS1. However, similar reductions in the intracellular abundance of NS1 were also observed. Individual siRNAs targeting VCP in the deconvolution screen also produced similar, albeit weaker, intracellular and extracellular NS1-reduced phenotypes. VCP is an ATPase that has been shown to play a key role in the biogenesis and maintenance of DENV replication organelles [395], and the pharmacological inhibition of this host factor results in reduced viral RNA replication and infectious virus production for multiple orthoflavivirus species [394]. While our results indicate that the accumulation of extracellular NS1 was reduced in VCP siRNA-treated cells, in considering the accompanied reduction of intracellular NS1, this more likely represents a consequence of reduced viral RNA replication and/or protein synthesis rather than a direct effect on NS1 secretion. As such, for the aim of identifying host cell factors associated with NS1 secretion, VCP likely represents a false hit. However, this supports the utility of the DENV2-NS1-NLuc reporter virus as a valuable tool that can be harnessed to interrogate host factors that critically impact DENV infection. In this context, further examination of our customised membrane-trafficking siRNA screen data revealed that the HERPUD1 siRNA pool reduced both intracellular and extracellular NS1-NLuc luciferase levels to ~75% of the NTC, suggesting that this gene may act in a pathway that favours DENV infection. Indeed, HERPUD1 has been identified as an interacting partner of DENV2 NS4B [384], a viral protein that plays essential roles in viral replication [140]. Conversely, several of our siRNA pools (e.g.: IP6K3, CDC42, CBLB, ARPC5, RAB3D, EPN3, PDCD6IP) enhanced the intracellular and extracellular accumulation of NS1-NLuc levels by ~50% and ~25% of the corresponding NTC levels,

respectively, suggesting that these genes may be involved in pathways that limit DENV infection. Of course, any interpretation of this screens' data must be considered within the parameters of the screen strategy (e.g.: targeted membrane-trafficking siRNA treatment of cells post-infection). Clearly, harnessing the DENV2-NS1-NLuc reporter virus to further interrogate DENV2 biology using alternative functional genomics and/or chemical compound screens would be invaluable.

The identification of DNM1 as a determinant of NS1 secretion is also intriguing. Three dynamin genes are encoded within the mammalian genome (DNM1-3) with high homology but differing tissue-specific expression patterns [423], and all were targeted in our membrane-trafficking siRNA screen (Figure 3.04). The protein products of these genes share ~80% homology and perform similar functions, primarily in regulating clathrin-mediated endocytosis [396]. Given that the best categorised role of dynamins is in clathrin-mediated endocytosis [424], it is difficult to reconcile how the siRNA-mediated depletion of DNM1 leads to an apparent reduction in NS1 secretion. Moreover, in non-neuronal cells DNM1 protein is largely maintained in an inactive state mediated by glycogen synthase kinase-3β (GSK3β)-dependent phosphorylation [425]. Interestingly, GSK-3β has recently been revealed as playing an essential role in DENV sNS1-mediated endothelial hyperpermeability *in vitro* and vascular leak *in vivo* [275]. Thus, exploring the role of DNM1, and the potential connection between DNM1 and GSK-3β, in sNS1 biology is warranted. Also interestingly, while dynamin isoforms share similar functions, they also perform non-redundant roles in clathrin-mediated endocytosis in non-neuronal cells [424], and the results of our siRNA screen may reflect this. While cells treated with siRNAs targeting DNM1 reduced the extracellular accumulation of NS1-NLuc, this was not observed with the other DNM isoforms. On the contrary, cells treated with siRNA pools targeting DNM2 or DNM3 displayed increased abundances of intracellular NS1-NLuc (138% and 126% of NTC, respectively, and both ≥1 SD above the mean of the NTC) and extracellular NS1-NLuc (17% and 13% of NTC, respectively). Importantly, a previous study has shown that dynamins are involved in sNS1 internalisation. Using a pool of siRNAs that target both DNM1 and DNM2, Wang *et al*. demonstrated that the silencing of these genes in human endothelial cells prevents sNS1 internalisation and sNS1-mediated EGL disruption [219]. This information reinforces an important point that is crucial to the interpretation of the results of our screens. For our siRNA screen that measures intracellular and secreted NS1-NLuc in cell culture lysates and supernatants, respectively, it is important to consider the localization, traffic and roles of the various subpopulations of NS1. NS1 is synthesised in the ER and trafficked to multiple destinations: intracellular NS1 is largely associated with the viral replication complexes; GPI-anchored NS1 is plasma membrane-bound and cell-surface-exposed; NS1 is secreted into the extracellular milieu; secreted NS1 (sNS1) can also bind and internalise into cells, with cell surface binding and internalisation shown to be two distinct processes [219]. Our NS1-NLuc-containing cell culture lysates would be expected to include intracellular (non-secreted) NS1, GPI-anchored NS1, cell-surface-bound sNS1, and internalised

sNS1. Our supernatants would be expected to only contain freely circulating sNS1 and potentially intracellular NS1 released by virus-induced cell death, although data provided in Chapter 4 indicates that virus-induced cell death does not result in the accumulation of extracellular NS1 that is detectable by quantitative Western blotting. As such, the treatment of cells with siRNAs that impact any of these processes would influence our results. Given that cells treated with siRNAs targeting DNM2 or DNM3 displayed increased intracellular and extracellular NS1-NLuc levels relative to the NTC, it cannot be ruled out that siRNA-induced knockdown of DNM2 or DNM3 leads to enhanced NS1-NLuc expression or stability. However, it is also possible that these results reflect the role of DNM2 and DNM3 in the internalisation of sNS1. Conceivably, the treatment of cells with siRNAs that allow cell surface binding but prevent the internalisation of sNS1 may display: (i) increased levels of intracellular NS1-NLuc, existing as cell-surface-bound but not internalized; and (ii) increased extracellular levels of sNS1, given the reduced ability of sNS1 internalisation. Thus, our results may further substantiate DNM2, and now implicate DNM3, has playing a pivotal role in the internalisation of sNS1. Given the intriguing results obtained here for DNM1-3, further exploration of the roles of dynamin isoforms in sNS1 biology and sNS1-mediated pathology is justified.

The prominent feature of the siRNA screen results was the high confidence identification of COPI components as important determinants of NS1 secretion. Specifically, our screen identified COPA, COPB2, and COPG1 as the top-ranking hits. Each of the siRNA treatments targeting these COPI components resulted in increased or unaffected intracellular abundances of NS1-NLuc and reduced extracellular abundances of NS1-NLuc. This resulted in a large reduction in the NS1-NLuc secretion ratios, indicating that NS1-NLuc secretion efficiency was severely impeded by COPI component siRNA treatment. In the deconvolution siRNA screen, multiple individual siRNAs targeting these genes induced a strong NS1-NLuc secretion efficiency-reducing phenotype, thus confirming COPA, COPB2, and COPG1 as important determinants of NS1-NLuc secretion. Given that several genes that encode components of the multi-subunit COPI complex were identified as involved in the secretion of our NS1-NLuc fusion protein, we focussed our attention towards understanding COPI and validating its components, including its effector, GBF1, as critical host cellular factors involved in NS1 secretion.

COPI is a highly conserved protein complex that coats transport vesicles that shuttle protein and lipid cargo between cellular compartments. The complex consists of seven coatomer subunits [426]. Mechanistically, COPI vesicle formation requires GBF1-catalysed hydrolysis of GDP for GTP on ADP-ribosylation factors (ARF) [403, 427]. Activated ARFs then recruit preassembled cytosolic heptameric COPI complexes to a donor membrane [428]. The continued recruitment of COPI complexes to the nascent vesicle results in membrane destabilisation and ultimately culminates in

vesicle scission [429]. The newly formed COPI coated vesicle, complete with membrane bound and luminal cargo is then disseminated to its target acceptor membrane location [430]. The best categorised role of COPI coated vesicles is their involvement in the bi-directional trafficking of proteins and lipids within the early secretory pathway [334]. COPI coated vesicles function in intra-Golgi trafficking mediating anterograde and retrograde transport [336, 431]. They also mediate Golgi-to-ER recycling of escaped ER-resident proteins, thus maintaining the structural and functional integrity of these organelles [338]. Several studies have implicated COPI components as performing a role in endosomal transport and function [339-342]. More recently, COPI has been demonstrated to perform roles in a wealth of processes including lipid metabolism [343], autophagy [344], mRNA localisation [345], nuclear envelope disassembly [346], and neurogenesis [347, 348]. Regarding COPI vesicle regulators, GBF1 is well documented as being involved in multiple aspects of orthoflavivirus replication (reviewed in [370]). In addition, several ARFs have also been shown to play overlapping and redundant roles in DENV biology [57, 362]. While these components regulate COPI vesicle formation, it must be noted that they have multiple effectors [326, 432, 433]. However, given that the effects of GBF1 and ARF inhibition on orthoflavivirus biology can be phenocopied by COPI component depletion [57], this strongly suggests that COPI is involved in multiple aspects of the orthoflavivirus life cycle. Crucially, a recent study by Iglesias *et al* [57] demonstrated that DENV utilises COPI for the trafficking of capsid protein between the ER and lipid droplets, highlighting that the exploitation of COPI machinery by DENV is not limited to the canonical role of COPI in the secretory pathway. Given the diverse roles of COPI and its regulators in orthoflavivirus biology, to focus specifically on NS1 secretion while minimising pleiotropic effects, we concentrated our attention towards perturbing the COPI pathway at later stages of infection.

We confirmed the efficacy of our siRNA pools to knockdown their intended target mRNA expression using RT-qPCR. The expression of each gene of interest was substantially knockdown at 24 hours post-siRNA treatment. To confirm this was inducing a knockdown of the cognate protein, we employed indirect immunofluorescence microscopy and quantitation of cellular fluorescence intensity as a readout of COPI protein abundance. Importantly, target protein abundance was reduced in cells treated with our siRNAs. However, the level of protein knockdown was not as pronounced as the level of mRNA knockdown for any of our genes of interest. This low level of protein knockdown may be explained given that our genes of interest have been categorised as essential for optimal proliferation [406]. The largest siRNA-induced protein knockdown observed was in COPG1 silenced cells. Interestingly, COPG1 has a paralogous gene, COPG2. These paralogs share ~80% protein sequence identity, and each isoform can be incorporated into heptameric coatomer complexes. Proteomic profiling of COPI coated vesicles generated with these different isoforms has revealed that protein cargo constituents are striking similar [434], indicating that COPG1- and COPG2-dominated COPI vesicles exhibit functional redundancy. It is possible that

COPG2 compensated for the loss of COPG1 in COPG1-silenced cells. However, immunoelectron microscopy has revealed that these isoforms exhibit differential localisation patterns, with COPG1 preferentially localised to the cis-Golgi and COPG2 predominantly localising to the trans-Golgi [353], suggesting paralog-specific roles may influence COPI vesicle biology. Importantly, it has been shown that coatomer complexes are relatively stable and display a half-life of ~28 hours *in vitro* [405], thus providing an additional explanation for the moderate reductions in COPI protein abundances induced by our siRNA treatment. Other groups interrogating the impact of COPI silencing on virus biology have employed COPI siRNA treatment of cells prior to infection with varying success [57, 435]. Nonetheless, given that our aim was focussed on exploring the roles of COPI in DENV NS1 secretion, to alleviate potential consequences of COPI protein knockdown on alternative viral processes such as virus entry, genome replication, and protein synthesis, our preference was to knockdown COPI protein in a population of cells in which infection had already been established. As such, it was necessary to attempt to balance: (i) DENV-infected cell viability; (ii) timing and efficiency of COPI siRNA treatment; (iii) COPI protein knockdown levels; and (iv) viral load sufficient to obtain quantifiable intracellular and extracellular NS1 abundances. Under these constraints, we reasoned that a ~20 – 60% reduction in target protein abundance was sufficient to warrant further interrogation of COPI protein involvement in NS1 secretion using our experimental strategy.

We next assessed the impact of COPI siRNA treatment on DENV-infected Huh-7.5 cell viability and infectious DENV production. Importantly, we were able to show that Huh-7.5 cell viability was largely unaffected by COPI siRNA treatment, and that infectious DENV production was unaltered by COPI silencing. These data indicated that COPI siRNA treatment does not impair DENV RNA replication, virion assembly, or virion egress when COPI gene knockdown is applied at 4 hours post-DENV infection. This is in contrast to the results obtained by Tongmuang *et al*, who reported that the siRNA-mediated depletion of COPG1 in Huh-7 cells resulted in a 10-fold reduction in DENV production [435]. However, in addition to using a different yet related cell line, dissimilar experimental strategies were employed. Tongmuang and colleagues treated Huh-7 cells with COPG1-targeting siRNAs twice at 24 hour intervals prior to infection. In our experiments, the absence of any siRNA-mediated impact on Huh-7.5 cell viability and infectious DENV production confirms that our experimental strategy was a viable approach to interrogate the role of COPI components in NS1 secretion. Importantly, COPI component depletion resulted in a decrease in the extracellular levels of DENV NS1, coincident with increased or unchanged intracellular levels of NS1, indicating that COPI siRNA-mediated depletion impairs the efficient secretion of NS1 in DENV-infected cells. These results reflected the data acquired in the original and deconvolution siRNA screens, thus confirming that the siRNA-mediated depletion of COPI components exerts an impact on wildtype DENV NS1 secretion. Similar reductions in NS1 secretion efficiency were observed in experiments using WNV/KUNV-infected Huh-7.5 cells, indicating that the molecular mechanism exploited to achieve NS1 secretion may be a conserved feature within the Orthoflavivirus genus. While the modest levels of NS1 secretion inhibition observed here may reflect incomplete protein knockdown, these results may also reflect the possible existence

of multiple mechanisms that may be exploited by achieve NS1 secretion from human cells. However, further studies are required to definitively determine whether COPI machinery is essential for NS1 secretion or whether alternative pathways contribute. Taken together, these validation studies confirmed that COPI components are important determinants of NS1 secretion in orthoflavivirus-infected mammalian cells.

To confirm the role of COPI components in NS1 secretion using an siRNA-independent approach, we attempted to completely ablate expression of our genes of interest at the DNA level by employing CRISPR-Cas9 technology. Through analysing genetic modifications at the DNA level using TIDE, and quantifying target protein abundance by indirect immunofluorescence microscopy, we determined that the genome editing efficiency and protein knockout outcomes of our CRISPR-Cas9 experiments failed to generate cells that were completely deficient in COPI target protein. This result was consistent with previous studies that similarly failed to generate knockout cell lines that were completely deficient in COPI subunits [436]. Further, these results were not unexpected given that our genes of interest have been defined as ‘essential for optimal proliferation’ [406]. Considering their essential roles in maintaining the structure and function of the Golgi apparatus and the ER [338, 376], two organelles of critical importance to eukaryotic cells, our inability to knockout these genes using CRISPR technology is not surprising. While some groups have attempted to generate short-term, inducible COPI component knockout polyclonal cell lines for immediate experimental analysis [437], given the largely unaffected levels of COPI component protein that we observed in our CRISPR-Cas9-treated cells, we sought to identify an alternative strategy to perturb the COPI pathway. To circumvent the lethality imposed by essential gene knockout, we explored the use of a small panel of recently identified loss-of-function COPI SNP variants. At the molecular level, these rare genetic variants can impart COPI trafficking defects [410, 412, 438]. Interestingly and perhaps coincidentally, these pathogenic variants manifest disease phenotypes that are strikingly similar to orthoflavivirus-associated pathologies [411, 412, 439]. By overexpressing wildtype or deleterious COPI alleles in cells co-transfected with a T7 RNA polymerase-driven replication-independent DENV NS1-5 expression vector, we were able to assess the impact of COPI perturbation on NS1 secretion independently from genome replication and infectious virus production. Cells transfected with the wildtype COPB2 variant expression plasmid displayed a two-fold increase in NS1 secretion, suggesting that the availability of COPB2, but not COPA nor COPG1, protein may represent a bottleneck and be a limiting factor in DENV NS1 secretion. Surprisingly, the overexpression of the dominant-negative COPA-E241K variant also increased NS1 secretion efficiency. This COPA variant contains a mutation within the WD40 domain that causes deficiencies in Golgi-to-ER trafficking and leads to increases in ER stress [410, 439]. Whether the observed two-fold increase in NS1 secretion is a direct effect of COPA-E241K expression remains unclear. It is possible that NS1 secretion may be favoured under conditions of enhanced ER stress induced by COPA-E241K

expression. Alternatively, it is also possible that NS1 secretion is achieved via a non-canonical COPI function whereby the WD40 domain may be dispensable or inhibitory to NS1 secretion. Further investigation of how the overexpression of the COPA-E241K variant enhances NS1 secretion is warranted. Similarly to COPA-E241K, COPB2-R254C and COPG1-K652E have also been shown to induce defects in Golgi-to-ER trafficking and aberrant cellular responses. However, these allelic variants are not dominant-negative and as such their ectopic expression in the wildtype Huh-7.5 background may have masked any potential impact on NS1 secretion. Despite our inability to generate COPI component knockout cell lines by CRISPR-Cas9 technology, the use of genome editing to introduce these SNPs in the place of wildtype genes in Huh-7.5 cells presents an attractive approach to explore the emerging roles of COPI in orthoflavivirus biology. Moreover, given the impact of overexpression of COPA-E241K on enhancing NS1 secretion observed here, it would be interesting the assess the impact of this mutation on alternate aspects of DENV biology including infectious virus production.

As an additional and alternative mechanism to perturb the COPI pathway, we functionally inhibited COPI vesicle formation using the small molecule inhibitor Golgicide A (GCA). This compound is routinely utilised to study secretory pathway trafficking and COPI function given its potent and specific inhibition of GBF1. Moreover, GCA is frequently employed to study virus biology, thus making GCA well-suited to our aim of interrogating the role of COPI in DENV NS1 secretion. While it is well documented that GCA mediates a variety of impacts on orthoflavivirus biology [370], most studies have employed this compound at the early stages of infection. Here, we functionally inhibited GBF1 using GCA at a later stage of infection and found that GCA reduced infectious DENV production in a dose-dependent manner. Consistent with a GCA-mediated defect in infectious virus assembly and release, a concomitant increase in the intracellular abundance of DENV viral RNA was also observed. Using a DENV subgenomic replicon to study the impact of GCA-mediated GBF1 inhibition on DENV RNA replication, we found that DENV genome replication levels were unaffected by the addition of GCA at the concentrations employed. Collectively, these results confirm that GCA acts to inhibit the assembly and/or release of infectious DENV virions. Interestingly, despite a dose-dependent reduction in infectious DENV production, both DENV and WNV/KUNV NS1 secretion was observed to be reduced only at the highest GCA dose applied. Indeed, this confirms that GCA-mediated GBF1 inhibition can act to reduce orthoflavivirus NS1 secretion. Importantly, our results indicate that infectious DENV production is more sensitive than NS1 secretion to the impact of GCA-mediated GBF1 inhibition. These data further support the conclusion that multiple mechanisms may be exploited by DENV to achieve NS1 secretion from human cells.

Given the importance of the viral virulence factor NS1, many genetic, biochemical and imaging studies have been performed to interrogate NS1 secretion biology. While these studies have been integral to defining sNS1 structure and key functional residues that are critical to its secretion, major gaps exist in our understanding of how NS1 secretion is achieved from infected mammalian cells. The dogmatic view of NS1 secretion from mammalian cells centres around the canonical secretion pathway [52]. Specifically, this model stated that NS1 is translated into the ER as a soluble monomer and becomes glycosylated by the addition of high-mannose moieties at N130 and N207 [90, 91, 178, 213]. Newly synthesised NS1 monomers rapidly homodimerize to form partially hydrophobic membrane-associated NS1 dimers, the predominant intracellular NS1 form [90, 91]. It has been suggested that secretion-destined membrane-associated NS1 dimers preferentially localise to the sites of nascent lipid droplets on the luminal side of the ER [99], or to cholesterol-rich microdomains within the Golgi [95, 230]. This has been proposed as a mechanism to concentrate secretion-destined NS1 dimers, with three dimers coming together to pinch off from the membrane, converting them into a small soluble NS1 hexamer and collecting the lipid component that fills the hexamers central channel [99]. While not a strict prerequisite to achieve NS1 secretion [213, 218, 440], the secreted form of NS1 possesses a complex-type glycan at N130 [213]. It is assumed that the additional processing of the N130 glycan occurs following ER-to-Golgi translocation given that, in uninfected cells, the machinery responsible for this maturation resides in the Golgi [90]. It is important to note, however, that orthoflaviviruses dramatically and extensively remodel the intracellular secretory pathway architecture [173, 441, 442], and hijack and re-localise a multitude of host proteins [384, 385, 443], including inducing the redistribution of key components of glycosylation machinery [444]. Accordingly, uninfected cells are not representative of DENV-infected or NS1-expressing cells. Nonetheless, following its passage through the Golgi, secretion-destined NS1 is thought to then traffic from the trans-Golgi network to the plasma membrane where it is secreted from the cell as a hexameric glycolipoprotein [52, 445]. The present study confirms COPI components as important determinants of DENV and WNV/KUNV NS1 secretion and this is compatible with the hypothesis that NS1 is secreted from infected mammalian cells via the canonical secretion pathway. However, the results of our GCA experiments are particularly intriguing. It is well established that DENV virions mature as they traffic through the secretory pathway prior to being released from the cell as fully infectious virions. Analogously, secretion-destined NS1 is believed to be matured in the Golgi as it traffics through the secretory pathway prior to being released from the cell. While the relatively low concentrations of GCA employed in our study revealed a dose-dependent reduction in infectious DENV production, NS1 secretion was only observed to be inhibited at the highest dose applied (5 μM). Furthermore, while 5 μM GCA induced a dramatic decrease in NS1 secretion, our confocal microscopy analyses revealed that there was no significant impact of GCA on NS1 and Golgi marker GM130 co-localisation. Given the additional and emerging roles of COPI beyond intra-Golgi and Golgi-to-ER trafficking, coupled with the recent demonstration the DENV exploits a non-canonical role of COPI for trafficking capsid protein, alternative roles of COPI involvement in NS1 certainly

warrant consideration. Potential sites of COPI involvement in NS1 secretion are shown in Figure 3.18. Future studies further interrogating the contribution that COPI coated vesicles, their activators, and their vesicle constituents play in orthoflavivirus NS1 secretion will be integral to defining the role(s) of COPI in NS1 secretion and may provide additional targets for NS1-specific anti-orthoflaviviral therapies.

3.4: Conclusion

The aim of this Chapter was to identify and interrogate human host cellular factors that are associated with DENV NS1 secretion. Using an siRNA screen approach, we have identified components of the COPI complex as important human host cellular factors that are involved in DENV NS1 secretion. Using additional genetic and pharmacological approaches, we have demonstrated the importance of the COPI machinery in NS1 secretion by DENV and the closely related Australian-endemic WNV/KUNV. The identification of COPI components as important determinants of NS1 secretion may aid in the identification of novel targets for anti-orthoflaviviral therapies.

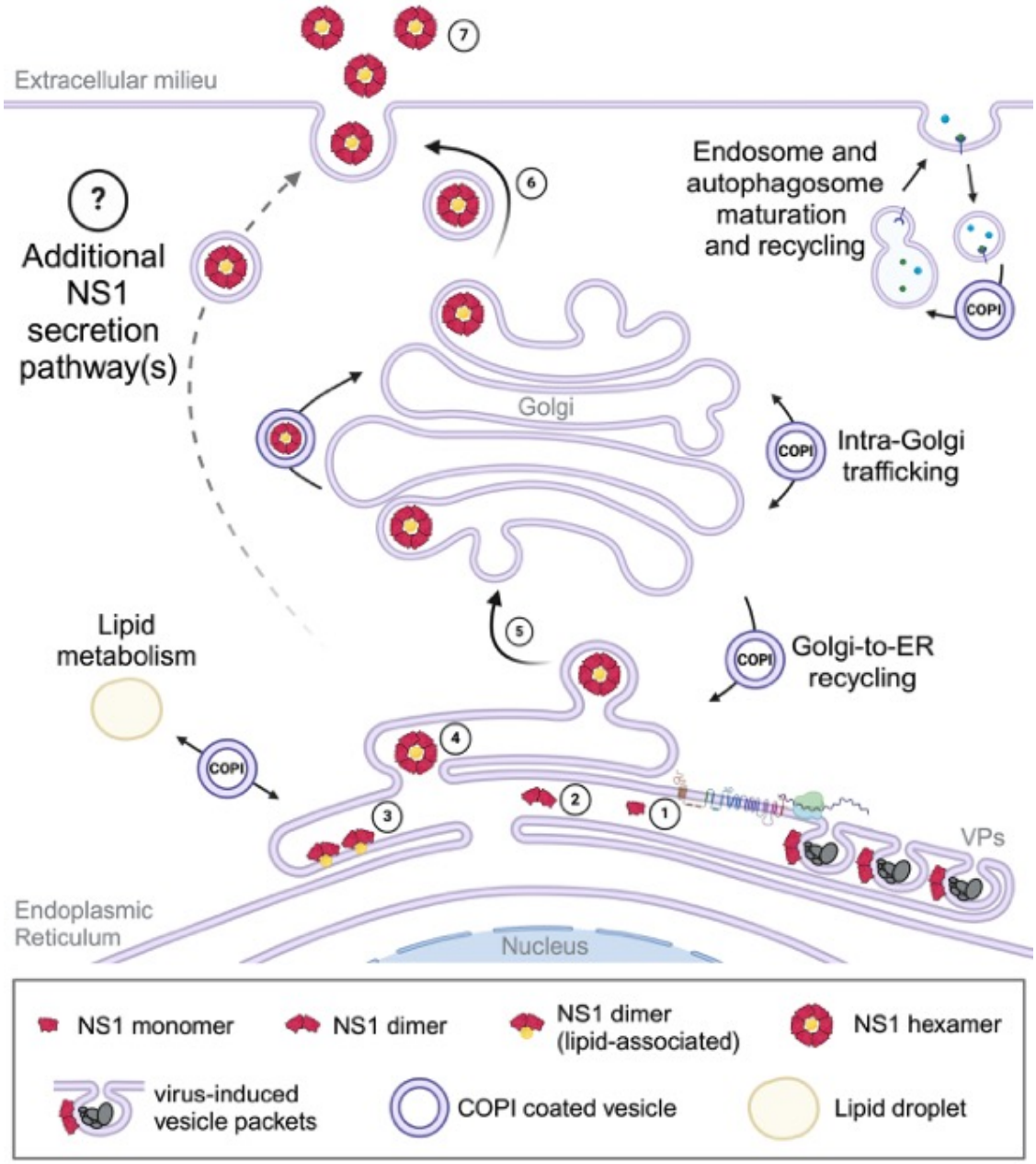

FIGURE 3.17. Potential sites of COPI involvement in DENV NS1 secretion. (1) DENV NS1 is translated into the ER as a soluble monomer and modified by the addition of high-mannose glycans at N130 and N207. (2) Soluble monomers rapidly homodimerize to form a partially hydrophobic and membrane-associated dimer, the predominant intracellular NS1 form that plays a critical role in viral genome replication (vesicle packet (VPs). (3) Membrane-associated NS1 dimers are proposed to concentrate at sites of nascent lipid droplets within the ER or cholesterol-rich microdomains within the Golgi. (4) Three membrane-associated dimers come together and pinch off from the membrane to form a soluble NS1 hexamer that is stabilised by a central lipid component. (5) Secretion-destined NS1 is proposed to traffic from the ER to the Golgi for additional processing of the N130 moiety to a complex-type glycan. (6) NS1 is proposed to be dispatched from the trans-Golgi network to the plasma membrane where it is released into the extracellular environment. (7) Secreted NS1 promotes viral propagation and contributes to dengue disease pathogenesis through a variety of pathways. Potential sites of COPI participation in NS1 secretion are shown (see Discussion). Created with BioRender.

Chapter 4

Identifying human host cell factors associated with DENV sNS1 internalisation

4.1: Introduction

The secreted form of orthoflavivirus NS1 can bind and internalise into a variety of host cell types [208, 209], and these processes elicit important biological impacts for both the virus and the host. DENV sNS1 is efficiently endocytosed by human hepatocyte-derived cells, and the pretreatment of cells with sNS1 prior to DENV infection leads to enhanced endocytic activity and increased cellular susceptibility to infection [277]. Similarly, sNS1 is endocytosed by human monocyte-derived dendritic cells (mo-DC) and the pretreatment of mo-DCs with sNS1 results in a greater proportion of infected cells following DENV inoculation [269]. In murine macrophages, sNS1 has been shown to induce the accumulation of lipid rafts in the plasma membrane facilitating DENV attachment [226]. This sNS1-induced enhancement of DENV infection is not a phenomenon limited to cells of mammalian origin; sNS1 has been shown to be efficiently endocytosed by mosquito cells, and significant increases in infectious DENV production are seen in mosquito cells following sNS1 pretreatment [233]. Hence, the interaction of sNS1 with uninfected DENV-target cells exerts an effect that acts to promote DENV infection. In the extracellular environment, sNS1 has been shown to bind a variety of complement proteins, and these interactions can trigger both protective and pathogenic effects [207]. sNS1 can bind with the complement regulatory plasma protein C4BP. This interaction has been shown to recruit the sNS1-C4BP complex to the surface of host cells to attenuate complement activation, thus facilitating immune evasion [257]. The binding of highly purified sNS1 to TLR4 on mouse bone marrow-derived macrophages and human peripheral blood mononuclear cells potently induces the transcription of proinflammatory cytokines [210]. This interaction between sNS1 and TLR4 contributes to the dysregulation of proinflammatory cytokines that can act to alter endothelial cell permeability and contribute to vascular leakage – a key symptom of severe dengue disease. In the extracellular environment, sNS1 forms high-affinity interactions with high-density lipoproteins (HDL). This sNS1-HDL complex triggers the production of proinflammatory cytokine production in macrophages to a greater extent than sNS1 or HDL alone [227]. Clearly, the interactions between sNS1 and extracellular host factors adds a layer of complexity to sNS1-host cell interactions, through which sNS1 can contribute to dengue disease. The molecular mechanism for this sNS1-HDL complex-induced host cell response remains to be defined, thus highlighting the importance of defining sNS1-host cell interactions. Additionally, the binding and internalisation of orthoflavivirus sNS1 by lineage-specific endothelial cells directly contributes to endothelial cell hyperpermeability and vascular leakage in a manner that reflects disease tropism [208]. Here, the sNS1-induced activation of endothelial cell enzymes, including heparinases and sialidases, results in cleavage of components of the endothelial glycocalyx layer and endothelial cell adherens junctions, thus disrupting endothelial cell barrier integrity. [211, 275]. Critically, this ability of sNS1 to directly induce endothelial barrier dysfunction and vascular leakage has been demonstrated to be dependent upon the internalisation of sNS1 [219].

Given the importance of sNS1 binding and internalisation into host cells, several studies have been performed to interrogate these processes. As described previously (see Introduction section 1.9 & 1.10), the near-ubiquitously expressed glycosaminoglycans, heparin sulfate and chondroitin sulfate E, can act as attachment factors to facilitate sNS1 host cell interactions [209]. In addition to TLR4 [210, 265], it was recently demonstrated that sNS1 can directly interact with the host cell-surface exposed HDL receptor, scavenger receptor class B type1 (SRB1) [233]. Given the confirmed interaction between sNS1 and HDL [227], it is possible that complexes formed between sNS1 and host factors in the extracellular environment may greatly enhance the repertoire of receptors that sNS1 can exploit to facilitate sNS1-host cell binding and internalisation. Endocytosis of sNS1 has been shown to occur in a clathrin- and dynamin-dependent manner [219]. Following internalisation, sNS1 first co-localises with markers of the early endosome (EEA1 and Rab5) [219], and then markers of the late endosome (Rab7, and LBPA) [270, 277]. Interestingly, the stability of internalised sNS1 appears to be cell type-dependent. Using immunofluorescence confocal microscopy to examine the intracellular distribution of internalised sNS1 in lung and brain endothelial cells briefly exposed to sNS1, Wang *et al* revealed intracellular sNS1 signal was greatest at 15 minutes post-inoculation and lost within 3 hours, suggesting internalised sNS1 may be degraded in these cell types [219]. However, in umbilical vein endothelial cells inoculated with sNS1, intracellular sNS1 signal was shown to steadily accumulate with time until at least 6 hours post-inoculation, with sNS1 puncta converging into larger aggregates [270]. Interestingly, in cell lines derived from human hepatocytes, a major target of sNS1 *in vivo* [277], internalised sNS1 was shown to be stable for at least 48 hours [277]. While these studies have provided much insight into the sNS1 binding and internalisation process, a more complete picture of the human host factors involved in sNS1 binding and internalisation is required.

The aim of this chapter was to generate a more comprehensive profile of the human host proteins that are associated with the early events of sNS1 internalisation. To achieve this aim we employed the engineered plant peroxidase, APEX2, that functions as a labelling enzyme that allows spatially-resolved proteomic mapping in live cells [446]. A schematic overview of APEX2-based proximity labelling in live cells is shown in Figure 4.01. Here, APEX2 is fused to a protein of interest and expressed within cells. These cells can then be treated with biotin-phenol and, in the presence of hydrogen peroxide, APEX2 generates short lived biotin-phenoxyl radicals which can covalently tag proximal proteins within a ~20 nm radius. These biotinylated proteins can then be enriched by streptavidin-based affinity purification and identified by mass spectrometry. Given that our protein of interest is sNS1, we employed our previously developed DENV2-NS1-APEX2 virus that contains APEX2 embedded within NS1 (Figure 4.02A) [94]. This DENV2-NS1-APEX2 virus has previously been characterised in the human hepatocyte-derived Huh-7.5 cell line [94]. Despite containing the APEX2 tag within NS1, when expressed intracellularly the NS1-APEX2 fusion protein displays wildtype-like NS1 localisation patterns (Figure 4.02B). This DENV2-NS1-APEX2 variant is infectious, albeit highly attenuated (Figure 4.02C). Importantly, similarly to wildtype NS1, the NS1-APEX2 fusion

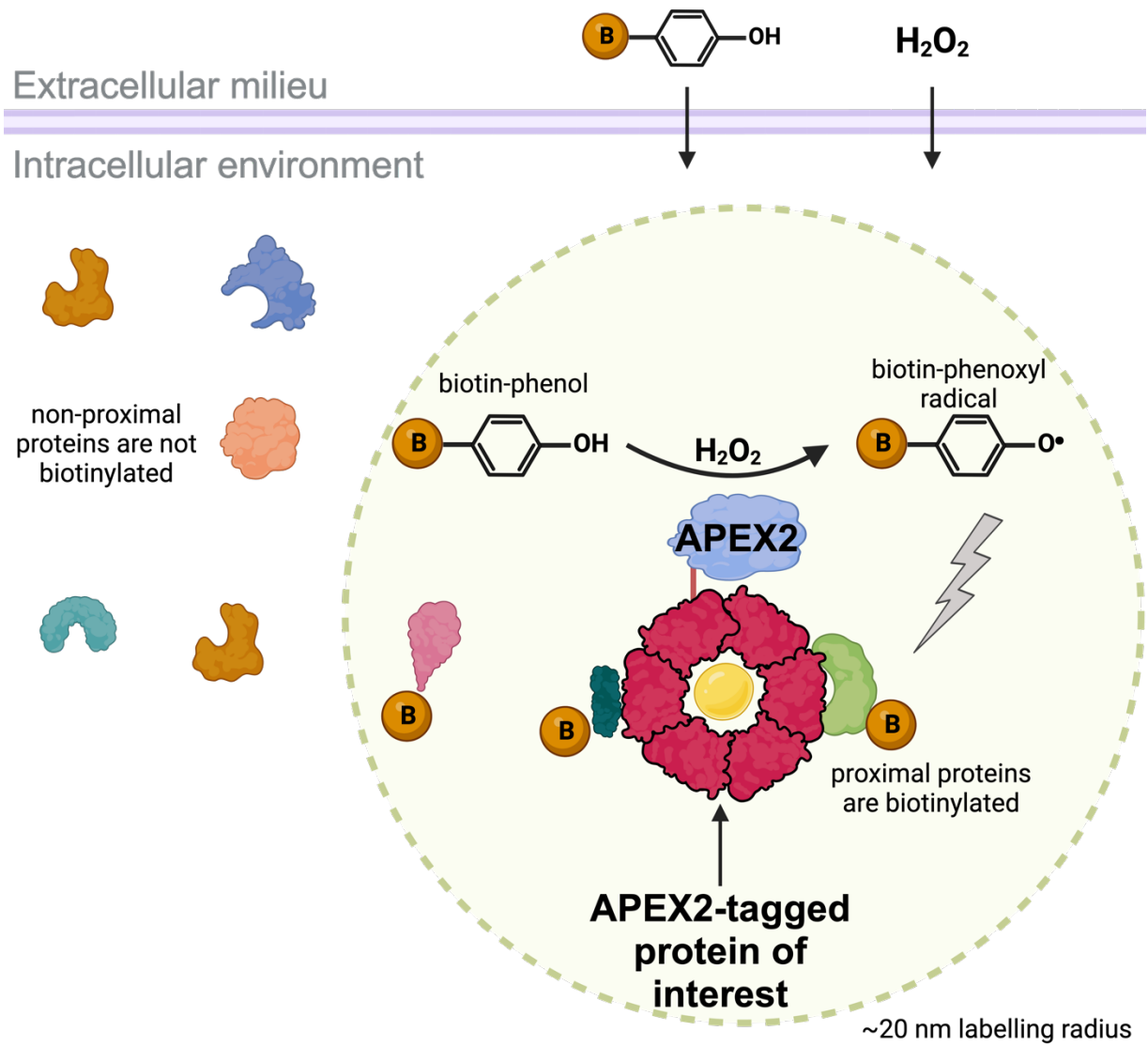

FIGURE 4.01. APEX2 proximity-based labelling allows the spatial and temporal mapping of protein networks within live cells. A protein of interest is genetically fused to the next-generation plant-based peroxidase, APEX2. A cell containing the APEX2-tagged protein of interest is provided with biotin-phenol and H_2O_2 substrates. In the presence of H_2O_2, APEX2 catalyses the oxidation of biotin-phenol to short-lived biotin-phenoxyl radicals. The localised release of these biotin-phenoxyl radicals react with electron-dense amino acids in proteins within close proximity (~20 nm diameter) provides spatial resolution as only proteins within the immediately proximal environment become biotinylated. The rapid labelling kinetics (~1 minute) provides temporal resolution. As tagged proteins are biotinylated, they can be recovered by affinity purification using streptavidin-coated beads and identified by mass spectrometry. Created in BioRender (https://BioRender.com).

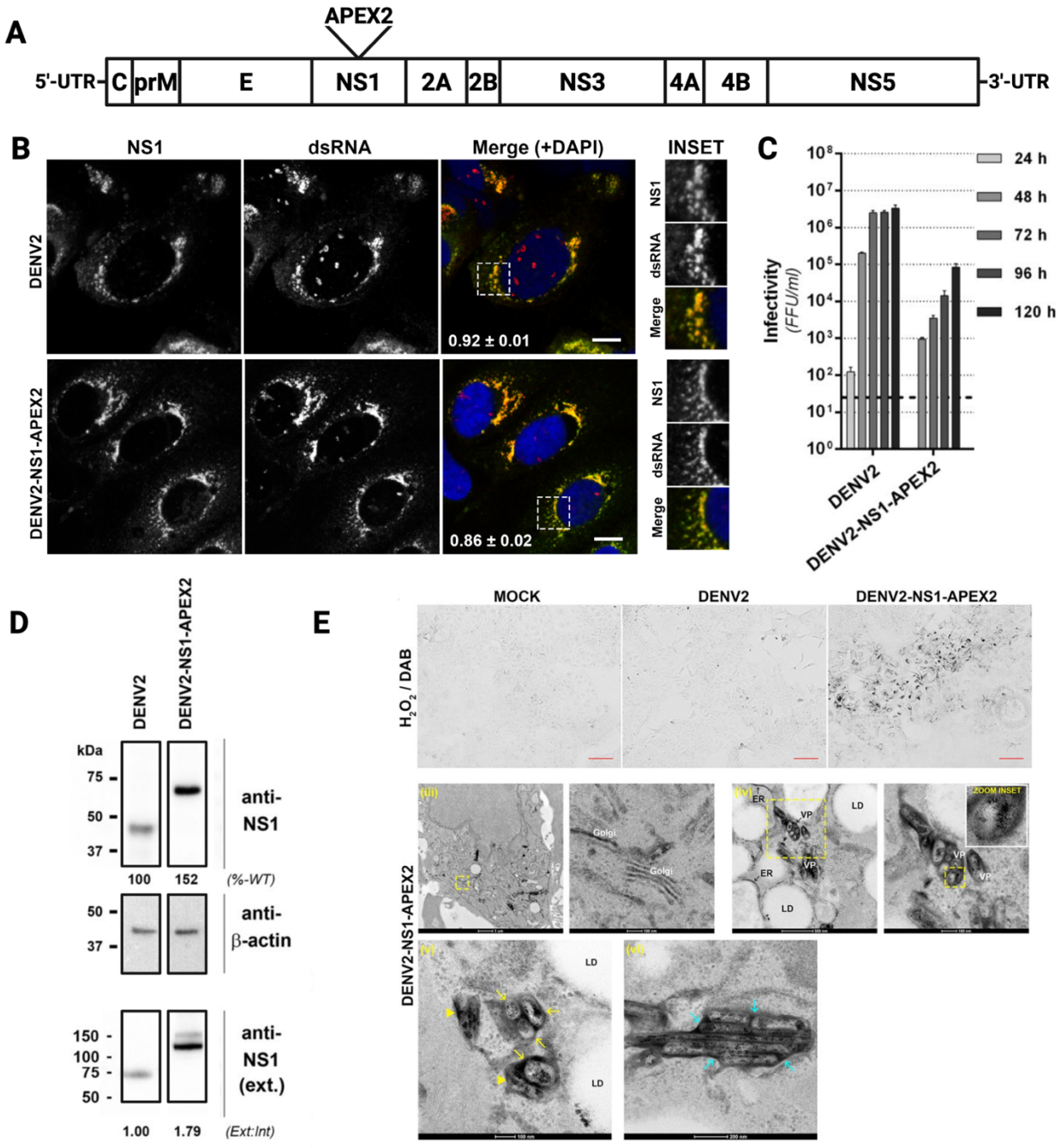

FIGURE 4.02. DENV2-NS1-APEX2 virus has been fully characterised. (A) DENV2 (16681) was modified by the insertion of the APEX2 gene (783 nt) within NS1 between Lys-174 and Gln-175. To assess the impact of the APEX2 insertion on various aspects of DENV2 and NS1 biology, Huh-7.5 cells were electroporated with *in vitro* transcribed DENV2 or DENV—NS1-APEX2 RNA and cultured for 4 days. (B) NS1-APEX2 fusion protein localisation with respect to dsRNA is unaltered by the APEX2 insertion. (C) DENV2-NS1-APEX2 is infectious but appreciably attenuated. (D) Western blot analysis confirms intracellular and extracellular NS1-APEX2 is readily detected by the anti-NS1 MAb 4G4 under nonreducing and nondenaturing conditions, indicating that the fusion protein retains the native epitope conformation that is recognised by 4G4 and contains the expected increase in molecular weight (~28 kDa). (E) NS1-APEX2 allows high-resolution electron microscopy analyses of NS1 localisation within infected cells. Adapted from Eyre *et al.* 2017.

protein is efficiently secreted from infected cells into cell culture supernatants (Figure 4.02D). Additionally, despite being embedded within NS1, the APEX2 tag is functionally active and has been demonstrated to have practical applications in electron microscopy, allowing high-resolution imaging of intracellular NS1 (Figure 4.02E). Given that this DENV2-NS1-APEX2 strain produces a secreted NS1-APEX2 (sNS1-APEX2) fusion protein, this resource could be employed for spatially and temporally resolved proteomic mapping to identify human host factors that are involved in sNS1 internalisation. Figure 4.03 provides a schematic overview of this experimental strategy. Briefly, Huh-7.5 cells are transfected with infectious *in vitro* transcribed DENV2-NS1-APEX2 RNA. sNS1-APEX2 can then be recovered from infected cell culture supernatant. This sNS1-APEX2-containing cell culture supernatant can then be inoculated onto naïve Huh-7.5 cells to allow sNS1-directed binding and internalisation. These cells can then be treated with biotin-phenol and hydrogen peroxide reagents to allow APEX2-catalysed biotinylation of sNS1-APEX2 proximal proteins. Whole cell lysates can then be prepared and employed for enrichment of biotinylated proteins using streptavidin-coated magnetic beads and identification by mass spectrometry.

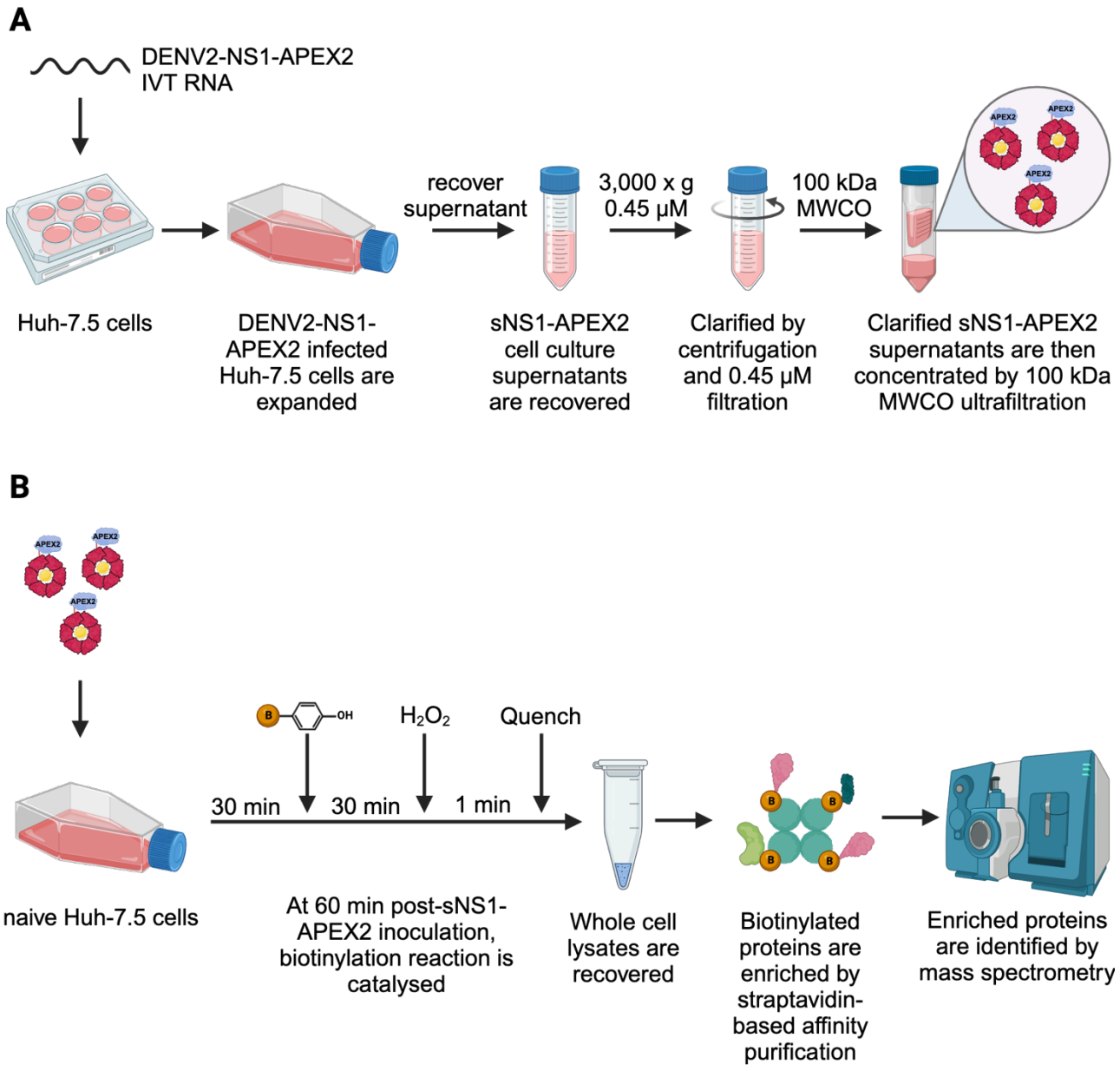

FIGURE 4.03. Schematic overview of the APEX2-based proximity labelling of sNS1 proximal proteins following internalisation into Huh-7.5 cells. (A) sNS1-APEX2 is recovered from DENV2-NS1-APEX2 transfected Huh-7.5 cell culture supernatants. (B) The sNS1-APEX2-containing cell culture supernatants is inoculated onto naïve Huh-7.5 cells to allow sNS1 binding and internalisation. At 30 minutes post-inoculation, inoculum is replaced by biotin-phenol supplemented cell culture media and incubated for 30 minutes. At 60 minutes post-inoculation, H2O2 is added to the culture to catalyse the biotinylation of sNS1-APEX2 proximal host proteins. The labelling reaction is stopped after 1 minute by the addition of quenching reagents. Cell culture monolayers are then lysed. Whole cell lysates are enriched for biotinylated proteins using magnetic streptavidin beads. Digested peptides are then identified by mass spectrometry. Created in BioRender (https://BioRender.com).

4.2: Results

4.2.1: Assessing the impact of the APEX2 tag on sNS1 internalisation

As described above, the NS1-APEX2 fusion protein displays wildtype-like intracellular NS1 localisation and is secreted from DENV2-NS1-APEX2 transfected cells, indicating that the APEX2 tag does not exert a major impact on NS1. However, to confirm that there are no major APEX2 tag-associated defects on sNS1-APEX2 internalisation, we assessed the impact of the APEX2 tag on sNS1 internalisation by confocal immunofluorescence microscopy.

First to generate sNS1-APEX2, Huh-7.5 cells were transfected with *in vitro* transcribed DENV2-NS1-APEX2 RNA. sNS1-APEX2-containing cell culture supernatant was then collected, clarified by centrifugation and filtered using a 0.45 μM filter. Naïve Huh-7.5 cells were inoculated with this clarified sNS1-APEX2 cell culture supernatant and incubated for 6 hours at 37°C in a humidified 5% CO_2 incubator to allow sNS1 binding and internalisation. As an sNS1 negative control, naïve Huh-7.5 cells were mock inoculated with fresh DMEM in parallel. At 6 hours post-inoculation, cells were extensively washed, fixed using 4% PFA, permeabilised using 0.1%(v/v) Triton X-100, and processed for indirect immunofluorescent labelling of internalised sNS1 in a manner consistent with the method employed by Alcala *et al* [233]. NS1 was labelled using mouse anti-NS1 (4G4) primary antibody followed by AlexaFluor 555-conjugated anti-mouse IgG, and cells were counterstained with DAPI. As additional controls to enable discrimination of NS1-specific immunolabelling, sNS1-APEX2 and mock inoculated cells were processed by omitting the anti-NS1 primary antibody. Confocal fluorescence microscopy revealed specific staining of NS1 that was unique to sNS1-APEX2 inoculated cells that were processed with anti-NS1 antibody (Figure 4.04). In addition to diffuse NS1 staining patterns throughout the cytoplasm, discreet punctate structures were also observed. Of note, intensely stained very large punctate structures were observed in the perinuclear region with nuclear deformations apparent. Collectively, these data provide evidence that indicates that sNS1-APEX2 is internalised by Huh-7.5 cells, suggesting that the APEX2 tag does not impact sNS1 internalisation.

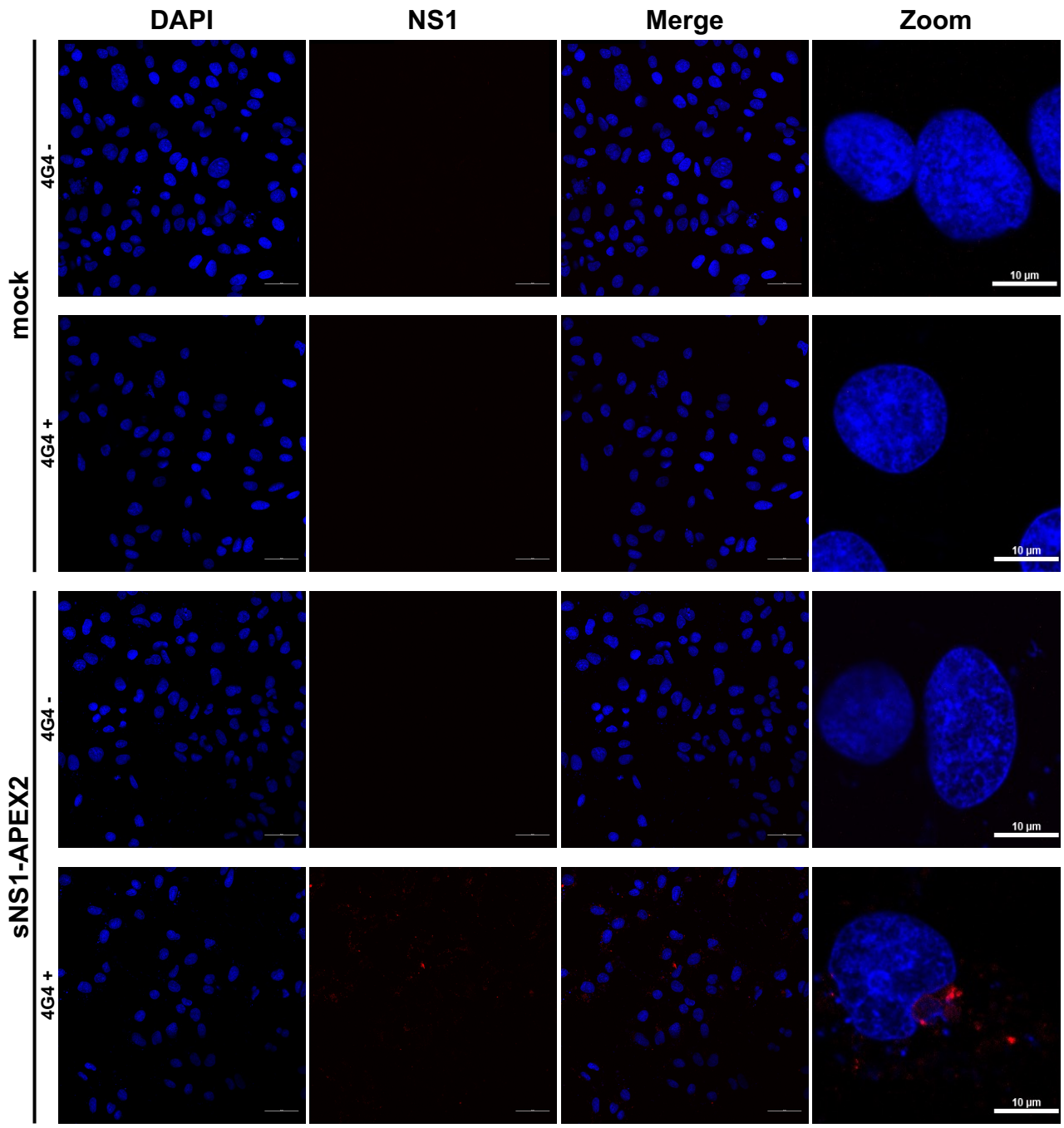

FIGURE 4.04. sNS1-APEX2 is internalised by Huh-7.5 cells. Huh-7.5 cells were inoculated with sNS1-APEX2-containing cell culture supernatants. At 6 hours post-internalisation, cells were extensively washed, fixed in 4% PFA, and permeabilised using triton-X. Cells were then stained for indirect immunofluorescent labelling using mouse anti-NS1 followed by Alexa-Fluor 555-conjugated anti-mouse IgG (red) and counter stained with DAPI. To discriminate NS1-specific labelling, sNS1-APEX2 inoculated and mock inoculated cells were stained by omitting the anti-NS1 primary antibody. Samples were then imaged using confocal fluorescence microscopy. Scale bars are 10 µM.

4.2.2: Optimising the yield of secreted NS1-APEX2 fusion protein

Our confocal immunofluorescence data indicated that sNS1-APEX2 is internalised into Huh-7.5 cells. However, the level of NS1 staining that was observed was substantially lower than that observed in other sNS1 internalisation studies that employed highly purified sNS1 (see: [233, 277]). Importantly, while the APEX2 protein has been genetically engineered to display increased sensitivity over its APEX predecessor, one of the major limitations of APEX2-catalysed proximity labelling in live cells is that low expression or low abundance of the APEX2-tagged protein of interest can lead to undetectable biotinylation activity [446]. Given these concerns, several strategies were designed to attempt to enhance the production, recovery, and concentration of sNS1-APEX2 from DENV2-NS1-APEX2 transfected cell culture supernatant.

4.2.2.1: Attempts to generate a lab-adapted DENV2-NS1-APEX2 variant

Our laboratory previously generated a panel of NS1-tagged virus variants, including a variant that harbours the red fluorescent protein mScarlet [94]. Like DENV2-NS1-APEX2, this DENV2-NS1-mScarlet variant displayed highly attenuated growth kinetics. Previous work within our group that sought to restore the fitness of this DENV2-NS1-mScarlet variant through adaptive laboratory evolution in Huh-7.5 cells led to the identification of four high-frequency mutations (Figure 4.05A). When introduced into the DENV2-NS1-mScarlet parent, these 'lab adapted' mutations restored DENV2-NS1-mScarlet fitness to near-wildtype levels (Figure 4.05B). As such, to assess whether these lab-adapted mutations may similarly restore the fitness of the DENV2-NS1-APEX2 variant to near-wildtype levels, and thus potentially enhance sNS1-APEX2 production in cell culture, these mutations were also introduced into DENV2-NS1-APEX2. To assess the impact of these mutations on DENV2-NS1-APEX2 fitness, *in vitro* transcribed RNA of DENV2, DENV2-NS1-APEX2, or the newly constructed DENV2-NS1-APEX2-Lab-Adapted variant were transfected into Huh-7.5 cells. Virus-containing cell culture supernatants were collected every 24 hours for 7 days and processed to assess infectivity by focus forming assay (FFA) (Figure 4.05 C). As expected, DENV2 displayed robust infectious virus production which peaked at 5 days post-transfection and then decreased concomitant with virus-induced cytopathic effects (CPE). Consistent with its attenuation, DENV2-NS1-APEX2 infectious virus production was appreciably impaired, as compared to wildtype DENV2, and a CPE-induced decline in infectivity was not observed within the experimental timeframe. Importantly, this suggests that DENV2-NS1-APEX2 infectious virus production may continue to increase past 7 days post-transfection and, thus, may require extended propagation times for the maximum accumulation of sNS1-APEX2. Interestingly, the DENV2-NS1-APEX2-Lab-Adapted variant exhibited severely attenuated infectious virus production suggesting that the four DENV2-NS1-mScarlet fitness-restoring mutations may be DENV2-NS1-mScarlet stain-specific and not a generalised NS1-insert fitness-restoring feature. As such, the use of this severely attenuated DENV2-NS1-APEX2-Lab-Adapted variant was discontinued.

A

NS1 NS4B

	K174S (39%)		Q175E (59%)		N222T (99%)		V219A (46%)	
	codon	amino acid	codon	amino acid	codon	amino acid	codon	amino acid
pFK-DVs Parent	AAA	K	CAG	Q	AAC	N	GTG	V
pFK-DVs	AAA	K	CAG	Q	AAC	N	GTG	V
Lab Adapted	AGT	S	GAG	E	ACC	T	GCG	A
DENV1	TCC	S	TAC	Y	ACA	T	GTG	V
DENV2	AAA	K	CAG	Q	AAC	N	GTC	V
DENV3	GTC	V	TAC	Y	ACC	T	GTT	V
DENV4	GGA	G	AGT	S	ACA	T	GTA	V

pFK-DVs Parent	NC_001474.2
DENV1	NC_001477.1
DENV2	MF459663.3
DENV3	NC_001475.2
DENV4	NC_002640.1

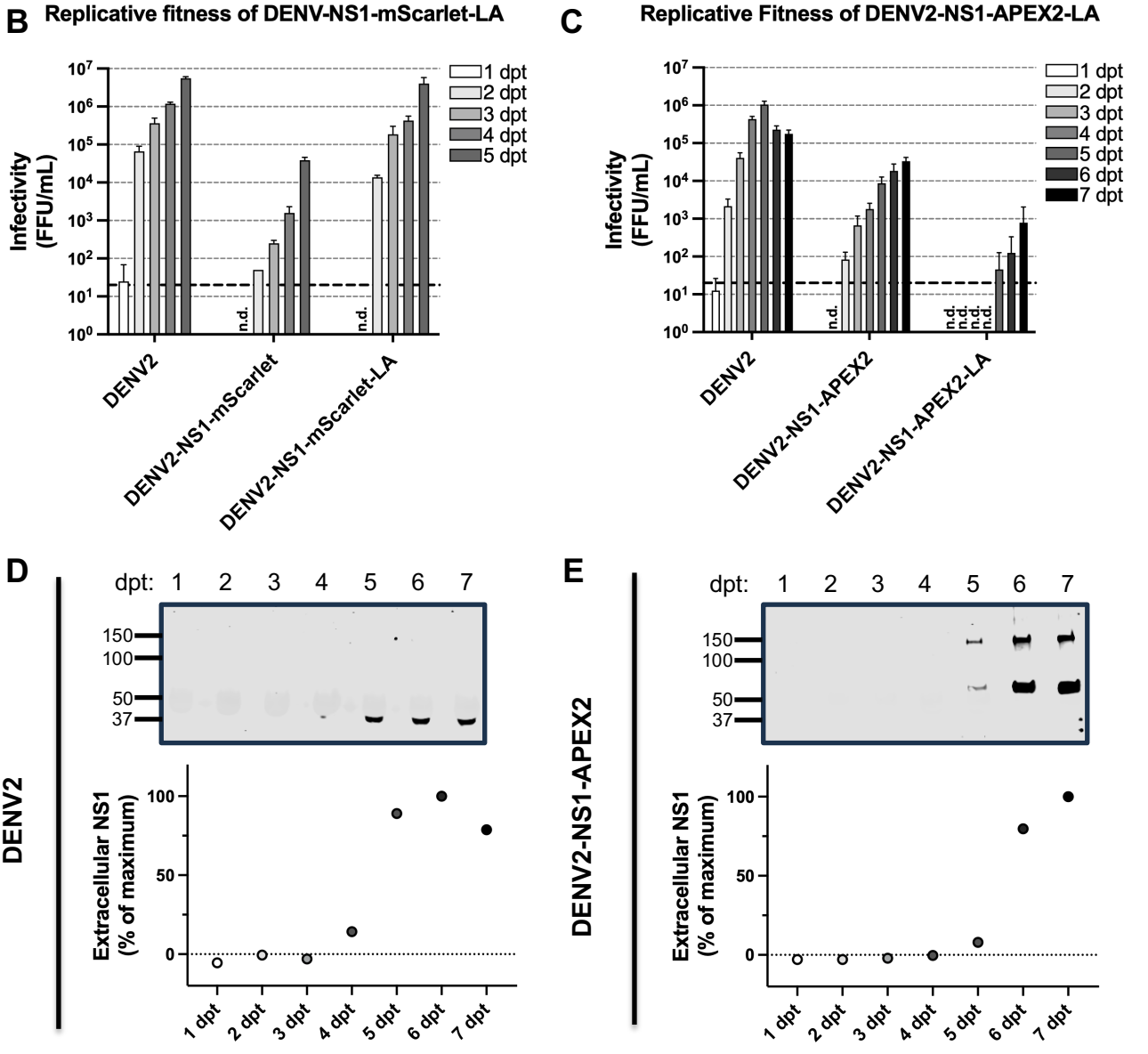

FIGURE 4.05. DENV2 NS1 secretion tracks similarly with infectious virus production. Previous work within our group identified 4 mutations that restored the fitness of the DENV2-NS1-mScarlet reporter virus (A & B) (unpublished data). Huh-7.5 cells were transfected with *in vitro* transcribed RNA of the indicated constructs, and cell culture supernatants were collected for 7 days to assess the impact of these four mutations on DENV2-NS1-APEX2-LA (lab adapted) viral fitness by FFA (C). DENV2 and DENV2-NS1-APEX2 supernatants were then subjected to SDS-PAGE and Western blot analysis to monitor the extracellular accumulation of sNS1 (D) and sNS1-APEX2 (E).

4.2.2.2: Assessing the relationship between secreted NS1 and infectious virus production

To determine the optimal timing for the maximum recovery of sNS1-APEX2 from transfected cell culture supernatant, we monitored the extracellular accumulation of sNS1 in transfected cell culture supernatant. For this, the DENV2 and DENV2-NS1-APEX2 cell culture supernatant collected above, were used to measure extracellular sNS1 abundance by quantitative Western blot analysis (Figure 4.05D & E). These data indicated that NS1 secretion tracks similarly, albeit delayed, with infectious virus production, most likely as a result of increased viral load within the cell culture system. Importantly, consistent with the CPE-induced decrease in wildtype infectious DENV production (Figure 4.05C, DENV2), the extracellular abundance of wildtype sNS1 was similarly observed to decrease at the later timepoint. Also importantly, consistent with the infectivity data (Figure 4.05C, DENV2-NS1-APEX2), the extracellular abundance of sNS1-APEX2 was not observed to peak and decline, suggesting that the extracellular abundance of sNS1-APEX2 may continue to increase beyond 7 days post-transfection. Collectively, these data indicated that to maximise the yield of the sNS1-APEX2 recovery from DENV2-NS1-APEX2 transfected cells, cell culture supernatant should be collected at the first sign of CPE – which may extend beyond 7 days post-transfection.

4.2.2.3: Comparing the effect of DENV2-NS1-APEX2 RNA transfection and infection on sNS1-APEX2 production

Given that the data above indicated that the extracellular levels of sNS1 increase with increasing viral load, we next explored whether infection rather than *in vitro* transcribed RNA transfection may be a viable method to enhance the production and recovery of sNS1-APEX2-containing cell culture supernatant. To evaluate this, Huh-7.5 cells were infected with DENV2-NS1-APEX2 (MOI ~1) or transfected with *in vitro* transcribed DENV2-NS1-APEX2 RNA. Cell culture supernatant was recovered every 24 hours until the first sign of virus-induced CPE (6 days post-infection; 8 days post-transfection) and subjected to SDS-PAGE and Western blot analysis to monitor the extracellular accumulation of sNS1-APEX2 (Figure 4.06). As expected, the abundance of extracellular sNS1-APEX2 increased with time for both infected and transfected cell culture treatments. Importantly, however, while both treatments produced Western blot banding patterns consistent with the sNS1-APEX2 fusion protein (Figure 4.06 black arrows), banding patterns more closely reflecting untagged sNS1 (Figure 4.06 grey arrows) were also observed in cells infected with DENV2-NS1-APEX2 at 6 days post-infection. For studies involving DENV2 reporter viruses in our laboratory, infectious virus stocks are generated by collecting virus-containing cell culture supernatant from tissue culture cells transfected with *in vitro* transcribed viral RNA [447]. As such, by 6 days post-infection when CPE occurred in cells infected with DENV2-NS1-APEX2, this virus had effectively propagated in cells for approximately 13 days. The presence of this band that is more consistent with untagged NS1 suggests that the DENV2-NS1-APEX2 virus may evolve in Huh-7.5 cells to remove part or all of the

APEX2 insert. Given that this APEX2-removed, more wildtype-like form of sNS1 would represent a contaminant that could confound our sNS1-APEX2 proximity biotinylation experiments, infection as a strategy to harvest sNS1-APEX2 was discontinued.

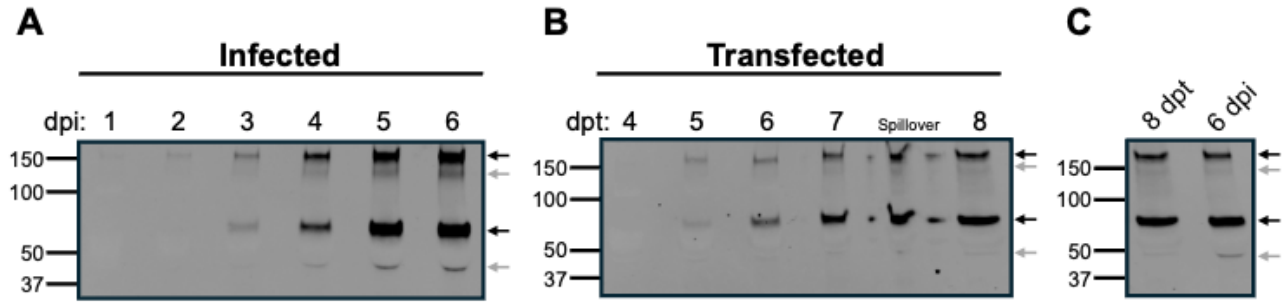

FIGURE 4.06. DENV2-NS1-APEX2 may evolve in Huh-7.5 cells to remove part or all of the APEX2 insert. Huh-7.5 cells were (A) infected with DENV2-NS1-APEX2 (MOI ~1) or (B) transfected with *in vitro* transcribed DENV2-NS1-APEX2 RNA. Cell culture supernatants were collected every 24 hours until CPE (6 days post-infection; 8 days post-transfection) and subjected to SDS-PAGE and Western blot analysis to monitor the extracellular accumulation of sNS1-APEX2. Side-by-side comparison of sNS1-APEX2 collected at CPE from DENV2-NS1-APEX2 transfected (8 dpt) and infected (6 dpi) (C) Huh-7.5 cells. Black arrows highlight bands corresponding to sNS1-APEX2; grey arrows highlight bands corresponding to untagged sNS1.

4.2.2.4: Concentrating sNS1-APEX2 using a 100 kDa molecular weight cutoff filter.

Given the unsuccessful attempts to enhance the accumulation of sNS1-APEX2 in cell culture supernatant, we sought to concentrate sNS1-APEX2 from sNS1-APEX2-containing cell culture supernatant by ultrafiltration using a 100 kDa molecular weight cutoff (MWCO) filter. A schematic overview of this strategy is shown in Figure 4.03A. For this, Huh-7.5 cells were transfected with *in vitro* transcribed DENV2-NS1-APEX2 RNA. At the first signs of CPE (8 days post-transfection), cell culture supernatant was recovered, clarified by centrifugation and filtered through a 0.45 μM filter. This clarified cell culture supernatant was then concentrated approximately 10-fold by ultrafiltration. The retentate was then thoroughly resuspended to recover concentrated sNS1-APEX2.

To confirm that this ultrafiltration process allowed the concentration and recovery of sNS1-APEX2, the input, retentate, and flow-through fractions were subjected to SDS-PAGE and Western blot analysis to visualise sNS1-APEX2 (Figure 4.07). Total protein staining was performed for the purpose of sNS1-APEX2 protein quantification (Figure 4.07A). Importantly, however, this revealed that the 100 kDa MWCO ultrafiltration process concentrated components of foetal bovine serum (FBS) present in the cell culture medium. Given the total protein stain signal intensity saturation, quantitative analysis of sNS1-APEX2 abundance was precluded. Nonetheless, the relative abundance of sNS1-APEX2 within the input and retentate fractions, coupled with the apparent absence of sNS1-APEX2 within the flow-through fraction confirmed that sNS1-APEX2 is concentrated and recovered by this ultrafiltration process (Figure 4.07 B & C). To assess the impact of this ultrafiltration process on the infectious DENV2-NS1-APEX2 virus contained within the cell culture supernatant, the input, retentate, and flow-through fractions were processed to assess infectivity (Figure 4.07D). Compared to the input fraction, the retentate fraction contained approximately 10-fold greater DENV titers. No infectious virus was detected in the flow-through fraction. These data indicated that infectious DENV2-NS1-APEX2 virus can be concentrated using a 100 kDa MWCO filter and that this ultrafiltration process does not adversely impact infectivity. Collectively, these data confirmed that a 100 kDa MWCO filter can be used to concentrate sNS1-APEX2 and infectious DENV2-NS1-APEX2 virions from the cell culture supernatant of Huh-7.5 cells transfected with *in vitro* transcribed DENV2-NS1-APEX2 RNA.

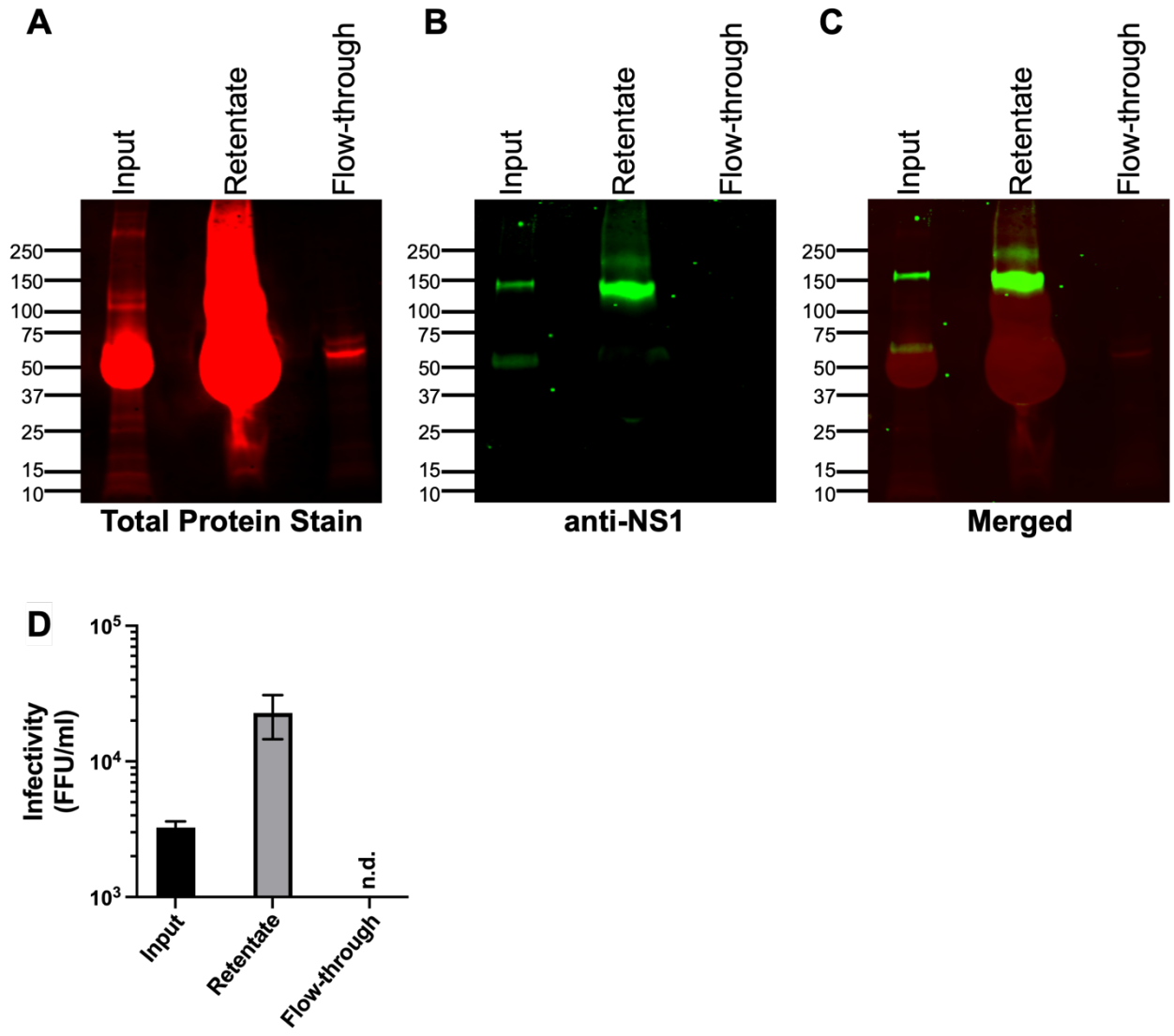

FIGURE 4.07. 100 kDa MWCO ultrafiltration can be used to concentrate sNS1-APEX2 and infectious DENV2-NS1-APEX2 virus. Huh-7.5 cells were transfected with *in vitro* transcribed DENV2-NS1-APEX2 RNA and cultured for 8 days. Cell culture supernatants were then collected, clarified by centrifugation and 0.4 M filtration. Clarified supernatants were then subjected to 100 kDa MWCO filtration. The input, retentate, and flow-through fractions were subjected to SDS-PAGE and Western blot analysis (A-C) using REVERT 700 Total protein stain (LI-COR) (B) and mouse anti-NS1 in conjunction with anti-mouse 800 to visualise extracellular sNS1-APEX2 (B & C). Each fraction was assessed for infectivity by FFA (D).

4.2.3: Design and construction of the controls for the sNS1-APEX2 biotinylation experiments

We determined that the use of sNS1-APEX2 proximity labelling-coupled quantitative proteomics experiments to identify the human host cell factors involved in the early events of sNS1 internalisation required two controls: (i) an APEX2-omitted negative control (mock inoculum) to distinguish sNS1-APEX2-catalysed biotinylation from background, and (ii) an untagged APEX2-only control to distinguish sNS1-specific interactions from potential APEX2-specific interactions.

4.2.3.1: APEX2-omitted control (mock-inoculum)

As a negative control to separate sNS1-APEX2-catalysed biotinylation from background, we opted to recover spent culture media from uninfected Huh-7.5 cells. This mock inoculum recovered from uninfected Huh-7.5 cells would not be expected to contain the same constituents as those recovered from DENV-infected cells; namely infectious virus, sNS1, and host cell factors that are secreted in response to DENV infection. Nevertheless, we employed this simple and reproducible control as a standard of comparison.

4.2.3.2: DENV-driven secreted APEX2 control (sAPEX2 inoculum)

To separate sNS1-specific interactions from potential APEX2-specific interactions, we designed an APEX2 control construct that could be secreted from Huh-7.5 cells (Figure 4.08A). To this end, we engineered an APEX2 gene construct that encodes: (i) a mouse IgK signal peptide at the N-terminus of the APEX2 protein to drive APEX2 secretion from mammalian cells, and (ii) a myc-tag at the 3' end of the APEX2 gene for straightforward detection of the APEX2 protein. Moreover, to ensure that the secreted APEX2 (sAPEX2) control inoculum is comparable to the experimental sNS1-APEX2 inoculum, this construct was introduced between T2A and P2A self-cleaving peptide encoding sequences in the full-length infectious DENV2 cDNA vector [299]. As such, by transfecting Huh-7.5 cells with infectious *in vitro* transcribed RNA from this DENV2-IgK-APEX2-myc construct, the expression of this APEX2 protein would be: (i) controlled by DENV replication; (ii) cleaved from the viral polypeptide and unattached to any viral protein, and; (iii) secreted from infected Huh-7.5 cells. Moreover, the secreted APEX2 (sAPEX2) control inoculum recovered from infected cells would contain: (i) wildtype untagged sNS1; (ii) infectious virus, and; (iii) host cell factors secreted in response to DENV infection.

4.2.4: Characterisation of the DENV2-IgK-APEX2-myc virus

4.2.4.1: DENV2-IgK-APEX2-myc variant is infectious

To assess the replicative fitness of this control construct, Huh-7.5 cells were transfected with *in vitro* transcribed RNA of DENV2 or DENV2-IgK-APEX2-myc. Virus-containing cell culture supernatant were collected every 24 hours for 7 days and processed to assess infectivity by FFA (Figure 4.08B). These data revealed that the growth kinetics of the DENV2-IgK-APEX2-myc variant are attenuated relative to the wildtype DENV2. This reduction in replicative fitness is comparable to that of the DENV2-NS1-APEX2 variant (Figure 4.05C), raising the possibility that the presence of the engineered APEX2 peroxidase contributes to the diminished DENV replication capacity. Regardless, the similar levels of attenuation shared between DENV2-NS1-APEX2 and DENV2-IgK-APEX2-myc would likely be beneficial for the downstream APEX2-based proximity-dependent biotinylation experiments given that the cell culture supernatant used to generate inoculum would be collected from cells that are infected to similar levels and thus may be expected to contain comparable levels of infectious virus and host cell factors that are released in response to DENV infection.

4.2.4.2: DENV2-IgK-APEX2-myc virus secretes untagged sAPEX2 and sNS1

To confirm that the DENV2-IgK-APEX2-myc virus secretes NS1 and APEX2, the virus-containing cell culture supernatant collected above was subjected to SDS-PAGE and Western blot analysis (Figure 4.08 C&D). As expected, quantitative Western blot analysis of the cell culture supernatant using an anti-NS1 antibody revealed that extracellular sNS1 exhibits a molecular weight consistent with wildtype untagged NS1 (Figure 4.08 C & E). Moreover, similar to DENV2 and DENV2-NS1-APEX2, the extracellular accumulation of sNS1 appeared to increase with infectious virus production. Key to this control, however, Western blot analysis of the cell culture supernatant using an anti-myc antibody revealed the presence of an anti-Myc reactive band that is consistent with the expected molecular weight (~27 kDa) of the Myc-tagged sAPEX2 protein (Figure 4.08 D & E), indicating that the APEX2 protein is secreted from infected Huh-7.5 cells.

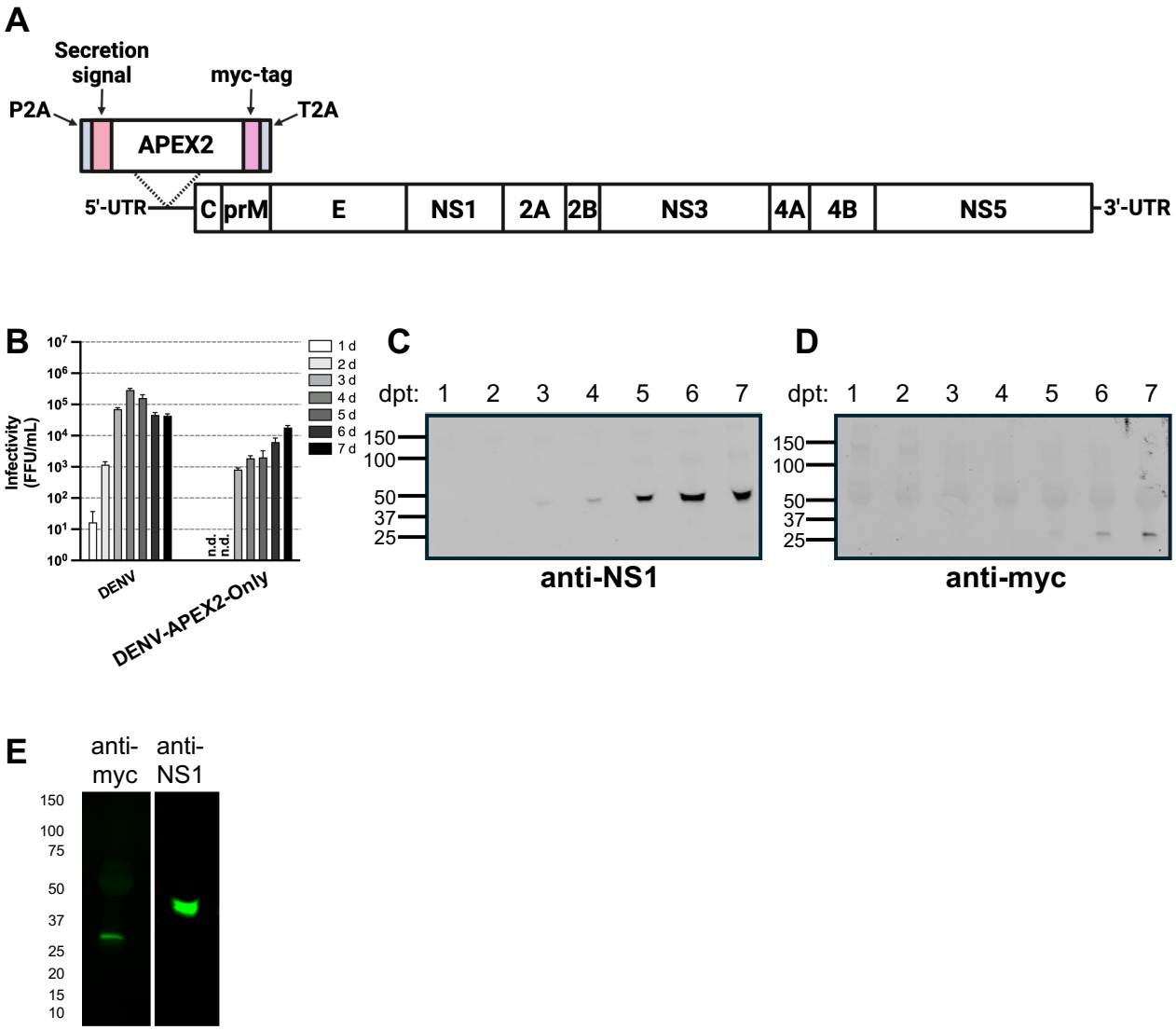

FIGURE 4.08. 100 kDa MWCO ultrafiltration can be used to concentrate sNS1-APEX2 and infectious DENV2-NS1-APEX2 virus. Schematic diagram the DENV2-IgK-APEX2-myc construct (A). Huh-7.5 cells were transfected with *in vitro* transcribed DENV2-IgK-APEX2-myc RNA and cell culture supernatants were collected for 7 days. Cell culture supernatants were processed to assess infectivity by FFA (B), and to monitor the extracellular accumulation of sNS1 (C) and sAPEX2-myc (D) by quantitative Western blot analysis (C). 7 days post-transfection supernatants were processed for Western blot analysis using mouse anti-myc (left) and mouse anti-NS1 primary antibodies in conjunction with anti-mouse 800 CW to visualise sAPEX2 and sNS1, respectively (E).

4.2.4.3: The APEX2 protein within DENV2-IgK-APEX2-myc virus is catalytically active

To confirm that the DENV2-IgK-APEX2-myc variant expresses a catalytically active APEX2 protein, we employed confocal immunofluorescence microscopy to visualise APEX2-catalysed biotinylation. For this, Huh-7.5 cells were transfected with *in vitro* transcribed RNA from DENV2-IgK-APEX2-myc or DENV2-NS1-APEX2. At 8 days post-transfection, live cells were incubated with biotin-phenol for 30 minutes. Cells were then treated for 1 minute with 1 mM H_2O_2 to allow APEX2-catalysed biotinylation of proximal proteins before the labelling reaction was stopped by the addition of quencher solution. As a negative control, untransfected Huh-7.5 cells were similarly treated. Cells were then fixed and stained with mouse anti-NS1 followed by anti-mouse AlexaFluor 555 and streptavidin-AlexaFluor 488 conjugate to visualise NS1 and biotinylated protein, respectively (Figure 4.09). Untransfected Huh-7.5 cells did not display NS1 staining. Despite the absence of APEX2, untransfected Huh-7.5 cells did, however, display weak streptavidin-Alexa Fluor staining of mitochondria. This is not unexpected, given that the mitochondrial matrix contains endogenously biotinylated proteins that result from the activity of the four endogenously expressed mammalian biotin protein ligases (3 of which are mitochondria-associated; 1 is cytosolic) [297, 448]. Both DENV2-NS1-APEX2 and DENV2-IgK-APEX2-myc RNA transfected cells displayed intense juxtanuclear NS1 staining patterns consistent with wildtype-like intracellular NS1 localisation. As expected, DENV2-NS1-APEX2 transfected cells displayed biotinylation patterns that heavily overlapped with NS1 staining in a manner consistent with previous studies in our laboratory. DENV2-IgK-APEX2-myc RNA transfected cells displayed NS1 and biotinylation staining patterns that exhibited a moderate level of overlap. However, the degree of overlap was not as pronounced as the DENV2-NS1-APEX2 patterns, as expected, given that the NS1 and APEX2 proteins are not fused in this DENV construct. Importantly, the biotinylation patterns observed in DENV2-IgK-APEX2-myc RNA transfected cells were markedly different to those observed in untransfected cells, indicating that the Myc-tagged APEX2 protein exhibits robust catalytic activity.

Collectively, these data indicated that the DENV2-IgK-APEX2-myc variant: (i) expresses a catalytically active APEX2 protein; (ii) replicates with attenuated kinetics not dissimilar to DENV2-NS1-APEX2; (iii) secretes untagged sNS1; (iv) secretes infectious virus, and; (iv) importantly, secretes sAPEX2 protein. As such, this DENV2-IgK-APEX2-myc variant could be utilised to provide a resource of sAPEX2 control inoculum that can be employed in downstream biotinylation experiments to differentiate sAPEX2-specfic interactions from sNS1-APEX2-specific interactions.

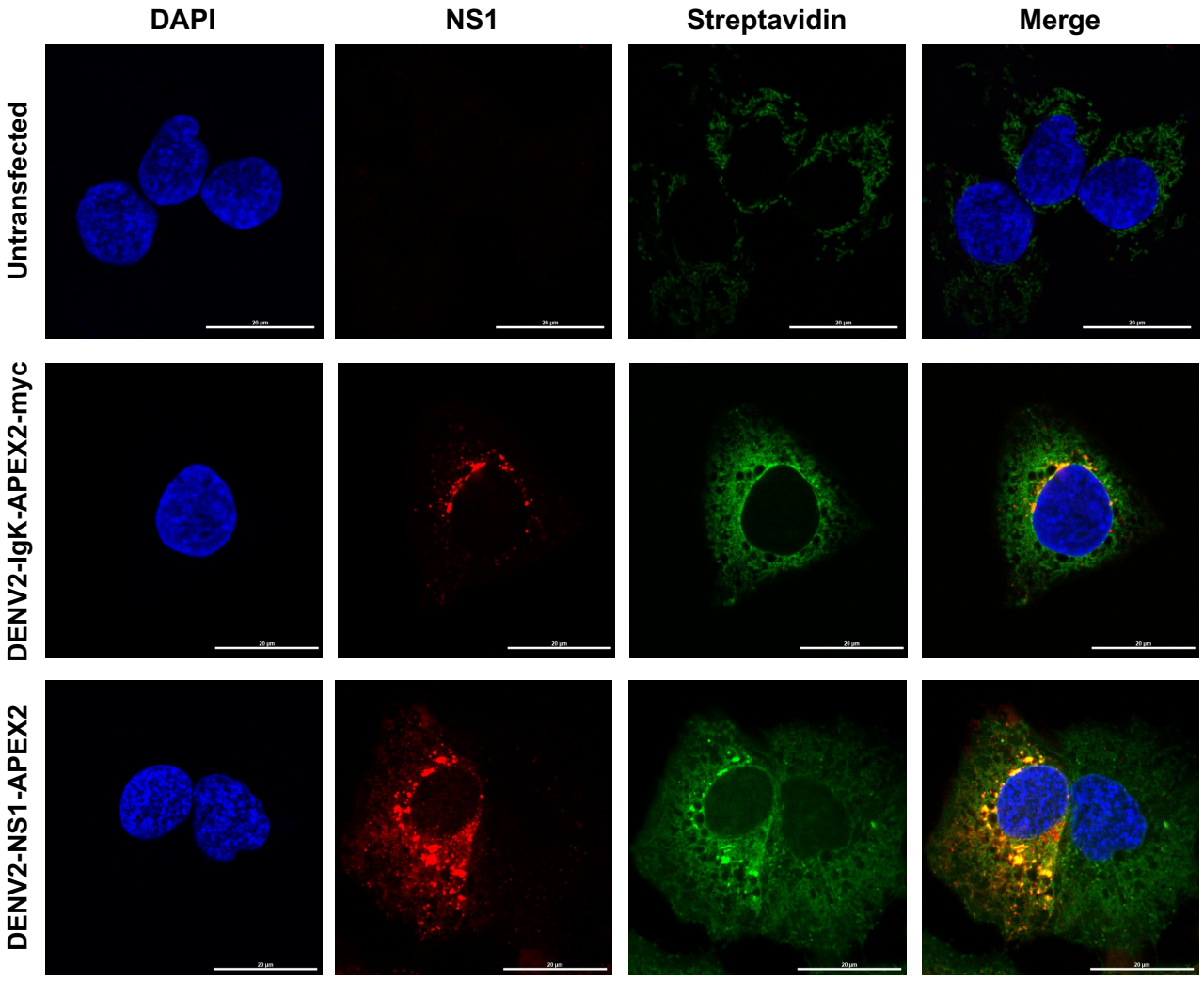

FIGURE 4.09. DENV2-IgK-APEX2-myc displays wildtype-like NS1 localisation and exhibits APEX2 catalytic activity. Huh-7.5 cells were transfected with *in vitro* transcribed DENV2-NS1-APEX2 or DENV2-IgK-APEX2-myc RNA. Untransfected Huh-7.5 cells served as a negative control. At 8 days post-transfection, cells were treated with biotin-phenol (500 mM final concentration) for 30 minutes. To allow APEX2-catalysed biotinylation, cells were treated with H_2O_2 (1 mM final concentration) for precisely one minute. This reaction was stopped by removing the cell culture media and washing the cells in quenching solution. Cells were then fixed in 4% PFA, permeabilised by triton-X, and processed for indirect immunofluorescent labelling using a mouse anti-NS1 primary antibody. To visualise NS1 and biotinylated protein, cells were then labelled using an AlexaFluor 555-conjugated anti-mouse IgG and streptavidin-AlexaFluor 488 conjugate, respectively. Cells were counter stained with DAPI. Samples were then imaged using confocal fluorescence microscopy.

4.2.5: Confirming the peroxidase activity of internalised sNS1-APEX2

The peroxidase activity of NS1-APEX2 has been shown to be functionally active in cells transfected with *in vitro* transcribed DENV2-NS1-APEX2 RNA, and this has been demonstrated to have practical applications in electron microscopy [94]. Moreover, the data presented in Figure 4.09 indicates that intracellularly expressed NS1-APEX2 is capable of APEX2-catalysed biotinylation, indicating that it has practical applications in APEX2-based proximity labelling in live cells. To confirm that the catalytic activity of APEX2 is functionally active following sNS1 internalisation into naïve Huh-7.5 cells and is capable of biotinylating endogenous proximal proteins, we employed confocal immunofluorescent microscopy and Western blot analysis for characterisation.

4.2.5.1: APEX2 is catalytically active following sNS1-APEX2 internalisation

To visualise sNS1-APEX2-catalysed biotinylation following internalisation into Huh-7.5 cells, ultrafiltration-recovered sNS1-APEX2 was inoculated onto naïve Huh-7.5 cells. In parallel, naïve Huh-7.5 cells were inoculated with ultrafiltration-recovered mock inoculum or ultrafiltration-recovered sAPEX2 control inoculum. To confirm that the ultrafiltration process used to concentrate cell culture supernatant inoculum does not interfere with APEX2-catalysed biotinylation, Huh-7.5 cells were inoculated with complete DMEM only. As a positive control for APEX2-catalysed biotinylation, Huh-7.5 cells transfected with *in vitro* transcribed DENV2-NS1-APEX2 RNA were also included. Huh-7.5 were inoculated with the described treatments and incubated for 30 minutes at 37°C in 5% CO_2. At 30 minutes post-inoculation, cells were extensively washed and incubated in complete DMEM supplemented with 500 mM biotin-phenol for 30 minutes at 37°C 5% CO_2. To catalyse the biotinylation reaction at 60 minutes post-inoculation, cells were treated for precisely 1 minute with H_2O_2 before the biotinylation labelling reaction was stopped by the addition of quencher solution. Cells were then extensively washed, fixed and stained for immunofluorescence microscopy using mouse anti-NS1 primary antibody followed by anti-mouse AlexaFluor 555 and streptavidin-AlexaFluor 488 conjugate to visualise NS1 and biotinylated protein, respectively (Figure 4.10). As expected, the positive control cells transfected with DENV2-NS1-APEX2 RNA displayed robust NS1-APEX2-dependent biotinylation staining patterns that exhibited remarkable overlap. As expected, the media only and ultrafiltration-recovered mock controls did not display any NS1 staining and only displayed weak mitochondrial streptavidin-AlexaFluor staining patterns indicative of endogenously biotinylated proteins. Despite containing abundant sNS1 as observed by Western blot analysis, the ultrafiltration-recovered sAPEX2 control inoculum displayed very little NS1 staining. The biotinylation patterns observed for this treatment was similar to the mock inoculum control, suggesting that the sAPEX2 protein may not be internalised by Huh-7.5 cells to a level detectable using this immunofluorescence microscopy technique. Importantly, Huh-7.5 cells inoculated with ultrafiltration-recovered sNS1-APEX2 displayed robust NS1 staining, consistent with internalised sNS1, indicating

that the ultrafiltration process employed to concentrate sNS1 does not impact sNS1-APEX2 internalisation. Also importantly, the observed NS1 signal was largely encompassed by streptavidin-Alexa Fluor staining patterns, confirming that the APEX2 portion of sNS1-APEX2 retains its catalytic activity post-internalisation. Taken together, these data indicated that following sNS1-mediated internalisation into Huh-7.5 cells, sNS1-APEX2 is capable of APEX2-catalysed biotinylation in a proximal manner.

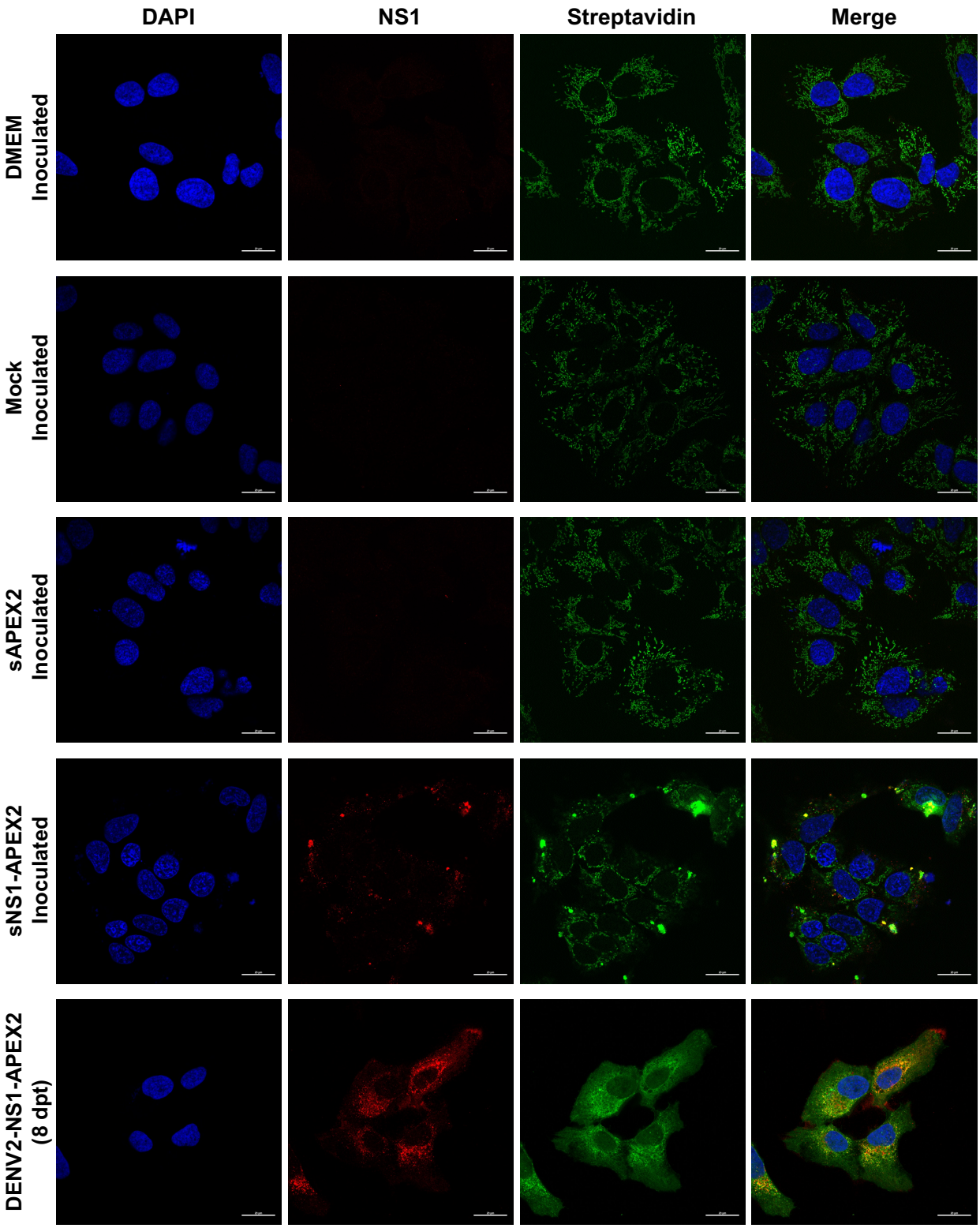

FIGURE 4.10. APEX2 is catalytically active following sNS1-APEX2 internalisation into Huh-7.5 cells. Huh-7.5 cells were inoculated with 100 kDa MWCO ultrafiltered supernatants containing sNS1-APEX2, sAPEX2, or APEX2-omitted (Mock). Huh-7.5 cells transfected with *in vitro* transcribed DENV2-NS1-APEX2 RNA served as a positive control for APEX2-catalysed biotinylation. To confirm the ultrafiltration process does not impact the biotinylation process, Huh-7.5 cells were inoculated with complete DMEM. Cells were subjected to APEX2-catalysed biotinylation and processed to visualise NS1 (red), biotinylated protein (green) and nuclei (blue) as described in Methods and Materials.

4.2.5.2: APEX2 can biotinylate endogenous protein following sNS1-APEX2 internalisation

While our confocal immunofluorescence data indicated that internalised sNS1-APEX2 was catalytically active, this technique cannot discriminate APEX2 self-biotinylation from the biotinylation of endogenous proximal proteins. To assess whether internalised sNS1-APEX2 can biotinylate proximal host proteins, a streptavidin Western blot analysis of whole cell lysates was performed. Here, Huh-7.5 cells were inoculated with sNS1-APEX2 inoculum. As an APEX2-deficient negative control, Huh-7.5 cells were treated with complete media. As a positive control for APEX2-catalysed biotinylation, Huh-7.5 cells transfected with a plasmid construct that expresses a catalytically active and cytosol-localised APEX2 protein were also included. At 30 minutes post-inoculation, cells were processed for APEX2-mediated proximity biotinylation (see Methods and Materials section 2.3.7 for details). Whole cell lysates were subjected to SDS-PAGE and Western blot analysis using a streptavidin fluorescent conjugate to visualise biotinylated protein (Figure 4.11). As expected, the plasmid-driven cytosolic APEX2 positive control produced strong streptavidin staining patterns throughout the lane, indicating that a variety of proteins of varying molecular weights were biotinylated by APEX2 activity. Streptavidin banding patterns were also detected throughout the sNS1-APEX2 lane. However, the staining intensity was only slightly more pronounced than that of the mock control. Importantly, the anti-β-actin loading control indicated that the mock control lane was loaded with substantially more protein (4-fold) than the sNS1-APEX2 lane, suggesting that the streptavidin signal in the sNS1-APEX2 is markedly underrepresented. Despite the substantially lower abundance of protein loaded, the streptavidin signal in the sNS1-APEX2 lane indicated the presence of biotinylated protein above background (mock) levels. These data suggest that internalised sNS1-APEX2 can biotinylate proximal host proteins.

Collectively, these immunofluorescence microscopy and Western blot data used to characterise the activity of internalised sNS1-APEX2 indicate that the sNS1-APEX2 fusion protein has practical applications for proximity-dependent biotinylation in live cells and may allow the identification of human host cell factors associated with the early events of sNS1 internalisation.

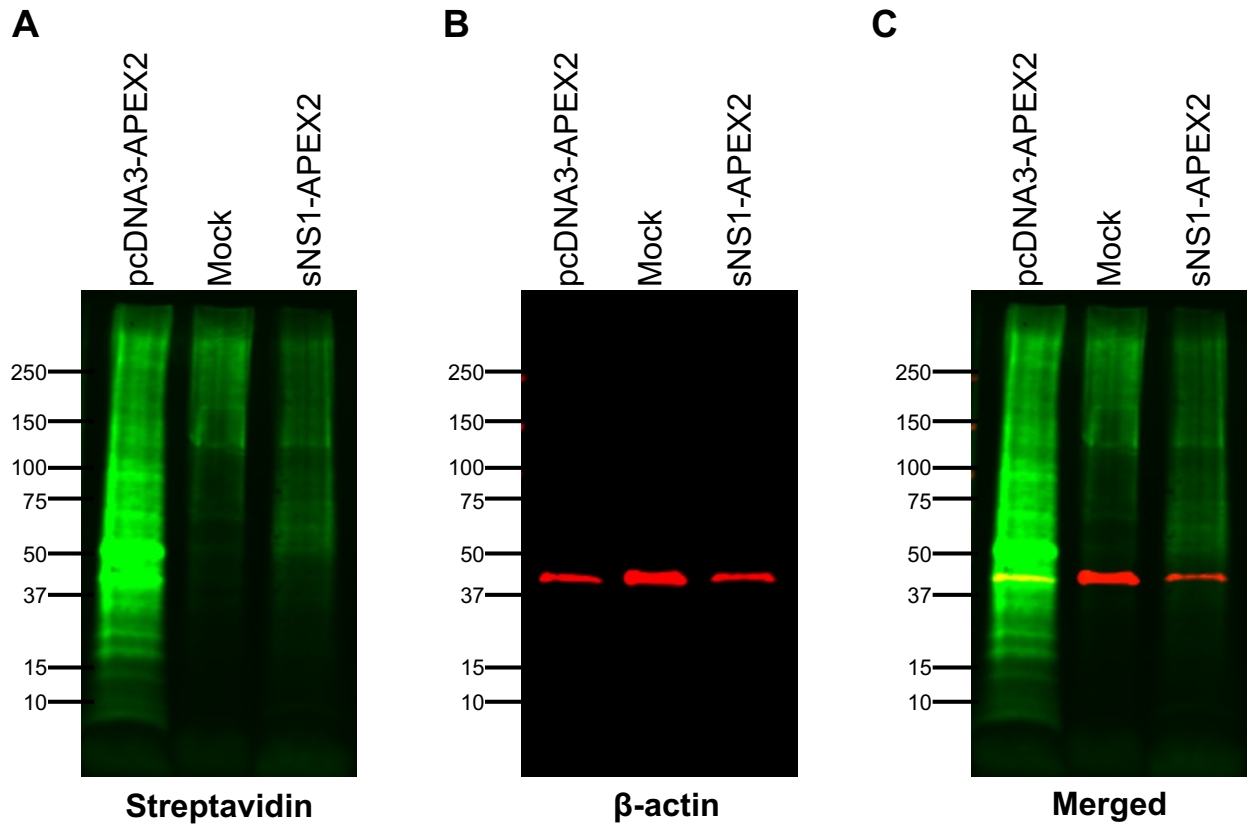

FIGURE 4.11. Internalised sNS1-APEX2 can biotinylate proximal proteins in Huh-7.5 cells. Huh-7.5 cells were inoculated with 100 kDa MWCO ultrafiltered supernatants containing sNS1-APEX2 for 30 minutes. Huh-7.5 cells transfected with a plasmid construct that expresses cytoplasmically-localised APEX2 cDNA served as a positive control for APEX2-catalysed biotinylation. Mock inoculated cells served as a negative control. At 30 minutes post-inoculation, media was replaced with complete DMEM supplemented with biotin-phenol (500 mM final concentration) and incubated for a further 30 minutes. To allow APEX2-catalysed biotinylation, cells were treated with H_2O_2 (1 mM final concentration) for precisely one minute. This reaction was stopped by removing the cell culture media and washing the cells in quenching solution. Cells culture monolayer were then lysed in RIPA buffer and whole cell lysates were subjected to SDS-PAGE and Western blot analysis using IRDye 800CW-conjugated streptavidin to visualise biotinylated protein (A) rabbit anti-β-actin and goat anti-rabbit IRDye 680CW for normalisation (B). 700 nm and 800 nm channels are merged in C.

4.2.6: Generating practicable quantities of sNS1-APEX2, sAPEX2, and mock inoculum

The methods used to generate sufficient volumes of inoculum for the proximity-dependent biotinylation experiments are detailed in the Methods and Materials section (2.3.7.1). Briefly, Huh-7.5 cells were transfected with *in vitro* transcribed DENV2-NS1-APEX2 or DENV2-IgK-APEX2-myc RNA in 6-well plates. For the negative control mock inoculum, untransfected Huh-7.5 cells were processed similarly. At 3 days post-transfection cells were expanded into 175 cm^2 tissue culture flasks. Given that the ultrafiltration process was shown to co-concentrate components of FBS, which may act to interfere with sNS1-host cell binding and/or internalisation, the concentration of FBS was adjusted with FBS-free media to a final concentration of 2% (v/v). At 7 days post-transfection, CPE was observed in DENV2-NS1-APEX2 transfected cells. cell culture supernatant were collected, clarified by centrifugation, filtered through a 0.45 µM filter, and concentrated approximately 10-fold by ultrafiltration using a 100 kDa MWCO filter. Inoculum samples were then stored at -80°C. For the cell culture supernatant and ultrafiltered inoculum, infectivity was assessed by FFA, and extracellular sNS1-APEX2 and s-APEX2-myc were assessed by SDS-PAGE and Western blot analysis (Figure 4.12). This revealed comparable levels of infectious DENV2-NS1-APEX2 and DENV2-IgK-APEX2-myc were contained within the concentrated inoculum (Figure 4.12 A & C). Additionally, sNS1-APEX2 (Figure 4.12B), sNS1 and sAPEX2-myc (Figure 4.12D) were retained and concentrated in the inoculum.

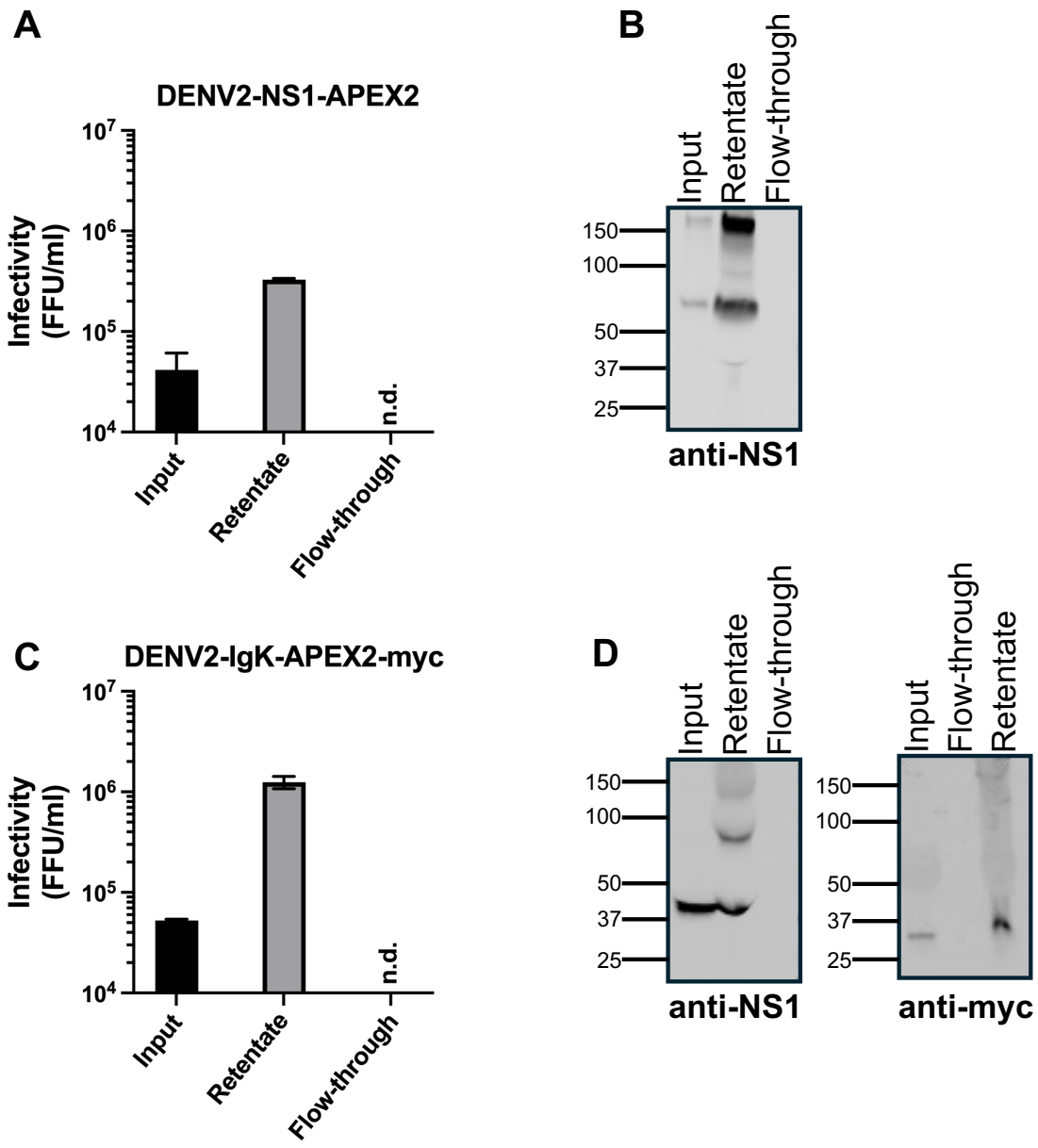

FIGURE 4.12. Generating practicable quantities of sNS1-APEX2 and sAPEX2-myc fusion proteins. Huh-7.5 cells were transfected with *in vitro* transcribed DENV2-NS1-APEX2 or DENV2-IgK-APEX2-myc RNA and propagated as described in Methods and Materials. Cell culture supernatants were collected at CPE, and centrifuge clarified cell-free supernatants were subjected to 100 kDa MWCO ultrafiltration. The ultrafiltration fractions (input, retentate, and flow-through) were processed to assess infectivity by FFA (A & C). SDS-PAGE and Western blot analysis were used to confirm the presence of sNS1-APEX2 (B), sNS1 and sAPEX2-myc (D).

4.2.7: APEX2-catalysed biotinylation of internalised sNS1 proximal proteins

To identify the human host proteins associated with sNS1 internalisation by APEX2-based proximity biotinylation, the experimental approach shown in Figure 4.03B was performed. Complete details of the methods employed are detailed in the Methods and Materials section (2.3.7.2). Briefly, Huh-7.5 cells were inoculated with ultrafiltration-recovered sNS1-APEX2, sAPEX2, or mock inoculum and returned to culture for 30 minutes. Each treatment was performed in quadruplicate. At 30 minutes post-inoculation, inoculum was removed, cells were washed in media and returned to culture for 30 minutes in biotin-phenol-supplemented media. At 60 minutes post-inoculation, H_2O_2 was added to catalyse the biotinylation reaction for precisely 1 minute. Cells were then immediately washed in quenching solution and then lysed on ice in quencher solution-supplemented RIPA buffer. Whole cell lysates were homogenised, clarified by centrifugation, and stored at -20°C. Samples were then delivered to collaborators (Nusha Chegeni, Alex Colella, Tim Chataway) at Flinders Omics for streptavidin-based affinity purification and identification by mass spectrometry as described in the Methods and Materials section (2.3.7.2) and Appendix VI. Briefly, clarified whole cell lysate samples were enriched for biotinylated proteins using Sulfo-NHS-Acetate-treated streptavidin magnetic beads. Following Lys-C and trypsin digestions, eluted peptides were analysed with a Dionex Ultimate 3000 UPLC coupled with a Thermo Fusion Lumos tandem mass spectrometer (Orbitrap Fusion™ Lumos™ Tribrid™ Mass Spectrometer, ThermoFisher Scientific). Peptide sequence identification was determined by matching to a human protein database using the Proteome Discoverer Program (software 2.4.1.15).

A total of 1,183 proteins were identified in our samples. Of these, 1,076 were identified with high confidence and 107 with medium confidence. Statistical analyses of label-free quantification intensities were performed to visualise significantly enriched proteins when comparing sNS1-APEX2 vs sAPEX2 samples or sNS1-APEX2 vs mock samples. The hits were ranked by mean enrichment of the four replicates with a set cutoff of ≥2-fold enrichment with an abundance ratio adjusted p-value ≤0.05. Using this hit selection criteria, a total of 45 proteins were identified as significantly enriched in sNS1-APEX2 vs sAPEX2 samples (Figure 4.13). A total of 21 proteins were identified as significantly enriched in sNS1-APEX2 vs mock samples (Figure 4.14).

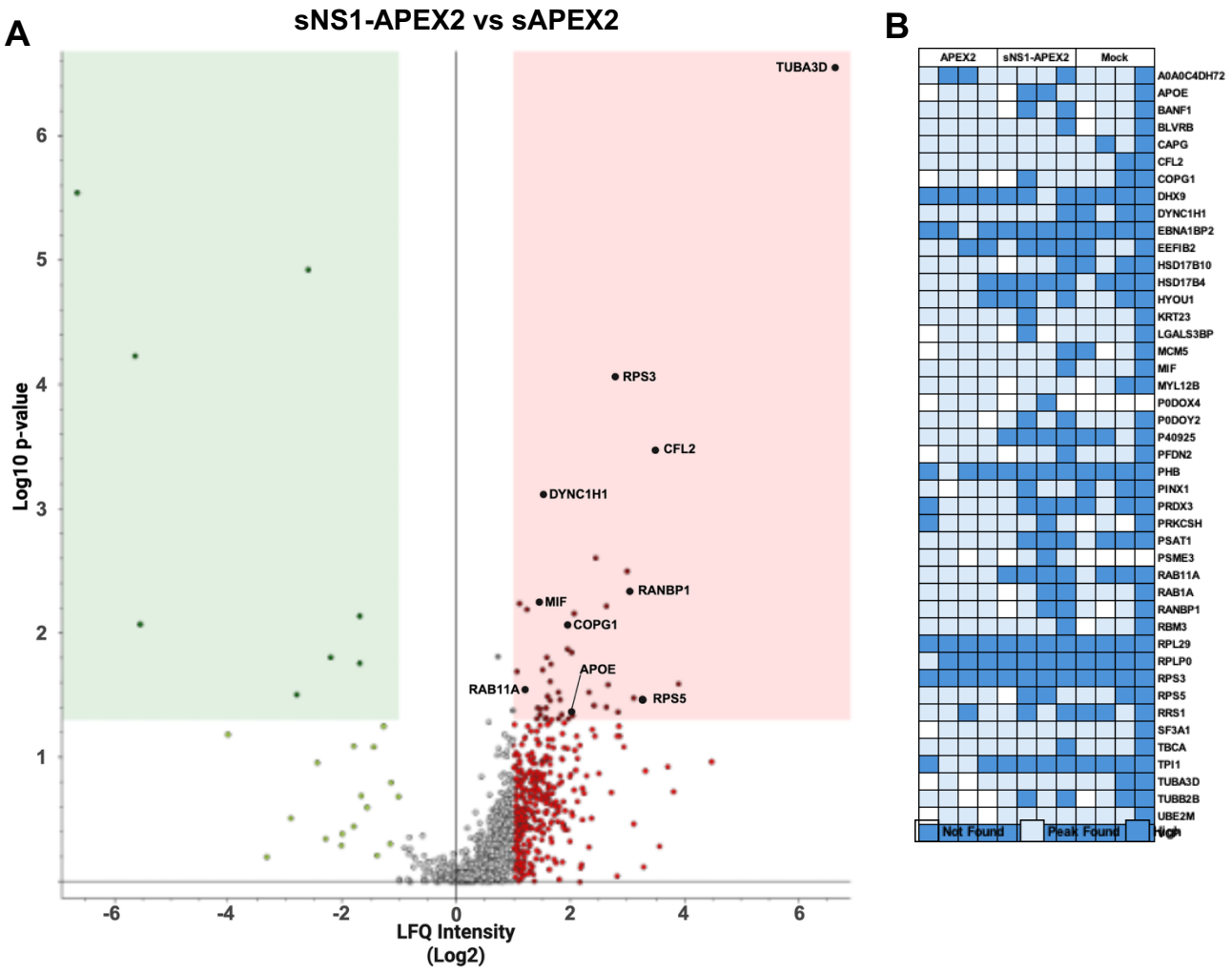

FIGURE 4.13. Quantitative analysis of sNS1-APEX2 vs sAPEX2 proximity labelled cells. (A) Volcano plot of proteins enriched in sNS1-APEX2 inoculated vs sAPEX2 inoculated Huh-7.5 cells. Proteins within the pink box are determined as significantly enriched ≥ 2-fold ($p \leq 0.05$). (B) Frequency map illustrating the degree to which proteins were identified for each individual replicate.

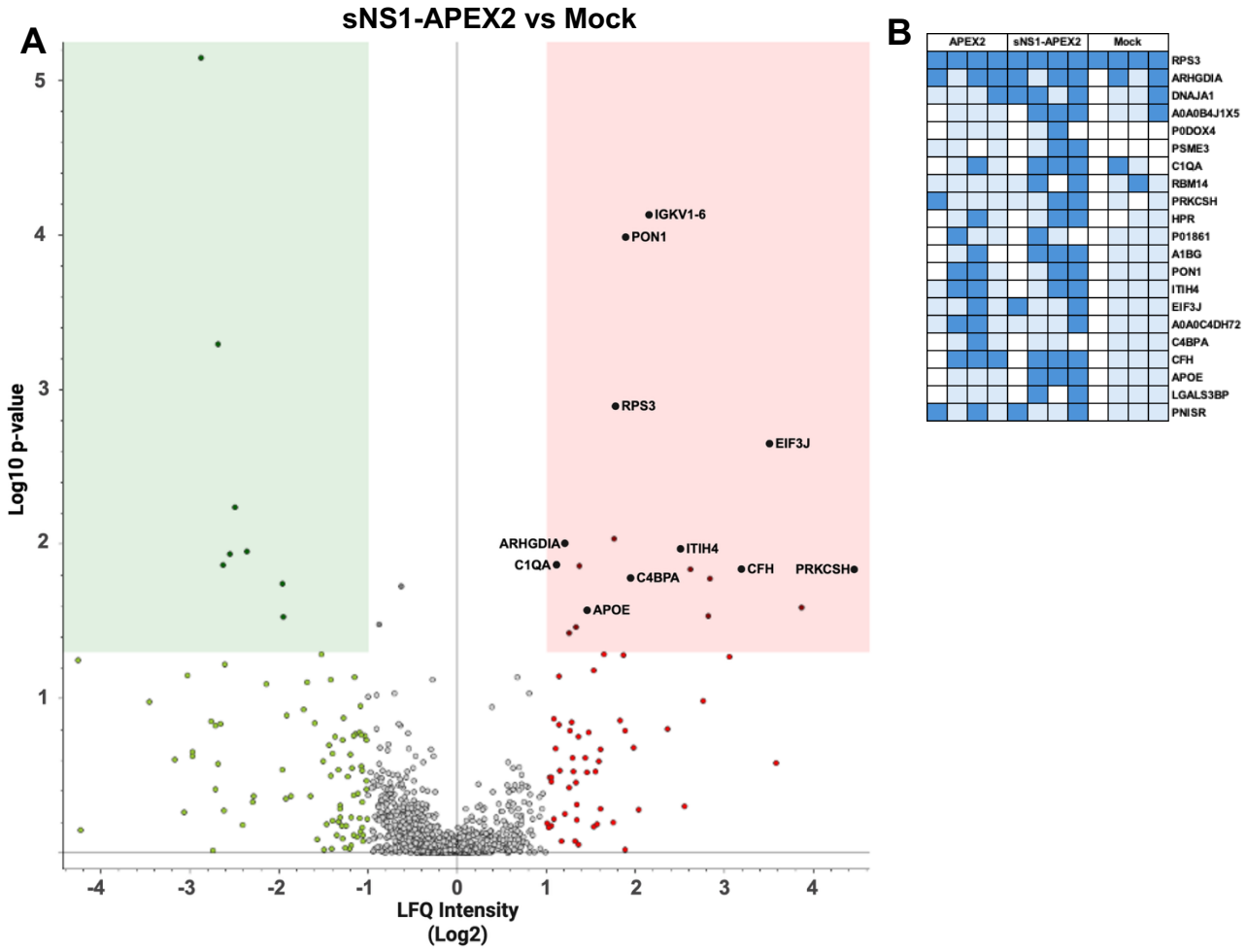

FIGURE 4.14. Quantitative analysis of sNS1-APEX2 vs Mock proximity labelled cells. (A) Volcano plot of proteins enriched in sNS1-APEX2 inoculated vs Mock inoculated Huh-7.5 cells. Proteins within the pink box are determined as significantly enriched ≥ 2-fold ($p \leq 0.05$). (B) Frequency map illustrating the degree to which proteins were identified for each individual replicate.

To provide further confidence that the sNS1-APEX2 enriched proteins identified in our study are likely to be associated with sNS1, we compared our hits with the previously published NS1 interactome that was generated by Hafirassou and colleagues using a FLAG- and HA-tagged NS1 DENV2 subgenomic replicon expressed in Raji, HeLa, and HAP1 cells with NS1 interacting proteins retrieved from cell lysates using tandem affinity co-IP [222] (Figure 4.15). Overlap of the proteins identified in all three cell lines of the previously published NS1 interactome with the enriched hits identified in our sNS1-APEX2 vs sAPEX2 and sNS1-APEX2 vs mock analyses revealed a total correlation of 2 proteins. Comparison of the 45 enriched hits identified for sNS1-APEX2 vs APEX2 with the published NS1 interactome revealed an overlap of a further 19 proteins. Of the 21 hits identified for sNS1-APEX2 vs mock, an additional 3 proteins were identified as shared with the previously published NS1 interactome. Despite the differences in the methodologies used to identify sNS1-associated and NS1-associted proteins, the substantial level of overlap strongly supports the validity of our results. In our study, a total of 7 proteins were identified as significantly enriched in both sNS1-APEX2 vs sAPEX2 and sNS1-APEX2 vs mock samples. Importantly, the identification of APOE in our study is consistent with the recently identified interaction between sNS1 and HDL or LDL complexes that have been observed both *in vitro* and *in vivo* [227]. These sNS1-lipoprotein complexes that have been observed in DENV infected patient sera have been shown to acquire an APOE positive phenotype over time [227]. The identification of APOE, a host protein known to associate with sNS1 in the extracellular environment confirms that our data set contains human proteins known to associate with sNS1. Moreover, it also confirms that our data set contains biologically relevant human host factors that associate with sNS1 in DENV-infected patients.

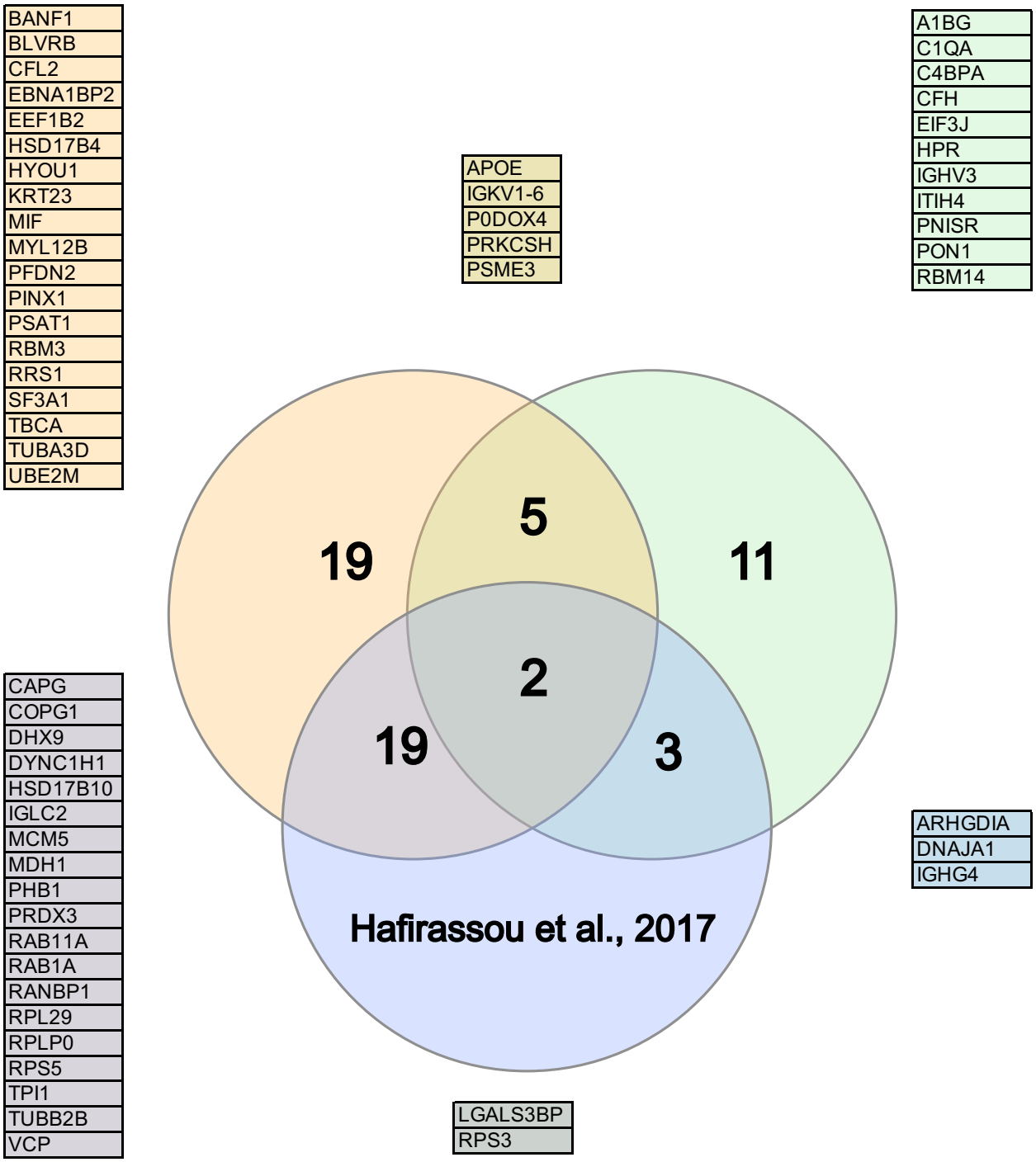

FIGURE 4.15. Comparison of internalised sNS1-APEX2 enriched proteins with intracellularly-expressed NS1 interactome. Venn diagram depicting Huh-7.5 endogenous proteins that were enriched in sNS1-APEX2 vs sAPEX2 (left) and sNS1-APEX2 vs Mock (right) samples with the previously identified NS1 interactome generated by Hafirassou *et al*., 2017. Venn diagram created with https://www.interactivenn.net/. (Heberle *et al*., 2015).

To associate the sNS1-APEX2 enriched proteins with biological processes, gene ontology (GO) analyses were performed using Metascape. Interestingly, when comparing sNS1-APEX2 vs sAPEX2 enriched proteins, most identified proteins are connected to *N*-linked glycosylation and eukaryotic translation elongation (Figure 4.16A). This result is intriguing given that the sNS1-APEX2 inoculum also contains infectious DENV2-NS1-APEX2 virus, raising the possibility that the translation of nascent NS1-APEX2 may have contributed to the identification of our hits. When comparing sNS1-APEX2 samples to the mock control, most enriched proteins relate to regulation of complement cascade, HDAC6 interactions, platelet degranulation and regulation of innate immune responses (Figure 4.17A), likely reflecting the lack of infectious virus present in the cell culture system the was used to propagate the mock inoculum. Nonetheless, it is well documented that sNS1 interacts with a variety of complement proteins in the extracellular environment. C1QA and C4BPA have previously been identified as direct interacting partners of sNS1. Thus, the identification of these host proteins confirms that our study has identified sNS1 interacting proteins.

Next, to associate our enriched proteins with cellular components, GO analyses were performed using STRING. Consistent with the biological processes associated with translation, ribonucleoprotein complexes were enriched in sNS1-APEX2 vs sAPEX2 samples (Figure 4.16B). For the sNS1-APEX2 vs mock hits, an enrichment in extracellular components is observed (Figure 4.17B). Interestingly, an enrichment in extracellular exosome components were observed for both sNS1-APEX2 vs sAPEX2 and sNS1-APEX2 vs mock identified hits. This result is consistent with recent data that revealed DENV sNS1 is a component of extracellular vesicles [449], and sNS1 can associate with exosomes in the extracellular environment [450]. The enrichment of cellular components known to be associated with sNS1 provides further support that the proteins identified in this study are sNS1-associated.

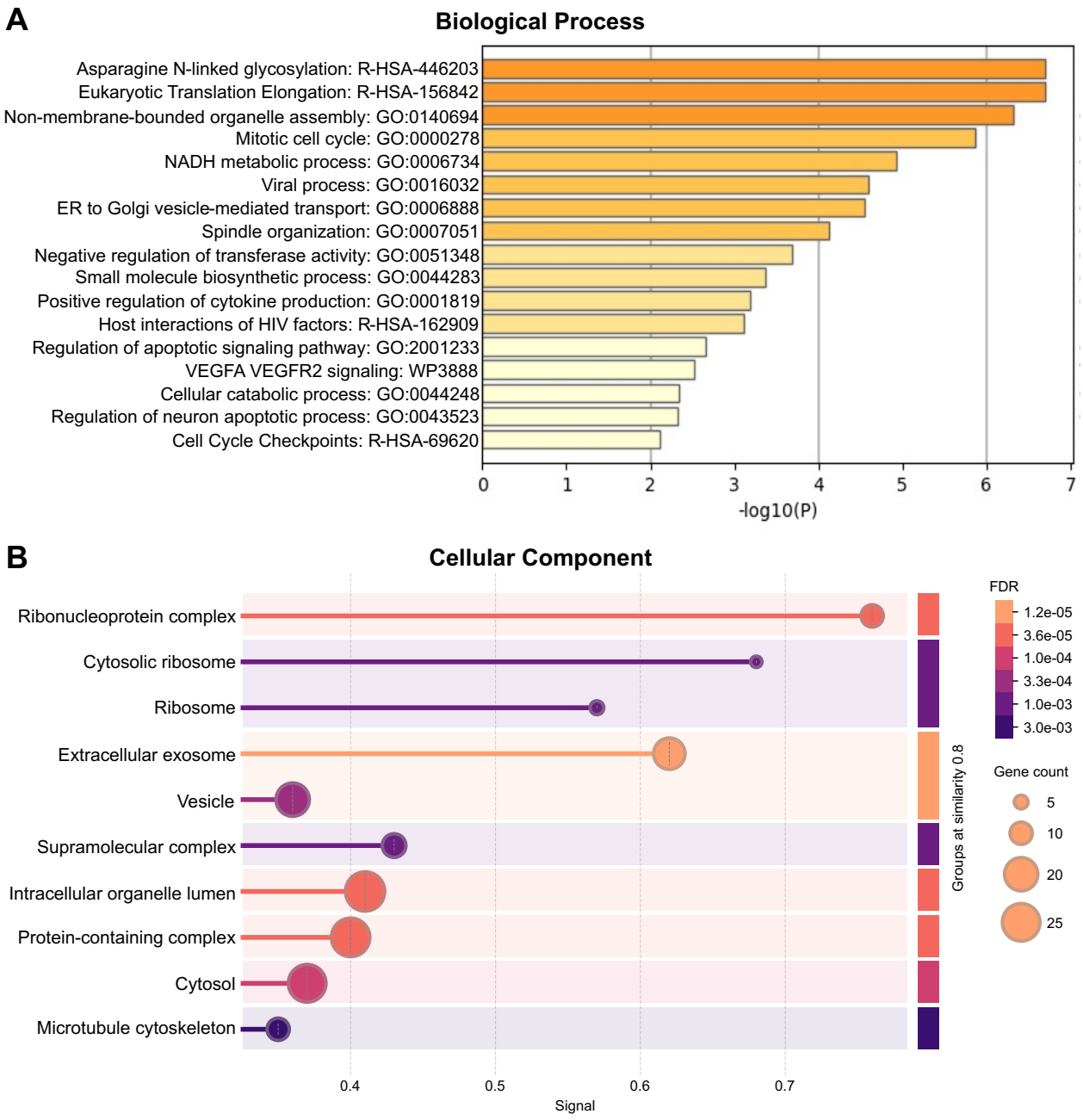

FIGURE 4.16. Gene ontology enrichment analysis of enriched sNS1-APEX2 vs sAPEX2 proteins. (A) Gene ontology (GO) analysis of biological processes were identified using Metascape database (http://metascape.org (Zhou *et al*., 2019), accessed 19 December 2024)), top enrichment biological processes are coloured by –log10 (p-value). (B) GO cellular components were identified using STRING database (https://string-db.org/ (accessed 19 December 2024)), terms are grouped by similarity score ≥0.8.

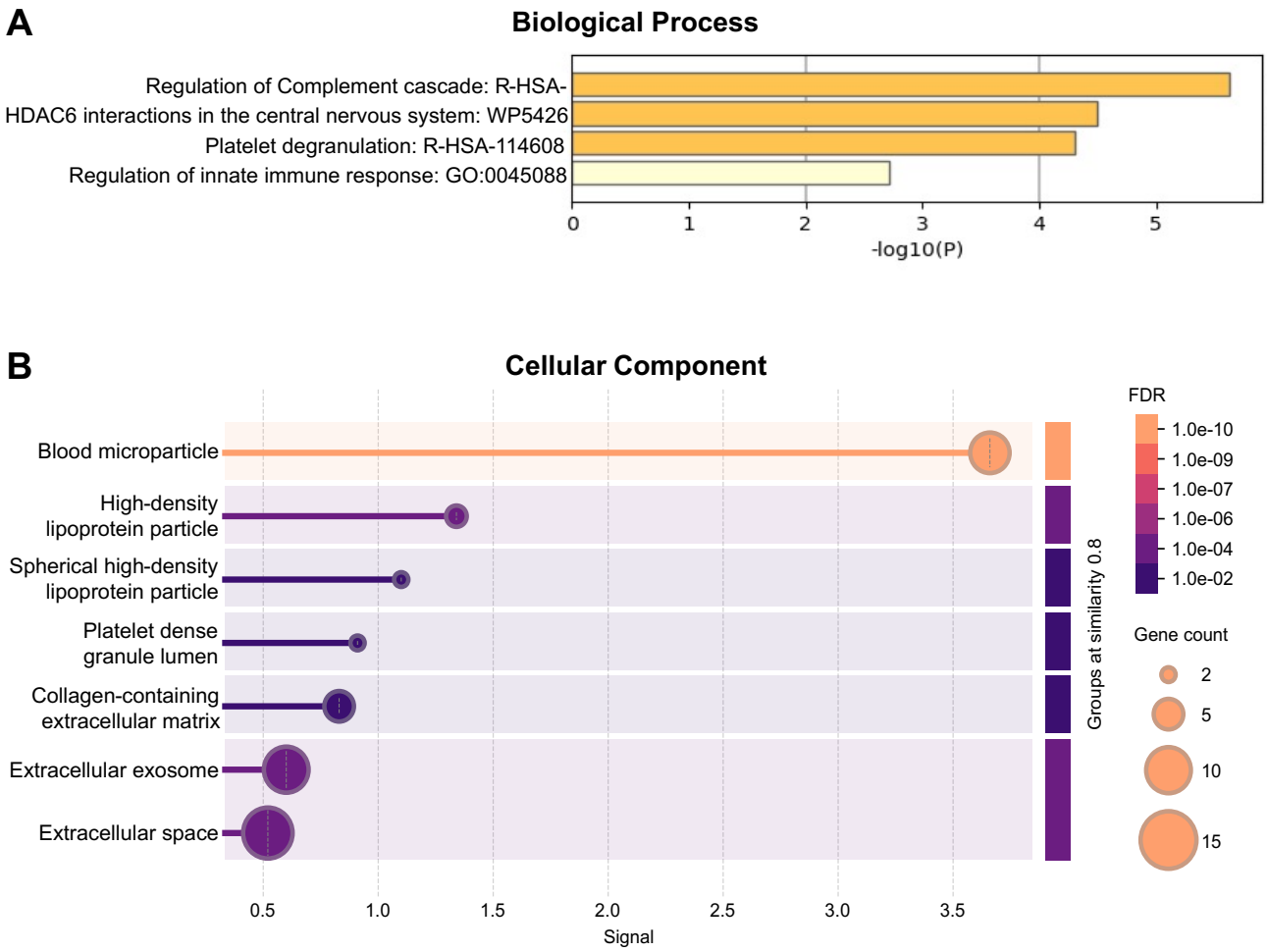

FIGURE 4.17. Gene ontology enrichment analysis of enriched sNS1-APEX2 vs sAPEX2 proteins. (A) Gene ontology (GO) analysis of biological processes were identified using Metascape database (http://metascape.org (Zhou *et al*., 2019), accessed 19 December 2024)), top enrichment biological processes are coloured by –log10 (p-value). (B) GO cellular components were identified using STRING database (https://string-db.org/ (accessed 19 December 2024)), terms are grouped by similarity score ≥0.8.

To evaluate functional and physical associations between the sNS1-APEX2 enriched hits, a protein-protein interaction (PPI) network was constructed using STRING. Additionally, to provide further confidence that the enriched hits are associated with the early events of sNS1 internalisation rather than nascent NS1 translation, proteins identified as cellular components of extracellular exosomes are highlighted in red (Figure 4.18). Interestingly, several of the ribosomal proteins that were enriched in the sNS1-APEX2 vs sAPEX2 samples and contributing to the biological process of eukaryotic translation are categorised as extracellular exosome components, suggesting that the identification of these proteins may be the result of sNS1 inoculation rather than nascent NS1 translation. As shown in Figure 4.18, several functional and/or physical interactions exist between several of our identified hits. Importantly, these analyses revealed a network that connects VCP, a pro-orthoflaviviral host factor [451] that colocalises with JEV NS1 in infected cells [394], with several proteins that play key roles in intracellular trafficking. DYNC1H1 (dynein cytoplasmic 1 heavy chain 1) is a major component of cytoplasmic dynein 1 which is the main retrograde motor that carries cargo along microtubules [452]. TUBA3D (tubulin alpha 3D) and TUBB2B (tubulin beta 2B) are alpha- and beta-tubulins, respectively. Tubulin is a major constituent of microtubules, which are main components of the cytoskeleton and are involved in intracellular transport. TBCA (tubulin folding co-factor A) is a chaperone that assists in tubulin folding. Additionally, the network that connects the Rab GTPases Rab1A, Rab11A, with COPG1 is intriguing given that these Rabs are associated with regulating endosomal trafficking and that COPG1 is a component of the coatomer protein complex I that coats intracellular transport vesicles. The identification of functional and/or physical associations that link known NS1 interacting proteins with proteins involved in endosomal trafficking and retrograde motility suggests that these human host factors may be associated with the intracellular transport of internalised sNS1.

Collectively, the analyses presented above provide several lines of evidence that indicate our sNS1-APEX2-based proteomic analysis has identified a broad range of human host proteins that are associated with the early events of sNS1 internalisation. Our data set contains several proteins that are known to associate or directly interact with sNS1 in the extracellular environment. Moreover, several of our protein hits are categorised as components of exosomes, a human host factor that sNS1 is also known to interact with in the extracellular environment. The identification of these host proteins indicates that interactions between sNS1 and extracellular factors may be important for facilitating sNS1-host cell binding and/or internalisation. Additionally, the identification of human host proteins known to be involved in endosomal trafficking strongly suggests that our data has identified human host proteins that are associated with the intracellular transport of internalised sNS1. Taken together, these data indicate that this study has provided a more comprehensive profile of the human host proteins that are associated with the early events of sNS1 internalisation into human hepatic cells, a major target of sNS1 *in vivo*.

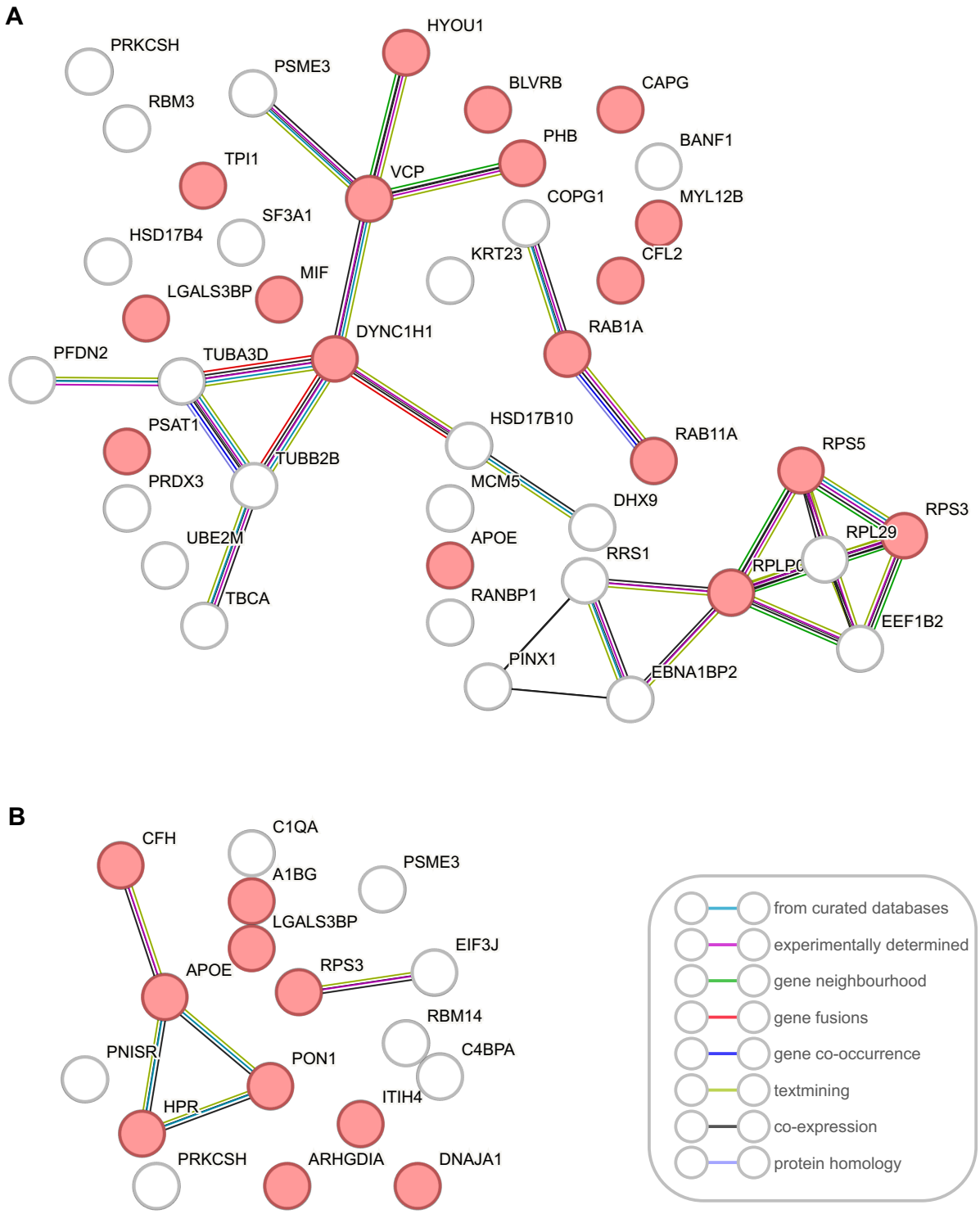

FIGURE 4.18. Protein-protein interaction networks of the internalised sNS1-APEX2 enriched proteins. STRING database-generated protein-protein interaction network displaying the significantly enriched (≥ 2-fold; p-value ≤ 0.05) proteins identified in the sNS1-APEX2 vs sAPEX2 (A) and sNS1-APEX2 vs Mock (B) analyses. Confidence score threshold was set at 0.7 (high confidence) for both analyses. Nodes represent proteins and the connecting lines indicate functional and physical associations. Connecting lines are coloured based on evidence of interaction (inset box). STRING database (https://string-db.org/ (accessed 19 December 2024)).

4.3: Discussion

sNS1 is bound and internalised by a variety of human host cell types [208, 209]. This process has been shown to exert several functions including enhancing cellular susceptibility to infection [269, 277], and inducing aberrant cytokine production that can disrupt endothelial cell monolayer integrity and contribute to vascular leakage [210, 264]. Moreover, the internalisation of sNS1 by endothelial cells has been shown to directly disrupt the endothelial glycocalyx layer and induce endothelial cell hyperpermeability and vascular leakage [211, 219]. As such, identifying the human host proteins that are involved in sNS1 internalisation is of critical importance and could contribute to the development of antiviral therapies to alleviate the pathologies associated with DENV infection. Therefore, the aim of this chapter was to identify candidate human host proteins associated with the early events of sNS1 internalisation.

A recently developed method that has garnered much attention is APEX2-based peroxidase catalysed proximity labelling [296, 297]. A protein of interest is fused to APEX2, an engineered ascorbate peroxidase that allows promiscuous and rapid biotinylation of proximal proteins in live cells. In the presence of biotin-phenol and H_2O_2, APEX2 generates biotin-phenoxyl radicals that covalently tag proximal proteins within a 20 nm radius. Since the tagged endogenous proteins are biotinylated, this can be coupled with streptavidin-based affinity purification and mass spectrometry. Our laboratory previously generated a DENV2-NS1-APEX2 construct that contains the APEX2 tag embedded within NS1. This fully infectious virus was previously characterised in Huh-7.5 cells. In *in vitro* transcribed RNA transfected Huh-7.5 cells, this NS1-APEX2 fusion protein displays wildtype-like intracellular NS1 localisation, NS1-APEX2 secretion, and has been demonstrated to have practical applications in APEX2-based electron microscopy [94]. Given the aim of this chapter, we recovered the secreted NS1-APEX2 (sNS1-APEX2) fusion protein from DENV2-NS1-APEX2 transfected Huh-7.5 cell culture supernatant. This sNS1-APEX2-containing cell culture supernatant was inoculated onto naïve Huh-7.5 cells to allow the spatially resolved proteomic mapping of the human host proteins associated with sNS1 internalisation.

First, we confirmed that the sNS1-APEX2 fusion protein is internalised into Huh-7.5 cells. Confocal immunofluorescence microscopy revealed that internalised sNS1 was distributed diffusely throughout the cytoplasm and strong NS1 signal appeared as large punctate structures in the perinuclear region. It is worth noting that the fixation and labelling process employed in this study was similar in method to the sNS1 internalisation study performed by Alcala *et al* [233]. However, the inclusion of a glycine-acid wash step to remove surface-bound uninternalized sNS1 prior to fixation, as performed by Wang *et al* [219], may have been a valuable approach to run in parallel, to

distinguish internalised sNS1 from cell surface-bound sNS1. Nonetheless, our data was consistent with previous studies interrogating sNS1 internalisation in human hepatocytes [233, 277], strongly supporting the conclusion that sNS1-APEX2 is internalised into Huh-7.5 cells. Next, we confirmed that internalised sNS1-APEX2 retained its APEX2 catalytic activity to ensure its ability to biotinylate endogenous proteins within close proximity to internalised sNS1. Confocal immunofluorescence microscopy and Western blot analyses were utilised for functional characterisation. Our results revealed that sNS1-APEX2 is internalised in an sNS1-dependent manner and can biotinylate sNS1-APEX2 proximal endogenous proteins in an APEX2-dependent manner. This confirmed that internalised sNS1-APEX2 could be utilised for proximity-dependent biotinylation in live cells.

As a control for the sNS1-APEX2 proximity labelling experiments to separate sNS1-specific from any potential APEX2-specific interactions, we developed a DENV-driven APEX2 construct for which APEX2 is unattached to any DENV protein and is secreted from infected Huh-7.5 cells via a signal peptide. Using confocal immunofluorescence microscopy, we confirmed that this DENV-driven APEX2 protein is functionally active, allowing APEX2-catalysed biotinylation in live cells, and that the secreted APEX2 (sAPEX2) protein accumulates in infected cell culture supernatant. Importantly, we demonstrated that this DENV construct is infectious and replicates with similar kinetics to that of the DENV2-NS1-APEX2 strain. Moreover, the NS1 expressed by this strain was shown to display wildtype-like intracellular distribution and is secreted into cell culture supernatant. Thus, similarly to the sNS1-APEX2 experimental inoculum that co-contains sNS1-APEX2 and infectious DENV2-NS1-APEX2 virus, the sAPEX2 control inoculum also contains sNS1 and infectious virus. As a negative control for the sNS1-APEX2 proximity labelling experiments to separate sNS1-APEX2 specific interactions from background, we opted to recover cell culture supernatant from untransfected Huh-7.5 cells for a simple and reproducible mock-inoculum control as a standard of comparison.

Several approaches were employed to attempt to increase the yield of the sNS1-APEX2 fusion protein from DENV2-NS1-APEX2 transfected cells. Ultimately, we employed a 100 kDa MWCO ultrafiltration technique to concentrate sNS1-APEX2 cell culture supernatant. This ultrafiltration process was shown to successfully concentrate sNS1-APEX2 and infectious DENV2-NS1-APEX2 virions. While the presence of DENV virions may act to influence the binding and internalisation of sNS1, we reasoned that for our sNS1-APEX2 proximity biotinylation experiments, the presence of infectious virus in the inoculum more accurately reflects the true biological scenario *in vivo*. However, this ultrafiltration process simultaneously co-concentrated components of the FBS present in the cell culture media. Here, we reasoned that highly concentrated FBS in the sNS1-APEX2 inoculum may interfere with sNS1-mediated host cell binding and/or internalisation. To circumvent this, when DENV2-NS1-APEX2 transfected Huh-7.5 cells were propagated to generate sNS1-APEX2 cell

culture supernatant, culture media was added during cell expansion to dilute the final FBS concentration from our laboratory standard 10% (v/v) to approximately 2% (v/v) over the course of 7 days.

Previous studies have shown that internalised sNS1 co-localises with Rab5 positive early endosomes before transitioning to Rab7 positive late endosomes at 1.5 hours and 6 hours post-inoculation, respectively. We designed our methodology such that we could capture the sNS1-associated host factors that precede these events. By incubating cells with ultrafiltered sNS1-APEX2 inoculum for 30 minutes, then removing the inoculum and incubating cells for a further 30 minutes in biotin-phenol-supplemented media before catalysing the biotinylation reaction for precisely 1 minute, our approach should identify sNS1 proximal host proteins up to and including 1 hour post inoculation. Our results revealed a total of 45 proteins that were significantly enriched ≥2-fold in sNS1-APEX2 vs APEX2 samples, and 21 proteins that were significantly enriched ≥2-fold in sNS1-APEX2 vs mock samples. Comparisons of these hits with the previously published NS1 interactome revealed a considerable degree of overlap [222], providing confirmation that our sNS1 proteomic data contains proteins previously identified as NS1 interacting partners, thus supporting the validity of our results. The degree of overlap shared between our study and the previously published study is particularly intriguing given the differences in the experimental methods used to identify sNS1 and NS1 associated host proteins. DENV NS1 is a multifunctional protein that is trafficked to several intracellular and extracellular locales where it performs a variety of roles. The previously published NS1 interactome was generated by tandem affinity co-immunoprecipitation of whole cell lysates prepared from HA- and FLAG-tagged NS1-modified DENV2 subgenomic replicon-harbouring Raji, HeLa, and HAP1 cells. Importantly, it should be noted that subgenomic replicon-encoded NS1 is secreted. This process should therefore allow the identification of host proteins that are capable of interacting directly (and to a lesser extent indirectly) with intracellular NS1, cell surface-exposed NS1, cell surface-bound sNS1 and internalised sNS1. Given the relative abundance, however, this study is biased towards identifying intracellular NS1 interacting partners. The sNS1-APEX2 biotinylation approach in our study, however, strongly favours identification of internalised sNS1 proximal host cell proteins that are associated with the early events (up to and including 1 hour post inoculation) of sNS1 internalisation in live cells. Given that we recovered sNS1-APEX2 from infected cell culture supernatants, our data likely includes host proteins that associate with sNS1 in the extracellular environment or that are co-secreted with sNS1. Also, given the presence of infectious virus in the inoculum, it cannot be excluded that our study also contains host factors associated with genome translation. While this does highlight the difficulty in working with a multifunctional viral protein that performs a variety of roles, it also suggests that these shared proteins are likely of particular importance to multiple aspects of NS1 and sNS1. Thus, these proteins may represent valuable candidates for host-directed antiviral therapeutics.

Our study identified several proteins that are known to associate with extracellular sNS1, either through direct interactions with sNS1 or indirectly by association with sNS1-host factor complexes. Interestingly, the human host protein APOE was significantly enriched in our study. It was recently revealed that sNS1 forms a high-affinity interaction with APOA1-containing high-density lipoproteins (HDL) and a lower-affinity interaction with APOB-containing low-density lipoproteins (LDL) in the extracellular environment, with sNS1 docking onto the lipoprotein surface [227]. In DENV-infected patient plasma, these sNS1-lipoprotein complexes acquire an APOE positive phenotype during the course of infection [227]. While sNS1-HDL complexes have been shown to stimulate the production of proinflammatory cytokines in human primary macrophages, the biological relevance of this sNS1-APOE interaction remains to be determined. Nonetheless, the identification of APOE in this work confirms that our study has identified sNS1-host factor interactions that are observed *in vivo*. This indicates that our data set could be further explored to identify novel sNS1-host factor interactions that occur in DENV-infected patients.

Several components of the complement system were also observed as significantly enriched in our study. The identification of the complement protein C1QA in our study is consistent with the identification of this protein as an NS1 interacting partner in a yeast two-hybrid screening study that was subsequently confirmed by co-IP [453]. Additionally, C4BPA, which was identified in our study, has previously been demonstrated to directly interact with sNS1 [257]. Importantly, sNS1 has been shown to bind C4BP in solution and recruit it to the surface of mammalian cells [257]. The enrichment of C4BPA in our study indicates that extracellular sNS1-host factor interactions that facilitate sNS1-host cell interactions and elicit important biological effects have been identified in our study. As such, our hits could be mined to identify additional extracellular host factors that facilitate sNS1-host cell interactions.

Factor H, a complement regulatory factor that acts to prevent complement activation, was also identified as a hit in our study. Lower levels of circulating Factor H are found in patients with DHF than patients with DF and this imbalance is suggested to be associated with exacerbated complement activity that contributes to dengue disease severity [454]. Factor H has been identified as an interacting partner of NS1 from WNV [455], but this interaction is not observed with DENV NS1 [455, 456]. The APEX2-based proximity-dependent labelling used in this study biotinylates proximal proteins; thus, it is likely that only a fraction of our hits reflect direct sNS1 interactors. However, the identification of sNS1 proximal proteins is of interest, given that host factors that form proximal associations rather than direct interactions, may also impart important biological effects. Thus, in addition to identifying human host proteins that directly interact with sNS1, our data likely contains sNS1-associated host proteins that are of both physiological and biological relevance.

For the enriched proteins identified in sNS1-APEX2 samples as compared to sAPEX2 samples, GO analyses revealed an enrichment of biological processes related to *N*-linked glycosylation and eukaryotic translation. Given that the sNS1-APEX2 inoculum contained infectious DENV2-NS1-APEX2 virus, this may have been the result of translation of nascent NS1-APEX2. Indeed, the identification of the ribosomal proteins RPS3, RPS5, RPL29, and RPLP0 in our study, is consistent with previous studies that have identified these proteins as NS1 interacting partners in DENV-infected [457], or DENV subgenomic replicon transfected [222], mammalian cells. While our biotinylation reaction was catalysed for only 1 minute at 60 minutes post-inoculation, a timepoint preceding positive-sense viral RNA amplification in human hepatic cell culture systems [458], it is possible that the APEX2-based proximity labelling method is sensitive enough to detect input strand DENV protein translation, particularly in a polysome setting [459]. However, given that ribosomal proteins also exhibit extra-ribosomal functions, it is possible that the proteins shared between this study and the previously identified NS1 interactome represent host cell proteins that are of critical importance to multiple aspects both NS1 and sNS1 biology. Interestingly, additional GO analyses revealed that several of these ribosomal proteins that contribute to the biological processes of translation are also components of extracellular exosomes. Extracellular vesicles, including exosomes, act in intercellular communication by transferring donor cell RNA and proteins, including the ribosomal proteins identified here, to a recipient cell by fusing directly with the plasma membrane to release luminal content or by being internalised by endocytosis in a clathrin-dependent manner [460]. It is well recognised that extracellular vesicle secretion is enhanced in the context of orthoflavivirus infection of both mammalian and arthropod cells [461]. Over the last decade, the emerging role of orthoflavivirus-modified extracellular vesicles as conveyors of virus, infectious and subgenomic RNA and viral proteins has revealed a role of these vesicles in modulating host cell physiology and enhancing viral transmission and pathogenicity [462, 463]. Indeed, NS1 has been identified as a component of extracellular vesicles as a membrane-bound and possibly luminal component [449, 450]. As such, the identification of these hits as putative sNS1 associated proteins may be the result of sNS1 interactions with extracellular vesicles that may act to favour sNS1 internalisation. The experiments performed in this study do not allow one to distinguish whether these putative sNS1 interactions are the result of associations of sNS1 or nascent NS1 translation. It would be invaluable to perform a co-IP or targeted mass spectrometry analyses of the inoculum and post-inoculated whole cell lysates to confirm where these putative NS1 interactions have occurred. It is intriguing to consider that sNS1 may hijack ribosomal protein-containing extracellular vesicles as a mechanism to subvert the host immune response or to sequester pre-translation machinery to expedite viral protein synthesis during subsequent infection. These processes could conceivably contribute to the NS1-induced enhancement of infection that is observed when uninfected cells are pretreated with sNS1.

The high spatial and temporal resolution provided by APEX2-based proximity labelling provides our study with the ability to identify both direct interacting and proximal sNS1 proteins that are associated with sNS1 internalisation. The PPI network generated in this study revealed several functional and physical associations exist between our hits. The inclusion of previously identified NS1 interactors with novel host proteins identified here, suggests that these proteins may represent host cellular factors that are associated with the intracellular trafficking of sNS1 following internalisation. The physical and functional network that connects VCP, a pro-orthoflaviviral host factor [390-393] that colocalises with JEV NS1 in infected cells [394], with cytoplasmic dynein (DYNC1H1) and tubulin proteins (TUBB2B, TUBA3D, TBCA) suggests that these proteins may be associated with the intracellular trafficking of internalised sNS1 [464]. Additionally, the coatomer protein complex I subunit, COPG1, and the small GTPases, RAB1 and RAB11, would also make interesting candidates given their role in the trafficking of intracellular vesicles [465]. Exploring how these proteins and their associated pathways influence the intracellular trafficking of internalised sNS1 represents a fascinating area of research.

4.4: Conclusion

The aim of this chapter was to generate a more comprehensive profile of the human host proteins that are associated with the early events of sNS1 internalisation. This was achieved by using a secreted NS1-APEX2 fusion protein that allows proximity-dependent biotinylation in live cells, which revealed a list of several host proteins that are putatively associated with sNS1 internalisation. Collectively, the identification of several proteins known to interact with DENV NS1 in both the extracellular and intracellular environment strongly supports the validity of our results. Moreover, the inclusion of these known sNS1 interacting proteins with the putative sNS1 interacting proteins identified in this study in protein-protein interaction networks indicate that functional linkages exist between these proteins. Taken together our study has provided a more complete picture of the molecular machinery involved in the early events of DENV sNS1 internalisation into human hepatic cells, a major target of sNS1. Future work interrogating how these host factors may be involved with sNS1 internalisation may contribute to the identification of targets for host-directed therapeutics.

Chapter 5

Final discussion

DENV is the most prevalent mosquito-borne human viral pathogen. Distributed throughout the tropical and subtropical world, half of the world's population live in at-risk areas [24, 28]. Over the last two decades, a ten-fold increase in the incidence of dengue has been reported by the World Health Organization [27], resulting in the emergence of dengue as a global health problem. In 2019, 129 countries reported cases of dengue, with approximately 56.7 million new cases and 36,055 related deaths reported [27, 28]. There are currently two licensed DENV vaccines, Dengvaxia and Qdenga, however, neither vaccine provides long-lasting immune protection against all DENV serotypes and the use of Dengvaxia and, to a lesser extent Qdenga, in seronegative individuals is not recommended [466]. Moreover, there are no dengue-specific therapeutics to prevent dengue disease progression, thus necessitating a better understanding of DENV biology. Of particular interest is the identification of DENV-host molecular interactions as this may reveal novel targets for both virus- and host-directed therapeutics.

DENV is a member of the Orthoflavivirus genus and shares a high level of genetic similarity with other genera members including the Australian-endemic West Nile virus Kunjin subtype (WNV/KUNV). The highly condensed ~11 kb single stranded positive sense RNA genome encodes a 3,411 amino acid polyprotein which is cleaved into three structural and seven non-structural proteins. Garnering much recent attention is the non-structural protein 1 (NS1), a 352 aa protein that has a molecular weight of 45 – 55 kDa dependent upon its glycosylation status. This multifunctional virulence factor exhibits multiple oligomeric states and is found in a variety of intra- and extracellular locales. In the intracellular environment, NS1 plays essential roles in viral RNA replication [93, 95, 96] and virus particle assembly [97]. In infected cells, a portion of NS1 is observed to be plasma membrane-associated and cell surface-exposed [196], and this NS1 form has been shown to facilitate intracellular signal transduction [197]. NS1 is also secreted into the extracellular environment and significant levels of secreted NS1 (sNS1) are found in patient sera [199, 202-204]. Indeed, high levels of sNS1 in hospitalised DENV-infected individuals have been correlated with adverse disease outcomes [206]. In the extracellular environment, sNS1 has been linked to dengue disease pathogenesis through a variety of pathways [95, 96]. sNS1 can elicit the production of cross-reactive antibodies that can damage endothelial cells and platelets [96]. sNS1 can also interfere with components of the complement system to modulate their activity and alter the host immune response [207]. Through binding to immune cells, sNS1 can stimulate the production of proinflammatory cytokines that can disrupt endothelial cell integrity [210]. Additionally, sNS1 is efficiently endocytosed by a variety of uninfected cell types [208, 209], and through unknown mechanisms can contribute to enhanced susceptibility to infection [277]. The internalisation of sNS1 by endothelial cells has been shown to directly contribute to endothelial cell hyperpermeability and vascular leakage [219] – a key symptom of severe disease. Given the diverse roles of sNS1 in dengue pathogenesis, defining the

human host cellular factors associated with NS1 secretion and sNS1 internalisation is of critical importance.

The first aim of this project was to identify and interrogate the human host cell factors that are associated with DENV NS1 secretion. To achieve this aim, we performed a customised membrane-trafficking siRNA screen in human hepatocellular Huh-7.5 cells infected with our previously characterised DENV2-NS1-NLuc reporter virus [94]. Our results revealed COPA, COPB2, and COPG1 as the top three hits whose depletion reduced the extracellular accumulation of sNS1. These are three of the seven subunits of the coatomer protein complex I (COPI) that coats transport vesicles and is best known for its role in trafficking proteins within the early secretory pathway [334, 376]. Our deconvolution siRNA screen revealed that multiple siRNAs targeting these COPI components also induced a similar NS1 secretion-impairing phenotype, thus implicating COPI as an important determinant of DENV NS1 secretion. Given the importance of COPI in mediating protein trafficking within the early secretory pathway, the exploitation of COPI components and their associated pathways to achieve NS1 secretion is not surprising. As such, we chose to focus our investigation on the role of COPI components in orthoflavivirus NS1 secretion. Additionally, given the role of GBF1 as a master regulator of COPI vesicle formation [371], the role of GBF1 in NS1 secretion was also explored.

Validation studies in Huh-7.5 cells confirmed that COPI component siRNA treatment substantially reduced target mRNA abundance, however only a modest reduction in cognate protein was observed. In DENV infected Huh-7.5 cells, our COPI component siRNA treatment did not impact intracellular viral RNA abundance or infectious virus production. Importantly, however, our COPI component siRNA treatment did reduce NS1 secretion efficiency in both DENV- and WNV/KUNV-infected cells, indicating that these related viruses may exploit similar mechanisms to achieve NS1 secretion. Given that NS1 secretion-impairing phenotypes were achieved by individually targeting three components of the COPI complex and the COPI vesicle regulator, GBF1, this substantiated COPI as an important determinant of NS1 secretion. Moreover, this indicates that the requirement for COPI components to achieve efficient NS1 secretion may be a feature conserved within the Orthoflavivirus genus. Given the modest reductions in COPA, COPB2, COPG1, and GBF1 protein abundance incurred by our siRNA treatment, attempts were made to genetically ablate these components using CRISPR-Cas9 technology. However, consistent with previous studies [437], attempts to generate cells completely deficient in COPI component protein were not successful, likely due to the essential nature of these genes [406]. Future studies further interrogating the role of COPI in NS1 secretion could involve the use of inducible shRNA or CRISPR-inhibition (CRISPRi) knockdown approaches in stable cell lines as this may enable more potent COPI protein knockdown

in an entire cell population, without the potentially confounding effects of sustained knockdown or knockout on cell proliferation. It is important to note, however, that our wildtype DENV and WNV/KUNV experimental systems were constrained by the requirement to balance cell viability, knockdown of genes that have been categorised as 'essential for optimal proliferation', productive DENV infection, Western blot-quantifiable NS1 protein production and secretion, and focus the impact of COPI depletion on NS1 secretion while mitigating the potential impact of COPI depletion on alternative aspects of the DENV lifecycle [57, 435]. As such, in the context of a fully infectious orthoflavivirus system, the use of stable cell lines capable of inducible COPI component knockdown would need to be similarly balanced against potential pleiotropic effects of COPI depletion, which may vary greatly even between closely related viruses [467]. The use of NS1-expressing plasmid systems could also facilitate the simple and systematic examination of COPI component silencing on a greater diversity of orthoflavivirus NS1 species and variants to explore genera-wide and species- or serotype-specific effects. Moreover, panels of different cell types that display inducible knockdown of COPI components would facilitate the examination of host cell type-specific effects of COPI depletion on NS1 secretion.

To perturb the COPI pathway, we examined the impact of overexpressing wildtype and deleterious SNP COPI variants. Wildtype COPB2 overexpression was found to enhance NS1 secretion, further confirming COPI as an important determinant of NS1 secretion efficiency and suggesting that the availability of COPB2 protein may be a limiting factor for NS1 secretion. Intriguingly, while overexpression of wildtype COPA did not impact NS1 secretion, NS1 secretion was enhanced in cells expressing the dominant-negative COPA-E241K variant. This variant contains a mutation within the WD40 domain, a region that is critical for mediating cargo-selective interactions via dilysine motifs contained within ER-resident proteins to mediate their retrieval from the Golgi to the ER [468]. Golgi-to-ER trafficking is one of the best categorised roles of COPI coated vesicles and, indeed, this COPA-E241K variant exhibits an impaired ability to bind to dilysine motif-containing cargo and this has been shown to impair Golgi-to-ER retrograde trafficking [410]. However, COPI has also been demonstrated to play a variety of roles in endosomal transport and function [339-342], lipid metabolism [343], autophagy [344, 469, 470] mRNA localisation [345], nuclear envelope disassembly [346], and neurogenesis [347, 348]. It is possible that the WD40 domain of COPA, that is critical for its role in Golgi-to-ER trafficking, may be dispensable or even inhibitory to these alternative COPI pathways. Thus, it is conceivable that the requirement of COPI for efficient NS1 secretion may be due to additional and/or alternative COPI functions beyond its role in early secretory pathway trafficking. Cells expressing the COPA SNP variant COPA-D243G that similarly contains a mutation within the WD40 domain and displays defective Golgi-to-ER trafficking, also exhibits increased autophagosome and endolysosome size [410]; intracellular organelles that have recently been identified as playing roles in non-canonical secretion pathways [471] (discussed

below). Given the NS1 secretion-enhancing phenotype observed in cells transfected with the COPA-E241K variant, future studies of the localisation of NS1 with respect to these organelles that possess secretory capacity may be worthwhile. Importantly, however, the COPA-E241K variant is a genetic cause of COPA syndrome, a rare genetic immune-mediated disorder that exhibits features of both autoimmune and autoinflammatory disorders [439]. As such, cells that express this COPA variant also display physiological perturbations, which may may act to influence cellular secretion. Compared with cells overexpressing COPA-WT, cells overexpressing the COPA-E241K variant exhibit enhanced ER stress [410], which can induce protein secretion through unconventional pathways [306]. Moreover, one of the pathological consequences of COPA-E241K expression, is defective Golgi-to-ER retrieval of the innate immune adapter molecule, STING (Stimulator of interferon genes) [472]. This COPA-E241K-induced Golgi mislocalisation and hyperactivation of STING results in increased Type I IFN signalling [437]. As such, by co-transfecting an ER-stress- and type I IFN signalling-inducing plasmid with an NS1-expressing plasmid, we may have created an environment within this cell culture system that is more reflective of DENV infection, which itself may be critical to enhancing NS1 secretion efficiency [473]. Thus, while of the role of COPA-E241K in NS1 secretion is intriguing and warrants exploration, future investigations must consider the influence of heterologous expression of COPA-E241K on other host factors and pathways that may indirectly impact upon NS1 secretion, particularly in the context of a fully infectious DENV system.

To further confirm the involvement of COPI in NS1 secretion we employed Golgicide A (GCA) to pharmacologically inhibit the catalytic activity of GBF1 which prevents Arf activation and COPI vesicle formation [474]. By treating DENV- or WNV/KUNV-infected cells with increasing concentrations of GCA (1 – 5 μM), we found NS1 secretion was reduced in the presence of 5 μM GCA, thus confirming that GCA reduces NS1 secretion. Despite GCA being a Golgi-dispersing agent [474], we found that this 5 μM GCA-induced reduction in NS1 secretion appeared independent of changes to gross Golgi morphology as no apparent differences in NS1 and the Golgi marker GM130 staining patterns were observed by confocal immunofluorescence microscopy. Moreover, co-localisation analysis indicated no significant impact on NS1 co-localisation with GM130. Interestingly, however, while NS1 secretion was reduced at the highest GCA dose applied, infectious DENV titers were reduced in a dose-dependent manner. This indicates that infectious DENV production is more sensitive than NS1 secretion to the effects of GCA-mediated GBF1 inhibition. Interestingly, this observation that infectious DENV production is more sensitive than NS1 secretion to the effects of GCA-mediated GBF1 inhibition contrasts with our siRNA data. In our experiments, siRNA-mediated depletion of GBF1 (and only depleted by 17% relative to the NTC) was sufficient to reduce NS1 secretion but was insufficient to reduce infectious DENV production. Of course, these two techniques used to interfere with GBF1 differ in their mechanism of action. GCA inhibits the catalytic activity of GBF1 by binding to the GBF1-Arf-GDP protein-protein interface, thus preventing Arf activation [474].

On the other hand, siRNA treatment reduces the total cellular levels of GBF1, however residual GBF1 is presumably catalytically active. As detailed in the Introduction, GBF1 is a 200 kDa protein that contains the conserved catalytic Sec7 domain responsible for GDP-to-GTP transfer to Arfs for Arf activation, and a further 5 conserved non-catalytic domains, the function(s) of which are ill-defined [357, 367, 475]. GBF1 is essential to the replication cycles of a variety of +ssRNA virus families and its proviral roles have been shown to be dependent on both catalytic and non-catalytic activities [370]. Given that differing effects on NS1 secretion and infectious virus production were obtained in this study when GBF1 was modulated by siRNA or GCA treatment, dissecting the role(s) of GBF1 in NS1 secretion certainly warrants further investigation. Similar to the COPI-SNP and NS1-NS5 polyprotein co-expression experiments employed in this study, future studies could employ the GBF1 variants GBF1-M832L and GBF1-E794K that are GCA-resistant and catalytically inactive, respectively [371], to explore the functional role(s) of GBF1 in NS1 secretion. Moreover, the utilisation of truncated GBF1 mutants that were employed by Belov *et al* to study the impact of GBF1 on poliovirus replication could also provide insights into the features and functions of GBF1 that are important in NS1 secretion [476].

Collectively, this work that aimed to identify and interrogate the human host cell factors associated with NS1 secretion has revealed the COPI subunits: COPA, COPB2, and COPG1 as important determinants of efficient NS1 secretion. Additionally, we have demonstrated that GBF1, the master regulator of COPI vesicle formation, is also an important determinant of NS1 secretion. However, several lines of evidence suggest that the role of COPI in NS1 secretion may extend beyond the canonical roles of COPI in early secretory pathway trafficking, and these pathways warrant investigation. In the context of NS1 secretion, exploring the role that COPI plays in lipid droplet (LD) metabolism is an attractive future research direction, given that DENV has previously been shown to exploit this GBF1/Arf/COPI pathway for the trafficking of Capsid between the ER and LDs [57]. The confirmed exploitation of this COPI pathway by DENV may also facilitate efficient NS1 secretion given that LDs are cytosolic organelles composed of a hydrophobic core of neutral lipids, predominantly triacylglycerol and cholesterol esters, enclosed within a phospholipid monolayer. These LD components, triacylglycerol and cholesterol esters, have been identified as the predominant lipid components that stabilise the hexameric form of sNS1 [99]. Based on the lipid content of hexameric sNS1, it has been proposed that intracellular dimeric NS1 preferentially localises at the sites of nascent LDs on the luminal side of the ER to concentrate NS1 dimers, with three dimers coming together to pinch of from the membrane to form the soluble NS1 hexamer complete with the lipid component [99]. It was recently demonstrated that COPI can act directly on the surface of LDs, budding COPI coated nano-LDs in a process that promotes the development of membrane bridges between the LD and ER [477, 478]. This COPI-driven process facilitates the reabsorption of LDs back into the ER [479]. Conceivably, the role of COPI in forming these physical

associations between LDs and the ER may be exploited by DENV to provide the triacylglycerol and cholesterol ester resource that facilitates NS1 hexamerisation and/or stabilisation. Accordingly, this GBF1/Arf/COPI LD pathway that is exploited by DENV should be investigated for its potential importance to NS1 secretion. Additionally, exploring the emerging role of COPI in endosome and autophagosome function and trafficking [480] also represents an attractive focus of future research, as this may also play a role in NS1 secretion. While endosomes and autophagosomes are well-understood to be involved in degradative processes, over the last decade a growing body of evidence has confirmed a role for these components in cellular secretion [471, 481-483]. Termed secretory autophagy, autophagosome-like vesicles complete with recruited cargo can be released via the plasma membrane for secretion into the extracellular environment as membrane-bound extracellular vesicles. Additionally, autophagosomes can fuse with endosomes or multivesicular bodies to form amphisomes, which also fuse with the plasma membrane to achieve secretion [471]. It is well understood that DENV interferes with autophagic machinery to enhance viral replication [484], and NS1 alone is sufficient to induce autophagosome formation [264, 485]. Viral RNA and viral proteins, including NS1, co-localise with autophagy markers in DENV infected cells [449]. Indeed, it has been shown that DENV-infected cells release infectious autophagy-related extracellular vesicles that promote transmission [486], and these infectious autophagy-associated extracellular vesicles contain NS1 [449]. In the extracellular environment, sNS1 has been shown to interact with and become a membrane-bound component of extracellular vesicles [450]. However, immunogold labelling and transmission electron microscopy of purified autophagosomes recovered from DENV-infected cells has revealed that NS1 is a luminal component of these vesicles [487]. Indeed, the inhibition of infectious autophagy-related vesicle egress from DENV infected cells also induces a reduction in NS1 secretion [488]. Collectively, these data suggest that secretory autophagy represents an additional and non-canonical secretion pathway that DENV may exploit to achieve NS1 secretion. Given that COPI and NS1 have each been associated with these intracellular organelles that can facilitate the secretion of both extracellular vesicles or their luminal content, this hypothesis warrants consideration. The possibility that NS1 secretion is achieved through the release of extracellular vesicles is consistent with our proteomic analyses of the host factors that are involved in NS1 binding and internalisation (Chapter 4) that revealed a significant enrichment of extracellular exosome-associated proteins as host factors that are associated with sNS1 internalisation. Future studies into this possibility could benefit from the use of the COPA-E241K variant, given that cells expressing a similar WD40 mutation-containing variant (COPA-D243G) display enlarged endosomes and autophagosomes, which may be linked to its NS1 secretion-enhancing phenotype.

While we have identified COPI as an important determinant of NS1 secretion and thereby contributed to a better understanding of the human host factors associated with NS1 secretion, more work is

required to define the molecular mechanism(s) of NS1 secretion. Given the essential nature of COPI components, targeting COPI as a therapeutic intervention to prevent pathologies associated with sNS1 is unlikely. However, the work presented here, that reveals COPI as an important determinant of NS1 secretion, opens avenues for future investigations to further interrogate the role of COPI in NS1 secretion, which may lead to the identification of druggable targets.

Given the importance of sNS1 internalisation to DENV biology and dengue pathology, we sought to identify the human host proteins that are associated with the early events of sNS1 internalisation (Chapter 4). To this end we employed our previously developed DENV2-NS1-APEX2 virus that harbours the engineered plant peroxidase, APEX2, embedded within NS1 [94]. When genetically fused to a protein of interest, APEX2 can catalyse the biotinylation of proximal proteins within live cells, thus allowing spatially restricted labelling for proteomic profiling [297]. The fully infectious, albeit attenuated, DENV2-NS1-APEX2 construct secretes NS1-APEX2 (sNS1-APEX2) fusion protein from infected cells. Thus, sNS1-APEX2-containing cell culture supernatants were inoculated onto naïve cells to allow sNS1-mediated binding and internalisation and APEX2-mediated proximity-dependent biotinylation of internalised sNS1 proximal host factors in live cells for subsequent purification and identification by quantitative mass spectrometry.

Characterisation studies performed in this work indicated that the sNS1-APEX2 is internalised into naïve Huh-7.5 cells in an sNS1-dependent manner. Moreover, internalised sNS1-APEX2 was shown to be catalytically active, allowing the biotinylation of sNS1-APEX2 proximal host proteins. This confirmed the practicability of sNS1-APEX2 for APEX2-based proximity labelling to identify internalised sNS1 proximal proteins. For the proximity biotinylation experiments we designed a DENV2-IgK-APEX2-myc control construct that can be transfected into cells for the DENV2-driven expression of a secreted APEX2 (sAPEX2) protein that is unattached to any viral protein. Characterisation studies in Huh-7.5 cells transfected with IVT DENV2-IgK-APEX2-myc RNA confirmed that this variant displays wildtype-like intracellular NS1 localisation, NS1 secretion, infectious virus production, APEX2 secretion and functionality of the APEX2 to biotinylate proximal host proteins. This sAPEX2-containing cell culture supernatant served as an APEX2-only control to allow the differentiation between sNS1-dependent and APEX2-dependent interactions with host proteins. For an APEX2-deficient (mock) inoculum we employed similarly concentrated cell culture supernatants that were collected from parallel uninfected cells. Given the appreciable attenuation of the DENV2-NS1-APEX2 variant, several strategies were explored to enhance the production, recovery, and concentration of sNS1-APEX2 from from DENV2-NS1-APEX2 transfected cell culture supernatants. Ultimately, we chose to concentrate the sNS1-APEX2 in the cell culture supernatants using a 100 kDa MWCO ultrafiltration technique. This process was shown to concentrate sNS1-

APEX2, infectious virus, and components of FBS that were present in the cell culture media. To lessen potential inhibitory actions of highly concentrated FBS within our experimental and control inoculums, FBS was diluted during the propagation and expansion of cell cultures that were used to generate experimental and control inoculums (Figure 4.1A).

To identify the human host cell proteins involved in the early events of sNS1 internalisation, cells were incubated with ultrafiltered inoculum for 30 minutes. Inoculum was then replaced with biotin-phenol-containing media and incubated for a further 30 minutes before the biotinylation reaction was catalysed for precisely 1 minute. This timeframe was employed to reveal the host proteins that are associated with the early events of sNS1 binding and internalisation and intracellular trafficking, up to and including 1 hour post-inoculation. Whole cell lysates were enriched for biotinylated protein using streptavidin-based affinity purification and enriched peptides were identified using label-free quantitative LC-MS/MS.

Our analyses revealed 45 and 21 sNS1-associated human host proteins that were significantly enriched ≥ 2-fold in sNS1-APEX2 vs sAPEX2 and sNS1-APEX2 vs mock samples, respectively. Comparisons of our sNS1-associated proteomes with a previously published NS1 interactome generated in DENV subgenomic replicon-expressing cells revealed substantial overlap, confirming the validity of our work, and indicating that these host proteins may be associated with multiple aspects of NS1 and sNS1 biology. Importantly, several host proteins known to directly interact or associate with sNS1 in the extracellular environment were identified in our study. It was recently shown that sNS1 dissociates onto HDL and LDL complexes and that sNS1-lipoprotein complexes acquire an APOE positive phenotype in DENV-infected patient sera during the course of infection [227]. The identification of APOE in our study confirms that our data set contains sNS1-host factor associations that reflect the physiological conditions observed *in vivo*. This indicates that our data could be mined to identify novel sNS1-host protein interactions that occur in DENV-infected patients. The complement protein C1Q is also considered to represent a bona fide direct interacting partner of sNS1 [453], however it remains unclear whether this interaction plays a role in complement activation or immune evasion. The identification of C1QA confirms that our data set contains host proteins that directly interact with sNS1 thorough which proviral or antiviral effects may be elicited. Thus, further examination of our data set may reveal sNS1-host protein interactions that are important for promoting or limiting DENV infection. sNS1 has been shown to bind the complement regulatory factor, C4BP, and this sNS1-C4BP complex is recruited to the host cell surface to attenuate complement activation [257]. The identification of C4BP in our study confirms that our data contains sNS1-host factor interactions that are known to confer important biological effects. The identification of host proteins known to interact with sNS1 in the extracellular environment suggests

that some of the proteins identified in our study may represent interactions that occurred in the DENV2-NS1-APEX2 transfected cell culture system used to generate sNS1-APEX2 inoculum, as opposed to interactions that occurred with target cells following inoculation. Nonetheless, the identification of human host proteins that interact with sNS1 in the extracellular environment is of critical importance. Moreover, these proteins fit the aim of identifying human host proteins that are associated with the early events of sNS1 internalisation given that extracellular sNS1-host protein complexes may facilitate sNS1-host cell interactions, as evidenced by sNS1-C4BP. Importantly, given that we have identified human host proteins that have previously been shown to associate with sNS1 in DENV infected patients and exert important biological effects, our data should be mined to identify novel sNS1-host protein interactions that are crucial to DENV and dengue disease.

Intriguingly, gene ontology (GO) analyses revealed an enrichment of host proteins associated with extracellular exosomes. Indeed, sNS1 has been identified as a component of extracellular exosomes as a membrane-bound component [450] and possibly luminal content [463]. Exosomes are functional extracellular vesicles that facilitate intercellular communication. These vehicles carry a complex cargo of nucleic acids, lipids, and proteins including ribosomal proteins, cytokines, and growth factors from a donor cell to a recipient cell. Over the last decade, the emerging role of orthoflavivirus-modified extracellular vesicles as conveyors of virus, infectious and subgenomic viral RNA, and viral proteins has revealed several roles of extracellular vesicles in modulating host cell physiology, enhancing viral transmission and pathogenicity [462, 463]. Exosomes can dock with recipient cells through direct interactions with extracellular receptors and can be internalised through a wide variety of mechanisms including clathrin-mediated endocytosis, phagocytosis, lipid raft-mediated endocytosis, micropinocytosis and caveolin-mediated endocytosis [460]. It is intriguing to consider that NS1 may hijacking extracellular vesicles in the extracellular environment and become a membrane-bound component, to facilitate sNS1 host cell binding and internalisation. Supporting this hypothesis, complement factor h (CFH), a regulatory factor that acts to prevent complement activation, was identified as an sNS1 proximal protein in our study. CFH has been identified as an interacting partner of NS1 from WNV [455], but this interaction is not observed with DENV NS1 [455, 456]. However, our APEX2-based work should identify sNS1 proximal proteins, not just direct interactors. Complement components exhibit complex interactions with extracellular vesicles [489], and the presence of CFH on extracellular vesicles protects against complement-mediated destruction [490], thus providing an opportunity for close associations between DENV sNS1 and CFH via an extracellular vesicle scaffold. Importantly, CFH can bind to a variety of host cell ligands, including the glycosaminoglycan heparin sulfate [491], a host cell factor that is important for sNS1-host cell binding [209].

Several ribosomal proteins (RP) were enriched in our study, and many of these have previously been identified in other DENV NS1-based proteomics studies [384, 457]. As our inoculum contained infectious DENV2-NS1-APEX2, it is possible that some translation of nascent NS1-APEX2 may have occurred during the short time-frame of inoculation and contributed to the biotinylation and capture of host factors involved in early translation. However, many of the RPs identified in our study are also bona fide components of exosomes [492], suggesting that these sNS1-RP associations may have occurred in the cell culture system used to generate sNS1-APEX2 cell culture supernatant. Under this hypothesis, it is possible that these associations occurred in the cell culture supernatant given that sNS1 can associate with extracellular vesicles in solution [450]. Alternatively, given that NS1 may be secreted as luminal content of extracellular vesicles [463], it is also possible that these associations occurred in the intracellular environment prior to secretion. Adding complexity, RPs also exhibit extra-ribosomal functions that can modulate cellular processes, and extra-ribosomal functions are certainly manipulated by viruses [493]. The consistent identification of RPS3 as a component of the (s)NS1 interactome in multiple studies is interesting, despite differences in experimental methodologies, both virological and technical. RPS3 is a component of the 40S subunit that participates in ribosomal maturation and translation initiation [494]. An extra-ribosomal function of RPS3, however, is exerted through its interaction with the NF-Kβ subunit, p65. This RPS3-p65 interaction promotes the nuclear accumulation of the NF-Kβ complex resulting in the transcriptional upregulation of NF-Kβ target genes [495]. Conceivably, the hijacking of RPS3 by (s)NS1 to manipulate these (or other [493]) RPS3 functions would be beneficial to DENV in DENV-infected cells. However, RPS3 is also a verified component of exosomes and RPS3-rich exosomes can trigger alterations to recipient cell phenotypes [496]. Moreover, RPS3 has been demonstrated to act as an exosomal RNA-binding protein that may be important for facilitating intercellular transport of specific RNA species [497]. Indeed, both fully infectious and immune-modulating subgenomic DENV viral RNA species are trafficked in extracellular vesicles [449, 498, 499]. It is intriguing to consider that sNS1 may be hijacking these intercellular communication vehicles, as sNS1 in the extracellular environment or possibly as NS1 within infected cells prior to secretion, to interfere with recipient cell physiology. Based on the two functions of RPS3 mentioned above, the hijacking of RPS3- or other RP-rich exosomes by NS1 could facilitate manipulation of immune signalling or translation machinery sequestration. One or both of these processes could potentially help to establish uninfected cells as more susceptible to subsequent infection. Further interrogation of NS1-positive extracellular vesicles is certainly warranted. In this context, APEX2 has been demonstrated to have practical applications in proximity-dependent RNA labelling [500]. If NS1 is a luminal component of extracellular vesicles, as has been suggested [463], future work employing sNS1-APEX2-based proximity labelling of proteins and nucleic acids could help to characterise the molecular inventory contained within NS1-positive extracellular vesicles.

Our protein-protein interaction network analyses revealed functional and/or physical associations that connect several proteins involved in intracellular trafficking pathways, suggesting that these human host factors may be involved in the intracellular trafficking of internalised sNS1. Our study identified two Rab GTPases, Rab1A and Rab11A as sNS1 proximal host factors. Rab GTPases are principal regulators of intracellular membrane trafficking that are responsible for coordinating the biogenesis, transport, and fusion of membrane-bound organelles and vesicles [501]. As such, Rab GTPases are commonly used as markers of various intracellular organelles. Using fixed cell confocal immunofluorescence microscopy of sNS1 inoculated endothelial cells, it has been shown that sNS1 co-localises with clathrin at 30 minutes post-inoculation and partially co-localises with the early endosome marker, Rab5, and the lysosomal cysteine protease, cathepsin L, at 90 minutes post-inoculation [219]. Our experimental approach, however, should capture the host proteins that are in close proximity to internalised sNS1 up to and including 1 hour post-internalisation. Thus, the identification of Rab1A and Rab11A is intriguing. Rab GTPases function as molecular switches by cycling between a GEF-catalysed GTP activated state and a GAP-catalysed GDP inactivated state [502]. To modulate membrane trafficking processes, Rab GTPases interact with various and diverse effectors including vesicular coat proteins, motor proteins, tethering complexes and SNARES [382, 503]. Some Rab effectors were identified in our study, including the COPI component COPG1, and the dynein motor component DYNC1H1. Given the diversity of Rab GTPase effectors and the diverse functions they perform [504], it is likely that other Rab effectors that influence downstream events following sNS1 internalisation remain to be identified. A major role of Rab11A is to regulate the slow recycling pathway that transports endocytosed receptors from early endosomes back to the plasma membrane [505]. As our methodology restricted sNS1 internalisation to 1 hour, the identification of Rab11A here suggests that our data set may also include co-internalised plasma membrane receptors and/or co-factors that are important for sNS1 host cell binding and internalisation. Interestingly, in endothelial cells, this Rab11A-dependent recycling pathway has been demonstrated to be essential for mediating VE-cadherin recycling to adherens junctions to maintain and control endothelial barrier integrity [506]. This may be relevant to the recent demonstration by Wang *et al* that sNS1-mediated endothelial hyperpermeability and EGL disruption is dependent upon sNS1 internalisation [219]. Moreover, in hepatocyte-derived Huh-7 cells, internalised sNS1 has been shown to be stable for up to 48 hours within intracellular membrane-bound organelles that are characteristic of late endosomes and, to a lesser extent, multivesicular bodies or autophagosomes [277]. It is therefore tempting to speculate that the hijacking of this Rab11A-mediated recycling pathway may prevent plasma membrane receptor recycling and maintain sNS1-host cell receptor-mediated signalling. Additionally, Rab11A has been shown to play a role in lysosome exocytosis [507], a cellular process involved in plasma membrane and extracellular matrix remodelling, repair, and degradation [508]. Consistent with this, sNS1 stimulation of endothelial cells has been shown to increase the activity of the lysosomal protease Cathepsin L and its activation of heparinase [211], and that sNS1 induces the degradation of sialic acid and

shedding of heparin sulfate from the endothelial glycocalyx layer [211]. However, it must be noted that Rab11A also coordinates crosstalk between the Golgi, trans-Golgi network, autophagosomes and MVBs [509]. Additionally, while Rab1A is associated with the trafficking of early endocytic vesicles [510], a major role of Rab1A is to mediate vesicular transport from the ER to the ERGIC [511]. Thus, it cannot be ignored that these factors may have been identified due to nascent NS1-APEX2 translation. However, the identification of DYNC1H1, a component of cytoplasmic dynein which carries cargo along microtubules in a retrograde manner, and the tubulin-related components (TUBA3D, TUBB2B, and TBCA) supports the hypothesis that these host factors are associated with the intracellular trafficking of internalised sNS1 [512]. Further interrogation of the potential roles of Rab GTPases and their effectors in the intracellular trafficking of sNS1 is certainly warranted. Future studies could employ the constitutively active Rab11A-Q70L and the dominant negative Rab11A-S25N Rab11A variants to examine the role of Rab11A in the intracellular trafficking of sNS1. Moreover, by combining the commercially available fluorescently tagged Rab11A variants with our DENV2 reporter viruses that feature fluorescent protein tags within NS1 and secrete fluorescently tagged sNS1, advanced microscopy techniques could be employed to examine the nature and behaviour of internalised sNS1 trafficking.

While we have generated a robust candidate list of human host cell factors associated with the sNS1 internalisation, this sNS1-APEX2 based study has certain caveats. The sNS1-APEX2 fusion protein was propagated in the Huh-7.5 cells, a human hepatocellular carcinoma-derived cell line, transfected with infectious IVT DENV2-NS1-APEX2 RNA. Accordingly, these cancer cells and unanticipated properties and effects of the APEX2-tagged reporter virus and its delivery, may have contributed to the inappropriate identification of or failure to observe virus-host interactions that otherwise occur during exposure of primary cells to wildtype NS1 that is encoded by wildtype DENV. Moreover, given the difficulties in generating practicable yields of sNS1-APEX2, these cells were propagated in FBS-limited media and cell culture supernatants were subjected to 100 kDa MWCO ultrafiltration. This methodology used to generate sNS1-APEX2 inoculum may have introduced biases with respect to which sNS1-host factor complexes were isolated in the inoculum. Furthermore, while reflective of what occurs during a natural DENV infection, the presence of infectious virus within these cells would have inevitably influenced the cellular secretome, likely contributing to the enrichment of immune-related components. The striking enrichment of host proteins associated with exosomes is consistent with both the DENV-induced enhanced secretion of extracellular vesicles, and the known association between extracellular sNS1 and exosomes. However, it should be noted, that exosomes secretion is enhanced, and their luminal content is influenced, under conditions of nutrient deprivation [513], which may have occurred as a result of limited FBS availability. Moreover, the use of a 100 kDa MWCO ultrafiltration process is one of several methods often employed for exosome purification [514], thus this process may have enriched for, or even driven, sNS1-exosome associations in the

inoculum. We chose to investigate the host factors associated with sNS1 internalisation in Huh-7.5 cells given that: (i) hepatocytes are a major target of sNS1 *in vivo* [277]; (ii) internalised sNS1 is remarkably stable in human hepatocytes [277] and; (iii) the pretreatment of hepatocytes with sNS1 enhances subsequent infection [277] through an unknown mechanism, thus providing an interesting avenue of research moving forward. However, the human host factors associated with sNS1 internalisation would be influenced by cell type-specific differences. Given that sNS1 internalisation by endothelial cells contributes directly to EGL disruption and vascular leakage [219], it would also be of interest to repeat or extend these studies using cell lines that are more biologically relevant to dengue disease pathology. Moreover, given that sNS1 can act as a PAMP and stimulate the production and release of proinflammatory cytokines and chemokines that can contribute to vascular leakage [210], additional studies in immune cells would be invaluable. However, in this context, host cell binding rather than internalisation may be the critical factor, further highlighting the importance of identifying host cell receptors that facilitate sNS1 attachment. In our study, we employed the engineered peroxidase APEX2 which exhibits robust catalytic activity in reducing environments given that it lacks disulfide bonds and calcium binding sites [446]. APEX2 proximity labelling is most reliable when the protein of interest is present in the intracellular environment and associated with intracellular structures, organelles, and membranes [297], thus making sNS1-APEX2 well suited to identify host factors associated with internalised sNS1. In contrast to APEX2, HRP exhibits robust catalytic activity in oxidising environments including the extracellular space and can be used for proximity-dependent biotinylation [289]. An HRP-tagged sNS1 fusion protein would be extremely useful for cell-surface proteomic profiling to identify sNS1- binding host cell factors at the cell surface. Finally, in this work, we employed a label-free proteomics approach. While the use of SILAC-based labelling is a favoured approach in quantitative proteomics and has been employed within our laboratory for tissue culture-based quantitative proteomics experiments, the use of SILAC in these experiments was deemed prohibitive given the large-scale nature of the cell culture propagation required to generate sufficient quantities of sNS1-APEX2 cell culture supernatants. However, it may have been beneficial to include TMT or iTRAQ labelling to ensure more reproducible protein quantification and minimise the variability that is otherwise associated with separate mass spectrometry runs and separate sample preparation, separation and data acquisition processes. Furthermore, a thoughtfully developed SILAC labelling approach may have enabled distinguishment of whether an identified NS1-host protein associations occurred in the infected ‘producer’ cells, cell free supernatants or target cells following inoculation, while also achieving superior protein quantification. In our experiments, we performed 4 replicates per treatment to increase statistical power for label-free quantification. Nevertheless, given the inherent variability associated with label-free quantification, statistical significance thresholds should be considered cautiously so as to not overlook potentially critical sNS1 interactors. Moreover, given the challenges of reliably measuring peptide abundances in low-abundance ranges using Proteome Discoverer software [515], critical but infrequent host factor interactions may have been masked. This could be of significant

importance given that the identification of Rab11A suggests that host cell receptors exploited by sNS1 to achieve binding and internalisation may be contained within our data set. Given the comparatively low abundance of plasma membrane proteins relative to cytosolic proteins, additional data mining and/or alternative proximity biotinylation and quantitative proteomics methods may be required to identify these plasma membrane host factors. Indeed, more comprehensive data analyses employing additional bioinformatic normalization processes and tools are currently being performed by collaborators. Given the promising results generated by our innovative approach to identify the human host factors associated with the early events of DENV sNS1 internalisation, future studies could employ a similar APEX2-based approach to identify the sNS1 interactome of other orthoflaviviruses as this may reveal targets for pan-orthoflavivirus antiviral therapies.

Concluding Remarks

The work presented in this thesis aimed to identify the human host cell factors that are associated with the processes of DENV NS1 secretion and sNS1 internalisation. Our innovative customised membrane-trafficking siRNA screen revealed, for the first time, the coatomer protein complex I (COPI) as an important determinant of NS1 secretion. Further interrogation of these components in follow-up gene-silencing, overexpression, and pharmacological inhibitor-based experiments confirmed the involvement of COPI and the master regulator of COPI vesicle formation, GBF1, in both DENV and WNV/KUNV NS1 secretion, indicating that the exploitation of COPI to achieve efficient NS1 secretion may be a feature conserved within the Orthoflavivirus genus. This work that pinpoints COPI as a key player in NS1 secretion paves the way for future studies to identify the precise molecular mechanism(s) of COPI's involvement in NS1 secretion. Additionally, our APEX2-based proteomic profiling experiments has revealed a broad profile of candidate human host proteins associated with the early events of sNS1 internalisation in human cells. Our identification of human host proteins that are known to associate with sNS1 in DENV infected patients confirms the physiological relevance of our novel data set. Moreover, the identification of human host proteins that interact with sNS1 and elicit important biological effects for the virus or the host confirms the biological relevance of our novel data set. The proteins identified in our data set perform a wide variety of roles that may act to influence sNS1-human host cell binding and intracellular trafficking of internalised sNS1. The work presented here can be used to guide future studies to reveal human host factors that are critical to sNS1 internalisation. Collectively, the confirmation of COPI as a key player in NS1 secretion coupled with the generation of candidate list of human host factors associated with sNS1 internalisation may aid in the identification of novel targets for anti-orthoflaviviral therapies.

Appendices

Appendix I: Buffers, media and solutions

Acetone:methanol fixative solution

100 mg/mL Ampicillin

Biotin phenol solution

20% D-glucose solution

Dimethyl sulfoxide (DMSO)

Dulbeccos Phosphate buffered saline

Foetal bovine serum (FBS)

20% Glucose solution

80% Glycerol solution

Hydrogen peroxide solution

Lauria Bertani Lennox media

Lauria Bertani Lennox agar plates supplemented with ampicillin sodium salt

MilliQ water

1x Phosphate buffered saline

10% Sodium dodecyl sulfate (SDS)

3M Sodium acetate (NaAc) (pH 5.5)

1M Sodium acsorbate solution

1M Sodium azide

4M Sodium chloride

100x Streptomycin-Penicillin

Super optimal broth with catabolite repression (SOC)

1M Tris (pH 8.0)

20x Tris-acetate-EDTA buffer (TAE)

10x Tris-buffered-saline (TBS)

10x Tris-glycine-SDS (TGS)

62.5mM Tris-HCl (pH 6.7)

Trolox solution

10x TBS	
Reagent	Weight (g)
Tris base (MW 121.1 g)	24
NaCl (MW 58.4 g)	88
Dissolve in 900 mL distilled H2O	
Adjust pH to 7.6 with 12 N HCl	
H2O	To 1L

Trypsin-EDTA

20x TAE	
Reagent	Quantity
Tris Base	97g
H2O	700mL
Glacial Acetic Acid	22.8mL
0.5M EDTA (pH 8.0)	40mL
H2O	To 1L

Lauria Bertani (with/without agar)	
Reagent	Weight (g)
NaCl	10
Tryptone	10
Yeast Extract	5
Agar (Optional)	15
Dissolve in 900 mL H2O	
Adjust pH to 7.0 with 5 N NaOH	
H2O	To 1L

Acetone:Methanol Fixative	
Reagent	Volume (mL)
Acetone	5
Methanol	5
Total	10

RIPA Buffer (25 mL)	
Reagent	Volume
1 M Tris, pH 7	1
4 M NaCl	0.9375
10% SDS	0.25
Sodium Deoxycholate	0.125 g
Triton X-100	0.25
MQ H2O	22.4375
Protease Cocktail Inhibitor	1x
Total	25 mL

5% BSA	
Reagent	Quantity
5% BSA	2.5 g
H2O	to 50 mL

NP-40 Lysis Buffer	
Reagent	Volume (mL)
1M Tris-HCl (pH 8)	2
4M NaCl	1.5
NP-40* (IGEPAL® CA630)	0.4
dH2O	36.1
Total	40

4x Reducing Loading buffer (30% Glycerol)	
Reagent	Volume
0.5 M Tris-HCl, pH 6.8	1
Glycerol (80%)	3
10% (w/v) SDS	1.6
2-mercaptoethanol	0.4
1% (w/v) bromophenol blue	0.4
H2O	1.6
Total	8

4x Non-Reducing Loading Buffer (30% Glycerol)	
Reagent	Volume
0.5 M Tris-HCl, pH 6.8	1
10% (w/v) SDS	1.6
Glycerol (80%)	3
1% (w/v) bromophenol blue	0.4
H2O	2
Total	8

Protease Inhibitor Cocktail	
Reagent	**Volume (uL)**
NP-40	495
Proteinase Inhibitor	5
Total	500

Running Buffer	
Reagent	Volume (mL)
H20	900
10x Tris Glycine SDS	100
Total	1000

Western Blot Wet Transfer Buffer	
Reagent	Volume / Mass
Tris (g)	3.03
Glycine (g)	14.4
H2O (mL)	800
Methanol (mL)	200
Total	1 L

TBS (with/without Tween 20)	
Reagent	Volume (mL)
10x TBS	100
H2O	900
Tween 20 (Optional)	1
Total	1000

2x Freezing Mix	
Reagent	Volume per cryotube (mL)
50% DMEM	0.25
30% FCS	0.15
20% DMSO	0.1
Total	0.5
Filter through 0.2 uM filter!!!!	

Biotin-Phenol (-80*C)
Stock = 500mM; Working = 500µM; 1uL stock to 900µL DMEM
400µL/well * 7.5 wells = 3mL total
Add 3uL BP Stock to 2997 µL pre-warmed DMEM

H2O2 Solution (100 mM)
30% Sigma solution = 10 M in H2O
Working = 100 mM; 1mL 30% Sigma in 100 Dulbeccos PBS
4µL/well * 7.5 wells = 30µL required
Add 0.3uL 30% H2O2 to 30 uL PBS

Quencher Solution		
Reagent	Stock	Dilution
10 mM Sodium Ascorbate	1000 mM	1/100
5 mM Trolox	500 mM	1/100
10 mM Sodium Azide	1000 mM	1/100
Dulbecco's PBS	Neat	Neat

Sodium Ascorbate (1000 mM)	
Sodium Ascorbate (powder)	2.5 g
MQ H2O	to 12.6 mL

Trolox (500 mM)	
Trolox (powder)	0.1 g
DMSO	799 uL

Sodium Azide (1000 mM) (stored -20*C)	
10% Azide solution	1mL
MQ H2O	538 uL
total	1.538 mL

Appendix II: Synthetic Oligonucleotides and Gene Fragments

Generating SNP COPI-GFP cDNA expression constructs	
Name	Sequence
COPA E241K 1 Fwd	CTGGCGCATGAATGAATCAAAGGCATGGaAGGTTGATACCTGC
COPA E241K 1 Rev	GCAGGTATCAACCTtCCATGCCTTTGATTCATTCATGCGCCAG
COPA E241K 2 Fwd	GCATGGaAGGTTGATACCTGCCGGGGCCATTACAAC
COPA E241K 2 Rev	GTTGTAATGGCCCCGGCAGGTATCAACCTtCCATGC
COPB2 R254C Fwd	CAGAAGATGGAACAGTAtGTATTTGGCATTCAAGCACC
COPB2 R254C Rev	GGTGCTTGAATGCCAAATACaTACTGTTCCATCTTCTG
COPG1 K652E Fwd	GTATGTCATCCGCTGCACCgAACACACCTTCACCAAC
COPG1 K652E Rev	GTTGGTGAAGGTGTGTTcGGTGCAGCGGATGACATAC

RT-qPCR primers	
Name	Sequence
RPLP0 Sense	AGATGCAGCAGATCCGCAT
RPLP0 Antisense	GGATGGCCTTGCGCA
DENV2 Sense	ATCCTCCTATGGTACGCACAAA
DENV2 Antisense	CTCCAGTATTATTGAAGCTGCTATCC
KiCq Start COPA FH1	ATGAATATCCCTGGATTCTGAG
KiCq Start COPA RH1	AAACACAGGTTCTAGATTGC
KiCq Start COPB2 FH1	ATGGAACAGTACGTATTTGG
KiCq Start COPB2 RH1	GACATTGTTTGACCCTCTTAG
KiCq Start COPG1 FH1	CCTCACCAAGATTCTTTATCTC
KiCq Start COPG1 RH1	GATCATTGGACTGAAAGAGC
KiCq Start GBF1 FH1	ATTGCTCTCTAAGGTCTTCC
KiCq Start GBF1 RH1	GCATGTACTTGTCCATGAAG

COPI CRISPR-Cas9 Guide cDNA	
Name	Sequence
COPA Guide RNA 1 Oligo #1	CACCGTGGAAGTCAATGCCTCGCAC
COPA Guide RNA 1 Oligo #2	AAACGTGCGAGGCATTGACTTCCAC
COPA Guide RNA 2 Oligo #1	CACCGGTCACGATCGTGGAGTAAAC
COPA Guide RNA 2 Oligo #2	AAACGTTTACTCCACGATCGTGACC
COPB2 Guide RNA 1 Oligo #1	CACCGTTCGTCACCAAACTTCACTT
COPB2 Guide RNA 1 Oligo #2	AAACAAGTGAAGTTTGGTGACGAAC
COPB2 Guide RNA 2 Oligo #1	CACCGCTTGATAGTCCTGTCCAAAG
COPB2 Guide RNA 2 Oligo #2	AAACCTTTGGACAGGACTATCAAGC
COPG1 Guide RNA 1 Oligo #1	CACCGTAGCACATCCGACGGAGTGT
COPG1 Guide RNA 1 Oligo #2	AAACACACTCCGTCGGATGTGCTAC
COPG1 Guide RNA 2 Oligo #1	CACCGGGGGACCACGGAAGCGACCG
COPG1 Guide RNA 2 Oligo #2	AAACCGGTCGCTTCCGTGGTCCCCC
GBF1 Guide RNA 1 Oligo #1	CACCGCGTGCCCACAAAACGAGCAT
GBF1 Guide RNA 1 Oligo #2	AAACATGCTCGTTTTGTGGGCACGC
GBF1 Guide RNA 2 Oligo #1	CACCGTTGGTTAGGTGGGCACCCAC
GBF1 Guide RNA 2 Oligo #2	AAACGTGGGTGCCCACCTAACCAAC

Appendix II: Synthetic Oligonucleotides and Gene Fragments

COPI CRISPR-Cas9 genomic DNA PCR	
COPA Guide 1 Fwd Primer	TCTGATAGCCAAAAATTGGCG
COPA Guide 1 Rev Primer	TATAGGTTGCTAGTCTCTGGC
COPA Guide 2 Fwd Primer	AGAGAAATTAAGTGGTCTACCAAAATC
COPA Guide 2 Rev Primer	GAAAGATAGTCCATGCTTGTGG
COPB2 Guide 1 Fwd Primer	GCTTAATACATGTTGCAGTGAGG
COPB2 Guide 1 Rev Primer	TTTCAGTTTCTCTTTAGGACAGC
COPB2 Guide 2 Fwd Primer	AAGTATGTGATCTTCCTGTTCG
COPB2 Guide 2 Rev Primer	CAAAGTTAATCTATGTCAAAAGCAAGG
COPG1 Guide 1 and 2 Fwd Primer	TATCACCTAAGCTAGACTGTGG
COPG1 Guide 1 and 2 Rev Primer	TCAAAACCAAACAGGTCATCC
COPG1 NEWER Guide 1 and 2 Fwd Primer	AGGCAAGTGACATTTGCTCC
COPG1 NEWER Guide 1 and 2 Rev Primer	GATCTCAGCTCACTGCAACC
COPG1 TIDE Fwd (KiCq)	CCTCACCAAGATTCTTTATCTC
COPG1 TIDE Rev	CTAACTGAACCTACAAATCAATG
GBF1 Guide 1 and 2 Fwd Primer	ACTTATTTGGCTATTTCTCGTGG
GBF1 Guide 1 Rev Primer	AGTGTGGAGGCTCTTTTTATCC

COPI CRISPR-Cas9 Genomic PCR Amplicon Sequencing Primers	
COPA Guide 1 Seq Primer	GCCCCTCTCATCTTCTGC
COPA Guide 2 Seq Primer	ATTAGCCGGGTATGGTGG
COPB2 Guide 1 Seq Primer	TTGCTGTGTTGTCCAGG
COPB2 Guide 2 Seq Primer	GCATAATATTAGCCCAGG
COPG1 Guide 1 Seq Primer	AAGAAATAAGAGAACTGAGC
COPG1 Guide 2 Seq Primer	GTTGCATACCCAGAAAGC
COPG1 TIDE Fwd (KiCq)	CCTCACCAAGATTCTTTATCTC
COPG1 TIDE Rev	CTAACTGAACCTACAAATCAATG
GBF1 Guide 1 Seq Primer	AGGAATTACTGTGATAAACAAGG
GBF1 Guide 2 Seq Primer	GTTCTCAGAGCAGACTCC

Sanger Sequencing Primers	
T7 Fwd_SJ	TAATACGACTCACTATAGGG
SP6 Rev_SJ	ATTTAGGTGACACTATAG
CMV_FPseq	CGCAAATGGGCGGTAGGCGTG
pLENTI6 RPSEQ2	CAAACTCATTACTAACCGGTAC
COPA_800 Rev_SJ	ACGGCACAAGATACATTG
COPA_754 Fwd_SJ	ATGAATCAAAGGCATGGG
COPA_1523 Rev_SJ	GCTGACCAGATAACGTATTTC
COPA_1460 Fwd_SJ	CTCTATCACACTCTTTGACG
COPA_2318 Rev_SJ	CCACAGTTCTTCAGGATC
COPA_2243 Fwd_SJ	TGCTGAGATCAGAAAGG
COPA_3076 Rev_SJ	GTCATTAAGCTTCAGGC
COPA_3014 Fwd_SJ	TATGGCTATCCTAATCG
COPB2_428_Fwd_SJ	ATTATGTTATGCAGATTGTGATC
COPB2_1161_Fwd_SJ	CTTTGGATCTGCTCAGG
COPB2_1853_Fwd_SJ	GGACCAGAGTTGCACAC
COPB2_2542_Fwd_SJ	ACAGCTCAACAGGAAC
COPG1_397_Fwd_SJ	GATAGCACCATGCTGCAG
COPG1_1087_Fwd_SJ	CAGATCTCCTCCTTCATG
COPG1_1786_Fwd_SJ	ATCACAGCAGTCAAACAGC
COPG1_2477_Fwd_SJ	ACACGTTGCTCCTGGCTG
GBF1_Seq_FP1	AGCCGGAGGCATGAGTG
GBF1_Seq_FP2	CCGTCACTTATTCCAG
GBF1_Seq_FP3	CCTGCCAGATCCACG
GBF1_Seq_FP4	TGACCTCTTCACCATG
GBF1_Seq_FP5	AGAGATGCTGCTAAG
GBF1_Seq_FP6	AGTGTGTGGAATCGCTG

Appendix III: Antibodies

Antibody	Manufacturer
Mouse anti-NS1 (4G4)	Mozzy Mabs
Mouse anti-Capsid (6F3.1)	Prof. John Aaskov (Brisbane, Aust.)
Mouse anti-B-actin (8H10D10)	Cell Signaling Technology
Mouse anti-B-actin (AC-15)	Sigma-Aldrich
Rabbit anti-B-actin (13E5)	Cell Signaling Technology
Mouse anti-COPA (H-3):sc-398099	Santa Cruz Biotechnology
Rabbit anti-COPB2 (ab2899)	Abcam
Rabbit anti-COPG1 (PA5-65194)	ThermoFisher
Rabbit anti-GBF1 (ab86071)	Abcam
Rabbit anti-GM130	Cell Signaling Technology
Goat anti-mouse IgG, AF-488 (A11001)	Invitrogen
Goat anti-mouse IgG, AF-555 (A21422)	Invitrogen
Goat anti-rabbit IgG, AF-488 (A11008)	Invitrogen
Streptavidin, AF-488 Conjugate (S11223)	Invitrogen

Appendix IV: Plasmid Maps

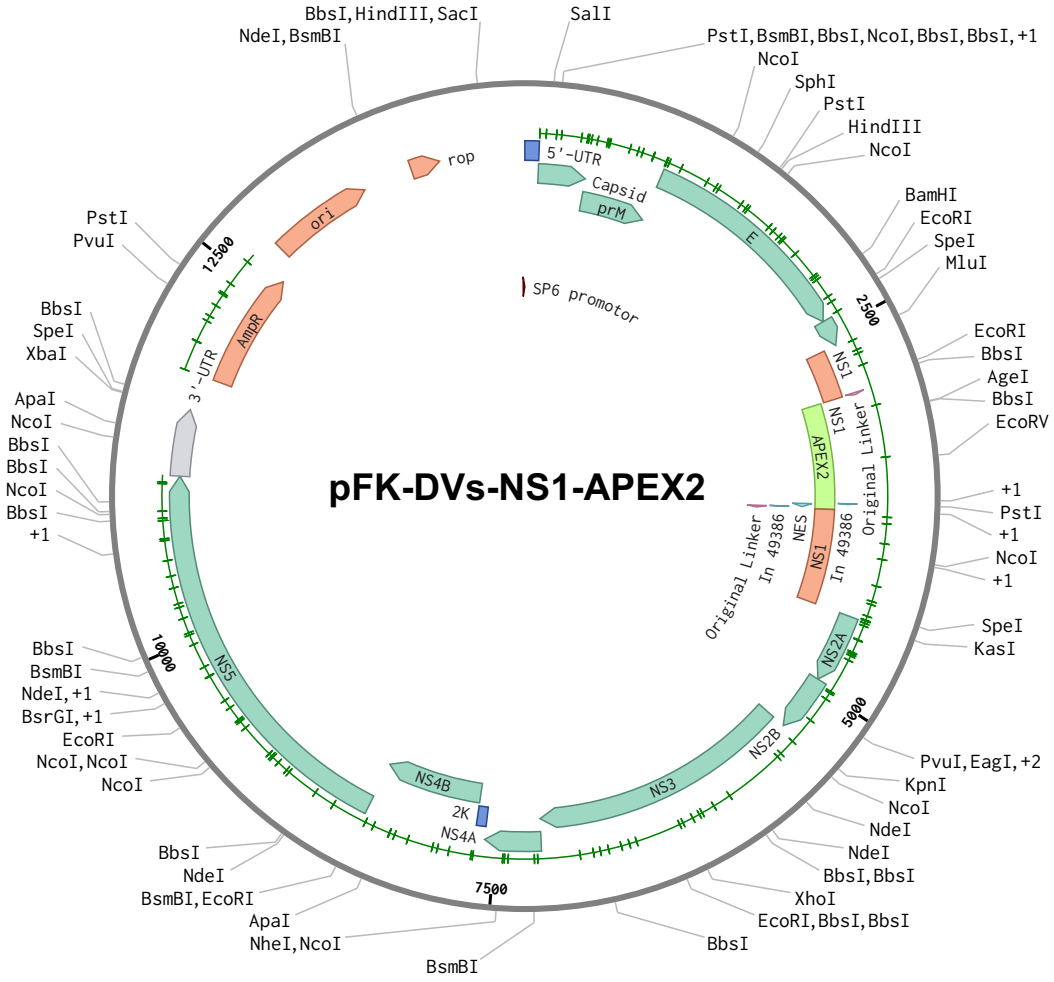

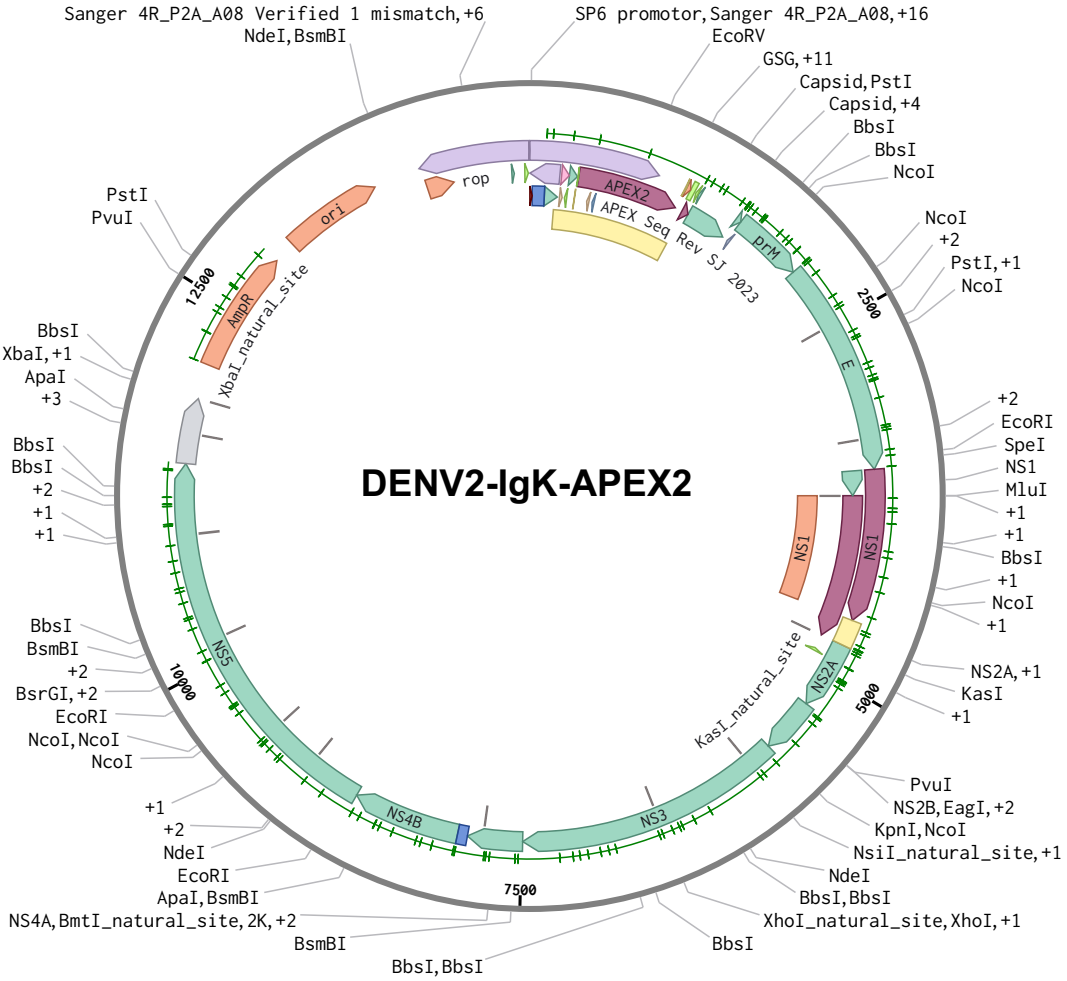
DENV2-IgK-APEX2
Sanger 4R_P2A_A08 Verified 1 mismatch, +6
NdeI, BsmBI
SP6 promotor, Sanger 4R_P2A_A08, +16
EcoRV
GSG, +11
Capsid, PstI
Capsid, +4
BbsI
BbsI
NcoI
NcoI
+2
PstI, +1
NcoI
+2
EcoRI
SpeI
NS1
MluI
+1
+1
BbsI
+1
NcoI
+1
NS2A, +1
KasI
+1
PvuI
NS2B, EagI, +2
KpnI, NcoI
NsiI_natural_site, +1
NdeI
BbsI, BbsI
XhoI_natural_site, XhoI, +1
BbsI
BbsI, BbsI
BsmBI
NS4A, BmtI_natural_site, 2K, +2
ApaI, BsmBI
EcoRI
NdeI
+2
+1
NcoI
NcoI, NcoI
EcoRI
BsrGI, +2
+2
BsmBI
BbsI
BbsI
+1
+1
+2
ApaI
+3
XbaI, +1
BbsI
PvuI
PstI
rop
ori
AmpR
XbaI_natural_site
APEX2
APEX Seq Rev SJ 2023
prM
E
NS1
NS1
NS2A
KasI_natural_site
NS3
NS4B
NS5
2500
5000
7500
10000
12500

DENV2-IgK-APEX2-myc (14883 bp)

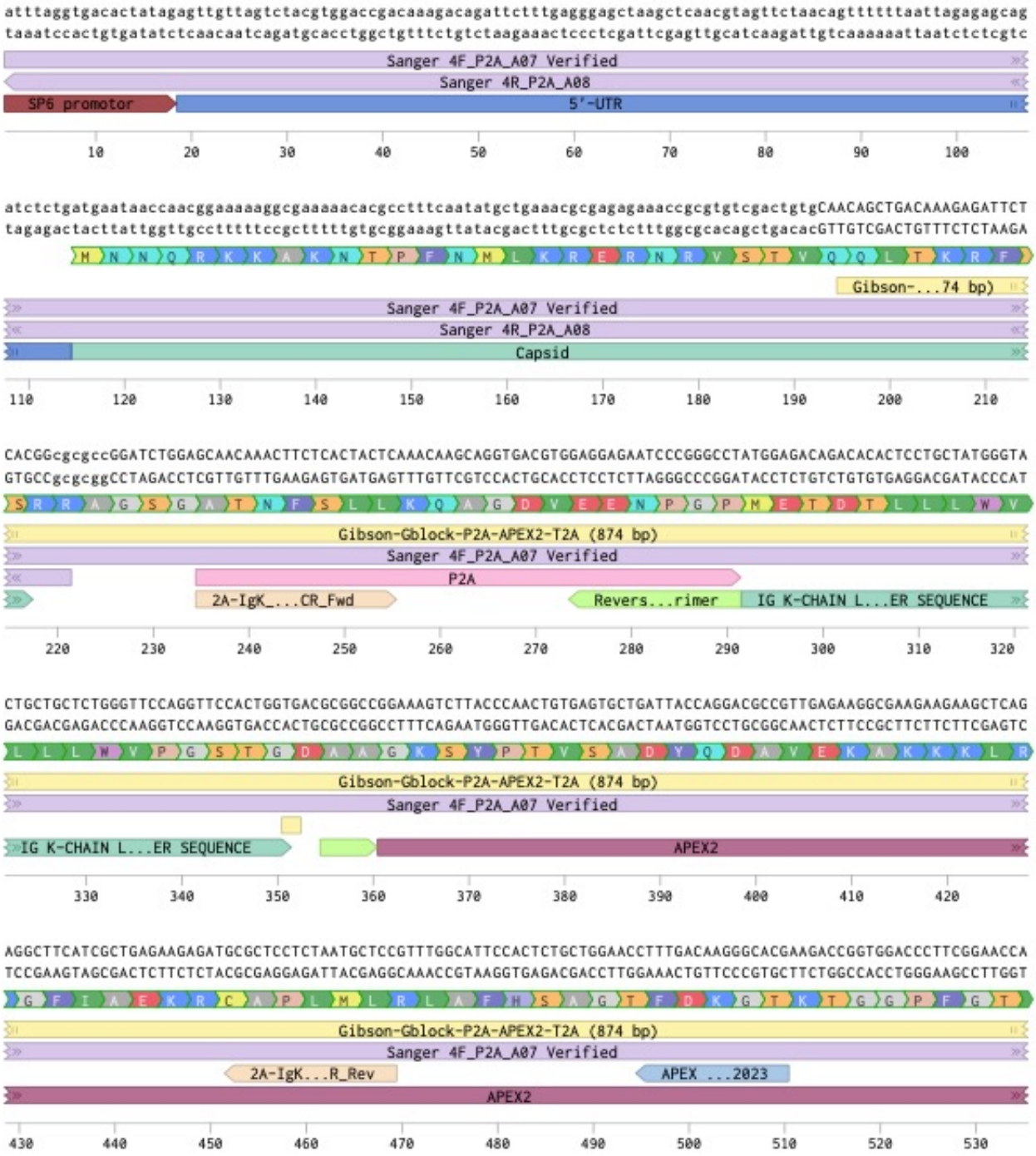

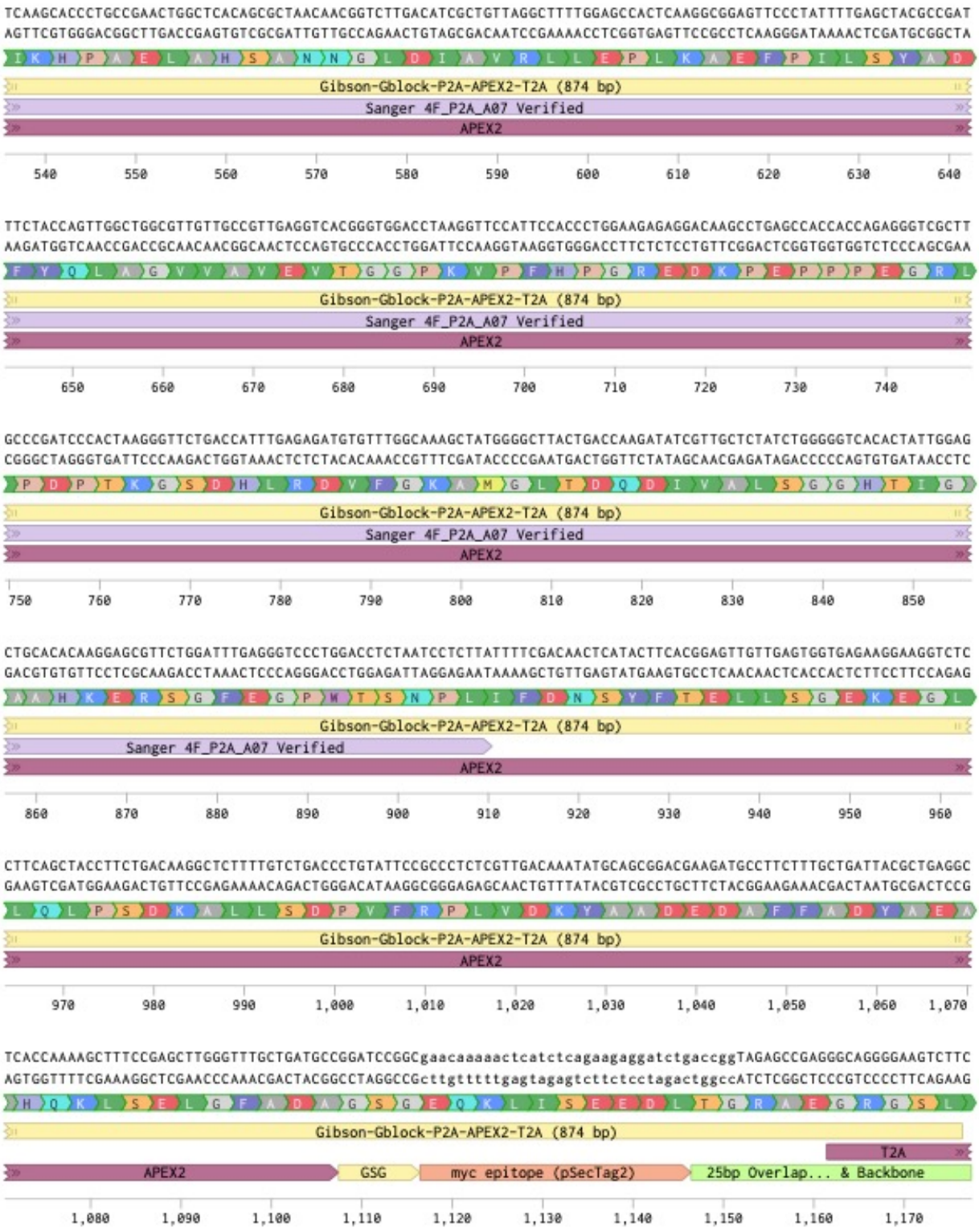
TCAAGCACCCTGCCGAACTGGCTCACAGCGCTAACAACGGTCTTGACATCGCTGTTAGGCTTTTGGAGCCACTCAAGGCGGAGTTCCCTATTTTGAGCTACGCCGAT
AGTTCGTGGGACGGCTTGACCGAGTGTCGCGATTGTTGCCAGAACTGTAGCGACAATCCGAAAACCTCGGTGAGTTCCGCCTCAAGGGATAAAACTCGATGCGGCTA
IKHPAELAHSANNGLDIAVRLLEPLKAEFPILSYAD
Gibson-Gblock-P2A-APEX2-T2A (874 bp)
Sanger 4F_P2A_A07 Verified
APEX2
540 550 560 570 580 590 600 610 620 630 640
TTCTACCAGTTGGCTGGCGTTGTTGCCGTTGAGGTCACGGGTGGACCTAAGGTTCCATTCCACCCTGGAAGAGAGGACAAGCCTGAGCCACCACCAGAGGGTCGCTT
AAGATGGTCAACCGACCGCAACAACGGCAACTCCAGTGCCCACCTGGATTCCAAGGTAAGGTGGGACCTTCTCTCCTGTTCGGACTCGGTGGTGGTCTCCCAGCGAA
FYQLAGVVAVEVTGGPKVPFHPGREDKPEPPPEGRL
Gibson-Gblock-P2A-APEX2-T2A (874 bp)
Sanger 4F_P2A_A07 Verified
APEX2
650 660 670 680 690 700 710 720 730 740
GCCCGATCCCACTAAGGGTTCTGACCATTTGAGAGATGTGTTTGGCAAAGCTATGGGGCTTACTGACCAAGATATCGTTGCTCTATCTGGGGGTCACACTATTGGAG
CGGGCTAGGGTGATTCCCAAGACTGGTAAACTCTCTACACAAACCGTTTCGATACCCCGAATGACTGGTTCTATAGCAACGAGATAGACCCCCAGTGTGATAACCTC
PDPTKGSDHLRDVFGKAMGLTDQDIVALSGGHTIG
Gibson-Gblock-P2A-APEX2-T2A (874 bp)
Sanger 4F_P2A_A07 Verified
APEX2
750 760 770 780 790 800 810 820 830 840 850
CTGCACACAAGGAGCGTTCTGGATTTGAGGGTCCCTGGACCTCTAATCCTCTTATTTTCGACAACTCATACTTCACGGAGTTGTTGAGTGGTGAGAAGGAAGGTCTC
GACGTGTGTTCCTCGCAAGACCTAAACTCCCAGGGACCTGGAGATTAGGAGAATAAAAGCTGTTGAGTATGAAGTGCCTCAACAACTCACCACTCTTCCTTCCAGAG
AAHKERSGFEGPWTSNPLIFDNSYFTELLSGEKEGL
Gibson-Gblock-P2A-APEX2-T2A (874 bp)
Sanger 4F_P2A_A07 Verified
APEX2
860 870 880 890 900 910 920 930 940 950 960
CTTCAGCTACCTTCTGACAAGGCTCTTTTGTCTGACCCTGTATTCCGCCCTCTCGTTGACAAATATGCAGCGGACGAAGATGCCTTCTTTGCTGATTACGCTGAGGC
GAAGTCGATGGAAGACTGTTCCGAGAAAACAGACTGGGACATAAGGCGGGAGAGCAACTGTTTATACGTCGCCTGCTTCTACGGAAGAAACGACTAATGCGACTCCG
LQLPSDKALLSDPVFRPLVDKYAADEDAFFADYAEA
Gibson-Gblock-P2A-APEX2-T2A (874 bp)
APEX2
970 980 990 1,000 1,010 1,020 1,030 1,040 1,050 1,060 1,070
TCACCAAAAGCTTTCCGAGCTTGGGTTTGCTGATGCCGGATCCGGCgaacaaaaactcatctcagaagaggatctgaccggTAGAGCCGAGGGCAGGGGAAGTCTTC
AGTGGTTTTCGAAAGGCTCGAACCCAAACGACTACGGCCTAGGCCGcttgtttttgagtagagtcttctcctagactggccATCTCGGCTCCCGTCCCCTTCAGAAG
HQKLSELGFADAGSGEQKLISEEDLTGRAEGRGSL
Gibson-Gblock-P2A-APEX2-T2A (874 bp)
T2A
APEX2
GSG
myc epitope (pSecTag2)
25bp Overlap... & Backbone
1,080 1,090 1,100 1,110 1,120 1,130 1,140 1,150 1,160 1,170

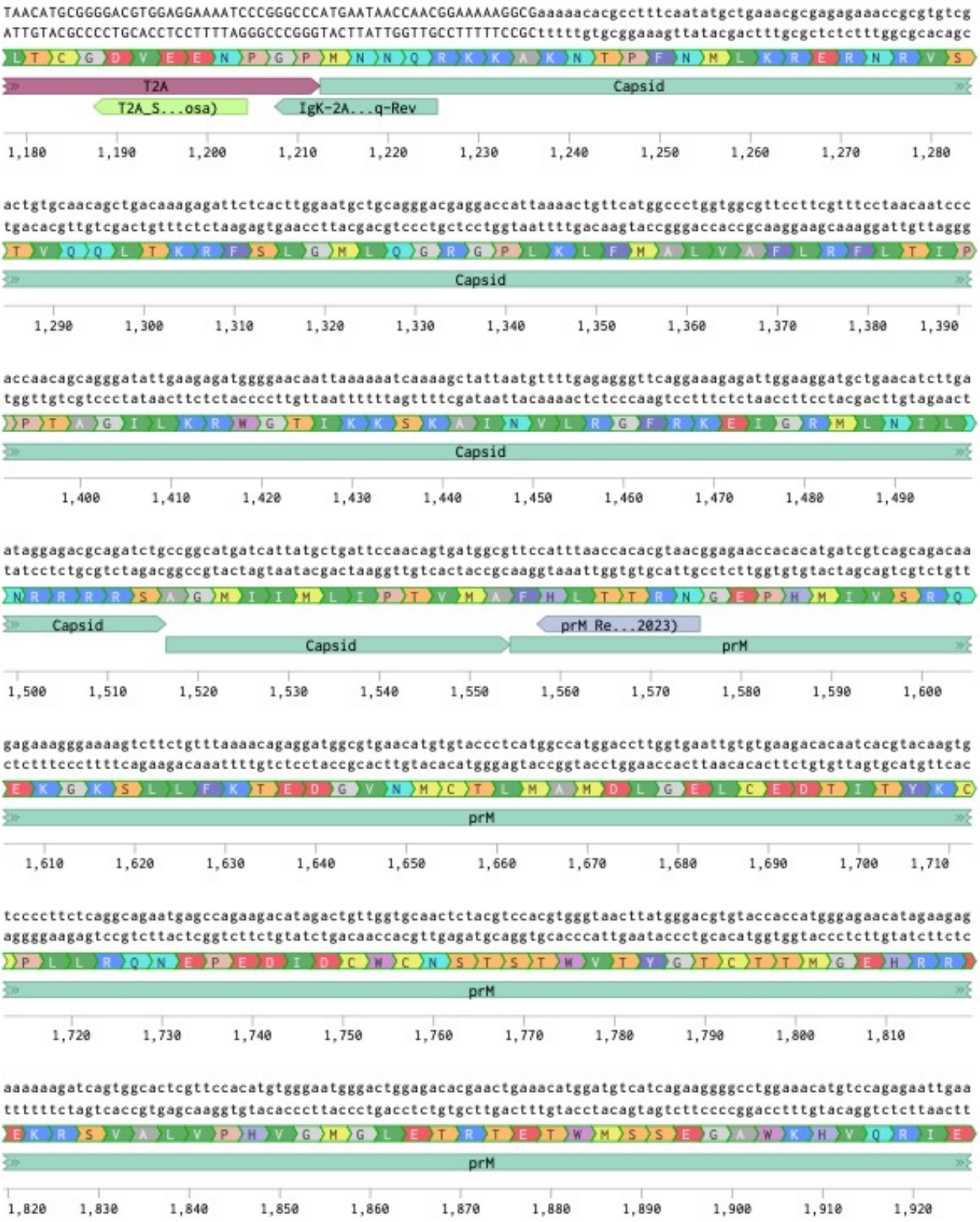
TAACATGCGGGGACGTGGAGGAAAATCCCGGGCCCATGAATAACCAACGGAAAAAGGCGaaaaacacgcctttcaatatgctgaaacgcgagagaaaccgcgtgtcg
ATTGTACGCCCCTGCACCTCCTTTTAGGGCCCGGGTACTTATTGGTTGCCTTTTTCCGCtttttgtgcggaaagttatacgactttgcgctctctttggcgcacagc
L T C G D V E E N P G P M N N Q R K K A K N T P F N M L K R E R N R V S
T2A
Capsid
T2A_S...osa)
IgK-2A...q-Rev
1,180 1,190 1,200 1,210 1,220 1,230 1,240 1,250 1,260 1,270 1,280
actgtgcaacagctgacaaagagattctcacttggaatgctgcagggacgaggaccattaaaactgttcatggccctggtggcgttccttcgtttcctaacaatccc
tgacacgttgtcgactgtttctctaagagtgaaccttacgacgtccctgctcctggtaatttgacaagtaccgggaccaccgcaaggaagcaaaggattgttaggg
T V Q Q L T K R F S L G M L Q G R G P L K L F M A L V A F L R F L T I P
Capsid
1,290 1,300 1,310 1,320 1,330 1,340 1,350 1,360 1,370 1,380 1,390
accaacagcagggatattgaagagatggggaacaattaaaaaatcaaaagctattaatgttttgagagggttcaggaaagagattggaaggatgctgaacatcttga
tggttgtcgtccctataacttctctacccctttgttaatttttagttttcgataattacaaaactctcccaagtcctttctctaaccttcctacgacttgtagaact
P T A G I L K R W G T I K K S K A I N V L R G F R K E I G R M L N I L
Capsid
1,400 1,410 1,420 1,430 1,440 1,450 1,460 1,470 1,480 1,490
ataggagacgcagatctgccggcatgatcattatgctgattccaacagtgatggcgttccatttaaccacacgtaacggagaaccacacatgatcgtcagcagacaa
tatcctctgcgtctagacggccgtactagtaatacgactaaggttgtcactaccgcaaggtaaattggtgtgcattgcctcttggtgtgtactagcagtcgtctgtt
N R R R R S A G M I I M L I P T V M A F H L T T R N G E P H M I V S R Q
Capsid
prM Re...2023)
Capsid
prM
1,500 1,510 1,520 1,530 1,540 1,550 1,560 1,570 1,580 1,590 1,600
gagaaagggaaaagtcttctgtttaaaacagaggatggcgtgaacatgtgtaccctcatggccatggaccttggtgaattgtgtgaagacacaatcacgtacaagtg
ctctttccctttcagaagacaaattttgtctcctaccgcacttgtacacatgggagtaccggtacctggaaccacttaacacacttctgtgttagtgcatgttcac
E K G K S L L F K T E D G V N M C T L M A M D L G E L C E D T I T Y K C
prM
1,610 1,620 1,630 1,640 1,650 1,660 1,670 1,680 1,690 1,700 1,710
tcccctttctcaggcagaatgagccagaagacatagactgttggtgcaactctacgtccacgtgggtaacttatgggacgtgtaccaccatgggagaacatagaagag
aggggaagagtccgtcttactcggtcttctgtatctgacaaccacgttgagatgcaggtgcacccattgaataccctgcacatggtggtaccctcttgtatcttctc
P L L R Q N E P E D I D C W C N S T S T W V T Y G T C T T M G E H R R
prM
1,720 1,730 1,740 1,750 1,760 1,770 1,780 1,790 1,800 1,810
aaaaaagatcagtggcactcgttccacatgtgggaatgggactggagacacgaactgaaacatggatgtcatcagaaggggcctggaaacatgtccagagaattgaa
ttttttctagtcaccgtgagcaaggtgtacacccttaccctgacctctgtgcttgactttgtacctacagtagtcttccccggacctttgtacaggtctcttaactt
E K R S V A L V P H V G M G L E T R T E T W M S S E G A W K H V Q R I E
prM
1,820 1,830 1,840 1,850 1,860 1,870 1,880 1,890 1,900 1,910 1,920

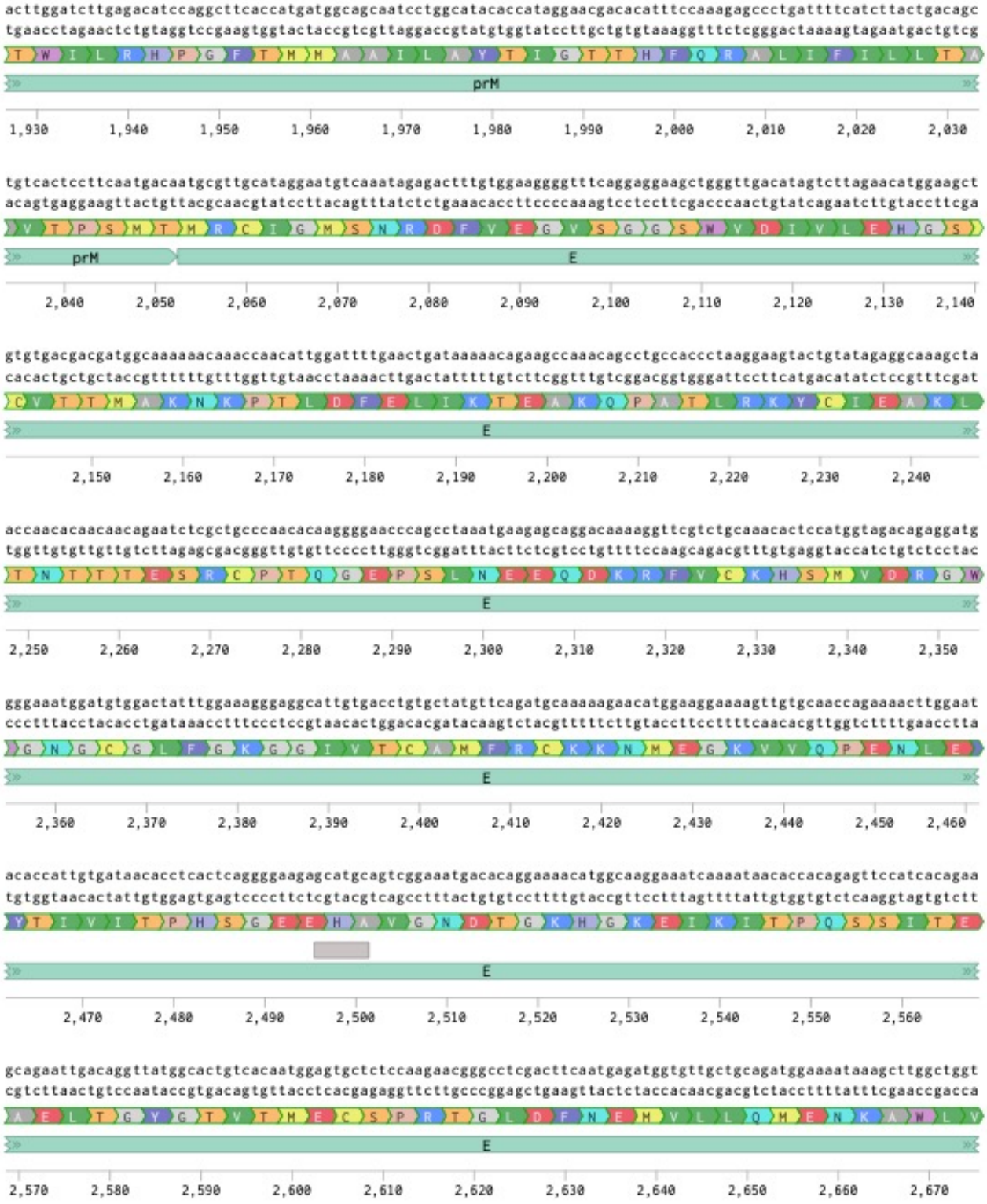
prM
1,930
1,940
1,950
1,960
1,970
1,980
1,990
2,000
2,010
2,020
2,030
prM
E
2,040
2,050
2,060
2,070
2,080
2,090
2,100
2,110
2,120
2,130
2,140
E
2,150
2,160
2,170
2,180
2,190
2,200
2,210
2,220
2,230
2,240
E
2,250
2,260
2,270
2,280
2,290
2,300
2,310
2,320
2,330
2,340
2,350
E
2,360
2,370
2,380
2,390
2,400
2,410
2,420
2,430
2,440
2,450
2,460
E
2,470
2,480
2,490
2,500
2,510
2,520
2,530
2,540
2,550
2,560
E
2,570
2,580
2,590
2,600
2,610
2,620
2,630
2,640
2,650
2,660
2,670

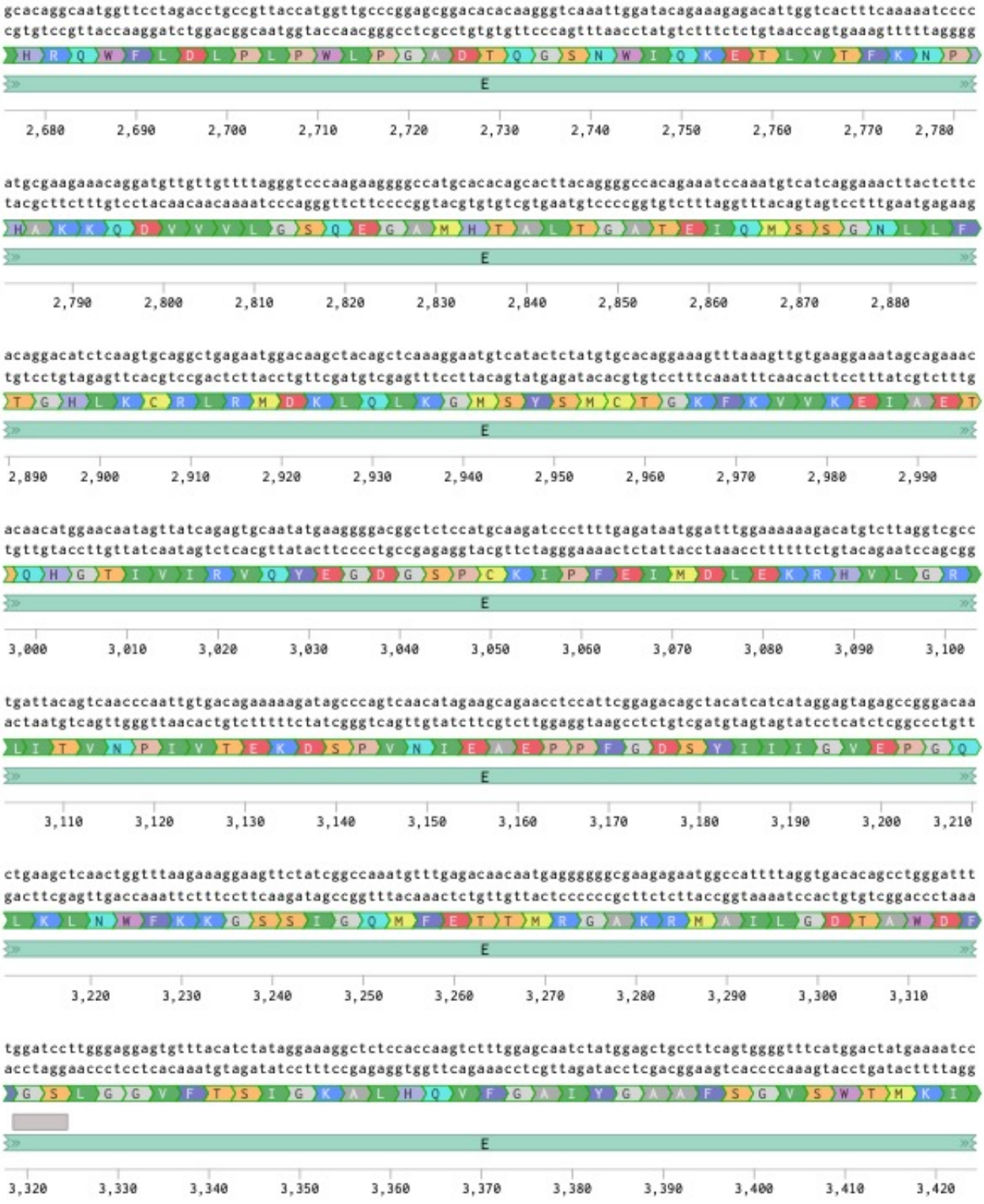
gcacaggcaatggttcctagacctgccgttaccatggttgcccggagcggacacacaagggtcaaattggatacagaaagagacattggtcactttcaaaaatcccc
cgtgtccgttaccaaggatctggacggcaatggtaccaacgggcctcgcctgtgtgttcccagtttaacctatgtctttctctgtaaccagtgaaagtttttagggg
H R Q W F L D L P L P W L P G A D T Q G S N W I Q K E T L V T F K N P
E
2,680 2,690 2,700 2,710 2,720 2,730 2,740 2,750 2,760 2,770 2,780
atgcgaagaaacaggatgttgttgttttagggtcccaagaaggggccatgcacacagcacttacaggggccacagaaatccaaatgtcatcaggaaacttactcttc
tacgcttctttgtcctacaacaacaaaatcccagggttcttccccggtacgtgtgtcgtgaatgtccccggtgtctttaggtttacagtagtcctttgaatgagaag
H A K K Q D V V V L G S Q E G A M H T A L T G A T E I Q M S S G N L L F
E
2,790 2,800 2,810 2,820 2,830 2,840 2,850 2,860 2,870 2,880
acaggacatctcaagtgcaggctgagaatggacaagctacagctcaaaggaatgtcatactctatgtgcacaggaaagtttaaagttgtgaaggaaatagcagaaac
tgtcctgtagagttcacgtccgactcttacctgttcgatgtcgagtttccttacagtatgagatacacgtgtcctttcaaatttcaacacttcctttatcgtctttg
T G H L K C R L R M D K L Q L K G M S Y S M C T G K F K V V K E I A E T
E
2,890 2,900 2,910 2,920 2,930 2,940 2,950 2,960 2,970 2,980 2,990
acaacatggaacaatagttatcagagtgcaatatgaaggggacggctctccatgcaagatccctttgagataatggatttggaaaaaagacatgtcttaggtcgcc
tgttgtaccttgttatcaatagtctcacgttatacttcccctgccgagaggtacgttctagggaaaactctattacctaaacctttttttctgtacagaatccagcgg
Q H G T I V I R V Q Y E G D G S P C K I P F E I M D L E K R H V L G R
E
3,000 3,010 3,020 3,030 3,040 3,050 3,060 3,070 3,080 3,090 3,100
tgattacagtcaacccaattgtgacagaaaaagatagcccagtcaacatagaagcagaacctccattcggagacagctacatcatcataggagtagagccgggacaa
actaatgtcagttgggttaacactgtctttttctatcgggtcagttgtatcttcgtcttggaggtaagcctctgtcgatgtagtagtatcctcatctcggccctgtt
L I T V N P I V T E K D S P V N I E A E P P F G D S Y I I I G V E P G Q
E
3,110 3,120 3,130 3,140 3,150 3,160 3,170 3,180 3,190 3,200 3,210
ctgaagctcaactggtttaagaaaggaagttctatcggccaaatgtttgagacaacaatgaggggggcgaagagaatggccattttaggtgacacagcctgggattt
gacttcgagttgaccaaattctttccttcaagatagccggtttacaaactctgttgttactccccccgcttctcttaccggtaaaatccactgtgtcggaccctaaa
L K L N W F K K G S S I G Q M F E T T M R G A K R M A I L G D T A W D F
E
3,220 3,230 3,240 3,250 3,260 3,270 3,280 3,290 3,300 3,310
tggatccttgggaggagtgtttacatctataggaaaggctctccaccaagtctttggagcaatctatggagctgccttcagtggggtttcatggactatgaaaatcc
acctaggaaccctcctcacaaatgtagatatcctttccgagaggtggttcagaaacctcgttagatacctcgacggaagtcaccccaaagtacctgatacttttagg
G S L G G V F T S I G K A L H Q V F G A I Y G A A F S G V S W T M K I
E
3,320 3,330 3,340 3,350 3,360 3,370 3,380 3,390 3,400 3,410 3,420

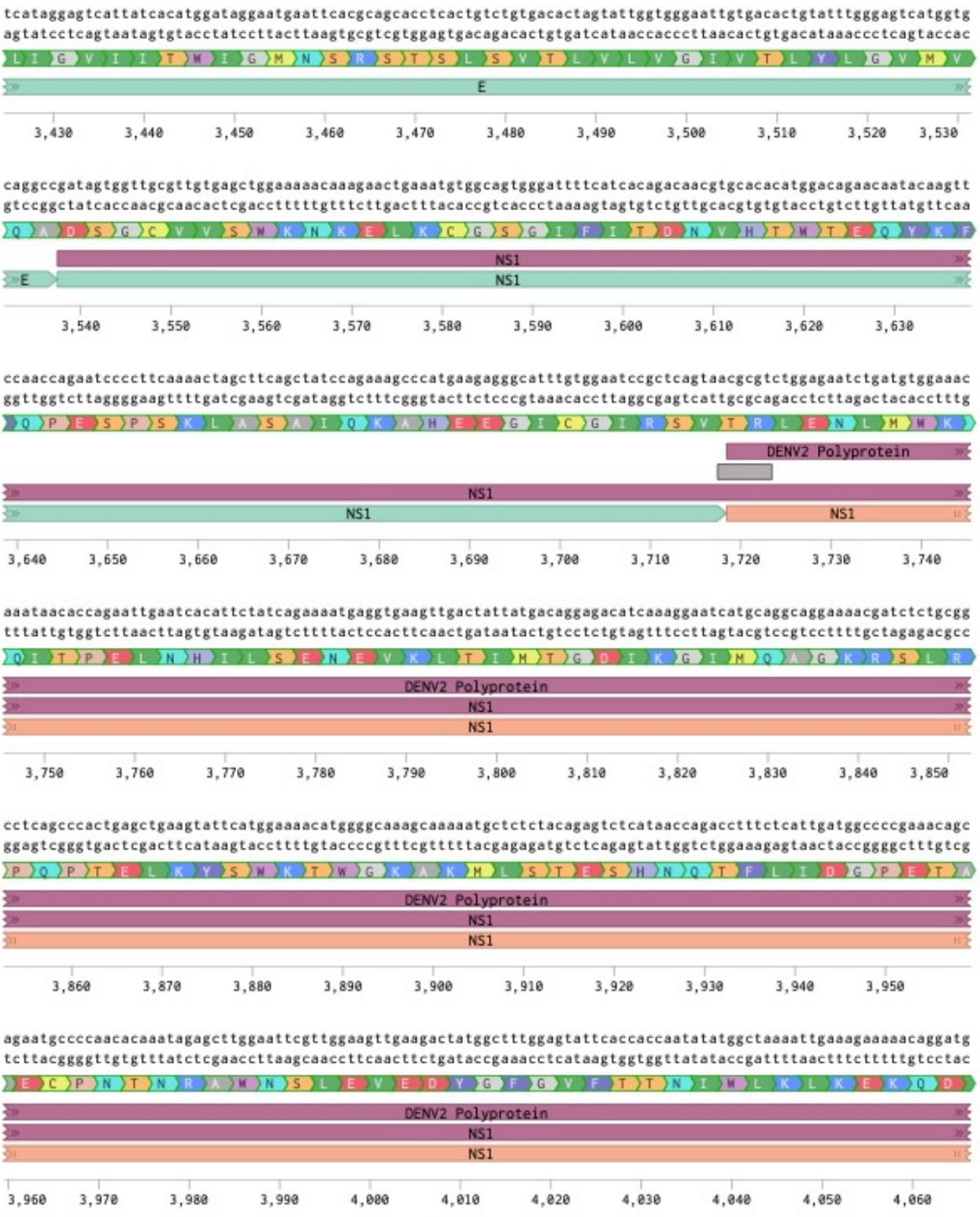
tcataggagtcattatcacatggataggaatgaattcacgcagcacctcactgtctgtgacactagtattggtgggaattgtgacactgtatttgggagtcatggtg
agtatcctcagtaatagtgtacctatccttacttaagtgcgtcgtggagtgacagacactgtgatcataaccacccttaacactgtgacataaaccctcagtaccac
L I G V I I T M I G M N S R S T S L S V T L V L V G I V T L Y L G V M V
E
3,430 3,440 3,450 3,460 3,470 3,480 3,490 3,500 3,510 3,520 3,530
caggccgatagtggttgcgttgtgagctggaaaaacaaagaactgaaatgtggcagtgggattttcatcacagacaacgtgcacacatggacagaacaatacaagtt
gtccggctatcaccaacgcaacactcgacctttttgtttcttgactttacaccgtcaccctaaaagtagtgtctgttgcacgtgtgtacctgtcttgttatgttcaa
Q A D S G C V V S W K N K E L K C G S G I F I T D N V H T W T E Q Y K F
NS1
E
NS1
3,540 3,550 3,560 3,570 3,580 3,590 3,600 3,610 3,620 3,630
ccaaccagaatccccttcaaaactagcttcagctatccagaaagcccatgaagagggcatttgtggaatccgctcagtaacgcgtctggagaatctgatgtggaaac
ggttggtcttaggggaagttttgatcgaagtcgataggtctttcgggtacttctcccgtaaacaccttaggcgagtcattgcgcagacctcttagactacacctttg
Q P E S P S K L A S A I Q K A H E E G I C G I R S V T R L E N L M W K
DENV2 Polyprotein
NS1
NS1
NS1
3,640 3,650 3,660 3,670 3,680 3,690 3,700 3,710 3,720 3,730 3,740
aaataacaccagaattgaatcacattctatcagaaaatgaggtgaagttgactattatgacaggagacatcaaaggaatcatgcaggcaggaaaacgatctctgcgg
tttattgtggtcttaacttagtgtaagatagtcttttactccacttcaactgataatactgtcctctgtagtttccttagtacgtccgtccttttgctagagacgcc
Q I T P E L N H I L S E N E V K L T I M T G D I K G I M Q A G K R S L R
DENV2 Polyprotein
NS1
NS1
3,750 3,760 3,770 3,780 3,790 3,800 3,810 3,820 3,830 3,840 3,850
cctcagcccactgagctgaagtattcatggaaaacatggggcaaagcaaaaatgctctctacagagtctcataaccagacctttctcattgatggccccgaaacagc
ggagtcgggtgactcgacttcataagtacctttgtaccccgtttcgtttttacgagagatgtctcagagtattggtctggaaagagtaactaccggggctttgtcg
P Q P T E L K Y S W K T W G K A K M L S T E S H N Q T F L I D G P E T A
DENV2 Polyprotein
NS1
NS1
3,860 3,870 3,880 3,890 3,900 3,910 3,920 3,930 3,940 3,950
agaatgccccaacacaaatagagcttggaattcgttggaagttgaagactatggctttggagtattcaccaccaatatatggctaaaattgaaagaaaaacaggatg
tcttacggggttgtgtttatctcgaaccttaagcaaccttcaacttctgataccgaaacctcataagtggtggttatataccgattttaactttctttttgtcctac
E C P N T N R A W N S L E V E D Y G F G V F T T N I W L K L K E K Q D
DENV2 Polyprotein
NS1
NS1
3,960 3,970 3,980 3,990 4,000 4,010 4,020 4,030 4,040 4,050 4,060

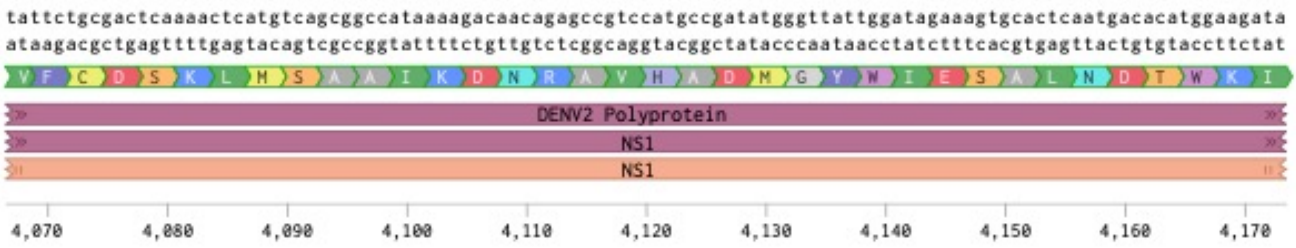
tattctgcgactcaaaactcatgtcagcggccataaaagacaacagagccgtccatgccgatatgggttattggatagaaagtgcactcaatgacacatggaagata
ataagacgctgagttttgagtacagtcgccggtattttctgttgtctcggcaggtacggctatacccaataacctatctttcacgtgagttactgtgtaccttctat
V F C D S K L M S A A I K D N R A V H A D M G Y W I E S A L N D T W K I
DENV2 Polyprotein
NS1
NS1
4,070
4,080
4,090
4,100
4,110
4,120
4,130
4,140
4,150
4,160
4,170

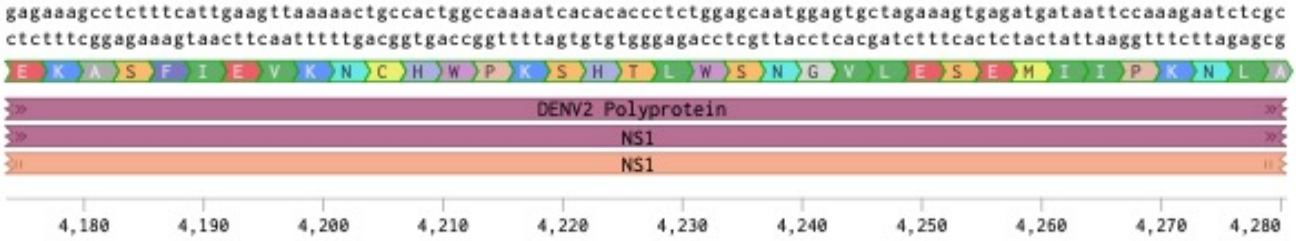
gagaaagcctctttcattgaagttaaaaactgccactggccaaaatcacacaccctctggagcaatggagtgctagaaagtgagatgataattccaaagaatctcgc
ctctttcggagaaagtaacttcaatttttgacggtgaccggttttagtgtgtgggagacctcgttacctcacgatctttcactctactattaaggtttcttagagcg
E K A S F I E V K N C H W P K S H T L W S N G V L E S E M I I P K N L A
DENV2 Polyprotein
NS1
NS1
4,180
4,190
4,200
4,210
4,220
4,230
4,240
4,250
4,260
4,270
4,280

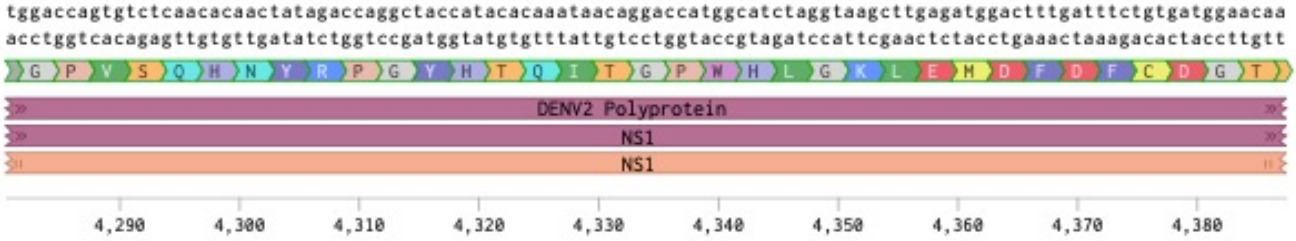
tggaccagtgtctcaacacaactatagaccaggctaccatacacaaataacaggaccatggcatctaggtaagcttgagatggactttgatttctgtgatggaacaa
acctggtcacagagttgtgttgatatctggtccgatggtatgtgtttattgtcctggtaccgtagatccattcgaactctacctgaaactaaagacactaccttgtt
G P V S Q H N Y R P G Y H T Q I T G P W H L G K L E M D F D F C D G T
DENV2 Polyprotein
NS1
NS1
4,290
4,300
4,310
4,320
4,330
4,340
4,350
4,360
4,370
4,380

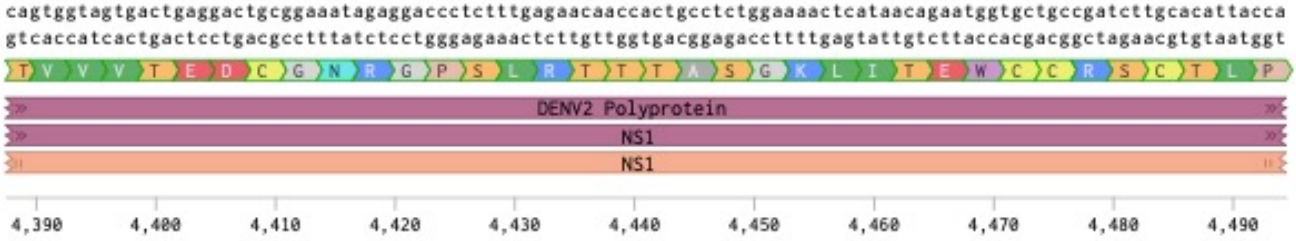
cagtggtagtgactgaggactgcggaaatagaggaccctctttgagaacaaccactgcctctggaaaactcataacagaatggtgctgccgatcttgcacattacca
gtcaccatcactgactcctgacgcctttatctcctgggagaaactcttgttggtgacggagacctttgagtattgtcttaccacgacggctagaacgtgtaatggt
T V V V T E D C G N R G P S L R T T T A S G K L I T E W C C R S C T L P
DENV2 Polyprotein
NS1
NS1
4,390
4,400
4,410
4,420
4,430
4,440
4,450
4,460
4,470
4,480
4,490

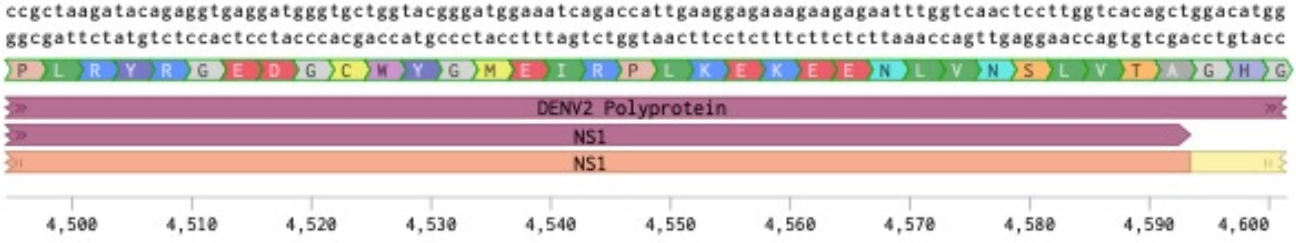
ccgctaagatacagaggtgaggatgggtgctggtacgggatggaaatcagaccattgaaggagaaagaagagaatttggtcaactccttggtcacagctggacatgg
ggcgattctatgtctccactcctacccacgaccatgccctacctttagtctggtaacttcctctttcttctcttaaaccagttgaggaaccagtgtcgacctgtacc
P L R Y R G E D G C W Y G M E I R P L K E K E E N L V N S L V T A G H G
DENV2 Polyprotein
NS1
NS1
4,500
4,510
4,520
4,530
4,540
4,550
4,560
4,570
4,580
4,590
4,600

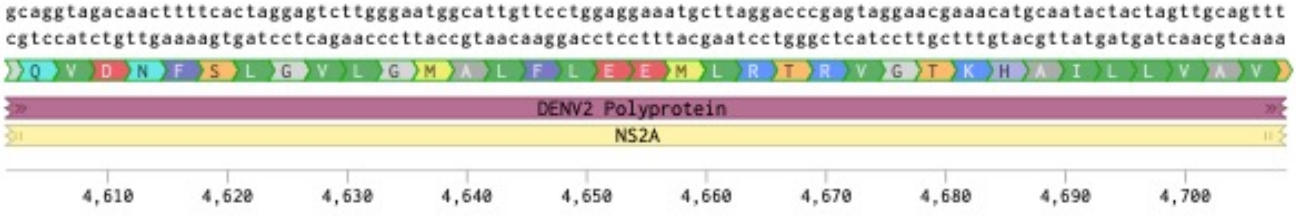
gcaggtagacaacttttcactaggagtcttgggaatggcattgttcctggaggaaatgcttaggacccgagtaggaacgaaacatgcaatactactagttgcagttt
cgtccatctgttgaaaagtgatcctcagaacccttaccgtaacaaggacctcctttacgaatcctgggctcatccttgctttgtacgttatgatgatcaacgtcaaa
Q V D N F S L G V L G M A L F L E E M L R T R V G T K H A I L L V A V
DENV2 Polyprotein
NS2A
4,610
4,620
4,630
4,640
4,650
4,660
4,670
4,680
4,690
4,700

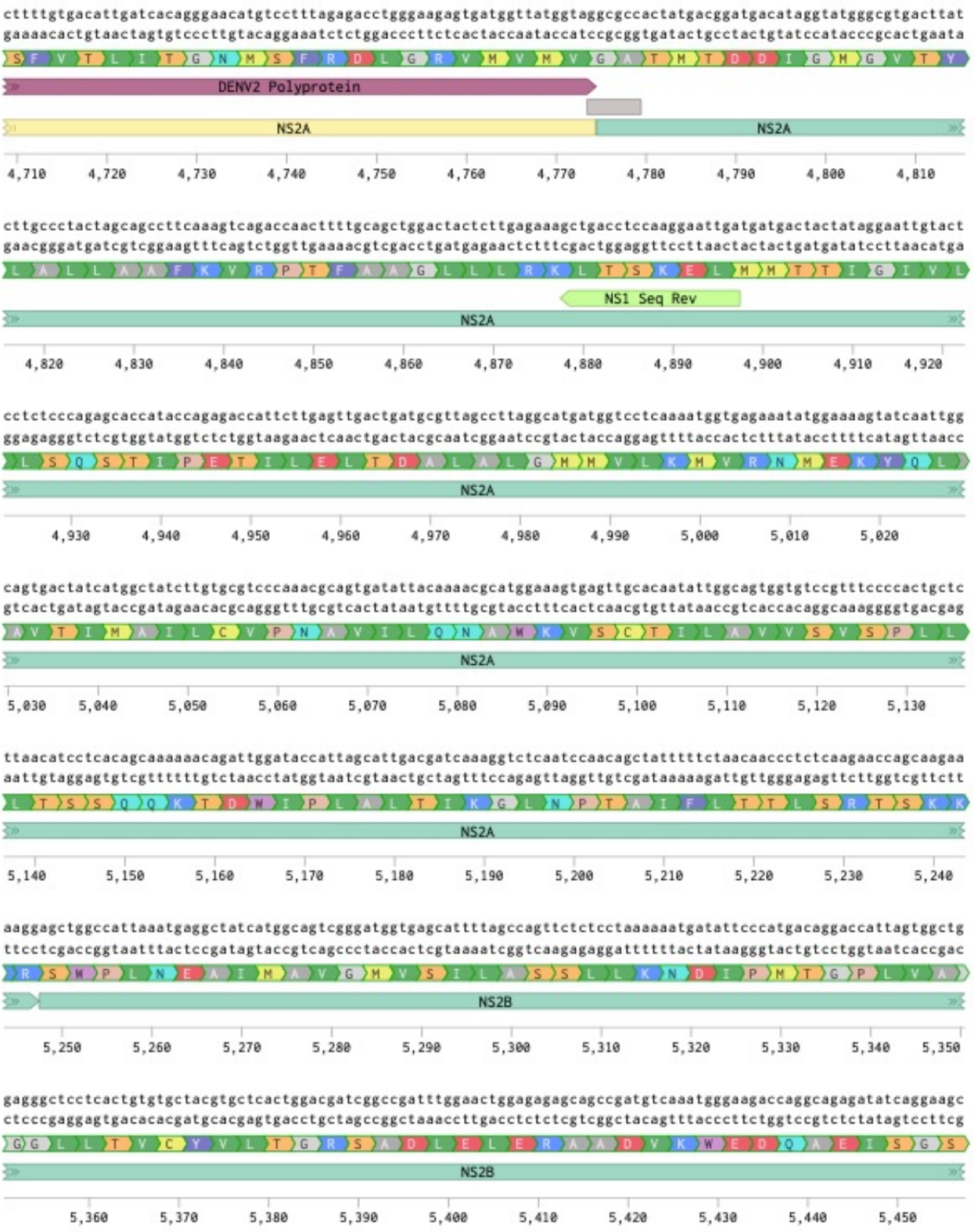
ctttgtgacattgatcacagggaacatgtcctttagagacctgggaagagtgatggttatggtaggcgccactatgacggatgacataggtatgggcgtgacttat
gaaaacactgtaactagtgtcccttgtacaggaaatctctggacccttctcactaccaataccatccgcggtgatactgcctactgtatccatacccgcactgaata
DENV2 Polyprotein
NS2A
NS2A
4,710 4,720 4,730 4,740 4,750 4,760 4,770 4,780 4,790 4,800 4,810
cttgccctactagcagccttcaaagtcagaccaacttttgcagctggactactcttgagaaagctgacctccaaggaattgatgatgactactataggaattgtact
gaacgggatgatcgtcggaagtttcagtctggttgaaaacgtcgacctgatgagaactctttcgactggaggttccttaactactactgatgatatccttaacatga
NS1 Seq Rev
NS2A
4,820 4,830 4,840 4,850 4,860 4,870 4,880 4,890 4,900 4,910 4,920
cctctcccagagcaccataccagagaccattcttgagttgactgatgcgttagccttaggcatgatggtcctcaaaatggtgagaaatatggaaaagtatcaattgg
ggagagggtctcgtggtatggtctctggtaagaactcaactgactacgcaatcggaatccgtactaccaggagttttaccactctttataccttttcatagttaacc
NS2A
4,930 4,940 4,950 4,960 4,970 4,980 4,990 5,000 5,010 5,020
cagtgactatcatggctatcttgtgcgtcccaaacgcagtgatattacaaaacgcatggaaagtgagttgcacaatattggcagtggtgtccgtttccccactgctc
gtcactgatagtaccgatagaacacgcagggtttgcgtcactataatgttttgcgtacctttcactcaacgtgttataaccgtcaccacaggcaaaggggtgacgag
NS2A
5,030 5,040 5,050 5,060 5,070 5,080 5,090 5,100 5,110 5,120 5,130
ttaacatcctcacagcaaaaaacagattggataccattagcattgacgatcaaaggtctcaatccaacagctatttttctaacaaccctctcaagaaccagcaagaa
aattgtaggagtgtcgttttttgtctaacctatggtaatcgtaactgctagtttccagagttaggttgtcgataaaaagattgttgggagagttcttggtcgttctt
NS2A
5,140 5,150 5,160 5,170 5,180 5,190 5,200 5,210 5,220 5,230 5,240
aaggagctggccattaaatgaggctatcatggcagtcgggatggtgagcattttagccagttctctcctaaaaaatgatattcccatgacaggaccattagtggctg
ttcctcgaccggtaatttactccgatagtaccgtcagccctaccactcgtaaaatcggtcaagagaggatttttttactataagggtactgtcctggtaatcaccgac
NS2B
5,250 5,260 5,270 5,280 5,290 5,300 5,310 5,320 5,330 5,340 5,350
gagggctcctcactgtgtgctacgtgctcactggacgatcggccgatttggaactggagagagcagccgatgtcaaatgggaagaccaggcagagatatcaggaagc
ctcccgaggagtgacacacgatgcacgagtgacctgctagccggctaaaccttgacctctctcgtcggctacagtttacccttctggtccgtctctatagtccttcg
NS2B
5,360 5,370 5,380 5,390 5,400 5,410 5,420 5,430 5,440 5,450

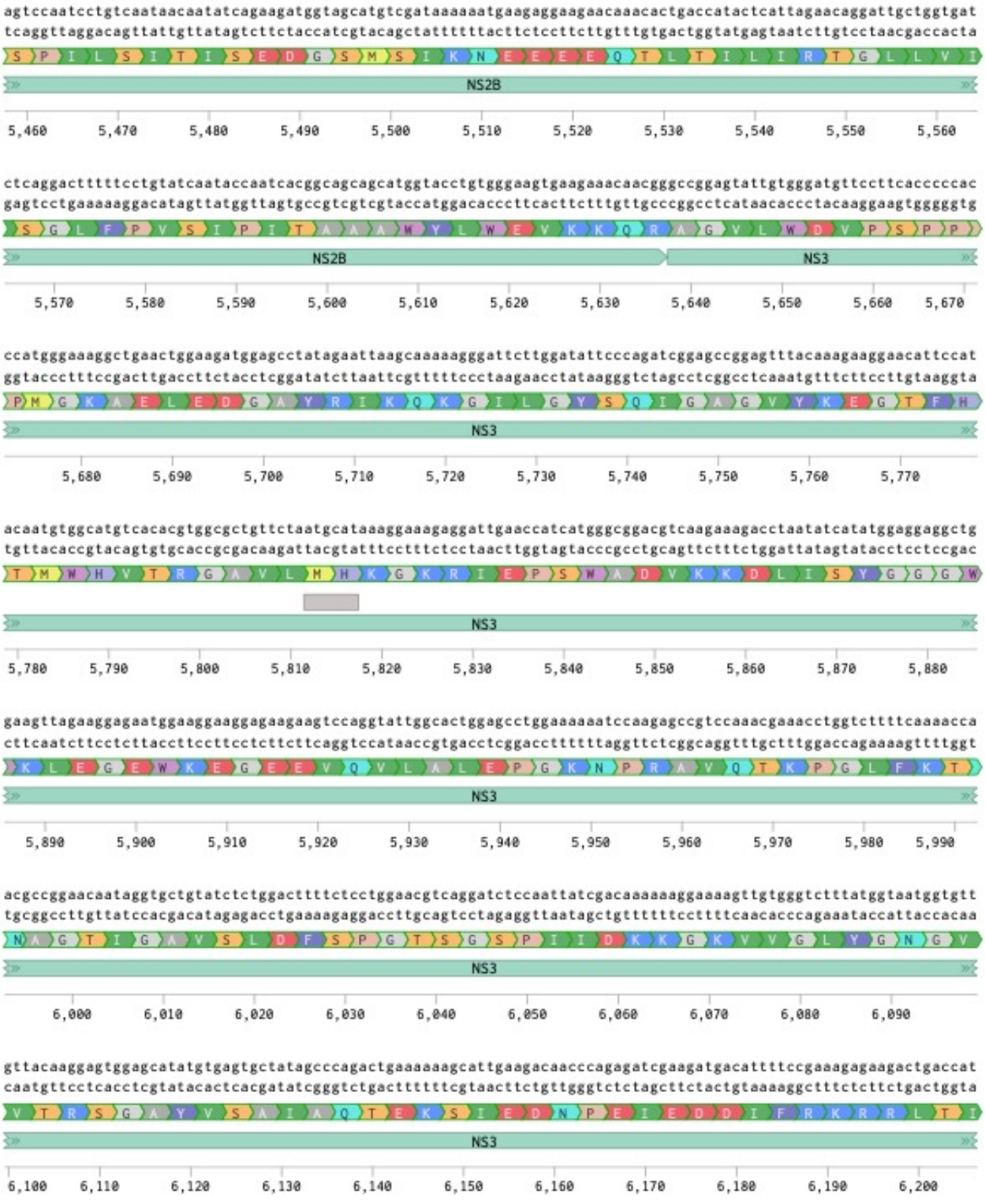
agtccaatcctgtcaataacaatatcagaagatggtagcatgtcgataaaaaatgaagaggaagaacaaacactgaccatactcattagaacaggattgctggtgat
tcaggttaggacagttattgttatagtcttctaccatcgtacagctatttttttacttctccttcttgtttgtgactggtatgagtaatcttgtcctaacgaccacta
S P I L S I T I S E D G S M S I K N E E E E Q T L T I L I R T G L L V I
NS2B
5,460 5,470 5,480 5,490 5,500 5,510 5,520 5,530 5,540 5,550 5,560
ctcaggacttttttcctgtatcaataccaatcacggcagcagcatggtacctgtgggaagtgaagaaacaacgggccggagtattgtgggatgttccttcacccccac
gagtcctgaaaaaggacatagttatggttagtgccgtcgtcgtaccatggacacccttcacttctttgttgcccggcctcataacaccctacaaggaagtgggggtg
S G L F P V S I P I T A A A W Y L W E V K K Q R A G V L W D V P S P P
NS2B
NS3
5,570 5,580 5,590 5,600 5,610 5,620 5,630 5,640 5,650 5,660 5,670
ccatgggaaaggctgaactggaagatggagcctatagaattaagcaaaaagggattcttggatattcccagatcggagccggagtttacaaagaaggaacattccat
ggtacccttccgacttgaccttctacctcggatatcttaattcgtttttccctaagaacctataagggtctagcctcggcctcaaatgtttcttccttgtaaggta
P M G K A E L E D G A Y R I K Q K G I L G Y S Q I G A G V Y K E G T F H
NS3
5,680 5,690 5,700 5,710 5,720 5,730 5,740 5,750 5,760 5,770
acaatgtggcatgtcacacgtggcgctgttctaatgcataaaggaaagaggattgaaccatcatgggcggacgtcaagaaagacctaatatcatatggaggaggctg
tgttacaccgtacagtgtgcaccgcgacaagattacgtatttccttttctcctaacttggtagtacccgcctgcagttctttctggattatagtatacctcctccgac
T M W H V T R G A V L M H K G K R I E P S W A D V K K D L I S Y G G G W
NS3
5,780 5,790 5,800 5,810 5,820 5,830 5,840 5,850 5,860 5,870 5,880
gaagttagaaggagaatggaaggaaggagaagaagtccaggtattggcactggagcctggaaaaaatccaagagccgtccaaacgaaacctggtcttttcaaaacca
cttcaatcttcctcttaccttccttcctcttcttcaggtccataaccgtgacctcggacctttttttaggttctcggcaggtttgctttggaccagaaaagttttggt
K L E G E W K E G E E V Q V L A L E P G K N P R A V Q T K P G L F K T
NS3
5,890 5,900 5,910 5,920 5,930 5,940 5,950 5,960 5,970 5,980 5,990
acgccggaacaataggtgctgtatctctggacttttctcctggaacgtcaggatctccaattatcgacaaaaaaggaaaagttgtgggtctttatggtaatggtgtt
tgcggccttgttatccacgacatagagacctgaaaagaggaccttgcagtcctagaggttaatagctgtttttttccttttcaacacccagaaataccattaccacaa
N A G T I G A V S L D F S P G T S G S P I I D K K G K V V G L Y G N G V
NS3
6,000 6,010 6,020 6,030 6,040 6,050 6,060 6,070 6,080 6,090
gttacaaggagtggagcatatgtgagtgctatagcccagactgaaaaaagcattgaagacaacccagagatcgaagatgacatttttccgaaagagaagactgaccat
caatgttcctcacctcgtatacactcacgatatcgggtctgacttttttcgtaacttctgttgggtctctagcttctactgtaaaaggctttctcttctgactggta
V T R S G A Y V S A I A Q T E K S I E D N P E I E D D I F R K R R L T I
NS3
6,100 6,110 6,120 6,130 6,140 6,150 6,160 6,170 6,180 6,190 6,200

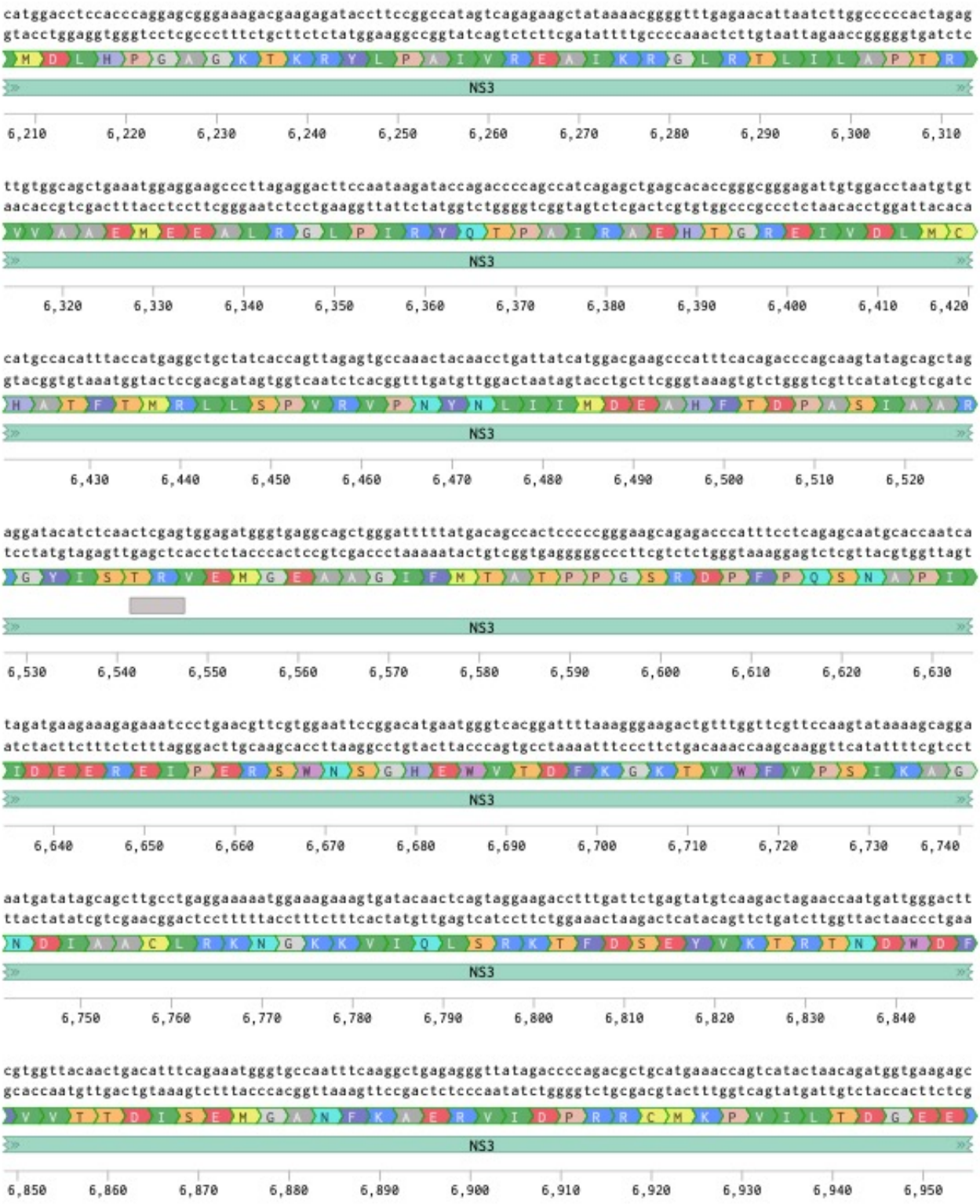
catggacctccacccaggagcgggaaagacgaagagataccttccggccatagtcagagaagctataaaacggggtttgagaacattaatcttggcccccactagag
gtacctggaggtgggtcctcgccctttctgcttctctatggaaggccggtatcagtctcttcgatattttgccccaaactcttgtaattagaaccgggggtgatctc
M D L H P G A G K T K R Y L P A I V R E A I K R G L R T L I L A P T R
NS3
6,210 6,220 6,230 6,240 6,250 6,260 6,270 6,280 6,290 6,300 6,310
ttgtggcagctgaaatggaggaagcccttagaggacttccaataagataccagaccccagccatcagagctgagcacaccgggcgggagattgtggacctaatgtgt
aacaccgtcgactttacctccttcgggaatctcctgaaggttattctatggtctggggtcggtagtctcgactcgtgtggcccgccctctaacacctggattacaca
V V A A E M E E A L R G L P I R Y Q T P A I R A E H T G R E I V D L M C
NS3
6,320 6,330 6,340 6,350 6,360 6,370 6,380 6,390 6,400 6,410 6,420
catgccacatttaccatgaggctgctatcaccagttagagtgccaaactacaacctgattatcatggacgaagcccatttcacagacccagcaagtatagcagctag
gtacggtgtaaatggtactccgacgatagtggtcaatctcacggtttgatgttggactaatagtacctgcttcgggtaaagtgtctgggtcgttcatatcgtcgatc
H A T F T M R L L S P V R V P N Y N L I I M D E A H F T D P A S I A A R
NS3
6,430 6,440 6,450 6,460 6,470 6,480 6,490 6,500 6,510 6,520
aggatacatctcaactcgagtggagatgggtgaggcagctgggatttttatgacagccactcccccgggaagcagagacccatttcctcagagcaatgcaccaatca
tcctatgtagagttgagctcacctctacccactccgtcgaccctaaaaatactgtcggtgagggggcccttcgtctctgggtaaaggagtctcgttacgtggttagt
G Y I S T R V E M G E A A G I F M T A T P P G S R D P F P Q S N A P I
NS3
6,530 6,540 6,550 6,560 6,570 6,580 6,590 6,600 6,610 6,620 6,630
tagatgaagaaagagaaatccctgaacgttcgtggaattccggacatgaatgggtcacggattttaaagggaagactgtttggttcgttccaagtataaaagcagga
atctacttctttctctttagggacttgcaagcaccttaaggcctgtacttacccagtgcctaaaatttcccttctgacaaaccaagcaaggttcatattttcgtcct
I D E E R E I P E R S W N S G H E W V T D F K G K T V W F V P S I K A G
NS3
6,640 6,650 6,660 6,670 6,680 6,690 6,700 6,710 6,720 6,730 6,740
aatgatatagcagcttgcctgaggaaaaatggaaagaaagtgatacaactcagtaggaagacctttgattctgagtatgtcaagactagaaccaatgattgggactt
ttactatatcgtcgaacggactccttttttaccttttctttcactatgttgagtcatccttctggaaactaagactcatacagttctgatcttggttactaaccctgaa
N D I A A C L R K N G K K V I Q L S R K T F D S E Y V K T R T N D W D F
NS3
6,750 6,760 6,770 6,780 6,790 6,800 6,810 6,820 6,830 6,840
cgtggttacaactgacatttcagaaatgggtgccaatttcaaggctgagagggttatagaccccagacgctgcatgaaaccagtcatactaacagatggtgaagagc
gcaccaatgttgactgtaaagtctttacccacggttaaagttccgactctcccaatatctggggtctgcgacgtactttggtcagtatgattgtctaccacttctcg
V V T T D I S E M G A N F K A E R V I D P R R C M K P V I L T D G E E
NS3
6,850 6,860 6,870 6,880 6,890 6,900 6,910 6,920 6,930 6,940 6,950

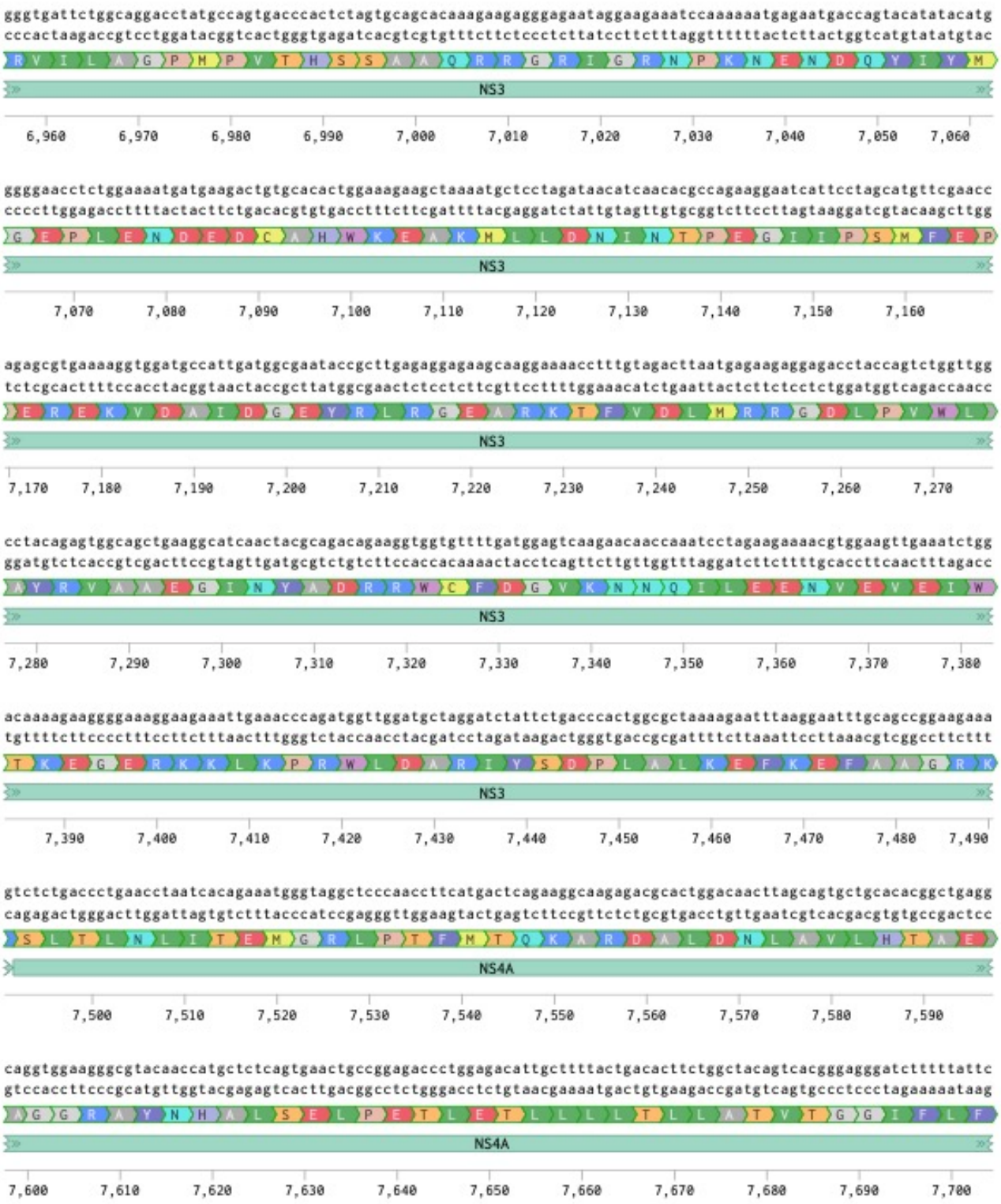
gggtgattctggcaggacctatgccagtgacccactctagtgcagcacaaagaagagggagaataggaagaaatccaaaaaatgagaatgaccagtacatatacatg
cccactaagaccgtcctggatacggtcactgggtgagatcacgtcgtgtttcttctccctcttatccttctttaggttttttactcttactggtcatgtatatgtac
R V I L A G P M P V T H S S A A Q R R G R I G R N P K N E N D Q Y I Y M
NS3
6,960 6,970 6,980 6,990 7,000 7,010 7,020 7,030 7,040 7,050 7,060
ggggaacctctggaaaatgatgaagactgtgcacactggaaagaagctaaaatgctcctagataacatcaacacgccagaaggaatcattcctagcatgttcgaacc
ccccttggagacctttttactacttctgacacgtgtgacctttcttcgattttacgaggatctattgtagttgtgcggtcttccttagtaaggatcgtacaagcttgg
G E P L E N D E D C A H W K E A K M L L D N I N T P E G I I P S M F E P
NS3
7,070 7,080 7,090 7,100 7,110 7,120 7,130 7,140 7,150 7,160
agagcgtgaaaaggtggatgccattgatggcgaataccgcttgagaggagaagcaaggaaaacctttgtagacttaatgagaagaggagacctaccagtctggttgg
tctcgcacttttccacctacggtaactaccgcttatggcgaactctcctcttcgttccttttggaaacatctgaattactcttctcctctggatggtcagaccaacc
E R E K V D A I D G E Y R L R G E A R K T F V D L M R R G D L P V W L
NS3
7,170 7,180 7,190 7,200 7,210 7,220 7,230 7,240 7,250 7,260 7,270
cctacagagtggcagctgaaggcatcaactacgcagacagaaggtggtgttttgatggagtcaagaacaaccaaatcctagaagaaaacgtggaagttgaaatctgg
ggatgtctcaccgtcgacttccgtagttgatgcgtctgtcttccaccacaaaactacctcagttcttgttggtttaggatcttcttttgcaccttcaactttagacc
A Y R V A A E G I N Y A D R R W C F D G V K N N Q I L E E N V E V E I W
NS3
7,280 7,290 7,300 7,310 7,320 7,330 7,340 7,350 7,360 7,370 7,380
acaaaagaaggggaaaggaagaaattgaaacccagatggttggatgctaggatctattctgacccactggcgctaaaagaatttaaggaatttgcagccggaagaaa
tgttttcttccccttttccttctttaactttgggtctaccaacctacgatcctagataagactgggtgaccgcgattttcttaaattccttaaacgtcggccttctttt
T K E G E R K K L K P R W L D A R I Y S D P L A L K E F K E F A A G R K
NS3
7,390 7,400 7,410 7,420 7,430 7,440 7,450 7,460 7,470 7,480 7,490
gtctctgaccctgaacctaatcacagaaatgggtaggctcccaaccttcatgactcagaaggcaagagacgcactggacaacttagcagtgctgcacacggctgagg
cagagactgggacttggattagtgtctttacccatccgagggttggaagtactgagtcttccgttctctgcgtgacctgttgaatcgtcacgacgtgtgccgactcc
S L T L N L I T E M G R L P T F M T Q K A R D A L D N L A V L H T A E
NS4A
7,500 7,510 7,520 7,530 7,540 7,550 7,560 7,570 7,580 7,590
caggtggaagggcgtacaaccatgctctcagtgaactgccggagaccctggagacattgcttttactgacacttctggctacagtcacgggagggatctttttattc
gtccaccttcccgcatgttggtacgagagtcacttgacggcctctgggacctctgtaacgaaaatgactgtgaagaccgatgtcagtgccctccctagaaaaataag
A G G R A Y N H A L S E L P E T L E T L L L L T L L A T V T G G I F L F
NS4A
7,600 7,610 7,620 7,630 7,640 7,650 7,660 7,670 7,680 7,690 7,700

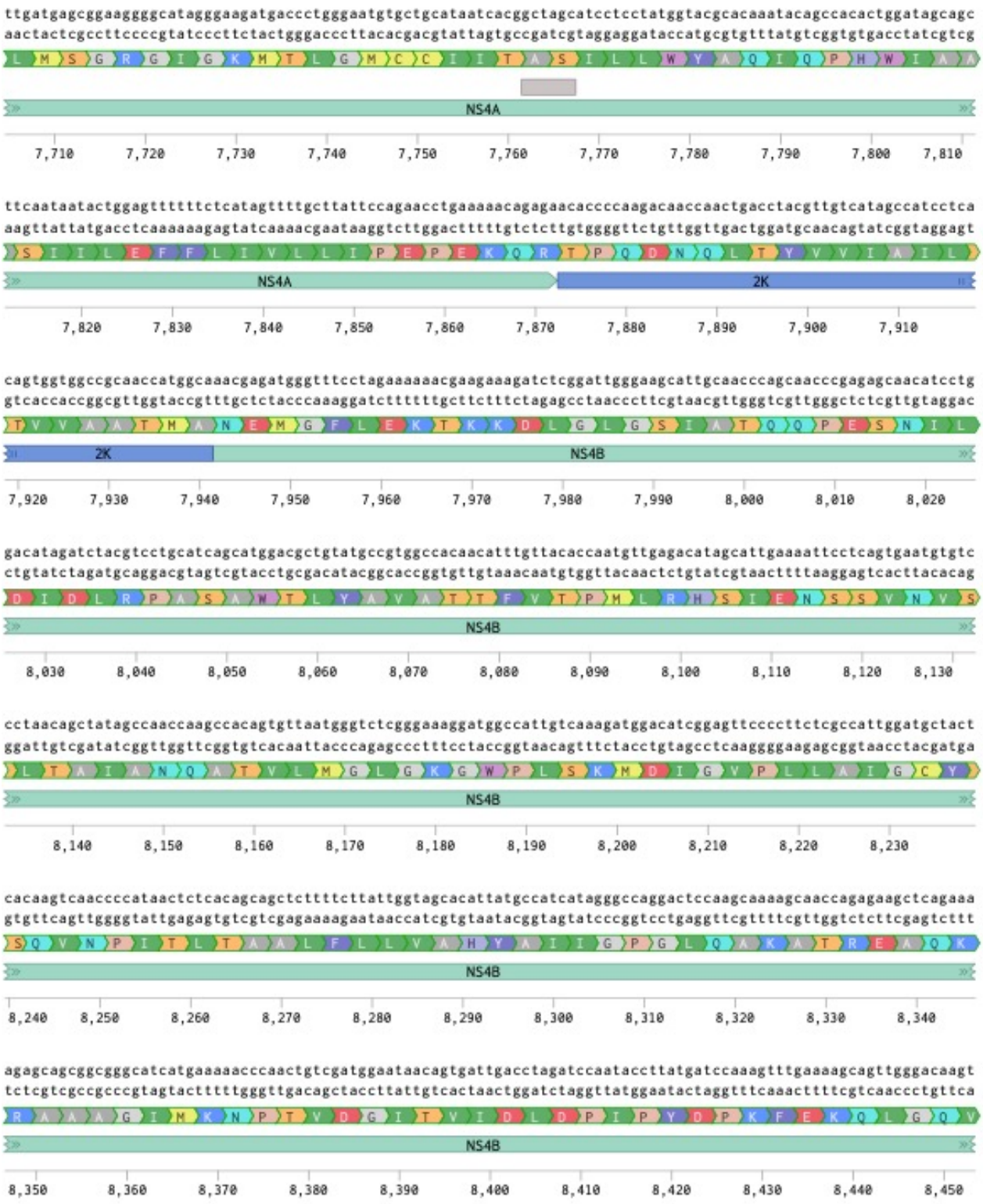
ttgatgagcggaaggggcatagggaagatgaccctgggaatgtgctgcataatcacggctagcatcctcctatggtacgcacaaatacagccacactggatagcagc
aactactcgccttccccgtatcccttctactgggacccttacacgacgtattagtgccgatcgtaggaggataccatgcgtgtttatgtcggtgtgacctatcgtcg
L M S G R G I G K M T L G M C C I I T A S I L L W Y A Q I Q P H W I A A
NS4A
7,710 7,720 7,730 7,740 7,750 7,760 7,770 7,780 7,790 7,800 7,810
ttcaataatactggagttttttctcatagttttgcttattccagaacctgaaaaacagagaacaccccaagacaaccaactgacctacgttgtcatagccatcctca
aagttattatgacctcaaaaaagagtatcaaaacgaataaggtcttggacttttgtctcttgtggggttctgttggttgactggatgcaacagtatcggtaggagt
S I I L E F F L I V L L I P E P E K Q R T P Q D N Q L T Y V V I A I L
NS4A
2K
7,820 7,830 7,840 7,850 7,860 7,870 7,880 7,890 7,900 7,910
cagtggtggccgcaaccatggcaaacgagatgggtttcctagaaaaaacgaagaaagatctcggattgggaagcattgcaacccagcaacccgagagcaacatcctg
gtcaccaccggcgttggtaccgtttgctctacccaaaggatctttttgcttctttctagagcctaacccttcgtaacgttgggtcgttgggctctcgttgtaggac
T V V A A T M A N E M G F L E K T K K D L G L G S I A T Q Q P E S N I L
2K
NS4B
7,920 7,930 7,940 7,950 7,960 7,970 7,980 7,990 8,000 8,010 8,020
gacatagatctacgtcctgcatcagcatggacgctgtatgccgtggccacaacatttgttacaccaatgttgagacatagcattgaaaattcctcagtgaatgtgtc
ctgtatctagatgcaggacgtagtcgtacctgcgacatacggcaccggtgttgtaaacaatgtggttacaactctgtatcgtaacttttaaggagtcacttacacag
D I D L R P A S A W T L Y A V A T T F V T P M L R H S I E N S S V N V S
NS4B
8,030 8,040 8,050 8,060 8,070 8,080 8,090 8,100 8,110 8,120 8,130
cctaacagctatagccaaccaagccacagtgttaatgggtctcgggaaaggatggccattgtcaaagatggacatcggagttccccttctcgccattggatgctact
ggattgtcgatatcggttggttcggtgtcacaattacccagagccctttcctaccggtaacagtttctacctgtagcctcaaggggaagagcggtaacctacgatga
L T A I A N Q A T V L M G L G K G W P L S K M D I G V P L L A I G C Y
NS4B
8,140 8,150 8,160 8,170 8,180 8,190 8,200 8,210 8,220 8,230
cacaagtcaaccccataactctcacagcagctcttttcttattggtagcacattatgccatcatagggccaggactccaagcaaaagcaaccagagaagctcagaaa
gtgttcagttggggtattgagagtgtcgtcgagaaaagaataaccatcgtgtaatacggtagtatcccggtcctgaggttcgttttcgttggtctcttcgagtcttt
S Q V N P I T L T A A L F L L V A H Y A I I G P G L Q A K A T R E A Q K
NS4B
8,240 8,250 8,260 8,270 8,280 8,290 8,300 8,310 8,320 8,330 8,340
agagcagcggcgggcatcatgaaaaacccaactgtcgatggaataacagtgattgacctagatccaatacttatgatccaaagtttgaaaagcagttgggacaagt
tctcgtcgccgcccgtagtacttttgggttgacagctaccttattgtcactaactggatctaggttatggaatactaggtttcaaacttttcgtcaaccctgttca
R A A A G I M K N P T V D G I T V I D L D P I P Y D P K F E K Q L G Q V
NS4B
8,350 8,360 8,370 8,380 8,390 8,400 8,410 8,420 8,430 8,440 8,450

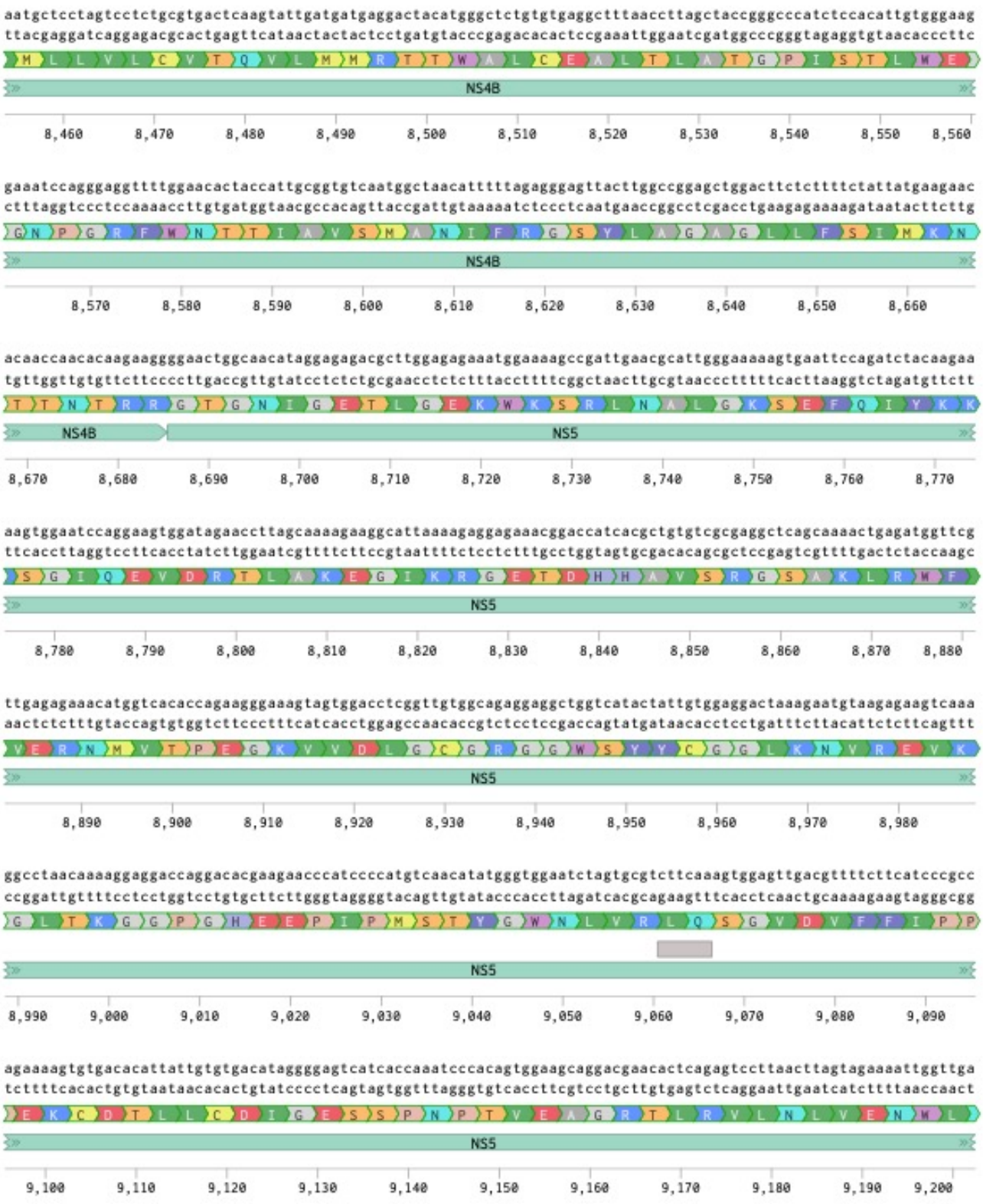
aatgctcctagtcctctgcgtgactcaagtattgatgatgaggactacatgggctctgtgtgaggctttaaccttagctaccgggcccatctccacattgtgggaag
ttacgaggatcaggagacgcactgagttcataactactactcctgatgtacccgagacacactccgaaattggaatcgatggcccgggtagaggtgtaacacccttc
M L L V L C V T Q V L M M R T T W A L C E A L T L A T G P I S T L M E
NS4B
8,460 8,470 8,480 8,490 8,500 8,510 8,520 8,530 8,540 8,550 8,560
gaaatccagggaggttttggaacactaccattgcggtgtcaatggctaacatttttagagggagttacttggccggagctggacttctcttttctattatgaagaac
ctttaggtccctccaaaaccttgtgatggtaacgccacagttaccgattgtaaaaatctccctcaatgaaccggcctcgacctgaagagaaaagataatacttcttg
G N P G R F M N T T I A V S M A N I F R G S Y L A G A G L L F S I M K N
NS4B
8,570 8,580 8,590 8,600 8,610 8,620 8,630 8,640 8,650 8,660
acaaccaacacaagaaggggaactggcaacataggagagacgcttggagagaaatggaaaagccgattgaacgcattgggaaaaagtgaattccagatctacaagaa
tgttggttgtgttcttcccctgaccgttgtatcctctctgcgaacctctctttacctttcggctaacttgcgtaaccctttttcacttaaggtctagatgttctt
T T N T R R G T G N I G E T L G E K W K S R L N A L G K S E F Q I Y K K
NS4B
NS5
8,670 8,680 8,690 8,700 8,710 8,720 8,730 8,740 8,750 8,760 8,770
aagtggaatccaggaagtggatagaaccttagcaaaagaaggcattaaaagaggagaaacggaccatcacgctgtgtcgcgaggctcagcaaaactgagatggttcg
ttcaccttaggtccttcacctatcttggaatcgttttcttccgtaattttctcctctttgcctggtagtgcgacacagcgctccgagtcgttttgactctaccaagc
S G I Q E V D R T L A K E G I K R G E T D H H A V S R G S A K L R W F
NS5
8,780 8,790 8,800 8,810 8,820 8,830 8,840 8,850 8,860 8,870 8,880
ttgagagaaacatggtcacaccagaagggaaagtagtggacctcggttgtggcagaggaggctggtcatactattgtggaggactaaagaatgtaagagaagtcaaa
aactctctttgtaccagtgtggtcttccctttcatcacctggagccaacaccgtctcctccgaccagtatgataacacctcctgatttcttacattctcttcagttt
V E R N M V T P E G K V V D L G C G R G G W S Y Y C G G L K N V R E V K
NS5
8,890 8,900 8,910 8,920 8,930 8,940 8,950 8,960 8,970 8,980
ggcctaacaaaaggaggaccaggacacgaagaacccatccccatgtcaacatatgggtggaatctagtgcgtcttcaaagtggagttgacgttttcttcatcccgcc
ccggattgttttcctcctggtcctgtgcttcttgggtaggggtacagttgtatacccaccttagatcacgcagaagtttcacctcaactgcaaaagaagtagggcgg
G L T K G G P G H E E P I P M S T Y G W N L V R L Q S G V D V F F I P P
NS5
8,990 9,000 9,010 9,020 9,030 9,040 9,050 9,060 9,070 9,080 9,090
agaaaagtgtgacacattattgtgtgacataggggagtcatcaccaaatcccacagtggaagcaggacgaacactcagagtccttaacttagtagaaaattggttga
tcttttcacactgtgtaataacacactgtatcccctcagtagtggtttagggtgtcaccttcgtcctgcttgtgagtctcaggaattgaatcatcttttaaccaact
E K C D T L L C D I G E S S P N P T V E A G R T L R V L N L V E N W L
NS5
9,100 9,110 9,120 9,130 9,140 9,150 9,160 9,170 9,180 9,190 9,200

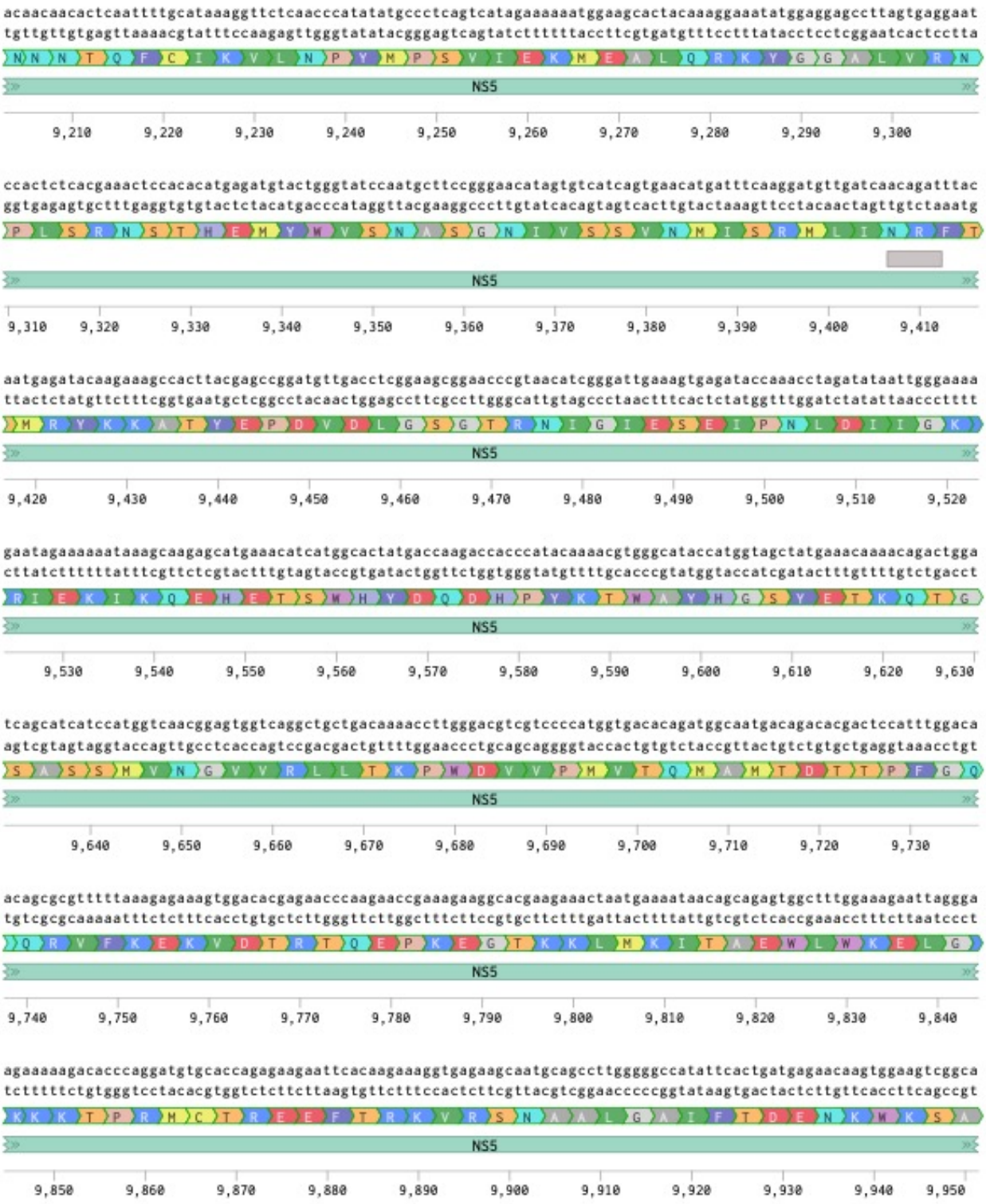
acaacaacactcaattttgcataaaggttctcaacccatatatgccctcagtcatagaaaaaatggaagcactacaaaggaaatatggaggagccttagtgaggaat
tgttgttgtgagttaaaacgtatttccaagagttgggtatatacgggagtcagtatctttttttaccttcgtgatgtttcctttatacctcctcggaatcactcctta
NNNTQFCIKVLNPYMPSVIEKMEALQRKYGGALVRN
NS5
9,210 9,220 9,230 9,240 9,250 9,260 9,270 9,280 9,290 9,300
ccactctcacgaaactccacacatgagatgtactgggtatccaatgcttccgggaacatagtgtcatcagtgaacatgatttcaaggatgttgatcaacagatttac
ggtgagagtgctttgaggtgtgtactctacatgacccataggttacgaaggcccttgtatcacagtagtcacttgtactaaagttcctacaactagttgtctaaatg
PLSRNSTHEMYMVSNASGNIVSSVNMISRMLINRFT
NS5
9,310 9,320 9,330 9,340 9,350 9,360 9,370 9,380 9,390 9,400 9,410
aatgagatacaagaaagccacttacgagccggatgttgacctcggaagcggaacccgtaacatcgggattgaaagtgagataccaaacctagatataattgggaaaa
ttactctatgttctttcggtgaatgctcggcctacaactggagccttcgccttgggcattgtagccctaactttcactctatggtttggatctatattaaccctttt
MRYKKATYEPDVDLGSGTRNIGIESEIPNLDIIGK
NS5
9,420 9,430 9,440 9,450 9,460 9,470 9,480 9,490 9,500 9,510 9,520
gaatagaaaaaataaagcaagagcatgaaacatcatggcactatgaccaagaccacccatacaaaacgtgggcataccatggtagctatgaaacaaaacagactgga
cttatctttttttatttcgttctcgtactttgtagtaccgtgatactggttctggtgggtatgttttgcacccgtatggtaccatcgatactttgttttgtctgacct
RIEKIKQEHETSWHYDQDHPYKTWAYHGSYETKQTG
NS5
9,530 9,540 9,550 9,560 9,570 9,580 9,590 9,600 9,610 9,620 9,630
tcagcatcatccatggtcaacggagtggtcaggctgctgacaaaaccttgggacgtcgtccccatggtgacacagatggcaatgacagacacgactccatttggaca
agtcgtagtaggtaccagttgcctcaccagtccgacgactgttttggaaccctgcagcaggggtaccactgtgtctaccgttactgtctgtgctgaggtaaacctgt
SASSMVNGVVRLLTKPWDVVPMVTQMAMTDTTPFGQ
NS5
9,640 9,650 9,660 9,670 9,680 9,690 9,700 9,710 9,720 9,730
acagcgcgtttttaaagagaaagtggacacgagaacccaagaaccgaaagaaggcacgaagaaactaatgaaaataacagcagagtggctttggaaagaattaggga
tgtcgcgcaaaaatttctctttcacctgtgctcttgggttcttggctttcttccgtgcttctttgattacttttattgtcgtctcaccgaaacctttcttaatccct
QRVFKEKVDTRTQEPKEGTKKLMKITAEWLWKELG
NS5
9,740 9,750 9,760 9,770 9,780 9,790 9,800 9,810 9,820 9,830 9,840
agaaaaagacacccaggatgtgcaccagagaagaattcacaagaaaggtgagaagcaatgcagccttgggggccatattcactgatgagaacaagtggaagtcggca
tctttttctgtgggtcctacacgtggtctcttcttaagtgttctttccactcttcgttacgtcggaacccccggtataagtgactactcttgttcaccttcagccgt
KKKTPRMCTREEFTRKVRSNAALGAIFTDENKMKSA
NS5
9,850 9,860 9,870 9,880 9,890 9,900 9,910 9,920 9,930 9,940 9,950

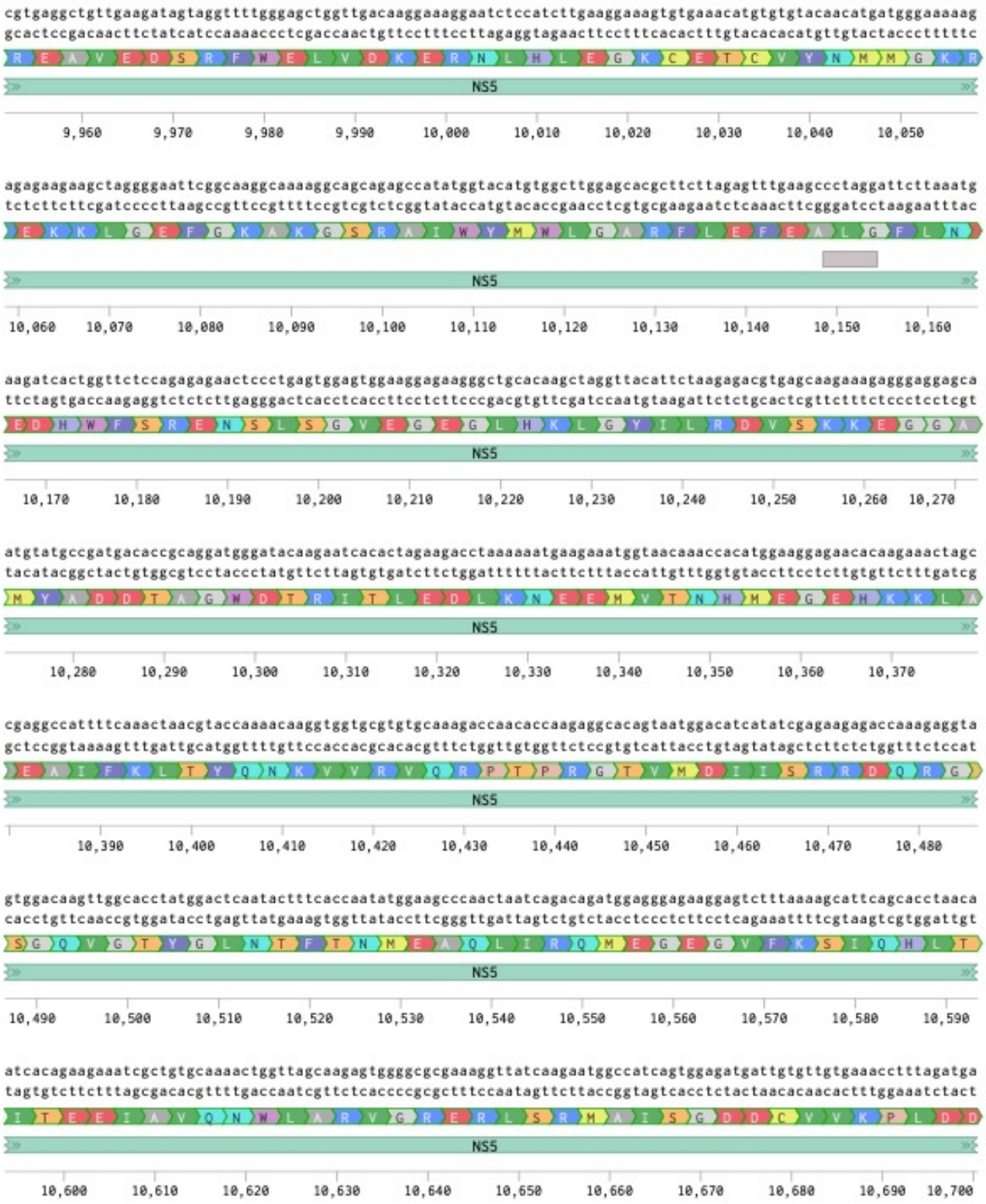
cgtgaggctgttgaagatagtaggttttgggagctggttgacaaggaaaggaatctccatcttgaaggaaagtgtgaaacatgtgtgtacaacatgatgggaaaaag
gcactccgacaacttctatcatccaaaaccctcgaccaactgttcctttccttagaggtagaacttcctttcacactttgtacacacatgttgtactaccctttttc
R E A V E D S R F W E L V D K E R N L H L E G K C E T C V Y N M M G K R
NS5
9,960 9,970 9,980 9,990 10,000 10,010 10,020 10,030 10,040 10,050
agagaagaagctaggggaattcggcaaggcaaaaggcagcagagccatatggtacatgtggcttggagcacgcttcttagagtttgaagccctaggattcttaaatg
tctcttcttcgatcccctttaagccgttccgttttccgtcgtctcggtataccatgtacaccgaacctcgtgcgaagaatctcaaacttcgggatcctaagaatttac
E K K L G E F G K A K G S R A I W Y M W L G A R F L E F E A L G F L N
NS5
10,060 10,070 10,080 10,090 10,100 10,110 10,120 10,130 10,140 10,150 10,160
aagatcactggttctccagagagaactccctgagtggagtggaaggagaagggctgcacaagctaggttacattctaagagacgtgagcaagaaagagggaggagca
ttctagtgaccaagaggtctctcttgagggactcacctcaccttcctcttcccgacgtgttcgatccaatgtaagattctctgcactcgttctttctccctcctcgt
E D H W F S R E N S L S G V E G E G L H K L G Y I L R D V S K K E G G A
NS5
10,170 10,180 10,190 10,200 10,210 10,220 10,230 10,240 10,250 10,260 10,270
atgtatgccgatgacaccgcaggatgggatacaagaatcacactagaagacctaaaaaatgaagaaatggtaacaaaccacatggaaggagaacacaagaaactagc
tacatacggctactgtggcgtcctaccctatgttcttagtgtgatcttctggatttttttacttctttaccattgtttggtgtaccttcctcttgtgttctttgatcg
M Y A D D T A G W D T R I T L E D L K N E E M V T N H M E G E H K K L A
NS5
10,280 10,290 10,300 10,310 10,320 10,330 10,340 10,350 10,360 10,370
cgaggccattttcaaactaacgtaccaaaacaaggtggtgcgtgtgcaaagaccaacaccaagaggcacagtaatggacatcatatcgagaagagaccaaagaggta
gctccggtaaaagtttgattgcatggttttgttccaccacgcacacgtttctggttgtggttctccgtgtcattacctgtagtatagctcttctctggtttctccat
E A I F K L T Y Q N K V V R V Q R P T P R G T V M D I I S R R D Q R G
NS5
10,390 10,400 10,410 10,420 10,430 10,440 10,450 10,460 10,470 10,480
gtggacaagttggcacctatggactcaatactttcaccaatatggaagcccaactaatcagacagatggagggagaaggagtctttaaaagcattcagcacctaaca
cacctgttcaaccgtggatacctgagttatgaaagtggttataccttcgggttgattagtctgtctacctccctcttcctcagaaattttcgtaagtcgtggattgt
S G Q V G T Y G L N T F T N M E A Q L I R Q M E G E G V F K S I Q H L T
NS5
10,490 10,500 10,510 10,520 10,530 10,540 10,550 10,560 10,570 10,580 10,590
atcacagaagaaatcgctgtgcaaaactggttagcaagagtggggcgcgaaaggttatcaagaatggccatcagtggagatgattgtgttgtgaaacctttagatga
tagtgtcttctttagcgacacgttttgaccaatcgttctcaccccgcgctttccaatagttcttaccggtagtcacctctactaacacaacactttggaaatctact
I T E E I A V Q N W L A R V G R E R L S R M A I S G D D C V V K P L D D
NS5
10,600 10,610 10,620 10,630 10,640 10,650 10,660 10,670 10,680 10,690 10,700

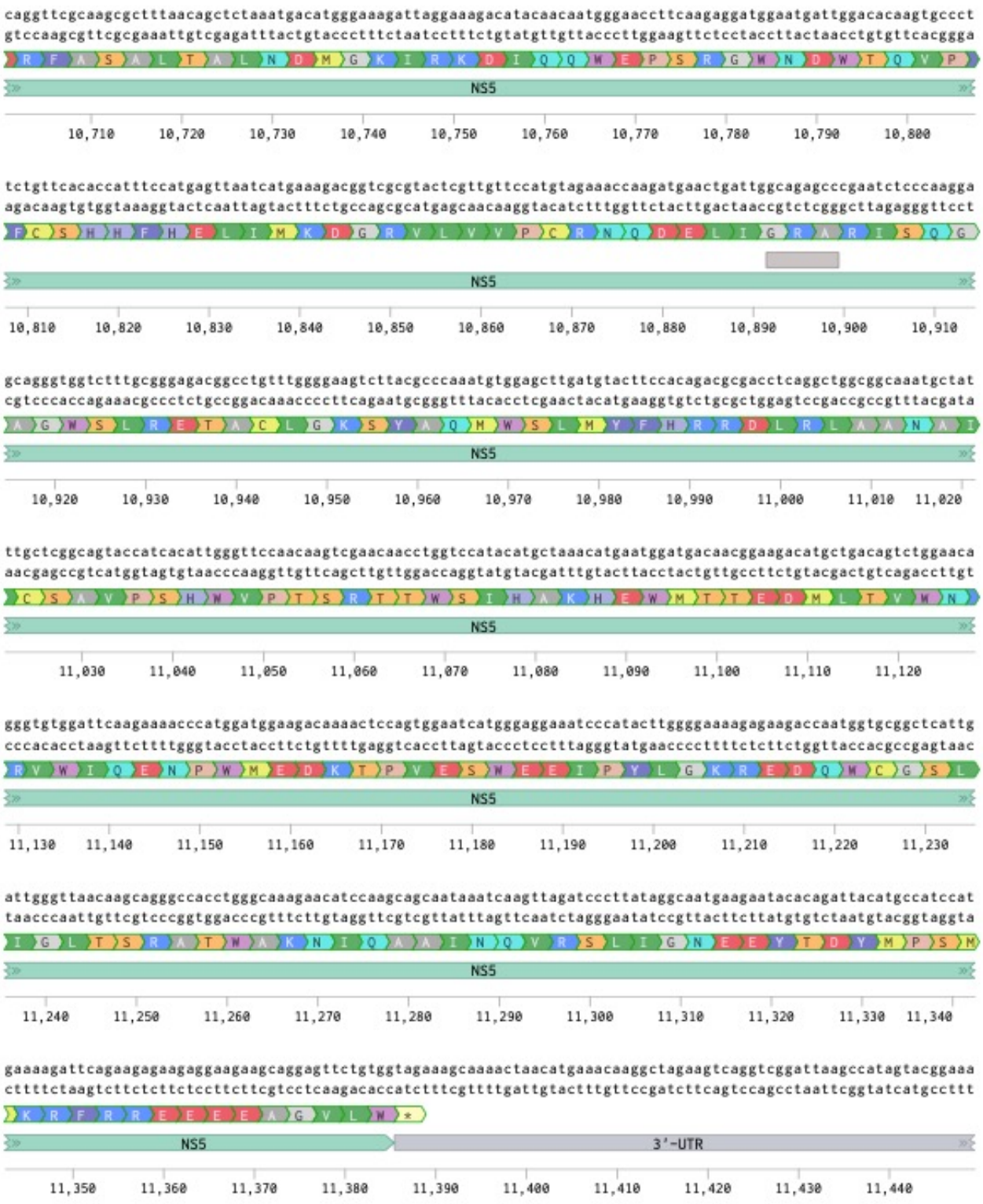
caggttcgcaagcgctttaacagctctaaatgacatgggaaagattaggaaagacatacaacaatgggaaccttcaagaggatggaatgattggacacaagtgccct
gtccaagcgttcgcgaaattgtcgagatttactgtacccttttctaatcctttctgtatgttgttacccttggaagttctcctaccttactaacctgtgttcacggga
R F A S A L T A L N D M G K I R K D I Q Q W E P S R G W N D W T Q V P
NS5
10,710 10,720 10,730 10,740 10,750 10,760 10,770 10,780 10,790 10,800
tctgttcacaccatttccatgagttaatcatgaaagacggtcgcgtactcgttgttccatgtagaaaccaagatgaactgattggcagagcccgaatctcccaagga
agacaagtgtggtaaaggtactcaattagtactttctgccagcgcatgagcaacaaggtacatctttggttctacttgactaaccgtctcgggcttagagggttcct
F C S H H F H E L I M K D G R V L V V P C R N Q D E L I G R A R I S Q G
NS5
10,810 10,820 10,830 10,840 10,850 10,860 10,870 10,880 10,890 10,900 10,910
gcagggtggtctttgcgggagacggcctgtttggggaagtcttacgcccaaatgtggagcttgatgtacttccacagacgcgacctcaggctggcggcaaatgctat
cgtcccaccagaaacgccctctgccggacaaaccccttcagaatgcgggtttacacctcgaactacatgaaggtgtctgcgctggagtccgaccgccgtttacgata
A G W S L R E T A C L G K S Y A Q M W S L M Y F H R R D L R L A A N A I
NS5
10,920 10,930 10,940 10,950 10,960 10,970 10,980 10,990 11,000 11,010 11,020
ttgctcggcagtaccatcacattgggttccaacaagtcgaacaacctggtccatacatgctaaacatgaatggatgacaacggaagacatgctgacagtctggaaca
aacgagccgtcatggtagtgtaacccaaggttgttcagcttgttggaccaggtatgtacgatttgtacttacctactgttgccttctgtacgactgtcagaccttgt
C S A V P S H W V P T S R T T W S I H A K H E W M T T E D M L T V W N
NS5
11,030 11,040 11,050 11,060 11,070 11,080 11,090 11,100 11,110 11,120
gggtgtggattcaagaaaacccatggatggaagacaaaactccagtggaatcatgggaggaaatcccatacttggggaaaagagaagaccaatggtgcggctcattg
cccacacctaagttcttttgggtacctaccttctgttttgaggtcaccttagtaccctcctttagggtatgaaccccttttctcttctggttaccacgccgagtaac
R V W I Q E N P W M E D K T P V E S W E E I P Y L G K R E D Q W C G S L
NS5
11,130 11,140 11,150 11,160 11,170 11,180 11,190 11,200 11,210 11,220 11,230
attgggttaacaagcagggccacctgggcaaagaacatccaagcagcaataaatcaagttagatcccttataggcaatgaagaatacacagattacatgccatccat
taacccaattgttcgtcccggtggacccgtttcttgtaggttcgtcgttatttagttcaatctagggaatatccgttacttcttatgtgtctaatgtacggtaggta
I G L T S R A T W A K N I Q A A I N Q V R S L I G N E E Y T D Y M P S M
NS5
11,240 11,250 11,260 11,270 11,280 11,290 11,300 11,310 11,320 11,330 11,340
gaaaagattcagaagagaagaggaagaagcaggagttctgtggtagaaagcaaaactaacatgaaacaaggctagaagtcaggtcggattaagccatagtacggaaa
cttttctaagtcttctcttctcctttcttcgtcctcaagacaccatctttcgttttgattgtacttttgttccgatcttcagtccagcctaatttcggtatcatgccttt
K R F R R E E E E A G V L W *
NS5
3'-UTR
11,350 11,360 11,370 11,380 11,390 11,400 11,410 11,420 11,430 11,440


3'-UTR
11,460 11,470 11,480 11,490 11,500 11,510 11,520 11,530 11,540 11,550
3'-UTR
11,560 11,570 11,580 11,590 11,600 11,610 11,620 11,630 11,640 11,650 11,660
3'-UTR
11,670 11,680 11,690 11,700 11,710 11,720 11,730 11,740 11,750 11,760 11,770
3'-UTR
11,780 11,790 11,800 11,810 11,820 11,830 11,840 11,850 11,860 11,870
11,880 11,890 11,900 11,910 11,920 11,930 11,940 11,950 11,960 11,970 11,980
M S I Q
AmpR
11,990 12,000 12,010 12,020 12,030 12,040 12,050 12,060 12,070 12,080 12,090
H F R V A L I P F F A A F C L P V F A H P E T L V K V K D A E D Q L G A
AmpR
12,100 12,110 12,120 12,130 12,140 12,150 12,160 12,170 12,180 12,190
R V G Y I E L D L N S G K I L E S F R P E E R F P M M S T F K V L L C
AmpR
12,200 12,210 12,220 12,230 12,240 12,250 12,260 12,270 12,280 12,290 12,300

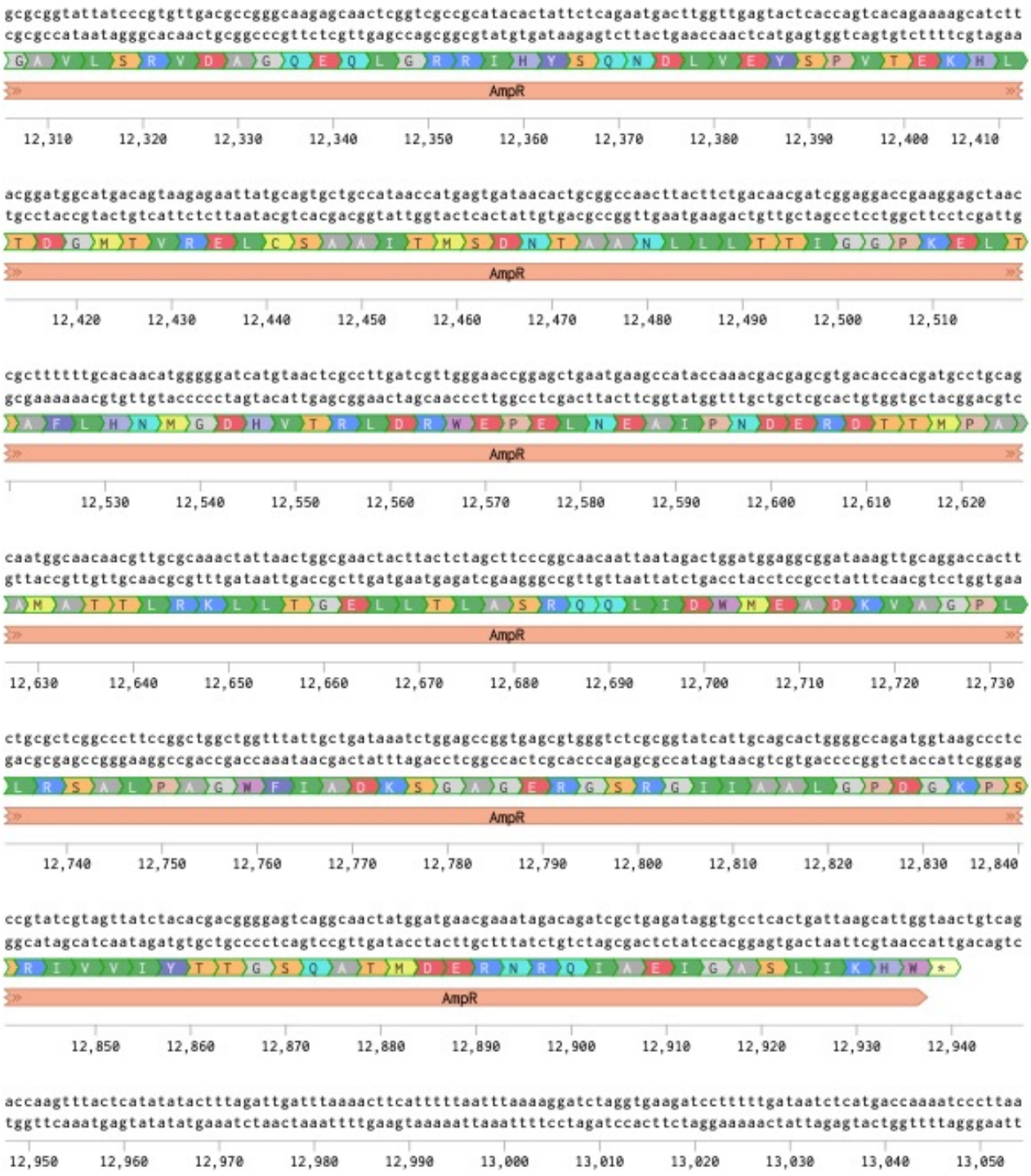
gcgcggtattatcccgtgttgacgccgggcaagagcaactcggtcgccgcatacactattctcagaatgacttggttgagtactcaccagtcacagaaaagcatctt
cgcgccataatagggcacaactgcggcccgttctcgttgagccagcggcgtatgtgataagagtcttactgaaccaactcatgagtggtcagtgtcttttcgtagaa
G A V L S R V D A G Q E Q L G R R I H Y S Q N D L V E Y S P V T E K H L
AmpR
12,310 12,320 12,330 12,340 12,350 12,360 12,370 12,380 12,390 12,400 12,410
acggatggcatgacagtaagagaattatgcagtgctgccataaccatgagtgataacactgcggccaacttacttctgacaacgatcggaggaccgaaggagctaac
tgcctaccgtactgtcattctcttaatacgtcacgacggtattggtactcactattgtgacgccggttgaatgaagactgttgctagcctcctggcttcctcgattg
T D G M T V R E L C S A A I T M S D N T A A N L L L T T I G G P K E L T
AmpR
12,420 12,430 12,440 12,450 12,460 12,470 12,480 12,490 12,500 12,510
cgctttttgcacaacatgggggatcatgtaactcgccttgatcgttgggaaccggagctgaatgaagccataccaaacgacgagcgtgacaccacgatgcctgcag
gcgaaaaaacgtgttgtacccccctagtacattgagcggaactagcaacccttggcctcgacttacttcggtatggtttgctgctcgcactgtggtgctacggacgtc
A F L H N M G D H V T R L D R W E P E L N E A I P N D E R D T T M P A
AmpR
12,530 12,540 12,550 12,560 12,570 12,580 12,590 12,600 12,610 12,620
caatggcaacaacgttgcgcaaactattaactggcgaactacttactctagcttcccggcaacaattaatagactggatggaggcggataaagttgcaggaccactt
gttaccgttgttgcaacgcgtttgataattgaccgcttgatgaatgagatcgaagggccgttgttaattatctgacctacctccgcctatttcaacgtcctggtgaa
A M A T T L R K L L T G E L L T L A S R Q Q L I D M M E A D K V A G P L
AmpR
12,630 12,640 12,650 12,660 12,670 12,680 12,690 12,700 12,710 12,720 12,730
ctgcgctcggcccttccggctggctggtttattgctgataaatctggagccggtgagcgtgggtctcgcggtatcattgcagcactggggccagatggtaagccctc
gacgcgagccgggaaggccgaccgaccaaataacgactatttagacctcggccactcgcacccagagcgccatagtaacgtcgtgaccccggtctaccattcgggag
L R S A L P A G W F I A D K S G A G E R G S R G I I A A L G P D G K P S
AmpR
12,740 12,750 12,760 12,770 12,780 12,790 12,800 12,810 12,820 12,830 12,840
ccgtatcgtagttatctacacgacggggagtcaggcaactatggatgaacgaaatagacagatcgctgagataggtgcctcactgattaagcattggtaactgtcag
ggcatagcatcaatagatgtgctgcccctcagtccgttgatacctacttgctttatctgtctagcgactctatccacggagtgactaattcgtaaccattgacagtc
R I V V I Y T T G S Q A T M D E R N R Q I A E I G A S L I K H W *
AmpR
12,850 12,860 12,870 12,880 12,890 12,900 12,910 12,920 12,930 12,940
accaagtttactcatatatactttagattgatttaaaacttcatttttaatttaaaaggatctaggtgaagatccttttgataatctcatgaccaaaatcccttaa
tggttcaaatgagtatatatgaaatctaactaaatttttgaagtaaaaattaaattttcctagatccacttctaggaaaaactattagagtactggttttagggaatt
12,950 12,960 12,970 12,980 12,990 13,000 13,010 13,020 13,030 13,040 13,050


cgtgagttttcgttccactgagcgtcagaccccgtagaaaagatcaaaggatcttcttgagatccttttttttctgcgcgtaatctgctgcttgcaaacaaaaaaaccc
gcactcaaaagcaaggtgactcgcagtctggggcatcttttctagtttcctagaagaactctaggaaaaaaagacgcgcattagacgacgaacgtttgtttttttgg
ori
13,060 13,070 13,080 13,090 13,100 13,110 13,120 13,130 13,140 13,150 13,160
accgctaccagcggtggtttgtttgccggatcaagagctaccaactctttttccgaaggtaactggcttcagcagagcgcagataccaaatactgtccttctagtgt
tggcgatggtcgccaccaaacaaacggcctagttctcgatggttgagaaaaaggcttccattgaccgaagtcgtctcgcgtctatggtttatgacaggaagatcaca
ori
13,170 13,180 13,190 13,200 13,210 13,220 13,230 13,240 13,250 13,260
agccgtagttaggccaccacttcaagaactctgtagcaccgcctacatacctcgctctgctaatcctgttaccagtggctgctgccagtggcgataagtcgtgtctt
tcggcatcaatccggtggtgaagttcttgagacatcgtggcggatgtatggagcgagacgattaggacaatggtcaccgacgacggtcaccgctattcagcacagaa
ori
13,270 13,280 13,290 13,300 13,310 13,320 13,330 13,340 13,350 13,360 13,370
accgggttggactcaagacgatagttaccggataaggcgcagcggtcgggctgaacgggggggttcgtgcacacagcccagcttggagcgaacgacctacaccgaact
tggcccaacctgagttctgctatcaatggcctattccgcgtcgccagcccgacttgccccccaagcacgtgtgtcgggtcgaacctcgcttgctggatgtggcttga
ori
13,380 13,390 13,400 13,410 13,420 13,430 13,440 13,450 13,460 13,470 13,480
gagatacctacagcgtgagctatgagaaagcgccacgcttcccgaagggagaaaggcggacaggtatccggtaagcggcagggtcggaacaggagagcgcacgaggg
ctctatggatgtcgcactcgatactctttcgcggtgcgaagggcttccctctttccgcctgtccataggccattcgccgtcccagccttgtcctctcgcgtgctccc
ori
13,490 13,500 13,510 13,520 13,530 13,540 13,550 13,560 13,570 13,580
agcttccaggggaaacgcctggtatctttatagtcctgtcgggtttcgccacctctgacttgagcgtcgatttttgtgatgctcgtcaggggggcggagcctatgg
tcgaaggtccccctttgcggaccatagaaatatcaggacagcccaaagcggtggagactgaactcgcagctaaaaacactacgagcagtccccccgcctcggatacc
ori
13,600 13,610 13,620 13,630 13,640 13,650 13,660 13,670 13,680 13,690
aaaaacgccagcaacgcggccttttacggttcctggccttttgctggccttttgctcacatgttctttcctgcgttatcccctgattctgtggataaccgtattac
tttttgcggtcgttgcgccggaaaaatgccaaggaccggaaaacgaccggaaaacgagtgtacaagaaaggacgcaataggggactaagacacctattggcataatg
ori
13,700 13,710 13,720 13,730 13,740 13,750 13,760 13,770 13,780 13,790 13,800
cgcctttgagtgagctgataccgctcgccgcagccgaacgaccgagcgcagcgagtcagtgagcgaggaagcggaagagcgcctgatgcggtattttctccttacgc
gcggaaactcactcgactatggcgagcggcgtcggcttgctggctcgcgtcgctcagtcactcgctccttcgccttctcgcggactacgccataaaagaggaatgcg
13,810 13,820 13,830 13,840 13,850 13,860 13,870 13,880 13,890 13,900 13,910
atctgtgcggtatttcacaccgcatatggtgcactctcagtacaatctgctctgatgccgcatagttaagccagtatacactccgctatcgctacgtgactgggtca
tagacacgccataaagtgtggcgtataccacgtgagagtcatgttagacgagactacggcgtatcaattcggtcatatgtgaggcgatagcgatgcactgacccagt
13,920 13,930 13,940 13,950 13,960 13,970 13,980 13,990 14,000 14,010


tggctgcgccccgacacccgccaacacccgctgacgcgccctgacgggcttgtctgctcccggcatccgcttacagacaagctgtgaccgtctccgggagctgcatg
accgacgcggggctgtgggcggttgtgggcgactgcgcgggactgcccgaacagacgagggccgtaggcgaatgtctgttcgacactggcagaggccctcgacgtac
Sang...tch
14,020 14,030 14,040 14,050 14,060 14,070 14,080 14,090 14,100 14,110 14,120
tgtcagaggttttcaccgtcatcaccgaaacgcgcgaggcagctgcggtaaagctcatcagcgtggtcgtgaagcgattcacagatgtctgcctgttcatccgcgtc
acagtctccaaaagtggcagtagtggctttgcgcgctccgtcgacgccatttcgagtagtcgcaccagcacttcgctaagtgtctacagacggacaagtaggcgcag
rop
Sanger 4R_P2A_A08 Verified 1 mismatch
14,130 14,140 14,150 14,160 14,170 14,180 14,190 14,200 14,210 14,220 14,230
cagctcgttgagtttctccagaagcgttaatgtctggcttctgataaagcgggccatgttaagggcggttttttcctgtttggtcactgatgcctccgtgtaagggg
gtcgagcaactcaaagaggtcttcgcaattacagaccgaagactatttcgcccggtacaattcccgccaaaaaaggacaaaccagtgactacggaggcacattcccc
rop
Sanger 4R_P2A_A08 Verified 1 mismatch
14,240 14,250 14,260 14,270 14,280 14,290 14,300 14,310 14,320 14,330
gatttctgttcatgggggtaatgataccgatgaaacgagagaggatgctcacgatacgggttactgatgatgaacatgcccggttactggaacgttgtgagggtaaa
ctaaagacaagtacccccattactatggctactttgctctctcctacgagtgctatgcccaatgactactacttgtacgggccaatgaccttgcaacactcccattt
Sanger 4R_P2A_A08 Verified 1 mismatch
14,340 14,350 14,360 14,370 14,380 14,390 14,400 14,410 14,420 14,430 14,440
caactggcggtatggatgcggcgggaccagagaaaaatcactcagggtcaatgccagcgcttcgttaatacagatgtaggtgttccacagggtagccagcagcatcc
gttgaccgccatacctacgccgccctggtctcttttttagtgagtcccagttacggtcgcgaagcaattatgtctacatccacaaggtgtcccatcggtcgtcgtagg
Sanger 4R_P2A_A08 Verified 1 mismatch
14,450 14,460 14,470 14,480 14,490 14,500 14,510 14,520 14,530 14,540 14,550
tgcgatgcagatccggaacataatggtgcagggcgctgacttccgcgtttccagactttacgaaacacggaaaccgaagaccattcatgttgttgctcaggtcgcag
acgctacgtctaggccttgtattaccacgtcccgcgactgaaggcgcaaaggtctgaaatgctttgtgccttttggcttctggtaagtacaacaacgagtccagcgtc
Sanger 4R_P2A_A08 Verified 1 mismatch
14,560 14,570 14,580 14,590 14,600 14,610 14,620 14,630 14,640 14,650
acgttttgcagcagcagtcgcttcacgttcgctcgcgtatcggtgattcattctgctaaccagtaaggcaaccccgccagcctagccgggtcctcaacgacaggagc
tgcaaaacgtcgtcgtcagcgaagtgcaagcgagcgcatagccactaagtaagacgattggtcattccgttggggcggtcggatcggcccaggagttgctgtcctcg
IgK_...Fwd
Sanger 4R_P2A_A08 Verified 1 mismatch
14,670 14,680 14,690 14,700 14,710 14,720 14,730 14,740 14,750 14,760
acgatcatgcgcacccgtggccaggacccaacgctgcccgagatgcgccgcgtgcggctgctggagatggcggacgcgatggatatgttctgccaagctaagcttga
tgctagtacgcgtgggcaccggtcctgggttgcgacgggctctacgcggcgcacgccgacgacctctaccgcctgcgctacctatacaagacggttcgattcgaact
Sec_P-APEX2-T_Fwd
Sanger 4R_P2A_A08 Verified 1 mismatch
14,770 14,780 14,790 14,800 14,810 14,820 14,830 14,840 14,850 14,860 14,870
gctctctagc
cgagagatcg
14,880

Appendix V: Supplementary Material (Customised membrane-trafficking siRNA Screen and Deconvolution Screen)

(i) Membrane-trafficking siRNA library

Gene Symbol	GENEID	GINumber	Gene Accession	Pool Catalog Number	Sequence
ACTR2	10097	205361120	NM_005722	L-012076-02	GAAAGAGCAUUUAUCGUUU
					GAACAUGGAUCUUAGAGUC
					AGAAUGGAAUGGACUCUUA
					UGGUGUGACUGUUCGAUAA
ACTR3	10096	34452698	NM_005721	L-012077-00	GCAGUAAAGGAGCGCUAUA
					GUGAUUGGCAGCUGUAUUA
					GGAAUUGAGUGGUGGUAGA
					GCCAAAACCUAUUGAUGUA
ADAM10	102	73747882	NM_001110	L-004503-00	CAUCUGACCCUAAACCAAA
					CAAGGGAAGGAAUAUGUAA
					GAACUAUGGGUCUCAUGUA
					CGAGAGAGUUAUCAAAUGG
AMPH	273	21536422	NM_139316	L-011569-00	GAACUUCACCCGACGCUUA
					UCACAGAGUCGCUGCAUGA
					GAGGAUAUUUAGCAGCAAU
					GACAAGCACUGAUUUGGUA
AP1B1	162	22027652	NM_145730	L-011200-00	UAGACGAGCUUAUCUGCUA
					CCACUCAGGACUCAGAUAA
					GGAAGGCUGUGCGUGCUAU
					CUAAGGACUUGGACUACUA
AP1M1	8907	18105005	NM_032493	L-013196-00	UAUCACGCUUCGAGAAUGA
					GCCCAAUGAUGCCGACUCA
					CGAGAUCCCUUACUUCACU
					GAAGGCAUCAAGUAUCGGA
AP1M2	10053	14916516	NM_005498	L-012056-00	GGUCUUCAUUGAUGUCAUA
					CCACUGAUCUGGAUUGAGU
					AGAGAAACGUCGUGAUUUG
					CCGAGGGUAUCAAGUAUAA
AP2A1	160	19913415	NM_130787	L-012492-00	CCGAUGAGUUGCUGAAUAA
					GGAGCAAUGCCAAGCAGAU
					CCAAGAAGGUGCAGCAUUC
					GCAAGAAGAACCCAGAUGA
AP2A2	161	71725392	NM_012305	L-012812-00	GAAUUUAGGUCGGAUGUUU
					GCCCAUCACUCUCAACAAA
					CCGAAUUGCUGGUGAUUAC
					GCACUUGGGUGUGGUAACU
AP2B1	163	71773037	NM_001282	L-003627-00	GUACAAUGAUCCCAUCUAU
					UGAAUUAUGUGGUCCAAGA
					GAUGUUGACUUUGUUCGAA
					CAACAAGUAUGAAAGUAUC

Gene Symbol	GENEID	GINumber	Gene Accession	Pool Catalog Number	Sequence
AP2M1	1173	68799813	NM_001025205	L-008170-00	GUUAAGCGGUCCAACAUUU
					GCGAGAGGGUAUCAAGUAU
					AGUUUGAGCUUAUGAGGUA
					GAACCGAAGCUGAACUACA
AP3D1	8943	40018647	NM_003938	L-016014-00	CUACAGGGCUCUGGAUAUU
					GGACGAGGCAAAAUACAUA
					GAAGGACGUUCCCAUGGUA
					CAAAGUCGAUGGCAUUCGG
AP4E1	23431	75812964	NM_007347	L-021474-00	GAGAAUUCAUCUGGAUAUA
					UCGAAUACUUUGCACGAUA
					CAAGUUAGCCCAACAAGGA
					GGUCUAGGAUCAGAAAGUA
ARF1	375	66879658	NM_001658	L-011580-00	UGACAGAGAGCGUGUGAAC
					CGGCCGAGAUCACAGACAA
					ACGAUCCUCUACAAGCUUA
					GAACCAGAAGUGAACGCGA
ARF6	382	6996000	NM_001663	L-004008-00	CGGCAUUACUACACUGGGA
					UCACAUGGUUAACCUCUAA
					GAGCUGCACCGCAUUAUCA
					GAUGAGGGACGCCAUAAUC
ARFIP2	23647	38569401	NM_012402	L-012820-00	GCUAGGAGCCGUGAACUUC
					CAUUGUGUCUGGUGGCUAU
					GCACAAAGCAACUGUUAUC
					GGAGGAAUUUGGCUACAAU
ARPC1B	10095	22907055	NM_005720	L-012082-00	GAGAGUAACCGUAUUGUGA
					UAGACUCGCUGCACAAGAA
					CGUGUGAUCUCCAUCUGUU
					UCGCGACUCUGGCCUCUGA
ARPC2	10109	23238209	NM_005731	L-012081-00	CCAUGUAUGUUGAGUCUAA
					GCUCUAAGGCCUAUAUUCA
					GGACAGAGUCACAGUAGUC
					GUACGGGAGUUUCUUGGUA
ARPC3	10094	23397667	NM_005719	L-005284-00	GAUGAGAGCCUAUUUACAA
					AAAUGUAUACGCUGGGAAU
					GAAUGAAGCUGAUAGGACC
					AUACAGAUAUUGUGGAUGA
ARPC4	10093	68161510	NM_001024960	L-008571-00	GAACUUCUUUAUCCUUCGA
					UAAACCAUCUGGCUGGAUC
					GAAGAGUUCCUUAAGAAUU
					GAGAUGAAGCUGUCAGUCA
ARPC5	10092	23238212	NM_005717	L-012080-00	GCAGGCAGCAUUGUCUUGA
					GUGUGGAUCUCCUAAUGAA
					GAAUAUGACGAGAACAAGU
					GCAGUUCAAUCUCUGGACA
ARRB1	408	58219794	NM_020251	L-011971-00	UGGAUAAGGAGAUCUAUUA
					AUGGAAAGCUCACCGUCUA
					GAACUGCCCUUCACCCUAA
					GAACGAGACGCCAGUAGAU

Gene Symbol	GENEID	GINumber	Gene Accession	Pool Catalog Number	Sequence
ARRB2	409	39812054	NM_199004	L-007292-00	CGAACAAGAUGACCAGGUA
					CGGCGUAGACUUUGAGAUU
					GGGCUUGUCCUUCCGCAAA
					UAGAUCACCUGGACAAAGU
ASAP2	8853	4502248	NM_003887	L-011544-00	GAAAUAAGCGGAGCGGAAA
					GCAAAGCUCAACCUGCUAA
					GAAGGCCUCCAUCGAGAUA
					CUACGGAUCUUCACACGAU
ATG12	9140	38261968	NM_004707	L-010212-00	GAACACCAAGUUUCACUGU
					GCAGUAGAGCGAACACGAA
					GGGAAGGACUUACGGAUGU
					GGGAUGAACCACAAAGAAA
ATM	472	73486662	NM_138292	L-003201-00	GCAAAGCCCUAGUAACAUA
					GGUGUGAUCUUCAGUAUAU
					GAGAGGAGACAGCUUGUUA
					GAUGGGAGGCCUAGGAUUU
ATP6V0A1	535	77539781	NM_005177	L-017618-00	GAACUUACCGAGAGAUAAA
					CGGCCGAUGUUUACUUAUA
					GUUCAGUGGUCGAUACAUU
					CCAGCUCCGUAUACUAUUA
BECN1	8678	19923741	NM_003766	L-010552-00	GAUACCGACUUGUUCCUUA
					GGAACUCACAGCUCCAUUA
					CUAAGGAGCUGCCGUUAUA
					GAGAGGAGCCAUUUAUUGA
BIN1	274	21536416	NM_139351	L-008246-00	GACAUCAAGUCACGCAUUG
					GAACAGCCGCGUAGGUUUC
					ACAACGACCUGCUGUGGAU
					CCAGCAACGUGCAGAAGAA
CAMK1	8536	21536281	NM_003656	L-004940-00	AGAUACAGCUCUAGAUAAG
					GAAGAUAAGAGGACGCAGA
					UGAAAUACCUGCAUGACCU
					GAAUGAUGCCAAACUCUUU
CAV1	857	15451855	NM_001753	L-003467-00	CUAAACACCUCAACGAUGA
					GCAAAUACGUAGACUCGGA
					GCAGUUGUACCAUGCAUUA
					GCAUCAACUUGCAGAAAGA
CAV2	858	38176291	NM_198212	L-010958-00	AGAUUGGGAUACUGUAAUA
					GUAAAGACCUGCCUAAUGG
					GUAGGACGAUGCUUCUCUU
					UAUCAUUGCUCCAUUGUGU
CAV3	859	15451858	NM_001234	L-011229-00	UCAAGGUGGUGCUGCGGAA
					GCCCAGAUCGUCAAGGAUA
					GGACAUAGUCAAGGUGGAU
					UGCCAUGCAUUAAGAGCUA
CBL	867	52426744	NM_005188	L-003003-00	AAUCAACUCUGAACGGAAA
					GACAAUCCCUCACAAUAAA
					UAGCCCACCUUAUAUCUUA
					GGAGACACAUUUCGGAUUA

Gene Symbol	GENEID	GINumber	Gene Accession	Pool Catalog Number	Sequence
CBLB	868	54112419	NM_170662	L-003004-00	GAACAUCACAGGACUAUGA
					GUACUGGUCCGUUAGCAAA
					GGUCGAAUUUUGGGUAUUA
					UAUCAGCAUUUACGACUUA
CBLC	23624	20149595	NM_012116	L-006962-00	CAUUUGAGCUCUGCAAGAU
					GAACAGCAGUGACCAGGAA
					GGCCAACACUCCUCAAGAA
					GCAACAAGGAUGUGAAGAU
CDC42	998	16357471	NM_044472	L-005057-00	CGGAAUAUGUACCGACUGU
					GCAGUCACAGUUAUGAUUG
					GAUGACCCCUCUACUAUUG
					CUGCAGGGCAAGAGGAUUA
CFL1	1072	49472823	NM_005507	L-012707-00	CCUCUAUGAUGCAACCUAU
					CAUGGAAGCAGGACCAGUA
					UAAAUGGAAUGUUGUGGAG
					ACUCUGUGCUUGUCUGUUU
CIB1	10519	9951921	NM_006384	L-012261-00	CGGCUUAGUGCGUCUGAGA
					GAGCGAAUCUGCAGGGUCU
					CCAAAGACAGCCUUAGCUU
					UGAACUGCCUCACGGGAGA
CIB2	10518	44921612	NM_006383	L-012230-00	GGGCUUUGCUGACUUCGAG
					AAGAGCAGCUAGACAACUA
					GCGACAAGGUCAUUGAGGA
					GAACCUCACUUUCAACGAC
CIB3	117286	42718009	NM_054113	L-012901-00	CCCGCGACCUCAAGGCUUA
					UCAUGAGGCUCUUCUAUCG
					GUGAGAAGGUGCUGGAUGA
					CCAGAGGAUUGCCCAGGUA
CLINT1	9685	37537713	NM_014666	L-021406-00	GCUCCUAGCUUACCUCAUA
					CAGCAGCCAUCACUGAAUA
					AUUCAGAGAUCGAGUCUAA
					UGGUAAGGAUCAAGGUAUA
CLTA	1211	4502898	NM_001833	L-004002-00	AGACAGUUAUGCAGCUAUU
					CCAAUUCUCGGAAGCAAGA
					AGUAAUGAAUGGUGAAUAC
					CCAAAGAUGUCUCCCGCAU
CLTB	1212	32483393	NM_001834	L-004003-00	GGAACCAGCGCCAGAGUGA
					CAUCUAAGGUCACGGAACA
					GCACAGAGUGGGAGAAGGU
					GGAAACGGCUGCAAGAGCU
CLTC	1213	41327727	NM_004859	L-004001-01	GAGAAUGGCUGUACGUAAU
					UGAGAAAUGUAAUGCGAAU
					GCAGAAGAAUCAACGUUAU
					CGUAAGAAGGCUCGAGAGU
CLTCL1	8218	4502902	NM_001835	L-011611-00	CCGAGUGGCUUGUCAAUUU
					GCACAUCAUUGAAGUUGGA
					CCAUGAAGAUGUUUGAUAG
					GAAUUAAUCCAGCUAACAU

Gene Symbol	GENEID	GINumber	Gene Accession	Pool Catalog Number	Sequence
COPA	1314	6996002	NM_004371	L-011835-00	ACUCAGAUCUGGUGUAAUA
					GCAAUAUGCUACACUAUGU
					GAACAUUCGUGUCAAGAGU
					GCGGAGUGGUUCCAAGUUU
CYTH3	9265	33946275	NM_004227	L-019268-00	GGGAAUUCAGUUUCUAAUA
					GAACGAGCCAUUUAAGAUC
					GAGAAGGCCUAAAUAAGAC
					AGAGAUCCCUUCUAUGACA
DAB2	1601	4503250	NM_001343	L-008522-00	GAACCAGCCUUCACCCUUU
					CAAAGGAUCUGGGUCAACA
					GAUCUAAACUCUGAAAUCG
					AAACUGAAAUCGGGUGUUG
DIAPH1	1729	31742531	NM_005219	L-010347-00	GAAGUGAACUGAUGCGUUU
					GAAGUUGUCUGUUGAAGAA
					GAUAUGAGAGUGCAACUAA
					GCGAGCAAGUGGAGAAUAU
DNM1	1759	59853098	NM_004408	L-003940-00	GAGAAUCUGUCCUGGUACA
					GAAUAUCCAUGGCAUUAGA
					GCAGUUCGCCGUAGACUUU
					CACAGAAUAUGCCGAGUUC
DNM2	1785	56549124	NM_001005362	L-004007-00	GGCCCUACGUAGCAAACUA
					GAGAUCAGGUGGACACUCU
					CCGAAUCAAUCGCAUCUUC
					GAGCGAAUCGUCACCACUU
DNM3	26052	42544242	NM_015569	L-013931-00	GAAAGCUUGUCCUGGUAUA
					CGGAAAGGAUUGUUGCUAA
					GACCAGGUAUUGCUAUUGA
					GGGAUGAGAUGCUUCGAAU
EEA1	8411	55770887	NM_003566	L-004012-00	GCAGUCAGCUGGAAAGUCA
					GAAGCAACGGUUCAGAAUA
					GUUCAAACACUAAUGGAUA
					GAACCUUGAAGCUUUAUUA
EFS	10278	14589875	NM_032459	L-012094-00	GAGAUGGUGCAGUGUGUAA
					CGUCAGCCUUACUCAAUUU
					GCAAUUCACUACCCUGCUC
					GAUGGAGGAUGACCCAGCA
EPN1	29924	41350200	NM_013333	L-004724-00	ACUAAUCCCUUCCUCCUAU
					GAACGUGCGUGAGAAAGCU
					GAUCAAGGUUCGAGAGGCC
					GGAAGACGCCGGAGUCAUU
EPN2	22905	41327739	NM_148921	L-004725-00	AGACUACGCUGUUGGAUUU
					GAAGAAAGCCGAAGGGACA
					CCUUUGAGCUCUUCAGUAA
					GAACAAUUACUCAGAGGCA
EPN3	55040	8923677	NM_017957	L-021006-00	GUACAAGGCUCUAACAUUG
					GAACCGUCCUGUCCCGAAG
					CUAGUUCGCUCAUGUCCGA
					GGACUUGGCUGACAUCUUC

Gene Symbol	GENEID	GINumber	Gene Accession	Pool Catalog Number	Sequence
EPS15	2060	56682951	NM_001981	L-004005-00	AUAAAGAUAUGGACGGAUU
					UGAAUUAACUAGUCAGGAA
					CAAGUGAGGUUCAGGAUCU
					CUUAAUCAGUCAGAAGUUA
EPS15L1	58513	10864046	NM_021235	L-004006-00	GAAGUUACCUUGAGCAAUC
					CAAUAGUGCUGAAGGCUUU
					GUAAAGGGUUCUUGGACAA
					GCAACAACACGCAAGAGUU
ERC1	23085	38045893	NM_178038	L-010942-00	GCGGACAAUUGAACGCUUA
					UGAAAGAACGGGUCAAAUC
					CAAUAUAGCUCUCUUGGAG
					GCACAAAUGUUAGAGGAGG
EZR	7430	21614498	NM_003379	L-017370-00	GCGCGGAGCUGUCUAGUGA
					GCGCAAGGAGGAUGAAGUU
					GGAAUCAACUAUUUCGAGA
					GCUCAAAGAUAAUGCUAUG
FYN	2534	23510363	NM_153048	L-003140-00	CGGAUUGGCCCGAUUGAUA
					GGACUCAUAUGCAAGAUUG
					GAAGCCCGCUCCUUGACAA
					GGAGAGACAGGUUACAUUC
GIT1	28964	41393572	NM_014030	L-020565-00	GGACGACGCCAUCUAUUCA
					CGAGCUGCUUGUAGUGUAU
					CCGCACACCCAUUGACUAU
					GCUCAGAGAAGAUCCAUUU
GORASP1	64689	29826292	NM_031899	L-013510-00	GAUCUCUACCACAGAAUAA
					GAGGACUUCUUUACGCUCA
					GAACUGACCACCACAGCUG
					CUGGAGGUGUUCAAUAUGA
GRB2	2885	45359858	NM_203506	L-019220-00	UGAAUGAGCUGGUGGAUUA
					AGGCAGAGCUUAAUGGAAA
					CGAAGAAUGUGAUCAGAAC
					GAAAGGAGCUUGCCACGGG
HGS	9146	24496766	NM_004712	L-016835-00	GAGGUAAACGUCCGUAACA
					GCACGUCUUUCCAGAAUUC
					AAAGAACUGUGGCCAGACA
					GAACCCACACGUCGCCUUG
HIP1	3092	38045918	NM_005338	L-005001-00	GCAAAUCACAGAUCGAAGA
					GAGCCUGUCUGAGAUAGAA
					GAACAGCGAUAUAGCAAGC
					GCAGUGAUCCCUUCAAUUU
HIP1R	9026	48762941	NM_003959	L-027079-00	CUGUGGAGAUGUUUGAUUA
					UGGCUGACCUCUUCGAUCA
					UGAAUGCACUGGAGGGUGA
					GCAGGAAUGUUCUCGCACA
IP6K3	117283	78191796	NM_054111	L-006739-00	GGAAUGAGCACACCACCUA
					ACAUGAGCGUGAUGAAGUA
					UCUAUCAGUUCCUACAUAA
					GUUCAUACCGCUUCUAUUC

Gene Symbol	GENEID	GINumber	Gene Accession	Pool Catalog Number	Sequence
ITSN1	6453	47717124	NM_001001132	L-008365-00	GAUAUCAGAUGUCGAUUGA
					GAACGAAAGAUCAUAGAAU
					CGACAAGGCCGGAGUCUUC
					GCACAGAUAUGGGCACUAG
ITSN2	50618	22325382	NM_147152	L-009841-00	GAUCAAACGUGACAAGUUG
					CCAAACAUGUGGGCUAUUA
					CCUCAUGGGUCAUCUUAUA
					GGUGAAUUAUAGAGCAUUA
LIMK1	3984	8051614	NM_016735	L-007730-00	GAGCAUGACCCUCACGAUA
					GAAGCGAGUUGCCCGUGUG
					GCCCAGAUGUGAAGAAUUC
					GGAGACCGGAUCUUGGAAA
MAP1LC3A	84557	31563517	NM_181509	L-013579-00	GGACGGCUUCCUCUAUAUG
					CGGUGAUCAUCGAGCGCUA
					UCGCGGACAUCUACGAGCA
					UGAGCGAGUUGGUCAAGAU
MAP4K2	5871	22035599	NM_004579	L-003587-00	GCGCAAAGGUGGCUACAAU
					GGACAGGGACACAAUCCUA
					GGAAUGACCGCUUGUGGAU
					CGCCCAAACUGAGAGAUAA
MAPK8IP1	9479	20986517	NM_005456	L-003595-00	GAAGACUACUGGUACGAGG
					AGGACACACUGAAUAAUAA
					GAUAUCAUCCAAAGAACAA
					GGGAAUAAAUGUAGCCACU
MAPK8IP2	23542	21237774	NM_139124	L-012462-00	AGUUUGAGAUGAUCGAUGA
					GGACAGCCCUGACCUCACU
					GAAACUGACCGUCCACCUG
					ACCAAGAGCACCUGGCGUA
MAPK8IP3	23162	41350322	NM_033392	L-003596-00	GCAUGGCUGUUGUGUACGA
					CAAGAACUAUGCCGAUCAG
					GCAGAGCGCAGUCACAUCA
					CGAGUGGUCUGAUGUUCAA
NEDD4	4734	38257154	NM_006154	L-007178-00	GGAGGGAACAUACAAAGUA
					GAUCACAAUUCCAGAACGA
					GAACUAGAGCUUCUUAUGU
					CCAAUGAUCUAGGGCCUUU
NEDD4L	23327	21361471	NM_015277	L-007187-00	AAGGGAAUAUAUCGACUUA
					GAAUAUCGCUGGAGACUCU
					GAUCAUAACACAAAGACUA
					GUACAUAUGCGGUCAAAGA
NSF	4905	11079227	NM_006178	L-009401-00	GAAAAUCGCCAAUCAAUUA
					GGAUAGGAAUCAAGAAGUU
					CAAUAGACCAGAUCUGAUA
					UCUCUUGGCUCGACAGAUU
PACSIN1	29993	47834327	NM_020804	L-007735-00	CGAGAAAGGCCCACAGUAU
					CAAGAAGGCCUACCAUUUG
					GAACAGCAGCUACAUCCAU
					UGACAGAGGCAGACAAGGU

Gene Symbol	GENEID	GINumber	Gene Accession	Pool Catalog Number	Sequence
PACSIN3	29763	34147484	NM_016223	L-015343-00	CCAACUACGUGGAGUGUGU
					ACAAUCAGCCGGAAAGAGA
					GGACAUGGAACAGGCCUUU
					AGACAAAAGCUCAGUAUGA
PAK1	5058	42794768	NM_002576	L-003521-00	ACCCAAACAUUGUGAAUUA
					GGAGAAAUUACGAAGCAUA
					UCAAAUAACGGCCUAGACA
					CAUCAAAUAUCACUAAGUC
PDCD6IP	10015	48255927	NM_013374	L-004233-00	CAGAUCUGCUUGACAUUUA
					UCGAGACGCUCCUGAGAUA
					GCGUAUGGCCAGUAUAAUA
					GUACCUCAGUCUAUAUUGA
PI4KA	5297	4505806	NM_002650	L-006776-00	GCUAUGUGCGGGAGUAUAU
					GAUCGAGCGUCUCAUCACA
					GUGGCCAACUGGAGAUCUA
					GGAACGAAGUGACCCGUCU
PICALM	8301	56788367	NM_001008660	L-004004-00	CAACAGGCAUGAUAGGAUA
					GUUCAAAGAUGCCAUUAGA
					GUAAUGGCCUAUCCUGCUA
					CAUUACAACUCAUCAUUUG
PIK3C2G	5288	15451927	NM_004570	L-006773-00	GAACUUUGCUGUCGUGCUU
					GCAAAAGGCUUGAUAGAGA
					ACAACUAGGUCGAUUGAAA
					GAACCCUGCCCUAUGUAUA
PIK3CG	5294	21237724	NM_002649	L-005274-00	GCUGAAGCGUGGUUUAAGA
					CCCGAAAGCUUUAGAGUUC
					GAAUUGCUCUGGCAUUUUA
					GACGUCAGUUCCCAAGUUA
PIP5K1A	8394	4505814	NM_003557	L-004780-00	ACACAGUACUCAGUUGAUA
					GCACAACGAGAGCCCUUAA
					GUGGUUCCCUAUUCUAUGU
					GUAAGACCCUGCAGCGUGA
RAB11A	8766	34485712	NM_004663	L-004726-00	GCAACAAUGUGGUUCCUAU
					CAAGAGCGAUAUCGAGCUA
					GUGCAGUGCUGUCAGAACA
					GAGAUUUACCGCAUUGUUU
RAB11B	9230	4758985	NM_004218	L-004727-00	UAACGUAGAGGAAGCAUUC
					GAGUACGACUACCUAUUCA
					UCGCCAAGCACCUGACCUA
					CAACUUGUCCUUCAUCGAG
RAB11FIP5	26056	24308074	NM_015470	L-004298-00	GUACGUCGGUGGUGGAGAA
					CCUGAGCGCCAGUAUGUUU
					GCGAUGAGGCCAACCAGAU
					GGUACAAGCUGCACUCCAA
RAB1A	5861	41350195	NM_004161	L-008283-00	CAGCAUGAAUCCCGAAUAU
					GUAGAACAGUCUUUCAUGA
					GGAAACCAGUGCUAAGAAU
					UGAGAAGUCCAAUGUUAAA

Gene Symbol	GENEID	GINumber	Gene Accession	Pool Catalog Number	Sequence
RAB29	8934	4506374	NM_003929	L-010556-00	GAGAACGGUUUCACAGGUU
					CAGGACAGCUUCAGCAAAC
					GGACCAGAUUGACCGGUUC
					GCUAGUAGUGUUUGGCUUA
RAB2A	5862	4506364	NM_002865	L-010533-00	GAAGGAGUCUUUGACAUUA
					GCAGGAGCUUUACUAGUUU
					GUGCUCGAAUGAUAACUAU
					GCUUAUUGCUACAGUUUAC
RAB3A	5864	34147654	NM_002866	L-009668-00	GAAGAUGUCCGAGUCGUUG
					UCAAGACCAUCUAUCGCAA
					GUUCAAGAUUCUCAUCAUC
					GAGGCAAGCGCCAAGGACA
RAB3B	5865	19923749	NM_002867	L-008825-00	GGACACAGACCCGUCGAUG
					CUACUCAGAUCAAGACCUA
					CAAAGGAGAACAUCAGUGU
					UUAAACUGCUUAUCAUUGG
RAB3C	115827	34147545	NM_138453	L-008520-00	UGAGCGAGGUCAACAUUUA
					GGAUCGAUUUCAAAGUAAA
					GUACAAGAUUGGUCAACUC
					GCCAUGGGCUUUAUUUUAA
RAB3D	9545	18677727	NM_004283	L-010822-00	GUUCAAACUGCUACUGAUA
					GUACUGUGGGCAUCGAUUU
					UGACAUCGCCAAUCAGGAA
					GGACGAACGUGUUGUGCCU
RAB4A	5867	19923259	NM_004578	L-008539-00	GCUCAGGAGUGUGGUUGUU
					UACAAUGCGCUUACUAAUU
					GAUAAUAAAUGUUGGUGGU
					GAACGAUUCAGGUCCGUGA
RAB4B	53916	82659106	NM_016154	L-008780-00	GCACUAUCCUCAACAAGAU
					AGAAUAAGUUCAAACAGGA
					AAUCAUGUCUCCUUCAUCA
					UCAGUGACGCGGAGUUAUU
RAB5A	5868	31543538	NM_004162	L-004009-00	GCAAGCAAGUCCUAACAUU
					UGACACUACAGUAAAGUUU
					GGAAGAGGAGUAGACCUUA
					AGAGUCCGCUGUUGGCAAA
RAB5B	5869	33943097	NM_002868	L-004010-00	GGAGCGAUAUCACAGCUUA
					GAAAGUCAAGCCUGGUAUU
					CAACAAACGUAUGGUGGAG
					AAGCUGCAAUCGUGGUUUA
RAB5C	5878	41393544	NM_004583	L-004011-00	UCAUUGCACUCGCGGGUAA
					GAACAAGAUCUGUCAAUUU
					GCAAUGAACGUGAACGAAA
					GCUAAGAAGCUUCCCAAGA
RAB6A	5870	38679893	NM_002869	L-008975-00	GUGGAUUGAUGAUGUCAGA
					CCAAAGAGCUGAAUGUUAU
					GAGCAAAGCGUUGGAAAGA
					GAAAGAGGAAGUGAUGUUA

Gene Symbol	GENEID	GINumber	Gene Accession	Pool Catalog Number	Sequence
RAB6B	51560	51036600	NM_016577	L-008548-00	GCUGAUAAGAGGCAGAUAA
					CAACAGACCUCUAAGUGGA
					GAGUUAAGGUUCCAUAAUA
					UCAGGAAAGUUGAGUGUAA
RAB7B	338382	38490536	NM_177403	L-018225-00	GUAGGGCUCUGUCGAGGUA
					GAAACUCAUUAUCGUCGGA
					UCAAUGUGGUGCAAGCGUU
					GGAAGUAGCUCAAGGCUGG
RAB8A	4218	40548385	NM_005370	L-003905-00	CAGGAACGGUUUCGGACGA
					GAAUUAAACUGCAGAUAUG
					GAACAAGUGUGAUGUGAAU
					GAACUGGAUUCGCAACAUU
RAB8B	51762	62865646	NM_016530	L-008744-00	GCAAUUGACUAUGGGAUUA
					GAACAAUCACGACAGCGUA
					GAUCAAAGAAGACCAGUUU
					CGAUAGAACUAGAUGGAAA
RAC1	5879	38505163	NM_006908	L-003560-00	GUGAUUUCAUAGCGAGUUU
					GUAGUUCUCAGAUGCGUAA
					AUGAAAGUGUCACGGGUAA
					GAACUGCUAUUUCCUCUAA
RHOA	387	50593005	NM_001664	L-003860-00	CGACAGCCCUGAUAGUUUA
					GACCAAAGAUGGAGUGAGA
					GCAGAGAUAUGGCAAACAG
					GGAAUGAUGAGCACACAAG
ROCK1	6093	4885582	NM_005406	L-003536-00	CUACAAGUGUUGCUAGUUU
					UAGCAAUCGUAGAUACUUA
					CCAGGAAGGUAUAUGCUAU
					GCCAAUGACUUACUUAGGA
ROCK2	9475	41872582	NM_004850	L-004610-00	GCAACUGGCUCGUUCAAUU
					UAGAAUAUGUGGCCUAGAA
					GAAACUAAUAGGACACUAA
					CAAACUUGGUAAAGAAUUG
SAR1A	56681	21361614	NM_020150	L-016756-00	GAGCAAGCACGUCGCGUUU
					UAUAUUGACUGAUGUUUGG
					GAGGAUGUCUUUAUUCUAA
					GCAUGCAUUUCGUUUAUUA
SEC13	6396	34335133	NM_183352	L-012351-00	CAUGUGAGCUGGUCCAUCA
					GGUCGUGUGUUCAUUUGGA
					CCAUCUCCCUGCUGACUUA
					GUAAUUAACACUGUGGAUA
SH3GLB1	51100	21359904	NM_016009	L-017086-00	AGAAUUGGAUGCUCACUUA
					UCAACAAGUGGCCUAGUAA
					AAACGUCAGCCUUAAAUUU
					UUAAGUAGGUGGACUAUGG
SH3GLB2	56904	24431995	NM_020145	L-015810-00	GCAAAGCUCGGGUGCUCUA
					GACUAGACCUCGUAAUUAC
					GCUCUGGAAUGAUGAAGUG
					CCACGACGGUGCCUGACUU

Gene Symbol	GENEID	GINumber	Gene Accession	Pool Catalog Number	Sequence
SNAP91	9892	7662227	NM_014841	L-032296-00	GCAUAGACCUGUUUAGUAC
					CUACAAUGAUGGUGUUAUU
					GCUAAAGAGUAUGCCAAUA
					GAGCAAGUUGGUAUUGAUA
SNX1	6642	71772739	NM_148955	L-017518-00	GAAAAGAAGUGAUACGGUU
					GGAAAGAGCUAGCGCUGAA
					CAAAGGCCAUCUCCUAAUG
					GAAAGGGACUUCGAGAGGA
SNX2	6643	23111037	NM_003100	L-017520-00	CCACAGAAGUUGUAUUAGA
					GUGCUGCCAUGUUAGGUAA
					AAUGAUGGUUGCUAACAAA
					UGAAUCGGAUGCAUGGUUU
STAU1	6780	82659088	NM_017454	L-011894-00	GCAGGGAGUUUGUGAUGCA
					UAAUAAAGAGGAUGAGUUC
					CGAGUAAAGCCUAGAAUCA
					CGGAUGCAGUCCACCUAUA
SYNJ1	8867	44921605	NM_003895	L-019486-00	GAAGCAAUUUCGCAGCAUA
					GUUCUGAGCCUAAAUGGUA
					AAACAGAACAGGUUGUGUA
					UCUCCAAACCCAUUUAUUA
SYNJ2	8871	52851404	NM_003898	L-012624-00	GGACGUAGCCAUCGACACA
					UCACAAGUUUGGACUAUGA
					GAAUUGAGCGCAGGGAAUA
					ACCCUAAACUGUUGAAUAA
SYT1	6857	5032138	NM_005639	L-020044-00	GCAAUUUACUUUCAAGGUA
					GGGCACAUCUGAUCCUUAC
					GAUCGUUUCUCUAAGCAUG
					GUAAGAGGCUGAAGAAGAA
SYT2	127833	31560862	NM_177402	L-018809-00	GUAAAGGUGCCUAUGAACA
					GAUCGCCAUUGCUGUGGUU
					GAACGAAGCCAUAGGCAAG
					AGACCAAAGUCCAUCGGAA
TNIK	23043	55741806	NM_015028	L-004542-00	GAACAUACGGGCAAGUUUA
					UAAGCGAGCUCAAAGGUUA
					CGACAUACCCAGACUGAUA
					GACCGAAGCUCUUGGUUAC
TSG101	7251	18765712	NM_006292	L-003549-00	CCGUUUAGAUCAAGAAGUA
					CUCCAUACCCAUCCGGAUA
					CCACAACAAGUUCUCAGUA
					CCAAAUACUUCCUACAUGC
VAMP1	6843	40549443	NM_016830	L-012497-00	UAACAUGACCAGUAACAGA
					GGCAGGAGCAUCACAAUUU
					CCAUCAUCGUGGUAGUUAU
					GUGGACAUCAUACGUGUGA
VAMP2	6844	7657674	NM_014232	L-012498-00	GCGCAAAUACUGGUGGAAA
					CAUCAUAGUUUACUUCAGC
					GGGAGUGAUUUGCGCCAUC
					UCAUGAGGGUGAACGUGGA

Gene Symbol	GENEID	GINumber	Gene Accession	Pool Catalog Number	Sequence
VAPA	9218	37588849	NM_194434	L-021382-00	CCUGAGAGAUGAAGGUUUA
					UAGGGAAAUUCAUCUUGUA
					GGAUAAACCUGGAUCAACC
					GGCAAAACCUGAUGAAUUA
VAPB	9217	40806212	NM_004738	L-017795-00	UGUUACAGCCUUUCGAUUA
					CCACGUAGGUACUGUGUGA
					GCUCUUGGCUCUGGUGGUU
					GUAAUUAUUGGGAAGAUUG
VAV2	7410	40549447	NM_003371	L-005199-00	CUGAAAGUCUGCCACGAUA
					UGGCAGCUGUCUUCAUUAA
					GUGGGAGGGUCGUCUGGUA
					GCCGCUGGCUCAUCGAUUG
VCP	7415	7669552	NM_007126	L-008727-00	GCAUGUGGGUGCUGACUUA
					CAAAUUGGCUGGUGAGUCU
					CCUGAUUGCUCGAGCUGUA
					GUAAUCUCUUCGAGGUAUA
VPS36	51028	71051597	NM_016075	L-004701-00	AAACCGAGCUCGAGGAAUG
					CGACUGAUUUGGAGAGAUC
					CAAAGAACAUGGCCAGAUU
					GGGAAUAGCUAACCCAGUU
VPS4A	27183	17865806	NM_013245	L-013092-00	CCACAAACAUCCCAUGGGU
					CCGAGAAGCUGAAGGAUUA
					UCAAAGAGAACCAGAGUGA
					GAAUAACAAUGAUGGGACU
WAS	7454	4507908	NM_000377	L-028294-00	GCCGAGACCUCUAAACUUA
					UGACUGAGUGGCUGAGUUA
					GAAUGGAUUUGACGUGAAC
					GACCUAGCCCAGCUGAUAA
WASF1	8936	68161503	NM_001024936	L-011557-00	AAACAAGACCUCAGACAUA
					CAACUAAGUAGCCUAAGUA
					UAGAUUGGUUGGAGUAAGA
					CCAUCAACCCUACCUGUAA
WASF2	10163	45007036	NM_006990	L-012141-00	GGAUUUGGGUCUCCAGGGA
					CAAGAGAAGCGGGAUGUUG
					GCAAAUGGUUGUAGUAAUU
					GGGCAGAGCUUUCUCAGUU
WASF3	10810	62865897	NM_006646	L-012301-00	CAUCGGACGUUACGGAUUA
					GCUAACAACUUCUACAUCA
					CAGCGAACUUGAAUGUGUA
					GGCUGAAGUUCUAUACUGA
NTC				D-001810-10	UGGUUUACAUGUCGACUAA
					UGGUUUACAUGUUGUGUGA
					UGGUUUACAUGUUUUCUGA
					UGGUUUACAUGUUUUCCUA
FLuc				FLuc 1	GGAAAGACGAUGACGGAAA
				FLuc 2	GCUACAUUCUGGAGACAUA
NLuc				NLuc 1	CAAAUGGGCCAGAUCGAAA
				NLuc 2	CGAACAUGAUCGACUAUUU

(ii) Custom additions to the siRNA library

Gene Symbol	GENEID	GINumber	Gene Accession	Pool Catalog Number	Sequence
ARF4	378	6995998	NM_001660	L-011582-00	AGACAACCAUUCUGUAUAA
					GCUAUGGCCAUCAGUGAAA
					GAACUGGUCUGUAUGAAGG
					GGGCUUCAGUCUCUUCGUA
ARL1	400	33946322	NM_001177	L-019265-01	AUGUAGAGACGGUGACGUA
					CGAAUGAUACCAAACGUUU
					GGGAUAAUUUGAUCGAAUC
					CUGUUUGGAACUCGGGAAA
C1QA	712	7705752	NM_015991	L-013136-00	CCAUAUCGCUGGCCUCUAU
					GCACUGUACCCGGCUACUA
					CGUGGCAUCCCGGGAAUUA
					GAUGGCUGGUGCUCUGUGU
C4A	720	67190747	NM_007293	L-011002-00	GCGCAACCCUGUACGACUA
					UCAAAGGCCACGUCGAGUA
					GAGUACGGCUUCCAGGUUA
					UGUUGAAGGUCCUGAGUUU
CCT2	10576	57165416	NM_006431	L-020107-00	GCACAACAUUAUCCUCAAA
					AAAGUUAGCUGUAGAAGCA
					GAAGUUAAAUUCCGUCAAG
					UGACACAGCUUGCCAAUAG
CCT3	7203	58761483	NM_001008800	L-018339-00	GAGCAGGCCUGUUGGAAAU
					GCCCAUGCCUUGACAGAAA
					GCUGCAGACUUAUAAGACA
					GACAGACAAUAAUCGCAUU
CCT5	22948	58331232	NM_012073	L-012797-00	CAAAUGGGCUUGAUAAGAU
					GAAGCAACAGCAUGUCAUA
					GCGGAGAGACGUUGACUUU
					ACAGAUAUCUCUUGCAACA
CCT6B	10693	58331172	NM_006584	L-020161-00	GCGAGUAGAAGAUGCAUUU
					GAUGAAGCAUAAAUUAGGA
					GGUACUACUUCAAAUGUUC
					GAGUUUGGGAUAAUUAUUG
CCT7	10574	58331184	NM_001009570	L-020115-00	CCAAAGUUGUCUUGUCCAA
					UAGAGAAGAUCCAUCAUUC
					GAGUAGACAUCAACAACGA
					GGACAUUGCUGACAACUUU
CDIPT	10423	22027476	NM_006319	L-009631-01	GUCACAAGAUGAUCGACUU
					GCCAAGAAGAAGUGACGCU
					GGCAUAUAGUAGCUGCUUA
					CACCUUGUGUGCUGGGAAU
CHP1	11261	37622888	NM_007236	L-021437-01	ACGCAUGAUGGUCGGAGUA
					CGUUACUGCGGGACGAAGA
					GGCAAAUGUUAAUGACGGA
					GCACUUUGCUUUUCGACUA

Gene Symbol	GENEID	GINumber	Gene Accession	Pool Catalog Number	Sequence
COG1	9382	82546870	NM_018714	L-013309-01	CCAGGAAAUUAAUCGGGUU
					UGAAGGGUCUCGCGGGAAU
					AACCAGAAACAUCGAAACA
					CUGUAUGGUUCAAGUAGUA
COMMD4	54939	88703049	NM_017828	L-016966-02	GGGCUGAGGAGAAGGGUGU
					UGAAUAGGUUGGCAGGUGU
					AGGACCUUUCCCAGCAUUA
					AAAGGCAAUUGUUGGCUGU
COPB2	9276	4758031	NM_004766	L-019847-00	GGACACACCCAUUAUGUUA
					GCAGAUGACCGUCUUGUUA
					GAUAUUGACACAACAGAUA
					GAUAUGGGCAGUUGUGAAA
COPG1	22820	35250828	NM_016128	L-019138-00	GCACAAACACACUCAAUGA
					UGUCAGAAAUCUCGGAUGA
					GCAAACACGCCGUCCUUAU
					UGAGUGCUCUGGCGAAGUU
DDOST	1650	34147559	NM_005216	L-015786-01	CGGGAGACUCAUUCGCUUU
					GGGCAGUGAGUGCGGGAUU
					ACACGCAGUAUGAGCGCUU
					UCAAGUUGCCCGACGUGUA
EI24	9538	55956767	NM_001007277	L-019879-00	GCCAUUUGGUUUCAGGAUA
					CCACGUAUUGUUAGUAGAA
					GGUAACAGCCCGAAUUAUC
					GUUAGUCUCCUGCAUAUGU
ERLEC1	27248	20070263	NM_015701	L-010658-00	GAAUACUGCUAGAGCUUAU
					CCUCACUCCUGUCAAUAUA
					CGAAGUAUGUCAUGGAAAA
					GGUUGAAUCUCCAGUGAUC
GBF1	8729	4758415	NM_004193	L-019783-00	GAUGAGGGCUUCCACAUUG
					CAACACACCUACUAUCUCU
					GAGAAGCUAGCAAUACUGA
					CCACUGCUGUCACUCUCUA
GRM4	2914	4504140	NM_000841	L-005619-00	GCACCAACCGUGAGCGAAU
					GCGCAUGGACCCUGUAGAU
					CAACAGCCGCUACGACUUC
					CACCAACCAUGCAAUCUAG
HERPUD1	9709	58530858	NM_001010990	L-020918-00	CGACAGUACUACAUGCAAU
					GGGCCACCGUUGUUAUGUA
					GGCUUCAGCUUUCCUGGUU
					GCGGAUGAAUGCACAAGGU
LPCAT1	79888	33946290	NM_024830	L-010289-00	GAUCAGACACAUUUCGAAA
					GAACUCUGAUCCAGUAUAU
					GGAGGAAGGUUGUGGACUU
					CCACAGGUUUGCAGAAAUG
MAGT1	84061	141801933	NM_032121	L-018190-02	GCACGAGACUUGCUUAAUA
					UAUAGUAGCCUCAGAAGAA
					ACAGAUUGACCACGGGAAU
					GUUCCGUCGCCUUGUGAAA
PDIA3	2923	67083697	NM_005313	L-003674-00	GGAAUAGUCCCAUUAGCAA
					GGGCAAGGACUUACUUAUU
					AGACCCAAAUAUCGUCAUA
					GAGGAGUUCUCGCGUGAUG

Gene Symbol	GENEID	GINumber	Gene Accession	Pool Catalog Number	Sequence
QSOX2	169714	55770903	NM_181701	L-018803-01	CUGCAGAACCACACGGAAG
					GGUCGCAUGGAUUGAUUAA
					CGAUCUGAGUUGAGGGGUU
					GACCUGAUCCCGUAUGAAA
RAB10	10890	33695094	NM_016131	L-010823-00	GCAAGGGAGCAUGGUAUUA
					CACGUUAGCUGAAGAUAUC
					GAUGAUGCCUUCAAUACUA
					GAAUAGACUUCAAGAUCAA
RPN1	6184	62739176	NM_002950	L-018903-01	CGACAGAGUGAGCGAAAUG
					GAAUAGGCCUUUACCGUCA
					UGAUCAAUGAGGACGUGAA
					CAAUUUGGAAGUACGUGAA
RPN2	6185	35493915	NM_002951	L-011765-01	CUGCUGUGCUCUCGCAUAA
					UGGAAACAACAGCGUUAUU
					CAUGACGUGGAGAGACUAA
					CCGUAGAGCUCAGAGUCAA
SCAMP3	10067	16445420	NM_052837	L-013442-00	GAAGGGCAACACAGCAGUA
					GAGUGACAGUUCAUUCAAU
					CACAGAACCUAAGAACUAU
					GCAGAGGAGUUGGACCGAA
SCFD1	23256	33469977	NM_182835	L-010943-01	AAGCAUUGGUGCACGAUGU
					GACAAGAAACUUCGAGAAA
					GUGCCAGGAUCUUCGAAAU
					GAUAUCACAGACACGGAAA
SEC22B	9554	34335289	NM_004892	L-011963-00	AAUAGUGUAUGUCCGAUUC
					GCUAAGCAACUCUUUCGAA
					CCUAGAAGAUUUGCACUCA
					GAAGCACUCUCAGCAUUGG
SLC35A2	7355	5032210	NM_005660	L-007538-01	CAGAAGAGGGGUAACGUGA
					AGAAUAACCUCCAGUAUGU
					CGGAAGUGCUCAAAGGUCU
					UAGCUGUGCUGGUGGUCCA
SLC35B2	347734	194018407	NM_178148	L-007543-02	GGUGAGCGCUUUACGGACU
					AGCUAUGGUUCUUCCGAUU
					GAAAAGCACAAGCGGUGUA
					GGGCACCCAUGUACCGGUA
STT3A	3703	34303951	NM_152713	L-017073-01	GCUGUAAUGGUGCGUCUAA
					UAUUAUUGGCUUCGUCAUA
					GCUUUGACCGUGUCCGAAA
					GGAUAUAUCUCCCGAUCUG
STT3B	201595	30578409	NM_178862	L-017859-01	GAGCAUCAACCUACGACUU
					GAUCACAAACCUCGAGUCA
					AGAUGAACAUGCACGAGUA
					ACAUAGCACUGGUGGGAAA
SURF4	6836	19593984	NM_033161	L-010622-01	CCACAAGGGUAGUCGAACA
					CGAAUAUUGGUAAGAUCGA
					GCUCCCUGUUAGUGCCGUA
					ACGUAUAUUUCAACGCCUU
TMEM165	55858	32189370	NM_018475	L-018846-01	GACCUUAGCCACCGGAACA
					GGGAGAUGUUGAAACGGGU
					CGGGAAGGCUUAAAGAUGA
					GCUCCAGUUCAUACCAAUA

(iii) Customised membrane-trafficking siRNA Screen Method

Formal methods

A siRNA library was prepared at 1μM in 1x siRNA buffer (Dharmacon cat# B-002000-UB-100) in 96-well plates (Eppendorf cat# 951040188). The library comprised a commercially available library targeting membrane trafficking proteins (Human ON-TARGETplus siRNA Library- Membrane trafficking – SMARTpool, Dharmacon cat# G-105500) and 37 additional siRNA SMARTpools (Dharmacon). Columns 1 and 12 of each library plate contained 2 wells of each control siRNA SMARTpool targeting RACK1, Firefly luciferase, Nanoluciferase, as well as a non-targeting control (total 4 data points/control/plate). The library was stored at -80C.

Huh7.5 cells were seeded into T75 flasks at $1.56x10^6$ cells per flask (20mL media). The following day, cells were transfected with DENV-NS1-NLuc RNA using DMRIE-C (8mL OptiMem with 47μL DMRIE-C and 39.6μg RNA, per flask) for 3 hours before transfection reagent was replaced with media. Two days after DENV-NS1-NLuc transfection, cells were reverse transfected with siRNA SMARTpool at a final concentration of 40nM in 96-well plates (Corning Costar cat #3596). Briefly, 4μL of 1μM each siRNA SMARTpool was incubated with 15.7μL OptiMem and 0.3μL Dharmafect4 for 20 minutes. DENV-NS1-NLuc transfected cells were then added at $1.25x10^4$cells/well/80μL). After 3 hours incubation at 37C, 5%CO_2, the supernatant was replaced with 100μL per well of media. For each experiment, each siRNA SMARTpool was transfected in triplicate. There were 3 independent experimental replicates for a total of 9 data points* per siRNA SMARTpool. Two days after siRNA SMARTpool reverse-transfection, supernatants were collected and centrifuged at 500g, 15C for 5 minutes. 25μL of clarified supernatant was combined with 25μL of 2x passive lysis buffer (Promega cat #E1941) and frozen at -20C. The remaining supernatant was stored at -80C. Cells were washed with 100μL of PBS, before being lysed with 50μL of 1x passive lysis buffer and stored at -20C.

Samples were assayed using the Nano-Glo Dual-luciferase reporter (NanoDLR) assay (Promega, cat# N1620). The day before each assay batch sample plates and Nano-Glo Dual-luciferase reporter assay (Promega) reagents were placed at 4C. The following day, 10μL of cell lysate or lysed-supernatant was transferred to a white 96-well plate (Perkin Elmer cat # 6005290) using a Janus liquid handler (Perkin Elmer). Immediately following transfer, 50μL per well of OneGlo reagent was dispensed and mixed (15 seconds shaking) using a BioTek 406 dispenser (BioTek). Plates were incubated at room temperature for 45 minutes before luminescence was read on an Ensight plate reader (0.1mm above plate, 0.1 second read, Perkin Elmer). Following plate reading, 50μL per well of NanoDLR Stop&Glo was added and the plate shaken. The plate was incubated for 45 minutes at room temperature before luminescence was read again using the same settings as the first read.

*due to automation error in the first round of NanoDLR assays, there is no assay data for lysates or supernatants corresponding to library plate 3. See the associated plate maps excel file for a list of these siRNA. Only the assay step failed and we could go back and assay the stored lysates and supernatants but we decided it was not worth it. Therefore there are only 6 data points for these siRNA, from assays on samples from experiments 2 and 3.

(iv) Customised membrane-trafficking siRNA Screen Data Analysis Method

Data structure and compilation

The luminescence readings after 45 min of incubation with the respective luciferase substrates were used to measure the enzymatic activity of NLuc and FLuc which is directly related to the relative quantities of both enzymes present in the samples. As described in the Materials and Methods, samples consisted of Passive Lysis Buffer (Promega)-inactivated supernatants and cell lysates collected after DENV transfection and siRNA mediated gene knockdown. Accordingly, every test siRNA- or control siRNA-transfected well generated 2 samples corresponding to lysates and supernatants and both NLuc and FLuc activities were measured in each sample, thus generating 4 data points per well (treatment). Accordingly, each plate generates one file containing the data of all wells within the plate for each luciferase reading. The table below summarises the luciferase readings and the variables names assigned to them:

Enzyme	Sample	Variable name
Firefly luciferase	Lysate	FLuc_Lys
Firefly luciferase	Culture supernatant	FLuc_Sup
NanoLuc luciferase	Lysate	NLuc_Lys
NanoLuc luciferase	Culture supernatant	FLuc_Sup

The data for all plates (all replicates) were exported as individual files (4 per each plate) from the Ensight multimode plate reader (Revvity) in a csv format. All data files were then compiled into one single database containing all readings from all plates using a Python script. During compilation the script also generated identifiers for all data points as for treatment (test siRNAs and controls), source sample, luciferase type, replicate number (within the plate) and experimental replicate number (plate replicate). This annotated database was then imported into Spotfire (TIBCO Spotfire Desktop 10.8.0) for further data processing and analysis.

The correctness of identifier assignment to data points was confirmed by crosschecking with the plate's layouts according to the experimental design using cross-tables, heatmaps and scatter plot visualisations in Spotfire.

Data exploration and Quality Control:

The data was assessed for quality using general statistics for central tendency and variability on controls (non-targeting siRNA control, NT_siRNA) such as mean, standard deviation and

coefficient of variation (%CV) on a per plate basis (4 NT_siRNA treated wells per plate). No significant differences were observed for control values across all plates, with the %CV remaining below 8%. Similarly, the %CV for all controls for each replica was below 10%.
A general exploration of the data was also carried out for the FLuc_Lys values on a per plate basis to assess variability and identify outliers. Outliers were identified using the inter-quartile range and upper and lower inner fences as boundaries and the corresponding data set (well) was removed from the analysis. After outlier removal, the %CV for FLuc_Lys values across all replicas remained below 15%.

FLuc activity in the lysates was not only used to assess consistency and variability but also for data normalization under the assumption that the knockdown of selected gene by siRNA transfection should not affect the FLuc expression. This was confirmed by comparing the average values of FLuc_Lys readings for every gene to the average values of the non-targeting siRNA control of the corresponding plate. Only siRNA pool targeting the gene RHOA consistently reduced the levels of NLuc_Lys, so this gene was removed from the analysis.
Because FLuc secretion to the culture media was not expected but also not relevant for the purposes of the screen, the readings corresponding to FLuc activity in the supernatants were not considered in the data analysis although they were measured and rendered almost undetectable levels, as expected.

Data Normalisation:

For calculation and data normalisation, all wells were considered as independent treatments and the replicates were only averaged after normalisation.
The NLuc relative levels (RL) in lysates and supernatants were calculated as ratios of Fluc_Lys values in order to normalise for variations of the cell densities. In this case:

$$RL\_NLuc\_Lys = \frac{NLuc\_Lys}{FLuc\_Lys} \qquad RL\_NLuc\_Sup = \frac{NLuc\_Sup}{FLuc\_Lys}$$

The NLuc secretion ratio (SR) to the media was also calculated as a ration of supernatant to lysates readings:

$$SR\_Nluc = \frac{NLuc\_Sup}{NLuc\_Lys}$$

Following this, NLuc RL and SR values were normalised as percentages of average values of the NT_siRNA controls of corresponding plates.

$$Normal\_NLuc\_Lys = \frac{RL\_NLuc\_Lys\ (well)}{Mean\ RL\_NLuc\_Lys\ (NT\_siRNA)} * 100$$

$$Normal\_NLuc\_Sup = \frac{RL\_NLuc\_Sup\ (well)}{Mean\ RL\_NLuc\_Sup\ (NT\_siRNA)} * 100$$

$$Normal\_SR\_NLuc = \frac{SR\_NLuc\ (well)}{Mean\ SR\_NLuc\ (NT\_siRNA)} * 100$$

Normalised values were then used for further calculations and identification of hits.

Identification of hits:

Several factors must be considered for identifying genes (hits) involved in NS1 secretion, when measuring the secretion levels after transient siRNA-mediated mRNA knockdown. For hits identification, four effects were considered as possible for any test siRNA and thus contributing to the overall effect on NLuc secretion as a measure of NS1 protein expression and release:

1. Cell toxicity, indirectly measured as a significant decrease of FLuc activity: **FLuc knockdown**.
2. Inhibition of NLuc activity in lysates, measured as a significant decrease of *Normal_NLuc_Lys* values: **NLuc_Lys knockdown.**
3. Inhibition of NLuc activity in supernatants, measured as a significant decrease of *Normal_NLuc_Sup* values: **NLuc_Sup knockdown.**
4. Inhibition of NLuc secretion, measured as a significant decrease of *Normal_SR-NLuc* values: **Secretion knockdown.**

For determining the knockdown effects, thresholds were calculated for all possible effects individually and Boolean values (TRUE or FALSE) were assigned to every test siRNA using conditional functions to test if the values fell over the respective threshold.

All thresholds (one for each possible effect) were calculated based on the central tendency and variation of the normalised values of NT_siRNA controls. For this, control values from all replicates were averaged and the mean and standard deviation values were used for threshold calculation. The threshold for FLuc knockdown, NLuc_Sup knockdown and NLuc_Lys knockdown was set at one standard deviations below the mean value while for Secretion knockdown, a threshold of two standard deviations from the mean was used.

To assist with hits identification a scoring system was developed, assigning numerical values (scores) to each knockdown effect according to the significance (relevancy) for the experimental model. The score values were selected in a way that the rank resulting from the addition of all scores (total scores) would generate a unique value for all possible combinations of effects. Scores were assigned to treatments based on the Boolean values after conditional comparison with respective thresholds.The scores for each effect are shown in the tables below:

Treatment scoring system according to the detected effects

Effect	**Parameter**	**Criteria**	**Threshold** (calculated from NT_siRNA control)	**Score**	
				TRUE	**FALSE**
Secretion knockdown	Normal_SR_NLuc	<	Mean SR_NLuc - 2SD	8	0
NO FLuc knockdown	FLuc	>	Mean FLuc - 1SD	4	0
NLucLys knockdown	Normal_NLuc_Lys	<	Mean Normal_NLuc_Lys - 1SD	2	0
NLucSup knockdown	Normal_NLuc_Sup	<	Mean Normal_NLuc_Sup - 1SD	1	0

Treatment classification based on the total scores

Treatment Classification	**Total Score**	**Effects**			
		Secretion knockdown	*NO FLuc knockdown*	*NLuc_Lys knockdown*	*NLuc_Sup knockdown*
HIT	≥ 12	T	T	T/F	T/F
Potential HIT	5 - 11	F	T	T	T/F
No Effect	< 5	F	T	F	F

T: True, F: False, T/F: either True or False

Based on the total score, each gene (siRNA pool) was classified into Hit, Potential Hit or No Effect.

- Hit: total score ≥ 12, suggesting that the gene knockdown resulted in no effect on FLuc levels but knocked down the secretion of NLuc.
- Potential Hits: total score 5 - 11, suggesting that the gene knockdown did not affect the FLuc expression, knocked down the NLuc expression but had no effect on the secretion.
- No effect: total score < 5, suggesting no effect at all in any of the enzyme's levels or a significant decrease of FLuc basal expression levels that could be considered as a toxic effect reducing cell viability.

Treatment	Total Score	FLucLys	%CV FLucLys	NLucLys	%CV NLucLys	NLucSup	%CV NLucSup	NLuc Secretion	%CV NLuc Secretion	Knockdown FLuc?	Knockdown NLucLys?	Knockdown NLucSup?	Knockdown Secretion?	POTENTIAL HITS
COPA	13	115.51	10.01	100.74	12.01	70.75	4.99	67.97	13.29	NO	NO	YES	YES	YES
COPB2	13	117.96	12.09	113.56	11.21	77.35	5.85	65.37	6.71	NO	NO	YES	YES	YES
COPG1	12	112.39	12.01	117.2	11.41	79.4	5.58	64.99	8.83	NO	NO	NO	YES	YES
Nluc_siRNA2	7	94.72	11.25	44.35	25.4	39.19	8.51	88.35	12.39	NO	YES	YES	NO	YES
RACK1_siRN	7	118.56	11.65	68.75	27.7	70.35	7.65	102.26	16.43	NO	YES	YES	NO	YES
VCP	7	117.54	8.88	73.21	12.8	64.32	7.65	84	11.45	NO	YES	YES	NO	YES
DNM1	5	112.3	6.13	90.76	20.36	76.91	6.1	80.97	7.09	NO	NO	YES	NO	YES
EEA1	5	120.07	12.29	83.67	12.53	72.92	7.66	84.14	13.48	NO	NO	YES	NO	YES
GRM4	5	100.78	14.19	85.23	37.51	70.65	9.13	82.51	7.01	NO	NO	YES	NO	YES
VAV2	5	113.56	8.94	93.3	30.52	75.83	8.38	77.96	8.73	NO	NO	YES	NO	YES
ACTR2	4	116.85	8.26	107.8	29.32	91.32	5.54	82.69	10.26	NO	NO	NO	NO	NO
ACTR3	4	130.04	8.38	100.79	23.6	91.19	3.46	88.53	10.65	NO	NO	NO	NO	NO
ADAM10	4	91.26	11.2	119	17.38	104.14	6.79	83.91	6.52	NO	NO	NO	NO	NO
AMPH	4	97.32	10.12	87.54	22.56	81.88	6.07	89.92	8.52	NO	NO	NO	NO	NO
AP1B1	4	86.95	11.33	93.81	30.74	88.82	5.77	89.98	7.79	NO	NO	NO	NO	NO
AP1M1	4	103.67	5.17	83.21	23.25	86.6	5.64	101.4	10.73	NO	NO	NO	NO	NO
AP1M2	4	98.54	6.32	139.66	22.75	122.72	6.94	85.51	9.84	NO	NO	NO	NO	NO
AP2A1	4	81.69	9.3	109.54	28.14	94.5	6.18	82.89	7.54	NO	NO	NO	NO	NO
AP2A2	4	92.65	11.12	95.87	29.39	87.38	7.26	86.98	8.11	NO	NO	NO	NO	NO
AP2B1	4	96.57	10.63	82.04	30.58	78.52	4.53	91.23	7.52	NO	NO	NO	NO	NO
AP2M1	4	82.73	7	118.28	26.76	94.16	3.34	76.33	8.48	NO	NO	NO	NO	NO
AP3D1	4	91.36	10.97	116.67	25.9	120.71	4.14	100.12	5.38	NO	NO	NO	NO	NO
AP4E1	4	94.96	8.29	131.47	23.07	105.62	7.1	77.21	9.98	NO	NO	NO	NO	NO
ARF1	4	85.38	10.32	100.68	18.59	89.85	6.96	85.61	8.03	NO	NO	NO	NO	NO
ARF4	4	96.51	6.86	125.32	21.09	121.41	7.16	94.71	11.58	NO	NO	NO	NO	NO
ARF6	4	88.77	8.12	101.76	19.35	99.49	6.31	94.63	10.88	NO	NO	NO	NO	NO
ARFIP2	4	98.92	3.95	130.41	24.75	111.4	3.36	83.7	12.75	NO	NO	NO	NO	NO
ARL1	4	95.4	22.52	100.1	22.99	99.81	21.01	97.06	11.47	NO	NO	NO	NO	NO
ARPC1B	4	117.08	8.03	123.65	22.96	104.43	5.1	81.9	12.18	NO	NO	NO	NO	NO
ARPC2	4	109.87	5.68	98.5	20.01	83.85	6.71	82.39	11.19	NO	NO	NO	NO	NO
ARPC3	4	106.77	7.1	134.17	19.93	116.6	4.41	83.69	10.78	NO	NO	NO	NO	NO
ARPC4	4	120.81	9.8	120.76	19.76	107.22	5.95	85.3	10.72	NO	NO	NO	NO	NO
ARPC5	4	99.87	12	148.39	29.06	130.56	10.31	84.52	10.15	NO	NO	NO	NO	NO
ARRB1	4	113.93	11.72	98.45	16.8	82.1	5.84	80.68	8.66	NO	NO	NO	NO	NO
ARRB2	4	107.28	9.29	112.05	15.47	93.72	6.08	80.44	6.81	NO	NO	NO	NO	NO
ASAP2	4	96.25	4.64	94.81	18.22	89.15	4.25	89.98	6.35	NO	NO	NO	NO	NO
ATG12	4	89.28	6.4	103.09	16.29	104.26	5.54	97.37	7.65	NO	NO	NO	NO	NO
ATM	4	96.36	7.16	122.08	19.12	102.77	7.03	80.76	8.46	NO	NO	NO	NO	NO
ATP6V0A1	4	103.73	5.92	116.35	15.09	96.07	6.49	79.27	6.92	NO	NO	NO	NO	NO
BECN1	4	100.05	4.1	98.78	12.11	88.88	5.98	86.02	9.4	NO	NO	NO	NO	NO
BIN1	4	95.16	7.22	92.5	20.77	88.87	2.45	92.55	7.68	NO	NO	NO	NO	NO
C1QA	4	98.28	10.12	91.22	29.53	86.23	7.29	92.35	5.91	NO	NO	NO	NO	NO
C4A	4	108.6	9.56	111.69	23.2	96.54	4.82	86.26	9.87	NO	NO	NO	NO	NO
CAMK1	4	106.95	8.62	83.21	20.53	78.71	5.54	91.26	10.41	NO	NO	NO	NO	NO
CAV1	4	100.64	6.14	123.08	13	108.79	4.87	84.6	6.03	NO	NO	NO	NO	NO
CAV2	4	92.79	6.35	130.41	14.19	110.1	6.88	80.92	8.74	NO	NO	NO	NO	NO
CAV3	4	107.67	7.26	129.75	11.67	107.77	8.32	79.47	9.38	NO	NO	NO	NO	NO
CBL	4	101.8	3.53	134.39	15.19	111.36	5.06	79.81	10.31	NO	NO	NO	NO	NO
CBLB	4	91.78	4.76	149.51	24.16	133.34	2.79	86.4	8.17	NO	NO	NO	NO	NO
CBLC	4	104.25	7.87	113.04	23.23	99.31	5.15	84.43	15.09	NO	NO	NO	NO	NO
CCT2	4	89.76	8.05	139.7	24.77	125.18	5.16	88.38	6.92	NO	NO	NO	NO	NO
CCT3	4	96.98	8.31	111.4	25.1	96.83	7.24	86.24	9.14	NO	NO	NO	NO	NO
CCT5	4	111.31	7.95	113.25	18.32	97.94	8.22	85.42	4.35	NO	NO	NO	NO	NO
CCT6B	4	91.92	7.17	122.16	17.48	102.27	6.07	83.69	8.7	NO	NO	NO	NO	NO
CCT7	4	96.54	7.33	128.22	20.45	110.37	8.01	85.64	9.47	NO	NO	NO	NO	NO
CDC42	4	89.76	4.69	150.98	12.35	134.09	3.7	85.39	5.2	NO	NO	NO	NO	NO
CDIPT	4	94.87	4.77	139.59	19.14	120.27	5.56	83.95	12.85	NO	NO	NO	NO	NO
CFL1	4	108	6.58	103.03	15.47	82.17	6.08	76.7	10.96	NO	NO	NO	NO	NO
CHP1	4	101.73	4.96	107.88	23.36	107.23	8.15	96.8	9.47	NO	NO	NO	NO	NO
CIB1	4	97.1	4.49	127.48	18.36	108.16	6.15	80.88	11.27	NO	NO	NO	NO	NO
CIB2	4	87.65	6.73	131.29	24.69	119.84	7.52	85.71	8.3	NO	NO	NO	NO	NO
CIB3	4	112.83	5.4	117.81	19.46	105.26	3.79	85.97	13.1	NO	NO	NO	NO	NO
CLINT1	4	103.41	12.53	135.97	23.99	113.3	5.66	79.98	9.96	NO	NO	NO	NO	NO
CLTA	4	95.12	6.01	123.12	20.67	99.88	6.13	78.01	10.85	NO	NO	NO	NO	NO
CLTB	4	99.47	3.91	95.85	17.53	81.51	5.13	81.3	8.63	NO	NO	NO	NO	NO
CLTC	4	109	4.58	93.67	17.58	78.57	4.98	80.54	8.64	NO	NO	NO	NO	NO
CLTCL1	4	92.5	5.88	125.82	18.08	105.8	7.67	81.18	7.3	NO	NO	NO	NO	NO
COG1	4	116.73	6.65	103.09	23.6	94.66	7.21	91.27	8.35	NO	NO	NO	NO	NO
COMMD4	4	95.07	7.61	112.99	28.51	97.17	8.14	84.98	7.89	NO	NO	NO	NO	NO
CYTH3	4	85.95	7.74	121.98	22.63	120.43	5.24	95.74	9.06	NO	NO	NO	NO	NO
DAB2	4	89.81	7.65	114.8	22.97	98.66	6.61	81.56	11.46	NO	NO	NO	NO	NO
DDOST	4	118.42	11.52	87.32	32.01	87.88	5.66	100.06	13.32	NO	NO	NO	NO	NO
DIAPH1	4	102.95	4.57	112.34	21.74	93.94	4.99	79.89	8.13	NO	NO	NO	NO	NO
DNM2	4	101.16	5.54	137.96	24.85	117.13	9.28	82.08	10.86	NO	NO	NO	NO	NO
DNM3	4	99.61	7.27	125.65	18.38	112.67	5.91	85.36	14.43	NO	NO	NO	NO	NO
EFS	4	97.65	5.67	125.47	12.75	108.66	6.51	82.57	12.9	NO	NO	NO	NO	NO
EI24	4	99.53	13.67	102.81	37.28	96.12	14.49	92.97	7.19	NO	NO	NO	NO	NO
EPN1	4	96.77	6.37	120.38	21.24	100.45	4.44	80.23	10.96	NO	NO	NO	NO	NO
EPN2	4	117.2	5.48	118.25	22.47	106.03	4.44	87.12	7.03	NO	NO	NO	NO	NO
EPN3	4	95.75	5.94	146.54	19.23	128.48	4.64	84.66	12.38	NO	NO	NO	NO	NO
EPS15	4	100.74	8.68	108.92	18.25	86.45	7.81	75.05	9.65	NO	NO	NO	NO	NO
EPS15L1	4	98.53	4.54	119.48	14.31	103.35	4.84	83.53	10.29	NO	NO	NO	NO	NO
ERC1	4	108.61	4.54	135.21	30.44	109.2	4.37	79.91	15.4	NO	NO	NO	NO	NO
ERLEC1	4	95.56	6.59	106.12	25.22	106.61	5.71	99.29	7.04	NO	NO	NO	NO	NO
EZR	4	98.57	6.14	106.9	20.92	91.91	6.44	82.26	10.4	NO	NO	NO	NO	NO
FYN	4	99.48	8.04	97.42	11.19	79.83	4.72	77.72	11.58	NO	NO	NO	NO	NO
GBF1	4	90.08	7.01	111.23	14.21	87.89	8.2	75.39	10.6	NO	NO	NO	NO	NO
GIT1	4	92.5	6.31	140.82	18.52	119.08	2.49	81.62	10.04	NO	NO	NO	NO	NO
GORASP1	4	115.79	8.72	92.19	23.19	82.89	5.75	86.2	8.27	NO	NO	NO	NO	NO
GRB2	4	104.31	7.91	100.66	22.32	83.19	6.8	79.63	8.63	NO	NO	NO	NO	NO
HERPUD1	4	105.8	8.76	75.19	24.83	77.65	3.45	103.14	7.24	NO	NO	NO	NO	NO
HGS	4	104.62	10.41	90.47	31.96	92.22	7.62	99.16	11.42	NO	NO	NO	NO	NO
HIP1	4	98.69	8.63	112.08	25.75	89.68	8.54	76.34	9.07	NO	NO	NO	NO	NO
HIP1R	4	88.13	8.44	108.4	18.7	100.11	4.04	89.32	9.13	NO	NO	NO	NO	NO
IP6K3	4	100.55	3.88	152.23	14.41	135.23	4.46	85.22	12.19	NO	NO	NO	NO	NO
ITSN1	4	98.51	4.71	103.08	11.79	89.63	4.39	83.53	8.06	NO	NO	NO	NO	NO
ITSN2	4	84.42	7.22	135.51	17.45	119.2	6.95	84.37	9.89	NO	NO	NO	NO	NO
LIMK1	4	103.87	7.56	122.75	24.01	98.99	5.63	77.19	9.43	NO	NO	NO	NO	NO
LPCAT1	4	108.52	7.64	120.95	21.55	98.51	4.47	78.58	6.92	NO	NO	NO	NO	NO

Treatment	Total Score	FLucLys	%CV FLucLys	NLucLys	%CV NLucLys	NLucSup	%CV NLucSup	NLuc Secretion	%CV NLuc Secretion	Knockdown FLuc?	Knockdown NLucLys?	Knockdown NLucSup?	Knockdown Secretion?	POTENTIAL HITS
MAGT1	4	102.41	7.11	92.94	29.47	87.35	8.88	93.61	7.68	NO	NO	NO	NO	NO
MAP1LC3A	4	109	6.74	111.05	16.11	96.62	6.97	84.32	10.21	NO	NO	NO	NO	NO
MAP4K2	4	101.9	6.21	117.06	11.63	96.63	6.27	78.8	7.26	NO	NO	NO	NO	NO
MAPK8IP1	4	103.36	8.23	98.1	30.59	102.21	3.32	102.8	12.36	NO	NO	NO	NO	NO
MAPK8IP2	4	120.79	12.64	105.24	30.36	85.08	6.53	77.23	7.76	NO	NO	NO	NO	NO
MAPK8IP3	4	112.48	12.35	118.43	22.61	91.97	4.26	75.3	7.45	NO	NO	NO	NO	NO
NEDD4	4	97.9	6.45	117.56	17.34	95.77	5.76	77.62	9.23	NO	NO	NO	NO	NO
NEDD4L	4	100.19	9.56	130.46	22.2	99.98	3.67	74.09	8.06	NO	NO	NO	NO	NO
NSF	4	99.57	5.9	114.71	23.21	98.47	6.45	82.41	9.13	NO	NO	NO	NO	NO
NT_siRNA	4	100	10.3	100	25.54	100	7.05	100	14.84	NO	NO	NO	NO	NO
PACSIN1	4	102.49	6.46	105.2	22.43	94.87	6.23	85.99	6.06	NO	NO	NO	NO	NO
PACSIN3	4	98.59	6.85	116.16	26.2	102.64	4.64	84.24	10.08	NO	NO	NO	NO	NO
PAK1	4	102.73	6.74	125.2	15.54	105.85	6.93	81.65	7.61	NO	NO	NO	NO	NO
PBS	4	95.92	8.26	99.51	21.06	92.12	8.15	92.23	8.27	NO	NO	NO	NO	NO
PDCD6IP	4	94.99	7.46	142.57	21.16	125.24	4.18	84.45	8.28	NO	NO	NO	NO	NO
PDIA3	4	95.36	6.44	101.17	23.02	104.57	8.06	101.99	6.51	NO	NO	NO	NO	NO
PI4KA	4	106.74	10.12	99.04	20.72	82	4.39	79.08	5.8	NO	NO	NO	NO	NO
PICALM	4	98.8	6.97	104.28	18.96	87.99	5.31	81.59	12.49	NO	NO	NO	NO	NO
PIK3C2G	4	105.17	5.84	125.57	20.63	103.43	6.41	79.9	14.03	NO	NO	NO	NO	NO
PIK3CG	4	89.32	8.41	128.8	18.99	106.81	2.73	79.49	8.78	NO	NO	NO	NO	NO
PIP5K1A	4	99.76	4.2	122.92	13.2	99.61	6.62	78.32	11.41	NO	NO	NO	NO	NO
QSOX2	4	102.06	5.62	121.5	23.11	102.56	4.11	81.22	13.9	NO	NO	NO	NO	NO
RAB10	4	109.5	6.32	119.92	20.49	107.2	10.2	85.24	13.6	NO	NO	NO	NO	NO
RAB11A	4	98.46	4.06	97.6	22.91	91.6	6.42	90.12	11.42	NO	NO	NO	NO	NO
RAB11B	4	93.7	6.71	124.5	25.15	122.18	4.45	95.04	13.26	NO	NO	NO	NO	NO
RAB11FIP5	4	101.02	4.77	124.99	31.14	112.09	5.45	87.78	10.21	NO	NO	NO	NO	NO
RAB1A	4	97.62	6.98	108.11	11.56	93.6	3.61	82.99	7.76	NO	NO	NO	NO	NO
RAB29	4	97.53	8.05	100.79	30.28	96.38	8.92	93.72	18.3	NO	NO	NO	NO	NO
RAB2A	4	100.12	8.13	103.97	16.36	90.94	3.94	83.21	7.6	NO	NO	NO	NO	NO
RAB3A	4	98.5	9.25	112.6	20.03	95.44	5.01	80.78	4.14	NO	NO	NO	NO	NO
RAB3B	4	100.06	6.66	119.99	22.72	102.26	2.98	81.78	6.26	NO	NO	NO	NO	NO
RAB3C	4	96.75	4.95	134.72	26.55	119.25	5.47	86.47	10.82	NO	NO	NO	NO	NO
RAB3D	4	93.89	8.7	148.13	16.47	119.38	4.58	77.34	9.55	NO	NO	NO	NO	NO
RAB4A	4	100.05	5.98	120.75	22.57	99.49	3.65	78.6	6.3	NO	NO	NO	NO	NO
RAB4B	4	106.02	5.13	113.47	18.95	100.61	2.5	85.36	10.71	NO	NO	NO	NO	NO
RAB5A	4	101.43	3.41	101.64	17.54	89.18	4.4	84.61	7.85	NO	NO	NO	NO	NO
RAB5B	4	106.45	3.92	104.58	23.27	92.04	4.06	84.97	6.28	NO	NO	NO	NO	NO
RAB5C	4	105.35	5.43	108.86	24.11	88.74	4.89	78.12	9.78	NO	NO	NO	NO	NO
RAB6A	4	107.38	3.76	119.42	14.12	98.04	5.15	78.87	4.96	NO	NO	NO	NO	NO
RAB6B	4	104.23	5.45	125.71	19.44	109.95	5.09	85.08	11.25	NO	NO	NO	NO	NO
RAB7B	4	116.87	6.67	106.02	18.9	88.69	3.77	80.98	9.42	NO	NO	NO	NO	NO
RAB8A	4	105.68	7.14	100.89	16.15	83.61	5.83	78.9	7.27	NO	NO	NO	NO	NO
RAB8B	4	101.29	6.44	138.42	20.72	113.59	6.25	80.16	10.44	NO	NO	NO	NO	NO
RAC1	4	103.7	8.04	100.49	22.86	83.1	6.32	79.11	9.4	NO	NO	NO	NO	NO
ROCK1	4	109.56	5.25	111.1	16.64	90.48	4.46	77.78	4.59	NO	NO	NO	NO	NO
ROCK2	4	85	6.42	129.2	28.7	126.98	5.09	96.49	14.23	NO	NO	NO	NO	NO
RPN1	4	110.69	5.99	86.18	27.7	88.24	4.55	101.09	13.07	NO	NO	NO	NO	NO
RPN2	4	98.88	10.52	108.19	19.04	93.01	7.52	84.26	7.25	NO	NO	NO	NO	NO
SAR1A	4	107.03	6.76	122.49	21.57	98.22	5.57	77.36	10.59	NO	NO	NO	NO	NO
SCAMP3	4	104.16	4.36	127.95	25.14	105.33	5.39	80.24	11.72	NO	NO	NO	NO	NO
SCFD1	4	98.52	10.03	120.63	32.85	97.97	5.36	77.95	10.38	NO	NO	NO	NO	NO
SEC13	4	104.14	3.63	98.65	15.18	83.32	4.83	80.87	7.44	NO	NO	NO	NO	NO
SEC22B	4	90.22	7.67	111.86	25.25	109.13	8.34	95.61	11.92	NO	NO	NO	NO	NO
SH3GLB1	4	98.45	6.28	127.26	15.24	110.53	4.52	84.19	7.85	NO	NO	NO	NO	NO
SH3GLB2	4	104.51	7.22	116.22	18.45	99.95	7.08	82.89	12.8	NO	NO	NO	NO	NO
SLC35A2	4	97.47	4.77	112.36	17.04	106.2	3.45	90.68	12.73	NO	NO	NO	NO	NO
SLC35B2	4	107.39	7.96	103.24	17.76	96.76	5.39	91.58	13.08	NO	NO	NO	NO	NO
SNAP91	4	99.13	9.47	129.69	18.12	109.35	5.58	81.36	6.91	NO	NO	NO	NO	NO
SNX1	4	104.42	5.28	125.4	22.46	101.75	6.15	78.78	11.83	NO	NO	NO	NO	NO
SNX2	4	103.27	2.64	112.37	20.56	100.25	5.95	85.31	7.43	NO	NO	NO	NO	NO
STAU1	4	104.11	6.51	122	22.96	103.47	4.06	82.09	13.58	NO	NO	NO	NO	NO
STT3A	4	95.01	7.54	110.47	25.68	109.23	4.89	97.29	10.72	NO	NO	NO	NO	NO
STT3B	4	87.99	8.28	102.89	23.17	98.56	2.96	95.9	10.39	NO	NO	NO	NO	NO
SURF4	4	91.46	10.28	127.9	28.87	105.89	6.9	79.77	11.62	NO	NO	NO	NO	NO
SYNJ1	4	99.98	7.03	99.37	14.47	95.74	9.3	92.25	12.35	NO	NO	NO	NO	NO
SYNJ2	4	96.54	6.85	88.87	14.24	84.87	6.07	91.78	19.41	NO	NO	NO	NO	NO
SYT1	4	95.39	8.82	102.8	14.73	88.28	6.19	81.61	7.89	NO	NO	NO	NO	NO
SYT2	4	104.65	4.09	136.76	20.22	122.95	4.3	86.58	13.54	NO	NO	NO	NO	NO
TMEM165	4	99.7	5.98	112.17	25.06	101.6	5.93	89.28	15.3	NO	NO	NO	NO	NO
TNIK	4	104.01	3.83	138.39	19.94	119.08	4.36	82.95	8.11	NO	NO	NO	NO	NO
TSG101	4	100.7	7.45	91.75	12.92	81.42	7.05	84.7	6.52	NO	NO	NO	NO	NO
VAMP1	4	99.85	2.3	124.14	21.01	106.54	5.57	82.86	13.39	NO	NO	NO	NO	NO
VAMP2	4	99.72	9.96	103.27	21.77	84.44	6.46	77.68	4.76	NO	NO	NO	NO	NO
VAPA	4	88.52	6.52	116.85	23.25	119.4	3.79	100.13	13.91	NO	NO	NO	NO	NO
VAPB	4	95.42	10.21	108.04	30.93	111.33	5.36	101.28	9.72	NO	NO	NO	NO	NO
VPS36	4	107.78	8.22	112.51	16.73	100.22	9.13	86.08	12.54	NO	NO	NO	NO	NO
VPS4A	4	109.53	8.42	119.45	17.44	107.6	3.53	86.59	9.61	NO	NO	NO	NO	NO
WAS	4	99.17	6.93	106.3	20.07	94.33	4.78	84.84	5.3	NO	NO	NO	NO	NO
WASF1	4	109.11	8.59	97.35	29.2	89.04	12.45	89.67	15.25	NO	NO	NO	NO	NO
WASF2	4	102.36	7.42	117.48	24.67	98.91	6.22	82.09	12.54	NO	NO	NO	NO	NO
WASF3	4	99.73	3.8	135.93	25.4	111.03	4.96	78.84	7.01	NO	NO	NO	NO	NO
Fluc_siRNA2	0	25.36	31.66	528.06	39.33	489.19	20.36	88.86	12.07	YES	NO	NO	NO	KILL CELLS
RHOA	0	67.04	6.76	145.85	21.45	145.33	5.19	96.47	12.15	YES	NO	NO	NO	KILL CELLS

(v) Deconvolution siRNA Library

Gene Symbol	GENEID	GINumber	GeneAccession	DuplexCatalogNumber	Sequence
COPA	1314	6996002	NM_004371	J-011835-05	ACUCAGAUCUGGUGUAAUA
				J-011835-06	GCAAUAUGCUACACUAUGU
				J-011835-07	GAACAUUCGUGUCAAGAGU
				J-011835-08	GCGGAGUGGUUCCAAGUUU
COPB2	9276	4758031	NM_004766	J-019847-06	GGACACACCCAUUAUGUUA
				J-019847-07	GCAGAUGACCGUCUUGUUA
				J-019847-08	GAUAUUGACACAACAGAUA
				J-019847-09	GAUAUGGGCAGUUGUGAAA
COPG1	22820	35250828	NM_016128	J-019138-05	GCACAAACACACUCAAUGA
				J-019138-06	UGUCAGAAAUCUCGGAUGA
				J-019138-07	GCAAACACGCCGUCCUUAU
				J-019138-08	UGAGUGCUCUGGCGAAGUU
DNM1	1759	59853098	NM_004408	J-003940-05	GAGAAUCUGUCCUGGUACA
				J-003940-06	GAAUAUCCAUGGCAUUAGA
				J-003940-07	GCAGUUCGCCGUAGACUUU
				J-003940-08	CACAGAAUAUGCCGAGUUC
EEA1	8411	55770887	NM_003566	J-004012-06	GCAGUCAGCUGGAAAGUCA
				J-004012-07	GAAGCAACGGUUCAGAAUA
				J-004012-08	GUUCAAACACUAAUGGAUA
				J-004012-09	GAACCUUGAAGCUUUAUUA
GBF1	8729	4758415	NM_004193	J-019783-05	GAUGAGGGCUUCCACAUUG
				J-019783-06	CAACACACCUACUAUCUCU
				J-019783-07	GAGAAGCUAGCAAUACUGA
				J-019783-08	CCACUGCUGUCACUCUCUA
GRM4	2914	4504140	NM_000841	J-005619-06	GCACCAACCGUGAGCGAAU
				J-005619-07	GCGCAUGGACCCUGUAGAU
				J-005619-08	CAACAGCCGCUACGACUUC
				J-005619-09	CACCAACCAUGCAAUCUAG
VAV2	7410	40549447	NM_003371	J-005199-05	CUGAAAGUCUGCCACGAUA
				J-005199-06	UGGCAGCUGUCUUCAUUAA
				J-005199-07	GUGGGAGGGUCGUCUGGUA
				J-005199-08	GCCGCUGGCUCAUCGAUUG
VCP	7415	7669552	NM_007126	J-008727-09	CAAAUUGGCUGGUGAGUCU
				J-008727-10	CCUGAUUGCUCGAGCUGUA
				J-008727-11	GUAAUCUCUUCGAGGUAUA
				J-008727-12	GCAUGUGGGUGCUGACUUA

(vi) Deconvolution siRNA Screen Method

A siRNA library was prepared at 1μM in 1x siRNA buffer (Cherry pick custom Dharmacon library (Ref# SO-2845356G)) in 96-well plates (Eppendorf cat# 951040188). The library comprised individual siRNA sequences picked from the pools selected as hits from the previous screen of siRNA targeting membrane trafficking proteins and other biological relevant genes. The library (1 plate) was remapped into two library plates to generate 3 replicates of each individual sequence and accommodate controls in columns 1-3 and source pools in remaining free wells. The controls were added in 6 replicates each per plate and included a non-targeting siRNA (NT_siRNA) and two SMARTpools targeting Firefly luciferase (FLuc) and Nanoluciferase (NLuc): FLuc2_siRNA and NLuc2_siRNA respectively. The library was stored at -80C.

Huh7.5 cells were seeded into 6-well plates at $1.2x10^5$ cells per well (2mL media) and transfected the next day with DENV-NS1-NLuc RNA using DMRIE-C (1mL OptiMem with 6μL DMRIE-C and 6μg RNA, per well). Cells were incubated for 3 hours before transfection reagent was replaced with media. Two days after DENV-NS1-NLuc transfection, cells were harvested and reverse transfected in 96-well plates (Corning Costar cat #3596). For reverse transfection, 4μL of 1μM each siRNA (40nM final concentration per well) from previously prepared library plate, 0.3μL Dharmafect4 and 15.7μL OptiMem were added to each well (20 □L total volume per well), incubated for 20 min at room temperature and DENV-NS1-NLuc transfected cells were then added at $1.25x10^4$cells/well/80μL). Cells were transfected for 3 h at 37°C, 5%CO_2 before the supernatant was replaced with 100μL per well of media. Two days after siRNA reverse-transfection, supernatants were collected and kept at 4°C before processing for storage and later Luciferase assay. Cells in every well were then assayed for viability using a Cell Titer Blue (CTB) kit (Promega, cat # G8081). CTB reagent was diluted 1:5 in complete media and 100□L was added to every well. Plates were incubated for 1h at 37°C, 5%CO_2 before reading florescence in an Ensight plate reader (Ex 560 nm, Em590 nm). During the CTB reagent incubation, supernatants were centrifuged at 500g, 15°C for 5 minutes and 25μL of clarified supernatant was combined with 25μL of 2x passive lysis buffer (Promega cat #E1941) and frozen at -20C. After fluorescence reading, cells were washed twice with 100μL of PBS, before being lysed with 50μL of 1x passive lysis buffer. Supernatant and lysates samples were stored at -20C until they were assayed for Firefly luciferase and Nanoluciferase activity.

Samples were assayed using the Nano-Glo Dual-luciferase reporter (NanoDLR) assay (Promega, cat# N1620). The day before each assay reagents were placed at 4C. For the assay, 10μL of cell lysate or supernatant was transferred to a white 96-well plate (Perkin Elmer cat # 6005290) and 50μL per well of OneGlo reagent was dispensed and mixed (15 seconds shaking) using a BioTek 406 dispenser (BioTek). Plates were incubated at room temperature for 45 minutes in the dark before luminescence was read on an Ensight plate reader (0.1mm above plate, 0.1 second read, Perkin Elmer). Following plate reading, 50μL per well of NanoDLR Stop&Glo was added, plate

shaken and incubated for 45 minutes at room temperature in the dark. Luminescence was read again using the same settings as the first read.

The screen included 2 independent experimental replicates. Each experiment included 3 replicates of each siRNA individual sequences or pools and 6 replicates of each control. A total of 6 data set per siRNA and 24 for each control were generated. As cells were assayed for viability and that each cell treatment was split into lysates and supernatants and further assayed for two luciferase enzymes, the total number of data points were 1728.

For the analysis, the data from luciferase activity in all samples was normalised to viability readings. Further normalisation was carried out using the NT_siRNA values as reference and the data expressed as a percentage of the mean of this control on per plate basis. In addition, the ratio of supernatant to lysate values was calculated for every well as an estimation of the secretion rate for each enzyme. The NT_siRNA values were used also for setting threshold values for each parameter (enzyme, sample and secretion ratio). For all parameter the threshold was set as 2 standard deviations below the mean of the NT_siRNA normalised values.

Individual scores per parameter were assigned to each siRNA rendering normalised values below the threshold. Total scores were then used to identify hits following the general consideration that hit sequences were not inhibiting the FLuc expression but knocking down NLuc secretion, at least.

(vii) Deconvolution siRNA Screen Data Analysis Method

Data handling and analysis of the deconvolution siRNA screen was very similar to that of the primary screen and thus only the main differences or additions are detailed below.

Data structure and compilation

For the deconvolution hit follow up, identified hits and selected genes were assayed as pooled (4 siRNA per pool as evaluated in primary screen) and individual siRNA in triplicates while 6 replicas of the non-targeting siRNA (NT-siRNA) control were included in each plate. Two experimental replicas using identical plate layouts were used.

Sample preparation and luciferase measurements were performed as described previously, so data sets with similar structures were generated. However, to counteract the possibility of direct effects of a test siRNA on FLuc expression levels, an additional measurement for cell viability was introduced. In addition to the luciferase assays, CellTiter-Blue (CTB; Promega) viability assays were also performed (as described in Materials and Methods), in order to normalise the data to the number of cells in the well.

Individual csv files in list format for each assay and sample were exported from the Ensight and compiled into a single database containing the annotated data points from all plates. Compilation of all files was carried out using the same Python script with minor adjustment for additional data.

Further data handling and analysis was done using Spotfire.

Data exploration and Quality Control:

The mean, standard deviation and %CV was calculated for the experimental replicates for each treatment on a per plate basis and used to assess data quality. In this case the central values and variability of the readings from CTB assays (viability) and RLU from FLuc were similar in the two experimental replicas and no significant effect was observed from any of the siRNAs on cell viability (toxicity) or FLuc expression. Similarly, outliers were detected on the control well and removed, resulting in %CV values lower than 10% for all plates and across the screen.

Data Normalisation:

Considering that CTB assays are a more accurate measurement of cell viability, this data was used to calculate the relative expression values for both FLuc_Lys and NLuc as a point of difference from the normalisation method used in the primary screen, where FLuc_Lys values were used as a reference.

This normalisation method used the following formulas:

$$RE\_FLuc = \frac{FLuc\_Lys}{CTB\ Viability}$$

$$RE\_NLuc\_Lys = \frac{NLuc\_Lys}{CTB\ Viability}$$

$$RE\_\ NLuc\_Sup = \frac{NLucSup}{CTB\ Viability}$$

The NLuc secretion ratio (SR) to the media was also calculated as a ration of supernatant to lysate readings:

$$SR\_Nluc = \frac{NLuc\_Sup}{NLuc\_Lys}$$

Further normalisation was carried out using the same approach. Briefly, Normal_NLuc_Sup, Normal_NLuc_Lys and Normal_SR_NLuc were calculated as percentages of the mean of corresponding averages from NT_siRNA controls in every plate. The calculation was performed as described before.

Hit identification:

After normalisation, the methodology for Hits identification and siRNA effect classification was based on the same principles and followed the same procedure as described for the primary screening.

Gene Symbol	Sequence ID	Sequence	Exp_Replica	Score	Hits	Knockdown FLuc	Knockdown NLucLys	Knockdown NLucSup	Knockdown Secretion
COPA	COPA-5	ACUCAGAUCUGGUGUAAUA	1	12	HIT	113.26	94.81	70.77	75.28
COPA	COPA-6	GCAAUAUGCUACACUAUGU	1	12	HIT	105.37	114.1	79.95	70.23
COPA	COPA-7	GAACAUUCGUGUCAAGAGU	1	12	HIT	130.05	103.34	69.37	67.32
COPA	COPA-8	GCGGAGUGGUUCCAAGUUU	1	12	HIT	121.33	120.82	69.23	59.61
COPB2	COPB2-6	GGACACACCCAUUAUGUUA	1	12	HIT	132.01	110.49	77.12	70.99
COPB2	COPB2-7	GCAGAUGACCGUCUUGUUA	1	4	No effect	127.59	123.74	97.63	79.33
COPB2	COPB2-8	GAUAUUGACACAACAGAUA	1	12	HIT	156.83	127.64	70.75	56.62
COPB2	COPB2-9	GAUAUGGGCAGUUGUGAAA	1	4	No effect	116.35	106.13	92.38	89.75
COPG1	COPG1-5	GCACAAACACACUCAAUGA	1	0	Reduced FLuc	82.66	94.18	79.47	86
COPG1	COPG1-6	UGUCAGAAAUCUCGGAUGA	1	12	HIT	106.68	91.35	64.63	71.24
COPG1	COPG1-7	GCAAACACGCCGUCCUUAU	1	4	No effect	128.21	119.38	96.66	83.2
COPG1	COPG1-8	UGAGUGCUCUGGCGAAGUU	1	12	HIT	130.43	91.19	68.73	76.42
DNM1	DNM1-5	GAGAAUCUGUCCUGGUACA	1	4	No effect	108.63	107.98	87	81.65
DNM1	DNM1-6	GAAUAUCCAUGGCAUUAGA	1	12	HIT	105.12	111.09	76.68	69.91
DNM1	DNM1-7	GCAGUUCGCCGUAGACUUU	1	12	HIT	125.74	116.2	80.75	69.94
DNM1	DNM1-8	CACAGAAUAUGCCGAGUUC	1	4	No effect	114.44	94.22	83.44	89.49
EEA1	EEA1-6	GCAGUCAGCUGGAAAGUCA	1	12	HIT	148.48	155.49	115.89	74.99
EEA1	EEA1-7	GAAGCAACGGUUCAGAAUA	1	4	No effect	123.03	117.31	93.36	81.23
EEA1	EEA1-8	GUUCAAACACUAAUGGAUA	1	4	No effect	127.13	117.8	100.19	85.49
EEA1	EEA1-9	GAACCUUGAAGCUUUAUUA	1	4	No effect	99.99	98.23	86.62	90.1
GBF1	GBF1-5	GAUGAGGGCUUCCACAUUG	1	0	Reduced FLuc	64.76	98.64	97.72	101.39
GBF1	GBF1-6	CAACACACCUACUAUCUCU	1	4	No effect	98.68	90.47	79.71	88.24
GBF1	GBF1-7	GAGAAGCUAGCAAUACUGA	1	4	No effect	115.51	100.76	93.31	93.38
GBF1	GBF1-8	CCACUGCUGUCACUCUCUA	1	4	No effect	89.43	114.32	96.34	84.65
GRM4	GRM4-6	GCACCAACCGUGAGCGAAU	1	4	No effect	102.26	113.85	110.01	97.52
GRM4	GRM4-7	GCGCAUGGACCCUGUAGAU	1	4	No effect	106.12	91.91	89.62	97.59
GRM4	GRM4-8	CAACAGCCGCUACGACUUC	1	4	No effect	121.75	126.35	106.77	84.93
GRM4	GRM4-9	CACCAACCAUGCAAUCUAG	1	4	No effect	121.45	115.46	116.66	102.23
VAV2	VAV2-5	CUGAAAGUCUGCCACGAUA	1	4	No effect	130.03	121.51	120.5	99.33
VAV2	VAV2-6	UGGCAGCUGUCUUCAUUAA	1	4	No effect	107.47	130.06	118.91	91.5
VAV2	VAV2-7	GUGGGAGGGUCGUCUGGUA	1	4	No effect	140.02	119.75	105.26	88.2
VAV2	VAV2-8	GCCGCUGGCUCAUCGAUUG	1	4	No effect	93.84	93.45	102.89	111.36
VCP	VCP-0	CAAAUUGGCUGGUGAGUCU	1	4	No effect	159.5	103.71	90.28	87.56
VCP	VCP-1	CCUGAUUGCUCGAGCUGUA	1	4	No effect	127.14	77.01	74.59	98.52
VCP	VCP-2	GUAAUCUCUUCGAGGUAUA	1	4	No effect	112.5	88.02	90.06	102.76
VCP	VCP-9	GCAUGUGGGUGCUGACUUA	1	4	No effect	132.81	94.17	79.17	84.96
(Empty)	Buffer	(Empty)	1	4	No effect	100.51	113.56	103.84	92.65
(Empty)	COPA	(Empty)	1	4	No effect	114.95	126.09	101.96	81.38
(Empty)	COPB2	(Empty)	1	4	No effect	109.99	127.47	134.98	107.77
(Empty)	COPG1	(Empty)	1	12	HIT	94.76	119.69	81.21	68.33
(Empty)	DNM1	(Empty)	1	4	No effect	116.33	106.25	105.46	99.27
(Empty)	EEA1	(Empty)	1	4	No effect	118.82	115.14	116.41	101.13
(Empty)	Fluc2_siRNA	(Empty)	1	0	Reduced FLuc	29.81	111.07	103.14	93.19
(Empty)	GBF1	(Empty)	1	4	No effect	90.92	112.6	95.73	85.72
(Empty)	GRM4	(Empty)	1	4	No effect	114.31	109.05	117.55	107.67
(Empty)	Nluc2_siRNA	(Empty)	1	7	Potential Hit	98.77	55.45	45.28	82.68
(Empty)	NT_siRNA	(Empty)	1	4	No effect	100	100	100	100
(Empty)	VAV2	(Empty)	1	4	No effect	128.72	127.73	105.87	84.3
(Empty)	VCP	(Empty)	1	4	No effect	103.9	90.1	95.48	106.62

Appendix VI: Supplementary Material (Mass Spectrometry)

(i) EZQ™ protein quantification of clarified whole cell lysate samples.

Estimation of Protein Concentration
Using EZQ™ Protein Quantification Kit

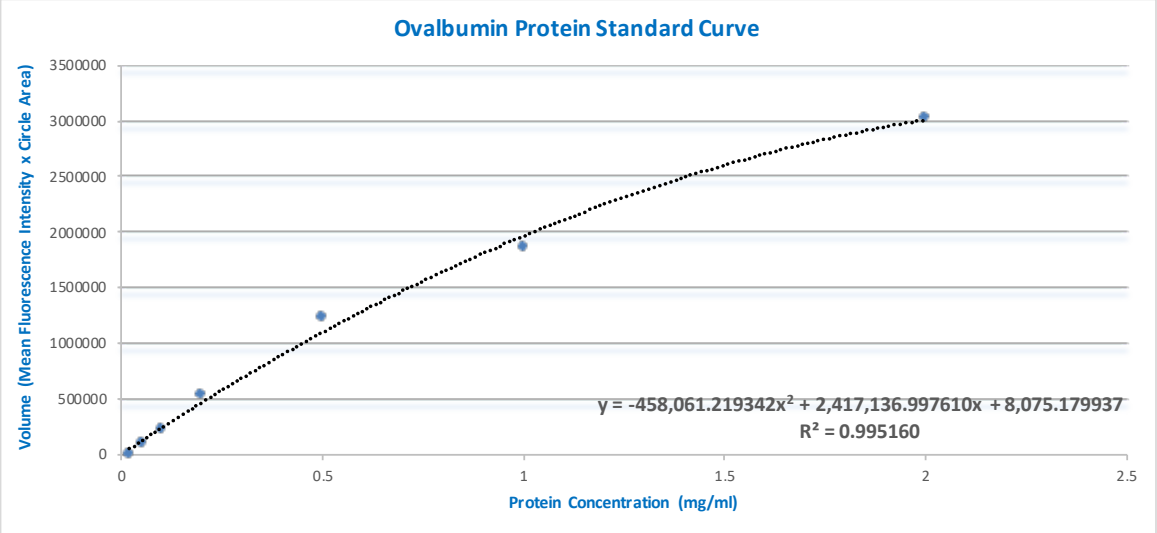

Insert	a	-458061.22
Insert	b	2,417,137.00
Insert	c	8,075.18

to solve for x, y must equal 0	$ax^2 + bx + c = 0$
to make y (volume) equal 0 volume must be deducted from both sides of the equation	$y-y = ax^2 + bx + c-y$
x can then be calculated through this equation:	
$x = \frac{-b \pm \sqrt{b^2-4ac}}{2a}$	

Standard Quadratic Equation

x = is the unknown protein concentration we are solving for

$y = ax^2+bx+c$

y = volume = (mean fluorescence intensity x area of circle)

a & **b** = equation parameters of the graph

c = constant value or y intercept of the parabola where the graph intersects the y-axis

Standard Curve:
Ovalbumin Protein Standards

Note: Copy/Paste "Adjusted Volume" values obtained from the Image Lab Software into the volume column below. These are values from each circle after background has been deducted.

Circle #	Standard Concentration (mg/ml) (Note: mg/ml = µg/µl)	Volume (y) (mean fluorescence intensity x circle area)	Average Volume (average of the triplicates)	y=0 (c minus average volume)	x (mg/ml) (calculated standard concentration)	Dilution Factor	Calculation of Ovalbumin Concentration (mg/ml) *(For Comparison Only)*	CV (%) (coefficient of variation)
1		2,847,197						
2		3,082,612						
3	2	3,157,369	3029060	-3.02E+06	2.03	**1**	2.0	5.3%
4		1,750,169						
5		1,783,130						
6	1	2,038,535	1857278	-1.85E+06	0.93	**2**	1.9	8.5%
7		1,234,126						
8		1,254,889						
9	0.5	1,198,988	1229334	-1.22E+06	0.57	**4**	2.3	2.3%
10		562,379						
11		526,196						
12	0.2	517,458	535344	-5.27E+05	0.23	**10**	2.3	4.4%
13		229,976						
14		226,633						
15	0.1	241,738	232782	-2.25E+05	0.09	**20**	1.9	3.4%
16		83,131						
17		93,199						
18	0.05	96,007	90779	-8.27E+04	0.03	**40**	1.4	7.5%
19		8,683						
20		5,749						
21	0.02	2345	7216	8.59E+02	0.00	**100**	0.0	28.8%

Unknown Protein Samples

Note: Copy/Paste "Adjusted Volume" Values obtained from the Image Lab Software into the volume column below. These are values from each circle after background has been deducted.

Circle #	Sample Name	Volume (y) (mean fluorescence intensity x circle area)	Average Volume (average of the triplicates)	y=0 (c minus average volume)	x (mg/ml) (unknown sample concentration)	Dilution Factor	Undiluted Sample Concentration (mg/ml)	CV (%) (coefficient of variation)
22		6,246						
23	dH2O	-9,635						
24		546	-948	9.02E+03	**0.00**	**1**	0.00	-848.8%
25		2,487,453						
26	NS1 #1 (neat)	2,819,849						
27		3,212,096	2839799	-2.83E+06	**1.76**	**1**	1.76	12.8%
28		2,992,451						
29	NS1 #2 (neat)	2,900,477						
30		2,800,574	2897834	-2.89E+06	**1.83**	**1**	1.83	3.3%
31		2,841,644						
32	NS1 #3 (neat)	2,852,693						
33		2,597,733	2764023	-2.76E+06	**1.67**	**1**	1.67	5.2%
34	NS1 #4 (neat)	2,818,287						
35		2,909,587						
36		2,790,955	2839610	-2.83E+06	**1.76**	**1**	1.76	2.2%
37		3,192,964						
38	IgK #1 (neat)	3,039,748						
39		3,035,400	3089370	-3.08E+06	**2.15**	**1**	2.15	2.9%
40		3,043,813						
41	IgK #2 (neat)	3,510,231					estimate	
42		3,322,858	3292301	-3.28E+06	**#NUM!**	**1**	2.30	7.1%
43		2,834,268						
44	IgK #3 (neat)	2,921,323						
45		3,331,954	3029181	-3.02E+06	**2.03**	**1**	2.03	8.8%
46	IgK #4 (neat)	2,982,290						
47		2,746,488						
48		3,086,892	2938556	-2.93E+06	**1.89**	**1**	1.89	5.9%
49		2,827,137						
50	SCM #1 (neat)	2,598,687						
51		2,714,517	2713447	-2.71E+06	**1.61**	**1**	1.61	4.2%
52		2,581,861						
53	SCM #2 (neat)	2,791,683						
54		2,842,558	2738701	-2.73E+06	**1.64**	**1**	1.64	5.0%
55		2,593,855						
56	SCM #3 (neat)	2,812,659						
57		2,708,523	2705012	-2.70E+06	**1.60**	**1**	1.60	4.0%
58	SCM #4	2,895,706						
59	(neat)	2,982,336						
60		2,734,979	2871007	-2.86E+06	**1.80**	**1**	1.80	4.4%

Sample	mg/ml
NS1 #1	1.76
NS1 #2	1.83
NS1 #3	1.67
NS1 #4	1.76
IgK #1	2.15
IgK #2	2.3
IgK #3	2.03
IgK #4	1.89
SCM #1	1.61
SCM #2	1.64
SCM #3	1.6
SCM #4	1.8

(ii) Method for the streptavidin bead enrichment of biotinylated protein.

APEX2 experiment, chemical acetylation of ligands, two-step digestion – Biotinylated Protein APEX2

Acetylation of Affinity Purification Ligands Using Sulfo-NHS-Acetate

(1) binding of the bait protein to an immobilized ligand,

(2) washing of the affinity matrix to remove nonspecifically bound proteins

(3) elution of bound bait proteins to enable downstream analysis of the sample via LC−MS

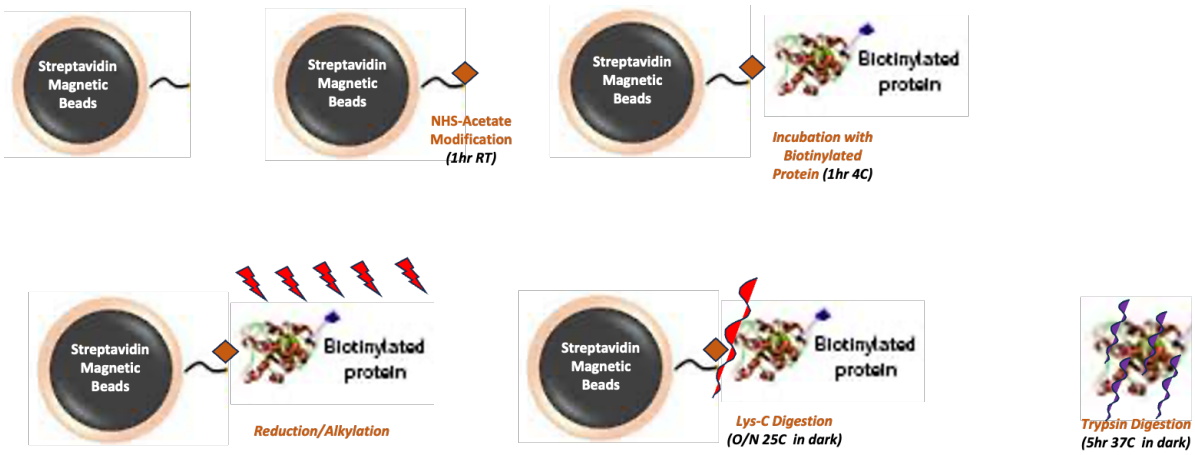

Beads:

Dynabeads M-280-Streptavidin (10mg/ml)

Binding Capacity:

Biotinylated Antibody: ~10ug/mg

Biotinylated Peptide: ~200 pmol / mg

Free Biotin: 650-900 pmol / mg

Streptavidin Bead Modification:

1. Transfer 100 µL of streptavidin magnetic beads into a maxymum recovery vial
    - = 1mg total bead
2. Place on magnet for 1 min. Remove supernatant.
3. Wash with 1ml of reaction buffer (50 mM HEPES-KOH, pH 7.8).
    - Vortex for 5 seconds (or keep on mixer for 5 minutes)
    - Place on magnet for 1 min. Discard wash.
4. Repeat wash step 2 more times for a total of 3 washes.
5. After discarding the final wash, resuspend the beads in 90 µL of reaction buffer.
6. Add 10 µL of Sulfo-NHS Acetate in an appropriate dilution to a final concentration of 5mM and incubate for 60 minutes at room temperature.
    - Make 50mM Stock (10ul in 100ul = 5mM final concentration)
    - Mw: 259.17 (50mM = 1mg in 77ul)
7. Place beads on magnet for 1 minute and remove supernatant.
8. Wash modified beads three times with 100 µL of 50mM ABC.
9. Resuspend modified beads in 100 µL PBST-azide (pH 6.8, 0.2% Tween 20, 0.02% sodium azide)

Cell Processing (Carried out by Steve):

1. Lyse cells in RIPA buffer (50 mM Tris, 150 mM NaCl, 0.1% SDS, 0.5% sodium deoxycholate, 1% TritonX-100, 1x protease inhibitor cocktail)
2. Centrifuge Lysate at 10 000g at 4°C.

NS1-APEX2 biotinylation to identify human host cell proteins involved in dengue virus NS1 internalisation.

There are three treatments:

- NS1: NS1-APEX2 fusion protein (Experimental)
- IgK: IgK-APEX2 (APEX2-Only control)
- SCM: Spent culture media (Mock control)

There are four replicates for each treatment.

The samples are whole cell lysates in ≥ 3mL RIPA buffer containing quenching solution (homogenised using 25G needle; centrifuged 15,000 x g 15 min 4*C).

The sample concentrations are below (Pierce, and Oriole normalised)

Sample	Pierce Concentration (ug/ul)	Oriole Normalised Concentration (ug/mL)	EZQ Concentrations (ug/ul)	Total Volume (mL)
NS1 #1	0.32352	323.52	1.76	3
NS1 #2	0.35841	358.41	1.83	3
NS1 #3	0.2935	293.5	1.67	3
NS1 #4	0.31552	315.52	1.76	3
IgK #1	0.40445	404.45	2.15	3
IgK #2	0.34256	342.56	2.3	3
IgK #3	0.40374	403.74	2.03	3
IgK #4	0.33146	331.46	1.89	3
SCM #1	0.3275	327.5	1.61	3
SCM #2	0.28554	285.54	1.64	3
SCM #3	0.3032	303.2	1.6	3
SCM #4	0.32756	327.56	1.8	3

RIPA Buffer	
Reagent	Volume (25mL)
1 M Tris, pH 7	1
4 M NaCl	0.9375
10% SDS	0.25
Sodium Deoxycholate	0.125 g
Triton X-100	0.25
MQ H2O (+ *Quencher Solution)	to 25mL
Protease Cocktail Inhibitor	1x

*Quencher solution: 10 mM Sodium Ascorbate, 5 mM Trolox, 10 mM Sodium Azide.

Purification:

1. Incubate the supernatant with S-NHS-Ac treated magnetic streptavidin beads for 1h at 4°C
   - *Place on thermomixer at 1000rpm*

Sample	EZQ Concentrations (ug/ul)	1mg (ul)	dh2O (ul)	final volume (ul)
NS1 #1	1.76	568	132	700
NS1 #2	1.83	546	154	700
NS1 #3	1.67	599	101	700
NS1 #4	1.76	568	132	700
IgK #1	2.15	465	235	700
IgK #2	2.3	435	265	700
IgK #3	2.03	493	207	700
IgK #4	1.89	529	171	700
SCM #1	1.61	621	79	700
SCM #2	1.64	610	90	700
SCM #3	1.6	625	75	700
SCM #4	1.8	556	144	700

2. Place sample on the magnet for 1-3 minute. Discard supernatant.
3. Wash beads 3 x with 500ul RIPA buffer.
   a. ~~a.~~ Vortex for 5 seconds ~~(or keep on vortex mixer for 5 minutes @2000 rpm)~~
   b. Place on magnet for 1 min. Discard wash.
4. Wash beads 5x with 50mM ABC Buffer.
   a. ~~Transfer samples to a fresh tube after the addition of ABC buffer~~
   b. Wash 2 x 500ul + 3 x 100ul washes
   c. Vortex for 5 seconds (or keep on mixer for 5 minutes)
   d. Place on magnet for 1 min. Discard wash.
5. Resuspend beads in 30 µL of 2 M urea (Sigma) in 50 mM ABC buffer

Reduction/Alkylation:

6. Reduce SNHS- Ac Beads using TCEP (0.2mM) for 30 minutes at RT
   a. Make 100mM TCEP. Dilute to 1mM then add 8.5ul to the sample.
7. Alkylate SNHS- Ac Beads using 1mM MMTS (S-methylmethanethiosulfonate, Fluka) in the dark at room temperature for 15 minutes.

a. Liquid Stock 1.337 g/ml = 1337 g/L : divided by 126.19 FW = 10.59M @97% purity = 10.59 x 0.97 = 10.2M
b. Dilute stock 1:1020 = 1ul in 1020 ul = 10mM
c. Add 5ul of 10mM stock

8. Quench the alkylation reaction by adding 0.1 mM TCEP or 5 mM DTT

LysC Digestion:

9. Elute the the reduced/alkylated proteins by digestion with 150 ng of Lys-C overnight at 25°C in the dark.
   - Resuspend 1ug freeze dried aliquot in 10ul dH_2O (=100ng/ul)
     - 2 vials were used.
   - Add 1.5 ul to each sample

10. Place tube on magnet and transfer the supernatant to a new vials

Trypsin Digestion:

11. Further digest the samples for 5 h at 37°C by the addition of 150 ng of Trypsin
    - Add 18ul dH_2O to 2ul (1ug/ul) vials of trypsin (=100ng/ul)
    - Add 1.5ul to each sample
12. Stop the proteolytic digestion was stopped by adding a 10% TFA solution to a final concentration of 0.5%.
    - Add 2.5ul of 10% stock

C18 Stagetip cleanup:

80% Acetonitrile / 0.1% Formic Acid	Stock Concentration	Final Concentration	for 10ml
Acetonitrile	100%	**80%**	**8000 µl**
Formic Acid	10%	**0.1%**	**100 µl**
dH2O			**1900 µl**

Disk	Tips used	C18 filters	Collection tube
C18	200ul white tips	3 x-small size disks 3 small size disks	maxymum recovery tube

1. Prepare C18 StageTips

2. Wet the C18 StageTip with 50 ul 80% Acetonitrile /0.1% FA. Discard the flowthrough.

Centrifuge	Time/Speed
Sigma	1 min @4000 rpm

3. Equilibrate the C18 StageTip with 50 ul Mass Spec Water (0.1% FA). Discard the flowthrough.

Centrifuge	Time/Speed
Sigma	1 min @4000 rpm

4. Place StageTips into clean 2ml Maxymum recovery tubes.

5. Apply sample to the StageTips. Keep flowthrough.

Sample	Time/Speed
54 ul	2 min @3000 rpm

6. Wash C18 StageTips with 100 ul Mass Spec Water (0.1% FA). Discard Flowthrough.

Centrifuge	Time/Speed
Sigma	2 min @4000 rpm

7. Place StageTips into clean 2ml Maxymum recovery tubes.

8. Elute with 200ul 80% Acetonitrile +0.1% Formic Acid.
-

Centrifuge	Time/Speed
Sigma	5 min @3000 rpm

9. Dry down the eluate in the vacuum concentrator.

10. Resuspend in 20 µL of 1% TFA +0.1%DDm.

Sample Resuspension

Sample	Resuspension Volume (ul)	Conc	Injection Volume (ul)	Transfer to MS vial
each	20	unknown	6	20

Chemical Acetylation Buffers

Sulfo-NHS Acetate (259.17 FW)	Amount	Actual
50mM Stock Solution	1 mg	2.4 mg
dH2O	77ul	184.8 ul

100mM TCEP (250.18 FW)	Amount	Actual	
TCEP	1 mg	1 mg	
dH2O	40 ul	40 ul	dilute 1:100 to obtain 1mM Concentration
10mM MMTS (126.19 FW)	**Amount**	**Actual**	
MMTS	1 in 1020 dilution of stock		
dH2O			
50mM ABC (79.05 FW)	**Amount**	**Actual**	
ABC	1 mg	147 mg	
dH2O	253 ul	37.2 ml	

2M Urea in 50mM ABC	FW	Amount
2M	60.06	60mg
50mM ABC		500ul

premade

Reaction Buffer	FW	Amount	
50mM HEPES	238.3	595.7 mg	
dH2O		40ml	
NaOH	adjust pH to 7.8		
dH2O		to 50ml	made fresh on 12/1/23

PBST Azide	Final Conc	Amount	premade
10x PBS	1x	5ml	
Tween 20	0.20%	100 ul	
Sodium Azide 1%	0.02%	1 ml	
dH2O		43.9 ml	
Final Volume		50ml	

(iii) Mass spectrometry

Liquid Chromatography Mass Spectrometry

Peptides were analysed with a Dionex Ultimate 3000 UPLC coupled with a Thermo, Fusion Lumos tandem mass spectrometer (Thermo Fisher Scientific, Waltham, Massachusetts, USA). An inhouse analytical column created from 75 µm inner diameter fused silica capillary with an integrated pulled tip emitter, packed with 1.5 µm ReproSil-Pur C18 beads (Dr. Maisch, Ammerbuch, Germany) to 25 cm, coupled with an inhouse packed trap column made from 150 µm inner diameter fused silica capillary, packed with 3 µm ReproSil-Pur C18 beads to 10mm were used. Mobile phase A was 0.1 % formic acid in water and mobile phase B was 0.1 % formic acid in 80 % acetonitrile. For each injection, 1 µg peptides were loaded and separated using a 120 min gradient from 3 to 31 % mobile phase B, followed by a 25 min washing and equilibration gradient. Samples were analysed using data dependent acquisition (DDA) utilizing a 3 second cycle time instrument method. Briefly, ms1 scans were performed using an orbitrap resolution of 60,000 and a scan range from 350m/z-2000m/z. A normalised AGC target of 1e6 with auto maximum injection time of 50ms. An intensity threshold of 5e4 and dynamic exclusion time of 45 sec was employed for all data dependent ms2 scans that were acquired at 15,000 resolution, AGC target 5e4, 30 % normalised collision energy (NCE) in the HCD cell, with dynamic maximum injection time mode used.

Lumos Data Dependent Analysis (DDA) Method

Liquid Chromatography

Instrument:	Dionex Ultimate 3000 UPLC (Thermo Fisher Scientific)
Mobile Phases:	Buffer A: Water, 0.1% Formic Acid
	Buffer B: 79.9% Acetonitrile, 20% Water, 0.1% Formic Acid
Trap Column:	PepMap™ 100 trap cartridge (0.3 x 5 mm, 5 µm C18, Thermo Fischer)
Analytical Column:	Inhouse pulled column created from 75 µm inner diameter fused silica capillary packed with 1.9 µm ReproSil-Pur C18 beads (Dr. Maisch, Ammerbuch, Germany) to 25cm

uHPLC Gradient

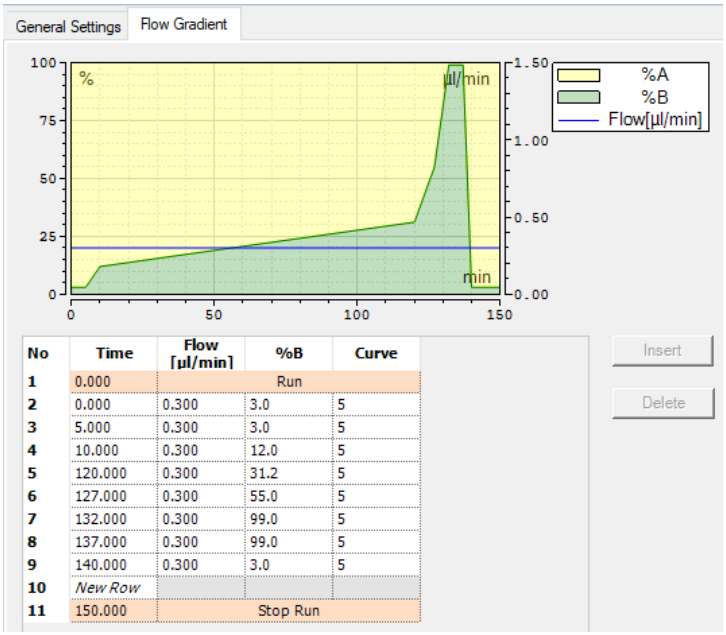

No	Time	Flow [µl/min]	%B	Curve
1	0.000	Run		
2	0.000	0.300	3.0	5
3	5.000	0.300	3.0	5
4	10.000	0.300	12.0	5
5	120.000	0.300	31.2	5
6	127.000	0.300	55.0	5
7	132.000	0.300	99.0	5
8	137.000	0.300	99.0	5
9	140.000	0.300	3.0	5
10	*New Row*			
11	150.000	Stop Run		

Mass Spectrometry

Instrument: Orbitrap Fusion™ Lumos™ Tribrid™ Mass Spectrometer (Thermo Fisher Scientific, Waltham, Massachusetts, USA)

MS Source: Nanospray Flex™ Ion Source (ES071, Thermo Fisher Scientific)

Column Oven: Nanospray Flex™ Column Oven (Sonation)

Oven Temp: 60°C

Spray Voltage: 2400 V

Ion Transfer Tube Temp: 275°C

Method Summary

Method Settings

Application Mode: **Peptide**

Method Duration (min): **140**

Global Parameters

Ion Source

Use Ion Source Settings from Tune: **True**

FAIMS Mode: **Not Installed**

MS Global Settings

Infusion Mode: **Liquid Chromatography**

Expected LC Peak Width (s): **30**

Advanced Peak Determination: **False**

Default Charge State: **2**

Enable Xcalibur AcquireX Ab method modifications: **False**

Internal Mass Calibration: **RunStart EASY-IC™**

Experiment #1 [MS_CV-30]

Start Time (min): **5**

End Time (min): **140**

Cycle Time (sec): **3**

Master Scan:

MS OT

Detector Type: **Orbitrap**

Orbitrap Resolution: **60000**

Mass Range: **Normal**

Use Quadrupole Isolation: **True**

Scan Range (m/z): **350-2000**

RF Lens (%): **40**

AGC Target: **Custom**

Normalized AGC Target (%): **250**

Maximum Injection Time Mode: **Custom**

Maximum Injection Time (ms): **50**

Microscans: **1**

Data Type: **Profile**

Polarity: **Positive**

Source Fragmentation: **Disabled**

Scan Description:

Filters:

MIPS

Monoisotopic Peak Determination: **Peptide**

Charge State

Include charge state(s): **2-7**

Include undetermined charge states: **False**

Dynamic Exclusion

Exclude after n times: **1**

Exclusion duration (s): **45**

Mass Tolerance: **ppm**

Low: **10**

High: **10**

Exclude Isotopes: **True**

Perform dependent scan on single charge state per precursor only: **False**

Exclude Within Cycle: **True**

Intensity

Filter Type: **Intensity Range**

Minimum Intensity: **5.0e4**

Maximum Intensity: **1.0e20**

Data Dependent

Data Dependent Mode: **Cycle Time**

Time between Master Scans (sec): **3**

Scan Event Type 1:

Scan:

ddMS² OT HCD

Isolation Mode: **Quadrupole**

Isolation Window (m/z): **1.4**

Isolation Offset: **Off**

Activation Type: **HCD**

Collision Energy Mode: **Fixed**

HCD Collision Energy Type: **Normalized**

HCD Collision Energy (%): **30**

Detector Type: **Orbitrap**

Orbitrap Resolution: **15000**

Mass Range: **Normal**

Scan Range Mode: **Define First Mass**

First Mass (m/z): **120**

AGC Target: **Custom**

Normalized AGC Target (%): **100**

Maximum Injection Time Mode: **Dynamic**

Microscans: **1**

Data Type: **Centroid**

Scan Description:

References

1. Gubler, D.J., *Dengue and dengue hemorrhagic fever.* Clin Microbiol Rev, 1998. **11**(3): p. 480-96.
2. Gubler, D.J., *Dengue/dengue haemorrhagic fever: history and current status.* Novartis Found Symp, 2006. **277**: p. 3-16; discussion 16-22, 71-3, 251-3.
3. Carey, D.E., *Chikungunya and dengue: a case of mistaken identity?* J Hist Med Allied Sci, 1971. **26**(3): p. 243-62.
4. Packard, R.M., *The Fielding H. Garrison Lecture:" Break-Bone" Fever in Philadelphia, 1780: Reflections on the History of Disease.* Bulletin of the History of Medicine, 2016. **90**(2): p. 193-221.
5. Brathwaite Dick, O., et al., *The history of dengue outbreaks in the Americas.* Am J Trop Med Hyg, 2012. **87**(4): p. 584-93.
6. Rose, N.H., et al., *Dating the origin and spread of specialization on human hosts in Aedes aegypti mosquitoes.* Elife, 2023. **12**.
7. Ashburn, P.M.C., C.F., *Experimental investigations regarding the etiology of dengue fever.* The Journal of infectious diseases, 1907: p. 440-475.
8. Bancroft, T.L., *On the aetiology of dengue fever.* Austral. Med. Gaz., 1906. **25**: p. 17-18.
9. Cleland, J.B. and B. Bradley, *Dengue Fever in Australia: Its History and Clinical Course, its Experimental Transmission by Stegomyia fasciata, and the results of Inoculation and other Experiments.* J Hyg (Lond), 1918. **16**(4): p. 317-418.
10. Kimura, R. and S. Hotta, *Studies on dengue: anti-dengue active immunization experiments in mice.* Jpn. J. Bacteriol, 1944. **1**: p. 96-99.
11. Sabin, A.B. and R.W. Schlesinger, *Production of immunity to dengue with virus modified by propagation in mice.* Science, 1945. **101**(2634): p. 640-642.
12. Sabin, A.B., *Research on dengue during World War II.* Am J Trop Med Hyg, 1952. **1**(1): p. 30-50.
13. Hammon, W.M., A. Rudnick, and G.E. Sather, *Viruses associated with epidemic hemorrhagic fevers of the Philippines and Thailand.* Science, 1960. **131**(3407): p. 1102-3.
14. Messina, J.P., et al., *Global spread of dengue virus types: mapping the 70 year history.* Trends Microbiol, 2014. **22**(3): p. 138-46.
15. Singh, N., et al., *Dengue in the Pacific--an update of the current situation.* Pac Health Dialog, 2005. **12**(2): p. 111-9.
16. *Dengue emergency in the Americas: time for a new continental eradication plan.* Lancet Reg Health Am, 2023. **22**: p. 100539.
17. Cardosa, J., et al., *Dengue virus serotype 2 from a sylvatic lineage isolated from a patient with dengue hemorrhagic fever.* PLoS Negl Trop Dis, 2009. **3**(4): p. e423.
18. Franco, L., et al., *First report of sylvatic DENV-2-associated dengue hemorrhagic fever in West Africa.* PLoS Negl Trop Dis, 2011. **5**(8): p. e1251.
19. Pyke, A.T., et al., *Complete Genome Sequence of a Highly Divergent Dengue Virus Type 2 Strain, Imported into Australia from Sabah, Malaysia.* Genome Announc, 2017. **5**(29).
20. Messina, J.P., et al., *The current and future global distribution and population at risk of dengue.* Nat Microbiol, 2019. **4**(9): p. 1508-1515.
21. Hales, S., et al., *Potential effect of population and climate changes on global distribution of dengue fever: an empirical model.* Lancet, 2002. **360**(9336): p. 830-4.
22. Stanaway, J.D., et al., *The global burden of dengue: an analysis from the Global Burden of Disease Study 2013.* Lancet Infect Dis, 2016. **16**(6): p. 712-723.
23. Zeng, Z., et al., *Global, regional, and national dengue burden from 1990 to 2017: A systematic analysis based on the global burden of disease study 2017.* EClinicalMedicine, 2021. **32**: p. 100712.
24. Bhatt, S., et al., *The global distribution and burden of dengue.* Nature, 2013. **496**(7446): p. 504-7.
25. Leung, X.Y., et al., *A systematic review of dengue outbreak prediction models: Current scenario and future directions.* PLoS Negl Trop Dis, 2023. **17**(2): p. e0010631.
26. Brady, O.J., et al., *Refining the global spatial limits of dengue virus transmission by evidence-based consensus.* PLoS Negl Trop Dis, 2012. **6**(8): p. e1760.

27. World-Health-Organization. *Disease Outbreak News; Dengue – Global situation*. (21 December 2023).
28. Ilic, I. and M. Ilic, *Global Patterns of Trends in Incidence and Mortality of Dengue, 1990-2019: An Analysis Based on the Global Burden of Disease Study.* Medicina (Kaunas), 2024. **60**(3).
29. Laverdeur, J., et al., *Dengue and chikungunya: future threats for Northern Europe?* Front Epidemiol, 2024. **4**: p. 1342723.
30. Akter, R., et al., *Spatial and temporal analysis of dengue infections in Queensland, Australia: Recent trend and perspectives.* PLoS One, 2019. **14**(7): p. e0220134.
31. Ryan, S.J., et al., *Global expansion and redistribution of Aedes-borne virus transmission risk with climate change.* PLoS Negl Trop Dis, 2019. **13**(3): p. e0007213.
32. Vasilakis, N., et al., *Fever from the forest: prospects for the continued emergence of sylvatic dengue virus and its impact on public health.* Nat Rev Microbiol, 2011. **9**(7): p. 532-41.
33. World-Health-Organization, *Dengue haemorrhagic fever : diagnosis, treatment, prevention and control, 2nd ed.* 1997.
34. World-Health-Organization, in *Dengue: Guidelines for Diagnosis, Treatment, Prevention and Control: New Edition*. 2009: Geneva.
35. World-Health-Organization, *Fact Sheets; Dengue and Severe Dengue.* 17 March 2023.
36. Alejandria, M.M., *Dengue haemorrhagic fever or dengue shock syndrome in children.* BMJ Clin Evid, 2015. **2015**.
37. Rodriguez-Manzano, J., et al., *Improving Dengue Diagnostics and Management Through Innovative Technology.* Curr Infect Dis Rep, 2018. **20**(8): p. 25.
38. Calisher, C.H., et al., *Antigenic relationships between flaviviruses as determined by cross-neutralization tests with polyclonal antisera.* Journal of general virology, 1989. **70**(1): p. 37-43.
39. Mustafa, M.S., et al., *Discovery of fifth serotype of dengue virus (DENV-5): A new public health dilemma in dengue control.* Med J Armed Forces India, 2015. **71**(1): p. 67-70.
40. Frasca, F., et al., *An update on the entomology, virology, pathogenesis, and epidemiology status of West Nile and Dengue viruses in Europe (2018–2023).* Tropical Medicine and Infectious Disease, 2024. **9**(7): p. 166.
41. Fernandez-Garcia, L., et al., *The internal ribosome entry site of the Dengue virus mRNA is active when cap-dependent translation initiation is inhibited.* J Virol, 2021. **95**(5).
42. Song, Y., et al., *Dengue and Zika Virus 5′ Untranslated Regions Harbor Internal Ribosomal Entry Site Functions.* mBio, 2019. **10**(2).
43. Filomatori, C.V., et al., *A 5′ RNA element promotes dengue virus RNA synthesis on a circular genome.* Genes Dev, 2006. **20**(16): p. 2238-49.
44. Alvarez, D.E., et al., *Long-range RNA-RNA interactions circularize the dengue virus genome.* J Virol, 2005. **79**(11): p. 6631-43.
45. Slonchak, A. and A.A. Khromykh, *Subgenomic flaviviral RNAs: What do we know after the first decade of research.* Antiviral Res, 2018. **159**: p. 13-25.
46. Manzano, M., et al., *Identification of cis-acting elements in the 3′-untranslated region of the dengue virus type 2 RNA that modulate translation and replication.* J Biol Chem, 2011. **286**(25): p. 22521-34.
47. Filomatori, C.V., et al., *Dengue virus genomic variation associated with mosquito adaptation defines the pattern of viral non-coding RNAs and fitness in human cells.* PLoS Pathog, 2017. **13**(3): p. e1006265.
48. Yu, L. and L. Markoff, *The topology of bulges in the long stem of the flavivirus 3′ stem-loop is a major determinant of RNA replication competence.* Journal of virology, 2005. **79**(4): p. 2309-2324.
49. Ng, W.C., et al., *The 5′ and 3′ untranslated regions of the flaviviral genome.* Viruses, 2017. **9**(6): p. 137.
50. Nasar, S., N. Rashid, and S. Iftikhar, *Dengue proteins with their role in pathogenesis, and strategies for developing an effective anti-dengue treatment: A review.* Journal of medical virology, 2020. **92**(8): p. 941-955.
51. Zeidler, J.D., et al., *Non-Canonical Roles of Dengue Virus Non-Structural Proteins.* Viruses, 2017. **9**(3).
52. Zhang, S., et al., *Secretory pathways and multiple functions of nonstructural protein 1 in flavivirus infection.* Frontiers in immunology, 2023. **14**: p. 1205002.

53. Diosa-Toro, M., et al., *Role of RNA-binding proteins during the late stages of Flavivirus replication cycle.* Virology Journal, 2020. **17**: p. 1-14.
54. Byk, L.A. and A.V. Gamarnik, *Properties and Functions of the Dengue Virus Capsid Protein.* Annu Rev Virol, 2016. **3**(1): p. 263-281.
55. Ma, L., et al., *Solution structure of dengue virus capsid protein reveals another fold.* Proc Natl Acad Sci U S A, 2004. **101**(10): p. 3414-9.
56. Samsa, M.M., et al., *Dengue virus capsid protein usurps lipid droplets for viral particle formation.* PLoS Pathog, 2009. **5**(10): p. e1000632.
57. Iglesias, N.G., et al., *Dengue Virus Uses a Non-Canonical Function of the Host GBF1-Arf-COPI System for Capsid Protein Accumulation on Lipid Droplets.* Traffic, 2015. **16**(9): p. 962-77.
58. Westaway, E.G., et al., *Proteins C and NS4B of the flavivirus Kunjin translocate independently into the nucleus.* Virology, 1997. **234**(1): p. 31-41.
59. Mori, Y., et al., *Nuclear localization of Japanese encephalitis virus core protein enhances viral replication.* J Virol, 2005. **79**(6): p. 3448-58.
60. Oh, W., et al., *Jab1 mediates cytoplasmic localization and degradation of West Nile virus capsid protein.* J Biol Chem, 2006. **281**(40): p. 30166-74.
61. Bulich, R. and J.G. Aaskov, *Nuclear localization of dengue 2 virus core protein detected with monoclonal antibodies.* J Gen Virol, 1992. **73 (Pt 11)**: p. 2999-3003.
62. Wang, S.H., et al., *Intracellular localization and determination of a nuclear localization signal of the core protein of dengue virus.* J Gen Virol, 2002. **83**(Pt 12): p. 3093-3102.
63. Sangiambut, S., et al., *Multiple regions in dengue virus capsid protein contribute to nuclear localization during virus infection.* J Gen Virol, 2008. **89**(Pt 5): p. 1254-1264.
64. Colpitts, T.M., et al., *Dengue virus capsid protein binds core histones and inhibits nucleosome formation in human liver cells.* PloS one, 2011. **6**(9): p. e24365.
65. Pong, W.L., et al., *RNA binding property and RNA chaperone activity of dengue virus core protein and other viral RNA-interacting proteins.* FEBS Lett, 2011. **585**(16): p. 2575-81.
66. Barnard, T.R., et al., *Molecular Determinants of Flavivirus Virion Assembly.* Trends Biochem Sci, 2021. **46**(5): p. 378-390.
67. Mebus-Antunes, N.C., et al., *The interaction of dengue virus capsid protein with negatively charged interfaces drives the in vitro assembly of nucleocapsid-like particles.* PLoS One, 2022. **17**(3): p. e0264643.
68. Jablunovsky, A. and J. Jose, *The Dynamic Landscape of Capsid Proteins and Viral RNA Interactions in Flavivirus Genome Packaging and Virus Assembly.* Pathogens, 2024. **13**(2).
69. Li, L., et al., *The flavivirus precursor membrane-envelope protein complex: structure and maturation.* Science, 2008. **319**(5871): p. 1830-4.
70. Hsieh, S.C., et al., *Highly conserved residues in the helical domain of dengue virus type 1 precursor membrane protein are involved in assembly, precursor membrane (prM) protein cleavage, and entry.* J Biol Chem, 2014. **289**(48): p. 33149-60.
71. Yu, I.M., et al., *Association of the pr peptides with dengue virus at acidic pH blocks membrane fusion.* J Virol, 2009. **83**(23): p. 12101-7.
72. Dias, R.S., et al., *DENV-3 precursor membrane (prM) glycoprotein enhances E protein immunogenicity and confers protection against DENV-2 infections in a murine model.* Hum Vaccin Immunother, 2021. **17**(5): p. 1271-1277.
73. Yu, I.M., et al., *Structure of the immature dengue virus at low pH primes proteolytic maturation.* Science, 2008. **319**(5871): p. 1834-7.
74. Zhang, W., et al., *Visualization of membrane protein domains by cryo-electron microscopy of dengue virus.* Nat Struct Biol, 2003. **10**(11): p. 907-12.
75. Kuhn, R.J., et al., *Structure of dengue virus: implications for flavivirus organization, maturation, and fusion.* Cell, 2002. **108**(5): p. 717-25.
76. Kielian, M. and F.A. Rey, *Virus membrane-fusion proteins: more than one way to make a hairpin.* Nature Reviews Microbiology, 2006. **4**(1): p. 67-76.
77. Modis, Y., et al., *Structure of the dengue virus envelope protein after membrane fusion.* Nature, 2004. **427**(6972): p. 313-9.
78. Watterson, D., B. Kobe, and P.R. Young, *Residues in domain III of the dengue virus envelope glycoprotein involved in cell-surface glycosaminoglycan binding.* J Gen Virol, 2012. **93**(Pt 1): p. 72-82.

79. Crill, W.D. and J.T. Roehrig, *Monoclonal antibodies that bind to domain III of dengue virus E glycoprotein are the most efficient blockers of virus adsorption to Vero cells.* Journal of virology, 2001. **75**(16): p. 7769-7773.
80. Crill, W.D. and G.-J.J. Chang, *Localization and characterization of flavivirus envelope glycoprotein cross-reactive epitopes.* Journal of virology, 2004. **78**(24): p. 13975-13986.
81. Sánchez-González, G., et al., *Probability of consolidation constrains novel serotype emergence in dengue fever virus.* Plos one, 2021. **16**(4): p. e0248765.
82. Modis, Y., et al., *A ligand-binding pocket in the dengue virus envelope glycoprotein.* Proc Natl Acad Sci U S A, 2003. **100**(12): p. 6986-91.
83. Pokidysheva, E., et al., *Cryo-EM reconstruction of dengue virus in complex with the carbohydrate recognition domain of DC-SIGN.* Cell, 2006. **124**(3): p. 485-93.
84. Mondotte, J.A., et al., *Essential role of dengue virus envelope protein N glycosylation at asparagine-67 during viral propagation.* J Virol, 2007. **81**(13): p. 7136-48.
85. Alen, M.M., et al., *Crucial role of the N-glycans on the viral E-envelope glycoprotein in DC-SIGN-mediated dengue virus infection.* Antiviral research, 2012. **96**(3): p. 280-287.
86. Zhang, Y., et al., *Conformational changes of the flavivirus E glycoprotein.* Structure, 2004. **12**(9): p. 1607-1618.
87. Klein, D.E., J.L. Choi, and S.C. Harrison, *Structure of a dengue virus envelope protein late-stage fusion intermediate.* J Virol, 2013. **87**(4): p. 2287-93.
88. Roby, J.A., et al., *Post-translational regulation and modifications of flavivirus structural proteins.* Journal of General Virology, 2015. **96**(Pt_7): p. 1551-1569.
89. Zheng, A., M. Umashankar, and M. Kielian, *In vitro and in vivo studies identify important features of dengue virus pr-E protein interactions.* PLoS pathogens, 2010. **6**(10): p. e1001157.
90. Winkler, G., et al., *Evidence that the mature form of the flavivirus nonstructural protein NS1 is a dimer.* Virology, 1988. **162**(1): p. 187-96.
91. Winkler, G., et al., *Newly synthesized dengue-2 virus nonstructural protein NS1 is a soluble protein but becomes partially hydrophobic and membrane-associated after dimerization.* Virology, 1989. **171**(1): p. 302-5.
92. Akey, D.L., et al., *Flavivirus NS1 structures reveal surfaces for associations with membranes and the immune system.* Science, 2014. **343**(6173): p. 881-5.
93. Mackenzie, J.M., M.K. Jones, and P.R. Young, *Immunolocalization of the dengue virus nonstructural glycoprotein NS1 suggests a role in viral RNA replication.* Virology, 1996. **220**(1): p. 232-40.
94. Eyre, N.S., et al., *Genome-Wide Mutagenesis of Dengue Virus Reveals Plasticity of the NS1 Protein and Enables Generation of Infectious Tagged Reporter Viruses.* J Virol, 2017. **91**(23).
95. Muller, D.A. and P.R. Young, *The flavivirus NS1 protein: molecular and structural biology, immunology, role in pathogenesis and application as a diagnostic biomarker.* Antiviral research, 2013. **98**(2): p. 192-208.
96. Glasner, D.R., et al., *The Good, the Bad, and the Shocking: The Multiple Roles of Dengue Virus Nonstructural Protein 1 in Protection and Pathogenesis.* Annu Rev Virol, 2018. **5**(1): p. 227-253.
97. Scaturro, P., et al., *Dengue virus non-structural protein 1 modulates infectious particle production via interaction with the structural proteins.* PLoS pathogens, 2015. **11**(11): p. e1005277.
98. Flamand, M., et al., *Dengue virus type 1 nonstructural glycoprotein NS1 is secreted from mammalian cells as a soluble hexamer in a glycosylation-dependent fashion.* J Virol, 1999. **73**(7): p. 6104-10.
99. Gutsche, I., et al., *Secreted dengue virus nonstructural protein NS1 is an atypical barrel-shaped high-density lipoprotein.* Proc Natl Acad Sci U S A, 2011. **108**(19): p. 8003-8.
100. Shu, B., et al., *CryoEM structures of the multimeric secreted NS1, a major factor for dengue hemorrhagic fever.* Nat Commun, 2022. **13**(1): p. 6756.
101. Pan, Q., et al., *The step-by-step assembly mechanism of secreted flavivirus NS1 tetramer and hexamer captured at atomic resolution.* Science advances, 2024. **10**(18): p. eadm8275.
102. Carpio, K.L. and A.D. Barrett, *Flavivirus NS1 and its potential in vaccine development.* Vaccines, 2021. **9**(6): p. 622.

103. Falgout, B. and L. Markoff, *Evidence that flavivirus NS1-NS2A cleavage is mediated by a membrane-bound host protease in the endoplasmic reticulum.* Journal of virology, 1995. **69**(11): p. 7232-7243.
104. Xie, X., et al., *Membrane topology and function of dengue virus NS2A protein.* J Virol, 2013. **87**(8): p. 4609-22.
105. Nemésio, H. and J. Villalaín, *Membrane interacting regions of Dengue virus NS2A protein.* The journal of physical chemistry B, 2014. **118**(34): p. 10142-10155.
106. Shrivastava, G., et al., *NS2A comprises a putative viroporin of Dengue virus 2.* Virulence, 2017. **8**(7): p. 1450-1456.
107. Mackenzie, J.M., et al., *Subcellular localization and some biochemical properties of the flavivirus Kunjin nonstructural proteins NS2A and NS4A.* Virology, 1998. **245**(2): p. 203-215.
108. Wu, R.-H., et al., *Scanning mutagenesis studies reveal a potential intramolecular interaction within the C-terminal half of dengue virus NS2A involved in viral RNA replication and virus assembly and secretion.* Journal of virology, 2015. **89**(8): p. 4281-4295.
109. Xie, X., et al., *Two distinct sets of NS2A molecules are responsible for dengue virus RNA synthesis and virion assembly.* J Virol, 2015. **89**(2): p. 1298-313.
110. Xie, X., et al., *Dengue NS2A Protein Orchestrates Virus Assembly.* Cell Host Microbe, 2019. **26**(5): p. 606-622 e8.
111. Dalrymple, N.A., V. Cimica, and E.R. Mackow, *Dengue Virus NS Proteins Inhibit RIG-I/MAVS Signaling by Blocking TBK1/IRF3 Phosphorylation: Dengue Virus Serotype 1 NS4A Is a Unique Interferon-Regulating Virulence Determinant.* mBio, 2015. **6**(3): p. e00553-15.
112. Li, Y., et al., *Membrane topology of NS2B of dengue virus revealed by NMR spectroscopy.* Biochimica et Biophysica Acta (BBA)-Biomembranes, 2015. **1848**(10): p. 2244-2252.
113. Leung, D., et al., *Activity of recombinant dengue 2 virus NS3 protease in the presence of a truncated NS2B co-factor, small peptide substrates, and inhibitors.* Journal of Biological Chemistry, 2001. **276**(49): p. 45762-45771.
114. Kim, Y.M., et al., *NMR analysis of a novel enzymatically active unlinked dengue NS2B-NS3 protease complex.* Journal of Biological Chemistry, 2013. **288**(18): p. 12891-12900.
115. Zuo, Z., et al., *Mechanism of NS2B-mediated activation of NS3pro in dengue virus: molecular dynamics simulations and bioassays.* Journal of virology, 2009. **83**(2): p. 1060-1070.
116. Falgout, B., et al., *Both nonstructural proteins NS2B and NS3 are required for the proteolytic processing of dengue virus nonstructural proteins.* J Virol, 1991. **65**(5): p. 2467-75.
117. Cahour, A., B. Falgout, and C.-J. Lai, *Cleavage of the dengue virus polyprotein at the NS3/NS4A and NS4B/NS5 junctions is mediated by viral protease NS2B-NS3, whereas NS4A/NS4B may be processed by a cellular protease.* Journal of virology, 1992. **66**(3): p. 1535-1542.
118. Aguirre, S., et al., *DENV inhibits type I IFN production in infected cells by cleaving human STING.* 2012.
119. Yu, C.-Y., et al., *Dengue virus targets the adaptor protein MITA to subvert host innate immunity.* PLoS pathogens, 2012. **8**(6): p. e1002780.
120. Aguirre, S., et al., *Dengue virus NS2B protein targets cGAS for degradation and prevents mitochondrial DNA sensing during infection.* Nat Microbiol, 2017. **2**: p. 17037.
121. Luo, D., et al., *Crystal structure of the NS3 protease-helicase from dengue virus.* Journal of virology, 2008. **82**(1): p. 173-183.
122. Xu, T., et al., *Structure of the Dengue virus helicase/nucleoside triphosphatase catalytic domain at a resolution of 2.4 A.* Journal of virology, 2005. **79**(16): p. 10278-10288.
123. Palacios-Rápalo, S.N., et al., *Nuclear localization of non-structural protein 3 (NS3) during dengue virus infection.* Archives of Virology, 2021. **166**: p. 1439-1446.
124. Luo, D., et al., *Flexibility between the protease and helicase domains of the dengue virus NS3 protein conferred by the linker region and its functional implications.* Journal of biological chemistry, 2010. **285**(24): p. 18817-18827.
125. Luo, D., et al., *Insights into RNA unwinding and ATP hydrolysis by the flavivirus NS3 protein.* The EMBO journal, 2008. **27**(23): p. 3209-3219.
126. Sampath, A., et al., *Structure-based mutational analysis of the NS3 helicase from dengue virus.* Journal of virology, 2006. **80**(13): p. 6686-6690.

127. Bartelma, G. and R. Padmanabhan, *Expression, purification, and characterization of the RNA 5'-triphosphatase activity of dengue virus type 2 nonstructural protein 3.* Virology, 2002. **299**(1): p. 122-132.
128. Chan, Y.K. and M.U. Gack, *A phosphomimetic-based mechanism of dengue virus to antagonize innate immunity.* Nature immunology, 2016. **17**(5): p. 523-530.
129. Miller, S., et al., *The non-structural protein 4A of dengue virus is an integral membrane protein inducing membrane alterations in a 2K-regulated manner.* J Biol Chem, 2007. **282**(12): p. 8873-82.
130. Lin, C., et al., *Cleavage at a novel site in the NS4A region by the yellow fever virus NS2B-3 proteinase is a prerequisite for processing at the downstream 4A/4B signalase site.* Journal of virology, 1993. **67**(4): p. 2327-2335.
131. Li, Y., et al., *Secondary structure and membrane topology of dengue virus NS4A protein in micelles.* Biochimica et Biophysica Acta (BBA)-Biomembranes, 2018. **1860**(2): p. 442-450.
132. Hung, Y.-F., et al., *Amino terminal region of dengue virus NS4A cytosolic domain binds to highly curved liposomes.* Viruses, 2015. **7**(7): p. 4119-4130.
133. Roosendaal, J., et al., *Regulated cleavages at the West Nile virus NS4A-2K-NS4B junctions play a major role in rearranging cytoplasmic membranes and Golgi trafficking of the NS4A protein.* Journal of virology, 2006. **80**(9): p. 4623-4632.
134. Teo, C.S.H. and J.J.H. Chu, *Cellular vimentin regulates construction of dengue virus replication complexes through interaction with NS4A protein.* Journal of virology, 2014. **88**(4): p. 1897-1913.
135. Aktepe, T.E., et al., *The host protein reticulon 3.1 A is utilized by flaviviruses to facilitate membrane remodelling.* Cell reports, 2017. **21**(6): p. 1639-1654.
136. He, Z., et al., *Dengue virus subverts host innate immunity by targeting adaptor protein MAVS.* Journal of virology, 2016. **90**(16): p. 7219-7230.
137. Li, Y., et al., *Secondary structure and membrane topology of the full-length dengue virus NS4B in micelles.* Angewandte Chemie, 2016. **128**(39): p. 12247-12251.
138. Miller, S., S. Sparacio, and R. Bartenschlager, *Subcellular localization and membrane topology of the dengue virus type 2 non-structural protein 4B.* Journal of Biological Chemistry, 2006. **281**(13): p. 8854-8863.
139. Naik, N.G. and H.-N. Wu, *Mutation of putative N-glycosylation sites on dengue virus NS4B decreases RNA replication.* Journal of Virology, 2015. **89**(13): p. 6746-6760.
140. Chatel-Chaix, L., et al., *A combined genetic-proteomic approach identifies residues within dengue virus NS4B critical for interaction with NS3 and viral replication.* Journal of virology, 2015. **89**(14): p. 7170-7186.
141. Zou, J., et al., *Characterization of dengue virus NS4A and NS4B protein interaction.* Journal of virology, 2015. **89**(7): p. 3455-3470.
142. Umareddy, I., et al., *Dengue virus NS4B interacts with NS3 and dissociates it from single-stranded RNA.* J Gen Virol, 2006. **87**(Pt 9): p. 2605-2614.
143. Zou, J., et al., *Mapping the interactions between the NS4B and NS3 proteins of dengue virus.* Journal of virology, 2015. **89**(7): p. 3471-3483.
144. Kundharapu, S. and T.K. Chowdary, *Dengue Virus NS4b N-Terminus Disordered Region Interacts with NS3 Helicase C-Terminal Subdomain to Enhance Helicase Activity.* Viruses, 2022. **14**(8).
145. Egloff, M.P., et al., *An RNA cap (nucleoside-2'-O-)-methyltransferase in the flavivirus RNA polymerase NS5: crystal structure and functional characterization.* The EMBO journal, 2002.
146. Sanford, T.J., et al., *Circularization of flavivirus genomic RNA inhibits de novo translation initiation.* Nucleic acids research, 2019. **47**(18): p. 9789-9802.
147. Daffis, S., et al., *2'-O methylation of the viral mRNA cap evades host restriction by IFIT family members.* Nature, 2010. **468**(7322): p. 452-456.
148. Yap, T.L., et al., *Crystal structure of the dengue virus RNA-dependent RNA polymerase catalytic domain at 1.85-angstrom resolution.* Journal of virology, 2007. **81**(9): p. 4753-4765.
149. Bujalowski, P.J., W. Bujalowski, and K.H. Choi, *Interactions between the dengue virus polymerase NS5 and stem-loop A.* Journal of virology, 2017. **91**(11): p. 10.1128/jvi. 00047-17.
150. Filomatori, C.V., et al., *RNA sequences and structures required for the recruitment and activity of the dengue virus polymerase.* J Biol Chem, 2011. **286**(9): p. 6929-39.

151. Cui, T., et al., *Recombinant dengue virus type 1 NS3 protein exhibits specific viral RNA binding and NTPase activity regulated by the NS5 protein.* Virology, 1998. **246**(2): p. 409-417.
152. Brand, C., M. Bisaillon, and B.J. Geiss, *Organization of the Flavivirus RNA replicase complex.* Wiley Interdisciplinary Reviews: RNA, 2017. **8**(6): p. e1437.
153. Tay, M.Y. and S.G. Vasudevan, *The transactions of NS3 and NS5 in flaviviral RNA replication.* Dengue and Zika: Control and Antiviral Treatment Strategies, 2018: p. 147-163.
154. Brooks, A.J., et al., *The interdomain region of dengue NS5 protein that binds to the viral helicase NS3 contains independently functional importin β1 and importin α/β-recognized nuclear localization signals.* Journal of Biological Chemistry, 2002. **277**(39): p. 36399-36407.
155. Kumar, A., et al., *Nuclear localization of dengue virus nonstructural protein 5 does not strictly correlate with efficient viral RNA replication and inhibition of type I interferon signaling.* Journal of virology, 2013. **87**(8): p. 4545-4557.
156. Hannemann, H., et al., *Serotype-specific differences in dengue virus non-structural protein 5 nuclear localization.* Journal of Biological Chemistry, 2013. **288**(31): p. 22621-22635.
157. Pryor, M.J., et al., *Nuclear localization of dengue virus nonstructural protein 5 Through Its Importin α/β–recognized nuclear localization sequences is integral to viral infection.* Traffic, 2007. **8**(7): p. 795-807.
158. Petit, M.J., et al., *Nuclear dengue virus NS5 antagonizes expression of PAF1-dependent immune response genes.* PLoS pathogens, 2021. **17**(11): p. e1010100.
159. De Maio, F.A., et al., *The dengue virus NS5 protein intrudes in the cellular spliceosome and modulates splicing.* PLoS pathogens, 2016. **12**(8): p. e1005841.
160. Mazzon, M., et al., *Dengue virus NS5 inhibits interferon-α signaling by blocking signal transducer and activator of transcription 2 phosphorylation.* The Journal of infectious diseases, 2009. **200**(8): p. 1261-1270.
161. Ashour, J., et al., *NS5 of dengue virus mediates STAT2 binding and degradation.* Journal of virology, 2009. **83**(11): p. 5408-5418.
162. Morrison, J., et al., *Dengue virus co-opts UBR4 to degrade STAT2 and antagonize type I interferon signaling.* PLoS pathogens, 2013. **9**(3): p. e1003265.
163. Begum, F., et al., *Insight into the tropism of dengue virus in humans.* Viruses, 2019. **11**(12): p. 1136.
164. Cruz-Oliveira, C., et al., *Receptors and routes of dengue virus entry into the host cells.* FEMS Microbiol Rev, 2015. **39**(2): p. 155-70.
165. Kim, S.Y., B. Li, and R.J. Linhardt, *Pathogenesis and inhibition of flaviviruses from a carbohydrate perspective.* Pharmaceuticals, 2017. **10**(2): p. 44.
166. Modhiran, N., et al., *Dual targeting of dengue virus virions and NS1 protein with the heparan sulfate mimic PG545.* Antiviral Res, 2019. **168**: p. 121-127.
167. Briant, L., et al., *Role of skin immune cells on the host susceptibility to mosquito-borne viruses.* Virology, 2014. **464**: p. 26-32.
168. Acosta, E.G., V. Castilla, and E.B. Damonte, *Alternative infectious entry pathways for dengue virus serotypes into mammalian cells.* Cell Microbiol, 2009. **11**(10): p. 1533-49.
169. Van Der Schaar, H.M., et al., *Dissecting the cell entry pathway of dengue virus by single-particle tracking in living cells.* PLoS pathogens, 2008. **4**(12): p. e1000244.
170. Acosta, E.G., V. Castilla, and E.B. Damonte, *Differential requirements in endocytic trafficking for penetration of dengue virus.* 2012.
171. Smit, J.M., et al., *Flavivirus cell entry and membrane fusion.* Viruses, 2011. **3**(2): p. 160-171.
172. Neufeldt, C.J., et al., *Rewiring cellular networks by members of the Flaviviridae family.* Nat Rev Microbiol, 2018. **16**(3): p. 125-142.
173. Welsch, S., et al., *Composition and three-dimensional architecture of the dengue virus replication and assembly sites.* Cell host & microbe, 2009. **5**(4): p. 365-375.
174. Keelapang, P., et al., *Alterations of pr-M cleavage and virus export in pr-M junction chimeric dengue viruses.* Journal of virology, 2004. **78**(5): p. 2367-2381.
175. Brandt, W.E., R.D. Cardiff, and P.K. Russell, *Dengue virions and antigens in brain and serum of infected mice.* J Virol, 1970. **6**(4): p. 500-6.
176. Rice, C.M., et al., *Nucleotide sequence of yellow fever virus: implications for flavivirus gene expression and evolution.* Science, 1985. **229**(4715): p. 726-33.

177. Song, H., et al., *Zika virus NS1 structure reveals diversity of electrostatic surfaces among flaviviruses.* Nat Struct Mol Biol, 2016. **23**(5): p. 456-8.
178. Falgout, B., R. Chanock, and C.J. Lai, *Proper processing of dengue virus nonstructural glycoprotein NS1 requires the N-terminal hydrophobic signal sequence and the downstream nonstructural protein NS2a.* J Virol, 1989. **63**(5): p. 1852-60.
179. Nowak, T., et al., *Analyses of the terminal sequences of West Nile virus structural proteins and of the in vitro translation of these proteins allow the proposal of a complete scheme of the proteolytic cleavages involved in their synthesis.* Virology, 1989. **169**(2): p. 365-376.
180. Hori, H. and C.J. Lai, *Cleavage of dengue virus NS1-NS2A requires an octapeptide sequence at the C terminus of NS1.* J Virol, 1990. **64**(9): p. 4573-7.
181. Wallis, T.P., et al., *Determination of the disulfide bond arrangement of dengue virus NS1 protein.* Journal of Biological Chemistry, 2004. **279**(20): p. 20729-20741.
182. Pryor, M.J. and P.J. Wright, *The effects of site-directed mutagenesis on the dimerization and secretion of the NS1 protein specified by dengue virus.* Virology, 1993. **194**(2): p. 769-780.
183. Akey, D.L., et al., *Structure-guided insights on the role of NS1 in flavivirus infection.* Bioessays, 2015. **37**(5): p. 489-94.
184. Lindenbach, B.D. and C.M. Rice, *trans-Complementation of yellow fever virus NS1 reveals a role in early RNA replication.* J Virol, 1997. **71**(12): p. 9608-17.
185. Muylaert, I.R., R. Galler, and C.M. Rice, *Genetic analysis of the yellow fever virus NS1 protein: identification of a temperature-sensitive mutation which blocks RNA accumulation.* J Virol, 1997. **71**(1): p. 291-8.
186. Khromykh, A.A., P.L. Sedlak, and E.G. Westaway, *cis- and trans-acting elements in flavivirus RNA replication.* J Virol, 2000. **74**(7): p. 3253-63.
187. Youn, S., et al., *Non-structural protein-1 is required for West Nile virus replication complex formation and viral RNA synthesis.* Virol J, 2013. **10**: p. 339.
188. Ci, Y., et al., *Zika NS1-induced ER remodeling is essential for viral replication.* J Cell Biol, 2020. **219**(2).
189. Tan, B.E.K., M.R. Beard, and N.S. Eyre, *Identification of Key Residues in Dengue Virus NS1 Protein That Are Essential for Its Secretion.* Viruses, 2023. **15**(5).
190. Lindenbach, B.D. and C.M. Rice, *Genetic interaction of flavivirus nonstructural proteins NS1 and NS4A as a determinant of replicase function.* J Virol, 1999. **73**(6): p. 4611-21.
191. Youn, S., et al., *Evidence for a genetic and physical interaction between nonstructural proteins NS1 and NS4B that modulates replication of West Nile virus.* J Virol, 2012. **86**(13): p. 7360-71.
192. Plaszczyca, A., et al., *A novel interaction between dengue virus nonstructural protein 1 and the NS4A-2K-4B precursor is required for viral RNA replication but not for formation of the membranous replication organelle.* PLoS Pathog, 2019. **15**(5): p. e1007736.
193. Rice, C.M., et al., *Partial N-terminal amino acid sequences of three nonstructural proteins of two flaviviruses.* Virology, 1986. **151**(1): p. 1-9.
194. Lee, J.M., A.J. Crooks, and J.R. Stephenson, *The synthesis and maturation of a non-structural extracellular antigen from tick-borne encephalitis virus and its relationship to the intracellular NS1 protein.* Journal of general virology, 1989. **70**(2): p. 335-343.
195. Mason, P.W., *Maturation of Japanese encephalitis virus glycoproteins produced by infected mammalian and mosquito cells.* Virology, 1989. **169**(2): p. 354-364.
196. Westaway, E.G. and M.R. Goodman, *Variation in distribution of the three flavivirus-specified glycoproteins detected by immunofluorescence in infected Vero cells.* Arch Virol, 1987. **94**(3-4): p. 215-28.
197. Jacobs, M.G., et al., *Dengue virus nonstructural protein 1 is expressed in a glycosyl-phosphatidylinositol-linked form that is capable of signal transduction.* FASEB J, 2000. **14**(11): p. 1603-10.
198. Noisakran, S., et al., *Association of dengue virus NS1 protein with lipid rafts.* J Gen Virol, 2008. **89**(Pt 10): p. 2492-2500.
199. Avirutnan, P., et al., *Vascular leakage in severe dengue virus infections: a potential role for the nonstructural viral protein NS1 and complement.* J Infect Dis, 2006. **193**(8): p. 1078-88.
200. Chung, K.M., et al., *Antibody recognition of cell surface-associated NS1 triggers Fc-γ receptor-mediated phagocytosis and clearance of West Nile virus-infected cells.* Journal of virology, 2007. **81**(17): p. 9551-9555.

201. Alcala, A.C., et al., *The dengue virus non-structural protein 1 (NS1) is secreted efficiently from infected mosquito cells.* Virology, 2016. **488**: p. 278-87.
202. Alcon, S., et al., *Enzyme-linked immunosorbent assay specific to Dengue virus type 1 nonstructural protein NS1 reveals circulation of the antigen in the blood during the acute phase of disease in patients experiencing primary or secondary infections.* J Clin Microbiol, 2002. **40**(2): p. 376-81.
203. Young, P.R., et al., *An antigen capture enzyme-linked immunosorbent assay reveals high levels of the dengue virus protein NS1 in the sera of infected patients.* J Clin Microbiol, 2000. **38**(3): p. 1053-7.
204. Libraty, D.H., et al., *High circulating levels of the dengue virus nonstructural protein NS1 early in dengue illness correlate with the development of dengue hemorrhagic fever.* J Infect Dis, 2002. **186**(8): p. 1165-8.
205. Fisher, R., et al., *The Role of NS1 Protein in the Diagnosis of Flavivirus Infections.* Viruses, 2023. **15**(2).
206. Ghetia, C., P. Bhatt, and C. Mukhopadhyay, *Association of dengue virus non-structural-1 protein with disease severity: a brief review.* Transactions of The Royal Society of Tropical Medicine and Hygiene, 2022. **116**(11): p. 986-995.
207. Conde, J.N., et al., *The complement system in flavivirus infections.* Frontiers in microbiology, 2017. **8**: p. 213.
208. Puerta-Guardo, H., et al., *Flavivirus NS1 Triggers Tissue-Specific Vascular Endothelial Dysfunction Reflecting Disease Tropism.* Cell Rep, 2019. **26**(6): p. 1598-1613 e8.
209. Avirutnan, P., et al., *Secreted NS1 of dengue virus attaches to the surface of cells via interactions with heparan sulfate and chondroitin sulfate E.* PLoS Pathog, 2007. **3**(11): p. e183.
210. Modhiran, N., et al., *Dengue virus NS1 protein activates cells via Toll-like receptor 4 and disrupts endothelial cell monolayer integrity.* Sci Transl Med, 2015. **7**(304): p. 304ra142.
211. Puerta-Guardo, H., D.R. Glasner, and E. Harris, *Dengue Virus NS1 Disrupts the Endothelial Glycocalyx, Leading to Hyperpermeability.* PLoS Pathog, 2016. **12**(7): p. e1005738.
212. Muller, D.A., et al., *Structure of the dengue virus glycoprotein non-structural protein 1 by electron microscopy and single-particle analysis.* J Gen Virol, 2012. **93**(Pt 4): p. 771-779.
213. Pryor, M.J. and P.J. Wright, *Glycosylation mutants of dengue virus NS1 protein.* J Gen Virol, 1994. **75 (Pt 5)**: p. 1183-7.
214. Pryor, M.J., et al., *Growth restriction of dengue virus type 2 by site-specific mutagenesis of virus-encoded glycoproteins.* J Gen Virol, 1998. **79 (Pt 11)**: p. 2631-9.
215. Crabtree, M.B., R.M. Kinney, and B.R. Miller, *Deglycosylation of the NS1 protein of dengue 2 virus, strain 16681: construction and characterization of mutant viruses.* Arch Virol, 2005. **150**(4): p. 771-86.
216. Tajima, S., T. Takasaki, and I. Kurane, *Characterization of Asn130-to-Ala mutant of dengue type 1 virus NS1 protein.* Virus Genes, 2008. **36**(2): p. 323-9.
217. Fan, J., Y. Liu, and Z. Yuan, *Critical role of Dengue Virus NS1 protein in viral replication.* Virol Sin, 2014. **29**(3): p. 162-9.
218. Somnuke, P., et al., *N-linked glycosylation of dengue virus NS1 protein modulates secretion, cell-surface expression, hexamer stability, and interactions with human complement.* Virology, 2011. **413**(2): p. 253-64.
219. Wang, C., et al., *Endocytosis of flavivirus NS1 is required for NS1-mediated endothelial hyperpermeability and is abolished by a single N-glycosylation site mutation.* PLoS Pathog, 2019. **15**(7): p. e1007938.
220. Post, P.R., R. Carvalho, and R. Galler, *Glycosylation and secretion of yellow fever virus nonstmctural protein NS1.* Virus research, 1991. **18**(2-3): p. 291-302.
221. Smith, G.W. and P.J. Wright, *Synthesis of proteins and glycoproteins in dengue type 2 virus-infected vero and Aedes albopictus cells.* Journal of General Virology, 1985. **66**(3): p. 559-571.
222. Hafirassou, M.L., et al., *A global interactome map of the dengue virus NS1 identifies virus restriction and dependency host factors.* Cell reports, 2017. **21**(13): p. 3900-3913.
223. Jacobs, S., J. Stephenson, and G. Wilkinson, *High-level expression of the tick-borne encephalitis virus NS1 protein by using an adenovirus-based vector: protection elicited in a murine model.* Journal of virology, 1992. **66**(4): p. 2086-2095.

224. Desprès, P., M. Girard, and M. Bouloy, *Characterization of yellow fever virus proteins E and NS1 expressed in Vero and Spodoptera frugiperda cells.* Journal of general virology, 1991. **72**(6): p. 1331-1342.
225. Flamand, M., V. Deubel, and M. Girard, *Expression and secretion of Japanese encephalitis virus nonstructural protein NS1 by insect cells using a recombinant baculovirus.* Virology, 1992. **191**(2): p. 826-836.
226. Coelho, D.R., et al., *ApoA1 Neutralizes Proinflammatory Effects of Dengue Virus NS1 Protein and Modulates Viral Immune Evasion.* J Virol, 2021. **95**(13): p. e0197420.
227. Benfrid, S., et al., *Dengue virus NS1 protein conveys pro-inflammatory signals by docking onto high-density lipoproteins.* EMBO Rep, 2022. **23**(7): p. e53600.
228. Chew, B.L.A., et al., *Secreted dengue virus NS1 from infection is predominantly dimeric and in complex with high-density lipoprotein.* Elife, 2024. **12**: p. RP90762.
229. Chew, B.L.A., et al., *Structural basis of Zika virus NS1 multimerization and human antibody recognition.* npj Viruses, 2024. **2**(1): p. 14.
230. Watterson, D., N. Modhiran, and P.R. Young, *The many faces of the flavivirus NS1 protein offer a multitude of options for inhibitor design.* Antiviral research, 2016. **130**: p. 7-18.
231. Alcalá, A.C., L.A. Palomares, and J.E. Ludert, *Secretion of nonstructural protein 1 of dengue virus from infected mosquito cells: facts and speculations.* Journal of virology, 2018. **92**(14): p. 10.1128/jvi. 00275-18.
232. Perera, D.R., et al., *Roles of NS1 Protein in Flavivirus Pathogenesis.* ACS Infectious Diseases, 2023. **10**(1): p. 20-56.
233. Alcala, A.C., et al., *Dengue Virus NS1 Uses Scavenger Receptor B1 as a Cell Receptor in Cultured Cells.* J Virol, 2022. **96**(5): p. e0166421.
234. Chen, H.-R., Y.-C. Lai, and T.-M. Yeh, *Dengue virus non-structural protein 1: a pathogenic factor, therapeutic target, and vaccine candidate.* Journal of biomedical science, 2018. **25**: p. 1-11.
235. Falconar, A.K., *Antibody responses are generated to immunodominant ELK/KLE-type motifs on the nonstructural-1 glycoprotein during live dengue virus infections in mice and humans: implications for diagnosis, pathogenesis, and vaccine design.* Clin Vaccine Immunol, 2007. **14**(5): p. 493-504.
236. Lin, C.-F., et al., *Liver injury caused by antibodies against dengue virus nonstructural protein 1 in a murine model.* Laboratory investigation, 2008. **88**(10): p. 1079-1089.
237. Sun, D.S., et al., *Antiplatelet autoantibodies elicited by dengue virus non-structural protein 1 cause thrombocytopenia and mortality in mice.* Journal of Thrombosis and Haemostasis, 2007. **5**(11): p. 2291-2299.
238. Lin, Y.-S., et al., *Molecular mimicry between virus and host and its implications for dengue disease pathogenesis.* Experimental Biology and Medicine, 2011. **236**(5): p. 515-523.
239. Lin, C.F., et al., *Antibodies from dengue patient sera cross-react with endothelial cells and induce damage.* J Med Virol, 2003. **69**(1): p. 82-90.
240. Cheng, H.-J., et al., *Anti-dengue virus nonstructural protein 1 antibodies recognize protein disulfide isomerase on platelets and inhibit platelet aggregation.* Molecular immunology, 2009. **47**(2-3): p. 398-406.
241. Cheng, H.J., et al., *Correlation between serum levels of anti-endothelial cell autoantigen and anti-dengue virus nonstructural protein 1 antibodies in dengue patients.* Am J Trop Med Hyg, 2015. **92**(5): p. 989-95.
242. Schlesinger, J.J., M.W. Brandriss, and E.E. Walsh, *Protection of mice against dengue 2 virus encephalitis by immunization with the dengue 2 virus non-structural glycoprotein NS1.* J Gen Virol, 1987. **68 (Pt 3)**: p. 853-7.
243. Zhang, Y.-M., et al., *Immunization of mice with dengue structural proteins and nonstructural protein NS1 expressed by baculovirus recombinant induces resistance to dengue virus encephalitis.* Journal of virology, 1988. **62**(8): p. 3027-3031.
244. Henchal, E., L. Henchal, and J. Schlesinger, *Synergistic interactions of anti-NS1 monoclonal antibodies protect passively immunized mice from lethal challenge with dengue 2 virus.* Journal of General Virology, 1988. **69**(8): p. 2101-2107.
245. Calvert, A.E., et al., *Non-structural proteins of dengue 2 virus offer limited protection to interferon-deficient mice after dengue 2 virus challenge.* Journal of General Virology, 2006. **87**(2): p. 339-346.

246. Beatty, P.R., et al., *Dengue virus NS1 triggers endothelial permeability and vascular leak that is prevented by NS1 vaccination.* Sci Transl Med, 2015. **7**(304): p. 304ra141.
247. Cheng, H.-J., et al., *Proteomic Analysis of Endothelial Cell Autoantigens Recognized by Anti-Dengue Virus Nonstructural Protein 1 Antibodies.* Experimental Biology and Medicine, 2009. **234**(1): p. 63-73.
248. Chen, M.-C., et al., *Deletion of the C-Terminal Region of Dengue Virus Nonstructural Protein 1 (NS1) Abolishes Anti-NS1-Mediated Platelet Dysfunction and Bleeding Tendency1.* The Journal of Immunology, 2009. **183**(3): p. 1797-1803.
249. Wan, S.W., et al., *Protection against dengue virus infection in mice by administration of antibodies against modified nonstructural protein 1.* PLoS One, 2014. **9**(3): p. e92495.
250. Hajishengallis, G., et al., *Novel mechanisms and functions of complement.* Nature immunology, 2017. **18**(12): p. 1288-1298.
251. Sarma, J.V. and P.A. Ward, *The complement system.* Cell and tissue research, 2011. **343**(1): p. 227-235.
252. Avirutnan, P., E. Mehlhop, and M.S. Diamond, *Complement and its role in protection and pathogenesis of flavivirus infections.* Vaccine, 2008. **26**: p. I100-I107.
253. Carr, J.M., et al., *Dengue virus and the complement alternative pathway.* FEBS letters, 2020. **594**(16): p. 2543-2555.
254. Avirutnan, P., et al., *Antagonism of the complement component C4 by flavivirus nonstructural protein NS1.* J Exp Med, 2010. **207**(4): p. 793-806.
255. Avirutnan, P., et al., *Complement-mediated neutralization of dengue virus requires mannose-binding lectin. mBio 2: e00276-11*. 2011, Published.
256. Thiemmeca, S., et al., *Secreted NS1 Protects Dengue Virus from Mannose-Binding Lectin-Mediated Neutralization.* J Immunol, 2016. **197**(10): p. 4053-4065.
257. Avirutnan, P., et al., *Binding of flavivirus nonstructural protein NS1 to C4b binding protein modulates complement activation.* J Immunol, 2011. **187**(1): p. 424-33.
258. Conde, J.N., et al., *Inhibition of the Membrane Attack Complex by Dengue Virus NS1 through Interaction with Vitronectin and Terminal Complement Proteins.* J Virol, 2016. **90**(21): p. 9570-9581.
259. Chakravarti, A. and R. Kumaria, *Circulating levels of tumour necrosis factor-alpha & interferon-gamma in patients with dengue & dengue haemorrhagic fever during an outbreak.* Indian J Med Res, 2006. **123**(1): p. 25-30.
260. Priyadarshini, D., et al., *Clinical findings and pro-inflammatory cytokines in dengue patients in Western India: a facility-based study.* PLoS One, 2010. **5**(1): p. e8709.
261. Malavige, G.N., et al., *Cellular and cytokine correlates of severe dengue infection.* PLoS One, 2012. **7**(11): p. e50387.
262. Tramontini Gomes de Sousa Cardozo, F., et al., *Serum from dengue virus-infected patients with and without plasma leakage differentially affects endothelial cells barrier function in vitro.* PLoS One, 2017. **12**(6): p. e0178820.
263. Rothman, A.L., *Immunity to dengue virus: a tale of original antigenic sin and tropical cytokine storms.* Nature Reviews Immunology, 2011. **11**(8): p. 532-543.
264. Chen, H.R., et al., *Dengue Virus Nonstructural Protein 1 Induces Vascular Leakage through Macrophage Migration Inhibitory Factor and Autophagy.* PLoS Negl Trop Dis, 2016. **10**(7): p. e0004828.
265. Chao, C.-H., et al., *Dengue virus nonstructural protein 1 activates platelets via Toll-like receptor 4, leading to thrombocytopenia and hemorrhage.* PLoS pathogens, 2019. **15**(4): p. e1007625.
266. Quirino-Teixeira, A.C., et al., *Inflammatory signaling in dengue-infected platelets requires translation and secretion of nonstructural protein 1.* Blood advances, 2020. **4**(9): p. 2018-2031.
267. Hottz, E.D., et al., *Platelets mediate increased endothelium permeability in dengue through NLRP3-inflammasome activation.* Blood, The Journal of the American Society of Hematology, 2013. **122**(20): p. 3405-3414.
268. Kar, M., et al. *Dengue virus entry and replication does not lead to productive infection in platelets*. in *Open forum infectious diseases*. 2017. Oxford University Press US.
269. Alayli, F. and F. Scholle, *Dengue virus NS1 enhances viral replication and pro-inflammatory cytokine production in human dendritic cells.* Virology, 2016. **496**: p. 227-236.

270. Barbachano-Guerrero, A., T.P. Endy, and C.A. King, *Dengue virus non-structural protein 1 activates the p38 MAPK pathway to decrease barrier integrity in primary human endothelial cells.* J Gen Virol, 2020. **101**(5): p. 484-496.
271. Glasner, D.R., et al., *Dengue virus NS1 cytokine-independent vascular leak is dependent on endothelial glycocalyx components.* PLoS pathogens, 2017. **13**(11): p. e1006673.
272. Wills, B.A., et al., *Size and charge characteristics of the protein leak in dengue shock syndrome.* J Infect Dis, 2004. **190**(4): p. 810-8.
273. Suwarto, S., et al., *Association of Endothelial Glycocalyx and Tight and Adherens Junctions With Severity of Plasma Leakage in Dengue Infection.* J Infect Dis, 2017. **215**(6): p. 992-999.
274. Pan, P., et al., *DENV NS1 and MMP-9 cooperate to induce vascular leakage by altering endothelial cell adhesion and tight junction.* PLoS Pathog, 2021. **17**(7): p. e1008603.
275. Puerta-Guardo, H., et al., *Flavivirus NS1 Triggers Tissue-Specific Disassembly of Intercellular Junctions Leading to Barrier Dysfunction and Vascular Leak in a GSK-3beta-Dependent Manner.* Pathogens, 2022. **11**(6).
276. Carroll, S.B., *Homeotic genes and the evolution of arthropods and chordates.* Nature, 1995. **376**(6540): p. 479-485.
277. Alcon-LePoder, S., et al., *The secreted form of dengue virus nonstructural protein NS1 is endocytosed by hepatocytes and accumulates in late endosomes: implications for viral infectivity.* J Virol, 2005. **79**(17): p. 11403-11.
278. Liu, J., et al., *Flavivirus NS1 protein in infected host sera enhances viral acquisition by mosquitoes.* Nat Microbiol, 2016. **1**(9): p. 16087.
279. Chen, J., M.M.-L. Ng, and J.J.H. Chu, *Activation of TLR2 and TLR6 by dengue NS1 protein and its implications in the immunopathogenesis of dengue virus infection.* PLoS pathogens, 2015. **11**(7): p. e1005053.
280. Modhiran, N., et al., *Dengue virus NS1 protein activates immune cells via TLR4 but not TLR2 or TLR6.* Immunology and cell biology, 2017. **95**(5): p. 491-495.
281. Powers, H.R. and D. Sahoo, *SR-B1's next top model: structural perspectives on the functions of the HDL receptor.* Current atherosclerosis reports, 2022. **24**(4): p. 277-288.
282. Kim, D.H. and J.J. Rossi, *RNAi mechanisms and applications.* Biotechniques, 2008. **44**(5): p. 613-616.
283. Alshaer, W., et al., *siRNA: Mechanism of action, challenges, and therapeutic approaches.* European journal of pharmacology, 2021. **905**: p. 174178.
284. Sigoillot, F.D. and R.W. King, *Vigilance and validation: Keys to success in RNAi screening.* ACS chemical biology, 2011. **6**(1): p. 47-60.
285. Echeverri, C.J., et al., *Minimizing the risk of reporting false positives in large-scale RNAi screens.* Nature methods, 2006. **3**(10): p. 777-779.
286. Mohr, S., C. Bakal, and N. Perrimon, *Genomic screening with RNAi: results and challenges.* Annual review of biochemistry, 2010. **79**(1): p. 37-64.
287. Jackson, A.L. and P.S. Linsley, *Recognizing and avoiding siRNA off-target effects for target identification and therapeutic application.* Nature reviews Drug discovery, 2010. **9**(1): p. 57-67.
288. Jones, C.E., et al., *Discovering antiviral restriction factors and pathways using genetic screens.* Journal of General Virology, 2021. **102**(5): p. 001603.
289. Niinae, T., Y. Ishihama, and K. Imami, *Biotinylation-based proximity labelling proteomics: basics, applications and technical considerations.* Journal of Biochemistry, 2021. **170**(5): p. 569-576.
290. Bosch, J.A., C.L. Chen, and N. Perrimon, *Proximity-dependent labeling methods for proteomic profiling in living cells: An update.* Wiley Interdisciplinary Reviews: Developmental Biology, 2021. **10**(1): p. e392.
291. Gillen, J. and A. Nita-Lazar, *Experimental analysis of viral–host interactions.* Frontiers in physiology, 2019. **10**: p. 425.
292. Caraballo, G.I., et al., *The dengue virus nonstructural protein 1 (NS1) interacts with the putative epigenetic regulator DIDO1 to promote flavivirus replication in mosquito cells.* Journal of virology, 2022. **96**(12): p. e00704-22.
293. Coyaud, E., et al., *Global interactomics uncovers extensive organellar targeting by Zika virus.* Molecular & Cellular Proteomics, 2018. **17**(11): p. 2242-2255.

294. Riva, L., et al., *Comparative analysis of Hepatitis C virus NS5A dynamics and localization in assembly-deficient mutants.* Pathogens, 2021. **10**(2): p. 172.
295. Martell, J.D., et al., *Engineered ascorbate peroxidase as a genetically encoded reporter for electron microscopy.* Nature biotechnology, 2012. **30**(11): p. 1143-1148.
296. Rhee, H.-W., et al., *Proteomic mapping of mitochondria in living cells via spatially restricted enzymatic tagging.* Science, 2013. **339**(6125): p. 1328-1331.
297. Hung, V., et al., *Spatially resolved proteomic mapping in living cells with the engineered peroxidase APEX2.* Nature protocols, 2016. **11**(3): p. 456-475.
298. Lobingier, B.T., et al., *An approach to spatiotemporally resolve protein interaction networks in living cells.* Cell, 2017. **169**(2): p. 350-360. e12.
299. Fischl, W. and R. Bartenschlager, *High-throughput screening using dengue virus reporter genomes.* Antiviral methods and protocols, 2013: p. 205-219.
300. Cerikan, B., et al., *A non-replicative role of the 3' terminal sequence of the dengue virus genome in membranous replication organelle formation.* Cell Reports, 2020. **32**(1).
301. Centofanti, S.M., *A microscopy-based analysis of host factors associated with the secretion of dengue virus NS1*, in *College of Medicine and Public Health*. 2021, Flinders University. p. 116.
302. Sanjana, N.E., O. Shalem, and F. Zhang, *Improved vectors and genome-wide libraries for CRISPR screening.* Nature methods, 2014. **11**(8): p. 783-784.
303. Nakabayashi, H., et al., *Growth of human hepatoma cell lines with differentiated functions in chemically defined medium.* Cancer research, 1982. **42**(9): p. 3858-3863.
304. Blight, K.J., et al., *Efficient replication of hepatitis C virus genotype 1a RNAs in cell culture.* Journal of virology, 2003. **77**(5): p. 3181-3190.
305. Eyre, N.S., et al., *Phosphorylation of NS5A Serine-235 is essential to hepatitis C virus RNA replication and normal replication compartment formation.* Virology, 2016. **491**: p. 27-44.
306. Rabouille, C., *Pathways of unconventional protein secretion.* Trends in cell biology, 2017. **27**(3): p. 230-240.
307. Viotti, C., *ER to Golgi-dependent protein secretion: the conventional pathway.* Unconventional protein secretion: methods and protocols, 2016: p. 3-29.
308. Lippincott-Schwartz, J., *Membrane Traffic and Compartmentalization within the Secretory Pathway*, in *Molecular Biology of Membrane Transport Disorders*, S.G. Schultz, et al., Editors. 1996, Springer US: Boston, MA. p. 1-9.
309. Braakman, I. and N.J. Bulleid, *Protein folding and modification in the mammalian endoplasmic reticulum.* Annual review of biochemistry, 2011. **80**(1): p. 71-99.
310. Sun, Z. and J.L. Brodsky, *Protein quality control in the secretory pathway.* Journal of Cell Biology, 2019. **218**(10): p. 3171-3187.
311. Schjoldager, K.T., et al., *Global view of human protein glycosylation pathways and functions.* Nature reviews Molecular cell biology, 2020. **21**(12): p. 729-749.
312. Szul, T. and E. Sztul, *COPII and COPI traffic at the ER-Golgi interface.* Physiology, 2011. **26**(5): p. 348-364.
313. Appenzeller-Herzog, C. and H.-P. Hauri, *The ER-Golgi intermediate compartment (ERGIC): in search of its identity and function.* Journal of cell science, 2006. **119**(11): p. 2173-2183.
314. Frappaolo, A., et al., *The close relationship between the Golgi trafficking machinery and protein glycosylation.* Cells, 2020. **9**(12): p. 2652.
315. De Matteis, M.A. and A. Luini, *Exiting the Golgi complex.* Nature reviews Molecular cell biology, 2008. **9**(4): p. 273-284.
316. Di Martino, R., L. Sticco, and A. Luini, *Regulation of cargo export and sorting at the trans-Golgi network.* FEBS letters, 2019. **593**(17): p. 2306-2318.
317. Ford, C., et al., *Cargo sorting at the trans-Golgi network at a glance.* Journal of Cell Science, 2021. **134**(23): p. jcs259110.
318. Stalder, D. and D.C. Gershlick. *Direct trafficking pathways from the Golgi apparatus to the plasma membrane*. in *Seminars in cell & developmental biology*. 2020. Elsevier.
319. Abrahamsen, H. and H. Stenmark, *Protein secretion: unconventional exit by exophagy.* Current Biology, 2010. **20**(9): p. R415-R418.
320. Filaquier, A., et al., *Roads and hubs of unconventional protein secretion.* Current Opinion in Cell Biology, 2022. **75**: p. 102072.

321. Noh, S.H., Y.J. Kim, and M.G. Lee, *Autophagy-related pathways in vesicular unconventional protein secretion.* Frontiers in Cell and Developmental Biology, 2022. **10**: p. 892450.
322. Chiritoiu-Butnaru, M., et al., *Unconventional protein secretion: From basic mechanisms to dysregulation in disease*. 2022, Frontiers Media SA. p. 1088002.
323. Schatz, M., P.B.V. Tong, and B. Beaumelle. *Unconventional secretion of viral proteins*. in *Seminars in cell & developmental biology*. 2018. Elsevier.
324. Kirkegaard, K., *Unconventional secretion of hepatitis A virus.* Proceedings of the National Academy of Sciences, 2017. **114**(26): p. 6653-6655.
325. Saraste, J. and K. Prydz, *Assembly and cellular exit of coronaviruses: Hijacking an unconventional secretory pathway from the pre-Golgi intermediate compartment via the Golgi ribbon to the extracellular space.* Cells, 2021. **10**(3): p. 503.
326. Robinson, M., et al., *Viral journeys on the intracellular highways.* Cellular and Molecular Life Sciences, 2018. **75**: p. 3693-3714.
327. Cohen, M.J., W.J. Chirico, and P.N. Lipke, *Through the back door: unconventional protein secretion.* The Cell Surface, 2020. **6**: p. 100045.
328. Bunz, M., M. Ritter, and M. Schindler, *HCV egress–unconventional secretion of assembled viral particles.* Trends in microbiology, 2022. **30**(4): p. 364-378.
329. Rothman, J.E. and F.T. Wieland, *Protein sorting by transport vesicles.* Science, 1996. **272**(5259): p. 227-234.
330. Barlowe, C.K. and E.A. Miller, *Secretory protein biogenesis and traffic in the early secretory pathway.* Genetics, 2013. **193**(2): p. 383-410.
331. Lee, C. and J. Goldberg, *Structure of coatomer cage proteins and the relationship among COPI, COPII, and clathrin vesicle coats.* Cell, 2010. **142**(1): p. 123-132.
332. Hughson, F.M., *Copy Coats: COPI Mimics Clathrin and COPII.* Cell, 2010. **142**(1): p. 19-21.
333. Budnik, A. and D.J. Stephens, *ER exit sites–localization and control of COPII vesicle formation.* FEBS letters, 2009. **583**(23): p. 3796-3803.
334. Glick, B.S. and A. Luini, *Models for Golgi traffic: a critical assessment.* Cold Spring Harb Perspect Biol, 2011. **3**(11): p. a005215.
335. Orci, L., et al., *Bidirectional transport by distinct populations of COPI-coated vesicles.* Cell, 1997. **90**(2): p. 335-349.
336. Pellett, P.A., et al., *Inter-Golgi transport mediated by COPI-containing vesicles carrying small cargoes.* Elife, 2013. **2**: p. e01296.
337. Rabouille, C. and J. Klumperman, *The maturing role of COPI vesicles in intra-Golgi transport.* Nature reviews Molecular cell biology, 2005. **6**(10): p. 812-817.
338. Lippincott-Schwartz, J., N.B. Cole, and J.G. Donaldson, *Building a secretory apparatus: role of ARF1/COPI in Golgi biogenesis and maintenance.* Histochemistry and cell biology, 1998. **109**(5): p. 449-462.
339. Whitney, J.A., et al., *Cytoplasmic coat proteins involved in endosome function.* Cell, 1995. **83**(5): p. 703-13.
340. Aniento, F., et al., *An endosomal beta COP is involved in the pH-dependent formation of transport vesicles destined for late endosomes.* J Cell Biol, 1996. **133**(1): p. 29-41.
341. Daro, E., et al., *Inhibition of endosome function in CHO cells bearing a temperature-sensitive defect in the coatomer (COPI) component epsilon-COP.* J Cell Biol, 1997. **139**(7): p. 1747-59.
342. Gu, F., et al., *Functional dissection of COP-I subunits in the biogenesis of multivesicular endosomes.* J Cell Biol, 1997. **139**(5): p. 1183-95.
343. Beller, M., et al., *COPI complex is a regulator of lipid homeostasis.* PLoS Biol, 2008. **6**(11): p. e292.
344. Razi, M., E.Y. Chan, and S.A. Tooze, *Early endosomes and endosomal coatomer are required for autophagy.* J Cell Biol, 2009. **185**(2): p. 305-21.
345. Zabezhinsky, D., et al., *An Essential Role for COPI in mRNA Localization to Mitochondria and Mitochondrial Function.* Cell Rep, 2016. **15**(3): p. 540-549.
346. Liu, J., et al., *The COPI complex functions in nuclear envelope breakdown and is recruited by the nucleoporin Nup153.* Dev Cell, 2003. **5**(3): p. 487-98.
347. Li, H., et al., *alpha-COP binding to the survival motor neuron protein SMN is required for neuronal process outgrowth.* Hum Mol Genet, 2015. **24**(25): p. 7295-307.

348. Jain Goyal, M., et al., *A paralog-specific role of COPI vesicles in the neuronal differentiation of mouse pluripotent cells.* Life Sci Alliance, 2020. **3**(9).
349. Pakdel, M. and J. von Blume, *Exploring new routes for secretory protein export from the trans-Golgi network.* Molecular Biology of the Cell, 2018. **29**(3): p. 235-240.
350. Rout, M.P. and M.C. Field, *The evolution of organellar coat complexes and organization of the eukaryotic cell.* Annual review of biochemistry, 2017. **86**(1): p. 637-657.
351. Bonifacino, J.S. and B.S. Glick, *The mechanisms of vesicle budding and fusion.* cell, 2004. **116**(2): p. 153-166.
352. Jarsch, I.K., F. Daste, and J.L. Gallop, *Membrane curvature in cell biology: An integration of molecular mechanisms.* Journal of Cell Biology, 2016. **214**(4): p. 375-387.
353. Moelleken, J., et al., *Differential localization of coatomer complex isoforms within the Golgi apparatus.* Proceedings of the National Academy of Sciences, 2007. **104**(11): p. 4425-4430.
354. Futatsumori, M., et al., *Identification and characterization of novel isoforms of COP I subunits.* The journal of biochemistry, 2000. **128**(5): p. 793-801.
355. Wegmann, D., et al., *Novel isotypic γ/ζ subunits reveal three coatomer complexes in mammals.* Molecular and cellular biology, 2004.
356. Béthune, J. and F.T. Wieland, *Assembly of COPI and COPII vesicular coat proteins on membranes.* Annual review of biophysics, 2018. **47**(1): p. 63-83.
357. Walton, K., et al., *Site-specific phosphorylations of the Arf activator GBF1 differentially regulate GBF1 function in Golgi homeostasis and secretion versus cytokinesis.* Scientific Reports, 2023. **13**(1): p. 13609.
358. Sztul, E., et al., *ARF GTPases and their GEFs and GAPs: concepts and challenges.* Molecular biology of the cell, 2019. **30**(11): p. 1249-1271.
359. Cavenagh, M.M., et al., *Intracellular distribution of Arf proteins in mammalian cells: Arf6 is uniquely localized to the plasma membrane.* Journal of Biological Chemistry, 1996. **271**(36): p. 21767-21774.
360. Popoff, V., et al., *Several ADP-ribosylation factor (Arf) isoforms support COPI vesicle formation.* Journal of Biological Chemistry, 2011. **286**(41): p. 35634-35642.
361. Nie, Z., D.S. Hirsch, and P.A. Randazzo, *Arf and its many interactors.* Current opinion in cell biology, 2003. **15**(4): p. 396-404.
362. Kudelko, M., et al., *Class II ADP-ribosylation Factors Are Required for Efficient Secretion of Dengue Viruses*.* Journal of Biological Chemistry, 2012. **287**(1): p. 767-777.
363. Pennauer, M., et al., *Shared and specific functions of Arfs 1–5 at the Golgi revealed by systematic knockouts.* Journal of Cell Biology, 2021. **221**(1): p. e202106100.
364. Jackson, C.L. and J.E. Casanova, *Turning on ARF: the Sec7 family of guanine-nucleotide-exchange factors.* Trends in cell biology, 2000. **10**(2): p. 60-67.
365. Pipaliya, S.V., et al., *Ancient complement and lineage-specific evolution of the Sec7 ARF GEF proteins in eukaryotes.* Molecular Biology of the Cell, 2019. **30**(15): p. 1846-1863.
366. Walton, K., A. Leier, and E. Sztul, *Regulating the regulators: role of phosphorylation in modulating the function of the GBF1/BIG family of Sec7 ARF-GEFs.* FEBS letters, 2020. **594**(14): p. 2213-2226.
367. Wright, J., R.A. Kahn, and E. Sztul, *Regulating the large Sec7 ARF guanine nucleotide exchange factors: the when, where and how of activation.* Cellular and molecular life sciences, 2014. **71**: p. 3419-3438.
368. Meissner, J.M., et al., *The Arf-GEF GBF1 undergoes multi-domain structural shifts to activate Arf at the Golgi.* Frontiers in Cell and Developmental Biology, 2023. **11**: p. 1233272.
369. Bhatt, J.M., et al., *Promiscuity of the catalytic Sec7 domain within the guanine nucleotide exchange factor GBF1 in ARF activation, Golgi homeostasis, and effector recruitment.* Molecular Biology of the Cell, 2019. **30**(12): p. 1523-1535.
370. Martinez, J.L. and C.F. Arias, *Role of the Guanine Nucleotide Exchange Factor GBF1 in the Replication of RNA Viruses.* Viruses, 2020. **12**(6).
371. García-Mata, R., et al., *ADP-ribosylation factor/COPI-dependent events at the endoplasmic reticulum-Golgi interface are regulated by the guanine nucleotide exchange factor GBF1.* Molecular biology of the cell, 2003. **14**(6): p. 2250-2261.
372. Casanova, J.E., *Regulation of Arf activation: the Sec7 family of guanine nucleotide exchange factors.* Traffic, 2007. **8**(11): p. 1476-1485.

373. Liu, Y., R.A. Kahn, and J.H. Prestegard, *Structure and membrane interaction of myristoylated ARF1.* Structure, 2009. **17**(1): p. 79-87.
374. Deng, Y., et al., *A COPI coat subunit interacts directly with an early-Golgi localized Arf exchange factor.* EMBO reports, 2009. **10**(1): p. 58-64.
375. Hamlin, J.N., et al., *Scyl1 scaffolds class II Arfs to specific subcomplexes of coatomer through the γ-COP appendage domain.* Journal of cell science, 2014. **127**(7): p. 1454-1463.
376. Arakel, E.C. and B. Schwappach, *Formation of COPI-coated vesicles at a glance.* Journal of cell science, 2018. **131**(5): p. jcs209890.
377. Beck, R., et al., *The COPI system: molecular mechanisms and function.* FEBS letters, 2009. **583**(17): p. 2701-2709.
378. Barlowe, C. and A. Helenius, *Cargo capture and bulk flow in the early secretory pathway.* Annual review of cell and developmental biology, 2016. **32**(1): p. 197-222.
379. Zerangue, N., et al., *Analysis of endoplasmic reticulum trafficking signals by combinatorial screening in mammalian cells.* Proceedings of the National Academy of Sciences, 2001. **98**(5): p. 2431-2436.
380. Paczkowski, J.E., B.C. Richardson, and J.C. Fromme, *Cargo adaptors: structures illuminate mechanisms regulating vesicle biogenesis.* Trends in cell biology, 2015. **25**(7): p. 408-416.
381. Bigay, J., et al., *Lipid packing sensed by ArfGAP1 couples COPI coat disassembly to membrane bilayer curvature.* Nature, 2003. **426**(6966): p. 563-566.
382. Cai, H., K. Reinisch, and S. Ferro-Novick, *Coats, tethers, Rabs, and SNAREs work together to mediate the intracellular destination of a transport vesicle.* Developmental cell, 2007. **12**(5): p. 671-682.
383. Taylor, R.J., G. Tagiltsev, and J.A. Briggs, *The structure of COPI vesicles and regulation of vesicle turnover.* FEBS letters, 2023. **597**(6): p. 819-835.
384. Shah, P.S., et al., *Comparative Flavivirus-Host Protein Interaction Mapping Reveals Mechanisms of Dengue and Zika Virus Pathogenesis.* Cell, 2018. **175**(7): p. 1931-1945 e18.
385. Hafirassou, M.L., et al., *A Global Interactome Map of the Dengue Virus NS1 Identifies Virus Restriction and Dependency Host Factors.* Cell Rep, 2017. **21**(13): p. 3900-3913.
386. Balsitis, S.J., et al., *Tropism of dengue virus in mice and humans defined by viral nonstructural protein 3-specific immunostaining.* The American journal of tropical medicine and hygiene, 2009. **80**(3): p. 416-424.
387. Eyre, N.S., et al., *Dynamic imaging of the hepatitis C virus NS5A protein during a productive infection.* Journal of virology, 2014. **88**(7): p. 3636-3652.
388. Tongmuang, N., et al., *Coat protein complex I facilitates dengue virus production.* Virus Res, 2018. **250**: p. 13-20.
389. Pontifex, C.S., et al., *Valosin-Containing Protein (VCP): A Review of Its Diverse Molecular Functions and Clinical Phenotypes.* International Journal of Molecular Sciences, 2024. **25**(11): p. 5633.
390. Phongphaew, W., et al., *Valosin-containing protein (VCP/p97) plays a role in the replication of West Nile virus.* Virus research, 2017. **228**: p. 114-123.
391. Ramanathan, H.N., et al., *A sensitive yellow fever virus entry reporter identifies valosin-containing protein (VCP/p97) as an essential host factor for flavivirus uncoating.* MBio, 2020. **11**(2): p. 10.1128/mbio. 00467-20.
392. Tabata, K., et al., *Endoplasmic reticulum-associated degradation controls virus protein homeostasis, which is required for flavivirus propagation.* Journal of Virology, 2021. **95**(15): p. 10.1128/jvi. 02234-20.
393. Anton, A., et al., *Valosin-containing protein ATPase activity regulates the morphogenesis of Zika virus replication organelles and virus-induced cell death.* Cellular Microbiology, 2021. **23**(4): p. e13302.
394. Sehrawat, S., et al., *Valosin-containing protein/p97 plays critical roles in the Japanese encephalitis virus life cycle.* Journal of Virology, 2021. **95**(11): p. 10.1128/jvi. 02336-20.
395. Mazeaud, C., et al., *The biogenesis of dengue virus replication organelles requires the ATPase activity of valosin-containing protein.* Viruses, 2021. **13**(10): p. 2092.
396. Ferguson, S.M. and P. De Camilli, *Dynamin, a membrane-remodelling GTPase.* Nature reviews Molecular cell biology, 2012. **13**(2): p. 75-88.
397. Jovic, M., et al., *The early endosome: a busy sorting station for proteins at the crossroads.* Histology and histopathology, 2010. **25**(1): p. 99.

398. Volpi, C., et al., *Opportunities and challenges in drug discovery targeting metabotropic glutamate receptor 4.* Expert Opinion on Drug Discovery, 2018. **13**(5): p. 411-423.
399. Clarke, P., et al., *Virus-induced transcriptional changes in the brain include the differential expression of genes associated with interferon, apoptosis, interleukin 17 receptor A, and glutamate signaling as well as flavivirus-specific upregulation of tRNA synthetases.* MBio, 2014. **5**(2): p. 10.1128/mbio. 00902-14.
400. Abe, K., et al., *Vav2 is an activator of Cdc42, Rac1, and RhoA.* Journal of Biological Chemistry, 2000. **275**(14): p. 10141-10149.
401. Norbury, A.J., et al., *Vav Proteins in Development of the Brain: A Potential Relationship to the Pathogenesis of Congenital Zika Syndrome?* Viruses, 2022. **14**(2).
402. Cowell, E., et al., *Vav proteins do not influence dengue virus replication but are associated with induction of phospho-ERK, IL-6, and viperin mRNA following DENV infection in vitro.* Microbiology Spectrum, 2024. **12**(1): p. e02391-23.
403. Garcia-Mata, R., et al., *ADP-ribosylation factor/COPI-dependent events at the endoplasmic reticulum-Golgi interface are regulated by the guanine nucleotide exchange factor GBF1.* Mol Biol Cell, 2003. **14**(6): p. 2250-61.
404. Bartlett, D.W. and M.E. Davis, *Insights into the kinetics of siRNA-mediated gene silencing from live-cell and live-animal bioluminescent imaging.* Nucleic acids research, 2006. **34**(1): p. 322-333.
405. Lowe, M. and T.E. Kreis, *In vivo assembly of coatomer, the COP-I coat precursor.* J Biol Chem, 1996. **271**(48): p. 30725-30.
406. Wang, T., et al., *Identification and characterization of essential genes in the human genome.* Science, 2015. **350**(6264): p. 1096-1101.
407. Park, J.S., et al., *A FACS-based genome-wide CRISPR screen reveals a requirement for COPI in Chlamydia trachomatis invasion.* IScience, 2019. **11**: p. 71-84.
408. Brinkman, E.K., et al., *Easy quantitative assessment of genome editing by sequence trace decomposition.* Nucleic acids research, 2014. **42**(22): p. e168-e168.
409. Adikusuma, F., et al., *Large deletions induced by Cas9 cleavage.* Nature, 2018. **560**(7717): p. E8-E9.
410. Watkin, L.B., et al., *COPA mutations impair ER-Golgi transport and cause hereditary autoimmune-mediated lung disease and arthritis.* Nature Genetics, 2015. **47**(6): p. 654-660.
411. DiStasio, A., et al., *Copb2 is essential for embryogenesis and hypomorphic mutations cause human microcephaly.* Hum Mol Genet, 2017. **26**(24): p. 4836-4848.
412. Bainter, W., et al., *Combined immunodeficiency due to a mutation in the γ1 subunit of the coat protein I complex.* The Journal of Clinical Investigation, 2021. **131**(3).
413. Shiri, A., et al., *Novel insight into the phenotype of microcephaly 19 in the patient with missense COPB2 mutation.* Eur J Med Genet, 2023. **66**(10): p. 104846.
414. Cerikan, B., et al., *A Non-Replicative Role of the 3′ Terminal Sequence of the Dengue Virus Genome in Membranous Replication Organelle Formation.* Cell Rep, 2020. **32**(1): p. 107859.
415. Saenz, J.B., et al., *Golgicide A reveals essential roles for GBF1 in Golgi assembly and function.* Nat Chem Biol, 2009. **5**(3): p. 157-65.
416. Westaway, E.G., *Proteins specified by group B togaviruses in mammalian cells during productive infections.* Virology, 1973. **51**(2): p. 454-65.
417. Mackenzie, J.M., M.K. Jones, and E.G. Westaway, *Markers for trans-Golgi membranes and the intermediate compartment localize to induced membranes with distinct replication functions in flavivirus-infected cells.* J Virol, 1999. **73**(11): p. 9555-67.
418. Mackenzie, J.M. and E.G. Westaway, *Assembly and maturation of the flavivirus Kunjin virus appear to occur in the rough endoplasmic reticulum and along the secretory pathway, respectively.* J Virol, 2001. **75**(22): p. 10787-99.
419. Carpp, L.N., et al., *Quantitative proteomic analysis of host-virus interactions reveals a role for Golgi brefeldin A resistance factor 1 (GBF1) in dengue infection.* Mol Cell Proteomics, 2014. **13**(11): p. 2836-54.
420. Rosales Ramirez, R. and J.E. Ludert, *The Dengue Virus Nonstructural Protein 1 (NS1) Is Secreted from Mosquito Cells in Association with the Intracellular Cholesterol Transporter Chaperone Caveolin Complex.* J Virol, 2019. **93**(4).
421. Nicholls, C.M., M. Sevvana, and R.J. Kuhn, *Structure-guided paradigm shifts in flavivirus assembly and maturation mechanisms.* Advances in virus research, 2020. **108**: p. 33-83.

422. Krzysztoń, R., et al., *Single-cell kinetics of siRNA-mediated mRNA degradation.* Nanomedicine: Nanotechnology, Biology and Medicine, 2019. **21**: p. 102077.
423. Cao, H., F. Garcia, and M.A. McNiven, *Differential distribution of dynamin isoforms in mammalian cells.* Molecular biology of the cell, 1998. **9**(9): p. 2595-2609.
424. Bhave, M., et al., *Early and nonredundant functions of dynamin isoforms in clathrin-mediated endocytosis.* Molecular biology of the cell, 2020. **31**(18): p. 2035-2047.
425. Mettlen, M., et al., *Regulation of clathrin-mediated endocytosis.* Annual review of biochemistry, 2018. **87**(1): p. 871-896.
426. Stenbeck, G., et al., *beta'-COP, a novel subunit of coatomer.* EMBO J, 1993. **12**(7): p. 2841-5.
427. Kawamoto, K., et al., *GBF1, a guanine nucleotide exchange factor for ADP-ribosylation factors, is localized to the cis-Golgi and involved in membrane association of the COPI coat.* Traffic, 2002. **3**(7): p. 483-95.
428. Hara-Kuge, S., et al., *En bloc incorporation of coatomer subunits during the assembly of COP-coated vesicles.* J Cell Biol, 1994. **124**(6): p. 883-92.
429. Arakel, E.C. and B. Schwappach, *Formation of COPI-coated vesicles at a glance.* J Cell Sci, 2018. **131**(5).
430. Arab, M., T. Chen, and M. Lowe, *Mechanisms governing vesicle traffic at the Golgi apparatus.* Current opinion in cell biology, 2024. **88**: p. 102365.
431. Orci, L., et al., *Bidirectional transport by distinct populations of COPI-coated vesicles.* Cell, 1997. **90**(2): p. 335-49.
432. Bhatt, J.M., et al., *Promiscuity of the catalytic Sec7 domain within the guanine nucleotide exchange factor GBF1 in ARF activation, Golgi homeostasis, and effector recruitment.* Mol Biol Cell, 2019. **30**(12): p. 1523-1535.
433. Cherfils, J., *Arf GTPases and their effectors: assembling multivalent membrane-binding platforms.* Curr Opin Struct Biol, 2014. **29**: p. 67-76.
434. Adolf, F., et al., *Proteomic profiling of mammalian COPII and COPI vesicles.* Cell reports, 2019. **26**(1): p. 250-265. e5.
435. Tongmuang, N., et al., *Coat protein complex I facilitates dengue virus production.* Virus research, 2018. **250**: p. 13-20.
436. Steiner, A., et al., *Deficiency in coatomer complex I causes aberrant activation of STING signalling.* Nat Commun, 2022. **13**(1): p. 2321.
437. Steiner, A., et al., *Deficiency in coatomer complex I causes aberrant activation of STING signalling.* Nature communications, 2022. **13**(1): p. 2321.
438. Deng, Z., et al., *A defect in COPI-mediated transport of STING causes immune dysregulation in COPA syndrome.* Journal of Experimental Medicine, 2020. **217**(11): p. e20201045.
439. Vece, T.J., et al., *Copa syndrome: a novel autosomal dominant immune dysregulatory disease.* Journal of clinical immunology, 2016. **36**: p. 377-387.
440. Youn, S., et al., *A short N-terminal peptide motif on flavivirus nonstructural protein NS1 modulates cellular targeting and immune recognition.* Journal of virology, 2010. **84**(18): p. 9516-9532.
441. Hassan, Z., et al., *How viruses hijack and modify the secretory transport pathway.* Cells, 2021. **10**(10): p. 2535.
442. Mackenzie, J., *Wrapping things up about virus RNA replication.* Traffic, 2005. **6**(11): p. 967-977.
443. Rastogi, M., N. Sharma, and S.K. Singh, *Flavivirus NS1: a multifaceted enigmatic viral protein.* Virology journal, 2016. **13**: p. 1-10.
444. Petrova, E., et al., *Uncovering flavivirus host dependency factors through a genome-wide gain-of-function screen.* Viruses, 2019. **11**(1): p. 68.
445. Alcala, A.C., L.A. Palomares, and J.E. Ludert, *Secretion of Nonstructural Protein 1 of Dengue Virus from Infected Mosquito Cells: Facts and Speculations.* J Virol, 2018. **92**(14).
446. Lam, S.S., et al., *Directed evolution of APEX2 for electron microscopy and proximity labeling.* Nature methods, 2015. **12**(1): p. 51-54.
447. Eyre, N.S., et al., *Identification of estrogen receptor modulators as inhibitors of flavivirus infection.* Antimicrobial agents and chemotherapy, 2020. **64**(8): p. 10.1128/aac. 00289-20.
448. Chapman-Smith, A. and J.E. Cronan Jr, *Molecular biology of biotin attachment to proteins.* The Journal of nutrition, 1999. **129**(2): p. 477S-484S.

449. Wu, Y.-W., et al., *Autophagy-associated dengue vesicles promote viral transmission avoiding antibody neutralization.* Scientific reports, 2016. **6**(1): p. 32243.
450. Safadi, D.E., et al., *Extracellular vesicles are conveyors of the NS1 toxin during dengue virus and Zika virus infection.* Viruses, 2023. **15**(2): p. 364.
451. Das, P. and J.P. Dudley, *How viruses use the VCP/p97 ATPase molecular machine.* Viruses, 2021. **13**(9): p. 1881.
452. Schiavo, G., et al., *Cytoplasmic dynein heavy chain: the servant of many masters.* Trends in neurosciences, 2013. **36**(11): p. 641-651.
453. Silva, E.M., et al., *Mapping the interactions of dengue virus NS1 protein with human liver proteins using a yeast two-hybrid system: identification of C1q as an interacting partner.* PloS one, 2013. **8**(3): p. e57514.
454. Nascimento, E.J., et al., *Alternative complement pathway deregulation is correlated with dengue severity.* PloS one, 2009. **4**(8): p. e6782.
455. Chung, K.M., et al., *West Nile virus nonstructural protein NS1 inhibits complement activation by binding the regulatory protein factor H.* Proc Natl Acad Sci U S A, 2006. **103**(50): p. 19111-6.
456. Kraivong, R., et al., *Complement alternative pathway genetic variation and dengue infection in the Thai population.* Clinical & Experimental Immunology, 2013. **174**(2): p. 326-334.
457. Cervantes-Salazar, M., et al., *Dengue virus NS1 protein interacts with the ribosomal protein RPL18: this interaction is required for viral translation and replication in Huh-7 cells.* Virology, 2015. **484**: p. 113-126.
458. Diamond, M.S., et al., *Modulation of dengue virus infection in human cells by alpha, beta, and gamma interferons.* Journal of virology, 2000. **74**(11): p. 4957-4966.
459. Diamond, M.S. and E. Harris, *Interferon inhibits dengue virus infection by preventing translation of viral RNA through a PKR-independent mechanism.* Virology, 2001. **289**(2): p. 297-311.
460. Gurung, S., et al., *The exosome journey: from biogenesis to uptake and intracellular signalling.* Cell Communication and Signaling, 2021. **19**(1): p. 47.
461. Martínez-Rojas, P.P., V. Monroy-Martínez, and B.H. Ruiz-Ordaz, *Role of extracellular vesicles in the pathogenesis of mosquito-borne flaviviruses that impact public health.* Journal of Biomedical Science, 2025. **32**(1): p. 4.
462. Reyes-Ruiz, J.M., et al., *The regulation of flavivirus infection by hijacking exosome-mediated cell–cell communication: new insights on virus–host interactions.* Viruses, 2020. **12**(7): p. 765.
463. Latanova, A., V. Karpov, and E. Starodubova, *Extracellular Vesicles in Flaviviridae Pathogenesis: Their Roles in Viral Transmission, Immune Evasion, and Inflammation.* International Journal of Molecular Sciences, 2024. **25**(4): p. 2144.
464. Valenzuela-Fernandez, A., et al., *HDAC6: a key regulator of cytoskeleton, cell migration and cell–cell interactions.* Trends in cell biology, 2008. **18**(6): p. 291-297.
465. Zhao, Y.G., P. Codogno, and H. Zhang, *Machinery, regulation and pathophysiological implications of autophagosome maturation.* Nature Reviews Molecular Cell Biology, 2021. **22**(11): p. 733-750.
466. Halstead, S.B., *Three dengue vaccines—what now.* N. Engl. J. Med, 2024. **390**: p. 464-465.
467. Gazina, E.V., et al., *Differential requirements for COPI coats in formation of replication complexes among three genera of Picornaviridae.* Journal of virology, 2002. **76**(21): p. 11113-11122.
468. Ma, W. and J. Goldberg, *Rules for the recognition of dilysine retrieval motifs by coatomer.* The EMBO journal, 2013. **32**(7): p. 926-937.
469. Zhang, Y., et al., *Loss of COPZ1 induces NCOA4 mediated autophagy and ferroptosis in glioblastoma cell lines.* Oncogene, 2021. **40**(8): p. 1425-1439.
470. Nie, J., et al., *COPI Vesicle Disruption Inhibits Mineralization via mTORC1-Mediated Autophagy.* International Journal of Molecular Sciences, 2023. **25**(1): p. 339.
471. Buratta, S., et al., *Lysosomal exocytosis, exosome release and secretory autophagy: the autophagic-and endo-lysosomal systems go extracellular.* International journal of molecular sciences, 2020. **21**(7): p. 2576.
472. Lepelley, A., et al., *Mutations in COPA lead to abnormal trafficking of STING to the Golgi and interferon signaling.* Journal of Experimental Medicine, 2020. **217**(11): p. e20200600.

473. Lee, Y.-R., et al., *Dengue virus-induced ER stress is required for autophagy activation, viral replication, and pathogenesis both in vitro and in vivo.* Scientific reports, 2018. **8**(1): p. 489.
474. Saenz, J.B., et al., *Golgicide A reveals essential roles for GBF1 in Golgi assembly and function.* Nature chemical biology, 2009. **5**(3): p. 157-165.
475. Bui, Q.T., M.-P. Golinelli-Cohen, and C.L. Jackson, *Large Arf1 guanine nucleotide exchange factors: evolution, domain structure, and roles in membrane trafficking and human disease.* Molecular Genetics and Genomics, 2009. **282**: p. 329-350.
476. Belov, G.A., et al., *Poliovirus replication requires the N-terminus but not the catalytic Sec7 domain of ArfGEF GBF1.* Cellular microbiology, 2010. **12**(10): p. 1463-1479.
477. Thiam, A.R., et al., *COPI buds 60-nm lipid droplets from reconstituted water–phospholipid–triacylglyceride interfaces, suggesting a tension clamp function.* Proceedings of the National Academy of Sciences, 2013. **110**(33): p. 13244-13249.
478. Wilfling, F., et al., *Arf1/COPI machinery acts directly on lipid droplets and enables their connection to the ER for protein targeting.* elife, 2014. **3**: p. e01607.
479. Olzmann, J.A. and P. Carvalho, *Dynamics and functions of lipid droplets.* Nature reviews Molecular cell biology, 2019. **20**(3): p. 137-155.
480. Gabriely, G., R. Kama, and J.E. Gerst, *Involvement of specific COPI subunits in protein sorting from the late endosome to the vacuole in yeast.* Molecular and cellular biology, 2007.
481. Ponpuak, M., et al., *Secretory autophagy.* Current opinion in cell biology, 2015. **35**: p. 106-116.
482. Tapia, D., et al., *Impact of interorganelle coordination between the conventional early secretory pathway and autophagy in cellular homeostasis and stress response.* Frontiers in Cell and Developmental Biology, 2023. **11**: p. 1069256.
483. Li, Q., et al., *Molecular mechanisms of secretory autophagy and its potential role in diseases.* Life Sciences, 2024: p. 122653.
484. Lee, Y.-R., et al., *Autophagic machinery activated by dengue virus enhances virus replication.* Virology, 2008. **374**(2): p. 240-248.
485. Wu, N., et al., *DENV-2 NS1 promotes AMPK-LKB1 interaction to activate AMPK/ERK/mTOR signaling pathway to induce autophagy.* Virology Journal, 2023. **20**(1): p. 231.
486. Cloherty, A.P., et al., *Dengue virus exploits autophagy vesicles and secretory pathways to promote transmission by human dendritic cells.* Frontiers in Immunology, 2024. **15**: p. 1260439.
487. Wu, S.-Y., et al., *The autophagosomes containing dengue virus proteins and full-length genomic RNA are infectious.* Viruses, 2021. **13**(10): p. 2034.
488. Li, M.Y., et al., *Lyn kinase regulates egress of flaviviruses in autophagosome-derived organelles.* Nature communications, 2020. **11**(1): p. 5189.
489. Karasu, E., et al., *Extracellular vesicles: packages sent with complement.* Frontiers in immunology, 2018. **9**: p. 721.
490. Bushey, R.T., et al., *Complement factor H protects tumor cell-derived exosomes from complement-dependent lysis and phagocytosis.* Plos one, 2021. **16**(6): p. e0252577.
491. Perkins, S.J., K.W. Fung, and S. Khan, *Molecular interactions between complement factor H and its heparin and heparan sulfate ligands.* Frontiers in immunology, 2014. **5**: p. 126.
492. Ochkasova, A., et al., *Two "Edges" in Our Knowledge on the Functions of Ribosomal Proteins: The Revealed Contributions of Their Regions to Translation Mechanisms and the Issues of Their Extracellular Transport by Exosomes.* International Journal of Molecular Sciences, 2023. **24**(14): p. 11458.
493. Zhao, Z., et al., *The Influence of Extra-Ribosomal Functions of Eukaryotic Ribosomal Proteins on Viral Infection.* Biomolecules, 2024. **14**(12): p. 1565.
494. Mitterer, V., et al., *Sequential domain assembly of ribosomal protein S3 drives 40S subunit maturation.* Nature communications, 2016. **7**(1): p. 10336.
495. Das, A.S., A. Basu, and R. Mukhopadhyay, *Ribosomal proteins: the missing piece in the inflammation puzzle?* Molecular and Cellular Biochemistry, 2024: p. 1-13.
496. Sun, M.-Y., et al., *Cisplatin-resistant gastric cancer cells promote the chemoresistance of cisplatin-sensitive cells via the exosomal RPS3-mediated PI3K-Akt-Cofilin-1 signaling axis.* Frontiers in Cell and Developmental Biology, 2021. **9**: p. 618899.

497. Statello, L., et al., *Identification of RNA-binding proteins in exosomes capable of interacting with different types of RNA: RBP-facilitated transport of RNAs into exosomes.* PloS one, 2018. **13**(4): p. e0195969.
498. Vora, A., et al., *Arthropod EVs mediate dengue virus transmission through interaction with a tetraspanin domain containing glycoprotein Tsp29Fb.* Proceedings of the National Academy of Sciences, 2018. **115**(28): p. E6604-E6613.
499. Yeh, S.-C., et al., *The anti-immune dengue subgenomic flaviviral RNA is present in vesicles in mosquito saliva and is associated with increased infectivity.* PLoS pathogens, 2023. **19**(3): p. e1011224.
500. Padrón, A., S. Iwasaki, and N.T. Ingolia, *Proximity RNA labeling by APEX-seq reveals the organization of translation initiation complexes and repressive RNA granules.* Molecular cell, 2019. **75**(4): p. 875-887. e5.
501. Hutagalung, A.H. and P.J. Novick, *Role of Rab GTPases in membrane traffic and cell physiology.* Physiological reviews, 2011. **91**(1): p. 119-149.
502. Lamber, E.P., A.-C. Siedenburg, and F.A. Barr, *Rab regulation by GEFs and GAPs during membrane traffic.* Current opinion in cell biology, 2019. **59**: p. 34-39.
503. Grosshans, B.L., D. Ortiz, and P. Novick, *Rabs and their effectors: achieving specificity in membrane traffic.* Proceedings of the National Academy of Sciences, 2006. **103**(32): p. 11821-11827.
504. Homma, Y., S. Hiragi, and M. Fukuda, *Rab family of small GTPases: an updated view on their regulation and functions.* The FEBS journal, 2021. **288**(1): p. 36-55.
505. Goldenring, J.R., *Recycling endosomes.* Current opinion in cell biology, 2015. **35**: p. 117-122.
506. Yan, Z., et al., *Rab11a mediates vascular endothelial-cadherin recycling and controls endothelial barrier function.* Arteriosclerosis, thrombosis, and vascular biology, 2016. **36**(2): p. 339-349.
507. Escrevente, C., et al., *Rab11 is required for lysosome exocytosis through the interaction with Rab3a, Sec15 and GRAB.* Journal of cell science, 2021. **134**(11): p. jcs246694.
508. Tancini, B., et al., *Lysosomal exocytosis: the extracellular role of an intracellular organelle.* Membranes, 2020. **10**(12): p. 406.
509. Moya-Alvarado, G., et al., *The Rab11-regulated endocytic pathway and BDNF/TrkB signaling: Roles in plasticity changes and neurodegenerative diseases.* Neurobiology of Disease, 2022. **171**: p. 105796.
510. Mukhopadhyay, A., et al., *Proteomic analysis of endocytic vesicles: Rab1a regulates motility of early endocytic vesicles.* Journal of cell science, 2011. **124**(5): p. 765-775.
511. Bhuin, T. and J.K. Roy, *Rab proteins: the key regulators of intracellular vesicle transport.* Experimental cell research, 2014. **328**(1): p. 1-19.
512. Reck-Peterson, S.L., et al., *The cytoplasmic dynein transport machinery and its many cargoes.* Nature reviews Molecular cell biology, 2018. **19**(6): p. 382-398.
513. Bec, N., et al., *Proteasome 19S RP and translation preinitiation complexes are secreted within exosomes upon serum starvation.* Traffic, 2019. **20**(7): p. 516-536.
514. Chen, J., et al., *Review on strategies and technologies for exosome isolation and purification.* Frontiers in bioengineering and biotechnology, 2022. **9**: p. 811971.
515. Palomba, A., et al., *Comparative evaluation of MaxQuant and proteome discoverer MS1-based protein quantification tools.* Journal of proteome research, 2021. **20**(7): p. 3497-3507.